Advances in Clinical and Experimental Medicine

MONTHLY ISSN 1899-5276 (PRINT) ISSN 2451-2680 (ONLINE) advances.umw.edu.pl

2026, Vol. 35, No. 2 (February)

Impact Factor (IF) – 1.9
Ministry of Science and Higher Education – 70 pts
Index Copernicus (ICV) – 161.00 pts

Wroclaw Medical University

Advances
in Clinical and Experimental
Medicine

Advances
in Clinical and Experimental Medicine

ISSN 1899-5276 (PRINT) ISSN 2451-2680 (ONLINE) advances.umw.edu.pl

MONTHLY 2026
Vol. 35, No. 2
(February)

Advances in Clinical and Experimental Medicine (*Adv Clin Exp Med*) publishes high-quality original articles, research-in-progress, research letters and systematic reviews and meta-analyses of recognized scientists that deal with all clinical and experimental medicine.

Editorial Office
ul. Marcinkowskiego 2–6
50-368 Wrocław, Poland
Tel.: +48 71 784 12 05
E-mail: acem.journal@umw.edu.pl

Publisher
Wroclaw Medical University
Wybrzeże L. Pasteura 1
50-367 Wrocław, Poland

Online edition is the original version of the journal

Editorial Policy

Advances in Clinical and Experimental Medicine (Adv Clin Exp Med) is an independent multidisciplinary forum for exchange of scientific and clinical information, publishing original research and news encompassing all aspects of medicine, including molecular biology, biochemistry, genetics, biotechnology and other areas. During the review process, the Editorial Board conforms to the "Uniform Requirements for Manuscripts Submitted to Biomedical Journals: Writing and Editing for Biomedical Publication" approved by the International Committee of Medical Journal Editors (www.ICMJE.org). The journal publishes (in English only) original papers and reviews. Short works considered original, novel and significant are given priority. Experimental studies must include a statement that the experimental protocol and informed consent procedure were in compliance with the Helsinki Convention and were approved by an ethics committee.

For all subscription-related queries please contact our Editorial Office: acem.journal@umw.edu.pl
For more information visit the journal's website: advances.umw.edu.pl

Pursuant to the ordinance of the Rector of Wroclaw Medical University No. 37/XVI R/2024, from March 1, 2024, authors are required to pay a fee for each manuscript accepted for publication in the journal Advances in Clinical and Experimental Medicine. The fee amounts to 1600 EUR for all types of papers.

Indexed in: MEDLINE, Science Citation Index Expanded, Journal Citation Reports/Science Edition, Scopus, EMBASE/Excerpta Medica, Ulrich's™ International Periodicals Directory, Index Copernicus

Typographic design: Piotr Gil, Monika Kolęda
DTP: Wydawnictwo UMW
Cover: Monika Kolęda
Printing and binding: Drukarnia I-BiS Bierońscy Sp.k.

Advances
in Clinical and Experimental Medicine

MONTHLY 2026, Vol. 35, No. 2 (February)

ISSN 1899-5276 (PRINT)
ISSN 2451-2680 (ONLINE)
advances.umw.edu.pl

Contents

Editorials

Original papers

Reviews

Internal peacekeepers and external mediators: A new model of peripheral immune tolerance involving regulatory T cells and mesenchymal stem cells

Phuc Van Pham[A–F]

VNUHCM-US Stem Cell Institute, University of Science, Vietnam National University Ho Chi Minh City, Vietnam

A – research concept and design; B – collection and/or assembly of data; C – data analysis and interpretation;
D – writing the article; E – critical revision of the article; F – final approval of the article

Advances in Clinical and Experimental Medicine, ISSN 1899–5276 (print), ISSN 2451–2680 (online) *Adv Clin Exp Med*. 2026;35(2):195–200

Address for correspondence
Phuc Van Pham
E-mail: phucpham@sci.edu.vn

Funding sources
None declared

Conflict of interest
None declared

Received on November 17, 2025
Reviewed on January 9, 2026
Accepted on January 11, 2026

Published online on January 23, 2026

Abstract

The 2025 Nobel Prize in Physiology or Medicine honored the seminal discovery that regulatory T cells (Tregs) restrain immune responses and prevent autoimmunity through peripheral immune tolerance. However, to obtain a holistic view of peripheral immune tolerance, it is also necessary to consider the role of mesenchymal stem/stromal cells (MSCs) in this process. Therefore, I propose a two-tier model that incorporates both Tregs and MSCs, with Tregs acting within the immune system as an "internal checkpoint" to temper effector cell activity, and tissue-resident MSCs – or "master signaling cells" – serving as an "external checkpoint." Injury- or pathogen-induced inflammation activates MSCs, which in turn secrete a broad repertoire of immunomodulatory molecules, create a local anti-inflammatory milieu, promote tissue repair, and directly dampen excessive immune activity at the site of damage. The concerted actions of Tregs and MSCs are essential for effective peripheral immune tolerance, shielding the host from pathogens and collateral tissue injury. This model helps explain the pathophysiology of autoimmunity and tumor immune evasion, as well as the therapeutic potential of MSC-based interventions.

Key words: inflammation, immune tolerance, autoimmunity, regulatory T cells, mesenchymal stem/stromal cell

Cite as
Pham PV. Internal peacekeepers and external mediators: A new model of peripheral immune tolerance involving regulatory T cells and mesenchymal stem cells. *Adv Clin Exp Med*. 2026;35(2):195–200. doi:10.17219/acem/216728

DOI
10.17219/acem/216728

Highlights

- This editorial expands on the 2025 Nobel Prize-recognized role of regulatory T cells by introducing mesenchymal stem/stromal cells (MSCs) as critical "external checkpoints" in immune regulation.
- Tissue-resident MSCs respond to inflammation by secreting immunosuppressive mediators, promoting tissue repair, and locally dampening excessive immune responses, complementing Treg-mediated immune control.
- The integrated Treg–MSC tolerance model provides new insights into autoimmune disease mechanisms and tumor immune evasion, and highlights the therapeutic potential of MSC-based immunomodulatory strategies.

Introduction

The 2025 Nobel Prize in Physiology or Medicine was awarded to Mary E. Brunkow, Fred Ramsdell, and Shimon Sakaguchi for their groundbreaking discovery of regulatory T cells (Tregs) and their role in maintaining immune homeostasis through peripheral immune tolerance.[1] Tregs monitor and suppress effector immune cells, preventing excessive immune responses and shielding host tissues from collateral damage.

Recent studies have revealed the widespread presence of another specialized cell population in most organs: mesenchymal stem/stromal cells (MSCs).[2–7] These adult stem cells possess potent immunomodulatory capacities and have been shown to directly curb excessive inflammatory responses within tissue niches.[8–11]

Building on these observations, I have developed a two-tier model of peripheral immune tolerance that integrates both Tregs and MSCs, with Tregs acting within the immune system as an "internal checkpoint" and tissue-resident MSCs serving as an "external checkpoint." I argue that durable peripheral immune tolerance – particularly in the context of pathogen-induced tissue injury – can be achieved only through the combined activities of these complementary regulatory cell types.

Tregs: The peacekeepers of the immune system

A brief overview of the immune system

The immune system functions as a living shield that protects the host from both exogenous pathogens and aberrant endogenous cells. It is composed of highly specialized cellular subsets that together form a multilayered defense mechanism. The first barrier consists of innate effector cells – macrophages, dendritic cells (DCs), and natural killer (NK) cells – that are capable of immediately eliminating exogenous threats.[12,13] Concomitantly, localized inflammation is initiated, facilitating leukocyte recruitment and the containment and destruction of the pathogen. The complement system, which enhances phagocytosis and helps regulate inflammation, is also an integral component of the innate immune response. Pathogens that evade the first line of defense are targeted by the antigen-specific (adaptive) immune response. Although slower to develop than innate immunity, the adaptive response is both potent and exquisitely targeted and confers long-term immunological memory. Two principal types of lymphocytes mediate adaptive immunity: B cells and T cells. B cells are activated by professional antigen-presenting cells (APCs), such as DCs and macrophages. Once activated, B cells secrete large quantities of antibodies that neutralize pathogens and opsonize them for phagocytosis. Some activated B cells differentiate into long-lived memory B cells, which enable more rapid responses upon re-exposure to the same antigen.[12] T cells are also activated by APCs. $CD4^+$ T helper (Th) cells orchestrate the adaptive immune response, whereas $CD8^+$ cytotoxic T lymphocytes (CTLs) directly lyse infected or transformed cells. Memory T cells are generated in parallel, ensuring a rapid response upon re-exposure to the antigen.[12] Collectively, the generation of memory B and T cells enables faster and more robust protection during subsequent encounters with the same pathogen.

Regulatory control of immune activity

The immune system must be tightly regulated to prevent collateral damage to host tissues, particularly in cases of molecular mimicry (i.e., when a pathogen expresses self-like antigens). A key regulatory mechanism that limits such "friendly fire" was elucidated by Brunkow, Ramsdell, and Sakaguchi, who were awarded the 2025 Nobel Prize in Physiology or Medicine for this work. They identified Tregs, a cell population that restrains autoreactive immune effector cells. This discovery helps explain why most individuals do not develop autoimmunity and how neoplastic cells can sometimes exploit immune tolerance.

Sakaguchi first postulated the existence of a suppressive T-cell subset in 1995, challenging the prevailing view that central immune tolerance in the thymus is sufficient.[14,15] In 2001, Brunkow and Ramsdell identified the genetic mutation in a mouse strain prone to fulminant autoimmunity: a loss-of-function mutation in the transcription factor FOXP3, a defect that was also found in humans.[16–18]

Sakaguchi subsequently demonstrated that FOXP3 is the master regulator specifying the lineage he had previously described, now formally termed regulatory T cells (Tregs).[19,20]

Tregs monitor and curb aberrant immune activity through multiple non-redundant mechanisms.[21–23] First, they modulate immune responses via cytokine-mediated suppression. Tregs secrete interleukin (IL)-10, which inhibits Th cells and macrophages; transforming growth factor beta (TGF-β), which limits T- and B-cell proliferation and activation; and IL-35, which restrains effector T (Teff) cells. Second, Tregs suppress immune effector cells through direct cell–cell contact. Tregs express CTLA-4 and thus outcompete Teff cells for binding to APCs by engaging the costimulatory ligands CD80/CD86. They also sequester IL-2 via the high-affinity IL-2 receptor α-chain (CD25), depriving effector cells of essential growth signals. Third, in certain contexts, Tregs can directly eliminate autoreactive T cells or overactivated APCs through granzyme- and perforin-dependent cytolysis. Finally, Tregs can exert suppressive effects through metabolic modulation. The ectonucleotidases CD39 and CD73 expressed on Tregs catalyze the conversion of pro-inflammatory extracellular ATP into immunosuppressive adenosine, which dampens Teff cell activity by binding to adenosine receptors. Through these varied mechanisms, Tregs modulate immune responses to ensure they are potent enough to eradicate pathogens, yet sufficiently restrained to preserve host tissue integrity. Thus, Tregs act as an indispensable "brake" on immune activation.

MSCs: Internal custodians of tissue homeostasis and external mediators of immune activity

Mesenchymal stem cells or master signaling cells?

Mesenchymal stem/stromal cells have long been appreciated for their capacity for self-renewal and multilineage differentiation. However, their more consequential properties may be mediated by their secretome – the rich repertoire of soluble factors and extracellular vesicles they release. Accordingly, it has recently been proposed that MSCs be renamed "master signaling cells".[24]

Colony-forming, plastic-adherent stromal cells were first reported by Friedenstein et al. in the late 1950s and 1960s[3]; however, it was not until 1991 that Caplan isolated such cells from bone marrow and characterized them.[4] Subsequently, MSC-like populations were identified in adipose tissue,[6] umbilical cord blood,[25] Wharton's jelly,[26] the placenta,[27] dental pulp,[28] the dermis,[29] and even hair follicles.[30] To harmonize the nomenclature, the International Society for Cell and Gene Therapy proposed 3 minimal criteria in 2006: 1) plastic adherence and fibroblast-like morphology; 2) expression of CD105, CD73, and CD90, with absence of CD14, CD34, CD45, and HLA-DR; and 3) trilineage differentiation in vitro into osteoblasts, chondrocytes, and adipocytes.[31]

Due to their favorable properties, MSCs are now used clinically across a broad range of applications. For example, off-the-shelf products such as Prochymal, Ryoncil, and Temcell HS are used to treat graft-versus-host disease,[32–34] whereas Cartistem[35] and StemOne[36] are utilized to treat osteoarthritic degeneration. The development of MSC-based therapies has ushered in a new era of regenerative medicine.

Intriguingly, the therapeutic efficacy of MSCs appears to depend less on their stemness (i.e., their capacity to directly replace lost cells) than on their potent secretome-mediated anti-inflammatory and immunomodulatory functions. This realization has prompted a terminological shift from referring to these cells as mesenchymal stem/stromal cells to referring to them as medicinal signaling cells. In a previously published article, this concept was further developed, and the term "master signaling cells" was proposed as a more accurate description of MSCs, given their role as ubiquitous tissue sentinels that orchestrate signaling networks to preserve organismal equilibrium.[24]

The immunomodulatory activity of MSCs

With regard to the anti-inflammatory and immunoregulatory effects of MSCs, they have been shown to promote immune tolerance.[32–36] Accordingly, MSCs functionally parallel Tregs by helping to maintain local immune quiescence.

When exposed to a pro-inflammatory milieu rich in interferon-gamma (IFN-γ), tumor necrosis factor alpha (TNF-α), and IL-1, MSCs become activated and upregulate inhibitory ligands, such as programmed death ligand 1 (PD-L1), Fas ligand (FasL), galectin-1, CD73, and human leukocyte antigen G (HLA-G).[37–39] Concurrently, MSCs secrete a spectrum of soluble mediators, including indoleamine 2,3-dioxygenase, prostaglandin E2, nitric oxide, TGF-β, and hepatocyte growth factor.[39,40] Through these factors, as well as direct cell–cell contact, MSCs suppress pro-inflammatory effector cells (i.e., Teff cells, NK cells, B cells, and DCs) while promoting the expansion of Tregs.[10,41,42] The net result is an anti-inflammatory, tolerogenic microenvironment that promotes tissue repair and minimizes immune-mediated collateral damage.

Discussion

Given that both Tregs and MSCs play vital roles in maintaining immune homeostasis, I propose a two-tier model of peripheral immune tolerance that incorporates these internal and external checkpoints acting sequentially

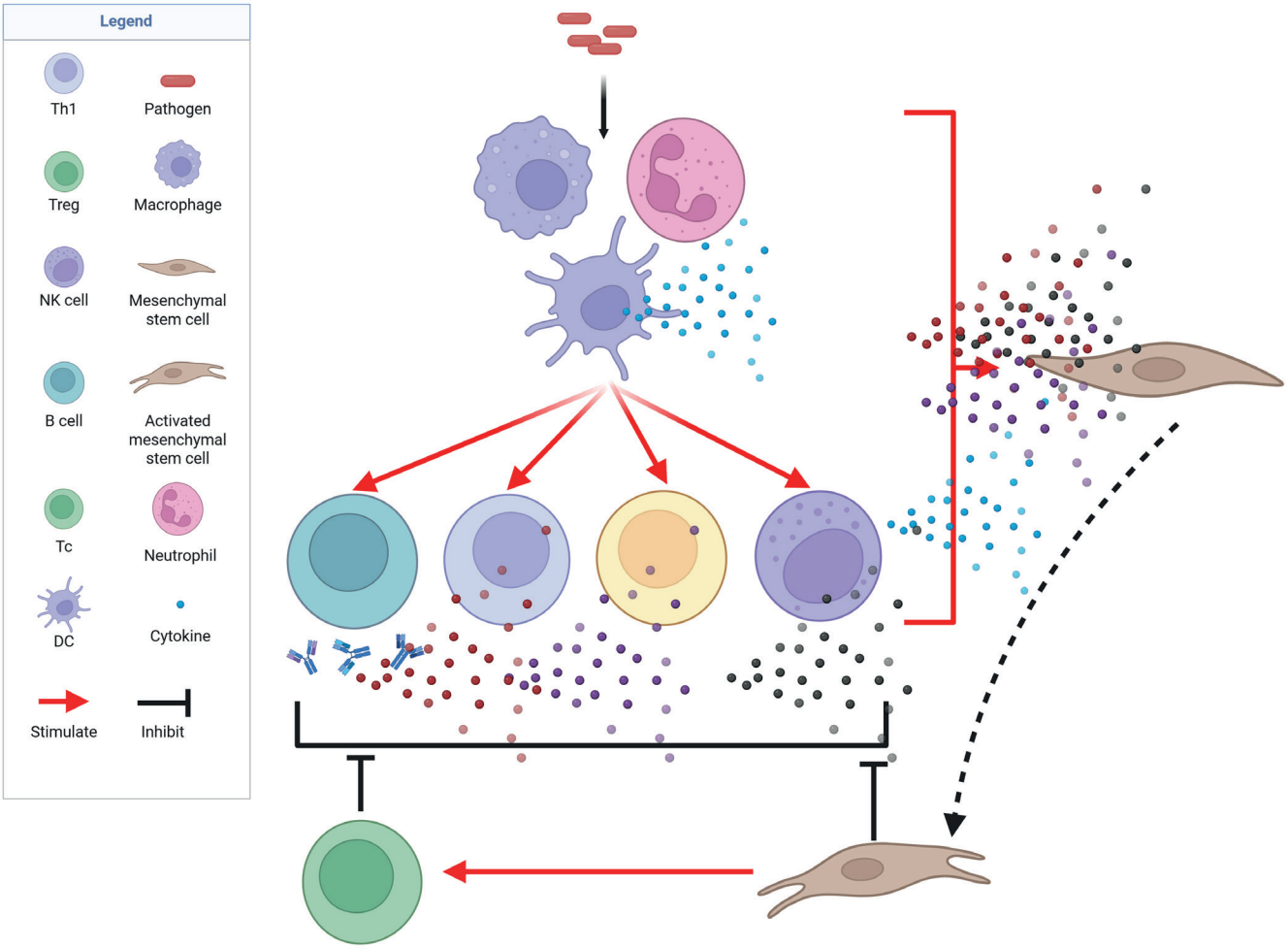

Fig. 1. A two-tier model of peripheral immune tolerance. When a pathogen invades the body, the immune system is activated to eradicate the harmful intruder. Concomitantly, regulatory T cells (Tregs) are induced in lymphoid organs to prevent excessive immune activation and systemic immunopathology. In parallel, inflammatory mediators released by immune cells reach the affected tissue and activate resident mesenchymal stem/stromal cells (MSCs). These MSCs adopt an anti-inflammatory, immunoregulatory phenotype that protects parenchymal cells from immune-mediated collateral damage during pathogen clearance (created with BioRender.com)

(Fig. 1). First, Tregs in secondary lymphoid organs curb the activity of adaptive immune effector cells. Then, once activated immune cells reach the site of infection or inflammation, resident or infiltrating MSCs are stimulated to locally dampen their effector functions.

This model helps explain the encouraging clinical outcomes observed with MSC infusion in several autoimmune settings.[43–47] However, a potential downside of MSC infusion is that the resulting broad immunosuppression may create a favorable environment for malignant cells, shielding them from CTL surveillance. The model also implies that autoimmune pathology may arise when both checkpoints are concurrently compromised.

The ubiquity of MSCs across virtually all organs likely reflects the critical importance of the tissue-level safeguard provided by these cells. Even in organs in which MSCs have not been conclusively identified, it is plausible that cells of analogous ontogeny persist in a dormant state or have differentiated into tissue-adapted subsets. Under homeostatic conditions, MSCs remain quiescent and help maintain local tissue equilibrium. When injury occurs, pro-inflammatory cytokines released by infiltrating immune cells activate MSCs, inducing a potent anti-inflammatory and immunomodulatory phenotype. Thus, MSCs provide a secondary defense mechanism within tissues. In contrast to Tregs, which primarily function to suppress inflammation, MSCs are multifunctional: they simultaneously temper immune activity and orchestrate tissue repair through a repertoire of paracrine and direct cell–cell mechanisms. Therefore, we propose that MSCs be regarded as a specialized, tissue-resident extension of the immune system – a gatekeeper population that shields host tissues from collateral damage inflicted by excessive immune activation.

Conclusions

The 2025 Nobel Prize in Physiology or Medicine was awarded for the identification of Tregs, which play a critical role in peripheral immune tolerance. Mesenchymal

stem cells also make substantial contributions to this process, serving as an external checkpoint in peripheral tissues. Thus, to more accurately describe the mechanisms underlying peripheral immune tolerance, I propose a two-tier model in which Tregs restrain immune responses at their source, whereas MSCs serve as tissue-resident gatekeepers that swiftly extinguish excessive inflammation and generate a pro-regenerative microenvironment. Concurrent failure of these complementary elements may drive autoimmune pathology, whereas excessive immunosuppression may allow tumors to evade immune surveillance. The central role of MSCs in peripheral immune tolerance reinforces the earlier suggestion that they be renamed "master signaling cells". In addition, the potent immunomodulatory capacity of MSCs and their ability to promote tissue repair render MSC-based interventions promising strategies for treating autoimmune diseases and tissue injury. In conclusion, my model acknowledges the roles of Tregs and MSCs in peripheral immune tolerance and highlights their contributions to ensuring that the immune system is powerful enough to eradicate pathogens, yet sufficiently restrained to safeguard the host.

Use of AI and AI-assisted technologies

Not applicable.

ORCID iDs

Phuc Van Pham https://orcid.org/0000-0001-7254-0717

References

1. Nobel Prize Organisation. Nober Prize 2025 in Physiology or Medicine: Press release. Stockholm, Sweden: Nobel Prize Organisation; 2025. https://www.nobelprize.org/prizes/medicine/2025/press-release. Accessed January 12, 2026.
2. Feng J, Mantesso A, De Bari C, Nishiyama A, Sharpe PT. Dual origin of mesenchymal stem cells contributing to organ growth and repair. *Proc Natl Acad Sci U S A*. 2011;108(16):6503–6508. doi:10.1073/pnas.1015449108
3. Friedenstein AJ, Chailakhyan RK, Latsinik NV, Panasyuk AF, Keiliss-Borok IV. Stromal cells responsible for transferring the microenvironment of the hemopoietic tissues: Cloning in vitro and retransplantation in vivo. *Transplantation*. 1974;17(4):331–340. doi:10.1097/00007890-197404000-00001
4. Caplan AI. Mesenchymal stem cells. *J Orthop Res*. 1991;9(5):641–650. doi:10.1002/jor.1100090504
5. Pittenger MF, Mackay AM, Beck SC, et al. Multilineage potential of adult human mesenchymal stem cells. *Science*. 1999;284(5411):143–147. doi:10.1126/science.284.5411.143
6. Zuk PA, Zhu M, Ashjian P, et al. Human adipose tissue is a source of multipotent stem cells. *Mol Biol Cell*. 2002;13(12):4279–4295. doi:10.1091/mbc.e02-02-0105
7. Toma JG, Akhavan M, Fernandes KJL, et al. Isolation of multipotent adult stem cells from the dermis of mammalian skin. *Nat Cell Biol*. 2001;3(9):778–784. doi:10.1038/ncb0901-778
8. Huang Y, Wu Q, Tam PKH. Immunomodulatory mechanisms of mesenchymal stem cells and their potential clinical applications. *Int J Mol Sci*. 2022;23(17):10023. doi:10.3390/ijms231710023
9. Sarsenova M, Kim Y, Raziyeva K, Kazybay B, Ogay V, Saparov A. Recent advances to enhance the immunomodulatory potential of mesenchymal stem cells. *Front Immunol*. 2022;13:1010399. doi:10.3389/fimmu.2022.1010399
10. Taşlı PN, Bozkurt BT, Kırbaş OK, Deniz-Hızlı AA, Şahin F. Immunomodulatory behavior of mesenchymal stem cells. In: Turksen K, ed. *Cell Biology and Translational Medicine*. Vol. 4. Advances in Experimental Medicine and Biology. Cham, Switzerland: Springer International Publishing; 2018:73–84. doi:10.1007/5584_2018_255
11. El-Sayed M, El-Feky MA, El-Amir MI, et al. Immunomodulatory effect of mesenchymal stem cells: Cell origin and cell quality variations. *Mol Biol Rep*. 2019;46(1):1157–1165. doi:10.1007/s11033-018-04582-w
12. Thaler MS, Klausner RD, Cohen HJ. *Medical Immunology*. Philadelphia, USA: Lippincott; 1977. ISBN:978-0-397-52081-7.
13. Paul WE, ed. *Fundamental Immunology*. 7th ed. Philadelphia, USA: Wolters Kluwer Health/Lippincott Williams & Wilkins; 2013. ISBN:978-1-4511-1783-7.
14. Sakaguchi S, Sakaguchi N, Asano M, Itoh M, Toda M. Immunologic self-tolerance maintained by activated T cells expressing IL-2 receptor α-chains (CD25). Breakdown of a single mechanism of self-tolerance causes various autoimmune diseases. *J Immunol*. 1995;155(3):1151–1164. doi:10.4049/jimmunol.155.3.1151
15. Sakaguchi S, Takahashi T, Nishizuka Y. Study on cellular events in postthymectomy autoimmune oophoritis in mice: I. Requirement of Lyt-1 effector cells for oocytes damage after adoptive transfer. *J Exp Med*. 1982;156(6):1565–1576. doi:10.1084/jem.156.6.1565
16. Brunkow ME, Jeffery EW, Hjerrild KA, et al. Disruption of a new forkhead/winged-helix protein, scurfin, results in the fatal lymphoproliferative disorder of the scurfy mouse. *Nat Genet*. 2001;27(1):68–73. doi:10.1038/83784
17. Bennett CL, Christie J, Ramsdell F, et al. The immune dysregulation, polyendocrinopathy, enteropathy, X-linked syndrome (IPEX) is caused by mutations of FOXP3. *Nat Genet*. 2001;27(1):20–21. doi:10.1038/83713
18. Wildin RS, Ramsdell F, Peake J, et al. X-linked neonatal diabetes mellitus, enteropathy and endocrinopathy syndrome is the human equivalent of mouse scurfy. *Nat Genet*. 2001;27(1):18–20. doi:10.1038/83707
19. Sakaguchi S. Regulatory T cells. *Cell*. 2000;101(5):455–458. doi:10.1016/S0092-8674(00)80856-9
20. Itoh M, Takahashi T, Sakaguchi N, et al. Thymus and autoimmunity: Production of $CD25^+CD4^+$ naturally anergic and suppressive T cells as a key function of the thymus in maintaining immunologic self-tolerance. *J Immunol*. 1999;162(9):5317–5326. doi:10.4049/jimmunol.162.9.5317
21. Wan YY. Regulatory T cells: Immune suppression and beyond. *Cell Mol Immunol*. 2010;7(3):204–210. doi:10.1038/cmi.2010.20
22. Sakaguchi S, Yamaguchi T, Nomura T, Ono M. Regulatory T cells and immune tolerance. *Cell*. 2008;133(5):775–787. doi:10.1016/j.cell.2008.05.009
23. Tian L, Humblet-Baron S, Liston A. Immune tolerance: Are regulatory T cell subsets needed to explain suppression of autoimmunity? *BioEssays*. 2012;34(7):569–575. doi:10.1002/bies.201100180
24. Pham PV. MSCs, but not mesenchymal stem cells. *Biomed Res Ther*. 2024;11(9):6797–6800. doi:10.15419/bmrat.v11i9.924
25. Lee OK, Kuo TK, Chen WM, Lee KD, Hsieh SL, Chen TH. Isolation of multipotent mesenchymal stem cells from umbilical cord blood. *Blood*. 2004;103(5):1669–1675. doi:10.1182/blood-2003-05-1670
26. Weiss ML, Medicetty S, Bledsoe AR, et al. Human umbilical cord matrix stem cells: Preliminary characterization and effect of transplantation in a rodent model of Parkinson's disease. *Stem Cells*. 2006;24(3):781–792. doi:10.1634/stemcells.2005-0330
27. Li CD, Zhang WY, Li HL, et al. Mesenchymal stem cells derived from human placenta suppress allogeneic umbilical cord blood lymphocyte proliferation. *Cell Res*. 2005;15(7):539–547. doi:10.1038/sj.cr.7290323
28. Gronthos S, Mankani M, Brahim J, Robey PG, Shi S. Postnatal human dental pulp stem cells (DPSCs) in vitro and in vivo. *Proc Natl Acad Sci U S A*. 2000;97(25):13625–13630. doi:10.1073/pnas.240309797
29. Sellheyer K, Krahl D. Skin mesenchymal stem cells: Prospects for clinical dermatology. *J Am Acad Dermatol*. 2010;63(5):859–865. doi:10.1016/j.jaad.2009.09.022
30. Gentile P, Scioli MG, Bielli A, Orlandi A, Cervelli V. Stem cells from human hair follicles: First mechanical isolation for immediate autologous clinical use in androgenetic alopecia and hair loss. *Stem Cell Investig*. 2017;4(7):58. doi:10.21037/sci.2017.06.04
31. Dominici M, Le Blanc K, Mueller I, et al. Minimal criteria for defining multipotent mesenchymal stromal cells: The International Society for Cellular Therapy position statement. *Cytotherapy*. 2006;8(4):315–317. doi:10.1080/14653240600855905

32. Kurtzberg J, Abdel-Azim H, Carpenter P, et al. A phase 3, single-arm, prospective study of remestemcel-L, ex vivo culture-expanded adult human mesenchymal stromal cells for the treatment of pediatric patients who failed to respond to steroid treatment for acute graft-versus-host disease. *Biol Blood Marrow Transplant*. 2020;26(5):845–854. doi:10.1016/j.bbmt.2020.01.018
33. Konishi A, Sakushima K, Isobe S, Sato D. First approval of regenerative medical products under the PMD Act in Japan. *Cell Stem Cell*. 2016;18(4):434–435. doi:10.1016/j.stem.2016.03.011
34. Etra A, Ferrara JLM, Levine JE. Remestemcel-L-rknd (Ryoncil): The first approved cellular therapy for steroid-refractory acute GVHD. *Blood*. 2025;146(16):1897–1901. doi:10.1182/blood.2025028553
35. Park YB, Ha CW, Lee CH, Yoon YC, Park YG. Cartilage regeneration in osteoarthritic patients by a composite of allogeneic umbilical cord blood-derived mesenchymal stem cells and hyaluronate hydrogel: Results from a clinical trial for safety and proof-of-concept with 7 years of extended follow-up. *Stem Cell Transl Med*. 2017;6(2):613–621. doi:10.5966/sctm.2016-0157
36. Gupta A. StemOneTM/Stempeucel®: CDSCO approved, adult human bone marrow-derived, cultured, pooled, allogenic mesenchymal stem cells for knee osteoarthritis. *Biomedicines*. 2023;11(11):2894. doi:10.3390/biomedicines11112894
37. López-García L, Castro-Manrreza ME. TNF-α and IFN-γ participate in improving the immunoregulatory capacity of mesenchymal stem/stromal cells: Importance of cell–cell contact and extracellular vesicles. *Int J Mol Sci*. 2021;22(17):9531. doi:10.3390/ijms22179531
38. Faghih M, Moshiri M, Mazrouei Arani N, et al. Evaluation of TNF-α and IFN-γ primed conditioned medium of mesenchymal stem cell in acetic acid-induced mouse model of acute colitis. *Cell Immunol*. 2024;405–406:104876. doi:10.1016/j.cellimm.2024.104876
39. Jiang W, Xu J. Immune modulation by mesenchymal stem cells. *Cell Prolif*. 2020;53(1):e12712. doi:10.1111/cpr.12712
40. Yi T, Song SU. Immunomodulatory properties of mesenchymal stem cells and their therapeutic applications. *Arch Pharm Res*. 2012;35(2):213–221. doi:10.1007/s12272-012-0202-z
41. Yarygin KN, Lupatov AYu, Sukhikh GT. Modulation of immune responses by mesenchymal stromal cells. *Bull Exp Biol Med*. 2016;161(4):561–565. doi:10.1007/s10517-016-3461-8
42. Castro-Manrreza ME, Montesinos JJ. Immunoregulation by mesenchymal stem cells: Biological aspects and clinical applications. *J Immunol Res*. 2015;2015:394917. doi:10.1155/2015/394917
43. Coulson-Thomas VJ, Coulson-Thomas YM, Gesteira TF, Kao WWY. Extrinsic and intrinsic mechanisms by which mesenchymal stem cells suppress the immune system. *Ocul Surf*. 2016;14(2):121–134. doi:10.1016/j.jtos.2015.11.004
44. Reddy BY, Xu DS, Hantash BM. Mesenchymal stem cells as immunomodulator therapies for immune-mediated systemic dermatoses. *Stem Cells Dev*. 2012;21(3):352–362. doi:10.1089/scd.2011.0404
45. El-Badri NS, Maheshwari A, Sanberg PR. Mesenchymal stem cells in autoimmune disease. *Stem Cells Dev*. 2004;13(5):463–472. doi:10.1089/scd.2004.13.463
46. Li A, Guo F, Pan Q, et al. Mesenchymal stem cell therapy: Hope for patients with systemic lupus erythematosus. *Front Immunol*. 2021;12:728190. doi:10.3389/fimmu.2021.728190
47. Zaripova LN, Midgley A, Christmas SE, et al. Mesenchymal stem cells in the pathogenesis and therapy of autoimmune and autoinflammatory diseases. *Int J Mol Sci*. 2023;24(22):16040. doi:10.3390/ijms242216040

Insights into brain oscillations and connectivity in neuropsychiatric disorders

Francesco Di Gregorio[A,D–F], Simone Battaglia[A,D–F]

Faculty of Psychology, eCampus University, Novedrate (Como), Italy

A – research concept and design; B – collection and/or assembly of data; C – data analysis and interpretation;
D – writing the article; E – critical revision of the article; F – final approval of the article

Advances in Clinical and Experimental Medicine, ISSN 1899–5276 (print), ISSN 2451–2680 (online) *Adv Clin Exp Med*. 2026;35(2):201–208

Address for correspondence
Simone Battaglia
E-mail: simone.battaglia@unibo.it

Funding sources
Simone Battaglia is supported by #NEXTGENERATIONEU (NGEU) and funded by the Ministry of University and Research (MUR), under the National Recovery and Resilience Plan (NRRP), project MNESYS (PE0000006) – A Multiscale Integrated Approach to the Study of the Nervous System in Health and Disease (DN. 1553, 11.10.2022), and by the Bial Foundation, Portugal (grant no. 235/22). Francesco Di Gregorio is supported by the Ministry of University and Research (MUR), Italy (grant No. P2022XAKXL). The views and opinions expressed are solely those of the authors and do not necessarily reflect those of the European Union. Neither the European Union nor the granting authorities can be held responsible for them.

Conflict of interest
None declared

Acknowledgements
The authors would like to express their gratitude to Valentina Francica and Chiara Di Fazio for their help and support.

Received on June 3, 2025
Reviewed on July 22, 2025
Accepted on November 4, 2025

Published online on November 20, 2025

Cite as
Di Gregorio F, Battaglia S. Insights into brain oscillations and connectivity in neuropsychiatric disorders. *Adv Clin Exp Med*. 2026;35(2):201–208. doi:10.17219/acem/213945

DOI
10.17219/acem/213945

Abstract

Electroencephalography has advanced from spectral analyses to integrate functional-connectivity and oscillatory metrics, offering mechanistic insights into network dysfunction across neurological and psychiatric disorders. Methodological advances, such as source reconstruction and brain modelling, enhance spatial precision and mitigate volume conduction. Empirical studies show that oscillatory brain activity and functional connectivity serve human cognition and their disruptions underlie symptoms in a variety of neuropsychiatric disorders. The study of the relation between brain oscillations and connectivity is pivotal for the advances in cognitive and clinical neuroscience. Crucially, integrating these biomarkers into machine-learning frameworks and closed-loop neuromodulation holds promise for personalized diagnostics and interventions.

Key words: neuropsychiatric disorders, electroencephalography, brain connectivity, brain oscillations, clinical neuroscience

Highlights

- EEG connectivity and oscillatory biomarkers reveal rhythm-specific network dysfunctions across neurological and psychiatric disorders.
- Alpha oscillations provide a unifying framework linking local neural activity with large-scale network coordination via thalamocortical circuits.
- Combining cross-frequency coupling, dynamic connectivity and graph-theoretical analyses enhances understanding of brain network dynamics.
- Multimodal and longitudinal EEG approaches enable precision diagnostics and personalized neuromodulation therapies.

Introduction

Electroencephalography (EEG) remains an irreplaceable neuroscientific technique for probing the temporal dynamics of neural activity, combining high temporal resolution with noninvasive, cost-effective implementation at the bedside.[1–3] Over the past 2 decades, EEG has evolved from simple spectral analyses to sophisticated functional connectivity metrics that capture interdependencies among cortical regions in both sensor and source spaces.[3–13] These advances have enabled the detection of subtle network dysfunctions that correlate with clinical phenotypes in neurological and psychiatric disorders, including emerging evidence for rhythm-specific network aberrations.[4,14–23] These approaches have promoted new insights into the neurophysiological substrates of cognition and the pathophysiology of psychiatric and neurological disorders, yet they also introduce methodological complexities that must be carefully managed.[24–27] In this editorial, we aim to synthesize the converging evidence on the link between brain oscillatory activity and connectivity into a focused perspective to explore pathophysiology in neurological and psychiatric disorders.

A primary challenge in EEG-based connectivity analysis arises from volume conduction and low spatial resolution at the scalp level: Signals recorded at nearby electrodes may reflect the same underlying neural source, inflating estimates of connectivity if uncorrected.[9,10,28–30] Source-reconstruction techniques (inverse solutions) can mitigate this issue by estimating activity within cortical nodes, but they demand accurate head models to solve the inverse problem reliably,[8,31–35] and recent reviews further underscore their broad antidepressant potential.[36,37] Consequently, the quality of the forward model and the choice of regularization parameters critically influence the accuracy of source-level connectivity estimates. Researchers must balance sensor-level convenience against the spatial precision afforded by source analyses, selecting methods that align with their hypotheses and experimental constraints. Standardized reporting of montage density, head model parameters and preprocessing pipelines is vital for reproducibility and cross-study comparisons.

Bridging connectivity and oscillatory frameworks

From a computational point of view, functional connectivity metrics and oscillatory dynamics are 2 sides of the same coin: While connectivity indices quantify the coordination between regions, oscillatory measures reflect the underlying rhythmic modes that facilitate or obstruct such coordination.[38–43] Phase-based, amplitude-based and information-theoretic metrics each interrogate these interactions from complementary angles: 1) Phase-lag index (PLI) and its variants assess the consistency of phase differences between signals, isolating genuine interregional coupling by minimizing zero-lag artifacts[10,31]; 2) Coherence metrics capture co-modulation of band-limited activities, reflecting how oscillatory fluctuations co-occur across the cortex[40,44,45]; 3) Mutual information (MI) and related entropy-based measures provide a nonlinear gauge of shared signal content, potentially revealing higher-order dependencies that linear metrics miss.[46,47] Finally, by integrating these classes of metrics, researchers can form a unified picture in which oscillations at distinct frequencies (e.g., alpha, theta) serve as communication channels whose efficacy is quantified by connectivity indices. This perspective allows for the computational integration between local oscillations and distributed functional connectivity, identifying oscillatory-specific brain functional networks. In neuroscience, the concept of metastability has been proposed as a signature that balance between these local and distributed activities in the brain. Specifically, metastability captures the brain's ability to balance functional segregation (specialized processing in localized regions) and integration (coordinated activity across distributed networks).[40,48,49] Metastable dynamics are thought to underpin key cognitive functions such as attention, working memory and consciousness by allowing the brain to flexibly reconfigure its network topology in response to internal and external demands.[50] Theoretical models often describe metastability using nonlinear dynamical systems and coupled oscillatory activities across brain areas, demonstrating how functional integration requires segregated brain areas to influence each other in a way that facilitates integration

and serve cognition and behavior.[51–53] Empirical evidence from electrophysiological (EEG/MEG) studies has shown that metastable patterns characterize both resting-state and task-related brain activity,[54] with alterations observed in neuropsychiatric disorders.[55–57]

Oscillations and connectivity: from neurology to psychiatry

Empirically, EEG-derived connectivity measures have elucidated network alterations across a spectrum of clinical conditions, revealing both shared and disorder-specific patterns for several health conditions, including neurodegenerative diseases.[58] In patients with the acute phase of ischemic and hemorrhagic stroke, a shift in spectral power characterized by reduced activity in higher frequency bands (alpha/mu: 8–13 Hz and beta: 14–30 Hz) alongside increased power in lower frequencies (delta: 1–3 Hz and theta: 4–7 Hz) has consistently been associated with unfavorable clinical outcomes.[13,19,59–66] In parallel, evidence suggests that stronger connectivity within the fronto-parietal motor network during the early post-stroke period correlates with more favorable motor recovery trajectories.[19,60] Conversely, increases in connectivity occurring at later stages have been linked to less optimal functional outcomes.[18,19,67–72]

In disorders of consciousness (DoC), patients with unresponsive wakefulness syndrome (UWS) or minimally conscious state (MCS) show reductions in functional connectivity and oscillatory brain dynamics within large-scale default mode and frontoparietal networks correlating with clinical severity and outcomes.[2,17,20,73–83] Mutual information and coherence metrics recorded in the acute post-injury phase can predict functional outcomes with up to ~83% accuracy, highlighting their prognostic utility.[2,17,20] Furthermore, combining multimodal connectivity metrics with complexity measures (e.g., permutation entropy) and local oscillatory activity can enhance predictive models,[84–87] reflecting the link between recovery trajectories and complex neural dynamics.

In patients with schizophrenia-spectrum disorders (SSD), alpha-band synchrony deficits in SSD manifest as both reduced posterior alpha power and weakened fronto-parietal connectivity, correlating with positive symptom severity and cognitive disorganization.[22,88,89] These aberrations align with a failure of pulsed inhibition mechanisms, leading to excessive cortical noise and impaired signal-to-noise gating.[90–94] Similarly, beta and gamma band connectivity alterations have been linked to negative symptoms and working-memory deficits, suggesting frequency-specific network dysfunction.[95–97] Integrative models propose that alterations in local processing and large-scale coordination underlie both perceptual distortions and executive dysfunction in SSD.[96]

In individuals with autism spectrum disorder (ASD), EEG studies have reported long-range underconnectivity in the alpha and beta frequency bands, accompanied by local hyperconnectivity, often manifesting as elevated short-range coherence, particularly in occipital, temporal and parietal regions.[98–100] Abnormal connectivity patterns, including alpha and theta coherence over frontal areas, have been implicated in atypical social perception and sensory integration.[98,101–103] Within the framework of predictive coding, these aberrant patterns are thought to reflect a deficiency in top-down predictive signaling and an overrepresentation of bottom-up error signals,[104] as a consequence of a core deficit in the flexibility.

In patients with attention-deficit/hyperactivity disorder (ADHD), EEG recordings typically show reduced posterior alpha power desynchronization and abnormal alpha and beta-based functional connectivity during sustained attention and cognitive tasks.[105–109] These alterations co-occur with weakened fronto-parietal connectivity, suggesting a functional breakdown in large-scale attentional and executive function networks.[110,111] Combined interventions using behavioral training and alpha-frequency transcranial alternating current stimulation (alpha-tACS) have shown preliminary success in enhancing oscillatory activity and improving executive function and attention performance.[112–115]

In major depressive disorder (MDD), elevated frontal alpha power, particularly in the left hemisphere, and a right-to-left alpha asymmetry are frequently reported EEG features (i.e., frontal alpha asymmetry, FAA), suggesting altered interhemispheric connectivity within the prefrontal cortex.[108,109] Although limited diagnostic value of FAA in MDD,[116–118] neuromodulation approaches targeting FAA have shown promising results in reducing depressive symptoms, especially those linked to motivational deficits.[119,120]

Taken together, this evidence supports and demonstrates the utility of EEG-derived connectivity and spectral metrics as robust biomarkers across diverse neuropsychiatric conditions (Table 1). Future work should focus on longitudinal, multimodal studies to validate these biomarkers and explore their relationship in cognition and in the diagnosis of neuropsychiatric disorders.[121]

Alpha activity as a unifying lens

Based on empirical evidence and computations needed to calculate functional connectivity measures, it is plausible to hypothesize a relation between local oscillatory metrics and oscillatory-based functional connectivity. Alpha oscillations (8–13 Hz) may represent the unifying lens to understand this relation. Alpha oscillations are the dominant rhythm in the human EEG and modulate perception, attention and memory. Translational evidence consistently report both disrupted local alpha-band activity and connectivity across several neuropsychiatric disorders.[21] For instance, in stroke and severe acquired

Table 1. Summary of the brain oscillatory pattern in the main neuropsychiatric disorders

Disorder	Spectral/connectivity alterations	Network involvement	Clinical/prognostic implications
Major depressive disorder (MDD)	Increased frontal alpha power (left > right); frontal alpha asymmetry (FAA).	Prefrontal interhemispheric connectivity.	FAA has limited diagnostic specificity but is a promising target for neuromodulation, particularly for motivational symptoms.
Schizophrenia-spectrum disorders (SSD)	Reduced posterior alpha power; ↓ fronto-parietal alpha connectivity; beta/gamma connectivity disruptions.	Large-scale fronto-parietal temporal and occipital oscillatory networks.	Alpha deficits correlate with positive symptoms; beta/gamma alterations correlate with negative symptoms and working-memory deficits; overall dysfunction reflects impaired local–global coordination.
Autism spectrum disorder (ASD)	Long-range underconnectivity (alpha, beta); local hyperconnectivity (occipito-temporo-parietal); abnormal frontal alpha/theta coherence.	Imbalance between local vs distributed networks.	Linked to atypical social perception and sensory integration; consistent with predictive coding deficits (↓ top-down, ↑ bottom-up error signaling).
Attention-deficit/hyperactivity disorder (ADHD)	Reduced posterior alpha desynchronization; altered alpha/beta connectivity during attention tasks.	Fronto-parietal attentional/executive networks.	Weakened large-scale connectivity underlies attentional/executive dysfunction; behavioral training + alpha-tACS enhances oscillatory activity and improves attention/executive performance.
Disorders of consciousness (UWS/MCS)	Global reductions in connectivity and oscillatory dynamics.	Default Mode Network (DMN), fronto-parietal networks.	Reduced connectivity correlates with clinical severity; mutual information/coherence metrics predict outcomes (~83% accuracy); multimodal indices enhance prognostic value.

brain injury, pronounced reductions in posterior alpha power, slowing of the individual alpha frequency (IAF) and weakened fronto-parietal connectivity correlate with attentional deficits and poor functional outcomes,[2,17–20,60] whereas in SSD, abnormal alpha-based connectivity is associated with psychotic symptoms and perceptual impairments.[95–97] The most probable neural substrate underlying the cross-diagnostic link between alpha oscillations and functional connectivity measures is the thalamus-cortical circuitry.[122–124] This brain network has been considered the generator of alpha oscillatory activity[125–128] and its dysfunctions yield disorder-specific connectivity signatures, ranging from hypoconnectivity in stroke to hyperconnectivity in ASD.[18,19,98,101–103] The hypothesis of the thalamus-cortical role in alpha generation forges the theoretical bridge between connectivity metrics and oscillatory measures, suggesting that optimized neuromodulation should aim to restore both rhythmic power and inter-regional synchrony. Clinically, integrating spectral and connectivity biomarkers into unified machine-learning frameworks can refine differential diagnosis, stratify patients for targeted interventions and monitor treatment response.[129,130] Establishing normative databases and open, multicenter repositories with standardized pipelines will be critical for validating hypothesis testing and improving treatment efficacy. Moreover, advances in real-time EEG processing and closed-loop neuromodulation can leverage these biomarkers for personalized treatments, such as alpha-modulation adapted to individual IAF.

Future directions

To enhance the translational impact of EEG connectivity and oscillatory research, future studies should pursue multimodal integration with structural and functional magnetic resonance imaging (MRI), as well as genomic and phenotypic data.[131] This integrative approach will enable the identification of neurogenetic factors that modulate rhythmic connectivity, facilitating the development of targeted interventions.[132–134] Longitudinal cohorts that track EEG connectivity trajectories across developmental stages and aging, alongside biomarkers of metabolites that modulate signals, will clarify how network dynamics confer vulnerability or resilience in neuropsychiatric conditions.[135]

Future research should prioritize integrative, mechanism-oriented approaches that leverage cross-frequency coupling (CFC), dynamic functional connectivity (dFC) and graph-theoretical metrics to resolve how multiscale oscillatory interactions map onto clinical phenotypes and treatment response. Cross-frequency coupling (particularly phase–amplitude coupling) has emerged as a reproducible index of mesoscale coordination and is differentially altered across psychiatric syndromes, suggesting both diagnostic and mechanistic utility.[136] Complementing CFC, dFC methods allow the characterization of transient network states and state-switching dynamics that are obscured by static connectivity estimates; these transient states are likely to index symptom-relevant fluctuations in cognition and arousal but require harmonized analytic standards to ensure reproducibility.[137] Graph-theoretical measures computed on EEG/MEG/fMRI networks can then quantify topology (e.g., hubness, modularity, efficiency) of both static and dynamic networks, providing compact biomarkers that are amenable to longitudinal tracking and to integration within predictive models.[138] We therefore advocate for: 1) multimodal pipelines that combine source-resolved electrophysiology with hemodynamic imaging, 2) standardized connectivity analysis workflows (including surrogate testing and cross-validation), and 3) translational studies that link topology and cross-frequency interactions to cellular and circuit-level mechanisms and to neuromodulatory

interventions. Collectively, these convergent approaches will improve mechanistic specificity and accelerate the translation of network biomarkers into personalized diagnostics and closed-loop therapeutics. In conclusion, by recognizing that oscillations and connectivity are inherently interdependent,[22,139] the field can accelerate the translation of EEG-derived metrics into precision diagnostics and personalized neuromodulation protocols.[140,141] This integrative framework not only deepens our mechanistic understanding of brain network dysfunction but also paves the way for novel therapeutic avenues that restore healthy rhythmic coordination across distributed neural circuits.[142,143]

Use of AI and AI-assisted technologies

Not applicable.

ORCID iDs

Francesco Di Gregorio https://orcid.org/0000-0002-3587-3149
Simone Battaglia https://orcid.org/0000-0003-4133-654X

References

1. Bareham CA, Roberts N, Allanson J, et al. Bedside EEG predicts longitudinal behavioural changes in disorders of consciousness. *NeuroImage Clin*. 2020;28:102372. doi:10.1016/j.nicl.2020.102372
2. Di Gregorio F, La Porta F, Petrone V, et al. Accuracy of EEG biomarkers in the detection of clinical outcome in disorders of consciousness after severe acquired brain injury: Preliminary results of a pilot study using a machine learning approach. *Biomedicines*. 2022;10(8):1897. doi:10.3390/biomedicines10081897
3. Di Gregorio F, Battaglia S. Advances in EEG-based functional connectivity approaches to the study of the central nervous system in health and disease. *Adv Clin Exp Med*. 2023;32(6):607–612. doi:10.17219/acem/166476
4. Baldassarre A, Ramsey LE, Siegel JS, Shulman GL, Corbetta M. Brain connectivity and neurological disorders after stroke. *Curr Opin Neurol*. 2016;29(6):706–713. doi:10.1097/WCO.0000000000000396
5. Bastos AM, Schoffelen JM. A tutorial review of functional connectivity analysis methods and their interpretational pitfalls. *Front Syst Neurosci*. 2015;9:175. doi:10.3389/fnsys.2015.00175
6. Cao J, Zhao Y, Shan X, et al. Brain functional and effective connectivity based on electroencephalography recordings: A review. *Hum Brain Mapp*. 2022;43(2):860–879. doi:10.1002/hbm.25683
7. Hallett M, De Haan W, Deco G, et al. Human brain connectivity: Clinical applications for clinical neurophysiology. *Clin Neurophysiol*. 2020;131(7):1621–1651. doi:10.1016/j.clinph.2020.03.031
8. Mahjoory K, Nikulin VV, Botrel L, Linkenkaer-Hansen K, Fato MM, Haufe S. Consistency of EEG source localization and connectivity estimates. *NeuroImage*. 2017;152:590–601. doi:10.1016/j.neuroimage.2017.02.076
9. Marinazzo D, Riera JJ, Marzetti L, Astolfi L, Yao D, Valdés Sosa PA. Controversies in EEG source imaging and connectivity: Modeling, validation, benchmarking. *Brain Topogr*. 2019;32(4):527–529. doi:10.1007/s10548-019-00709-9
10. Stam CJ, Nolte G, Daffertshofer A. Phase lag index: Assessment of functional connectivity from multichannel EEG and MEG with diminished bias from common sources. *Hum Brain Mapp*. 2007;28(11):1178–1193. doi:10.1002/hbm.20346
11. Vecchio F, Tomino C, Miraglia F, et al. Cortical connectivity from EEG data in acute stroke: A study via graph theory as a potential biomarker for functional recovery. *Int J Psychophysiol*. 2019;146:133–138. doi:10.1016/j.ijpsycho.2019.09.012
12. Di Biase L, Ricci L, Caminiti ML, Pecoraro PM, Carbone SP, Di Lazzaro V. Quantitative high density EEG brain connectivity evaluation in Parkinson's disease: The phase locking value (PLV). *J Clin Med*. 2023;12(4):1450. doi:10.3390/jcm12041450
13. Bentes C, Peralta AR, Viana P, et al. Quantitative EEG and functional outcome following acute ischemic stroke. *Clin Neurophysiol*. 2018;129(8):1680–1687. doi:10.1016/j.clinph.2018.05.021
14. Baldassarre A, Ramsey L, Rengachary J, et al. Dissociated functional connectivity profiles for motor and attention deficits in acute right-hemisphere stroke. *Brain*. 2016;139(7):2024–2038. doi:10.1093/brain/aww107
15. Bolwig TG. EEG and psychiatry: Time for a resurrection. *Acta Psychiatr Scand*. 2008;117(4):241–243. doi:10.1111/j.1600-0447.2008.01172.x
16. Cao KX, Ma ML, Wang CZ, et al. TMS-EEG: An emerging tool to study the neurophysiologic biomarkers of psychiatric disorders. *Neuropharmacology*. 2021;197:108574. doi:10.1016/j.neuropharm.2021.108574
17. Chennu S, Annen J, Wannez S, et al. Brain networks predict metabolism, diagnosis and prognosis at the bedside in disorders of consciousness. *Brain*. 2017;140(8):2120–2132. doi:10.1093/brain/awx163
18. Di Gregorio F, Petrone V, Casanova E, et al. Hierarchical psychophysiological pathways subtend perceptual asymmetries in neglect. *NeuroImage*. 2023;270:119942. doi:10.1016/j.neuroimage.2023.119942
19. Di Gregorio F, Lullini G, Orlandi S, et al. Clinical and neurophysiological predictors of the functional outcome in right-hemisphere stroke. *NeuroImage*. 2025;308:121059. doi:10.1016/j.neuroimage.2025.121059
20. Engemann DA, Raimondo F, King JR, et al. Robust EEG-based cross-site and cross-protocol classification of states of consciousness. *Brain*. 2018;141(11):3179–3192. doi:10.1093/brain/awy251
21. Ippolito G, Bertaccini R, Tarasi L, et al. The role of alpha oscillations among the main neuropsychiatric disorders in the adult and developing human brain: Evidence from the last 10 years of research. *Biomedicines*. 2022;10(12):3189. doi:10.3390/biomedicines10123189
22. Trajkovic J, Ricci G, Pirazzini G, et al. Aberrant functional connectivity and brain network organization in high-schizotypy individuals: An electroencephalography study. *Schizophr Bull*. 2025;51(5):1266–1281. doi:10.1093/schbul/sbaf004
23. Young MJ, Koch C, Claassen J, et al. An ethical framework to assess covert consciousness. *Lancet Neurol*. 2025;24(3):195–196. doi:10.1016/S1474-4422(24)00432-0
24. Battaglia S, Servajean P, Friston KJ. The paradox of the self-studying brain. *Phys Life Rev*. 2025;52:197–204. doi:10.1016/j.plrev.2024.12.009
25. Battaglia S, Nazzi C, Thayer JF. Genetic differences associated with dopamine and serotonin release mediate fear-induced bradycardia in the human brain. *Transl Psychiatry*. 2024;14(1):24. doi:10.1038/s41398-024-02737-x
26. Battaglia S, Nazzi C, Lonsdorf TB, Thayer JF. Neuropsychobiology of fear-induced bradycardia in humans: Progress and pitfalls. *Mol Psychiatry*. 2024;29(12):3826–3840. doi:10.1038/s41380-024-02600-x
27. Di Gregorio F, Battaglia S. The intricate brain–body interaction in psychiatric and neurological diseases. *Adv Clin Exp Med*. 2024;33(4):321–326. doi:10.17219/acem/185689
28. Nolte G, Bai O, Wheaton L, Mari Z, Vorbach S, Hallett M. Identifying true brain interaction from EEG data using the imaginary part of coherency. *Clin Neurophysiol*. 2004;115(10):2292–2307. doi:10.1016/j.clinph.2004.04.029
29. Nolte G, Ziehe A, Nikulin VV, et al. Robustly estimating the flow direction of information in complex physical systems. *Phys Rev Lett*. 2008;100(23):234101. doi:10.1103/PhysRevLett.100.234101
30. Vinck M, Oostenveld R, Van Wingerden M, Battaglia F, Pennartz CMA. An improved index of phase-synchronization for electrophysiological data in the presence of volume-conduction, noise and sample-size bias. *NeuroImage*. 2011;55(4):1548–1565. doi:10.1016/j.neuroimage.2011.01.055
31. Hardmeier M, Hatz F, Bousleiman H, Schindler C, Stam CJ, Fuhr P. Reproducibility of functional connectivity and graph measures based on the Phase Lag Index (PLI) and Weighted Phase Lag Index (wPLI) derived from high resolution EEG. *PLoS One*. 2014;9(10):e108648. doi:10.1371/journal.pone.0108648
32. Lehmann D, Faber PL, Gianotti LRR, Kochi K, Pascual-Marqui RD. Coherence and phase locking in the scalp EEG and between LORETA model sources, and microstates as putative mechanisms of brain temporo-spatial functional organization. *J Physiol (Paris)*. 2006;99(1):29–36. doi:10.1016/j.jphysparis.2005.06.005

33. Makeig S, Bell AJ, Tzyy-Ping J, Sejnowski TJ. Independent component analysis of electroencephalographic data. In: Touretzky DS, Mozer MC, Hasselmo ME, eds. *Advances in Neural Information Processing Systems 8: Proceedings of the 1995 Conference*. Cambridge, USA: MIT Press; 1996. https://papers.nips.cc/paper_files/paper/1995/hash/754dda4b1ba34c6fa89716b85d68532b-Abstract.html.
34. Mantini D, Franciotti R, Romani GL, Pizzella V. Improving MEG source localizations: An automated method for complete artifact removal based on independent component analysis. *NeuroImage*. 2008; 40(1):160–173. doi:10.1016/j.neuroimage.2007.11.022
35. Zhukov L, Weinstein D, Johnson C. Independent component analysis for EEG source localization. *IEEE Eng Med Biol Mag*. 2000;19(3):87–96. doi:10.1109/51.844386
36. Barbalho SM, Leme Boaro B, Da Silva Camarinha Oliveira J, et al. Molecular mechanisms underlying neuroinflammation intervention with medicinal plants: A critical and narrative review of the current literature. *Pharmaceuticals (Basel)*. 2025;18(1):133. doi:10.3390/ph18010133
37. Figueiredo Godoy AC, Frota FF, Araújo LP, et al. Neuroinflammation and natural antidepressants: Balancing fire with flora. *Biomedicines*. 2025;13(5):1129. doi:10.3390/biomedicines13051129
38. Cabral J, Hugues E, Sporns O, Deco G. Role of local network oscillations in resting-state functional connectivity. *NeuroImage*. 2011; 57(1):130–139. doi:10.1016/j.neuroimage.2011.04.010
39. Cohen MX. Multivariate cross-frequency coupling via generalized eigendecomposition. *eLife*. 2017;6:e21792. doi:10.7554/eLife.21792
40. Deco G, Kringelbach ML. Metastability and coherence: Extending the communication through coherence hypothesis using a whole-brain computational perspective. *Trends Neurosci*. 2016;39(3):125–135. doi:10.1016/j.tins.2016.01.001
41. Forrester M, Crofts JJ, Sotiropoulos SN, Coombes S, O'Dea RD. The role of node dynamics in shaping emergent functional connectivity patterns in the brain. *Netw Neurosci*. 2020;4(2):467–483. doi:10.1162/netn_a_00130
42. Modolo J, Hassan M, Wendling F, Benquet P. Decoding the circuitry of consciousness: From local microcircuits to brain-scale networks. *Netw Neurosci*. 2020;4(2):315–337. doi:10.1162/netn_a_00119
43. Tewarie P, Hunt BAE, O'Neill GC, et al. Relationships between neuronal oscillatory amplitude and dynamic functional connectivity. *Cereb Cortex*. 2019;29(6):2668–2681. doi:10.1093/cercor/bhy136
44. Fries P. A mechanism for cognitive dynamics: Neuronal communication through neuronal coherence. *Trend Cogn Sci*. 2005;9(10):474–480. doi:10.1016/j.tics.2005.08.011
45. Fries P. Rhythms for cognition: Communication through coherence. *Neuron*. 2015;88(1):220–235. doi:10.1016/j.neuron.2015.09.034
46. King JR, Sitt JD, Faugeras F, et al. Information sharing in the brain indexes consciousness in noncommunicative patients. *Curr Biol*. 2013;23(19):1914–1919. doi:10.1016/j.cub.2013.07.075
47. Riedl M, Müller A, Wessel N. Practical considerations of permutation entropy: A tutorial review. *Eur Phys J Spec Top*. 2013;222(2):249–262. doi:10.1140/epjst/e2013-01862-7
48. Deco G, Jirsa VK, McIntosh AR. Emerging concepts for the dynamical organization of resting-state activity in the brain. *Nat Rev Neurosci*. 2011;12(1):43–56. doi:10.1038/nrn2961
49. Hancock F, Rosas FE, Luppi AI, et al. Metastability demystified: The foundational past, the pragmatic present and the promising future. *Nat Rev Neurosci*. 2025;26(2):82–100. doi:10.1038/s41583-024-00883-1
50. Tognoli E, Kelso JAS. The metastable brain. *Neuron*. 2014;81(1):35–48. doi:10.1016/j.neuron.2013.12.022
51. Friston KJ. Transients, metastability, and neuronal dynamics. *NeuroImage*. 1997;5(2):164–171. doi:10.1006/nimg.1997.0259
52. Friston KJ. Functional and effective connectivity: A review. *Brain Connect*. 2011;1(1):13–36. doi:10.1089/brain.2011.0008
53. Tononi G. Consciousness and complexity. *Science*. 1998;282(5395): 1846–1851. doi:10.1126/science.282.5395.1846
54. Cabral J, Vidaurre D, Marques P, et al. Cognitive performance in healthy older adults relates to spontaneous switching between states of functional connectivity during rest. *Sci Rep*. 2017;7(1):5135. doi:10.1038/s41598-017-05425-7
55. Alderson TH, Bokde ALW, Kelso JAS, Maguire L, Coyle D. Metastable neural dynamics in Alzheimer's disease are disrupted by lesions to the structural connectome. *NeuroImage*. 2018;183:438–455. doi:10.1016/j.neuroimage.2018.08.033
56. Hellyer PJ, Scott G, Shanahan M, Sharp DJ, Leech R. Cognitive flexibility through metastable neural dynamics is disrupted by damage to the structural connectome. *J Neurosci*. 2015;35(24):9050–9063. doi:10.1523/JNEUROSCI.4648-14.2015
57. Lee WH, Doucet GE, Leibu E, Frangou S. Resting-state network connectivity and metastability predict clinical symptoms in schizophrenia. *Schizophr Res*. 2018;201:208–216. doi:10.1016/j.schres.2018.04.029
58. Tanaka M, Battaglia S, Liloia D. Navigating neurodegeneration: Integrating biomarkers, neuroinflammation, and imaging in Parkinson's, Alzheimer's and motor neuron disorders. *Biomedicines*. 2025; 13(5):1045. doi:10.3390/biomedicines13051045
59. Cassidy JM, Wodeyar A, Wu J, et al. Low-frequency oscillations are a biomarker of injury and recovery after stroke. *Stroke*. 2020;51(5): 1442–1450. doi:10.1161/STROKEAHA.120.028932
60. Cassidy JM, Wodeyar A, Srinivasan R, Cramer SC. Coherent neural oscillations inform early stroke motor recovery. *Hum Brain Mapp*. 2021;42(17):5636–5647. doi:10.1002/hbm.25643
61. Finnigan SP, Walsh M, Rose SE, Chalk JB. Quantitative EEG indices of sub-acute ischaemic stroke correlate with clinical outcomes. *Clin Neurophysiol*. 2007;118(11):2525–2532. doi:10.1016/j.clinph.2007.07.021
62. Finnigan S, Van Putten MJAM. EEG in ischaemic stroke: Quantitative EEG can uniquely inform (sub-)acute prognoses and clinical management. *Clin Neurophysiol*. 2013;124(1):10–19. doi:10.1016/j.clinph.2012.07.003
63. Gallina J, Pietrelli M, Zanon M, Bertini C. Hemispheric differences in altered reactivity of brain oscillations at rest after posterior lesions. *Brain Struct Funct*. 2022;227(2):709–723. doi:10.1007/s00429-021-02279-8
64. Leon-Carrion J, Martin-Rodriguez JF, Damas-Lopez J, Barroso Y Martin JM, Dominguez-Morales MR. Delta–alpha ratio correlates with level of recovery after neurorehabilitation in patients with acquired brain injury. *Clin Neurophysiol*. 2009;120(6):1039–1045. doi:10.1016/j.clinph.2009.01.021
65. Pietrelli M, Zanon M, Làdavas E, Grasso PA, Romei V, Bertini C. Posterior brain lesions selectively alter alpha oscillatory activity and predict visual performance in hemianopic patients. *Cortex*. 2019;121: 347–361. doi:10.1016/j.cortex.2019.09.008
66. Sheorajpanday RVA, Nagels G, Weeren AJTM, Van Putten MJAM, De Deyn PP. Quantitative EEG in ischemic stroke: Correlation with functional status after 6 months. *Clin Neurophysiol*. 2011;122(5):874–883. doi:10.1016/j.clinph.2010.07.028
67. Gale SD, Pearson CM. Neuroimaging predictors of stroke outcome: Implications for neurorehabilitation. *NeuroRehabilitation*. 2012;31(3): 331–344. doi:10.3233/NRE-2012-0800
68. Hoshino T, Oguchi K, Inoue K, Hoshino A, Hoshiyama M. Relationship between lower limb function and functional connectivity assessed by EEG among motor-related areas after stroke. *Top Stroke Rehabil*. 2021;28(8):614–623. doi:10.1080/10749357.2020.1864986
69. Kim B, Winstein C. Can neurological biomarkers of brain impairment be used to predict poststroke motor recovery? A systematic review. *Neurorehabil Neural Repair*. 2017;31(1):3–24. doi:10.1177/1545968316662708
70. Lim JS, Lee JJ, Woo CW. Post-stroke cognitive impairment: Pathophysiological insights into brain disconnectome from advanced neuroimaging analysis techniques. *J Stroke*. 2021;23(3):297–311. doi:10.5853/jos.2021.02376
71. Min YS, Park JW, Park E, et al. Interhemispheric functional connectivity in the primary motor cortex assessed by resting-state functional magnetic resonance imaging aids long-term recovery prediction among subacute stroke patients with severe hand weakness. *J Clin Med*. 2020;9(4):975. doi:10.3390/jcm9040975
72. Nicolo P, Rizk S, Magnin C, Pietro MD, Schnider A, Guggisberg AG. Coherent neural oscillations predict future motor and language improvement after stroke. *Brain*. 2015;138(10):3048–3060. doi:10.1093/brain/awv200
73. Bagnato S, Boccagni C, Prestandrea C, Sant'Angelo A, Castiglione A, Galardi G. Prognostic value of standard EEG in traumatic and non-traumatic disorders of consciousness following coma. *Clin Neurophysiol*. 2010;121(3):274–280. doi:10.1016/j.clinph.2009.11.008
74. Claassen J, Velazquez A, Meyers E, et al. Bedside quantitative electroencephalography improves assessment of consciousness in comatose subarachnoid hemorrhage patients. *Ann Neurol*. 2016;80(4): 541–553. doi:10.1002/ana.24752

75. Estraneo A, Loreto V, Guarino I, et al. Standard EEG in diagnostic process of prolonged disorders of consciousness. *Clin Neurophysiol*. 2016;127(6):2379–2385. doi:10.1016/j.clinph.2016.03.021
76. Gosseries O, Schnakers C, Ledoux D, et al. Automated EEG entropy measurements in coma, vegetative state/unresponsive wakefulness syndrome and minimally conscious state. *Funct Neurol*. 2011;26(1): 25–30. PMID:21693085. PMCID:PMC3814509.
77. O'Donnell A, Pauli R, Banellis L, et al. The prognostic value of resting-state EEG in acute post-traumatic unresponsive states. *Brain Commun*. 2021;3(2):fcab017. doi:10.1093/braincomms/fcab017
78. Rosanova M, Gosseries O, Casarotto S, et al. Recovery of cortical effective connectivity and recovery of consciousness in vegetative patients. *Brain*. 2012;135(4):1308–1320. doi:10.1093/brain/awr340
79. Sarasso S, Rosanova M, Casali AG, et al. Quantifying cortical EEG responses to TMS in (un)consciousness. *Clin EEG Neurosci*. 2014;45(1): 40–49. doi:10.1177/1550059413513723
80. Scarpino M, Lolli F, Hakiki B, et al. EEG and Coma Recovery Scale-Revised prediction of neurological outcome in disorder of consciousness patients. *Acta Neurol Scand*. 2020;142(3):221–228. doi:10.1111/ane.13247
81. Sitt JD, King JR, El Karoui I, et al. Large scale screening of neural signatures of consciousness in patients in a vegetative or minimally conscious state. *Brain*. 2014;137(8):2258–2270. doi:10.1093/brain/awu141
82. Stefan S, Schorr B, Lopez-Rolon A, et al. Consciousness indexing and outcome prediction with resting-state EEG in severe disorders of consciousness. *Brain Topogr*. 2018;31(5):848–862. doi:10.1007/s10548-018-0643-x
83. Tanaka M, Szabó Á, Vécsei L. Redefining roles: A paradigm shift in tryptophan–kynurenine metabolism for innovative clinical applications. *Int J Mol Sci*. 2024;25(23):12767. doi:10.3390/ijms252312767
84. Amiri M, Fisher PM, Raimondo F, et al. Multimodal prediction of residual consciousness in the intensive care unit: The CONNECT-ME study. *Brain*. 2023;146(1):50–64. doi:10.1093/brain/awac335
85. Coleman MR, Bekinschtein T, Monti MM, Owen AM, Pickard JD. A multimodal approach to the assessment of patients with disorders of consciousness. *Prog Brain Res*. 2009;177:231–248. doi:10.1016/S0079-6123(09)17716-6
86. Di Perri C, Bahri MA, Amico E, et al. Neural correlates of consciousness in patients who have emerged from a minimally conscious state: A cross-sectional multimodal imaging study. *Lancet Neurol*. 2016; 15(8):830–842. doi:10.1016/S1474-4422(16)00111-3
87. Gallucci A, Varoli E, Del Mauro L, et al. Multimodal approaches supporting the diagnosis, prognosis and investigation of neural correlates of disorders of consciousness: A systematic review. *Eur J Neurosci*. 2024;59(5):874–933. doi:10.1111/ejn.16149
88. Hinkley LBN, Vinogradov S, Guggisberg AG, Fisher M, Findlay AM, Nagarajan SS. Clinical symptoms and alpha band resting-state functional connectivity imaging in patients with schizophrenia: Implications for novel approaches to treatment. *Biol Psychiatry*. 2011;70(12): 1134–1142. doi:10.1016/j.biopsych.2011.06.029
89. Trajkovic J, Di Gregorio F, Ferri F, Marzi C, Diciotti S, Romei V. Resting state alpha oscillatory activity is a valid and reliable marker of schizotypy. *Sci Rep*. 2021;11(1):10379. doi:10.1038/s41598-021-89690-7
90. Braff DL. Prepulse inhibition of the startle reflex: A window on the brain in schizophrenia. *Curr Top Behav Neurosci*. 2010;4:349–371. doi:10.1007/7854_2010_61
91. Kumari V, Sharma T. Effects of typical and atypical antipsychotics on prepulse inhibition in schizophrenia: A critical evaluation of current evidence and directions for future research. *Psychopharmacology*. 2002;162(2):97–101. doi:10.1007/s00213-002-1099-x
92. Mena A, Ruiz-Salas JC, Puentes A, Dorado I, Ruiz-Veguilla M, De La Casa LG. Reduced prepulse inhibition as a biomarker of schizophrenia. *Front Behav Neurosci*. 2016;10:202. doi:10.3389/fnbeh.2016.00202
93. Radhu N, Garcia Dominguez L, Farzan F, et al. Evidence for inhibitory deficits in the prefrontal cortex in schizophrenia. *Brain*. 2015; 138(2):483–497. doi:10.1093/brain/awu360
94. Swerdlow NR, Weber M, Qu Y, Light GA, Braff DL. Realistic expectations of prepulse inhibition in translational models for schizophrenia research. *Psychopharmacology*. 2008;199(3):331–388. doi:10.1007/s00213-008-1072-4
95. Lynn PA, Sponheim SR. Disturbed theta and gamma coupling as a potential mechanism for visuospatial working memory dysfunction in people with schizophrenia. *Neuropsychiatr Electrophysiol*. 2016; 2(1):7. doi:10.1186/s40810-016-0022-3
96. Pittman-Polletta BR, Kocsis B, Vijayan S, Whittington MA, Kopell NJ. Brain rhythms connect impaired inhibition to altered cognition in schizophrenia. *Biol Psychiatry*. 2015;77(12):1020–1030. doi:10.1016/j.biopsych.2015.02.005
97. Senkowski D, Gallinat J. Dysfunctional prefrontal gamma-band oscillations reflect working memory and other cognitive deficits in schizophrenia. *Biol Psychiatry*. 2015;77(12):1010–1019. doi:10.1016/j.biopsych.2015.02.034
98. Ghuman AS, Van Den Honert RN, Huppert TJ, Wallace GL, Martin A. Aberrant oscillatory synchrony is biased toward specific frequencies and processing domains in the autistic brain. *Biol Psychiatry Cogn Neurosci Neuroimaging*. 2017;2(3):245–252. doi:10.1016/j.bpsc.2016.07.006
99. Kessler K, Seymour RA, Rippon G. Brain oscillations and connectivity in autism spectrum disorders (ASD): New approaches to methodology, measurement and modelling. *Neurosci Biobehav Rev*. 2016;71: 601–620. doi:10.1016/j.neubiorev.2016.10.002
100. O'Reilly C, Lewis JD, Elsabbagh M. Is functional brain connectivity atypical in autism? A systematic review of EEG and MEG studies. *PLoS One*. 2017;12(5):e0175870. doi:10.1371/journal.pone.0175870
101. Barnes SJK, Thomas M, McClintock PVE, Stefanovska A. Theta and alpha connectivity in children with autism spectrum disorder. *Brain Commun*. 2025;7(2):fcaf084. doi:10.1093/braincomms/fcaf084
102. Belmonte MK, Allen G, Beckel-Mitchener A, Boulanger LM, Carper RA, Webb SJ. Autism and abnormal development of brain connectivity. *J Neurosci*. 2004;24(42):9228–9231. doi:10.1523/JNEUROSCI.3340-04.2004
103. Uhlhaas PJ, Singer W. Neural synchrony in brain disorders: Relevance for cognitive dysfunctions and pathophysiology. *Neuron*. 2006;52(1):155–168. doi:10.1016/j.neuron.2006.09.020
104. Van De Cruys S, Evers K, Van Der Hallen R, et al. Precise minds in uncertain worlds: Predictive coding in autism. *Psychol Rev*. 2014; 121(4):649–675. doi:10.1037/a0037665
105. Alba G, Pereda E, Mañas S, et al. The variability of EEG functional connectivity of young ADHD subjects in different resting states. *Clin Neurophysiol*. 2016;127(2):1321–1330. doi:10.1016/j.clinph.2015.09.134
106. Debnath R, Miller NV, Morales S, Seddio KR, Fox NA. Investigating brain electrical activity and functional connectivity in adolescents with clinically elevated levels of ADHD symptoms in alpha frequency band. *Brain Res*. 2021;1750:147142. doi:10.1016/j.brainres.2020.147142
107. Lenartowicz A, Lu S, Rodriguez C, et al. Alpha desynchronization and frontoparietal connectivity during spatial working memory encoding deficits in ADHD: A simultaneous EEGfMRI study. *Neuroimage Clin*. 2016;11:210–223. doi:10.1016/j.nicl.2016.01.023
108. Lenartowicz A, Mazaheri A, Jensen O, Loo SK. Aberrant modulation of brain oscillatory activity and attentional impairment in attention-deficit/hyperactivity disorder. *Biol Psychiatry Cogn Neurosci Neuroimaging*. 2018;3(1):19–29. doi:10.1016/j.bpsc.2017.09.009
109. Murias M, Swanson JM, Srinivasan R. Functional connectivity of frontal cortex in healthy and ADHD children reflected in EEG coherence. *Cereb Cortex*. 2007;17(8):1788–1799. doi:10.1093/cercor/bhl089
110. Dipnall LM, Hourani D, Darling S, Anderson V, Sciberras E, Silk TJ. Fronto-parietal white matter microstructure associated with working memory performance in children with ADHD. *Cortex*. 2023;166: 243–257. doi:10.1016/j.cortex.2023.03.015
111. Parlatini V, Radua J, Robertsson N, et al. Asymmetry of attentive networks contributes to adult attention-deficit/hyperactivity disorder (ADHD) pathophysiology [published online as ahead of print on November 2, 2024]. *Eur Arch Psychiatry Clin Neurosci*. 2024. doi:10.1007/s00406-024-01927-4
112. Kannen K, Rasbach J, Fantazi A, et al. Alpha modulation via transcranial alternating current stimulation in adults with attention-deficit hyperactivity disorder. *Front Psychol*. 2024;14:1280397. doi:10.3389/fpsyg.2023.1280397
113. Yin Y, Wang X, Feng T. Noninvasive brain stimulation for improving cognitive deficits and clinical symptoms in attention-deficit/hyperactivity disorder: A systematic review and meta-analysis. *Brain Sci*. 2024;14(12):1237. doi:10.3390/brainsci14121237
114. Trajkovic J, Di Gregorio F, Marcantoni E, Thut G, Romei V. A TMS/EEG protocol for the causal assessment of the functions of the oscillatory brain rhythms in perceptual and cognitive processes. *STAR Protoc*. 2022;3(2):101435. doi:10.1016/j.xpro.2022.101435

115. Trajkovic J, Di Gregorio F, Thut G, Romei V. Transcranial magnetic stimulation effects support an oscillatory model of ERP genesis. *Curr Biol*. 2024;34(5):1048–1058.e4. doi:10.1016/j.cub.2024.01.069
116. Debener S, Beauducel A, Nessler D, Brocke B, Heilemann H, Kayser J. Is resting anterior EEG alpha asymmetry a trait marker for depression? *Neuropsychobiology*. 2000;41(1):31–37. doi:10.1159/000026630
117. Goldstein BL, Shankman SA, Kujawa A, Torpey-Newman DC, Olino TM, Klein DN. Developmental changes in electroencephalographic frontal asymmetry in young children at risk for depression. *Child Psychol Psychiatry*. 2016;57(9):1075–1082. doi:10.1111/jcpp.12567
118. Van Der Vinne N, Vollebregt MA, Van Putten MJAM, Arns M. Frontal alpha asymmetry as a diagnostic marker in depression: Fact or fiction? A meta-analysis. *Neuroimage Clin*. 2017;16:79–87. doi:10.1016/j.nicl.2017.07.006
119. Sun L, Peräkylä J, Hartikainen KM. Frontal alpha asymmetry, a potential biomarker for the effect of neuromodulation on brain's affective circuitry: Preliminary evidence from a deep brain stimulation study. *Front Hum Neurosci*. 2017;11:584. doi:10.3389/fnhum.2017.00584
120. Juhász L, Spisák K, Szolnoki BZ, et al. The power struggle: Kynurenine pathway enzyme knockouts and brain mitochondrial respiration. *J Neurochem*. 2025;169(5):e70075. doi:10.1111/jnc.70075
121. Szabó Á, Galla Z, Spekker E, et al. Oxidative and excitatory neurotoxic stresses in CRISPR/Cas9-induced kynurenine aminotransferase knockout mice: A novel model for despair-based depression and post-traumatic stress disorder. *Front Biosci (Landmark Ed)*. 2025;30(1):25706. doi:10.31083/FBL25706
122. Redinbaugh MJ, Phillips JM, Kambi NA, et al. Thalamus modulates consciousness via layer-specific control of cortex. *Neuron*. 2020;106(1):66–75.e12. doi:10.1016/j.neuron.2020.01.005
123. Saalmann YB, Pinsk MA, Wang L, Li X, Kastner S. The pulvinar regulates information transmission between cortical areas based on attention demands. *Science*. 2012;337(6095):753–756. doi:10.1126/science.1223082
124. Saalmann YB, Kastner S. Cognitive and perceptual functions of the visual thalamus. *Neuron*. 2011;71(2):209–223. doi:10.1016/j.neuron.2011.06.027
125. Halgren M, Ulbert I, Bastuji H, et al. The generation and propagation of the human alpha rhythm. *Proc Natl Acad Sci U S A*. 2019;116(47):23772–23782. doi:10.1073/pnas.1913092116
126. Schreckenberger M, Lange-Asschenfeldt C, Lochmann M, et al. The thalamus as the generator and modulator of EEG alpha rhythm: A combined PET/EEG study with lorazepam challenge in humans [published correction appers in: *Neuroimage*. 2006;32(1):485 doi:10.1016/j.neuroimage.2006.03.007]. *Neuroimage*. 2004;22(2):637–644. doi:10.1016/j.neuroimage.2004.01.047
127. Vijayan S, Kopell NJ. Thalamic model of awake alpha oscillations and implications for stimulus processing. *Proc Natl Acad Sci U S A*. 2012;109(45):18553–18558. doi:10.1073/pnas.1215385109
128. Tortora F, Hadipour AL, Battaglia S, Falzone A, Avenanti A, Vicario CM. The role of serotonin in fear learning and memory: A systematic review of human studies. *Brain Sci*. 2023;13(8):1197. doi:10.3390/brainsci13081197
129. Battaglia S, Fazio CD, Borgomaneri S, Avenanti A. Cortisol imbalance and fear learning in PTSD: Therapeutic approaches to control abnormal fear responses. *Curr Neuropharmacol*. 2025;23(7):835–846. doi:10.2174/1570159X23666250123142526
130. Battaglia S, Di Fazio C, Mazzà M, Tamietto M, Avenanti A. Targeting human glucocorticoid receptors in fear learning: A multiscale integrated approach to study functional connectivity. *Int J Mol Sci*. 2024;25(2):864. doi:10.3390/ijms25020864
131. Tanaka M, Szabó Á, Vécsei L, Giménez-Llort L. Emerging translational research in neurological and psychiatric diseases: From in vitro to in vivo models. *Int J Mol Sci*. 2023;24(21):15739. doi:10.3390/ijms242115739
132. Hernandez-Pavon JC, Schneider-Garces N, Begnoche JP, Miller LE, Raij T. Targeted modulation of human brain interregional effective connectivity with spike-timing dependent plasticity. *Neuromodulation*. 2023;26(4):745–754. doi:10.1016/j.neurom.2022.10.045
133. Di Gregorio F, La Porta F, Casanova E, et al. Efficacy of repetitive transcranial magnetic stimulation combined with visual scanning treatment on cognitive and behavioral symptoms of left hemispatial neglect in right hemispheric stroke patients: Study protocol for a randomized controlled trial. *Trials*. 2021;22(1):24. doi:10.1186/s13063-020-04943-6
134. Di Gregorio F, La Porta F, Lullini G, et al. Efficacy of repetitive transcranial magnetic stimulation combined with visual scanning treatment on cognitive-behavioral symptoms of unilateral spatial neglect in patients with traumatic brain injury: Study protocol for a randomized controlled trial. *Front Neurol*. 2021;12:702649. doi:10.3389/fneur.2021.702649
135. Tanaka M, Szatmári I, Vécsei L. Quinoline quest: Kynurenic acid strategies for next-generation therapeutics via rational drug design. *Pharmaceuticals (Basel)*. 2025;18(5):607. doi:10.3390/ph18050607
136. Yakubov B, Das S, Zomorrodi R, et al. Cross-frequency coupling in psychiatric disorders: A systematic review. *Neurosci Biobehav Rev*. 2022;138:104690. doi:10.1016/j.neubiorev.2022.104690
137. Hutchison RM, Womelsdorf T, Allen EA, et al. Dynamic functional connectivity: Promise, issues, and interpretations. *NeuroImage*. 2013;80:360–378. doi:10.1016/j.neuroimage.2013.05.079
138. Hallquist MN, Hillary FG. Graph theory approaches to functional network organization in brain disorders: A critique for a brave new small-world. *Netw Neurosci*. 2019;3(1):1–26. doi:10.1162/netn_a_00054
139. Jaeger C, Nuttall R, Zimmermann J, et al. Targeted rhythmic visual stimulation at individual participants' intrinsic alpha frequency causes selective increase of occipitoparietal BOLD-fMRI and EEG functional connectivity. *NeuroImage*. 2023;270:119981. doi:10.1016/j.neuroimage.2023.119981
140. Battaglia S, Nazzi C, Fullana MA, Di Pellegrino G, Borgomaneri S. 'Nip it in the bud': Low-frequency rTMS of the prefrontal cortex disrupts threat memory consolidation in humans. *Behav Res Ther*. 2024;178:104548. doi:10.1016/j.brat.2024.104548
141. Battaglia S, Nazzi C, Di Fazio C, Borgomaneri S. The role of pre-supplementary motor cortex in action control with emotional stimuli: A repetitive transcranial magnetic stimulation study. *Ann N Y Acad Sci*. 2024;1536(1):151–166. doi:10.1111/nyas.15145
142. Tanaka M. Beyond the boundaries: Transitioning from categorical to dimensional paradigms in mental health diagnostics. *Adv Clin Exp Med*. 2024;33(12):1295–1301. doi:10.17219/acem/197425
143. Tanaka M. From serendipity to precision: Integrating AI, multi-omics, and human-specific models for personalized neuropsychiatric care. *Biomedicines*. 2025;13(1):167. doi:10.3390/biomedicines13010167

Long-term safety and efficacy of loose combined cutting seton therapy for high anal fistula: Evidence from a prospective cohort study

Zhi Congcong[A], Cheng Yicheng[A], Li Xin[B], Shi Yuying[C], Liu Ningyuan[C], Zheng Lihua[D,F], Hou Wenxia[E,F]

2nd Department of Anorectal Surgery, China-Japan Friendship Hospital, Beijing, China

A – research concept and design; B – collection and/or assembly of data; C – data analysis and interpretation;
D – writing the article; E – critical revision of the article; F – final approval of the article

Advances in Clinical and Experimental Medicine, ISSN 1899–5276 (print), ISSN 2451–2680 (online) *Adv Clin Exp Med*. 2026;35(2):209–217

Address for correspondence
Zheng Lihua
E-mail: btv126@outlook.com

Funding sources
This study was supported by the Central High-Level Clinical Research Fund (grant No. 2022-NHLHCRF-LX-02-0121).

Conflict of interest
None declared

Received on December 21, 2024
Reviewed on March 27, 2025
Accepted on April 24, 2025

Published online on January 12, 2026

Abstract

Background. The healing rate after treatment in patients with high anal fistula (HAF) remains low. In individuals with HAF, the loose combined cutting seton (LCCS) technique has shown promising effectiveness, demonstrating a high cure rate, low incidence of incontinence and reduced pain levels.

Objectives. To assess the long-term efficacy and safety of LCCS technique in patients with HAF.

Materials and methods. The LCCS procedure was conducted in patients with HAF between December 2020 and February 2022. All participants were followed up for 12 months. The primary outcome was fistula healing, while secondary outcomes included fistula recurrence, visual analogue scale (VAS) pain score, severity of fecal incontinence, and quality of life.

Results. A total of 132 patients with HAF were included in the final analysis, with a mean follow-up duration of 17.0 ±3.8 months. At the 12-month follow-up, 130 patients (98.5%) achieved fistula healing. Among them, 103 patients who received primary HAF treatment at our center fully recovered, while 27 of 29 patients previously treated unsuccessfully at other hospitals achieved healing within 12 months, corresponding to a 93.1% success rate. Ninety patients (68.2%) reported no fecal incontinence at follow-up (Wexner Continence Grading Scale (WCGS) score = 0), and 42 patients had a WCGS score of 1. The LCCS procedure was associated with a persistently low risk of postoperative perianal discomfort, with 127 patients (96.2%) scoring 0 and only 5 (3.8%) scoring 1 on the VAS.

Conclusions. The LCCS technique is a safe and effective treatment for patients with HAF.

Key words: safety, efficacy, high anal fistula, loose combined cutting seton

Cite as
Congcong Z, Yicheng C, Xin L, et al. Long-term safety and efficacy of loose combined cutting seton therapy for high anal fistula: Evidence from a prospective cohort study. *Adv Clin Exp Med*. 2026;35(2):209–217. doi:10.17219/acem/204335

DOI
10.17219/acem/204335

Highlights

- High anal fistula (HAF) is an anorectal fistula with many external openings and channels, with the internal opening flowing through the deep layer of the external sphincter and impacting the upper two-thirds.
- The particular anatomical features of the human body present obstacles in treating this kind of AF, resulting in a high recurrence rate.
- The primary purpose of this study was to assess the long-term efficacy and safety of loose combined cutting seton (LCCS) in individuals with HAF.
- The evidence suggests that LCCS surgery for HAFs improves postoperative wound healing while reducing healing time, pain and complications, making it a valuable clinical practice for wider use.

Background

Anal fistula (AF) is a prevalent anorectal disorder, particularly affecting younger males. Epidemiological data estimate that AF affects approx. 8% of the population in Western countries and 3.6% in China.[1–3] High anal fistula (HAF) is characterized by multiple external openings and tracts, with the internal opening traversing the deep portion of the external sphincter, specifically involving the upper two-thirds of the muscle. The intricate anatomical features of the anorectal region present substantial challenges in the management of HAF, contributing to a significant recurrence rate.[4,5]

Inadequate treatment of HAF can disrupt the physiology of adjacent tissues and significantly affect patients' health and quality of life. Therapeutic objectives for HAF primarily focus on fistula healing, recurrence prevention and bowel function improvement.[5,6] Current clinical practice employs diverse therapeutic modalities to address HAF, including fibrin sealant, fistula plug, ligation of the inter-sphincteric fistula tract (LIFT), endorectal or dermal advancement flap, video-assisted AF treatment, and traditional Chinese medicine (TCM).[7–11] Despite these advances, reported healing rates remain suboptimal.[8,12]

Seton-based techniques have demonstrated efficacy in the management of HAF, offering high cure rate with a low risk of incontinence. Recent advancements in seton materials and application methods improved outcomes,[13,14] though reported recurrence rates still range from 8% to 22%. Clinical implementation remains heavily dependent on surgical expertise.[15–17] The loose seton technique facilitates effective drainage and accelerates the healing process while minimizing the risk of sphincter injury.[13] However, in some cases, excessive fibrosis may lead to treatment failure. Conversely, the cutting seton achieves definitive fistula resolution through progressive sphincter division; however, it is frequently associated with complications such as pain and fecal incontinence.[18]

To effectively manage HAF and improve patients' quality of life, it is essential to develop treatment approaches that achieve high healing rate while minimizing recurrence, incontinence and pain. Our prior retrospective study demonstrated that a combined virtual and solid wiring offers superior clinical outcomes compared to traditional solid seton techniques, particularly in reducing healing time and alleviating pain.[19] In this approach, the virtual seton facilitates drainage, whereas the solid seton progressively transects the fistulous tract. Nonetheless, the long-term postoperative recurrence, anal incontinence and recovery of anal function represent paramount determinants of surgical efficacy and quality of life following HAF repair. However, longitudinal data quantifying these critical long-term outcomes remain scarce.

Objectives

This prospective cohort study aims to evaluate the long-term efficacy and safety of loose combined cutting seton (LCCS) in patients with HAF.

Materials and methods

This was a prospective cohort study.

Study population

The study was conducted at the Anal and Intestinal Department of China-Japan Friendship Hospital (Beijing, China), a national referral center specializing in the treatment of over 1,000 patients annually with various types of AFs, serving individuals from across the country and abroad. This study included consecutive patients diagnosed with HAF who underwent surgical treatment at the Second Department of Anorectal Surgery of China-Japan Friendship Hospital between December 2020 and February 2022. The inclusion criteria were as follows: 1) individuals aged 18 years or older, and 2) a definitive diagnosis of HAF, including primary HAF and failed cases from other medical centers. The exclusion criteria included: 1) individuals with colorectal cancer, 2) inflammatory bowel disease (IBD) or intestinal tuberculosis, 3) autoimmune diseases, 4) coagulation dysfunction, 5) systemic infections related to acquired

immunodeficiency disease, 6) severe cardiopulmonary dysfunction, 7) life expectancy of less than 12 months, 8) pregnancy or lactation, and 9) inability to comply with long-term follow-up. Patients with missing primary indicators were also excluded from the final analysis. The study was approved by the Clinical Research Ethics Committee of China-Japan Friendship Hospital (approval No. 2022-KY-121-2), and written informed consent was obtained from all patients. This investigation adhered to the principles outlined in the Helsinki Declaration (2013 edition).

Surgery

All procedures were performed by the same surgical team (Z.L.H., C.Y.C., Z.C.C., and L.N.Y.) using the LCCS technique as previously described (Fig. 1).[19] Patients received general or epidural anesthesia and were positioned laterally to facilitate access to the fistula. Following standard perineal disinfection with 0.5% iodophor, the anal canal was adequately relaxed. A digital rectal examination was performed in conjunction with anorectal B-ultrasound findings to evaluate the internal opening of the fistula, its extent, the presence of branched tracts or necrotic tissue, and any indurated masses around the anorectal ring. A fistula probe was introduced through the external opening. If the fistula lacked an external opening, the distal end was excised to create an access point. The probe was introduced into the internal orifice along the fistula tract, and the fistula wall was meticulously dissected layer by layer to facilitate complete exposure. Tissue surrounding the internal orifice was excised to a margin of 0.5–1.0 cm. The probe was carefully advanced from the internal orifice upward through the fistula tract, assisted by curved hemostatic forceps, while a finger was inserted into the rectal cavity to locate the fistula apex. The forceps' tip was employed to access the stoma of the intestinal wall, which served as the focal point of the crisscrossed lumps. Subsequently, the examining finger was withdrawn, and 4 No. 10 silk threads were affixed to the fingertips at one end before being introduced into the enteric cavity. The threads were subsequently secured using hemostatic forceps, extracted from the stoma of the intestinal cavity along the fistula, tightened at both ends, and tied off for stabilization.

Postoperative wound management involved daily dressing changes adhering to standard disinfection protocols. Oil gauze was utilized to facilitate drainage, while standard gauze was used to secure external applications. All patients received intravenous analgesics (flurbiprofen axetil injection, 100 mg, each day) and antibiotics (etamycin sulfate and sodium chloride injection, 300 mL, each day) for 2 days post-surgery. The ligature was observed to loosen

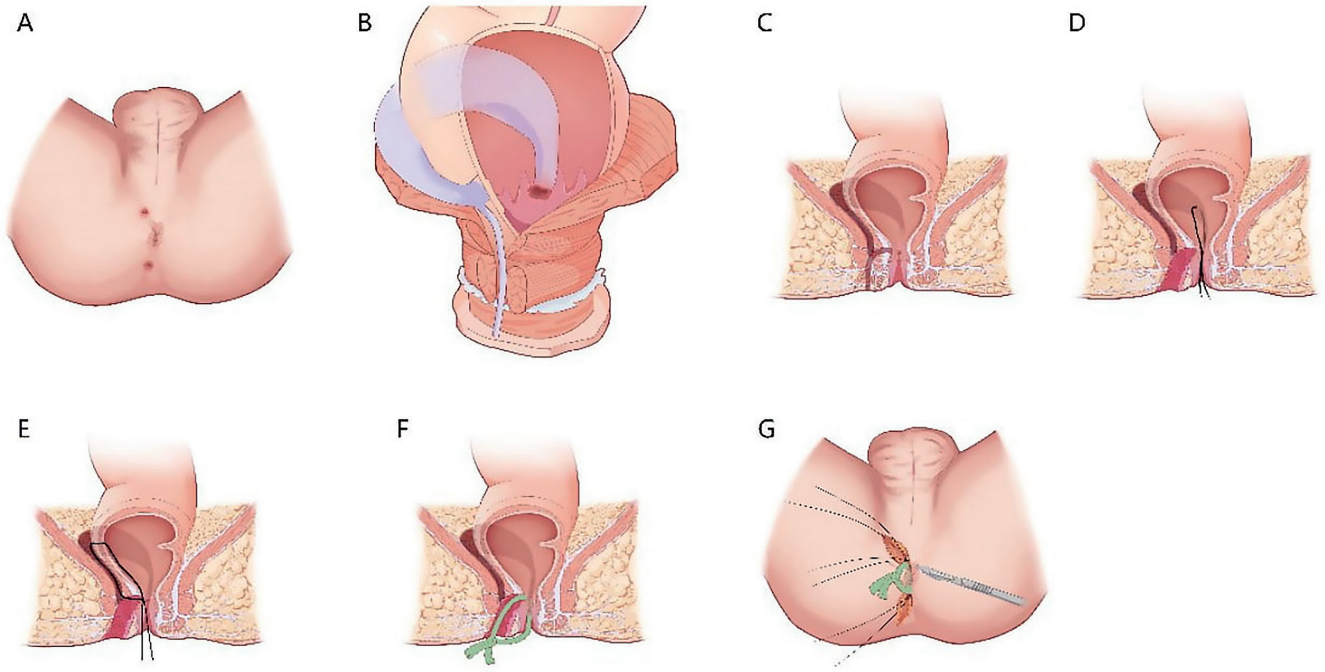

Fig. 1. Steps of the loose combined cutting seton (LCCS) procedure for high anal fistula (HAF). A. Using the right half of the horseshoe-shaped anal fistula (AF) as an example, 2 external openings are visible at 6 and 11 o'clock positions in the lithotomy position, and the right hemianal rectal ring was rigid; B. Stereoscopic representation in the sagittal plane: The fistula at 11 o'clock position in the lithotomy position passed through the depth of the external sphincter and intersected with the AF at 6 o'clock position in the lithotomy position on the rectal anal ring, forming an AF cavity; C. The skin and subcutaneous connective tissue were incised from the external opening at the 6 o'clock position in the lithotomy position to the dentate line at the same position; D. The AF cavity was explored at 6 o'clock position in the lithotomy position, an enterostomy was performed at the apex of the AF cavity at this position, and the line was connected to the top of the AF cavity at 6 o'clock position of the dentate line. At the same time, the skin and subcutaneous connective tissue were incised along the external opening at 11 o'clock position in the lithotomy position to the corresponding dentate line; E. The AF cavity was probed at the 11 o'clock position in the lithotomy position, and enterostomy was performed at the apex of the AF cavity at this position. The line was connected to the apex of the AF cavity at the 11 o'clock position of the dentate line; F. The incision was explored at the 6 and 11 o'clock position of the lithotomy, and the drainage lines were hung to ensure smooth drainage; G. Schematic diagram of the postoperative anatomy

on postoperative day 7 but was left in situ to maintain drainage. Based on the characteristics of the granulation tissue developing within the fistula tract, the silk thread was removed on postoperative day 20. Dressings were changed regularly thereafter until complete wound healing was achieved.

Data collection

Data were collected on patient demographics, medical history, comorbidities, fistula characteristics, surgical procedure, and clinical outcomes. Prior to the surgical procedure, all patients underwent a comprehensive baseline assessment, including routine blood tests, assessments of liver and renal function, and evaluation of blood glucose and lipid profiles. Furthermore, a subset of patients underwent endoanal ultrasonography and anorectal pressure manometry to determine the position of the internal orifice and the configuration of the fistula. Follow-up assessments were conducted at the outpatient clinic 12 months post-surgery. These evaluations included a physical examination (comprising anal inspection and digital rectal examination), endoanal ultrasonography and anorectal manometry. Patients experiencing severe symptoms or concerns regarding recurrence were advised to undergo additional clinical review.

Fistula healing was defined by the complete closure of the surgical incision, absence of secretions, and the lack of any detectable fistula as confirmed using endoanal ultrasonography. Recurrence was diagnosed if a patient met at least 1 of the following criteria: 1) non-healing of the surgical wound beyond 3 months, 2) persistent discharge beyond 3 months, 3) endoanal ultrasonography indicated the presence of the fistula, or 4) clinical necessity for reoperation.

A visual analogue scale (VAS) was employed to assess postoperative pain, with scores ranging from 0 (indicating no pain) to 10 (representing extremely severe pain). The severity of fecal incontinence was evaluated through the Wexner Continence Grading Scale (WCGS), encompassing 5 domains: solid, liquid, gas, pad wearing, and lifestyle alterations. Each domain was assigned a score ranging from 0 (indicating no incontinence) to 4 (indicating severe incontinence). The quality of life was evaluated using the 36-Item Short Form Survey (SF-36).

Outcomes

The primary outcome variable of this investigation was fistula healing rate. Secondary outcomes included the fistula recurrence rate, postoperative pain (VAS), fecal incontinence severity (WCGS), and quality of life (SF-36).

Statistical analyses

Continuous variables were reported as mean ± standard deviation (SD) for normal distributions tested by Kolmogorov–Smirnov test. Numerical and percentage representations were used for categorical variables. All statistical analyses were conducted using the SPSS v. 18.0 for Windows (SPSS Inc., Chicago, USA). A 2-sided p-value of less than 0.05 was deemed statistically significant. Missing data for certain variables were excluded from the analysis.

Results

Baseline characteristics

Following the application of the inclusion and exclusion criteria, 132 patients with HAF were included in the final analysis, comprising 114 men (86.4%) and 18 women (13.6%). Of these, 29 patients had previously undergone unsuccessful LIFT surgery at other medical centers. Detailed baseline characteristics prior to LCCS treatment are presented in Table 1 and Table 2.

Table 1. Baseline characteristics of 132 patients with HAF treated with loose combined cutting seton

Characteristics	Outcome
Age [years]#	36.4 ±8.7
Male, n (%)	114 (86.4)
BMI [kg/m^2]#	25.2 ±2.1
Hypertension, n (%)	5 (3.8)
Diabetes, n (%)	3 (2.3)
Current smoking, n (%)	29 (22.0)
Clinical presentation, n (%)	
Perianal mass	97 (73.5)
Perianal pain	116 (87.9)
Anal secretion	83 (62.9)
Fever	21 (15.9)
Anal pendant expansion	35 (26.5)
Duration of HAF [months]#	12.6 ±4.3
Number of external fistula orifices	
0	21 (15.9)
1	78 (59.1)
2	33 (25.0)
Number of fistula tracts	
1	94 (71.2)
2	38 (28.8)
Shape of fistula, n (%)	
Homotopic line	18 (13.6)
Full horseshoe	43 (32.6)
Semi-horseshoe	71 (53.8)
Position of internal orifice, n (%)	
1 and 6 o'clock	9 (6.8)
6 o'clock	111 (84.1)
7 o'clock	12 (9.1)

#mean ± standard deviation (SD); HAF – high anal fistula; BMI – body mass index.

Table 2. Continuous variables normality test results using the Kolmogorov–Smirnov test

Variables	D value	df	p-value
Age	0.572	131	0.568
BMI	0.328	131	0.743
Duration of HAF	0.614	131	0.540
Anal resting pressure	–0.493	131	0.623
Maximum systolic pressure	0.507	131	0.613
Rectal anal pressure difference	0.825	131	0.411
High pressure zone	0.716	131	0.475

HAF – high anal fistula; BMI – body mass index; df – degrees of freedom.

Secondary outcome

The WCGS assessment revealed that 90 patients (68.2%) exhibited no fecal incontinence during follow-up, corresponding to a WCGS score of 0. The remaining 42 patients reported a WCGS score of 1. The median total WCGS score was 0 (range: 0–12). The median total WCGS score was 0 for patient groups without previous surgery (range: 0–3) and 29 patients with failed surgeries before (range: 0–12). A total of 27 patients reported "occasional" liquid stool incontinence. Additionally, 5 patients experienced "occasional" flatus incontinence, and 9 patients reported "occasional" solid stool incontinence. Furthermore, 1 patient reported changes in their lifestyle. No patients exhibited anal itching (Table 4). At the 1-month postoperative follow-up, 127 patients (96.2%) reported a VAS pain score of 0, while 5 patients (3.8%) reported a score of 1. Notably, 3 of these patients no longer report any pain at the 3-month follow-up, suggesting that LCCS is associated with a long-term low risk of postoperative perianal pain. All patients achieved a final score of 100 in each SF-36 domain, indicating that the adverse effects of HAF on patients' general health, physical activities, physical health, emotional health, social activities, and pain were nearly eliminated during the long-term follow-up after LCCS surgery.

Anal inspection revealed scar-related clots formation in 6 patients (4.5%), while no malformations were observed in any of the patients. Digital rectal examination confirmed the absence of palpable masses, induration or tenderness in all patients. Endoanal ultrasonography was performed

Table 3. Postoperative Wexner Continence Grading Scale scores of 132 patients with HAF

Variables	Never	Occasionally	Sometimes	Usually	Always
Solid, n (%)	0	9 (6.8)	0	0	0
Liquid, n (%)	0	27 (20.5)	0	0	0
Flatus, n (%)	0	5 (3.8)	0	0	0
Wears pad, n (%)	0	0	0	0	0
Lifestyle alteration, n (%)	0	1 (0.8)	0	0	0

HAF – high anal fistula.

The median duration of HAF was 12 months (interquartile range (IQR): 2–36 months). The most common presenting symptoms were perianal pain (n = 116, 87.9%), perianal mass (n = 97, 73.5%), anal secretion (n = 83, 62.9%), anal pendent expansion (n = 35, 26.5%), and fever (n = 21, 15.9%). The majority of patients had a single fistula tract, characterized by 1 external orifice. The internal orifice was located at the 6 o'clock position in 111 (84.1%) patients and at 7 o'clock position in 12 (9.1%) patients, while an additional 9 patients (6.8%) exhibited internal orifices at both 1 and 6 o'clock, respectively. A semi-horseshoe shape fistula was identified in 71 patients (53.8%), a full horseshoe in 43 patients (32.6%) and homotopic line in 18 patients (13.6%). The preoperative laboratory findings of the patients are presented in Table 3. All patients exhibited normal liver function and renal function, with no significant abnormalities noted.

Primary outcome

The mean follow-up duration was 17.0 ±3.8 months. At the 12-month postoperative follow-up, 130 of 132 patients achieved fistula healing, yielding an overall healing rate of 98.5%. Among the 103 patients undergoing HAF treatment for the first time, the 12-month healing rate was 100%. Of 29 patients with prior treatment failures from external center, 27 achieved healing at 12-month follow-up, resulting in healing rate of 93.1%. Recurrence was observed in 2 patients at 10 and 11 months post-surgery, corresponding to an overall recurrence rate of 1.5%.

Table 4. Results of anorectal manometry in 132 patients at the end of 12-month follow-up

Variables	Value
Anal resting pressure [mm Hg], mean ±SD	77.2 ±5.7
Maximum systolic pressure [mm Hg], mean ±SD	140.5 ±11.4
Rectal anal pressure difference [mm Hg], mean ±SD	63.8 ±13.6
High pressure zone [cm], mean ±SD	4.1 ±0.3

SD – standard deviation.

Fig. 2. A patient with high anal fistula (HAF) operated for the first time. Man; 27 years old; 2-day disease duration; an external opening at 3 o'clock position in the truncal position; internal opening at points 6, 3 and 9 o'clock positions in the truncal position; most of the rectal anal ring in a rigid state. On the left, multiple incisions were made to thoroughly explore the anal fistula cavity and place drainage lines. On the right, the incision healed after 1 month, and the patient exhibited normal anal function without pain or exudation

Fig. 3. A patient with high anal fistula (HAF) was cured after treatment failed in an outside hospital. Man; 38 years old; disease course of 2 years; external mouth at 8 o'clock lithotomy position; internal mouth at 6 and 9 o'clock lithotomy position; most of the rectal anal ring in a rigid state. On the left, there is still a ruptured purulent discharge at 8 o'clock position. In the middle image, multiple incisions were used to thoroughly probe the anal fistula (AF) cavity and place drainage lines. On the right, the incisions healed after 1 month, and the patient's anal function was normal, without pain or exudation

in 132 patients postoperatively. The results indicated that all patients exhibited normal endoanal hypoechogenicity, with no evidence of gas or liquid shadow detected. Endoscopic ultrasonography identified a soft scar in 96 patients, accounting for 72.7% of the total cases.

Table 3 presents the results of postoperative anorectal manometry in 66 patients. The mean anal resting pressure, maximum systolic pressure and rectoanal pressure difference were 77.2 mm Hg, 140.5 mm Hg and 63.8 mm Hg, respectively. The mean high-pressure zone length was 4.1 cm. A recto-anal inhibitory reflex was observed in 57 patients (43.2%). Representative cases are illustrated in Fig. 2,3.

Safety

Throughout the postoperative hospitalization and follow-up period, no patients experienced fever, local swelling or pus in the surgical area. Additionally, there were no recorded cases of postoperative hemorrhage or subcutaneous hematoma.

Discussion

High anal fistula represents a complex subtype of AF characterized by intricate branching patterns, posing significant challenges in diagnosis and treatment. These complexities often lead to relapse or delayed healing following surgical intervention, resulting in substantial physical and psychological burdens that markedly impair patients' quality of life. As a national specialized center, our department has devoted the past decade to the clinical management and research of AF, particularly HAF. This work integrates the traditional principles of "deficiency and excess" with thread hanging technique. In this prospective cohort study, we observed a 3-month healing rate of 99.2% following treatment of HAF using a combination of deficiency and excess suturing, with the 12-month healing rate reaching 98.5%. Notably, primary intervention using this approach yielded 100% healing. Furthermore, over 2/3 of patients reported no postoperative fecal incontinence, while the remaining patients exhibited only minimal symptoms

(WCGS score of 1). Additionally, 96.2% of patients experienced complete resolution of anal or perianal pain after surgery with the combined deficiency and excess thread-hanging method.

Our clinical observations suggest that the anatomical morphology of HAF is not solely characterized by interwoven tubular infectious foci, as traditionally described, but rather by multiple lacuna-like infectious foci. Traditional tubular excision techniques carry the risk of leaving fissured extensions within these anatomical recesses, which may lead to incomplete resection and subsequent recurrence. Moreover, excessive excision of necrotic tissue may enlarge the size and depth of the AF cavity. The absence of oxygen in this space is attributed to the compression exerted by adjacent tissues, particularly the muscles, leading to a closed and hypoxic condition. This oxygen-deficient space fosters persistent or recurrent infection. This concept forms the basis of what we term the "lacuna theory" of HAF. Accordingly, we are actively refining our surgical protocol by incorporating virtual reality (VR)-assisted visualization into the thread-hanging technique. This approach underscores the meticulous excision of AF during the operation to thoroughly reveal the focus of the AF. It emphasizes meticulous excision of superficial necrotic tissue, coupled with manual exploration to delineate the pus cavity, thereby enhancing drainage. Solid thread suspension is employed for precise tissue incision, while virtual thread suspension facilitates effective drainage. Compared to conventional techniques, our treatment approach may involve a larger perianal incision; however, this allows for a more comprehensive exposure of the AF cavity.

The integration of VR and thread hanging facilitates effective drainage while minimizing harm to the anorectal ring, thus achieving radical fistula eradication and preserving anal sphincter function. Our findings indicate that the integration of deficiency and excess with thread-hanging therapy yields a significant healing rate. Patients who have not responded to previous treatments achieved a remarkable 12-month healing rate of 98.5%. During the 12-month postoperative follow-up, the majority of patients did not report any further incidents of fecal incontinence. In contrast, approx. 1/3 of the patients experienced occasional mild fecal incontinence, primarily attributed to unrelated intestinal inflammation. These outcomes suggest that our approach effectively preserves anal sphincter function. Additionally, the absence of pain in and around the anus indicates that this method may result in reduced local tissue damage, offering a more comprehensive and less invasive treatment option. The resolution of anal fistula, restoration of anal function and reduction of pain collectively contributed to an improved quality of life for patients.

Current international HAF management strategies include LIFT, fibrin glue sealant, AF plug, video-assisted AF treatment (VAAFT), photodynamic therapy (PDT), and fistula-tract laser closure (FiLaC™). Nonetheless, the healing rate associated with these treatments remains suboptimal. The LIFT procedure, first described by Rojanasakul et al., has been extensively evaluated.[20] A meta-analysis by Emile et al., encompassing 26 studies and 1,378 patients, reported a pooled success rate of 76% and a complication rate of 14%. Furthermore, this procedure is not appropriate for individuals with high-level trans-sphincter fistulas, anal fissures located above the sphincter, or cases with prior surgical scarring that complicates intersphincteric separation.[10] Lindsey et al. demonstrated that the healing rates for simple and complex AFs treated with fibrin glue were 50% and 69%, respectively.[21]

The findings from Adamina et al. indicated that AF suppositories may provide superior protection for anal function in complex AF; however, the cure rate remains approx. 50%.[22] Garg et al. conducted a systematic evaluation and meta-analysis involving 786 patients to assess the efficacy of VAAFT in treating AF. The findings indicated an overall success rate of 76.01% and a complication rate of 16.2%, with no reported cases of anal incontinence.[23] Arroyo et al. conducted a study involving PDT on 49 patients with complex AF, achieving an overall healing rate of 65.3%. One patient experienced phototoxicity, while 2 patients developed fever within 48 h post-surgery.[24] FiLaC, as studied by Marref et al. in 69 patients with a median follow-up of 6.3 months, achieved a healing rate of 45.6%, with no new cases of anal incontinence and stable outcomes in patients with pre-existing incontinence. Notably, a 60% healing rate was observed in high sphincter AF cases.[25] These findings highlight that, while alternative treatments offer benefits, their success rates remain suboptimal, and certain modalities carry a notable risk of complications.

In contrast to the aforementioned treatment methods, our approach integrating VR with thread hanging relies exclusively on conventional surgical instruments, eliminating the need for specialized equipment. This streamlined methodology significantly reduces operative duration, thereby lowering procedural costs and potentially decreasing anesthetic-related risks for patients. Furthermore, our strategy ensures comprehensive lesion exposure, facilitates effective drainage and necessitates prophylaxis with oral antibiotics for just 3–5 days during the perioperative period. By minimizing excessive debridement, this approach mitigates unnecessary tissue trauma. Our findings demonstrated no instances of postoperative systemic infections, with only 1 patient experiencing delayed incision healing within 1 month post-surgery, likely due to postoperative constipation, but without associated fever. Consequently, the approach we implemented offers significant security and ease of use. In clinical practice, it has been observed that certain patients may be able to forgo antibiotics following comprehensive debridement. This approach can minimize the likelihood of adverse reactions associated with antibiotic treatment, as well

as decrease the chances of bacterial resistance. Beyond the LCCS technique, emerging therapies such as platelet-rich plasma (PRP) warrant consideration, as prior studies have demonstrated its efficacy in various conditions, including HAF.[26,27] Future research should explore the integration of such adjunctive therapies to further optimize outcomes for HAF.

Limitations

Our investigation acknowledged certain limitations. Initially, it is important to note that this was a prospective cohort study rather than a randomized controlled trial (RCT). The primary rationale for employing this study design stems from our earlier clinical observations indicating a cure rate exceeding 95% for HAF treated with LCCS and thread-hanging therapy. In the context of a RCT, it is possible that certain patients within the control group could face preventable nonunion or recurrence. Second, this investigation was conducted at a single center, and our treatment methodologies and operational practices may vary from those of other medical institutions, potentially impacting the generalizability of our findings. Third, the inclusion of patients with prior unsuccessful treatments from other facilities may introduce heterogeneity in our cohort. Additionally, as a specialized center, our department manages a disproportionately high volume of HAF cases, which may contribute to selection bias. Fourth, the follow-up period was limited to 12 months, necessitating further investigation to ascertain the long-term efficacy of deficiency and excess combined with thread-hanging. Finally, this study did not include HAF resulting from tumors, IBD, intestinal tuberculosis, or other causes, which may restrict the applicability of our findings to these subgroups. Nonetheless, the effectiveness and safety of addressing deficiency and excess in conjunction with thread hanging for these patients require clarification through additional investigation.

Conclusions

The evidence from this study indicates that loose combined cutting seton surgery for HAFs significantly enhances postoperative wound healing, reduces healing time, alleviates pain, and lowers the rate of postoperative complications. These findings support its adoption as a valuable and effective approach in clinical practice, with potential for broader implementation.

Data Availability Statement

The datasets supporting the findings of this study are openly available in Zenodo at https://doi.org/10.5281/zenodo.15075155.

Consent for publication

Not applicable.

Use of AI and AI-assisted technologies

Not applicable.

ORCID iDs

Zhi Congcong https://orcid.org/0000-0003-3151-8382
Cheng Yicheng https://orcid.org/0000-0002-8714-6947
Li Xin https://orcid.org/0009-0001-7801-0239
Shi Yuying https://orcid.org/0000-0002-7803-8303
Liu Ningyuan https://orcid.org/0000-0002-1877-6136
Zheng Lihua https://orcid.org/0000-0003-0013-0545
Hou Wenxia https://orcid.org/0009-0000-9019-3261

References

1. Zanotti C, Martinez-Puente C, Pascual I, Pascual M, Herreros D, García-Olmo D. An assessment of the incidence of fistula-in-ano in four countries of the European Union. *Int J Colorectal Dis*. 2007;22(12):1459–1462. doi:10.1007/s00384-007-0334-7
2. Ommer A, Herold A, Berg E, et al. German S3 guidelines: Anal abscess and fistula (second revised version). *Langenbecks Arch Surg*. 2017;402(2):191–201. doi:10.1007/s00423-017-1563-z
3. Hokkanen SR, Boxall N, Khalid JM, Bennett D, Patel H. Prevalence of anal fistula in the United Kingdom. *World J Clin Cases*. 2019;7(14):1795–1804. doi:10.12998/wjcc.v7.i14.1795
4. Abdullaev Z, Agzamkhodjaev S, Chung JM, Lee SD. Risk factors for fistula recurrence after urethrocutaneous fistulectomy in children with hypospadias. *Turk J Urol*. 2021;47(3):237–241. doi:10.5152/tud.2020.20323
5. Chaveli Díaz C, Esquiroz Lizaur I, Eguaras Córdoba I, et al. Recurrence and incidence of fistula after urgent drainage of an anal abscess: Long-term results. *Cir Esp (Engl Ed)*. 2022;100(1):25–32. doi:10.1016/j.cireng.2021.11.012
6. He C, Chen Z, Liu S, Chen H, Zhang F. Prevalence and risk factors of interstitial lung disease in patients with primary Sjögren's syndrome: A systematic review and meta-analysis. *Int J Rheum Dis*. 2020;23(8):1009–1018. doi:10.1111/1756-185X.13881
7. Cheung F, Appleton N, Rout S, et al. Video-assisted anal fistula treatment: A high volume unit initial experience. *Ann R Coll Surg Engl*. 2018;100(1):37–41. doi:10.1308/rcsann.2017.0187
8. Handaya AY, Fauzi AR. Combined fistulotomy and contralateral anal internal sphincterotomy for recurrent and complex anal fistula to prevent recurrence. *Ann Coloproctol*. 2020;36(2):122–127. doi:10.3393/ac.2018.11.19
9. Jiang J, Zhang Y, Ding X, Zhang N, Ji L. Efficacy and safety of an innovatively modified cutting seton technique for the treatment of high anal fistula: A protocol for a randomized controlled trial. *Medicine (Baltimore)*. 2021;100(5):e24442. doi:10.1097/MD.0000000000024442
10. Emile SH, Khan SM, Adejumo A, Koroye O. Ligation of intersphincteric fistula tract (LIFT) in treatment of anal fistula: An updated systematic review, meta-analysis, and meta-regression of the predictors of failure. *Surgery*. 2020;167(2):484–492. doi:10.1016/j.surg.2019.09.012
11. Zwiep TM, Gilbert R, Boushey RP, et al. Comparison of ligation of the intersphincteric fistula tract and BioLIFT for the treatment of transsphincteric anal fistula: A retrospective analysis. *Dis Colon Rectum*. 2020;63(3):365–370. doi:10.1097/DCR.0000000000001573
12. Bakhtawar N, Usman M. Factors increasing the risk of recurrence in fistula-in-ano. *Cureus*. 2019;11(3):e4200. doi:10.7759/cureus.4200
13. Subhas G, Singh Bhullar J, Al-Omari A, Unawane A, Mittal VK, Pearlman R. Setons in the treatment of anal fistula: Review of variations in materials and techniques. *Dig Surg*. 2012;29(4):292–300. doi:10.1159/000342398
14. Mitalas LE, Van Wijk JJ, Gosselink MP, Doornebosch P, Zimmerman DDE, Schouten WR. Seton drainage prior to transanal advancement flap repair: Useful or not? *Int J Colorectal Dis*. 2010;25(12):1499–1502. doi:10.1007/s00384-010-0993-7

15. Choi D, Sung Kim H, Seo HI, Oh N. Patient-performed seton irrigation for the treatment of deep horseshoe fistula. *Dis Colon Rectum*. 2010;53(5):812–816. doi:10.1007/DCR.0b013e3181d2a8f9
16. Emile SH, Elfeki H, Thabet W, et al. Predictive factors for recurrence of high transsphincteric anal fistula after placement of seton. *J Surg Res*. 2017;213:261–268. doi:10.1016/j.jss.2017.02.053
17. Yan J, Ma L. Clinical effect of tunnel-like fistulectomy plus draining seton combined with incision of internal opening of anal fistula (TFSIA) in the treatment of high trans-sphincteric anal fistula. *Med Sci Monit*. 2020;26:e918228. doi:10.12659/MSM.918228
18. Patton V, Chen CM, Lubowski D. Long-term results of the cutting seton for high anal fistula. *ANZ J Surg*. 2015;85(10):720–727. doi:10.1111/ans.13156
19. Zhi C, Huang Z, Liu D, Zheng L. Long-term follow-up study of loose combined cutting seton surgery for patients with high anal fistula. *Ann Transl Med*. 2021;9(14):1160. doi:10.21037/atm-21-3242
20. Rojanasakul A, Pattanaarun J, Sahakitrungruang C, Tantiphlachiva K. Total anal sphincter saving technique for fistula-in-ano: The ligation of intersphincteric fistula tract. *J Med Assoc Thai*. 2007;90(3):581–586. PMID:17427539.
21. Lindsey I, Smilgin-Humphreys MM, Cunningham C, Mortensen NJM, George BD. A randomized, controlled trial of fibrin glue vs conventional treatment for anal fistula. *Dis Colon Rectum*. 2002;45(12):1608–1615. doi:10.1007/s10350-004-7247-0
22. Adamina M, Ross T, Guenin MO, et al. Anal fistula plug: A prospective evaluation of success, continence and quality of life in the treatment of complex fistulae. *Colorectal Dis*. 2014;16(7):547–554. doi:10.1111/codi.12594
23. Garg P, Singh P. Video-assisted anal fistula treatment (VAAFT) in cryptoglandular fistula-in-ano: A systematic review and proportional meta-analysis. *Int J Surg*. 2017;46:85–91. doi:10.1016/j.ijsu.2017.08.582
24. Arroyo A, Sánchez-Guillén L, Parra PA, et al. Photodynamic therapy for the treatment of complex anal fistula. *Lasers Surg Med*. 2020;52(6):503–508. doi:10.1002/lsm.23162
25. Marref I, Spindler L, Aubert M, et al. The optimal indication for FiLaC® is high trans-sphincteric fistula-in-ano: A prospective cohort of 69 consecutive patients. *Tech Coloproctol*. 2019;23(9):893–897. doi:10.1007/s10151-019-02077-9
26. Tawanwongsri W, Siri-archawawat D, Sindhusen S, Eden C. Therapeutic efficiency and safety assessment of intradermal platelet-rich plasma combined with oral tranexamic acid in patients with facial melasma [published online as ahead of print on June 27, 2024]. *Adv Clin Exp Med*. 2024. doi:10.17219/acem/187874
27. Wang Y, Rao Q, Ma Y, Li X. Platelet-rich plasma in the treatment of anal fistula: A systematic review and meta-analysis. *Int J Colorectal Dis*. 2023;38(1):70. doi:10.1007/s00384-023-04367-z

Comparative prognostic evaluation of SOFA and PSS scores in pediatric septic shock: A retrospective study

Chao Du[1,A–D], Xue Li[2,E,F]

[1] Department of Pediatric Intensive Care Unit, Shanxi Children's Hospital, Shanxi Maternal and Child Health Hospital, Taiyuan, China
[2] Shanxi Bethune Hospital, Shanxi Academy of Medical Sciences, Third Hospital of Shanxi Medical University, Tongji Shanxi Hospital, Taiyuan, China

A – research concept and design; B – collection and/or assembly of data; C – data analysis and interpretation;
D – writing the article; E – critical revision of the article; F – final approval of the article

Advances in Clinical and Experimental Medicine, ISSN 1899–5276 (print), ISSN 2451–2680 (online) *Adv Clin Exp Med*. 2026;35(2):219–229

Address for correspondence
Xue Li
E-mail: lixue@sxbqeh.com.cn

Funding sources
None declared

Conflict of interest
None declared

Received on March 24, 2025
Reviewed on April 26, 2025
Accepted on May 8, 2025

Published online on January 12, 2026

Abstract

Background. Septic shock in pediatric intensive care units (PICUs) requires accurate prognostic tools. The Sequential Organ Failure Assessment (SOFA) and the Phoenix Sepsis Score (PSS) are both widely used, yet their comparative effectiveness has not been fully established.

Objectives. To evaluate the prognostic sensitivity of the SOFA and PSS scores in predicting mortality among pediatric patients with septic shock, and to compare their performance across different patient subgroups.

Materials and methods. This retrospective study included 110 pediatric patients with septic shock admitted to the PICU of Shanxi Children's Hospital between 2020 and 2024. SOFA and PSS scores were recorded at admission, along with demographic, clinical, and outcome data. Patients with congenital organ abnormalities or severe inherited metabolic disorders were excluded. Predictive accuracy was assessed using correlation analyses and receiver operating characteristic (ROC) curve analysis.

Results. Both SOFA and PSS scores showed moderate correlations with mortality (SOFA: $r = 0.57$; PSS: $r = 0.56$), with SOFA demonstrating slightly higher overall predictive accuracy. PSS exhibited greater sensitivity in severe cases. Neurological and respiratory dysfunctions were the strongest predictors of mortality, whereas coagulation parameters had minimal prognostic value. Age-specific analysis revealed that SOFA was more accurate in patients aged 1–3 years and >7 years, while PSS outperformed SOFA in children aged 3–6 years.

Conclusions. Both SOFA and PSS scores are effective tools for predicting mortality in pediatric septic shock. SOFA demonstrated superior overall performance, whereas PSS showed advantages in specific age ranges and disease categories. Using the two scoring systems in combination may support more informed clinical decision-making.

Key words: SOFA score, pediatric septic shock, PSS score, prognostic evaluation, scoring system comparison

Cite as
Du C, Li X. Comparative prognostic evaluation of SOFA and PSS scores in pediatric septic shock: A retrospective study. *Adv Clin Exp Med*. 2026;35(2):219–229. doi:10.17219/acem/204830

DOI
10.17219/acem/204830

Highlights

- SOFA and Phoenix Sepsis Score (PSS) predict pediatric septic shock mortality effectively, with SOFA showing a slightly stronger overall correlation.
- PSS offers higher sensitivity in infants and younger children, while SOFA provides greater accuracy in older pediatric patients.
- Neurological and respiratory dysfunction drive mortality risk in both scoring systems, underscoring their prognostic importance.
- SOFA outperforms PSS in respiratory and postoperative cases, whereas PSS is more accurate in neurological and gastrointestinal disease contexts.
- Combining SOFA and PSS may optimize clinical decision-making, improving risk stratification and management in pediatric septic shock.

Background

Septic shock is one of the most critical and life-threatening conditions commonly encountered in pediatric intensive care units (PICUs), with a high incidence and mortality rate.[1,2] Accurate assessment of disease severity and prediction of mortality risk are essential for formulating appropriate treatment strategies and improving patient outcomes. However, predicting outcomes in pediatric septic shock remains a major clinical challenge due to heterogeneous presentations, rapidly evolving physiology, and varied responses to treatment.

Currently, various scoring systems are used in clinical practice to evaluate the severity of septic shock.[3–5] Among them, the Sequential Organ Failure Assessment (SOFA) score and the Phoenix Sepsis Score (PSS) are key tools for diagnosing pediatric sepsis.[6,7] The SOFA score quantifies organ dysfunction by evaluating multiple organ systems, including respiratory, circulatory, hepatic, coagulation, neurological, and renal functions, making it a general-purpose tool originally developed for adults.[8] In contrast, the PSS score is specifically designed for pediatric patients, focusing on indicators relevant to pediatric physiology to predict mortality risk.[7] It is a recently developed, pediatric-specific scoring system that incorporates age-adjusted physiological and clinical parameters tailored to pediatric patients' unique pathophysiology.[9]

Despite their widespread use, few studies have directly compared SOFA and PSS in pediatric septic shock, especially in terms of predictive accuracy across different age groups and disease categories.[10] Existing literature either focuses on adult populations or evaluates these tools independently, without highlighting how their structures and clinical applications differ. While SOFA provides a broad overview of organ failure, PSS integrates pediatric-specific variables, potentially offering better sensitivity in younger age groups.[11] This gap in comparative evidence limits clinicians' ability to choose the most effective prognostic tool in pediatric settings.

With the implementation of the 2024 International Consensus Criteria for Pediatric Sepsis and Septic Shock, the PSS has superseded the prior diagnostic criteria based on systemic inflammatory response syndrome (SIRS).[7] This new scoring system was created by a group of 35 pediatric experts from 6 continents, using data from international surveys, systematic reviews, meta-analyses, and a comprehensive dataset of over 3 million electronic health records from 10 sites on 4 continents.[1] Since the PSS has only recently been adopted, its comparative utility relative to established scoring systems such as SOFA remains insufficiently studied, especially in real-world PICU settings.

This study examines previously collected data from pediatric patients with septic shock who were treated in the PICU at Shanxi Children's Hospital, China between January 1, 2020, and December 31, 2024. It attempts to assess how well the SOFA and PSS scores predict the risk of mortality and which score is better at identifying individuals at higher risk. The study also looks at how different aspects of each grading system influence patient outcomes and analyzes their accuracy across disease categories. To our knowledge, this is one of the first studies to directly compare SOFA and the newly implemented PSS in a pediatric septic shock cohort, filling a critical evidence gap and providing practical insights to enhance risk stratification in clinical care.

Objectives

This study compared the ability of SOFA and PSS scores to predict death in pediatric septic shock and discovered which is more sensitive in identifying high-risk individuals. It also investigated how individual components of each score contribute to death prediction and compared their effectiveness across disease categories.

Materials and methods

Study population

This study comprised pediatric patients diagnosed with septic shock who were admitted to Shanxi Children's Hospital's Pediatric Intensive Care Unit between January 1, 2020,

and December 31, 2024. Patient selection was conducted retrospectively by reviewing electronic medical records.

Inclusion criteria were as follows: 1) patients meeting internationally recognized diagnostic criteria for pediatric septic shock;[12] 2) patients who underwent SOFA and PSS scoring immediately upon PICU admission, with all relevant subcomponent data recorded; and 3) patients with complete clinical records, including all required physiological and laboratory parameters to calculate both SOFA and PSS scores, as well as outcome data.

Exclusion criteria were as follows: 1) Patients with severe congenital organ malformations or uncontrolled severe inherited metabolic disorders; 2) Patients who had undergone major surgery or prolonged intensive care treatment prior to admission; 3) Patients with missing, incomplete, or inconsistent medical records that would prevent accurate SOFA or PSS scoring.

Patients with partially missing data were excluded only if the missing elements affected score computation. Otherwise, such cases were retained, and missing values were managed via cross-validation with laboratory and clinical notes.

This study was approved by the Institutional Review Board of Shanxi Bethune Hospital (approval No. IRB-WZ-2025-009).

Data collection

The following data were collected for each patient: general demographic information (age, sex, and disease category), disease-related information (diagnosis), and SOFA and PSS scores upon admission. The SOFA score included subcomponents for respiratory, coagulation, hepatic, circulatory, neurological, and renal function, whereas the PSS score included respiratory, circulatory (cardiovascular and mean arterial pressure), coagulation, and neurological function. Additionally, the final outcome (survival or death) within 72 h of PICU admission was recorded.

All SOFA and PSS scores were calculated retrospectively by 2 trained pediatric intensive care physicians working independently. To assess inter-observer variability, a random subset of 20 patient records was scored by both physicians. The inter-rater reliability was evaluated using the intraclass correlation coefficient (ICC), and discrepancies were resolved by consensus.

Scoring methods

The SOFA scoring system assesses 6 organ systems: respiratory, coagulation, hepatic, circulatory, neurological, and renal function. Each system is scored based on specific physiological indicators and laboratory test results, with a total score ranging from 0 to 24. Higher scores indicate greater severity of organ dysfunction.

The PSS scoring system is based on the 2024 International Consensus Criteria for Pediatric Sepsis and Septic Shock. It evaluates respiratory, circulatory, coagulation, and neurological functions to estimate the risk of death in pediatric patients.

Statistical analyses

Sample size justification

A total of 110 patients were included, based on the availability of complete and valid clinical data collected between 2020 and 2024. This sample size was considered adequate for exploratory analysis and subgroup comparisons, given the rarity and high-risk nature of pediatric septic shock.

Comparison of SOFA and PSS scores in predicting 72-hour mortality

Python software (https://www.python.org/) was used to analyze how well SOFA and PSS scores predict mortality. The point-biserial correlation coefficient was applied because the outcome variable (survival vs death) was binary. The predictive performance of both scoring systems was compared by examining the absolute values of their correlation coefficients, where higher values indicated stronger predictive accuracy.

We used Python to calculate Pearson's correlation coefficients to assess how each SOFA subcomponent relates to mortality. A coefficient with an absolute value closer to 1 signified a stronger association with patient outcomes. The significance of the correlation was evaluated using the p-value, with $p < 0.05$ considered statistically significant. Pearson's correlation coefficients and p-values were calculated for each PSS subcomponent to assess their association with mortality outcomes.

Patients were categorized into 4 age groups: <1 year, 1–3 years (including 3 years), 3–7 years (including 7 years), and >7 years. The distribution of patients in each group is shown in Supplementary Table 1. Python was used to calculate the impact of SOFA and PSS scores on mortality outcomes within each age group.

Using Python, we analyzed total SOFA and PSS scores by disease category, excluding the miscellaneous and Kawasaki disease groups, to evaluate their predictive performance for mortality. Sensitivity was calculated, and hypothesis testing was conducted to determine whether there was a significant difference between the 2 scoring systems in mortality prediction.

Receiver operating characteristic curves were generated using Python to determine the optimal thresholds for the 2 scoring systems (Fig. 1). Exceeding these thresholds is linked to a substantially higher risk of mortality.

Results

The prognostic accuracy of the SOFA and PSS scores in predicting mortality among pediatric patients with

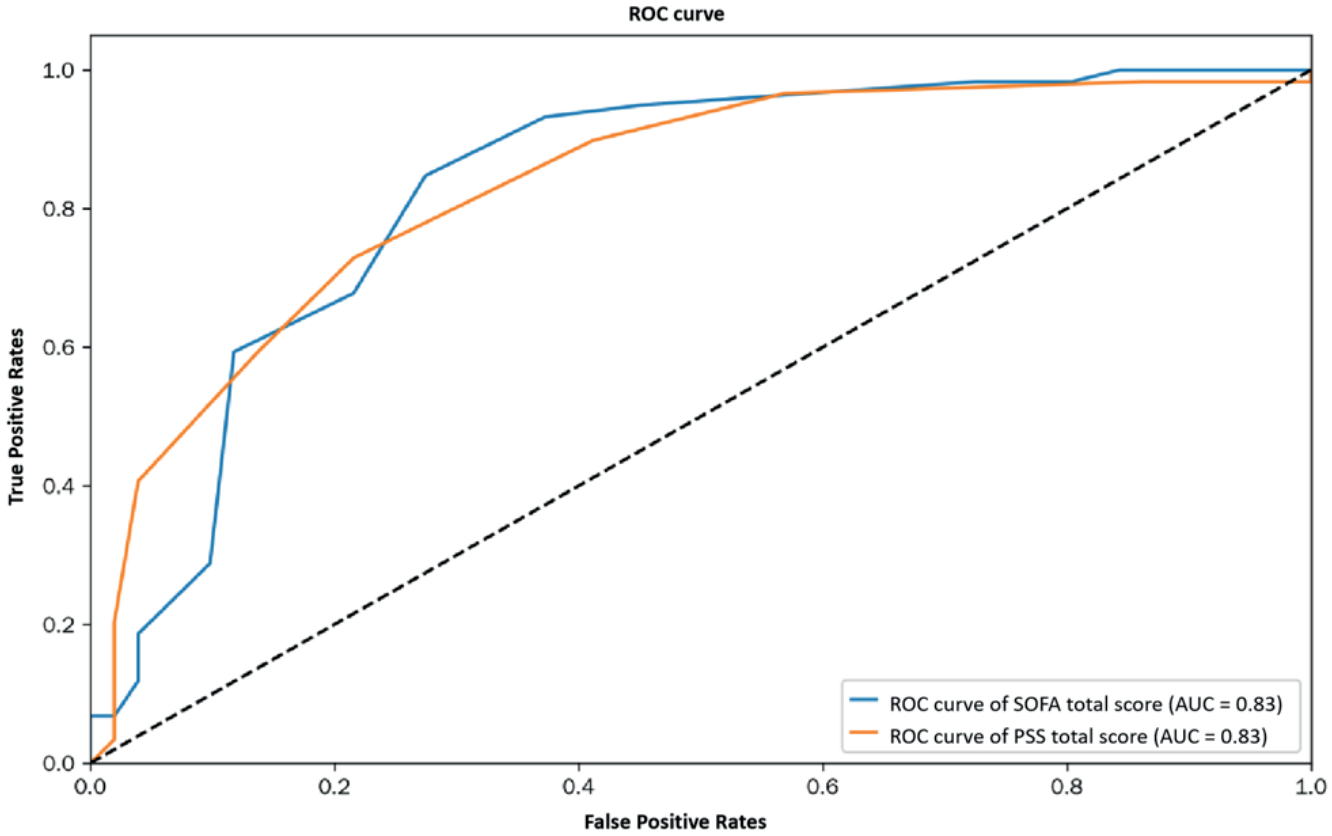

Fig. 1. Receiver operating characteristic (ROC) curve

septic shock in the PICU was assessed. We used correlation analysis, true positive rate (TPR) calculations, and subgroup analyses to evaluate their performance.

Overall correlation with mortality

As shown in Table 1, the SOFA score had a correlation coefficient of 0.57 with mortality, which falls into the category of a moderate positive correlation (defined as $0.4 \leq r < 0.7$). This suggests that higher SOFA scores were linked to an increased risk of death. The correlation was statistically significant, with a p-value of 7.04×10^{-11}, well below the standard 0.05 threshold. Similarly, the PSS score showed a moderate positive correlation with mortality ($r = 0.56$, $p = 2.26 \times 10^{-10}$), also confirming a significant association. A direct comparison of these values revealed that the SOFA score had a slightly stronger correlation with mortality than the PSS score, though the difference was minimal in predicting outcomes within 72 h of PICU admission.

Table 1. Comparison of predictive performance between SOFA and PSS scores

Scoring system	Correlation coefficient	p-value
SOFA score	0.571	7.040×10^{-11}
PSS score	0.559	2.260×10^{-10}

$p < 0.05$ is considered statistically significant; SOFA – Sequential Organ Failure Assessment; PSS – Phoenix Sepsis Score.

True positive rate performance

Table 2 provides further insights into the predictive performance of both scoring systems. The TPR analysis showed that higher SOFA scores were associated with an increased likelihood of correctly identifying non-survivors. This trend suggests that higher SOFA scores were associated with more accurate mortality predictions. In particular, in the highest score range (13.667, 15.333), the TPR reached 0.875, suggesting strong predictive accuracy. The PSS score exhibited a similar trend in Table 3, with higher score intervals corresponding to increased TPR. Notably, the highest TPR for the PSS score was 0.923

Table 2. True positive rate of SOFA score

SOFA score interval	True positive rate
(2.0, 3.667)	0.000
(3.667, 5.333)	0.143
(5.333, 7.0)	0.125
(7.0, 8.667)	0.200
(8.667, 10.333)	0.652
(10.333, 12.0)	0.793
(12.0, 13.667)	0.667
(13.667, 15.333)	0.875
(15.333, 17.0)	0.800

SOFA – Sequential Organ Failure Assessment.

Table 3. True positive rate of PSS score

PSS score interval	True positive rate
(0.0, 1.111)	–
(1.111, 2.222)	0.000
(2.222, 3.333)	0.063
(3.333, 4.444)	0.333
(4.444, 5.556)	0.500
(5.556, 6.667)	0.667
(6.667, 7.778)	0.688
(7.778, 8.889)	0.923
(8.889, 10.0)	0.923

PSS – Phoenix Sepsis Score.

in the (7.778, 8.889) and (8.889, 10.0) range, surpassing the TPR of the SOFA score in most intervals. This indicates that while both scoring systems were effective in identifying high-risk patients, the PSS score demonstrated slightly higher sensitivity in predicting mortality, particularly in the highest score ranges.

Subcomponent analysis

In Table 4, subcomponent analysis revealed that among the SOFA score components, the nervous system and respiratory sub-scores had the highest correlation with mortality, with correlation coefficients of 0.447 and 0.447, respectively. These findings indicate that neurological and respiratory dysfunctions were the most critical factors influencing patient outcomes in septic shock cases. The circulatory sub-score had a weaker but still significant correlation with mortality (0.317, $p < 0.05$), while the renal sub-score (0.203, $p = 0.033$) showed a marginally significant relationship. The hepatic and coagulation sub-scores, however, had lower correlation coefficients and p-values above 0.05, suggesting that their impact on mortality was not statistically significant.

For the PSS score subcomponents in Table 5, the respiratory sub-score demonstrated the strongest association with mortality, with a correlation coefficient of 0.460and a highly significant p-value (4.359×10^{-7}). The nervous system and cardiovascular sub-scores also had significant positive correlations with mortality (0.407229 and 0.391132, respectively, $p < 0.05$), reinforcing the importance of these physiological systems in predicting patient outcomes. The circulatory mean arterial pressure (MAP) sub-score (0.321, $p < 0.05$) exhibited a weaker but still significant relationship with mortality. In contrast, the coagulation sub-score showed no significant correlation with mortality, with a coefficient of only 0.029 and a p-value of 0.765, indicating its minimal contribution to prognosis.

Table 4. Pearson's correlation coefficients and p-values for SOFA subcomponents

SOFA subcomponent	Correlation coefficient	p-value
SOFA Score_Nervous System	0.447	9.543×10^{-7}
SOFA Score_Respiratory	0.447	9.682×10^{-7}
SOFA Score_Circulatory	0.317	7.261×10^{-4}
SOFA Score_Renal	0.203	3.333×10^{-2}
SOFA Score_Hepatic	0.156	1.032×10^{-1}
SOFA Score_Coagulation	0.077	4.250×10^{-1}

$p < 0.05$ is considered statistically significant; SOFA – Sequential Organ Failure Assessment.

Table 5. Pearson correlation coefficients and p-values for PSS subcomponents

PSS subcomponent	Correlation coefficient	p-value
PSS Score_Respiratory	0.460	4.359×10^{-7}
PSS Score_Nervous System	0.407	1.009×10^{-5}
PSS Score_Circulatory_Cardiovascular	0.391	2.390×10^{-5}
PSS Score_Circulatory_MAP	0.320	6.382×10^{-4}
PSS Score_Coagulation	0.029	7.652×10^{-1}

$p < 0.05$ is considered statistically significant; MAP – mean arterial pressure.

Age-stratified performance

Age-stratified analysis of predictive sensitivity in Table 6 revealed that the performance of the SOFA and PSS scores varied across different pediatric age groups. In patients aged 1–3 years, the SOFA score demonstrated higher sensitivity (0.688) compared to the PSS score (0.625), indicating better predictive ability for mortality in this subgroup. Conversely, in patients younger than 1 year, the PSS score exhibited greater sensitivity (0.733) than the SOFA score (0.600), suggesting that the PSS score was more effective in predicting mortality for this age group. In pediatric patients aged 3–7 years, the PSS score had higher sensitivity (0.750) compared to the SOFA score (0.625). However, in pediatric patients older than 7 years, the SOFA score (0.750) outperformed the PSS score (0.667). This demonstrates that the accuracy of both scoring systems varies by age, with SOFA being more accurate in older pediatric patients and PSS doing better in younger ones.

A χ^2 test was used to determine the relationship between SOFA and PSS scores and mortality in various age groups.

Table 6. Comparison of sensitivity of SOFA and PSS scores across different age groups

Age group	SOFA score sensitivity	PSS score sensitivity
1–3 years	0.688	0.625
<1 year	0.600	0.733
3–7 years	0.625	0.750
>7 years	0.750	0.667

SOFA – Sequential Organ Failure Assessment; PSS – Phoenix Sepsis Score.

Table 7. The χ^2 test results of SOFA and PSS scores across different age groups

Age group	SOFA score χ^2 value	SOFA score p-value	PSS score χ^2 value	PSS score p-value
1–3 years	3.646	0.056	6.317	0.012
<1 year	4.633	0.031	5.873	0.015
3–7 years	5.649	0.018	11.968	0.001
>7 years	5.462	0.019	3.723	0.054

$p < 0.05$ is considered statistically significant; SOFA – Sequential Organ Failure Assessment; PSS – Phoenix Sepsis Score.

The analysis compared the median values of both scores, which are displayed in Table 7. A $p < 0.05$ was judged statistically significant. The findings demonstrated that the accuracy of these scores varies with age. As a result, when applying these scores in clinical practice, age must be taken into account.

Overall, both SOFA and PSS scores were strongly related to death in pediatric septic shock patients, with SOFA performing marginally better in prediction. However, PSS was more sensitive in patients at higher risk, particularly in younger pediatric patients. According to subcomponent analysis, neurological and respiratory dysfunctions have the greatest impact on patient outcomes. Age-stratified analysis underlined the significance of tailoring the usage of these scores to the patient's age.

The usefulness of SOFA and PSS in predicting death differed by age group. The SOFA score in pediatric patients aged 1–3 years had a p-value of 0.056, which was somewhat higher than the 0.05 significance level. This indicated that its predictive value in this population was not statistically significant. On the other hand, the PSS score had a p-value of 0.012, showing a significant association with mortality. In infants under 1 year old, both SOFA ($p = 0.031$) and PSS ($p = 0.015$) scores revealed clear relationships with mortality risk. Similarly, in the 3–7 year age group, both scores were substantially linked with mortality, with the PSS score ($p = 0.001$) having a larger connection than the SOFA score ($p = 0.018$). Among pediatric patients older than 7 years, the SOFA score ($p = 0.019$) remained a significant predictor of mortality, whereas the PSS score ($p = 0.054$) was just above the statistical threshold, suggesting a weaker association. These findings highlight that the predictive performance of the SOFA and PSS scores varies by age, with PSS being more effective in younger pediatric patients and SOFA demonstrating better accuracy in older age groups.

Disease-specific sensitivity analysis

The study cohort included patients diagnosed with respiratory diseases, digestive system diseases, postoperative gastrointestinal conditions, neurological disorders, and hematologic diseases. Sensitivity analysis (Table 8) evaluated how well the SOFA and PSS scores predicted

Table 8. Comparison of SOFA and PSS scores across different diseases

Disease category	SOFA score sensitivity	PSS score sensitivity
Respiratory diseases	0.818	0.636
Digestive system diseases	0.667	0.778
Postoperative gastrointestinal conditions	0.889	0.778
Neurological disorders	0.333	0.600
Hematologic diseases	0.444	0.444

SOFA – Sequential Organ Failure Assessment; PSS – Phoenix Sepsis Score.

Table 9. Statistical significance of differences in mortality prediction (McNemar's test)

Disease category	McNemar's test p-value	Conclusion
Postoperative gastrointestinal conditions	0.375	no significant difference
Respiratory diseases	1.0	no significant difference
Digestive system diseases	1.0	no significant difference
Neurological disorders	0.219	no significant difference
Hematologic diseases	1.0	no significant difference

$p < 0.05$ is considered statistically significant.

mortality across these conditions. The SOFA score showed higher sensitivity (0.818) in respiratory diseases compared to the PSS score (0.636), indicating a stronger predictive ability in this category. However, in digestive system diseases, the PSS score (0.778) outperformed SOFA (0.667), suggesting better mortality prediction for these patients. For postoperative gastrointestinal conditions, SOFA (0.889) again had higher sensitivity than PSS (0.778), indicating its superior ability to assess mortality risk after surgery. Among patients with neurological disorders, the PSS score (0.600) was more effective than the SOFA score (0.333), suggesting stronger predictive power in this group. In hematologic diseases, both scores showed equal sensitivity (0.444), meaning their predictive accuracy was comparable. The McNemar's test (Table 9) found no statistically significant differences ($p > 0.05$) between the 2 scoring systems across these disease categories, indicating that while they differ in sensitivity for specific conditions, both provide valuable clinical insights without major disparities in overall predictive accuracy.

Threshold and ROC curve analysis

Threshold analysis (Fig. 1) identified critical score cutoffs for assessing mortality risk. A SOFA score above 10 was associated with a significantly increased risk of mortality, while a PSS score exceeding 6 also indicated a substantially elevated risk. These criteria are useful clinical

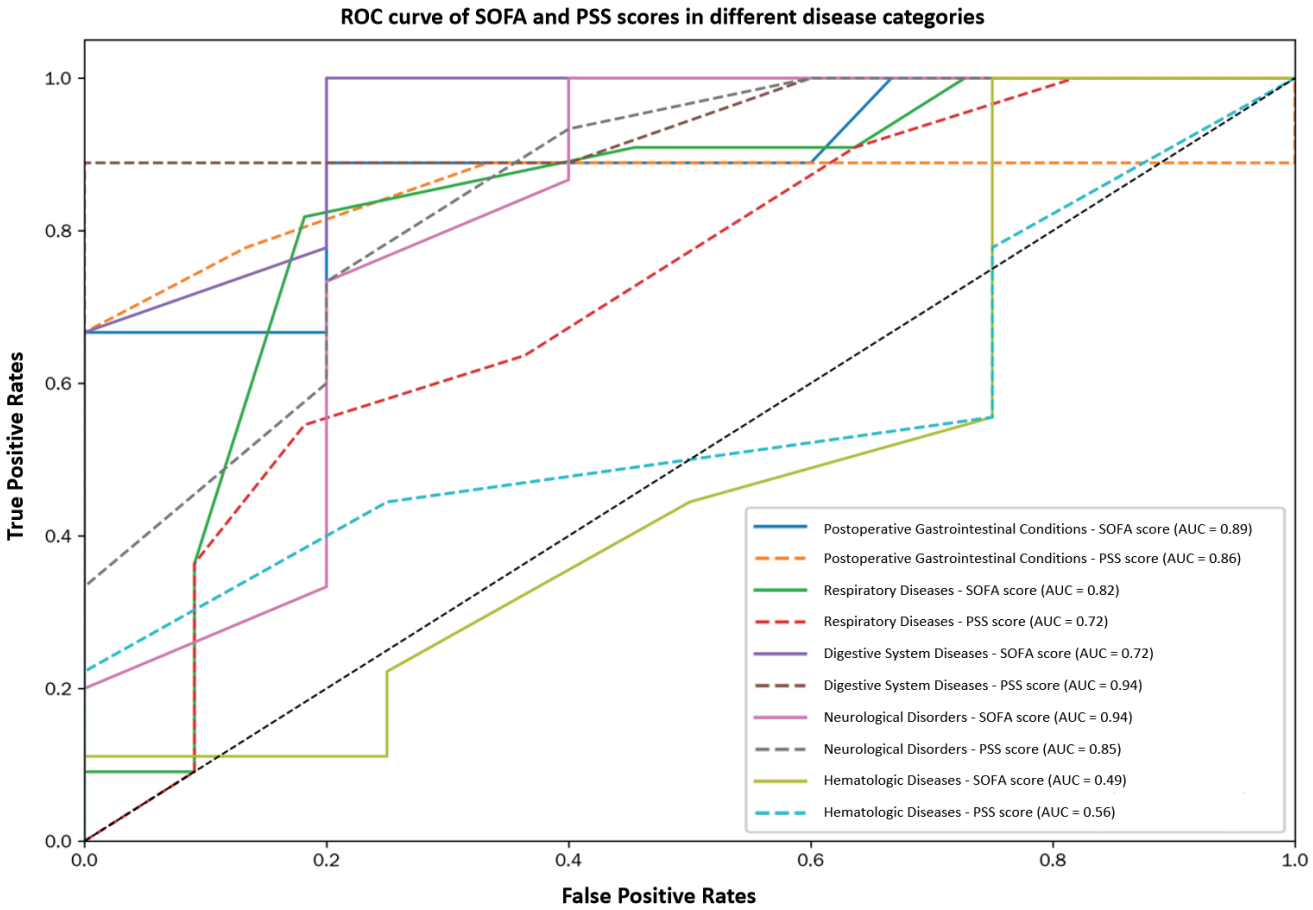

Fig. 2. Receiver operating characteristic (ROC) curve of Sequential Organ Failure Assessment (SOFA) and Phoenix Sepsis (PSS) scores in different disease categories

reference points for determining the severity of pediatric septic shock. Using Youden's index method, the study determined ideal cutoff values (Table 10) to aid in the differentiation of survivors and non-survivors across disease groups. These findings provide clinicians with a crucial tool for making early decisions and assessing risks in critically unwell pediatric patients.

We utilized receiver operating characteristic (ROC) curve analysis to determine how effectively SOFA and PSS scores predicted mortality across illness categories (Fig. 2).

Table 10. Mortality thresholds for SOFA and PSS scores in different disease categories

Disease category	SOFA score mortality threshold	PSS score mortality threshold
Respiratory diseases	10	7
Digestive system diseases	10	6
Postoperative gastrointestinal conditions	9	7
Neurological disorders	10	5
Hematologic diseases	9	9

SOFA – Sequential Organ Failure Assessment; PSS – Phoenix Sepsis Score.

In respiratory illnesses, the SOFA score had a greater AUC value. This suggested that it was more accurate in mortality prediction than the PSS score, which was still effective but significantly less precise. For digestive system illnesses, the SOFA score exhibited a somewhat lower balance of true and false positive rates, although both scores are still effective.

While the PSS score was equally useful but had a somewhat lower area under the curve (AUC) value, the SOFA score showed high prognostic ability in postoperative gastrointestinal problems. Both scores were helpful in determining mortality risk in neurological illnesses, although PSS outperformed SOFA. The PSS score had a marginally higher AUC value for hematologic disorders. In this category, the PSS score was therefore the more accurate predictor.

Overall, the SOFA score tended to produce ROC curves closer to the upper left corner, indicating better overall performance for mortality prediction. However, the PSS score consistently performed better than random chance and remained a useful method for assessing risk. These differences show the importance of opting for the most suitable scoring system based on patient's condition, so as to improve risk assessment and clinical decisions.

This study offers a detailed comparison of the SOFA and PSS scores in mortality prediction among pediatric septic shock patients. The results show that their accuracy depends on age and type of disease. The SOFA score was generally more effective for respiratory and postoperative gastrointestinal conditions. The PSS score was more effective for digestive system diseases and neurological disorders. The identification of threshold values in this study provides practical guidance for clinical risk assessment. Both scoring systems are valuable for disease severity evaluation, but their different strengths across subgroups show the need for a customized approach to patient management.

Discussion

Pediatric septic shock continues to present high mortality rates.[13] The disease can progress rapidly, and clinicians often lack objective tools for timely assessment.[14,15] The SOFA score has been adapted for pediatric use and is already applied in some clinical settings.[16] The introduction of the PSS in 2024 has broadened perspectives and has been practically applied, yet challenges persist in its usage.[17] Both scoring systems have their respective merits, and their superiority remains inconclusive. This study conducts a preliminary comparative analysis of the 2 scoring systems based on collected data, aiming to identify potential issues and provoke further reflection.

The findings confirm that higher SOFA and PSS scores are associated with increased mortality risk, consistent with known disease progression patterns. This reinforces both systems as valuable tools for initial risk stratification. However, mortality in low-scoring cases highlights the rapid progression of septic shock, where patients can deteriorate within a short period.[18] Lower-scoring cases tend to receive less attention compared to higher-scoring cases. Dynamic scoring at multiple time points, combined with the integration of real-time biomarkers such as B-type natriuretic peptide (BNP) and cardiac enzymes, may enhance early detection and improve risk prediction.[19–21]

The SOFA score has limitations when applied to children, as physiological parameters vary significantly across different pediatric age groups compared to adults.[22,23] For example, in the cardiovascular system assessment, the SOFA score categorizes MAP at a threshold of 70 mm Hg, which is not accurate for children. Before the introduction of the PSS score, modifications to the SOFA score were attempted to accommodate pediatric physiological characteristics,[16,24] but these adaptations were not widely adopted. In pediatric practice, vasoactive medication use is often utilized for scoring pediatric septic shock patients.[25,26] However, this method may overlook pediatric patients with a tendency for hypotension who have not yet received vasoactive medications, necessitating experienced clinicians to remain vigilant. The PSS builds on this approach by incorporating age-specific criteria.[21] Nevertheless, the MAP criteria in PSS remain stringent. Among all cases collected in this study, only 19 patients received a score ≥1 for MAP, with only 8 scoring 2, despite 59 mortality cases. In deceased patients, cardiovascular system scoring was relatively more objective than MAP-based scoring. While MAP scoring is significantly correlated with mortality, its stringent thresholds result in fewer qualifying patients, limiting its practical utility in cases of rapid disease progression and underestimating severity.

The PSS score omits liver and renal function assessments compared to the SOFA score, making it more convenient in clinical applications. Notably, PSS introduces the SpO_2/FiO_2 (S/F) ratio as a respiratory assessment parameter, providing a reliable evaluation method for hospitals without mechanical ventilation facilities.[7] This study found that liver and renal function assessments had a weaker predictive value for mortality, suggesting that PSS offers a more efficient approach. The evaluation of liver and kidney function often experiences delays, as it depends on laboratory tests. Given the rapid disease progression in critically ill pediatric patients, any delays in scoring could introduce biases in disease assessment. The PSS may offer a more time-efficient scoring system in emergency settings,[27] while the SOFA score's broader organ evaluation may offer advantages in complex or multi-system involvement.[28]

The age-dependent differences in mortality prediction between the 2 scoring systems present an interesting finding. In patients aged 1–3 years, the PSS score demonstrated superior predictive accuracy, whereas the SOFA score performed better in patients older than 7 years. Pediatric patients aged 1–3 years undergo rapid physiological changes and development,[29] and the PSS score, which accounts for pediatric physiology, may thus offer more accurate predictions in this group. In contrast, pediatric patients older than 7 years exhibit physiological parameters closer to adult levels, diminishing the advantages of the PSS score compared to SOFA. However, in pediatric patients younger than 1 year and those aged 3–7 years, no significant differences were observed between the 2 scoring systems. This could be attributed to the relatively small sample size, highlighting the need for further research with larger datasets. It may also reflect developmental physiology, as older children resemble adult profiles where SOFA parameters are more applicable, whereas PSS's pediatric-specific thresholds provide greater sensitivity in younger age groups.[29] For instance, infants under 1 year primarily undergo physical and neurological development, while the respiratory and cardiovascular systems remain relatively stable. Similarly, pediatric patients aged 3–7 experience slower growth, with minimal fluctuations in physiological parameters. Our findings are consistent with earlier studies suggesting that developmentally aligned tools enhance prediction accuracy in young patients.[29] These factors may contribute to the minimal differences observed between the 2 scoring

systems in these age groups. Further interdisciplinary exploration with developmental experts is warranted to refine these findings.

The performance of these 2 scoring systems varies slightly across different disease categories. Due to the limitations of the cases collected in this study, we primarily compared diseases of the respiratory, digestive, nervous, and hematologic systems. Our findings indicate that for patients with respiratory diseases, digestive diseases, and post-digestive tract surgery, the SOFA score outperforms the PSS score in mortality prediction. However, for neurological and hematologic diseases, the SOFA score is slightly less effective than the PSS score in predicting mortality. This discrepancy may be attributed to differences in the focus of each scoring system. The SOFA score emphasizes the overall assessment of multiple vital organs, whereas the PSS score primarily evaluates 4 key aspects: respiration, circulation, neurological function, and coagulation. In the context of this study, which focuses on pediatric septic shock, both scoring systems assign relatively high weights to the circulatory system. However, in pediatric patients with respiratory diseases, the respiratory system is often the first to be affected and may suffer the most severe impairment. As both scoring systems assign significant numerical values to respiratory dysfunction, the key difference lies in the assessment of other organ systems. The PSS score is relatively less comprehensive in evaluating these systems compared to the SOFA score, which may explain why the SOFA score exhibits higher sensitivity in predicting mortality for respiratory diseases.

For patients with digestive diseases or post-digestive tract surgery, the presence of both digestive tract involvement and shock may lead to severe disturbances in fluid-electrolyte balance and acid-base homeostasis,[30,31] potentially affecting the stability of the respiratory, neurological, and urinary systems. The SOFA score provides a more detailed assessment of the neurological and urinary systems than the PSS score, which likely accounts for its higher sensitivity in predicting mortality in these disease categories.

For neurological diseases, the PSS score classifies patients into broader categories, whereas the SOFA score offers a more detailed breakdown. As a result, the SOFA score is slightly more sensitive in predicting mortality for neurological conditions.

Compared to other illness types, both scores are less sensitive in predicting mortality in hematologic diseases. This implies that neither score is suitable for this patient population. As a result, hematologic problems require a more sophisticated system.

There are distinct trends in the mortality thresholds for PSS and SOFA scores. The SOFA score threshold is close to the median value of the overall score distribution. This suggests that it serves as a more reliable indicator of disease severity. Significant organ dysfunction and an increased risk of death are indicated when a patient's SOFA score is above this threshold. The PSS score, on the other hand, only substantially predicts mortality risk at higher levels; however, it also has a greater true positive rate within this range. This implies that the SOFA score is better for the slow and ongoing evaluation of illness progression, whereas the PSS score is better for identifying the most serious cases. This could explain SOFA's advantage in multi-organ dysfunction scenarios such as post-surgical shock, while PSS is more sensitive to localized dysfunctions.

Variability in management practices also affects patient outcomes. Variability in antibiotic choice, timing of vasoactive drug use, and supportive therapies may all impact patient prognosis.[32,33] Standardized care pathways and clearer scoring-based treatment thresholds could reduce this variation and improve outcomes.

In contrast to our results, previous studies have found conflicting trends. A previous study suggested that PSS had superior overall accuracy in a neonatal population,[34] whereas our data favors SOFA in older pediatric patients. This difference may be due to cohort variations, different inclusion criteria, or scoring implementation timing. These inconsistencies emphasize the need for multicenter validation across broader demographics.

These findings have important real-world implications. In emergency settings, the simplicity of the PSS and its reliance on fewer laboratory results make it particularly suitable for rapid triage.[35] SOFA, while more comprehensive, may better guide long-term ICU management or therapy escalation decisions.[36] Clinicians should consider using both scores complementarily – PSS for early warning and SOFA for monitoring disease trajectory.

Future directions should explore how treatment decisions (e.g., antibiotic initiation, ventilation, vasoactive support) correlate with score thresholds. Additionally, monitoring score trends over time could refine intervention strategies. For instance, rising scores may indicate the need for escalation, while declines could guide de-escalation. Artificial intelligence (AI) tools and wearable monitors could further personalize care, integrating real-time score updates into decision-making.

In summary, SOFA and PSS are both effective mortality predictors, each with distinct advantages. SOFA offers better overall performance, while PSS excels in early detection for certain age and disease groups. Their combined use may enhance prognostic accuracy and clinical decision-making. Further multicenter studies, score adaptations, and AI integration will be vital to optimizing care for pediatric septic shock.

Limitations

This study has notable limitations. One significant constraint is the relatively small sample size, limiting the collection of cases across different disease categories. For instance, there were a few cases of immunological and urinary system diseases complicated by septic shock, and

no cases of inherited metabolic disorders with septic shock were included. These omissions may introduce potential bias. Given the limitations of cases available at our hospital and our current research capacity, future efforts should focus on collecting a more comprehensive dataset to facilitate further investigations. This remains an intriguing area of research.

Conclusions

The central finding confirms that both SOFA and PSS scores are effective in predicting mortality, with SOFA exhibiting a slightly superior overall performance (correlation coefficient = 0.57 vs 0.56). While the difference in predictive strength was modest, SOFA's higher correlation and ROC performance (especially in respiratory and postoperative gastrointestinal cases) suggest it should be prioritized for general assessment and in patients aged 1–3 years and over 7 years.

However, PSS showed better sensitivity in high-score ranges and superior performance in patients younger than 1 year, pediatric patients aged 3–7 years, and in cases involving digestive and hematologic diseases. Specifically, PSS's respiratory sub-score (r = 0.460) was the most predictive component, while coagulation factors had minimal prognostic impact in both systems. Neurological and respiratory dysfunctions emerged as the strongest mortality predictors within the SOFA framework.

For clinical practice, we recommend using the SOFA score as the primary tool for general prognostic assessment in pediatric septic shock, particularly in respiratory or surgical gastrointestinal cases, and among patients aged 1–3 and >7 years. Conversely, the PSS score should be prioritized in infants and in patients presenting with digestive or hematologic conditions.

Their combined application may offer complementary insights and enhance decision-making accuracy in age- and disease-specific contexts. Future studies are encouraged to further refine scoring models for improved specificity and broader applicability across diverse pediatric subpopulations.

Data Availability Statement

The datasets supporting the findings of this study are openly available in Zenodo at https://doi.org/10.5281/zenodo.15081539.

Supplementary data

The supplementary materials are available at https://doi.org/10.5281/zenodo.15833612. The package includes the following files:

Supplementary Table 1 Distribution of patients across different age groups.

Consent for publication

Not applicable.

Use of AI and AI-assisted technologies

Not applicable.

ORCID iDs

Chao Du https://orcid.org/0009-0003-4997-9432
Xue Li https://orcid.org/0009-0009-0539-2027

References

1. Weiss SL, Peters MJ, Alhazzani W, et al. Surviving Sepsis Campaign International Guidelines for the Management of Septic Shock and Sepsis-Associated Organ Dysfunction in Children. *Pediatr Crit Care Med*. 2020;21(2):e52–e106. doi:10.1097/PCC.0000000000002198
2. Miranda M, Nadel S. Pediatric sepsis: A summary of current definitions and management recommendations. *Curr Pediatr Rep*. 2023;11(2):29–39. doi:10.1007/s40124-023-00286-3
3. Aggrawal K, Verma S, Stoltzfus MT, Singh B, Anamika F, Jain R. Tools for screening, predicting, and evaluating sepsis and septic shock: A comprehensive review. *Cureus*. 2024;16(8):e67137. doi:10.7759/cureus.67137
4. Thodphetch M, Chenthanakij B, Wittayachamnankul B, Sruamsiri K, Tangsuwanaruk T. A comparison of scoring systems for predicting mortality and sepsis in the emergency department patients with a suspected infection. *Clin Exp Emerg Med*. 2021;8(4):289–295. doi:10.15441/ceem.20.145
5. Reddy V, Reddy H, Gemnani R, Kumar S, Acharya S. Navigating the complexity of scoring systems in sepsis management: A comprehensive review. *Cureus*. 2024;16(2):e54030. doi:10.7759/cureus.54030
6. Balamuth F, Scott HF, Weiss SL, et al. Validation of the Pediatric Sequential Organ Failure Assessment Score and Evaluation of Third International Consensus Definitions for Sepsis and Septic Shock Definitions in the Pediatric Emergency Department. *JAMA Pediatr*. 2022;176(7):672. doi:10.1001/jamapediatrics.2022.1301
7. Schlapbach LJ, Watson RS, Sorce LR, et al. International Consensus Criteria for Pediatric Sepsis and Septic Shock. *JAMA*. 2024;331(8):665. doi:10.1001/jama.2024.0179
8. Moreno R, Rhodes A, Piquilloud L, et al. The Sequential Organ Failure Assessment (SOFA) score: Has the time come for an update? *Crit Care*. 2023;27(1):15. doi:10.1186/s13054-022-04290-9
9. Malik A, Taksande A, Meshram R. Pediatric Sequential Organ Assessment Score: A comprehensive review of the prognostic marker in the pediatric intensive care unit. *Cureus*. 2024;16(5):e60034. doi:10.7759/cureus.60034
10. van Wösten Asperen RM, La Roi-Teeuw HM, Tissing WJE, et al. The Phoenix Sepsis Score in pediatric oncology patients with sepsis at PICU admission: Test of performance in a European multicenter cohort, 2018–2020. *Pediatr Crit Care Med*. 2025;26(2):e177–e185. doi:10.1097/PCC.0000000000003683
11. Garvey M. Hospital-acquired sepsis, disease prevalence, and recent advances in sepsis mitigation. *Pathogens*. 2024;13(6):461. doi:10.3390/pathogens13060461
12. Sanchez-Pinto LN, Bennett TD, DeWitt PE, et al. Development and validation of the Phoenix Criteria for Pediatric Sepsis and Septic Shock. *JAMA*. 2024;331(8):675. doi:10.1001/jama.2024.0196
13. Rusmawatiningtyas D, Rahmawati A, Makrufardi F, et al. Factors associated with mortality of pediatric sepsis patients at the pediatric intensive care unit in a low-resource setting. *BMC Pediatr*. 2021;21(1):471. doi:10.1186/s12887-021-02945-0
14. Cruz AT, Lane RD, Balamuth F, et al. Updates on pediatric sepsis. 2020; *JACEP Open*. 1(5):981–993. doi:10.1002/emp2.12173
15. Peshimam N, Nadel S. Sepsis in children: State-of-the-art treatment. *Ther Adv Infect Dis*. 2021;8:20499361211055332. doi:10.1177/20499361211055332
16. Kashyap R, Sherani KM, Dutt T, et al. Current utility of Sequential Organ Failure Assessment Score: A literature review and future directions. *Open Respir Med J*. 2021;15(1):1–6. doi:10.2174/1874306402115010001

17. Msefula J, Kumwenda M, Calis JCJ. Pediatric Phoenix Sepsis Score validation challenges in low-resource settings and in the emergency department. *JAMA*. 2024;331(24):2134. doi:10.1001/jama.2024.8441
18. Bisarya R, Song X, Salle J, Liu M, Patel A, Simpson SQ. Antibiotic timing and progression to septic shock among patients in the ED with suspected infection. *Chest*. 2022;161(1):112–120. doi:10.1016/j.chest.2021.06.029
19. Fenta DA, Ali MM. Factors affecting quality of laboratory result during ordering, handling, and testing of the patient's specimen at Hawassa University College of Medicine and Health Science Comprehensive Specialized Hospital. *J Multidiscip Healthc*. 2020;13:809–821. doi:10.2147/JMDH.S264671
20. Mueller C, McDonald K, De Boer RA, et al. Heart Failure Association of the European Society of Cardiology practical guidance on the use of natriuretic peptide concentrations. *Eur J Heart Fail*. 2019;21(6):715–731. doi:10.1002/ejhf.1494
21. Yaluri N, Stančáková Yaluri A, Žeňuch P, Žeňuchová Z, Tóth Š, Kalanin P. Cardiac biomarkers and their role in identifying increased risk of cardiovascular complications in COVID-19 patients. *Diagnostics*. 2023;13(15):2508. doi:10.3390/diagnostics13152508
22. Jyotsna, Kumar R, Sharan S, Kishore S, Prakash J. The various scoring systems in pediatric intensive care units: A prospective observational study. *Cureus*. 2023;15(5):e39679. doi:10.7759/cureus.39679
23. Lalitha AV, Satish JK, Reddy M, Ghosh S, George J, Pujari C. Sequential Organ Failure Assessment Score as a predictor of outcome in sepsis in pediatric intensive care unit. *J Pediatr Intensive Care*. 2021;10(2):110–117. doi:10.1055/s-0040-1714705
24. Wang Z, He Y, Zhang X, Luo Z. Prognostic accuracy of SOFA and qSOFA for mortality among children with infection: A meta-analysis. *Pediatr Res*. 2023;93(4):763–771. doi:10.1038/s41390-022-02213-6
25. Da Silva PSL, Fonseca MCM. High-dose vasopressor therapy for pediatric septic shock: When is too much? *J Pediatr Intensive Care*. 2020;9(3):172–180. doi:10.1055/s-0040-1705181
26. Shah P, Petersen TL, Zhang L, Yan K, Thompson NE. Using Aggregate Vasoactive-Inotrope Scores to predict clinical outcomes in pediatric sepsis. *Front Pediatr*. 2022;10:778378. doi:10.3389/fped.2022.778378
27. Lashin HI, Sharif AF. Evaluation of various scoring systems as predictors of the need for intensive care unit admission and other adverse outcomes among patients with acute clozapine poisoning. *Toxicol Res*. 2023;12(3):468–479. doi:10.1093/toxres/tfad029
28. Wang X, Guo Z, Chai Y, et al. Application prospect of the SOFA score and related modification research progress in sepsis. *J Clin Med*. 2023;12(10):3493. doi:10.3390/jcm12103493
29. Saeed S, Elmorsy SA. Evaluation of the new poisoning mortality score in comparison with PSS and SOFA scoring systems to predict mortality in poisoned patients admitted to the intensive care unit. *Toxicol Res*. 2024;13(1):tfad113. doi:10.1093/toxres/tfad113
30. Utrilla Fornals A, Costas-Batlle C, Medlin S, et al. Metabolic and nutritional issues after lower digestive tract surgery: The important role of the dietitian in a multidisciplinary setting. *Nutrients*. 2024;16(2):246. doi:10.3390/nu16020246
31. Leigh S, Uhlig F, Wilmes L, et al. The impact of acute and chronic stress on gastrointestinal physiology and function: A microbiota–gut–brain axis perspective. *J Physiol*. 2023;601(20):4491–4538. doi:10.1113/JP281951
32. Ammar MA, Ammar AA, Wieruszewski PM, et al. Timing of vasoactive agents and corticosteroid initiation in septic shock. *Ann Intensive Care*. 2022;12(1):47. doi:10.1186/s13613-022-01021-9
33. Gras-Martín L, Plaza-Diaz A, Zarate-Tamames B, et al. Risk factors associated with antibiotic exposure variability in critically ill patients: A systematic review. *Antibiotics (Basel)*. 2024;13(9):801. doi:10.3390/antibiotics13090801
34. Hadzhieva-Hristova A, Krumova D, Stoeva T, Georgieva R, Iotova V. Assessment of Phoenix Sepsis Score, pSOFA, PELOD-2, and PRISM III in pediatric intensive care. *Children (Basel)*. 2025;12(3):262. doi:10.3390/children12030262
35. Van Der Slikke EC, Beumeler LF, Holmqvist M, Linder A, Mankowski RT, Bouma HR. Understanding post-sepsis syndrome: How can clinicians help? *Infect Drug Resist*. 2023;16:6493–6511. doi:10.2147/IDR.S390947
36. Lambden S, Laterre PF, Levy MM, Francois B. The SOFA score: Development, utility and challenges of accurate assessment in clinical trials. *Crit Care*. 2019;23(1):374. doi:10.1186/s13054-019-2663-7

Psychological distress in Chinese women with benign breast disease and breast cancer during diagnosis: A cross-sectional study

Yan Gao[1,2,A,B], Jintao Wang[3,B,C], Jun Guo[1,2,C,D], Jinnan Gao[1,2,E,F]

[1] Shanxi Bethune Hospital, Shanxi Academy of Medical Sciences, Tongji Shanxi Hospital, Third Hospital of Shanxi Medical University, Taiyuan, China
[2] Tongji Hospital, Tongji Medical College, Huazhong University of Science and Technology, Wuhan, China
[3] Department of Epidemiology, School of Public Health, Shanxi Medical University, Taiyuan China

A – research concept and design; B – collection and/or assembly of data; C – data analysis and interpretation;
D – writing the article; E – critical revision of the article; F – final approval of the article

Advances in Clinical and Experimental Medicine, ISSN 1899–5276 (print), ISSN 2451–2680 (online) *Adv Clin Exp Med*. 2026;35(2):231–241

Address for correspondence
Jinnan Gao
E-mail: Dr-gaojinnan@outlook.com

Funding sources
None declared

Conflict of interest
None declared

Acknowledgements
We extend our gratitude to all the patients who participated in this study. We also thank the data custodians of the Breast Surgery Department at Shanxi Bethune Hospital (Taiyuan, China) for providing access to the patient registry.

Received on November 19, 2024
Reviewed on March 2, 2025
Accepted on April 16, 2025

Published online on September 4, 2025

Abstract

Background. Research on the psychological distress experienced by women with benign breast disease (BBD) remains limited, though some evidence suggests it may resemble that of women with breast cancer (BC).

Objectives. This study aimed to use the Distress Thermometer (DT) to assess the levels of psychological distress and identify influencing factors during the diagnostic phase in patients with BC and BBD.

Materials and methods. From October 2022 to May 2023, a questionnaire survey incorporating the DT and Problem List (PL) was conducted among inpatients in the diagnostic phase for BC or BBD at the Breast Surgery Department of Shanxi Bethune Hospital (Taiyuan, China). Statistical analysis, including descriptive and inferential methods, was performed to examine factors affecting psychological distress in patients with BBD and BC.

Results. In this study, 373 participants were evaluated for psychological distress during the diagnostic phase. Among 255 patients diagnosed with BBD, the median distress score was 4, with a distress prevalence of 52%. The primary sources of distress included anxiety (43.5%), fear (21.2%), pain (7.1%), sleep disturbances (6.7%), and childcare responsibilities (5.1%). Among 118 BC patients, the median distress score was slightly higher at 4.5, with a distress prevalence of 63.6%. Key distress factors were anxiety (47.5%), fear (33.1%), financial worries (21.2%), depression (18.6%), and sadness (15.3%). Key predictors of distress varied between the 2 groups. For patients diagnosed with BBD, younger age, lower education levels, unemployment, and a higher Breast Imaging Reporting and Data System (BI-RADS®) classification significantly contributed to higher distress levels. In patients diagnosed with BC, younger age, lower education levels, and unemployment were the primary risk factors.

Conclusions. These findings underscore the psychological burden faced by both patient groups during diagnosis, highlighting the need for early identification and management of distress in this population.

Key words: psychological distress, breast cancer (BC), benign breast disease (BBD), distress thermometer (DT), predictors of distress

Cite as
Gao Y, Wang J, Guo J, Gao J. Psychological distress in Chinese women with benign breast disease and breast cancer during diagnosis: A cross-sectional study. *Adv Clin Exp Med*. 2026;35(2):231–241. doi:10.17219/acem/204102

DOI
10.17219/acem/204102

Highlights

- Amiodarone as a leading class III antiarrhythmic agent combines antiarrhythmic and vasodilator effects but carries a risk of hepatotoxicity.
- Amiodarone induces severe oxidative liver damage in rats, confirmed by biochemical, histopathological, and immunohistochemical analyses.
- Mitochondrial dysfunction underlies hepatocyte injury, with reduced ATP content and elevated ROS levels driving oxidative stress.
- Exogenous ATP and resveratrol supplementation mitigate liver damage, with resveratrol enhancing intracellular ATP production.
- Optimizing ATP dosing or combining ATP with resveratrol may offer a protective strategy against amiodarone-induced hepatic injury.

Background

Breast diseases are classified into benign breast disease (BBD) and malignant breast cancer (BC), with BBD accounting for approx. 75% of breast biopsy diagnoses.[1] A screening study of over 70,000 women reported a 44.7% prevalence of BBD.[2] Despite being less frequent, BC remains one of the most prevalent malignancies affecting women, with 2.3 million new cases reported globally in 2022.[3] In China, the incidence of BC has been increasing by 3% annually, with more younger women being diagnosed.[4]

Breast cancer patients often face significant psychological challenges due to changes in body function and appearance throughout diagnosis, treatment, and recovery.[5] High levels of psychological distress can lower their quality of life, reduce treatment adherence, and even increase the risk of suicidal behavior.[6] Research indicates that nearly half of women with BC experience distress, particularly around the time of diagnosis.[7,8] Even before a confirmed diagnosis, the uncertainty of potential cancer can heighten anxiety.[9]

While BC has high incidence and mortality rates, most palpable breast masses and lesions are benign, with a large portion of women presenting with breast complaints ultimately diagnosed with BBD.[10] Benign breast disease is common and comprises various histological subtypes characterized by changes in breast tissue. Unlike cancer, BBD is nonmalignant and not life-threatening, though some cases may progress to BC.[11] Studies have highlighted elevated psychological issues among women with BBD, occurring before, during, and even after the diagnostic phase.[12–14] This significant psychological burden is partly driven by prognostic uncertainty and the perceived risk of developing BC.[15] However, while most research has focused on distress in BC patients, few studies have examined psychological distress in those with BBD. This gap in knowledge makes it unclear whether the distress experienced by BBD patients is similar to that of BC patients, especially during the diagnostic phase.

Objectives

This study aimed to compare psychological distress levels in women diagnosed with BBD and BC during the diagnostic phase using the Distress Thermometer (DT), a validated, simple, and quick screening tool for distress. We further sought to identify the primary distress factors and predictors in each group, with the goal of informing early psychological support strategies for all women facing a breast disease diagnosis.

Materials and methods

Study design and setting

This study is a cross-sectional investigation that took place between October 2022 and May 2023, with participants being recruited from the inpatient Breast Surgery Department of Shanxi Bethune Hospital. The reporting of the study was based on the Strengthening the Reporting of Observational Studies in Epidemiology (STROBE) guidelines for the sake of transparency in research reporting.

The inclusion criteria were as follows: patients aged 18 years or older; breast ultrasound and/or mammography indicating a Breast Imaging Reporting and Data System (BI-RADS®) category 3 or higher; full insight into their health status; and the ability to read and write independently or with assistance from medical personnel to complete the questionnaire.

The exclusion criteria were communication barriers due to cognitive impairment or mental health disorder and a previous diagnosis of BC or other malignant neoplasms. Sample sizes were determined through power analysis to ensure statistical confidence, requiring a minimum of 327 participants for a 95% confidence level and a 5% margin of error. Anticipating a 10% non-response rate, the minimum target was set at 360 participants. This study achieved the goal, enrolling 373 participants to enable adequate statistical analysis.

The instrument: Distress Thermometer

The DT is designed to measure 1 aspect of psychological distress. It includes a visual analog single-item scale, that ranges from 0 (no distress) to 10 (mid-extreme distress). The higher the score, the greater the distress experienced. A previously established cut-off score of 4 indicates moderate-to-severe distress, suggesting a need for additional psychological support.[16] The DT has been widely used in oncology and other medical settings and has demonstrated strong reliability and validity across diverse populations, including Chinese patients.

The Problem List (PL) is a 42-item questionnaire that determines if patients have had any problems in the last week and what issues, if any, might be causing them distress. The items are structured into 5 categories: triaging problems (practical) with 12 items, emotional issues with 9 items, social difficulties with 6 items, religious/spiritual issues with 6 items, and physical problems with 9 items. Participants were asked to state if the problem had occurred in the past week by responding with a simple "yes" or "no" on the list. The PL has been culturally adapted and validated in different settings, including Chinese BC patients, where it had good test-retest reliability.

Data collection

Demographic information for all study participants was gathered using a structured questionnaire, which included age, education level, employment status, reproductive history, marital status, and type of medical insurance. Additionally, disease-related information was collected, including breast BI-RADS classification, clinical diagnoses, comorbidities such as diabetes, hypertension, cardiovascular diseases, and thyroid disorders, as well as a family history of BC and other tumors.

The inclusion of these demographic and clinical variables was based on prior research indicating their potential influence on psychological distress. For example, employment status and education level may affect coping strategies and access to healthcare, while BI-RADS classification directly reflects the severity of suspected disease and may heighten distress.

Statistical analyses

Descriptive statistics were used to calculate means, medians, frequencies, percentages, and interquartile ranges (IQRs) for patient characteristics, distress levels, and reported problems. The normality of continuous variables, such as age, was assessed separately for the BBD and BC groups using the Shapiro–Wilk test (Supplementary Table 1). In both groups, the test indicated non-normal distributions ($p < 0.001$). However, due to the sufficiently large sample sizes in each group ($n > 30$), the Central Limit Theorem supports the use of parametric tests, such as the t-test, and allows for the reporting of means and standard deviations (SD). Therefore, although age was not normally distributed, the use of parametric methods remains statistically justifiable in this context. Distress Thermometer scores were categorized into 2 levels: scores of 0–3 indicated mild distress, while scores of 4–10 indicated moderate-to-severe distress. Anxiety (A) scores and Depression (D) scores were also recorded. The χ^2 and Fisher's exact tests were employed to compare distress levels across groups with and without specific problems. Additionally, multivariate logistic regression analysis was conducted to identify factors significantly associated with distress, ensuring that predictor selection was based on clinical relevance and prior research. To verify logistic regression assumptions, linearity in the logit was tested using the Box–Tidwell procedure, showing a non-significant interaction term ($p > 0.05$), confirming linearity. The variance inflation factor (VIF) values remained below 2, indicating no multicollinearity. Model adequacy was assessed using the Hosmer–Lemeshow goodness-of-fit test ($\chi^2 = 6.73$, $p = 0.57$), confirming an acceptable fit (Supplementary Table 2). The Nagelkerke R^2 was higher in the BC group, indicating that the model accounted for a greater proportion of the variance in distress levels among BC patients compared to BBD patients (Tables 1,2). All analyses were performed using IBM SPSS Statistics v. 26 (IBM Corp., Armonk, USA), with a $p < 0.05$ considered statistically significant.

Ethics

This study complies with the ethical standards set forth in the Declaration of Helsinki and its later amendments. The research was approved by the Ethics Committee of Shanxi Bethune Hospital (Taiyuan, China; approval No. YXLL-2023-093), and written informed consent was obtained from all participants, ensuring that they fully understood the study's purpose, procedures, and their right to withdraw at any time without consequences.

Results

Patient characteristics

A total of 379 patients were surveyed, with 6 excluded due to incomplete clinical data (4 cases) and non-compliant diagnostic specimens (2 cases), resulting in a final sample of 373 participants. Among them, 255 patients were in the BBD group, and 118 were in the BC group. The age range for the BBD group was 14 –69 years, with a mean age of 40 ±11 years, while the BC group ranged from 27 to 83 years, with a mean age of 53 ±12 years. The BC group was significantly older than the BBD group ($p < 0.01$). Additionally, compared with the BC group, the BBD group had a significantly higher proportion of unmarried individuals ($p < 0.01$), fewer comorbidities ($p < 0.01$), and a greater proportion of nulliparous women ($p = 0.021$) (Table 3).

Table 1. The binary logistic regression model of psychological distress in benign breast disease

Benign breast disease		B	SE	χ^2	p-value	OR	95% CI
Age#		–0.032	0.016	4.002	<0.05[a]	0.97	0.94–0.99
Educational level	>9 years	0.721	0.294	6.016	<0.05[a]	2.06	1.16–3.66
	≤9 years					1	
Occupation	employed	0.612	0.305	4.024	<0.05[a]	1.84	1.01–3.35
	unmployed	–	–	–	–	1	
BI-RADS grade	4a	1.015	0.311	10.654	<0.01[a]	2.76	1.50–5.08
	3	–	–	–	–	1	

Nagelkerke R^2 = 0.436, Hosmer–Lemeshow test: test statistic: 104.92, p-value = 0.623. B (regression coefficient) indicates the strength and direction of the relationship between a predictor and psychological distress. #Age was entered into the logistic regression as a continuous variable. BI-RADS – Breast Imaging-Reporting and Data System; Categories 3 and 4a suggest low-to-moderate suspicion of malignancy; SE standard error; 95% CI – 95% confidence interval; OR – odds ratio. [a] p-value obtained using χ^2 test.

Table 2. The binary logistic regression model of psychological distress in breast cancer

Breast cancer		B	SE	χ^2	p-value	OR	95% CI
Age#		–0.043	0.022	3.896	<0.05[a]	0.96	0.92–0.99
Educational level	>9 years	1.034	0.516	4.020	<0.05[a]	2.81	1.02–7.73
	≤9 years	–	–	–	–	1	
Occupation	employed	1.863	0.528	12.458	<0.01[a]	6.44	2.29–18.12
	unemployed	–	–	–	–	1	

Nagelkerke R^2 = 0.314, Hosmer–Lemeshow test: test statistic: 62.05, p-value = 0.702. B (regression coefficient) indicates the strength and direction of the relationship between a predictor and psychological distress. #Age was entered into the logistic regression as a continuous variable. BI-RADS – Breast Imaging-Reporting and Data System. Categories 3 and 4a suggest low-to-moderate suspicion of malignancy; SE – standard error; 95% CI – 95% confidence interval; OR – odds ratio. [a] p-value obtained using χ^2 test.

Comparison of psychological distress between women with benign breast disease and breast cancer

Psychological distress was assessed using the DT, with a score of ≥4 indicating clinically significant distress. In the BC group, 63.6% of women reported psychological distress (score ≥ 4), with a median distress score of 4.5 (IQR = 3–6). In the BBD group, 52.2% of patients reported distress, with a median score of 4 (IQR = 2–5). Overall, psychological distress levels were higher in the BC group than in the BBD group (Fig. 1). The most frequently reported causes of psychological distress differed between the 2 groups. In the BC group, the main causes were worry or anxiety (47.4%), fear (33.0%), financial concerns (21.1%), sadness or depression (18.6%), and feelings of sorrow or loss (15.2%) (Fig. 2). In the BBD group, they were worry or anxiety (43.5%), fear (21.1%), pain (7.0%), sleep difficulties (6.6%), and childcare challenges (5.0%) (Fig. 3).

Factors associated with psychological distress in women with BBD and BC

To identify factors contributing to distress, patients were categorized based on their DT scores, with scores ≥4 indicating psychological distress and scores <4 indicating no distress. All variables were analyzed using t-tests or χ^2 tests. In the BBD group, univariate analysis showed significant differences in age, education level, marital status, employment status, parity, and BI-RADS classification. Multivariate regression analysis further identified several significant predictors of psychological distress. Younger patients had a higher likelihood of experiencing distress (OR = 0.97,

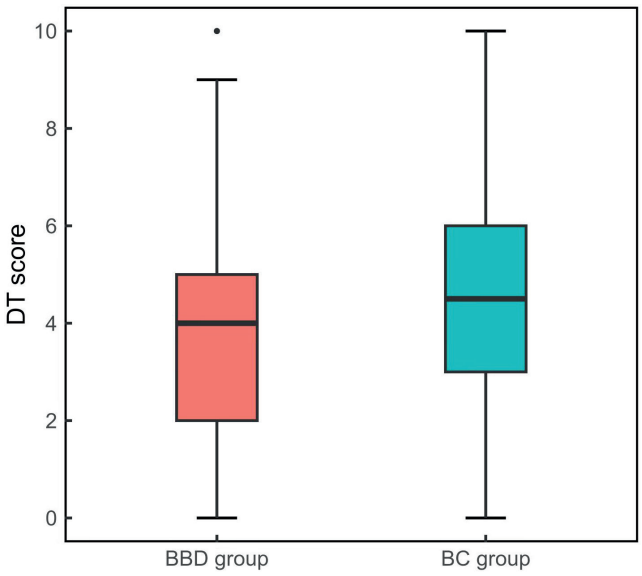

Fig. 1. Comparison of Distress Thermometer (DT) scores between the benign breast disease (BBD) group and the breast cancer (BC) group. The central line within each box represents the median DT score. The upper and lower edges of the box indicate the 75th percentile (Q3) and 25th percentile (Q1), respectively

Table 3. Sociodemographic and clinical characteristics of patients

Characteristics		Patients (%)		t/χ^2	p-value
		benign breast disease (n = 255)	breast cancer (n = 118)		
Age (mean ±SD)		40 ±11	53 ±12	3.36	<0.01[a]
Educational level	≤9 years	130 (51.0%)	72 (61.0%)	3.27	0.070[b]
	>9 years	125 (49.0%)	46 (39.0%)		
Marital status	single	31 (12.2%)	6 (5.1%)	4.52	<0.01[b]
	married	224 (87.8%)	112 (94.9%)		
Occupation	unemployed	130 (51.0%)	69 (58.5%)	1.82	0.177[b]
	employed	125 (49.0%)	49 (41.5%)		
Health insurance	resident	167 (65.5%)	84 (71.2%)	1.19	0.275[b]
	employee	88 (34.5%)	34 (28.8%)		
Comorbidities	no	203 (79.6%)	70 (59.3%)	16.92	<0.01[b]
	yes	52 (20.4%)	48 (40.7%)		
Family cancer history	no	220 (86.3%)	99 (83.9%)	0.37	0.544[b]
	Yes	35 (13.7%)	19 (16.1%)		
Childbearing status	no	36 (14.1%)	7 (5.9%)	5.30	0.021[b]
	yes	219 (85.9%)	111 (94.1%)		
BI-RADS	4c/5	–	96 (81.4%)	–	–
	4b	–	22 (18.6%)		
	4a	88 (34.5%)			
	3	167 (65.5%)			

SD – standard deviation; BI-RADS – Breast Imaging-Reporting and Data System: Categories 3 and 4a suggest low-to-moderate suspicion of malignancy, while 4b and 4c indicate increasing levels of concern. Category 5 is highly suggestive of malignancy; [a]p-value obtained using t-test; [b] p-value obtained using χ^2 test.

95% CI: 0.94–0.99, $p < 0.05$). Higher education was associated with greater distress (OR = 2.06, 95% CI: 1.16–3.66, $p = 0.01$), and employed women had higher distress levels (OR = 1.84, 95% CI: 1.01–3.35, $p < 0.05$). Additionally, women with higher BI-RADS scores experienced greater distress (OR = 2.76, 95% CI: 1.50–5.08, $p < 0.01$).

Differentiation by age, level of education, and employment status were revealed in the univariate analysis of the BC group. Multivariate regression analysis showed that distress levels were influenced by several factors. Younger women reported more distress (OR = 0.96, 95% CI: 0.92–0.99, $p < 0.05$). Women with higher levels of education were more likely to report distress (OR = 2.81, 95% CI: 1.02–7.73, $p < 0.05$), and employed patients reported significantly higher distress levels (OR = 6.44, 95% CI: 2.29–18.12, $p < 0.01$). Specific data are presented in Tables 1,2,4,5.

To summarize, psychological distress was prevalent in both groups but more common in BC patients (63.6%) as compared to those with BBD (52.2%). For both groups, anxiety and fear were the most marked sources, but in BC patients, financial concerns along with depression were more pronounced. Younger age, higher education, and employment status were significant predictors of distress in both groups. However, BI-RADS classification was another determinant for BBD patients. These conclusions call for further thought on the importance of proactive psychological screening and targeted interventions for women being diagnosed with breast diseases to optimize their mental health.

Discussion

As far as we know, this is the 1st research attempting to measure the distress levels of women with BC and BBD before the diagnosis is made. Two key findings emerged from this cross-sectional study. First, distress prevalence was higher in the BC group (63.6%) compared to the BBD group (52.2%). Second, age, education, and employment status were predictors of distress in both groups, while a higher BI-RADS grade was associated with increased distress levels in the BBD group.

Previous studies have primarily examined psychological distress in BC patients after diagnosis or during treatment. In Malaysia, 1 study reported a distress prevalence of 50.2% at diagnosis,[17] while a study conducted in the USA found a rate of 53.3% with Asian individuals having the highest percentage at 60.7% compared to other ethnic groups.[18] A study conducted in China among 137 patients undergoing chemotherapy reported a distress rate of 42.3%.[19] Our study suggests that BC patients often experience

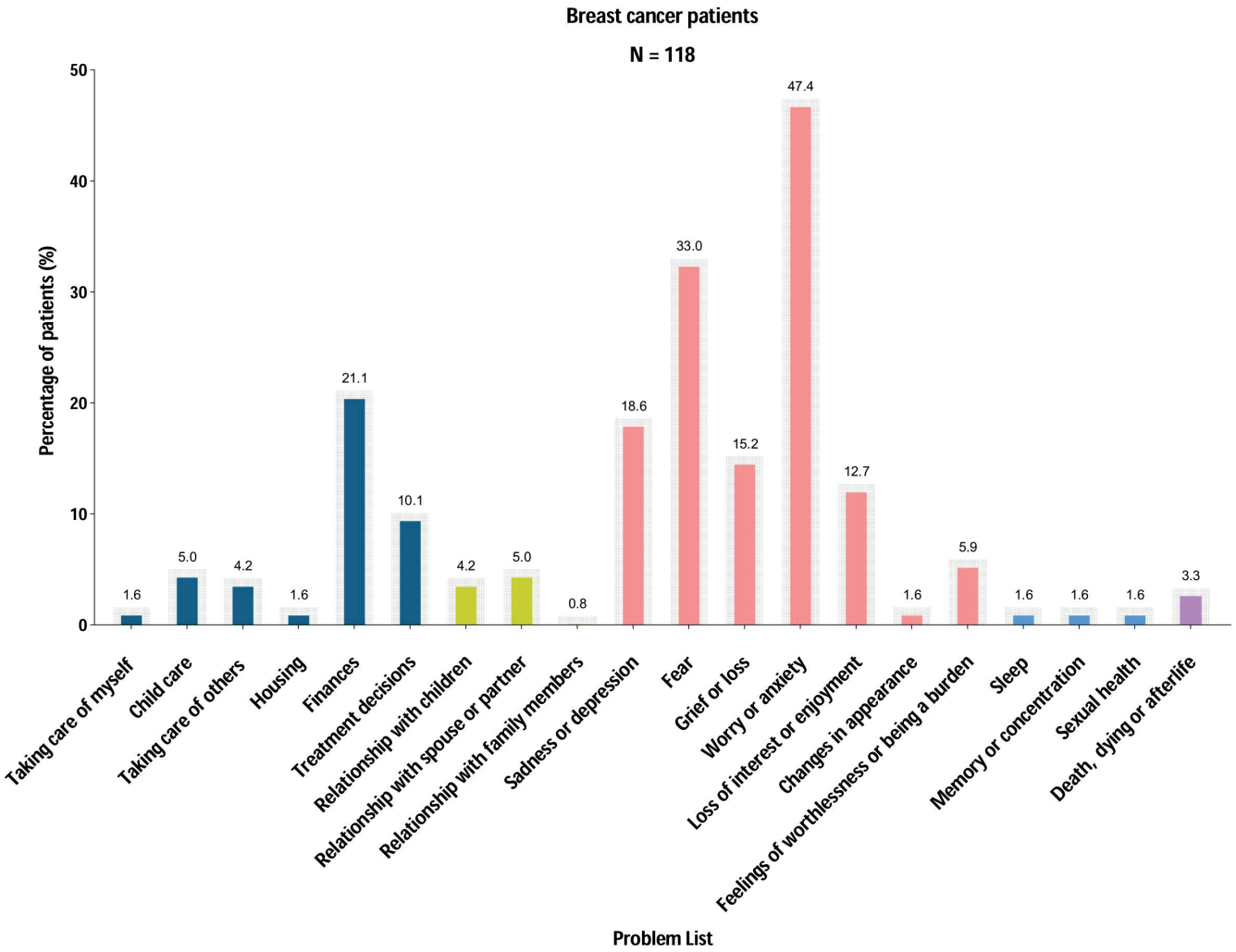

Fig. 2. Problem List (PL) of breast cancer (BC) patients

heightened psychological distress before receiving a diagnosis, with levels surpassing those observed during the treatment phase. This elevated pre-diagnosis distress may stem from cultural factors. Additionally, BC diagnosis often involves life-changing physical impacts and typically occurs between ages 45 and 55 – a stage where many women are managing significant family and financial responsibilities. These combined pressures contribute to increased psychological distress among Chinese BC patients before diagnosis.

Cultural perceptions of BC play a crucial role in shaping distress levels. In China, cancer is often perceived as a terminal illness, leading to heightened fear and anxiety even before a definitive diagnosis. Additionally, family expectations and social obligations contribute to distress, particularly for women who bear caregiving responsibilities. The stigma associated with a cancer diagnosis may further exacerbate psychological burdens, as individuals may fear social exclusion or discrimination.

A noteworthy finding from our study is the high level of pre-diagnostic distress reported among women with BBD. Prior research has shown that BBD patients can experience psychosocial challenges similar to those faced by BC patients.[20] Our findings are consistent with previous research showing that women attending a breast clinic for the 1st time often experience high levels of anxiety.[21] Psychological distress can emerge from the moment a breast lump is discovered and may persist through follow-up appointments for abnormal findings, regardless of whether the ultimate diagnosis is benign or malignant.[14,22,23] This heightened anxiety is understandable, as subjective symptoms can trigger fears of cancer, which in turn increase psychological distress. Therefore, it is essential for healthcare providers to offer psychological support to all patients awaiting diagnostic results, not just those at high risk of malignancy.[24]

Both groups of patients reported anxiety and fear during the diagnostic phase, which can be attributed to the uncertainty surrounding a potential cancer diagnosis. This uncertainty often leads to heightened feelings of anxiety and fear.[14,22,23] However, in the BC group, emotional distress was particularly prevalent before diagnosis, with 21% of patients indicating financial pressures. The costs associated with cancer treatment can be significant in China,

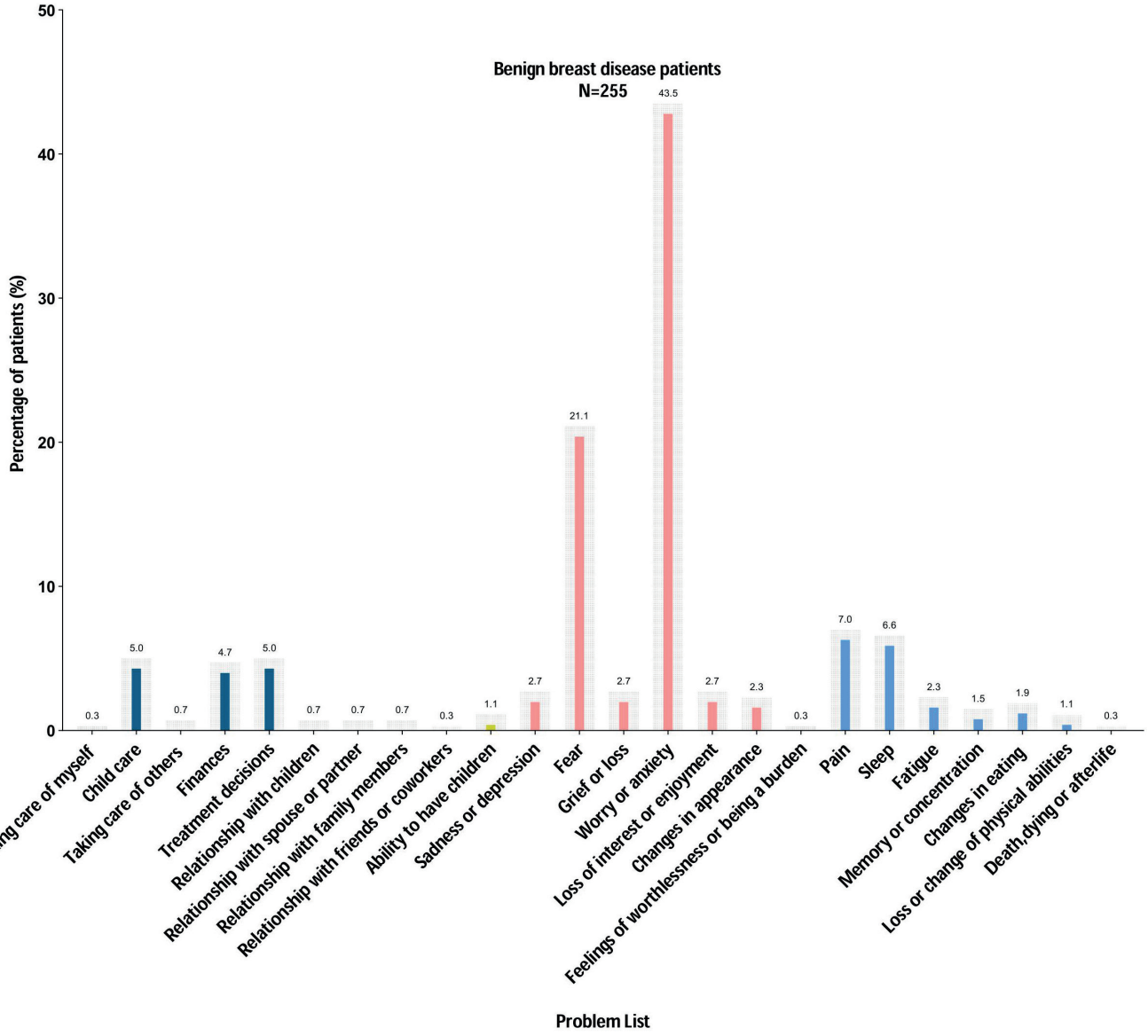

Fig. 3. Problem List (PL) of benign breast disease (BBD) patients

contributing to stress and financial strain for patients.[25,26] In contrast, women in the BBD group also identified childcare responsibilities as a factor of psychological distress. Given that BBD patients tend to be younger, concerns related to parenting may weigh more heavily on them. Previous research has shown that having children is a strong predictor of distress, particularly among younger women.[27]

Our study revealed a notable link between psychological distress and factors such as age, education level, and employment status in both the BBD and BC groups. Specifically, we found a negative correlation between age and psychological distress, indicating that younger individuals are more likely to experience higher levels of distress. This observation aligns with findings from various studies.[28,29] Younger BC patients often bear greater social roles and family responsibilities, which can substantially disrupt their work, academic pursuits, and family life during diagnosis and treatment. Furthermore, compared to older patients, younger individuals tend to have heightened concerns about their appearance and fertility, making it challenging for them to accept BC surgeries and subsequent treatments. Lastly, despite improvements in the 5-year survival rates for BC, younger patients often express greater anxiety about potential recurrence. These combined pressures contribute to increased psychological distress in this demographic.[30,31]

This study reveals that BC patients with higher educational attainment experience a greater prevalence of significant psychological distress, aligning with previous research conducted in China.[32] More educated individuals may have a deeper understanding of their diagnosis and treatment, making them more aware of potential health risks. Consequently, this knowledge can contribute to elevated levels of psychological distress.

Additionally, our findings indicate that individuals who are employed report higher levels of psychological distress

Table 4. One-variable analysis of predictors associated with psychological distress in benign breast disease

Characteristics		DT ≥ 4 (n = 133)	DT < 4 (n =1 22)	p-value
Age (mean ±SD)		37 ±10	42 ±11	<0.01[a]
Educational level	≤9 years	53 (39.8%)	77 (63.1%)	<0.01[b]
	>9 years	80 (60.2%)	45 (36.9%)	
Marital status	Single	22 (16.5%)	9 (7.4%)	0.025[b]
	Married	111 (83.5%)	113 (92.6%)	
Occupation	Unemployed	53 (39.8%)	77 (63.1%)	<0.01[b]
	Employed	80 (60.2%)	45 (36.9%)	
Health insurance	Resident	89 (66.9%)	78 (63.9%)	0.617[b]
	Employee	44 (33.1%)	44 (36.1%)	
Comorbidities	No	110 (82.7%)	93 (76.2%)	0.200[b]
	Yes	23 (17.3%)	29 (23.8%)	
Family cancer history	No	113 (85.0%)	107 (87.7%)	0.525[b]
	Yes	20 (15.0%)	15 (12.3%)	
Childbearing status	No	28 (21.1%)	8 (6.6%)	<0.01[b]
	Yes	105 (78.9%)	114 (93.4%)	
BI-RADS	4c/5	–	–	<0.01[b]
	4b	–	–	
	4a	54 (40.6%)	88 (52.5%)	
	3	79 (59.4%)	34 (47.5%)	

SD – standard deviation; DT – Distress Thermometer; A – anxiety score; D – depression score; BI-RADS – Breast Imaging-Reporting and Data System; [a] p-value obtained using t-test; [b] p-value obtained using χ^2 test.

Table 5. One-variable analysis of predictors associated with psychological distress in breast cancer

Characteristics		DT ≥ 4 (n = 75)	DT < 4 (n = 43)	p-value
Age (mean ±SD)		50 ±11	58 ±13	<0.01[a]
Educational level	≤9 years	38 (50.7%)	34 (79.1%)	<0.01[b]
	>9 years	37 (49.3%)	9 (20.9%)	
Marital status	Single	2 (2.7%)	4 (9.3%)	0.114[b]
	Married	73 (97.3%)	39 (90.7%)	
Occupation	Unemployed	32 (42.7%)	37 (86.0%)	<0.01[b]
	Employed	43 (57.3%)	6 (14.0%)	
Health insurance	Resident	49 (65.3%)	35 (81.4%)	0.064[b]
	Employee	26 (34.7%)	8 (18.6%)	
Comorbidities	No	45 (60.0%)	23 (53.5%)	0.491[b]
	Yes	30 (40.0%)	20 (46.5%)	
Family cancer history	No	65 (86.7%)	34 (79.1%)	0.280[b]
	Yes	10 (13.3%)	9 (20.9%)	
Childbearing status	No	4 (5.3%)	3 (7.0%)	0.716[b]
	Yes	71 (94.7%)	40 (93%)	
BI-RADS*	4c/5	62 (82.7%)	9 (20.9%)	<0.01[b]
	4b	13 (17.3%)	34 (79.1%)	
	4a	–	–	
	3	–	–	

SD – standard deviation; DT – Distress Thermometer; A – anxiety score; D – depression score; BI-RADS – Breast Imaging-Reporting and Data System; [a] p-value obtained using t-test; [b] p-value obtained using χ^2 test.

compared to those who are unemployed. Employed individuals may experience heightened psychological distress due to concerns about job security and financial stability resulting from their illness, especially in workplaces where health conditions may affect career prospects. The stress associated with work responsibilities can further exacerbate these feelings.[33] However, some studies suggest that unemployed individuals may also be particularly vulnerable to psychological distress due to financial insecurity and lack of social support.[34,35] Thus, additional research is warranted to identify the specific stressors affecting patients to better understand this relationship.

Our study highlights a link between higher BI-RADS classifications and increased distress levels. The BI-RADS provides a standardized framework for reporting breast pathology detected through mammography and ultrasound.[36] It helps categorize breast lesions based on their possibility of malignancy, with higher grades often leading to further testing or biopsies. Patients categorized as probably benign (BI-RADS 3) or with low suspicion (BI-RADS 4a) are frequently encountered and typically warrant short-interval follow-ups or biopsies.[37] This observation aligns with findings from earlier research showing that patients with higher BI-RADS scores report greater anxiety,[12,38] as elevated BI-RADS categories often necessitate further biopsies or surgical interventions, thereby amplifying the psychological burden on patients.

Limitations

While our findings provide valuable insights, this study has several limitations. First, the research was conducted with a relatively small sample of patients from a single center, which may restrict the broader applicability of the results. Future studies should incorporate multi-center data to capture a more diverse patient sample. As a second limitation of the study, it has relied on the experience of only inpatient individuals, which may lead to psychological neglect. Examining outpatient cases in future studies may provide a more comprehensive understanding of the psychological phenomena experienced by different patients. Moreover, the study was conducted in China, where cultural and socioeconomic factors may influence distress levels differently than in Western countries. While we identified key distress predictors, future research should explore additional psychological and social factors, such as coping mechanisms, social support networks, and access to mental health resources. Lastly, as a cross-sectional observational study, it only offers a snapshot of psychological distress at a specific moment. The absence of longitudinal data limits the ability to assess changes in distress over time. Future research should adopt longitudinal designs to monitor the progression of psychological distress and examine factors that may either intensify or alleviate these feelings, ultimately informing more effective management strategies.

Despite these limitations, our study highlights the need for early psychological support for both BC and BBD patients. Addressing distress during the diagnostic phase could improve patient wellbeing and enhance treatment outcomes. Future studies should explore targeted interventions, such as counseling and financial support programs, to help reduce psychological burdens in this patient population.

Conclusions

Psychological distress is often overlooked in breast disease patients, especially in China, where routine screenings are not yet standard practice. Additionally, there is a shortage of standardized assessment tools for evaluating psychological distress. This study highlights that psychological distress can arise not only from cancer diagnoses but also from benign tumors. Patients with breast diseases may encounter psychological challenges at various stages of their care. Therefore, it is crucial for medical institutions to prioritize the screening and management of psychological distress while increasing their focus on mental health. It is advisable for healthcare facilities to implement routine screenings for psychological distress at key stages of breast disease management, utilizing tools such as the DT. Early identification of distress can help provide timely psychological support, reduce anxiety, and improve overall wellbeing. Hospitals and clinics should also consider offering targeted interventions, such as counseling services, psychoeducational programs, and peer support groups, to address the specific concerns of different patient groups, especially to subgroups such as younger patients, those with lower educational levels, and individuals facing employment instability. By prioritizing mental health alongside physical treatment, medical institutions can enhance patient care, satisfaction, and quality of life.

This article is based on a previously available preprint posted on Research Square on Nov 29, 2023: "Prevalence and correlates of distress in Chinese women with benign breast disease". https://doi.org/10.21203/rs.3.rs-3639926/v1

Data Availability Statement

The datasets supporting the findings of this study are openly available in Zenodo at https://doi.org/10.5281/zenodo.14925760.

Supplementary data

The supplementary materials are available at https://doi.org/10.5281/zenodo.16014359. The package includes the following files:

Supplementary Table 1. Shapiro–Wilk test for normality of age in each group.

Supplementary Table 2. Logistic regression assumption tests.

Consent for publication

Not applicable.

Use of AI and AI-assisted technologies

Not applicable.

ORCID iDs

Imię Nazwisko https://orcid.org/0000-0000-0000-0000
Yan Gao https://orcid.org/0009-0007-7426-6169
Jintao Wang https://orcid.org/0009-0007-9789-1274
Jun Guo https://orcid.org/0009-0003-4916-5156
Jinnan Gao https://orcid.org/0000-0002-9163-9453

References

1. Sherman ME, Vierkant RA, Winham SJ, et al. Benign breast disease and breast cancer risk in the percutaneous biopsy era. *JAMA Surg*. 2024;159(2):193. doi:10.1001/jamasurg.2023.6382
2. Louro J, Román M, Posso M, et al. Differences in breast cancer risk after benign breast disease by type of screening diagnosis. *Breast*. 2020;54:343–348. doi:10.1016/j.breast.2020.09.005
3. Bray F, Laversanne M, Sung H, et al. Global cancer statistics 2022: GLOBOCAN estimates of incidence and mortality worldwide for 36 cancers in 185 countries. *CA Cancer J Clin*. 2024;74(3):229–263. doi:10.3322/caac.21834
4. Han B, Zheng R, Zeng H, et al. Cancer incidence and mortality in China, 2022. *J Nat Cancer Center*. 2024;4(1):47–53. doi:10.1016/j.jncc.2024.01.006
5. Guarino A, Polini C, Forte G, Favieri F, Boncompagni I, Casagrande M. The effectiveness of psychological treatments in women with breast cancer: A systematic review and meta-analysis. *J Clin Med*. 2020;9(1):209. doi:10.3390/jcm9010209
6. Matud MP, García MC. Psychological distress and social functioning in elderly Spanish people: A gender analysis. *Int J Environ Res Public Health*. 2019;16(3):341. doi:10.3390/ijerph16030341
7. Devarakonda SK, Timman R, Bouvy PF, et al. Trends in emotional functioning and psychosocial wellbeing in breast cancer survivors: A prospective cohort study using patient-reported outcome measures. *BMC Womens Health*. 2023;23(1):153. doi:10.1186/s12905-023-02243-0
8. Shahsavar Y, Choudhury A. Examining influential factors in newly diagnosed cancer patients and survivors: Emphasizing distress, self-care ability, peer support, health perception, daily life activity, and the role of time since diagnosis. *PLoS One*. 2023;18(9):e0291064. doi:10.1371/journal.pone.0291064
9. Bartley N, Napier C, Best M, Butow P. Patient experience of uncertainty in cancer genomics: A systematic review. *Genet Med*. 2020;22(9):1450–1460. doi:10.1038/s41436-020-0829-y
10. Wang Q, Yang Q, Li Z, et al. The application of methylene blue location technique in deep-seated benign breast tumor resection under endoscopy: A retrospective, single-institution analysis. *Gland Surg*. 2024;13(7):1269–1280. doi:10.21037/gs-24-139
11. Figueroa JD, Gierach GL, Duggan MA, et al. Risk factors for breast cancer development by tumor characteristics among women with benign breast disease. *Breast Cancer Res*. 2021;23(1):34. doi:10.1186/s13058-021-01410-1
12. Neeter LMFH, Nelemans PJ, Raat HPJ, et al. Contrast-enhanced mammography versus conventional imaging in women recalled from breast cancer screening (RACER trial): A multicentre, open-label, randomised controlled clinical trial. *Lancet Reg Health Eur*. 2024;44:100987. doi:10.1016/j.lanepe.2024.100987
13. Hulett JM, Cheng AL, Bormann JE, et al. An Internet Mantram Repetition Program to promote wellbeing in breast cancer survivors: A feasibility randomized controlled trial. *Integr Cancer Ther*. 2024;23:15347354241290504. doi:10.1177/15347354241290504
14. Fortin J, Leblanc M, Elgbeili G, Cordova MJ, Marin MF, Brunet A. The mental health impacts of receiving a breast cancer diagnosis: A meta-analysis. *Br J Cancer*. 2021;125(11):1582–1592. doi:10.1038/s41416-021-01542-3
15. Karveli S, Galanis P, Mitropoulou EM, Karademas E, Markopoulos C. The role of attachment styles on quality of life and distress among early-stage female breast cancer patients: A systematic review [published correction appears in *J Clin Psychol Med Settings*. 2023;30(4):740. doi:10.1007/s10880-023-09955-3]. *J Clin Psychol Med Settings*. 2023;30(4):724–739. doi:10.1007/s10880-023-09940-w
16. Riba MB, Donovan KA, Ahmed K, et al. NCCN Guidelines® Insights: Distress Management, Version 2.2023. Featured Updates to the NCCN Guidelines. *J Natl Compr Canc Netw*. 2023;21(5):450–457. doi:10.6004/jnccn.2023.0026
17. Vafaei Z, Najafian J, Shekarchizadeh M, et al. Perceived stress, anxiety, and depression in women with breast cancer: CIBC study. *J Cancer Res Ther*. 2023;19(7):1893–1898. doi:10.4103/jcrt.jcrt_2205_21
18. Fayanju OM, Ren Y, Stashko I, et al. Patient-reported causes of distress predict disparities in time to evaluation and time to treatment after breast cancer diagnosis. *Cancer*. 2021;127(5):757–768. doi:10.1002/cncr.33310
19. Zhao H, Li X, Zhou C, Wu Y, Li W, Chen L. Psychological distress among Chinese patients with breast cancer undergoing chemotherapy: Concordance between patient and family caregiver reports. *J Adv Nurs*. 2022;78(3):750–764. doi:10.1111/jan.15004
20. Gil-Olarte P, Gil-Olarte MA, Gómez-Molinero R, Guil R. Psychosocial and sexual wellbeing in breast cancer survivors undergoing immediate breast reconstruction: The mediating role of breast satisfaction. *Eur J Cancer Care (Engl)*. 2022;31(6):e13686. doi:10.1111/ecc.13686
21. Gutzeit A, Heiland R, Sudarski S, et al. Direct communication between radiologists and patients following imaging examinations: Should radiologists rethink their patient care? *Eur Radiol*. 2019;29(1):224–231. doi:10.1007/s00330-018-5503-2
22. Kim A, Chung KC, Keir C, Patrick DL. Patient-reported outcomes associated with cancer screening: A systematic review. *BMC Cancer*. 2022;22(1):223. doi:10.1186/s12885-022-09261-5
23. Ashour ASA, Abd-ElGawad M, Yohanna M, et al. Is music intervention effective in reducing anxiety and pain during breast biopsy procedure? A systematic review and meta-analysis of randomized controlled trials. *Support Care Cancer*. 2022;30(12):10379–10389. doi:10.1007/s00520-022-07414-7
24. Zainal NZ, Ng CG, Wong A, Andrew B, Mohd Taib NA, Low SY. Prevalence of depression, trait anxiety, and social support during the diagnostic phases of breast cancer. *J Taibah Univ Med Sci*. 2021;16(4):497–503. doi:10.1016/j.jtumed.2021.01.013
25. Ehsan AN, Wu CA, Minasian A, et al. Financial toxicity among patients with breast cancer worldwide: A systematic review and meta-analysis. *JAMA Netw Open*. 2023;6(2):e2255388. doi:10.1001/jamanetworkopen.2022.55388
26. Yu H, Li H, Zuo T, et al. Financial toxicity and psychological distress in adults with cancer: A treatment-based analysis. *Asia Pac J Oncol Nurs*. 2022;9(9):100069. doi:10.1016/j.apjon.2022.04.008
27. Graham-Wisener L, Dempster M, Sadler A, McCann L, McCorry NK. Validation of the Distress Thermometer in patients with advanced cancer receiving specialist palliative care in a hospice setting. *Palliat Med*. 2021;35(1):120–129. doi:10.1177/0269216320954339
28. Kasgri KA, Abazari M, Badeleh SM, Badeleh KM, Peyman N. Comprehensive review of breast cancer consequences for the patients and their coping strategies: A systematic review. *Cancer Control*. 2024;31:10732748241249355. doi:10.1177/10732748241249355
29. Phoosuwan N, Lundberg PC. Psychological distress and health-related quality of life among women with breast cancer: A descriptive cross-sectional study. *Support Care Cancer*. 2022;30(4):3177–3186. doi:10.1007/s00520-021-06763-z
30. Vazquez D, Rosenberg S, Gelber S, et al. Posttraumatic stress in breast cancer survivors diagnosed at a young age. *Psychooncology*. 2020;29(8):1312–1320. doi:10.1002/pon.5438
31. Kim J, Lee K. Lived experiences of breast cancer in patients under the age of 40: A phenomenological study. *Eur J Oncol Nurs*. 2023;65:102336. doi:10.1016/j.ejon.2023.102336

32. Sun KS, Lam TP, Lam KF, et al. Associations between demographic factors and psychological distress among Chinese residents in Hong Kong: beyond socioeconomic classes. *Psychol Health Med*. 2020;25(9): 1049–1061. doi:10.1080/13548506.2020.1714063
33. Forcino R, Lichtenstein J, Rotenberg S, et al. Work- and school-related distress among patients with cancer: Single-site retrospective chart review. *J Psychosoc Oncol*. 2023;41(2):242–249. doi:10.1080/07347332.2022.2090886
34. Okeke B, Hillmon C, Jones J, et al. The relationship of social determinants and distress in newly diagnosed cancer patients. *Sci Rep*. 2023;13(1):2153. doi:10.1038/s41598-023-29375-5
35. Achdut N, Refaeli T. Unemployment and psychological distress among young people during the COVID-19 pandemic: Psychological resources and risk factors. *Int J Environ Res Public Health*. 2020; 17(19):7163. doi:10.3390/ijerph17197163
36. Merjane V, Perin DMP, Bacha PMGE, Miranda BMM, Bitencourt AGV, lared W. Breast Imaging Reporting and Data System (BI-RADS®): A success history and particularities of its use in Brazil. *Rev Bras Ginecol Obstet*. 2024;46:e-rbgo6. doi:10.61622/rbgo/2024AR06
37. Berg WA. BI-RADS 3 on screening breast ultrasound: What is it and what is the appropriate management? *J Breast Imaging*. 2021;3(5): 527–538. doi:10.1093/jbi/wbab060
38. Budisavljevic A, Dedic Plavetic N, Klaric K, Kelemenic-Drazin R, Letica-Crepulja M. The impact of newly diagnosed early breast cancer on psychological resilience, distress levels, and the perception of health. *Int J Environ Res Public Health*. 2024;21(6):677. doi:10.3390/ijerph21060677

Cognitive impairment in liver transplant candidates: The role of blood ammonia level and three-point evaluation of brain MRI

Magdalena Grusiecka-Stańczyk[1,B–D,F], Maciej K. Janik[1,C–F], Piotr Olejnik[2,B,F], Aleksandra Golenia[3,B,C,E,F], Jolanta Małyszko[4,C,E,F], Joanna Raszeja-Wyszomirska[1,A,C–F]

[1] Department of Hepatology, Transplantology and Internal Medicine, Medical University of Warsaw, Poland
[2] Student, Faculty of Medicine, Medical University of Warsaw, Poland
[3] Department of Neurology, Medical University of Warsaw, Poland
[4] Department of Nephrology, Dialysis and Internal Medicine, Medical University of Warsaw, Poland

A – research concept and design; B – collection and/or assembly of data; C – data analysis and interpretation; D – writing the article; E – critical revision of the article; F – final approval of the article

Advances in Clinical and Experimental Medicine, ISSN 1899–5276 (print), ISSN 2451–2680 (online) *Adv Clin Exp Med*. 2026;35(2):243–251

Address for correspondence
Joanna Raszeja-Wyszomirska
E-mail: joanna.wyszomirska@wum.edu.pl

Funding sources
None declared

Conflict of interest
None declared

Received on July 17, 2024
Reviewed on November 22, 2024
Accepted on May 8, 2025

Published online on January 13, 2026

Abstract

Background. Cognitive impairment (CI) is common in patients with alcohol-use disorder (AUD)-related liver cirrhosis, especially those awaiting liver transplantation (LT). There are conflicting results in terms of the role of hepatic encephalopathy (HE) in CI development and persistence.

Objectives. This study investigated the impact of hyperammonemia on CI and evaluated the role of routine magnetic resonance imaging (MRI) in detecting CI among patients with AUD-related cirrhosis listed for LT at a single center.

Materials and methods. Fifty-two adults (36 males, 69%) with AUD-related liver cirrhosis (mean age: 51 ±11 years; mean Model for End-Stage Liver Disease (MELD) score 16 ±6) were evaluated. Cognitive function was assessed using the Addenbrooke's Cognitive Examination III (ACE-III), with scores below 82 indicating probable dementia. Magnetic resonance imaging evaluations focused on cortical-subcortical atrophy, vascular-origin changes, and chronic HE.

Results. Magnetic resonance imaging revealed HE-related changes in 38 patients (73%), vascular-origin changes in 32 patients (62%), and cortical-subcortical atrophy in 15 patients (29%). Cognitive impairment was present in 46 patients (88%), with 30 (58%) suspected of having dementia. Patients with MRI evidence of HE scored lower in the ACE III language subdomain ($p = 0.032$) and tended toward a higher Child–Pugh classification ($p = 0.083$). No significant differences were found in ACE-III results or clinical data between patients with and without vascular-origin changes or cortical–subcortical atrophy. Additionally, no correlations were observed between radiological findings, ammonia levels, ACE-III scores, and liver-related mortality.

Conclusions. These findings reveal a high prevalence of CI and significant MRI abnormalities in AUD patients awaiting LT. Further studies are needed to clarify the role of routine MRI in detecting cognitive deficits.

Key words: cognitive impairment, liver transplantation, brain magnetic resonance, alcohol-related liver cirrhosis, blood ammonia level

Cite as
Grusiecka-Stańczyk M, Janik MK, Olejnik P, Golenia A, Małyszko J, Raszeja-Wyszomirska J. Cognitive impairment in liver transplant candidates: The role of blood ammonia level and three-point evaluation of brain MRI. *Adv Clin Exp Med*. 2026;35(2):243–251. doi:10.17219/acem/204837

DOI
10.17219/acem/204837

Highlights

- Cognitive impairment was detected in 88% of AUD-related cirrhosis patients awaiting liver transplantation. Routine MRI showed brain atrophy or vascular changes in over 60% of candidates.
- No MRI features or ammonia levels significantly predicted cognitive performance.
- Liver functional reserve (Child-Pugh score) showed a non-significant trend with cognitive decline.

Background

Alcohol-use disorder (AUD), as defined by the Diagnostic and Statistical Manual of Mental Disorders (DSM-5), encompasses maladaptive patterns of alcohol use that lead to significant clinical consequences.[1] Chronic alcohol consumption often leads to liver cirrhosis, one of the primary indications for liver transplantation (LT).[2,3] Hepatic encephalopathy (HE), a severe neuropsychiatric syndrome associated with liver cirrhosis, arises from elevated ammonia and inflammation, resulting in low-grade cerebral edema, oxidative/nitrosative stress, inflammation, and disrupted brain oscillatory networks.[4] While blood ammonia serves as a biomarker with good negative predictive value for HE,[5,6] alcohol independently causes neurotoxic effects, damaging brain regions such as the frontal lobe, cerebellum and limbic system, including the hippocampus,[7,8] which further impairs brain function. Thus, chronic alcohol use and liver dysfunction are clearly linked to cognitive impairment (CI), likely through disruption of frontal–subcortical circuits and associated neurotransmitter imbalances.

Patients with liver cirrhosis commonly experience CI before LT, with recovery post-transplant varying in extent and timeline.[9,10] The history of HE appears to influence post-transplant recovery of brain function and connectivity.[8] Various factors, including minimal and overt HE, chronic alcohol use, and gut microbial dysbiosis, contribute to cognitive impairments in cirrhosis. Prolonged alcohol use is particularly associated with marked deficits in executive function, attention, motor skills, spatial reasoning, language, and memory.[11,12] Alcohol-induced neuroinflammation further reduces hippocampal white matter and prefrontal cortex volume, impairing memory and decision-making abilities.[7,13] Magnetic resonance imaging (MRI) remains a valuable tool for monitoring brain changes and evaluating recovery potential after transplantation, underscoring its importance in elucidating the neurobiological basis of CI in alcohol-related liver disease (ALD) and HE. Despite its clinical importance, detailed analysis of brain MRI findings is not readily available in routine practice.

In ALD, chronic alcohol consumption leads to significant cognitive deficits, particularly in executive function, memory and attention, through neurotoxic effects that disrupt glutamate and GABA neurotransmitter balance and impair the frontal–subcortical circuits essential for cognitive processing and behavioral regulation.[13] Alcohol also induces brain inflammation and oxidative stress, leading to structural and functional alterations. MRI studies show that patients with ALD often exhibit reduced gray matter in the frontal cortex and subcortical regions, changes that correlate with cognitive decline and increased susceptibility to HE.[13]

In HE, elevated ammonia disrupts astrocyte function, leading to increased glutamine levels, astrocyte swelling, and cerebral edema.[13] These changes impair neurotransmitter metabolism, manifesting as deficits in attention, reaction time and executive function. Hepatic encelopathy-related CI is associated with MRI abnormalities in the basal ganglia due to manganese deposition from chronic liver disease.[14] Ammonia accumulation also disrupts dopaminergic, glutamatergic and serotonergic pathways, further affecting frontal–subcortical circuits critical for cognitive processing.[14,15]

The MRI findings in HE patients frequently show basal ganglia abnormalities and cerebral edema, likely from astrocyte swelling and metabolic disruptions.[14,15] Even after transplantation, cognitive impairments, particularly in attention and executive function, often persist and are associated with reduced volumes in the frontal lobe and basal ganglia.[14,15] Cognitive deficits in ALD and HE primarily result from disruptions in frontal–subcortical circuits caused by alcohol-induced dysregulation of glutamate and GABA, compounded by the neurotoxic effects of ammonia, as noted above. Ammonia also damages astrocytes, which are essential for detoxification and neurotransmitter balance, further impairing neural communication between the basal ganglia and frontal cortex.[15] The impact of ammonia on astrocyte function underscores the need for early intervention to prevent cognitive decline in LT candidates.

Objectives

This study examines the predictive value of 3-point routine brain MRI evaluations for cognitive impairment in consecutive liver transplant candidates with alcohol use disorder-related liver cirrhosis at a single transplant center.

Materials and methods

Participants

A total of 52 adult patients (69% male, comprising 36 men and 16 women) with a mean age of 51 ±11 years, all diagnosed with AUD-related liver cirrhosis, were identified as potential candidates for LT in a single liver transplant center. The mean Model for End-Stage Liver Disease (MELD) score was 16 ±6, indicating an advanced stage of liver disease in the study cohort. The main indication for LT assessment in AUD patients was chronic liver failure (87%). However, 13% of patients had hepatocellular carcinoma (HCC) as the indication for LT.

Study design

All patients included in this cross-sectional, single-center study were admitted in 2023 to the Department of Hepatology, Transplantology, and Internal Medicine at the Medical University of Warsaw (Poland) for evaluation prior to listing for liver transplantation (LT). The work-up included biochemical and serological testing, cardiology and pulmonology assessments, and imaging studies, including brain MRI. The exclusion criteria included regular intake of hypnotics, severe overt HE and psychiatric or neurodegenerative diseases, making it impossible to perform the investigation. Blood ammonia levels were routinely measured as part of the laboratory work-up for all participants.

Cognitive assessment

Cognitive function was assessed using the Addenbrooke Cognitive Examination III (ACE III), which is a comprehensive tool designed to detect CI across various domains. A cutoff score of less than 82 on the ACE III was utilized to identify patients with a high likelihood of dementia. The ACE III covers cognitive domains such as attention, memory, verbal fluency, language, and visuospatial abilities. The Polish version is available free of charge.[16] The ACE-III has been previously validated against standard neuropsychological tests.[17] In addition, our center has prior experience with this tool, reflected in previously published projects.[18,19] All patients were routinely examined during their stay in the hospital by a psychiatrist dedicated to the transplant program, according to the pre-transplant work-up protocol, which consists of full psychiatric consultation, as well as the ACE III tool. The "liver-related mortality" was defined as a death occurring during the study.

Magnetic resonance imaging evaluation

Each patient underwent brain MRI using Siemens Magnetom Avanto 1.5T (Siemens AG, Erlangen, Germany) as part of their routine pre-transplant assessment. The MRI scans were evaluated using a standardized 3-point approach, focusing on the assessment of cortical-subcortical atrophy, a semi-quantitative evaluation of vascular-related changes, and the identification of features consistent with chronic HE. All MRI images were analyzed by experienced radiologists blinded to the cognitive functions assessment results and venous blood ammonia level. Organic brain changes in MRI, including cortical-subcortical atrophy, vascular-origin alterations and HE-related abnormalities, were systematically assessed and described using the Fazekas scale to ensure clarity and reproducibility. The results from these MRI scans were then correlated with cognitive test scores and clinical parameters.

Blood ammonia measurement

Fasting venous blood samples were collected from all subjects to assess blood ammonia concentration. Measurements were performed in ethylenediaminetetraacetic acid (EDTA) plasma using the enzymatic glutamate dehydrogenase (GLDH) method on the Dimension EXL analyzer (Siemens Healthineers, Forchheim, Germany). Reference values were 19–55 μg/dL.

Ethics

Appropriate informed consent was obtained from each patient included in the study. The study protocol was approved by the Bioethics Committee of the Medical University of Warsaw (approval No. KB/81/2022 and amendment No. KB42/A 2025) and was conducted in accordance with the ethical guidelines of the 1975 Declaration of Helsinki (6^{th} revision, 2008).

Statistical analyses

All statistical analyses were performed using IBM SPSS Statistics v. 29.0 (IBM Corp., Armonk, USA) and Python v. 3.10 (https://www.python.org/downloads/release/python-3100; SciPy and StatsModels packages) for advanced corrections. The normality of continuous variables was assessed using the Shapiro–Wilk and Kolmogorov–Smirnov tests. Due to the non-normal distribution of key variables, including MELD, ACE III scores, and blood ammonia levels, nonparametric tests were applied for both group comparisons and correlation analyses.

Continuous variables are presented as median (Q1–Q3) for non-normally distributed data and as mean ± standard deviation (SD) when normally distributed. Categorical variables are expressed as absolute numbers and percentages.

Group comparisons between patients with positive (ACE III < 82) and negative screening results were conducted using the Mann–Whitney U test for continuous variables and Pearson's χ^2 test or Fisher's exact test for categorical variables, depending on expected cell frequencies. The χ^2 test assumptions were verified by calculating expected

frequencies, which are presented in the Supplementary Table 1 (https://doi.org/10.5281/zenodo.17104342).

Correlations were evaluated using Spearman's rank correlation coefficient due to the nonparametric nature of the data. The analyses examined associations between MRI features (HE signs, vascular-origin changes and cortical–subcortical atrophy) and ACE-III total and domain scores; clinical parameters (Child–Pugh score, MELD score and blood ammonia) and cognitive function; and ACE-III total scores and both radiological features and clinical variables.

To control for multiple comparisons, the Benjamini–Hochberg false discovery rate (FDR) correction was applied across all sets of correlation analyses and group comparisons involving multiple variables. This method was chosen over Bonferroni to maintain statistical power while limiting false discoveries in an exploratory context.

Statistical results are reported with appropriate test statistics (U, χ^2, r), degrees of freedom where relevant and p-values rounded to 3 decimal places. The p-values less than 0.001 are reported as $p < 0.001$. An FDR-corrected $p < 0.05$ was considered statistically significant, and such results are marked with an asterisk in the tables.

Results

The clinical characteristics of the study cohort are summarized in Table 1. The median Model of End-Stage Liver Disease-Sodium (MELD-Na) score was 16 (Q1–Q3: 12–19) points, while the median Child–Pugh score was 8 (7–9) points. The median venous blood ammonia concentration was 83.5 µg/dL (Q1–Q3: 53–108), with 24 patients (46%) showing hyperammonemia, defined as > 55 µg/dL.

The median ACE III score across the entire cohort was 79 points (Q1–Q3: 69–88); 46 patients (88%) displayed impaired cognitive performance, as indicated by an ACE III score below 89 points, and 30 patients (58%) met the criteria for high probability of dementia, defined by an ACE III score below 82 points.

Radiological signs consistent with HE were observed in brain MRI scans of 38 patients (73%). These patients did not significantly differ from others in terms of age, sex, venous blood ammonia levels, MELD-Na scores, or total ACE III results (Mann–Whitney U test or Pearson's χ^2 test; all FDR-corrected $p > 0.05$). Although the uncorrected analysis showed lower language domain scores in patients with radiological signs of HE ($U = 207.5$, $p = 0.032$), this association was no longer significant after correction for multiple comparisons (FDR-adjusted $p = 0.067$). Similarly, a trend toward higher Child–Pugh classifications in these patients ($U = 338.5$, uncorrected $p = 0.083$) did not reach statistical significance after FDR correction.

Spearman's correlation analyses revealed no statistically significant associations, after correction for multiple comparisons, between any of the evaluated MRI features (HE, vascular-origin changes, cortical–subcortical atrophy) and ACE III total or domain scores. Full results are presented in Table 2.

Vascular-origin changes were reported in 32 patients (62%). Uncorrected comparisons showed a significant association with lower total ACE III scores (χ^2 test, $p = 0.045$), but this finding was not significant after FDR correction (adjusted $p = 0.090$). No associations were found between vascular-origin changes and clinical variables or hyperammonemia (FDR-adjusted $p > 0.05$).

Cortical–subcortical atrophy was identified in MRI scans of 15 patients (29%). Uncorrected analyses showed an association between atrophy and CI (χ^2 test, $p = 0.038$), but this finding did not remain significant after FDR correction (adjusted $p = 0.081$). No significant relationships were observed between cortical-subcortical atrophy and age, sex, ammonia levels (quantitative or categorical), MELD-Na, or Child–Pugh scores.

Table 1. Clinical characteristics of the study cohort and the subgroups of patients with positive and negative screening in ACE III Test for dementia (i.e., <82 points) in relation to demographic, clinical and imaging results

Variable	Total cohort (n = 52)	ACE III < 82 (n = 30)	ACE III ≥ 82 (n = 22)	Statistical test	Test statistic	p-value	FDR-corrected p-value
Age [years]	51.0 (44.0–59.0)	55.0 (44.5–59.0)	49.5 (43.8–54.5)	Mann–Whitney U	374.000	0.420	0.864
Gender (male %)	0 (0%)	0 (0%)	0 (0%)	Fisher's Exact	0.918	1.000	1.000
MELD score	15.0 (11.0–20.2)	16.0 (12.2–20.8)	13.0 (10.2–20.0)	Mann–Whitney U	370.000	0.463	0.864
Child–Pugh score	8.0 (7.0–10.0)	8.0 (7.2–11.0)	8.5 (6.0–9.8)	Mann–Whitney U	398.500	0.202	0.864
Blood ammonia [µg/dL]	73.0 (52.1–123.9)	80.2 (55.1–129.6)	64.3 (51.3–89.0)	Mann–Whitney U	370.000	0.464	0.864
MRI: signs of hepatic encephalopathy	38 (73%)	23 (77%)	15 (68%)	Fisher's Exact	0.652	0.540	0.864
MRI: vascular-origin changes	52 (100%)	30 (100%)	22 (100%)	χ^2	0.000	1.000	1.000
MRI: cortical-subcortical atrophy	52 (100%)	30 (100%)	22 (100%)	χ^2	0.000	1.000	1.000

All p-values were calculated using the Mann–Whitney U test or Fisher's exact test, where appropriate. False discovery rate (FDR) correction was applied using the Benjamini–Hochberg method. ACE III – Addenbrooke Cognitive Test III; HE – hepatic encephalopathy; MELD – Model of End-Stage Liver Disease; MRI – magnetic resonance imaging.

Table 2. Correlations between impairments in MRI of the brain and domains of The Addenbrooke Cognitive Test III in liver transplant recipients

MRI feature	ACE III domain	Spearman's r	p-value	n	FDR-corrected p-value
MRI: signs of hepatic encephalopathy	ACE III total	–0.169	0.231	52	0.655
MRI: signs of hepatic encephalopathy	Attention	–0.182	0.196	52	0.655
MRI: signs of hepatic encephalopathy	Memory	–0.009	0.951	52	0.951
MRI: signs of hepatic encephalopathy	Fluency	–0.096	0.498	52	0.748
MRI: signs of hepatic encephalopathy	Language	–0.299	0.032	52	0.555
MRI: signs of hepatic encephalopathy	Visuo-spatial abilities	–0.236	0.093	52	0.555
MRI: vascular-origin changes	ACE III Total	0.049	0.731	52	0.802
MRI: vascular-origin changes	Attention	0.258	0.065	52	0.555
MRI: vascular-origin changes	Memory	0.149	0.291	52	0.655
MRI: vascular-origin changes	Fluency	–0.11	0.437	52	0.748
MRI: vascular-origin changes	Language	0.064	0.652	52	0.782
MRI: vascular-origin changes	Visuo-spatial abilities	0.126	0.373	52	0.747
MRI: cortical-subcortical atrophy	ACE III Total	0.096	0.497	52	0.748
MRI: cortical-subcortical atrophy	Attention	0.074	0.603	52	0.775
MRI: cortical-subcortical atrophy	Memory	–0.044	0.757	52	0.802
MRI: cortical-subcortical atrophy	Fluency	0.08	0.574	52	0.775
MRI: cortical-subcortical atrophy	Language	0.198	0.16	52	0.655
MRI: cortical-subcortical atrophy	Visuo-spatial abilities	0.157	0.267	52	0.655

Spearman's rank correlation was used to assess the association between MRI features and cognitive test performance (ACE III total and domain scores). The p-values were corrected for multiple comparisons using the Benjamini–Hochberg False Discovery Rate (FDR) method. ACE III – Addenbrooke Cognitive Test III; HE – hepatic encephalopathy; MELD – Model of End-Stage Liver Disease; MRI – magnetic resonance imaging; *FDR-corrected $p < 0.05$.

Table 3. The correlations of ACE III total score and its domains with Child–Pugh Score, MELD-Na Score, and venous ammonia levels

Row type	Variable	ACE III	Attention	Memory	Fluency	Langugage	Visuo-spatial abilities
Spearman's r	Child–Pugh score	–0.283	–0.443*	–0.053	–0.223	–0.433*	–0.282
Spearman's r	MELD-Na score	–0.093	–0.226	0.045	–0.1	–0.222	–0.109
Spearman's r	venous ammonia level	–0.127	–0.243	–0.083	–0.076	–0.094	–0.247
p-value (FDR corrected)	Child–Pugh score	0.194	0.0123	0.753	0.226	0.0123	0.194
p-value (FDR corrected)	MELD-Na score	0.659	0.226	0.753	0.659	0.226	0.659
p-value (FDR corrected)	venous ammonia level	0.659	0.226	0.669	0.669	0.659	0.226

Spearman's rank correlation was used to assess associations between clinical parameters and ACE III total and domain scores; p-values were corrected for multiple comparisons using the Benjamini–Hochberg false discovery rate (FDR) method. ACE III – Addenbrooke Cognitive Test III; HE – hepatic encephalopathy; MELD – Model of End-Stage Liver Disease; MRI – magnetic resonance imaging. *FDR-corrected p-values < 0.05.

Table 3 presents the correlations between ACE III total and domain scores with clinical parameters, including blood ammonia, MELD-Na, and Child–Pugh scores. No significant correlations were observed between ammonia or MELD-Na and cognitive performance (Spearman's r, all FDR-adjusted $p > 0.05$). While uncorrected correlations suggested a relationship between Child–Pugh scores and ACE III total, attention, language, and visuospatial abilities, none of these remained significant after FDR correction. Scatterplots illustrating selected relationships between cognitive domains and clinical/imaging features are presented in Fig. 1.

Five patients (9.6%) died during the study period, all following liver transplantation due to infection and/or surgical complications. No significant differences in mortality were found between patients with or without radiological signs of HE, vascular-origin changes or cortical-subcortical atrophy, nor between CI groups (ACE III < 82 vs ≥ 82) (Pearson's χ^2 test, all $p > 0.05$).

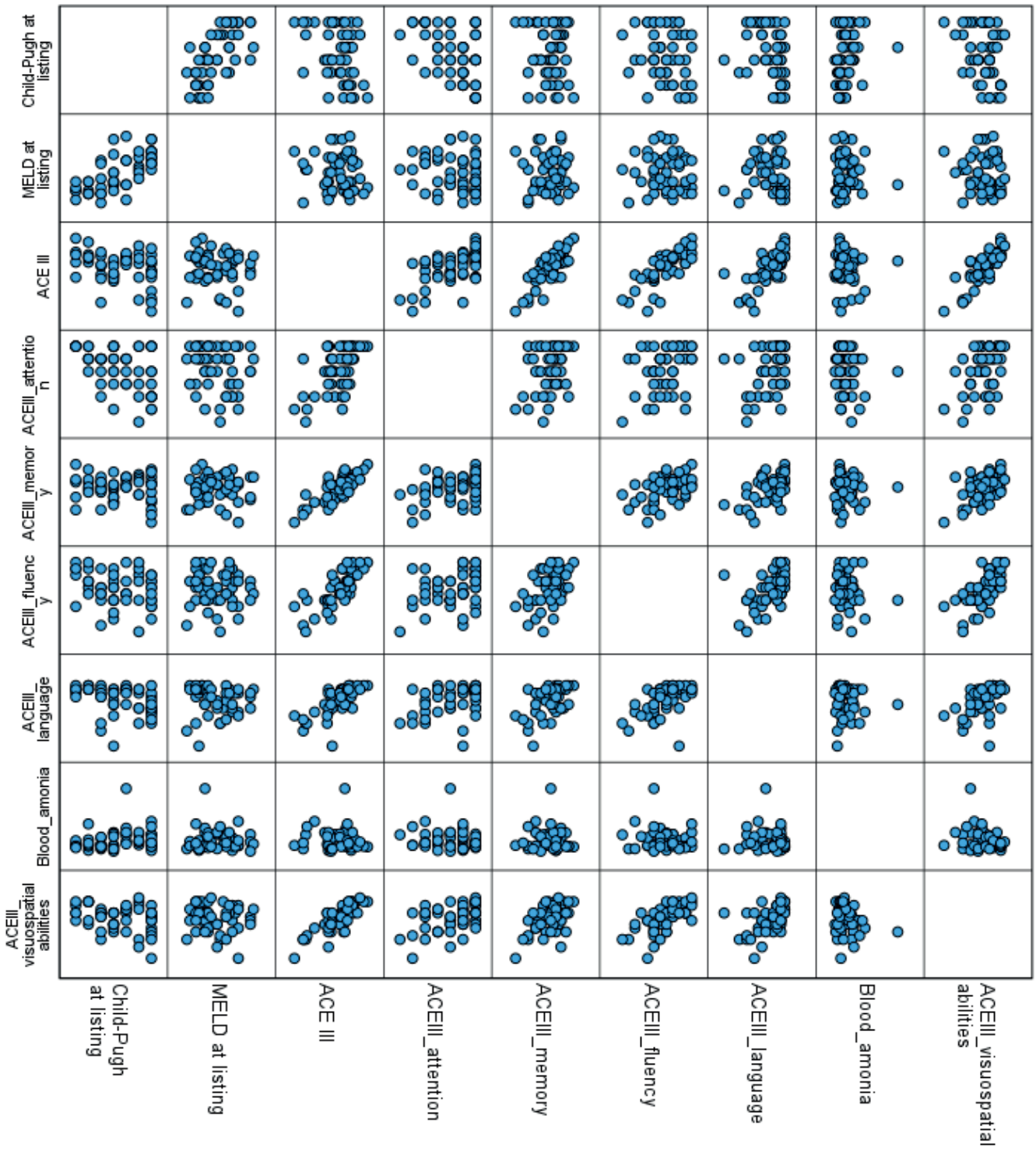

Fig. 1. Scatterplots illustrating the relationship between variables tested with Spearman's rank correlation coefficient

Discussion

The findings from this study confirm a high prevalence of CI among liver transplant candidates with end-stage liver disease (ESLD) related to AUD. This homogeneous cohort of AUD patients revealed a concerning frequency of structural brain changes on routine MRI. While numerous studies have investigated cognitive dysfunction in patients with hepatitis C and non-alcoholic fatty liver disease (NAFLD) using advanced imaging techniques (e.g., magnetic resonance spectroscopy (MRS), functional MRI,[20–22] such tools remain largely unavailable in routine pre-transplant care. Most standard clinical brain MRI reports do not include quantitative metrics such as mean diffusivity or fractional anisotropy.[23,24] Therefore, our study underscores the value of assessing cognitively vulnerable

ESLD patients using accessible and widely available neuroimaging tools.

Our data showed that vascular-origin changes and cortical-subcortical atrophy were frequent, even in a relatively young population (mean age: 51 years). Additionally, a striking proportion of patients demonstrated moderate-to-severe CI, with more than half meeting criteria for high dementia probability based on ACE III. This level of dysfunction may impact transplant candidacy through impaired treatment adherence and increased post-transplant risks, including graft rejection.[10]

Contrary to our initial assumptions, no significant correlations were found between radiological features and cognitive test scores after correction for multiple comparisons. Although patients with signs of HE showed lower scores in the language domain of the ACE III in uncorrected analysis, this finding did not remain statistically significant following FDR adjustment. Similarly, no MRI feature (including vascular-origin changes and atrophy) was significantly associated with cognitive performance in domain-level correlations.

These findings align with the growing understanding that blood ammonia levels, often central to the HE narrative, are unreliable markers of cognitive status in ESLD.[4–6] Our study confirms that ammonia levels were not correlated with ACE III total or domain scores, reinforcing the notion that multiple metabolic and systemic variables confound its interpretation.[25]

Contributing factors include individual variation in urea cycle function, dietary protein intake and hydration status, all of which can affect ammonia levels without reflecting cognitive decline. Additionally, limited access to anti-ammonia therapies (e.g., lactulose, rifaximin), whether due to cost constraints or poor adherence, may further confound this relationship in real-world settings.

The role of HE in long-term CI remains debated. Although LT improves ammonia clearance, persistent deficits post-transplantation have been widely reported.[12,26] Some studies suggest that structural brain damage from prior HE episodes may be irreversible,[9,27] whereas others report partial reversal of MRI abnormalities after transplantation.[28] Notably, Bajaj et al.[29] found that episodes of overt HE led to persistent deficits in working memory and response inhibition. Similarly, studies by Adejumo et al.[30] and Lopez-Franco et al.[31] point to a relationship between HE and dementia that may persist beyond the transplant period. However, evidence remains conflicting. While Ko et al.[32] did not find a clear link between pre- and post-transplant cognition, Berry et al.[33] highlighted pre-transplant CI as the strongest predictor of post-transplant dysfunction. Cheng et al.[34] demonstrated persistent abnormalities in functional brain connectivity in patients with prior HE, especially in regions responsible for higher-order cognition.

Our analysis identified a consistent, though uncorrected, association between cognitive performance and liver functional reserve, particularly the Child–Pugh score. This aligns with known links between advanced liver dysfunction, metabolic alterations and cognitive deficits.[35,36] However, after FDR correction, these associations lost statistical significance, suggesting the need for cautious interpretation. The trend may reflect the combined impact of malnutrition, systemic inflammation and energy metabolism deficits.[11,37]

The MELD score, which does not account for albumin or nutritional status, was not related to cognitive outcomes. This discrepancy further supports the theory that chronic nutritional deficits, captured in part by the Child–Pugh classification, may be more relevant in assessing cognitive vulnerability in this population. The high prevalence of CI in our ESLD cohort also exceeds that reported in kidney transplant recipients.[38]

Limitations

This single-center study addressed a critical gap in transplantology by focusing on AUD patients with ESLD – a clinically uniform group often underrepresented in cognitive research. Nevertheless, the sample size limits generalizability, and the lack of comprehensive neuropsychological testing or DSM-5-based diagnoses precludes a definitive classification of cognitive disorders.

While the ACE III is a robust screening tool, it cannot replace a detailed diagnostic evaluation. Additionally, the cross-sectional design prevents inferences regarding the trajectory of cognitive dysfunction, either pre- or post-transplant. Further studies should explore how routine MRI findings relate to post-LT outcomes, particularly in the presence or absence of HE history.

Conclusions

This study confirms the high prevalence of CI among liver transplant candidates with ESLD. Although structural brain abnormalities were frequently observed, they were not significantly associated with cognitive test outcomes after adjustment for multiple comparisons. Similarly, blood ammonia levels did not predict cognitive function.

Although subtle trends were observed between the Child–Pugh score and ACE III performance, these did not reach statistical significance after FDR correction. Our findings support growing evidence that cognitive dysfunction in ESLD may be multifactorial, involving metabolic, nutritional and neuroinflammatory pathways beyond hyperammonemia alone. Future research should aim to refine neuroimaging biomarkers and integrate broader systemic assessments to better characterize cognitive risk in this vulnerable population.

Supplementary data

The supplementary materials are available at https://doi.org/10.5281/zenodo.17104342. The package includes the following files:

Supplementary Table 1. Expected frequencies for categorical variables analyzed with the χ^2 test.

Data availability

The datasets generated and/or analyzed during the current study are available from the corresponding author on reasonable request.

Consent for publication

Not applicable

Use of AI and AI-assisted technologies

During the preparation of this work the authors used Chat GPT in order to improve language and readability. After using this tool/service, the authors reviewed and edited the content as needed and take full responsibility for the content of the publication.

ORCID iDs

Maciej K. Janik https://orcid.org/0000-0003-1941-0336
Piotr Olejnik https://orcid.org/0000-0003-1984-1566
Aleksandra Golenia https://orcid.org/0000-0002-7720-5253
Jolanta Małyszko https://orcid.org 0000-0001-8701-8171
Joanna Raszeja-Wyszomirska https://orcid.org/0000-0001-7204-9784

References

1. Gitto S, Aspite S, Golfieri L, et al. Alcohol use disorder and liver transplant: New perspectives and critical issues. *Korean J Intern Med*. 2020;35(4):797–810. doi:10.3904/kjim.2019.409
2. Ntandja Wandji LC, Ningarhari M, Lassailly G, et al. Liver transplantation in alcohol-related liver disease and alcohol-related hepatitis. *J Clin Exp Hepatol*. 2023;13(1):127–138. doi:10.1016/j.jceh.2022.06.013
3. Philip G, Hookey L, Richardson H, Flemming JA. Alcohol-associated liver disease is now the most common indication for liver transplant waitlisting among young American adults. *Transplantation*. 2022;106(10):2000–2005. doi:10.1097/TP.0000000000004202
4. Häussinger D, Dhiman RK, Felipo V, et al. Hepatic encephalopathy. *Nat Rev Dis Primers*. 2022;8(1):43. doi:10.1038/s41572-022-00366-6
5. Montagnese S, Rautou PE, Romero-Gómez M, et al. EASL Clinical Practice Guidelines on the management of hepatic encephalopathy. *J Hepatol*. 2022;77(3):807–824. doi:10.1016/j.jhep.2022.06.001
6. Vilstrup H, Amodio P, Bajaj J, et al. Hepatic encephalopathy in chronic liver disease: 2014 Practice Guideline by the American Association for the Study Of Liver Diseases and the European Association for the Study of the Liver. *Hepatology*. 2014;60(2):715–735. doi:10.1002/hep.27210
7. Harper C. The neuropathology of alcohol-related brain damage. *Alcohol Alcohol*. 2009;44(2):136–140. doi:10.1093/alcalc/agn102
8. Oscar-Berman M, Marinković K. Alcohol: Effects on neurobehavioral functions and the brain. *Neuropsychol Rev*. 2007;17(3):239–257. doi:10.1007/s11065-007-9038-6
9. Campagna F, Montagnese S, Schiff S, et al. Cognitive impairment and electroencephalographic alterations before and after liver transplantation: What is reversible? *Liver Transplant*. 2014;20(8):977–986. doi:10.1002/lt.23909
10. Golfieri L, Gitto S, Vukotic R, et al. Impact of psychosocial status on liver transplant process. *Ann Hepatol*. 2019;18(6):804–809. doi:10.1016/j.aohep.2019.06.011
11. King JA, Nephew BC, Choudhury A, Poirier GL, Lim A, Mandrekar P. Chronic alcohol-induced liver injury correlates with memory deficits: Role for neuroinflammation. *Alcohol*. 2020;83:75–81. doi:10.1016/j.alcohol.2019.07.005
12. Tryc AB, Pflugrad H, Goldbecker A, et al. New-onset cognitive dysfunction impairs the quality of life in patients after liver transplantation. *Liver Transplant*. 2014;20(7):807–814. doi:10.1002/lt.23887
13. Oscar-Berman M, Marinkovic K. Alcoholism and the brain: An overview. *Alcohol Res Health*. 2003;27(2):125–133. PMID:15303622. PMCID:PMC6668884.
14. Di Gregorio F, Battaglia S. Advances in EEG-based functional connectivity approaches to the study of the central nervous system in health and disease. *Adv Clin Exp Med*. 2023;32(6):607–612. doi:10.17219/acem/166476
15. Tanaka M, Vécsei L. A decade of dedication: Pioneering perspectives on neurological diseases and mental illnesses. *Biomedicines*. 2024;12(5):1083. doi:10.3390/biomedicines12051083
16. Sitek EJ, Barczak A, Senderecka M. A qualitative analysis of the ACE-III profile in the differential diagnosis of dementia syndromes. *Aktualn Neurol*. 2017;17(1):34–41. doi:10.15557/AN.2017.0004
17. Takenoshita S, Terada S, Yoshida H, et al. Validation of Addenbrooke's cognitive examination III for detecting mild cognitive impairment and dementia in Japan. *BMC Geriatr*. 2019;19(1):123. doi:10.1186/s12877-019-1120-4
18. Golenia A, Olejnik P, Żołek N, Wojtaszek E, Małyszko J. Cognitive impairment and anxiety are prevalent in kidney transplant recipients. *Kidney Blood Press Res*. 2023;48(1):587–595. doi:10.1159/000533755
19. Golenia A, Żołek N, Olejnik P, Żebrowski P, Małyszko J. Patterns of cognitive impairment in hemodialysis patients and related factors including depression and anxiety. *J Clin Med*. 2023;12(9):3119. doi:10.3390/jcm12093119
20. Petta S, Tuttolomondo A, Gagliardo C, et al. The presence of white matter lesions is associated with the fibrosis severity of nonalcoholic fatty liver disease. *Medicine (Baltimore)*. 2016;95(16):e3446. doi:10.1097/MD.0000000000003446
21. Prell T, Dirks M, Arvanitis D, et al. Cerebral patterns of neuropsychological disturbances in hepatitis C patients. *J Neurovirol*. 2019;25(2):229–238. doi:10.1007/s13365-018-0709-2
22. Weinstein G, Zelber-Sagi S, Preis SR, et al. Association of nonalcoholic fatty liver disease with lower brain volume in healthy middle-aged adults in the Framingham Study. *JAMA Neurol*. 2018;75(1):97. doi:10.1001/jamaneurol.2017.3229
23. Filipović B, Marković O, Đurić V, Filipović B. Cognitive changes and brain volume reduction in patients with nonalcoholic fatty liver disease. *Can J Gastroenterol Hepatol*. 2018;2018:9638797. doi:10.1155/2018/9638797
24. Thames AD, Castellon SA, Singer EJ, et al. Neuroimaging abnormalities, neurocognitive function, and fatigue in patients with hepatitis C. *Neurol Neuroimmunol Neuroinflammation*. 2015;2(1):e59. doi:10.1212/NXI.0000000000000059
25. Shawcross DL, Davies NA, Williams R, Jalan R. Systemic inflammatory response exacerbates the neuropsychological effects of induced hyperammonemia in cirrhosis. *J Hepatol*. 2004;40(2):247–254. doi:10.1016/j.jhep.2003.10.016
26. Skibsted Kornerup L, Pflugrad H, Weissenborn K, Vilstrup H, Dam G. Cognitive impairment after liver transplantation: Residual hepatic encephalopathy or posttransplant encephalopathy? *Hepat Med*. 2019;11:41–46. doi:10.2147/HMER.S144667
27. Garcia-Martinez R, Rovira A, Alonso J, et al. Hepatic encephalopathy is associated with posttransplant cognitive function and brain volume. *Liver Transplant*. 2011;17(1):38–46. doi:10.1002/lt.22197
28. Long LL, Li XR, Huang ZK, Jiang YM, Fu SX, Zheng W. Relationship between changes in brain MRI and ^{1}H-MRS, severity of chronic liver damage, and recovery after liver transplantation. *Exp Biol Med (Maywood)*. 2009;234(9):1075–1085. doi:10.3181/0903-RM-118

29. Bajaj JS, Schubert CM, Heuman DM, et al. Persistence of cognitive impairment after resolution of overt hepatic encephalopathy. *Gastroenterology*. 2010;138(7):2332–2340. doi:10.1053/j.gastro.2010.02.015
30. Adejumo A, Noll A, Rogal SS, et al. Dementia frequently coexists with hepatic encephalopathy but not other cirrhosis complications in US veterans. *Am J Gastroenterol*. 2023;118(3):475–480. doi:10.14309/ajg.0000000000002189
31. López-Franco Ó, Morin JP, Cortés-Sol A, et al. Cognitive impairment after resolution of hepatic encephalopathy: A systematic review and meta-analysis. *Front Neurosci*. 2021;15:579263. doi:10.3389/fnins.2021.579263
32. Ko D, Bratzke LC. Cognitive function in liver transplant recipients who survived more than 6 months. *Prog Transpl*. 2020;30(4):335–341. doi:10.1177/1526924820958144
33. Berry K, Ruck JM, Barry F, et al. Prevalence of cognitive impairment in liver transplant recipients. *Clin Transplant*. 2024;38(1):e15229. doi:10.1111/ctr.15229
34. Cheng Y, Zhang G, Shen W, et al. Impact of previous episodes of hepatic encephalopathy on short-term brain function recovery after liver transplantation: A functional connectivity strength study. *Metab Brain Dis*. 2018;33(1):237–249. doi:10.1007/s11011-017-0155-5
35. Sun B, Zhao Y, Lu W, Chen Y. The relationship of malnutrition with cognitive function in the older Chinese population: Evidence from the Chinese Longitudinal Healthy Longevity Survey Study. *Front Aging Neurosci*. 2021;13:766159. doi:10.3389/fnagi.2021.766159
36. Sun T, Feng M, Manyande A, Xiang H, Xiong J, He Z. Regulation of mild cognitive impairment associated with liver disease by humoral factors derived from the gastrointestinal tract and MRI research progress: A literature review. *Front Neurosci*. 2023;17:1206417. doi:10.3389/fnins.2023.1206417
37. Miarka M, Gibiński K, Janik MK, et al. Sarcopenia: The impact on physical capacity of liver transplant patients. *Life*. 2021;11(8):740. doi:10.3390/life11080740
38. Golenia A, Olejnik P, Grusiecka-Stańczyk M, et al. Cognitive impairment in patients awaiting kidney and liver transplantation: A clinically relevant problem? *Brain Behav*. 2024;14(8):e3647. doi:10.1002/brb3.3647

Outcomes of the toe PIP joint transfer for IIIB hypoplastic thumb: Is it justified when pollicization is denied?

Michał Górecki[A–E], Piotr Czarnecki[A,E,F], Ewa Bręborowicz[C], Leszek Romanowski[E,F]

Department of Traumatology, Orthopedics and Hand Surgery, Poznań University of Medical Sciences, Poland

A – research concept and design; B – collection and/or assembly of data; C – data analysis and interpretation;
D – writing the article; E – critical revision of the article; F – final approval of the article

Advances in Clinical and Experimental Medicine, ISSN 1899–5276 (print), ISSN 2451–2680 (online) *Adv Clin Exp Med*. 2026;35(2):253–263

Address for correspondence
Michał Górecki
E-mail: michalmgorecki@gmail.com

Funding sources
The research was financed by a Big Research Grant (No. 5330) from statutory funding for young researchers – doctoral students for 2022 from Poznan University of Medical Sciences.

Conflict of interest
None declared

Received on March 17, 2025
Reviewed on April 7, 2025
Accepted on June 9, 2025

Published online on September 17, 2025

Abstract

Background. Amputation followed by index finger pollicization is the gold-standard treatment for type III B thumb hypoplasia. However, despite its high success rate, some parents decline this procedure because it results in a four-finger hand.

Objectives. To evaluate the outcomes of reconstructive surgery in eight patients with type III B thumb hypoplasia, stabilized using a non-vascularized proximal interphalangeal (PIP) joint harvested from the foot when parental consent for pollicization was not granted.

Materials and methods. The study cohort comprised 8 postoperative patients (mean follow-up: 7 years) who underwent reconstructive stabilization of a hypoplastic thumb using a PIP joint from the foot. Hand function was evaluated by measuring range of motion (ROM), thumb stability and length, grip strength, and performance on a manual manipulation test. Donor-site morbidity was assessed via foot examination following PIP joint harvest. Functional outcomes were further analyzed using specialized patient-reported questionnaires.

Results. Most patients achieved good thumb stability and a functional passive range of motion. Reconstructed thumbs averaged approx. 75% of the length of a normal thumb, and grip strength measured about 50% of that in the contralateral hand. Donor-site assessment revealed toe shortening in the majority of cases but no deficits in ambulation or weight-bearing. The overall complication rate was 25%, and most patients and their parents reported satisfaction with the treatment.

Conclusions. Thumb reconstruction with a non-vascularized PIP joint yields enhanced stability and reduced hypermobility, with outcomes comparable to those reported for similar techniques. This approach represents a viable alternative for patients whose parents decline pollicization.

Key words: proximal interphalangeal joint, Blauth IIIB, PIP joint transfer, thumb stabilization, thumb hypoplasia

Cite as
Górecki M, Czarnecki P, Bręborowicz E, Romanowski L. Outcomes of the toe PIP joint transfer for IIIB hypoplastic thumb: Is it justified when pollicization is denied? *Adv Clin Exp Med*. 2026;35(2):253–263. doi:10.17219/acem/206081

DOI
10.17219/acem/206081

Highlights

- Long-term results after stabilization of hypoplastic thumb type III B using foot proximal interphalangeal (PIP) joint transfer delivers durable thumb stability and enhanced grip function.
- PIP joint transfer from the foot serves as a reliable reconstructive alternative when pollicization is not accepted by parents.
- Significant improvements in operated-hand grip strength and stability were documented in extended follow-up assessments.
- Outcomes comparable to established thumb reconstruction techniques validate the efficacy of this non-pollicization approach.
- Patient-centered surgical choice: This method respects parental preference by providing functional thumb reconstruction without pollicization.

Background

Congenital disabilities affect approx. 1% of newborns, and upper limb anomalies account for about 10% of these cases. Thumb hypoplasia or aplasia, a form of radial longitudinal deficiency, represents only 11% of all hand anomalies. This condition can occur as an isolated defect or in association with syndromes such as Holt–Oram, Rubinstein–Taybi, Apert, VACTERL association (vertebral defects, anal atresia, cardiac defects, tracheo-esophageal fistula, renal anomalies, and limb abnormalities), Fanconi anemia, or congenital radial deficiency.[1–3]

The modified Blauth classification system, which relies on clinical assessment and radiographic imaging, is used to determine the severity of thumb hypoplasia and guide the choice of surgical intervention.[4,5] Thumb hypoplasia significantly compromises hand grip function, thereby impacting both the physical and mental development of affected children.[6] Surgical intervention plays a key role in reducing disability, supporting development, and minimizing everyday functional limitations. Early treatment is critical to avoid maladaptive grip patterns, which can hinder rehabilitation and proper grasp development once embedded in the brain's cortical representation.[6–8]

The choice of surgical procedure depends on the severity of the thumb defect, and cosmetic and ethical factors are also considered, which increasingly influence parents' decision-making.[5,9–11] In cases of type III B thumb hypoplasia, as classified by the modified Blauth system, the condition is marked by thumb shortening and narrowing, flattening of the thumb web space, and underdeveloped thenar muscles. Additional characteristics include underdevelopment of the flexor pollicis longus (FPL), extensor pollicis longus (EPL), extensor pollicis brevis (EPB), and abductor pollicis longus (APL) tendons, as well as the proximal 2/3 of the first metacarpal, coupled with instability of the metacarpophalangeal (MP) and carpometacarpal (CMC) joints. The preferred treatment for this defect is thumb amputation followed by pollicization of the index finger, which delivers good functional outcomes and high patient satisfaction rates.[2,12–15]

Although effective, thumb amputation is often declined by parents because it results in a 4-fingered hand. The literature provides limited data on reconstructive methods to stabilize hypoplastic thumbs, where hypermobility and instability are major causes of dysfunction.[9–11,16–23]

Objectives

This study aimed to evaluate the outcomes of reconstructive surgery in 8 patients who underwent thumb stabilization procedures using a non-vascularized PIP joint harvested from the foot. These procedures were performed only in cases where parents declined pollicization.[24]

Materials and methods

Study design

This is a retrospective study evaluating the objective and subjective outcomes of surgical treatment of patients from the hand surgery department, with a minimum follow-up of 1 year. The data were summarized and interpreted, and appropriate conclusions were drawn, comparing the results with similar alternative treatment techniques in the literature.

As part of the basic statistical evaluation, the median value of the studied variables was presented, and, additionally, a correlation analysis was performed using Spearman's correlation coefficient. The confidence interval at which a result was considered statistically significant was adopted for $p < 0.05$.

Ethical approval was waived by the institute's Bioethics Committee, which determined that this study did not constitute a medical experiment requiring formal review. The research was conducted in accordance with the Declaration of Helsinki (2013 revision).

Participants

Between 2000 and 2022, our hand surgery department treated 25 patients with type III B thumb hypoplasia whose parents declined gold-standard pollicization – due to the resulting 4-fingered hand – and instead opted for alternative reconstructive techniques. For this reason, we proposed and performed an alternative reconstructive surgery by stabilizing the hypoplastic thumb using a non-vascularized PIP joint from the foot. An additional inclusion criterion required that the affected thumb have no history of prior surgical intervention. The surgical technique and related procedural details have been described comprehensively in an earlier publication (Fig. 1).[24]

Eight patients participated in the study, including 4 girls (50%) and 4 boys (50%), aged 3–15 years, with an average age of 8 years and 6 months. The defect was unilateral in 7 cases and an isolated thumb defect in 5 cases. Three cases involved a complex upper extremity defect, such as congenital radial deficiency. One patient had additional diagnoses of congenital hearing loss, hydrocephalus, and thumb aplasia in the contralateral hand. The children underwent between 1 and 4 surgeries (median: 1.5), with thumb stabilization using PIP joint graft often being the 1st procedure performed. Additional procedures included wrist centralization and ulnar bone lengthening. The age at the time of surgery ranged from 1 year to 3.5 years, with the median age of 1 year. Five right hands and 3 left hands underwent surgical procedures. The donor PIP joint was harvested from the right foot 7 times and from the left foot once. In 75% (6/8) of the cases, the grafts were obtained from the same side as the operated hand. The 3rd toe was most frequently used as the donor site, accounting for 63% of the cases, while the 4th and 2nd toes were used as the donor sites in 25% (2) and 12% (1) of the cases, respectively. One patient (No. 7) underwent a Huber opposition transfer 1 year after receiving the non-vascularized PIP joint graft from the toe to the hypoplastic thumb.[25]

The follow-up period ranged from 1 to 13 years, with a median of 6.5 years. Detailed patient data are provided in Table 1.

Table 1. Information about all the patients with Blauth type IIIB thumb hypoplasia in this study

Patient	Sex	Age at surgery [years]	Follow -up [years]	One-sided defect	Isolated defect	Operated side	Donor foot	Donor toe	Number of operations in the hand
1	M	1	3	yes	yes	L	R	IV	1
2	M	4	11	yes	yes	L	R	III	1
3	F	1	8	yes	no#	R	R	III	1
4	M	1	10	yes	no#	L	L	III	2
5	F	4	5	yes	yes	R	R	II	2
6	M	2	1	no*	yes	R	R	III	1
7	F	1	3	yes	yes	R	R	IV	2
8	F	1	14	yes	no#	R	R	III	4
Total/ median	M-4, F-4	1	6.5	7/8	5/8	L-3, R-5	L-1 R-7	III-5, IV-2, II-1	1.5

M – male; F – female; L – left; R – right; * thumb aplasia on the opposite side; #radial longitudinal deficiency.

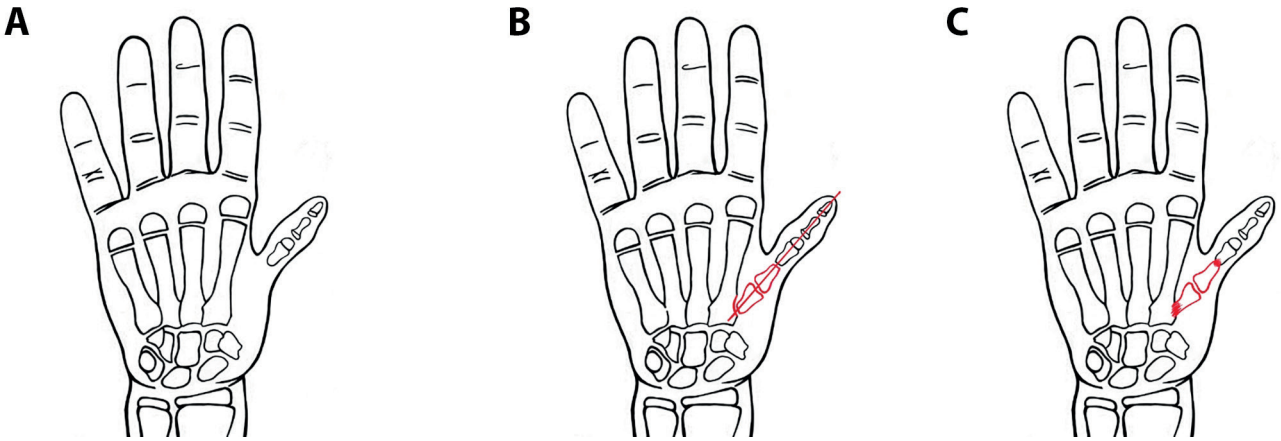

Fig. 1. Schematic drawing showing stabilization of the hypoplastic thumb type Blauth IIIB using a non-vascularized proximal interphalangeal (PIP) joint from the toe. A. Hypoplastic thumb type Blauth IIIB before the operation. B. Thumb after the procedure; the transferred joint and K-wire are marked in red. C. Thumb after obtaining bone union of the graft

Methods

The study on children and adolescents strictly adhered to ethical guidelines and the principles outlined in the Declaration of Helsinki. Before the commencement of the study, the entire process was thoroughly explained and presented to both the parents and the children. Participation in the study was entirely voluntary, and verbal consent was obtained from all the participants and their legal guardians, most often one of the parents. Ethical approval was waived by the Bioethics Committee of Poznan University of Medical Sciences, which issued a written waiver confirming that formal ethics review was not required for this non-experimental study

The first author examined all the patients under the supervision of the specialist. As part of the functional assessment, the passive range of motion in all joints of the hypoplastic thumb was measured using a goniometer and the point of maximum opposition. The stability of the transferred joint was evaluated with the dorsal shift test. It was performed by creating longitudinal traction to the thumb and then applying a palmar and dorsal pressure over the base of the 1st metacarpal to provoke subluxation of the joint.[26,27]

Sensation on the fingertip was assessed considering sensory discrimination using a standard 2-point discriminator.

The relative length of the hypoplastic thumb compared to the index finger was measured using the method developed by Goldfarb et al.[28] The norm refers to an adducted thumb, where the fingertip reaches 70% of the proximal phalanx length (AD/AB length ratio) and 32% of the index finger length (AD/AC length ratio).

The strength of the global and precise 2-point grip was assessed using equipment from Biometrics Ltd. E-LINK, Newport, UK; we used a Hand Accessory Kit (H400s) (Nine Mile Point Ind. Estate, Cwmfelinfach, Gwent, UK), specifically comprising the Dynamometer (G100) and Pinchmeter (P100). The examination was conducted according to the recommendations of the American Society of Hand Therapists (ASHT). A standard test position includes a seated posture with feet flat, elbow flexed at 90°, and wrist and forearm in a neutral position.[29–31] Three consecutive measurements were taken at 10-s intervals,[30] and the average value obtained from these trials was considered the maximum grip strength. Depending on the child's age, the dynamometer was set in 1 of the 5 standard test positions. The precision grip strength was assessed for 3 types of grips: Pincer, 3-point, and key (lateral). Results represent the mean of 3 measurements, expressed as a percentage of age- and gender-matched normative values[32] and of the contralateral healthy hand. The results were evaluated according to the scoring system by Percival et al.[33] and according to the hypoplastic thumb function assessment scale (WIMEC).[34]

The assessment of the hand's manipulative-manual functions and how the thumb was used in daily activities was based on our developed test. The tasks in the test required using the hypoplastic thumb with lateral, 2-point, 3-point, and global grips. During the 1st trial, the patient was instructed to perform each activity in the manner most convenient for them. If a substitute grip was used, the patient was asked to retry lifting the object or performing the task using the hypoplastic thumb.

During the test, the order of task execution was arbitrary, the time for each task was unlimited, and the tasks included lifting and placing various objects:

1. Coin – lateral/2-point grip;
2. Sheet of paper – lateral/2-point grip;
3. Small round ball – 3-point, 2-point, small concentric grip;
4. Round plastic button – lateral, 2-point, 3-point grip;
5. Lifting a pen – 3-point grip;
6. Drawing a circle/line or drawing – 3-point grip;
7. Plastic block (cuboid) – global grip;
8. Bottle – global grip (large concentric);
9. and 10. Lifting a wooden peg and placing it into a hole, and then removing it and placing it back on the table.

For completing a task using the hypoplastic thumb, the patient received 1 point; for completing a task with a substitute grip and then in the subsequent trial using the thumb, 2 points; for completing a task only using a substitute grip, 3 points; and if the task was impossible to complete, 4 points. The scoring range was 10–40 points, with fewer points indicating a better outcome. The point score was also converted to a percentage scale of 0–100% task completion according to the following formula:

% total manual-manipulative ability = (40 – [total points scored])/30 × 100%.

Subjective hand function assessment was conducted using the Michigan Hand Outcomes Questionnaire (MHQ). Depending on the child's age, the patient or the parent completed the test based on observations and conversations with the child. Because the test was initially designed for adults, the work module was modified to refer to school or household duties as work.

Additionally, an X-ray of the operated upper limb was performed during the check-up to assess the union of the transferred joint.

Results

The median passive range of motion for the hypoplastic thumb was 70° (range: 40–90°) at the interphalangeal (IP) joint, 35° (range: 5–45°) at the metacarpophalangeal (MP) joint, 75° (range: 30–90°) for radial abduction, and 70° (range: 10–90°) for palmar abduction. In 1 patient (No. 8), the first metacarpal was rigid with no passive motion; palmar and radial abduction measured 10° and 30°, respectively. Another patient (No. 7 after Huber opposition transfer) exhibited active palmar abduction up to 70° with an opposition strength of 4 on the Lovett scale.

In 6 patients, opposition was possible to the tip of the little finger, and, in the remaining 2, to the tip of the long finger. In 6 cases (75%), there was an improvement in the stability of the hypoplastic thumb base; 1 case showed partial improvement (13%), and in 1 case, there was no improvement in stability.

The sensation in the pulp of the hypoplastic thumb among all the examined patients remained within normal limits, not exceeding 5 mm in the 2-point discrimination test (2PD) (Table 2).

The median of the AD/AB and AD/AC ratios, which determine the relative length of the thumb, were 49 and 25, respectively. Compared to the values established in the literature by Goldfarb et al., this indicates a 25% shorter relative thumb length.[28]

For global grip strength, the median value was 44% relative to the opposite healthy hand and 23% relative to the norm appropriate for the patient's gender and age. Only 1 patient (No. 7) with active opposition after abductor digiti minimi muscle transfer could generate 2-point pinch strength, achieving 30% relative to the opposite healthy hand and 35% relative to the norm appropriate for the patient's gender and age.

The manual manipulation function of the hand was assessed using our test for all the patients, with an average final score of 23 points. The total manual–manipulative ability ranged from 33% to 100%, with a median score of 55% for all the patients. The most difficult task was lifting small objects such as coins or small balls, and the least difficult was lifting larger objects such as a glass or block. Initially, 75% of the patients performed most of the tasks using a substitute grip and, then, in subsequent trials, used the hypoplastic thumb. However, half of the patients immediately used the hypoplastic thumb for some tasks. Two patients performed all the tasks immediately using the hypoplastic thumb, while 3 used only the substitute grip. During the study, most of the patients used a substitute grip at least once. The grip most commonly employed was the pinch between the index and middle fingers, used by over 60% of patients (Table 3).

Table 2. Thumb range of motion and carpometacarpal (CMC) I stability after operation in study group

Patient	Thumb range of motion [°]					Stability of CMC I joint	2PD
	aIP	aMP	palmar abduction	radial abduction	opposition		
1	50	40	70	70	V	stable	≤5 mm
2	70	30	40	80	V	stable	≤5 mm
3	90	40	30	90	III	stable	≤5 mm
4	40	10	90	90	V	partially stable	≤5 mm
5	60	40	70	70	V	stable	≤5 mm
6	70	5	90	80	V	unstable	≤5 mm
7*	70	30	70#	70#	III	stable	≤5 mm
8	70	45	10	30	V	stable	≤5 mm
Total/ median	70	35	70	75	V-6; III-2		

*after Huber opposition transfer; #active movement; aIP – interphalangeal joint; aMP – metacaropophalangeal joint; CMC – carpometacarpal; 2PD – 2-point discrimination test.

Table 3. Thumb relative length, grip strength, and manual-manipulation test results in study group

Patient	Relative thumb length			Hand grip strength [%]		Precision grip strength [%]		Manual-manipulation test [%]
	AD/AB ratio	AD/AC ratio	percentage of the norm	healthy hand	norm	healthy hand	norm	
1	50	22	70	43	55	0	0	40
2	50	25	75	56	45	0	0	83
3	48	29	80	50	25	0	0	33
4	50	21	69	32	20	0	0	33
5	50	25	75	44	40	0	0	66
6	43	24	68	0	0	0	0	47
7*	45	26	92	100	20	30	35	100
8	33	21	56	0	0	0	0	63
Median	49	25	72	44	23	0	0	55

*after Huber opposition transfer. AB – the length of the proximal phalanx of the index finger; AC – the length of the entire index finger (proximal, middle, distal phalanges); AD – the position of the adducted thumb in relation to the index finger.

Upon analyzing hand function according to the Percival scale, the most significant percentages of results were rated as fair (50%) and poor (37%). Only 1 result was rated as good (13%). The median score among the studied group was 13 points. Using the WIMEC, the median score was 22 points (range: 19–23) out of a max of 25.

Based on the subjective assessment of hand function using the MHQ, the median score for all the patients was 61%. The highest scores were noted in the sections on satisfaction and work, at 69% and 55%, respectively. The lowest scores were observed in the Activities of Daily Living (ADL) and esthetic section, at 47% and 54%, respectively (Table 4; Fig. 2,3).

In 75% of cases, harvesting the PIP joint from the toe resulted in toe shortening, moderate in 5 patients and mild in 1 – though this did not pose a significant cosmetic concern. No patient experienced postoperative difficulties with ambulation or weight-bearing on the donor foot. However, 1 patient developed toe flaccidity after joint harvest, occasionally causing the toe to catch on footwear or when walking barefoot (Fig. 4).

Only in 2 cases (25%) did the harvested graft not achieve union with the 1st or 2nd metacarpal bone after 8 weeks of immobilization with K-wires. In one case, infection around the Kirschner wires caused hardware instability; in another, wire loosening alone was responsible. Both cases necessitated reoperation: The first involved graft restabilization only, while the second required pseudoarthrosis resection, defect reconstruction with a bone graft, and subsequent restabilization. After surgery, union was

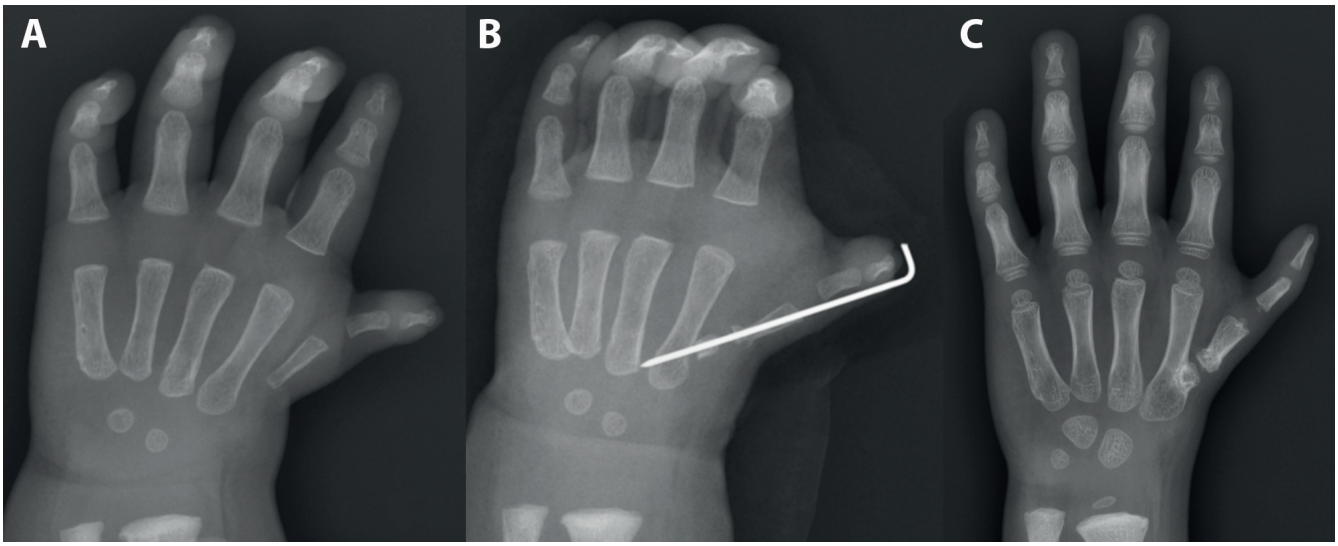

Fig. 2. X-ray of patient No. 1: hand in anterior–posterior (AP) position before the operation (A), after the operation (B), and after 3 years with full graft union and reconstructed carpometacarpal (CMC) I joint (C)

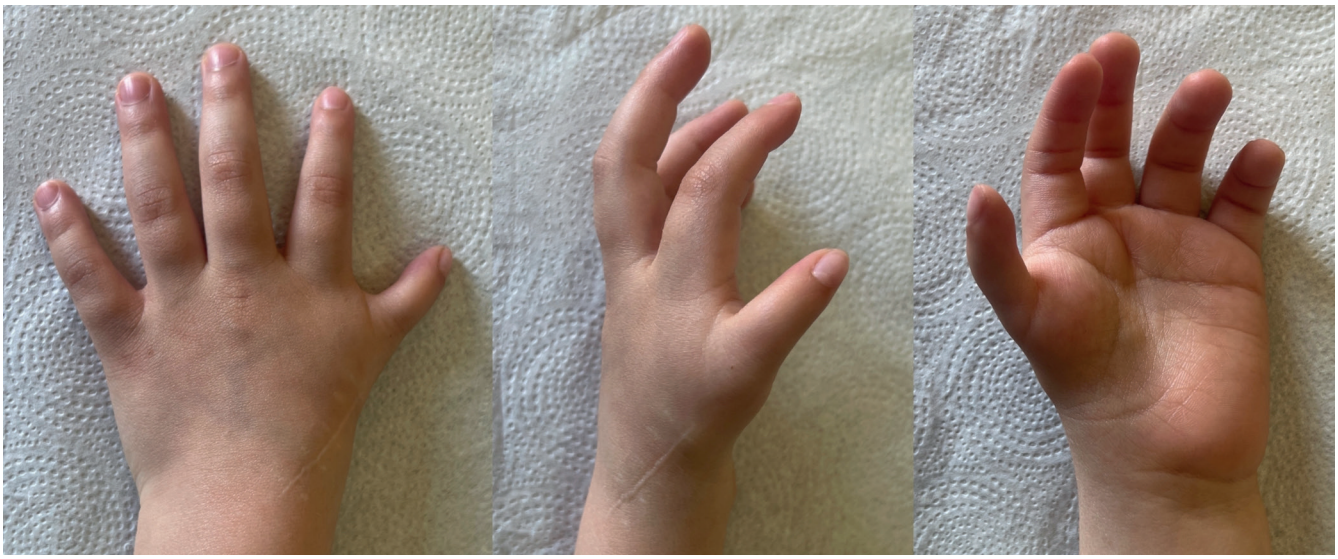

Fig. 3. Patient 1, 3 years after transfer of the proximal interphalangeal (PIP) joint, showing thumb shortening and thenar muscle atrophy, with the thumb in an intermediate position

Table 4. Hypoplastic thumb function assessment scales and Michigan Hand Questionnaire (MHQ) results in study group

Patient	Percival scale	WIMEC	Michigan Hand Questionnaire						
			hand function	ADL	work	pain	esthetic	satisfaction	overall
1	13	22	75	35.5	60	0	75	83	71
2	14	23	50	45.5	75	30	65	75	63
3	10	22	55	61.5	50	25	32	75	58
4	13	21	50	46	55	35	45	62.5	55
5	13	23	45	15	25	0	32	63	47
6	8	22	80	82	50	0	63	95	78
7*	16	22	65	65	100	0	65	60	75
8	11	19	35	47.5	55	35	0	58	45
Median	13	22	53	47	55	13	54	69	61

*after Huber opposition transfer; WIMEC – hypoplastic thumb function assessment scale; ADL – activities of daily living.

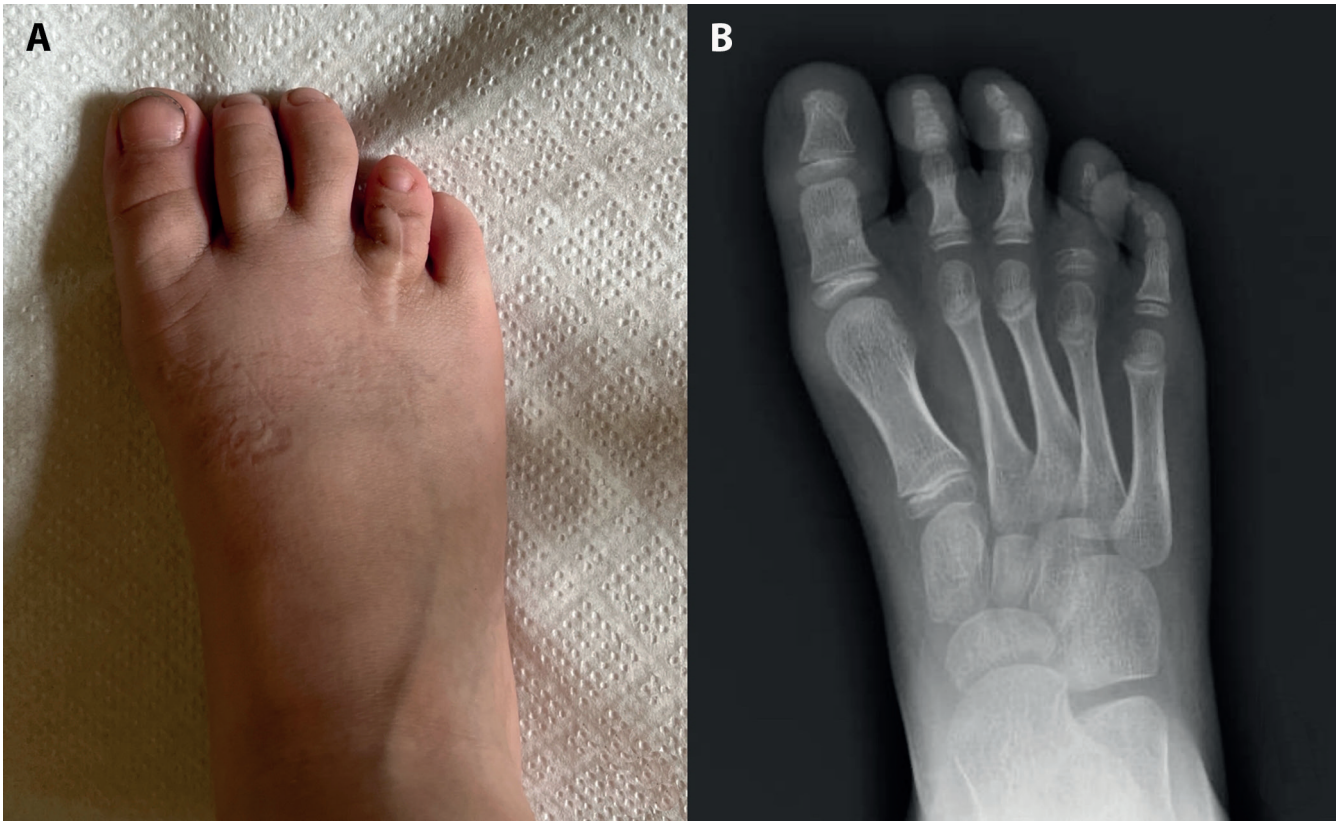

Fig. 4. Clinical photograph (A) and radiograph (B) of a patient's foot showing toe shortening, a change observed in most patients after proximal interphalangeal (PIP) joint graft harvesting

achieved only in 1 patient, while pseudoarthrosis persisted in the other, resulting in ongoing thumb instability. In this case, the parents ultimately opted for pollicization (all the functional results of this patient presented in the paper refer to the assessment before the pollicization) (Table 5).

There was no statistically significant correlation between the age at surgery and relative thumb length with the manual manipulation function test ($p = 0.256$ and $p = 0.417$) or MHQ score ($p = 0.923$ and $p = 0.493$) (Table 6).

Discussion

According to the modified Blauth classification, thumb amputation followed by index finger pollicization is widely regarded as the gold-standard treatment for type III B thumb hypoplasia, delivering optimal functional outcomes.[2] However, some parents decline this procedure due to concerns about its cosmetic effect, specifically, the resulting four-fingered hand. As a result, alternative reconstructive techniques aimed at preserving the hypoplastic thumb – with an emphasis on improving its stability,

Table 5. Foot assessment results, complications and reoperation rates

Patient	Donor foot assessment			Complications	Reoperations
	shortening	walking and bearing problems	cosmetic or functional problem		
1	yes	no	no	no	no
2	yes	no	no	no	no
3	yes	no	no	no	no
4	yes	no	no	no	no
5	no	no	no	graft nonunion	yes**
6	no	no	no	graft nonunion	yes, twice***
7	yes	no	no	no	no
8	yes	no	functional*	no	no
Total	6/8 (75%)	0/8 (0%)	1/8 (13%)	2/8 (25%)	3/8 (38%)

*limp and hooked toe; **resection of the pseudoarthrosis, filling the defect with a bone graft, and restabilization; ***graft restabilization/pollicization.

Table 6. The results of correlation between variables based on Spearman's correlation coefficient test

Correlated variables	Manual manipulation test	MHQ score
Age at surgery	$(r_s) = 0.456$/p-value = 0.256	$(r_s) = 0.041$/p-value = 0.923
Relative thumb length	$(r_s) = 0.335$/p-value = 0.417	$(r_s) = 0.286$/p-value = 0.493

MHQ – Michigan Hand Questionnaire

have been described in the literature. These reconstructive options include metatarsophalangeal (MTP) joint grafts (vascularized or non-vascularized), free phalanx grafts harvested from the toe, partial- or full-width metatarsal bone grafts, vascularized metatarsal transfers with full-thickness skin flaps, and non-vascularized structural grafts from the iliac crest.[9–11,14,17–19,23,35–39]

Autologous transfer of whole or partial PIP joints from the foot, using either vascularized or non-vascularized techniques, is well documented in both adult and pediatric populations as an alternative to arthrodesis or joint arthroplasty. Indications include congenital, traumatic, and post-infectious PIP joint deformities of the fingers.[40–42]

Kuzu et al.[41] reported on 7 adult patients who underwent vascularized transfer of the second toe PIP joint to the hand, demonstrating enhanced joint mobility. After 1 year, passive range of motion improved by 5–53°, and active range by 2–43°. In a separate series, Dautel et al.[40] evaluated 43 PIP joint reconstructions in children and adults over a 5-year follow-up, reporting a mean active range of 45° (range 34–79°). However, 2 transplanted joints developed complete ankyloses.

Our literature review revealed no reports of using a PIP joint transfer for type III B hypoplastic thumb reconstruction. However, some authors have described vascularized MTP joint grafts, with or without full-thickness skin flaps, as alternatives to pollicization.[14,18,36] In these series, 10 patients aged 1–16 years underwent the procedure: For younger children, parents declined pollicization, while older patients received surgery solely to improve thumb stability in the absence of prior pollicization. In all cases, adjunctive tendon transfers were performed to restore active thumb motion. Postoperative thumb stability improved in all cases. However, only Matsuzaki et al.[18] reported joint mobility, documenting radial abduction of up to 45° and palmar abduction of up to 75°. Some patients achieved global grip strength up to 3-fold higher, while key pinch strength remained 50% lower compared with pollicized individuals.[36] In contrast, a separate study reported grip strength at 40% and 2-point pinch strength at 14% relative to the contralateral healthy hand.[14] In 2 studies,[18,36] all the patients were able to grasp both small and large objects with the operated thumb, whereas, in the study by Foucher et al.,[14] over half of the patients could grasp small objects with the hypoplastic thumb but only used this grip occasionally during daily activities, with most being able to hold larger objects.

Another technique described in the literature involves free, non-vascularized grafting of the entire or partial proximal phalanx or metatarsal bone from the foot to the base of the hypoplastic thumb.[9–11,17] A total of 40 patients across 4 studies were operated on at an average age of just under 2 years, with an average follow-up of over 5 years. In total, 60% of the patients had a diagnosis of type III B thumb hypoplasia, while the remaining had type IIIC or IV (5% and 35%, respectively). Most patients underwent tendon transfers tailored to their specific requirements, primarily opponensplasty. Good stability of the reconstructed CMC joint was achieved in most cases, although instability persisted in 2 patients[10,17] (1 after half-width metatarsal transfer and the other after phalanx transfer). In 1 case,[17] partial instabilities were left uncorrected due to overall functional improvement.

In contrast, in another case,[10] complete instability required reoperation with vascularized MTP joint transfer, which improved thumb stability and function. Only the study by Kawabata et al.[17] evaluated the range of motion in the hypoplastic thumb, which averaged 35° of palmar abduction and 33° of radial abduction. The mean Kapandji score of all the patients was just under 6 points. All the studies assessed pinch grip strength, but only 3[9,10,17] compared it to that of the healthy contralateral hand, with an average strength of 31%. Chow et al.[10] also evaluated global grip strength, which averaged 61% compared to that of the healthy contralateral hand. In 1 study, Goldfarb and Manschke's method was used to compare the hypoplastic thumb's length to the index finger's proximal phalanx, finding it to be 57% of normal.[17] Most of the evaluated patients[9,11,17] could grasp smaller objects, though they more frequently used the hand for grasping larger objects. All the patients evaluated for donor site outcomes on the foot had no issues with walking, running, or weight-bearing, and shortening of the toe did not cause functional or cosmetic problems. The overall complication rate among all the patients was 18%. The most frequent complication was delayed or nonunion of the graft (four cases), with one instance each of donor-site mid-metatarsal fracture, fracture of the transferred metatarsal in the thumb, and first carpometacarpal (CMC I) joint instability. Based on 2 studies,[9,11] all the parents were postoperatively satisfied with the hypoplastic thumb's function and appearance.

In our clinical evaluation, after stabilizing the hypoplastic thumb with a PIP joint from the foot, we achieved improved thumb stability and reduced hypermobility, consistent with the results reported in the abovementioned studies. Similar to Chow et al.,[10] 1 of our cases experienced persistent instability due to graft nonunion with the second metacarpal despite reoperation, ultimately necessitating pollicization.

Consistent with earlier reports, our patients were able to grasp large objects because the stabilized opposable thumb provided counterpressure against the other fingers during a global grip. However, grasping smaller objects was more challenging for most of our patients than in the studies mentioned above, likely due to limited active thumb movement, as only 1 patient underwent tendon transfers for thumb opposition. Due to the lack of object standardization across all studies, the results remain inconclusive.

We achieved results regarding the radial and palmar abduction range of motion similar to those for the patient in the study by Matsuzaki et al.[18] and twice as good as those reported by Kawabata et al.[17] The mean Kapandji score in our study was similar to that in the studies mentioned above, averaging just under 6 points. We obtained comparable global grip strength results, with a median of 44% compared to the contralateral healthy hand, as reported by Foucher et al.[14] and Chow et al.,[10] where the average results were 40% and 61%, respectively. The relative length of the hypoplastic thumb compared to the proximal phalanx of the index finger (according to the method developed by Goldfarb et al.[28] was slightly more significant in our patients, measuring 72% compared to 57% in the study by Kawabata et al.[17]

In our study, only 1 patient (No. 7 after Huber opposition transfer) could generate 2-point pinch strength, likely due to the difficulty in overcoming the device's resistance, as the other patients lacked active adduction and thumb opposition. In this patient, grip strength was 34% of the normative value, comparable to the 31% average reported in previous studies. Similarly to the studies cited, long-term follow-up showed that patients and their parents were satisfied with the surgical outcomes and would opt for the procedure again.

In our study, similarly to the study by Garagnani et al.,[43] most patients had a shortened donor toe after the PIP graft was harvested. However, despite this, there were no significant functional foot issues or significant cosmetic concerns from either parents or patients.

The complication rate in our patient group was 25%, similar to the level reported in the reviewed studies (18%), with graft nonunion being the main issue, leading to CMC I joint instability. We performed reoperations in both cases, with union achieved in only 1, while instability persisted in the other, ultimately necessitating pollicization. In 1 case, graft nonunion resulted from infection around the Kirschner wires and subsequent hardware destabilization; in the other, nonunion was solely due to wire loosening. In the second case, despite graft restabilization, osseous union was not achieved. The patient presented with multiple congenital conditions, including thumb hypoplasia, congenital hearing loss, and hydrocephalus, which may have contributed to the nonunion. Ultimately, the parents consented to pollicization.

Our observations and the cited studies indicate that achieving improved thumb stability requires successful graft integration, regardless of the type of graft used.

If this surgical technique fails to achieve a satisfactory functional outcome for the patient, classical pollicization remains a viable option. In 1 of our cases, we performed pollicization with persistent thumb instability (during graft nonunion despite reoperation). We found no technical difficulties in performing pollicization as a secondary operation. No patient in our series required pollicization after achieving complete graft union, so we cannot directly assess this scenario. However, based on our experience, a prior successful graft union is unlikely to substantially alter the technical challenges or complication rates of subsequent pollicization.

In our work, we used the WIMEC scale to objectively assess the hypoplastic thumb function, a functional assessment score for congenital hypoplastic thumbs proposed by Mende et al. in 2021.[34] It is a basic score, applicable even in young and non-cooperative patients. Because the WIMEC scale has been described only recently, it awaits proper validation and reliability testing. Utilizing this scoring system enables precise comparison of preoperative and postoperative status and facilitates

benchmarking outcomes across different techniques and centers.[44,45] Currently, in the literature, only Sletten et al.[45] have used WIMEC as one of the methods for an objective postoperative outcome. He assessed the stability of the thumb's MP joint after ligament reconstruction with flexor digitorum superficialis in thumb hypoplasia type II and IIIA. Postoperatively, patients in the comparison groups achieved a mean WIMEC score of 30 points, surpassing our cohort's median score of 22 points, likely reflecting their less severe thumb hypoplasia.

None of the studies reviewed employed either the Percival scoring system or the Michigan Hand Outcomes Questionnaire (MHQ), precluding direct comparison with our findings.

Limitations

The small patient group is a limitation of this study. Also, a detailed subsequent evaluation with long-term follow-up would be preferable. It will be valuable to compare the obtained results with those for patients after index pollicization as the gold standard for treating grade IIIB thumb hypoplasia.

Conclusions

Patients who underwent hypoplastic thumb reconstruction using a non-vascularized PIP joint graft from the foot experienced improved thumb stability and reduced hypermobility. These outcomes are comparable to those reported for similar reconstructive techniques in the literature. This method may be considered an option for stabilizing a hypoplastic thumb in patients whose parents do not consent to pollicization.

To achieve a better functional effect, it is necessary to plan the required tendon transfers for a given patient in 1 or more stages of treatment. The most important condition for success is the bone union of the graft, regardless of its type, because its failure is the most common complication, resulting in no improvement in thumb stability. Harvesting a PIP joint from a toe most often leads to shortening of the toe but does not cause gait disturbances or problems with weight bearing.

At follow-up, both patients and their parents reported satisfaction with the surgical outcomes and expressed willingness to undergo the procedure again. However, we emphasize that this technique is not intended to replace pollicization as the gold-standard treatment but should be reserved for cases in which parental consent for pollicization is not granted.

Data Availability Statement

Data sharing is not applicable to this article, as all data are already included in the manuscript.

Consent for publication

Not applicable

Use of AI and AI-assisted technology

Not applicable

ORCID iDs

Michał Górecki https://orcid.org/0000-0001-9902-0770
Piotr Czarnecki https://orcid.org/0000-0002-2890-8139
Ewa Bręborowicz https://orcid.org/0000-0002-4184-4475

References

1. Sayadi L, Chopan M, Laub D. Thumb hypoplasia. *Eplasty*. 2015;15:ic62. PMID:26759691. PMCID:PMC4693184.
2. Tay SC, Moran SL, Shin AY, Cooney WP. The hypoplastic thumb. *J Am Coll Orthop Surg*. 2006;14(6):354–366. doi:10.5435/00124635-200606000-00005
3. Górecki M, Redman M, Romanowski L, Czarnecki P. Evaluation of the ulna lengthening by distraction osteogenesis in congenital radial deficiency. *Eur J Orthop Surg Traumatol*. 2022;33(5):1981–1987. doi:10.1007/s00590-022-03381-1
4. Tonkin MA. On the classification of congenital thumb hypoplasia. *J Hand Surg Eur Vol*. 2014;39(9):948–955. doi:10.1177/1753193413516246
5. Soldado F, Zlotolow DA, Kozin SH. Thumb hypoplasia. *J Hand Surg*. 2013;38(7):1435–1444. doi:10.1016/j.jhsa.2013.03.021
6. Tonkin MA. Assessment of surgery for the underdeveloped thumb. *J Hand Surg Eur Vol*. 2016;41(3):251–252. doi:10.1177/1753193415625146
7. Flatt AE. Our Thumbs. *Proc (Bayl Univ Med Cent)*. 2002;15(4):380–387. doi:10.1080/08998280.2002.11927870
8. Buck-Gramcko D. Congenital malformations of the hand and forearm. *Chirurgie de la Main*. 2002;21(2):70–101. doi:10.1016/S1297-3203(02)00103-8
9. Balakrishnan G, Vijayaragavan S, Somesh B. Restoration of five digit hand in type III B & C thumb hypoplasia: A game changer in surgical management. *Indian J Plast Surg*. 2020;53(3):349–356. doi:10.1055/s-0040-1718858
10. Chow CS, Ho PC, Tse WL, Hung LK. Reconstruction of hypoplastic thumb using hemi-longitudinal metatarsal transfer. *J Hand Surg Eur Vol*. 2012;37(8):738–744. doi:10.1177/1753193411432677
11. Liu B, Chen S, Chow ECS, Li P, Liu K, Yang C. Type IIIB and IV hypoplastic thumb reconstruction with non-vascularized fourth metatarsal. *J Hand Surg Eur Vol*. 2020;45(7):722–728. doi:10.1177/1753193420937547
12. Roper BA, Turnbull TJ. Functional assessment after pollicisation. *J Hand Surg*. 1986;11(3):399–403. doi:10.1016/0266-7681_86_90166-X
13. Kozin SH, Weiss AA, Webber JB, Betz RR, Clancy M, Steel HH. Index finger pollicization for congenital aplasia or hypoplasia of the thumb. *J Hand Surg*. 1992;17(5):880–884. doi:10.1016/0363-5023(92)90460-7
14. Foucher G, Medina J, Navarro R. Microsurgical reconstruction of the hypoplastic thumb, type IIIB. *J Reconstr Microsurg*. 2001;17(1):009–016. doi:10.1055/s-2001-12683
15. Sykes PJ, Chandraprakasam T, Percival NJ. Pollicisation of the index finger in congenital anomalies: A retrospective analysis. *J Hand Surg*. 1991;16(2):144–147. doi:10.1016/0266-7681(91)90164-J
16. Hu W, Gasnier P, Le Nen D, Kerfant N, Boloorchi A. Description of an original conservative method for the surgical management of the Blauth IIIb thumb hypoplasia: "relative lengthening - thumb stabilization" [in French]. *Ann Chir Plast Esthet*. 2012;57(4):342–349. doi:10.1016/j.anplas.2010.09.014
17. Kawabata H, Tamura D, Goldfarb CA. Treatment of blauth type IIIB thumb hypoplasia using a nonvascularized toe phalanx. *J Hand Surg*. 2021;46(1):68.e1–68.e7. doi:10.1016/j.jhsa.2020.07.007
18. Matsuzaki H, Toishi S, Yoshizu T. A Blauth IIIB hypoplastic thumb reconstructed with a vascularised metatarso-phalangeal joint transfer: a case report with 28 years of follow up. *Hand Surg*. 2009;14(1):63–68. doi:10.1142/S0218810409004244

19. Nakada M, Tada K, Nakajima T, Matsuta M, Tsuchiya H. A case of a 5-year-old boy with a Blauth type IIIB hypoplastic thumb reconstructed with a nonvascularized, hemilongitudinal metatarsal transfer. *Case Rep Orthop*. 2018;2018:8205285. doi:10.1155/2018/8205285
20. Nishijima N, Matsumoto T, Yamamuro T. Two-stage reconstruction for the hypoplastic thumb. *J Hand Surg*. 1995;20(3):415–419. doi:10.1016/S0363-5023(05)80098-X
21. Tan J, Tu YK. Comparative study of outcomes between pollicization and microsurgical second toe-metatarsal bone transfer for congenital radial deficiency with hypoplastic thumb. *J Reconstr Microsurg*. 2013;29(9):587–592. doi:10.1055/s-0033-1348063
22. Tu YK, Yeh WL, Sananpanich K, et al. Microsurgical second toe-metatarsal bone transfer for reconstructing congenital radial deficiency with hypoplastic thumb. *J Reconstr Microsurg*. 2004;20(3):215–225. doi:10.1055/s-2004-823109
23. Zhong W, Tian W, Zhao J, et al. Nonvascularized iliac crest bone graft for reconstruction of the first metacarpal in type IIIB thumb hypoplasia: A radiographic follow-up study. *J Hand Surg*. 2023;48(2):196.e1–196.e8. doi:10.1016/j.jhsa.2021.09.032
24. Górecki M, Czarnecki P, Romanowski L. Stabilization of the hypoplastic thumb type Blauth IIIB using a non-vascularized proximal interphalangeal joint from the toe as an alternative reconstruction when pollicization is not accepted: Description of the surgical technique. *Adv Clin Exp Med*. 2025;34(3):385–392. doi:10.17219/acem/186477
25. Huber E. Relief operation in the case of paralysis of the median nerve. *J Hand Surg*. 2004;29(1):35–37. doi:10.1016/j.jhsb.2003.10.003
26. Engelhardt TO, Djedovic G, Pedross F, Piza-Katzer H. Defining postoperative stability in children with radial polydactyly. *J Hand Surg Eur Vol*. 2016;41(3):275–280. doi:10.1177/1753193415613583
27. Choa RM, Parvizi N, Giele HP. A prospective case-control study to compare the sensitivity and specificity of the grind and traction-shift (subluxation-relocation) clinical tests in osteoarthritis of the thumb carpometacarpal joint. *J Hand Surg Eur Vol*. 2014;39(3):282–285. doi:10.1177/1753193413508714
28. Goldfarb CA, Gee AO, Heinze LK, Manske PR. Normative values for thumb length, girth, and width in the pediatric population. *J Hand Surg*. 2005;30(5):1004–1008. doi:10.1016/j.jhsa.2005.02.017
29. Mathiowetz V, Wiemer DM, Federman SM. Grip and pinch strength: Norms for 6- to 19-year-olds. *Am J Occup Ther*. 1986;40(10):705–711. doi:10.5014/ajot.40.10.705
30. Innes E. Handgrip strength testing: A review of the literature. *Aus Occup Therapy J*. 1999;46(3):120–140. doi:10.1046/j.1440-1630.1999.00182.x
31. Mathiowetz V, Kashman N, Volland G, Weber K, Dowe M, Rogers S. Grip and pinch strength: normative data for adults. *Arch Phys Med Rehabil*. 1985;66(2):69–74. PMID:3970660.
32. Protasewicz A. *Funkcja chwytna ręki po policyzacji palca promieniowego we wrodzonej hipoplazji kości promieniowej*. Rozprawa doktorska. Uniwersytet Medyczny im. Karola Marcinkowskiego w Poznaniu; 2006.
33. Percival NJ, Sykes PJ, Chandraprakasam T. A Method of Assessment of Pollicisation: *J Hand Surg*. Published online August 29, 2016. Accessed November 26, 2020. https://journals.sagepub.com/doi/10.1016/0266-7681%2891%2990163-I
34. Mende K, Tonkin MA. A functional assessment score for congenital hypoplastic thumbs. *J Hand Surg Eur Vol*. 2021;46(4):440–446. doi:10.1177/1753193421989925
35. Luangjarmekorn P, Pongernnak N, Kitidumrongsook P. Vascularized toe joint transfer for hypoplastic thumb type IV. *Tech Hand Up Extrem Surg*. 2021;25(4):226–234. doi:10.1097/BTH.0000000000000339
36. Shibata M, Yoshizu T, Seki T, Goto M, Saito H, Tajima T. Reconstruction of a congenital hypoplastic thumb with use of a free vascularized metatarsophalangeal joint. *J Bone Joint Surg*. 1998;80(10):1469–1476. doi:10.2106/00004623-199810000-00008
37. Tong DD, Wu LH, Li PC, et al. Reversed vascularized second metatarsal flap for reconstruction of Manske type IIIB and IV thumb hypoplasia with reduced donor site morbidity. *Chin Med J (Engl)*. 2019;132(21):2565–2571. doi:10.1097/CM9.0000000000000477
38. Liu B, Bai F, Chen S. Revisiting the management of Manske type 3B and 4 thumb hypoplasia. *J Hand Surg Eur Vol*. 2021;46(1):21–29. doi:10.1177/1753193420967240
39. Tonkin M. Surgical reconstruction of congenital thumb hypoplasia. *Indian J Plast Surg*. 2011;44(2):253. doi:10.4103/0970-0358.85347
40. Dautel G. Vascularized toe joint transfers to the hand for PIP or MCP reconstruction. *Hand Surg Rehabil*. 2018;37(6):329–336. doi:10.1016/j.hansur.2018.03.008
41. Kuzu İM, Kayan RB, Öztürk K, Güneren E. Functional improvement with free vascularized toe-to-hand proximal interphalangeal (PIP) joint transfer. *Plast Reconstr Surg Glob Open*. 2018;6(7):e1775. doi:10.1097/GOX.0000000000001775
42. Leclère FM, Haug L, Meier R, Surke C, Unglaub F, Vögelin E. Non-vascularized partial joint transfer for finger proximal interphalangeal joint reconstruction: A series of 9 patients. *Arch Orthop Trauma Surg*. 2020;140(1):139–144. doi:10.1007/s00402-019-03301-9
43. Garagnani L, Gibson M, Smith PJ, Smith GD. Long-term donor site morbidity after free nonvascularized toe phalangeal transfer. *J Hand Surg*. 2012;37(4):764–774. doi:10.1016/j.jhsa.2011.12.010
44. Mende K, Suurmeijer JA, Mason WTM, Smith BJ, Tonkin MA. A detailed analysis of long-term outcomes following reconstruction for congenital thumb hypoplasia. *J Hand Surg Eur Vol*. 2022;47(3):270–279. doi:10.1177/17531934211044653
45. Sletten IN, Jokihaara J, Stavenes AB, Winge MI. Satisfactory thumb metacarpophalangeal joint stability after ligament reconstruction with flexor digitorum superficialis in children with radial longitudinal deficiency. *J Hand Surg Eur Vol*. 2023;48(11):1151–1158. doi:10.1177/17531934231187813

Comparison of phonemic awareness in children with auditory processing disorder and children without auditory processing disorder using an objective test for assessing phonemic hearing: A preliminary study

Andrzej K. Konopka[1,A–D], Julia Pyttel[2,B–D], Anna Kasprzyk[3,D,E], Grażyna Mielnik-Niedzielska[4,E,F], Artur Niedzielski[3,E,F]

[1] Oticon Polska Sp. z o. o., Warsaw, Poland
[2] Audika, Warsaw, Poland
[3] Department of Pediatric Otolaryngology, Centre of Postgraduate Medical Education, Warsaw, Poland
[4] Department of Pediatric Otolaryngology, Phoniatrics and Audiology, Medical University of Lublin, Poland

A – research concept and design; B – collection and/or assembly of data; C – data analysis and interpretation; D – writing the article; E – critical revision of the article; F – final approval of the article

Advances in Clinical and Experimental Medicine, ISSN 1899–5276 (print), ISSN 2451–2680 (online) *Adv Clin Exp Med*. 2026;35(2):265–278

Address for correspondence
Andrzej K. Konopka
E-mail: andk@oticon.com

Funding sources
None declared

Conflict of interest
None declared

Received on July 22, 2024
Reviewed on December 24, 2024
Accepted on April 30, 2025

Published online on August 11, 2025

Cite as
Konopka AK, Pyttel J, Kasprzyk A, Mielnik-Niedzielska G, Niedzielski A. Comparison of phonemic awareness in children with auditory processing disorder and children without auditory processing disorder using an objective test for assessing phonemic hearing: A preliminary study. *Adv Clin Exp Med*. 2026;35(2):265–278. doi:10.17219/acem/204557

DOI
10.17219/acem/204557

Abstract

Background. Phonemic awareness is defined as the ability to break down a word into smaller units called phonemes or described as the ability to synthesize words from segments of one's own speech. Impaired phonemic hearing, depending on the degree of severity, hinders or prevents speech reception, disrupts the proper development of a child's pronunciation, may cause disorders in already developed speech, and complicates the acquisition of writing skills or disturbs the skill that has already been acquired.

Objectives. To create an objectified tool for phonemic hearing diagnostics to ensure that verbal material is always presented at the same intensity, from the same distance, and in the same direction. Another aim was to compare children with and without auditory processing disorder (APD) if they have disrupted phonemic hearing.

Materials and methods. A study involving 20 individuals was conducted using a sound level meter to determine the level of the auditory stimulus (therapist's voice) provided to patients during the diagnosis. Each participant in the study was tasked with repeating, in the most natural way for them, 2 pairs of words containing opposing sounds.

Results. The analysis revealed significant discrepancies both in the articulation of verbal material by different examiners and in the presentation of the same material by a single examiner using different methods. When the same phonemic opposition was presented in an identical manner by different diagnosticians, amplitude differences of up to 10.8 dB were observed, with a standard deviation (SD) of 2.5 dB. These findings underscored the need to develop an objectified tool for phonemic hearing diagnostics to ensure consistency and reliability in assessment.

Conclusions. In the research group encompassing children with APD, disorders within phonemic hearing occur more frequently and have a deeper nature. Phonemic hearing disorders in children are associated with significant difficulties in learning and daily functioning.

Key words: children, APD, phonemic awareness, auditory processing disorder

Highlights

- Phonemic hearing deficits in auditory processing disorder (APD): Children with APD exhibit significant impairments in phoneme discrimination, underscoring core processing challenges.
- 62.9% higher phonemic error rate vs peers: Quantitative analysis reveals that APD diagnoses correspond with a marked increase in phonemic mistakes compared to non-APD children.
- Early phonemic assessment and intervention boost outcomes: Timely diagnosis and targeted therapy for phonemic disorders enhance both academic performance and emotional well-being in APD-affected children.
- Specialized phonemic rehabilitation needed for APD: Results highlight the importance of developing and implementing tailored therapeutic protocols to address phonemic hearing issues in pediatric APD.

Background

The term "phonemic hearing" first emerged in Soviet research in the mid-20th century, particularly within the fields of neuropsychology and neurolinguistics.[1] Effective interpretation of acoustic signals requires not only intact auditory function but also the precise ability to differentiate between phonemes. Phonemic hearing is essential for speech development, literacy acquisition, and reading proficiency. It is commonly defined as the ability to segment words into their smallest sound units called phonemes[2] or to synthesize words from discrete speech sounds.[3] Impairments in phonemic hearing, depending on their severity, can hinder or even prevent effective speech perception. Such deficits may disrupt the development of correct pronunciation, contribute to speech disorders in children, and impede the acquisition of writing skills or interfere with skills that have already been established.

It is important to recognize that the primary function of language is communication.[4] This entails the exchange of information between individuals to promote mutual understanding. The communicative function of language enables us to convey specific content, emotions, and feelings through spoken or written words, thereby facilitating effective interpersonal interaction.

Phonemic awareness

Communication disorders may arise from an inability to differentiate the basic units of language, i.e., phonemes. In such cases, individuals struggle to distinguish between sounds that represent different phonemes within a given language. These difficulties are classified as phonemic hearing disorders and can be identified through assessments of phonemic awareness.[5]

Early research in this field was conducted in the 1950s by Wepman, who developed a test that involved distinguishing between pairs of words that differ by only 1 phoneme, such as: clothe/clove [ʒlotχe] [d͡ʒ̂ lɔtxɛ]/[ʒlove] [d͡ʒ̂ lɔvɛ], dim/din [dʹĩm] [dʲĩm]/[dʹĩn] [dʲĩn], leg/led [lek] [lɛk]/[let] [lɛt].[6]

A disorder in phonemic awareness is a significant impairment that can interfere with effective interaction with the environment. It also disrupts auditory perception, leading to misunderstandings of instructions and difficulties in following them. Additionally, it can hinder foreign language learning, as sounds that should be perceived as distinct may seem identical to the affected individual – e.g., mouse/house [mouse/mɔusɛ] and [χouse/xɔusɛ].

Phonemic hearing should be assessed in the individual's native language. Research has demonstrated that people interpret phonemes more accurately in their native tongue than in foreign languages. Therefore, conducting assessments in the native language is essential to avoid inaccurate results or misinterpretation.

Phonemic awareness disorders can lead to difficulties in everyday functioning and learning, potentially affecting an individual's self-esteem and social confidence.[7] Early identification and intervention are crucial to support effective communication and promote healthy cognitive and emotional development.

Phonemic awareness diagnostics

Contemporary tools for assessing phonemic awareness typically involve auditory tasks, such as identifying phonemic differences using rhyming word pairs. To reduce the risk of misinterpretation related to articulatory difficulties, these assessments are often supplemented with visual aids.

In English, common diagnostic tools include the Phonemic Synthesis Picture Pointing Test,[8] the Auditory Skills Assessment,[9] and PAT-2.[10] In Polish, resources such as *Phonemic and Phonematic Hearing – Theory and Practice* by Bronisław Rocławski (2016)[11] and *Examination and Shaping of Phonematic Hearing* by Irena Styczek (1982)[12] are frequently used.

However, many diagnostic tools and platforms developed over the past decade fail to utilize the full potential of modern computer and audiometric technologies commonly applied in hearing diagnostics. More critically, these tools often lack standardization and objectivity. Test outcomes can be influenced by numerous variables, including the examiner's voice volume, physical presence, and whether their mouth is obscured (e.g., by hands, papers, or books to prevent lip-reading). Additional factors such

as the patient's orientation (facing or side-facing the examiner), the distance between examiner and patient, and environmental conditions (e.g., reverberation, background noise) further contribute to variability. This lack of control makes it difficult to achieve reproducible and reliable assessments of phonemic hearing.[13]

An anonymous survey conducted among 15 experienced speech therapists, each with a minimum of three years of professional practice, highlighted the lack of consistency in current phonemic hearing assessment practices. The survey revealed considerable variation in key testing conditions. For instance, the distance between the examiner and the patient ranged from 25 to 100 cm, with a mean distance of 61.7 cm and a standard deviation (SD) of 17.8 cm.

Additionally, the patient's position relative to the examiner varied. In 73.3% of cases, patients sat facing the examiner with measures taken to prevent lip-reading, while in 26.7% of cases, they were seated beside the examiner. Among those seated face-to-face, 72.7% of examiners used a sheet of paper to cover the patient's mouth, 18.2% used their hand, and 9.1% used a book.

These discrepancies were further corroborated by sound level meter measurements and survey responses, both of which highlight a significant lack of consistency and standardization in phonemic hearing diagnostics.

Objectives

The main goal of this study was to develop an objective tool for diagnosing phonemic hearing. The tool was designed to ensure consistent presentation of verbal stimuli in terms of intensity, distance, and direction. A secondary objective of the study was to compare phonemic hearing abilities between children with and without APD to determine whether significant differences exist between the two groups.

Materials and methods

Study design and sample

To examine how professionals conduct phonemic awareness assessments, a study with 20 participants was carried out. A sound level meter measured the loudness of the therapist's voice during the diagnosis. Each participant was asked to naturally repeat 2 pairs of words that contain opposing sounds: "Tomek – domek" (t:d) and "dróżka – gruszka" (d:g). Based on these measurements, we calculated the amplitude differences for each therapist, referred to as Diff TD and Diff DG. The study was conducted in a medium-sized room measuring approx.16 m^2, resembling a typical speech therapy office. The participant was seated facing the sound level meter at a standard desk distance, replicating real-world assessment conditions. They were instructed to repeat the presented word pairs ("Tomek," "domek," "dróżka," "gruszka") with the opposing sounds in 5 different ways: With an uncovered mouth, covered by a sheet of paper, covered by a book, covered by a hand, and sitting sideways to the meter. These positions reflect common methods used by speech therapists during natural phonemic hearing tests.

Statistical analyses

All analyses were performed using the Automated Statistical Description System (System Zautomatyzowanego Tworzenia Opisu Statystycznego (SZTOS)). To assess the normality of the data, 2 Shapiro–Wilk tests were conducted. The results showed that the Diff DG measurements significantly deviated from a normal distribution (SW = 0.90; p = 0.034), while the Diff TD measurements were closer to normal (SW = 0.91; p = 0.078).

Since the Diff DG data did not follow a normal distribution, the nonparametric Wilcoxon signed-rank test was applied. In contrast, the Diff TD data met the assumptions of normality, allowing for the use of a one-sample Student's t-test. To compare amplitude measurement values across different methods of presenting verbal stimuli, a series of t-tests were conducted against reference values increasing in 0.5 dB increments.

Results

Preliminary results are presented in Table 1. Values highlighted in green represent the minimum, while those in red indicate the maximum, within the significance analysis of discrepancies. These discrepancies pertain to two key aspects: The variation observed when the same diagnostician presented phonemic oppositions using different methods, and the variation when the same phonemic opposition was presented by different diagnosticians.

The analysis revealed significant variability both in the articulation of verbal material by different examiners and in the presentation methods used by the same examiner. When the same phonemic opposition was presented in an identical manner by different diagnosticians, amplitude differences of up to 10.8 dB were observed (SD = 2.5 dB). In comparison, when the same diagnostician presented the opposition using different articulation methods, differences reached up to 8.4 dB (SD = 3.4 dB).

An analysis of amplitude intensities for the phonemic opposition t : d, which had an average of 3.88 dB PL in the tested group, showed a significant difference from the reference value range of 0 to 2.5 dB PL. For a reference value of 3 dB PL, the difference was at the borderline of statistical significance (p = 0.083). These results are shown in Table 2 and Fig. 1.

Similarly, for the phonemic opposition d:g, which had a mean amplitude of 4.34 dB PL, a significant difference was observed within the range of 0 to 2.5 dB PL (p = 0.010).

Table 1. Results of diagnostician's testing

Diagnostician	Phonemic opposition t : d										Phonemic opposition d : g									
	not covered	sheet	book	hand	side	AVG	Max	Min	Diff	StDev	not covered	sheet	book	hand	side	AVG	Max	Min	Diff	StDev
1	50.5	49.3	49.9	48.5	48.4	49.3	50.5	48.4	2.1	0.90	49.3	50.9	50.5	49.9	49.5	50.0	50.9	49.3	1.6	0.7
2	49.6	49.9	48.9	48.7	48.7	49.2	49.9	48.7	1.2[a]	0.55[a]	49.8	52.1	49.8	50.2	53.1	51.0	53.1	49.8[b]	3.3	1.5
3	50.1	50.1	48.4	50.6	48.6	49.6	50.6	48.4	2.2	0.99	50.0	49.1	49.1	51.3	50.1	49.9	51.3	49.1	2.2	0.9
4	49.3	49.4	55.2	50.2	55.1	51.8	55.2	49.3	5.9	3.04	55.4	49.2	55.0[b]	50.1	51.7	52.3	55.4	49.2	6.2	2.8
5	49.7	51.3	49.8	48.9	49.2	49.8	51.3	48.9	2.4	0.93	54.8	49.1	54.5	50.3	50.2	51.8	54.8	49.1	5.7	2.7
6	49.4	50.8	50.8	50.0	49.8	50.2	50.8	49.4	1.4	0.62	50.3	48.0	49.8	48.8	51.4	49.7	51.4	48.0	3.4	1.3
7	50.7	49.6	50.7	50.7	54.8	51.3	54.8	49.6[b]	5.2	2.01	49.7	49.8	49.6	50.2	48.0	49.5	50.2	48.0	2.2	0.8
8	49.2	49.8	57.0[b]	49.6	50.0	51.1	57.0[b]	49.2	7.8[b]	3.30[b]	49.5	49.4	51.3	51.3	50.6	50.4	51.3	49.4	1.9	0.9
9	47.2	47.2	49.4	50.4	48.2	48.5	50.4	47.2	3.2	1.40	48.0	51.6	55.0	51.4	55.5	52.3	55.5	48.0	7.5	3.1
10	47.4	48.5	49.7	47.8	50.9	48.9	50.9	47.4	3.5	1.44	50.5	50.2	47.9	47.9	47.3	48.8	50.5	47.3	3.2	1.5
11	46.4	47.7	49.0	53.4	47.8	48.9	53.4	46.4	7.0	2.70	48.5	47.7	47.4	49.8	47.6	48.2	49.8	47.4	2.4	1.0
12	47.5	47.6	48.6	47.4	48.7	48.0	48.7	47.4	1.3	0.63	49.7	46.9	48.6	46.5	49.1	48.2	49.7	46.5	3.2	1.4
13	52.1	50.9	48.7	47.8	49.0	49.7	52.1	47.8	4.3	1.75	55.0	48.2	48.3	49.4	47.5	49.7	55.0	47.5	7.5	3.1
14	49.2	51.0	48.3	50.0	48.9	49.5	51.0	48.3	2.7	1.05	53.1	49.6	48.9	47.1	52.0	50.1	53.1	47.1	6.0	2.4
15	47.7	48.7	47.5	49.1	48.1	48.2	49.1	47.5	1.6	0.67	48.8	49.2	48.9	49.4	50.9	49.4	50.9	48.8	2.1	0.9
16	48.4	52.0	49.3	48.1	45.9	48.7	52.0	45.9[a]	6.1	2.21	54.4	48.7	49.2	49.7	47.0	49.8	54.4	47.0	7.4	2.8
17	48.0	50.0	52.4	48.8	49.2	49.7	52.4	48.0	4.4	1.68	48.3	48.7	47.3	48.0	48.6	48.2	48.7	47.3	1.4[a]	0.6[a]
18	50.9	49.2	48.6	49.4	49.9	49.6	50.9	48.6	2.3	0.86	55.7	48.0	47.3	48.8	48.9	49.7	55.7[b]	47.3	8.4[b]	3.4[b]
19	47.7	49.4	46.2[a]	52.4	47.7	48.7	52.4	46.2	6.2	2.37	54.0	49.3	47.8	54.2	48.1	50.7	54.2	47.8	6.4	3.2
20	46.6	53.4	49.4	47.1	49.0	49.1	53.4	46.6	6.8	2.69	50.0	49.0	46.1[a]	48.6	51.0	48.9	51.0	46.1[a]	4.9	1.8
AVG	48.9	49.8	49.9	49.4	49.4	49.5	51.8	48.0	3.9	1.59	51.2	49.2	49.6	49.6	49.9	49.9	52.3	48.0	4.3	1.8
Max	52.1	53.4	57.0	53.4	55.1	51.8	57.0	49.6	7.8	3.30	55.7	52.1	55.0	54.2	55.5	52.3	55.7	49.8	8.4	3.4
Min	46.4	47.2	46.2	47.1	45.9	48.0	48.7	45.9	1.2	0.55	48.0	46.9	46.1	46.5	47.0	48.2	48.7	46.1	1.4	0.6
Diff	5.7	6.2	10.8[b]	6.3	9.2	3.9	8.3	3.7[a]	6.6	2.75	7.7	5.2	8.9[b]	7.7	8.5	4.1	7.0	3.7[a]	7.0	2.8
St. Dev.	1.6	1.5	2.5[b]	1.6	2.2	1.0[a]	2.1	1.1	2.2		2.7[b]	1.3	2.6	1.7	2.2	1.2	2.3	1.1[a]	2.3	1.0

a – minimum values; b – maximum values for significant analysis of the results in terms of discrepancies when examining different ways of presenting phonemic oppositions by the same diagnostician, as well as presenting the same phonemic opposition by different diagnosticians in the same manner.

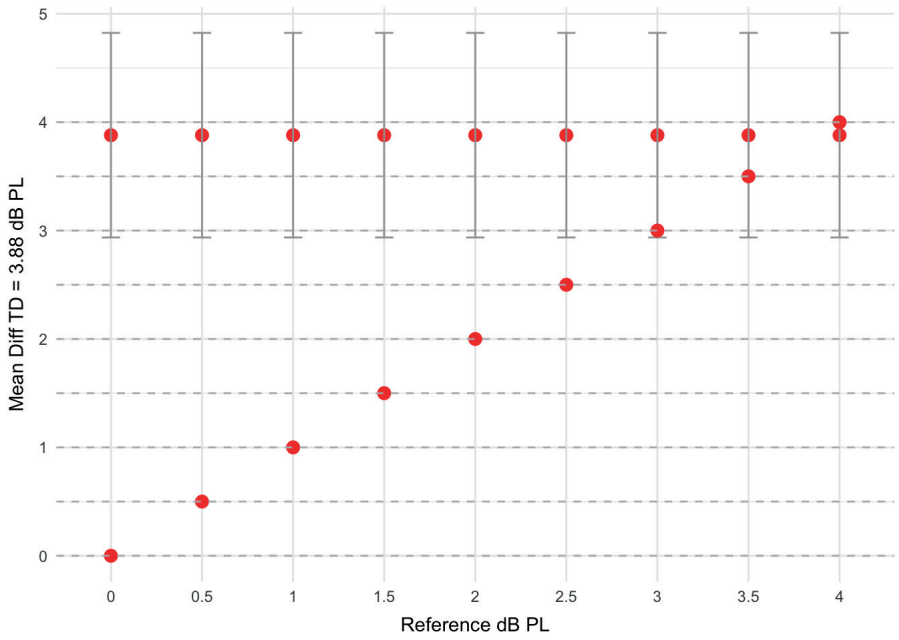

Fig. 1. Comparison of the phonemic opposition t : d measurement values from the sample with the corresponding reference values

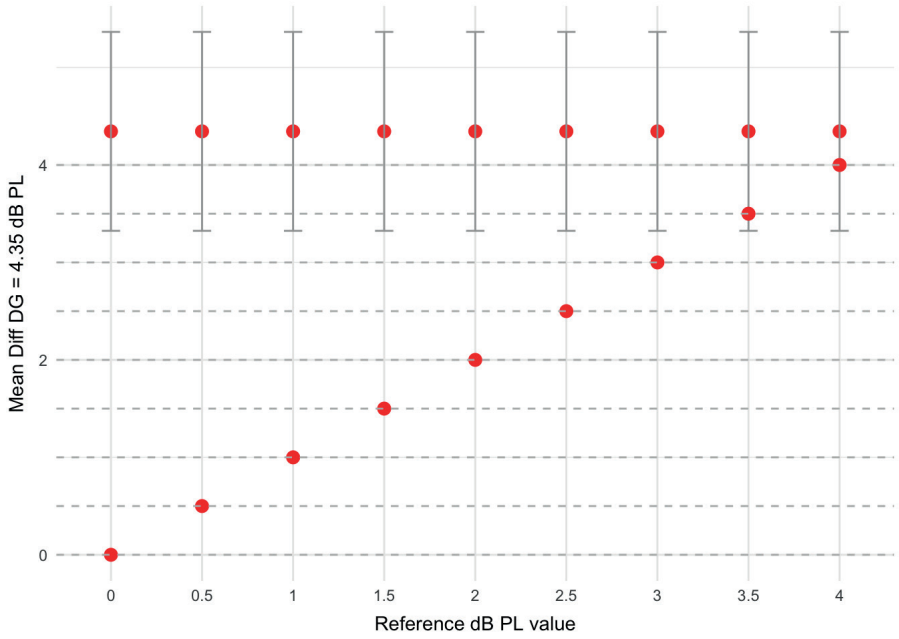

Fig. 2. Comparison of the phonemic opposition d : g measurement values from the sample with the corresponding reference values

These results are summarized in Table 3 and illustrated in Fig. 2. The observed variability exceeds the commonly accepted threshold for test-retest reliability in speech recognition tasks, which is 2 dB for typically functioning listeners.[14]

Discussion

The various discrepancies identified above, which adversely impact the consistency of test results, support the conclusion that an objective tool for phonemic hearing diagnostics is essential. Such a tool would ensure that verbal stimuli are consistently presented at the same intensity, distance, and direction. This level of standardization would enhance the repeatability and comparability of assessments – both across different patients and within repeated assessments of the same patient. Key factors influencing the reliability of these tests include procedural consistency, adherence to standardized protocols and diagnostic methods, and the use of uniform, calibrated equipment during testing.[15]

Audiological module for objective diagnosis of phonemic awareness

Considering the need for an objective diagnostic tool, an audiometric module was developed for assessing phonemic awareness. This tool is useful for specialists diagnosing

Table 2. Comparison of the phonemic opposition t : d measurement values from the sample with the corresponding reference values

M	ref	t	p-value
3.88	0.0	8.059	0.000
3.88	0.5	7.021	0.000
3.88	1.0	5.982	0.000
3.88	1.5	4.944	0.000
3.88	2.0	3.905	0.001
3.88	2.5	2.867	0.010
3.88	3.0	1.828	0.083
3.88	3.5	0.789	0.440
3.88	4.0	–0.249	0.806

M – mean level of the Diff t : d measurement in the tested sample; ref – reference value against which the Diff t : d value is tested; t – t-test Student value for a one-sample test.

Table 3. Comparison of the phonemic opposition d : g measurement values from the sample with the corresponding reference values

M	ref	V	p-value
4.34	0.0	210	0.000
4.34	0.5	210	0.000
4.34	1.0	210	0.000
4.34	1.5	209	0.000
4.34	2.0	196	0.001
4.34	2.5	174	0.010
4.34	3.0	154	0.070
4.34	3.5	141	0.200
4.34	4.0	125	0.500

M – mean level of the Diff d : g measurement in the tested sample; ref – reference value against which the Diff d : g value is tested; V – one-sample Wilcoxon signed rank test.

auditory processing disorders and related issues. The audiometer is equipped with a program containing 42 phonemic oppositions common in Polish. For each pair of rhyming words, 2 additional non-rhyming, differently sounding words are included to verify the patient's understanding and attention (Table 4).

The use of the Interacoustics AD 528 audiometer (Interacoustics A/S, Middelfart, Denmark), into which the diagnostic module is integrated, enables reliable phonemic hearing assessments. These assessments typically include evaluation of both air and bone conduction hearing. It is important to remember that phonemic awareness is fundamental to proper hearing function.

The dedicated audiometric module makes phonemic diagnosis objective and repeatable. The same narrator always delivers speech in the same manner, and the patient is positioned at the same distance from the speakers. The module also includes a photo-based book featuring modern graphics and vibrant colors. Photographs, rather than drawings, were intentionally used to make the assessment more appropriate for older patients and to avoid an infantilizing impression.

A dedicated diagnostic card accompanies the module, providing a clear and structured presentation of the phonemic assessment results. This facilitates subsequent diagnostic and therapeutic decision-making, including the need for further testing for APD or dyslexia, referrals for speech therapy, or the formulation of appropriate educational recommendations.

During the examination, the patient sits at a designated spot calibrated by the device, facing a centrally located speaker. In an open-field setting, phonemic hearing tests are conducted according to the following steps:

1. The examiner names objects depicted in photographs, and the patient is asked to point to the corresponding image (concept learning phase).
2. The examiner then asks targeted questions, and the patient selects the appropriate photograph in response.
3. If the patient responds correctly to all items, the examiner proceeds to the next phonemic opposition.
4. If any errors occur, the specific phonemic opposition is retested to confirm or clarify the result.

Repeated errors involving rhyming words may indicate a specific disturbance in the corresponding phonemic function. A higher number of errors across various items may suggest broader difficulties with phonemic awareness. Based on the results of these assessments, clinicians can confirm or rule out phonemic hearing disorders and identify appropriate therapeutic interventions.

Diagnosing phonemic functions is essential in evaluating learning difficulties, persistent articulation issues despite speech therapy and in diagnosing dyslexia.

Utilizing the audiometric module for assessing phonemic awareness in children with APD and children without APD

Given the complexity of APD symptoms and its various aspects, it is crucial to use diagnostic methods that can provide comprehensive insights into a patient's condition within the limited time of a consultation.[16] Having developed an objective tool for assessing phonemic hearing, a key question arises: Do children with APD, who have difficulties with learning, understanding complex commands, and recalling verbally delivered information, also experience more severe disruptions in phonemic hearing compared to children without APD? To explore this, in-depth diagnostics were conducted on 2 groups – children with APD and typically developing children (without higher auditory function disorders) – assuming that phonemic hearing issues might be more pronounced in the 1st group.

Study design and sample

The study involved 120 children aged 8–12 years (since auditory perception continues to develop until around age 7), divided into 2 groups of 60 each. All participants had normal hearing confirmed by audiometric and

Table 4. Examples of phonemic oppositions in Polish language

42 phonemic oppositions implemented for diagnosis with the audiometric module	Oppositive phonemes (Orthographic Polish Transcription)	Oppositive phonemes (International Phonetic Alphabet (IPA))
1	półki – bułki	[pu̯ʲki] [puwci] – [bu̯ʲki] [buwci]
2	łapa – ława	[u̯apa] [wapa] – [u̯ava] [wava]
3	paczki – kaczki	[paʧki] [paʧci] – [kaʧki] [kaʧci]
4	boli – goli	[bolʲi] [bɔlʲji] – [golʲi] [gɔlʲji]
5	bije – wije	[b̯ije] [bjijɛ] – [v̯ʲie] [vʲijɛ]
6	Burek – murek	[burek] [burɛk] – [murek] [murɛk]
7	beczki – teczki	[beʧki] [bɛʧci] – [teʧki] [tɛʧci]
8	Tomek – domek	[tõmek] [tõmɛk] – [dõmek] [dõmɛk]
9	kot – koc	[kot] [kɔt] – [koc] [kɔʦ]
10	taczki – kaczki	[taʧki] [taʧci] – [kaʧki] [kaʧci]
11	matka – maska	[matka] [matka] – [maska] [maska]
12	dróżka – gruszka	[druška] [druʃka] – [gruška] [gruʃka]
13	dęby – zęby	[demby] [dɛmbʲ] – [zemby] [zɛmbʲ]
14	kury – góry	[kury] [kurʲ] – [gury] [gurʲ]
15	gąbki – ząbki	[gõ̯bʲki] [gɔ̃wpci] – [zõ̯bʲki] [zɔ̃wpci]
16	liszki – liski	[liˑškʲi] [liˑʃci] – [liˑskʲi] [liˑsci]
17	nos – noc	[nos] [nɔs] – [noc] [nɔʦ]
18	sale – fale	[sale] [salɛ] – [fale] [falɛ]
19	kasa – Kasia	[kasa] [kasa] – [kaśa] [kaɕa]
20	nosze – noże	[noše] [nɔʃɛ] – [noże] [nɔʒɛ]
21	kaszka – kaczka	[kaška] [kaʃka] – [kačka] [kaʧka]
22	szałas – hałas	[šau̯as] [ʃawas] – [xau̯as] [xawas]
23	czapka – żabka	[čapkʲi] [ʧapci] – [žabkʲi] [ʒapci]
24	tacka – taczka	[tacʲki] [taʦci] – [tačʲki] [taʧci]
25	zebra – żebra	[zebra] [zɛbra] – [žebra] [ʒɛbra]
26	zagony – wagony	[zagõny] [zagɔ̃nʲ] – [vagõny] [vagɔ̃nʲ]
27	Basie – bazie	[baśe] [baɕɛ] – [baźe] [baʑɛ]
28	w lesie – w lecie	[v] [v] [leśe] [lɛɕɛ] – [v] [v] [leće] [lɛʨɛ]
29	bucik – budzik	[bućik] [buʨik] – [buʒik] [budʑik]
30	kura – kula	[kura] [kura] – [kula] [kula]
31	rama – jama	[rãma] [rãma] – [i̯ãma] [jãma]
32	mak – rak	[mak] [mak] – [rak] [rak]
33	mak – hak	[mak] [mak] – [χak] [xak]
34	murek – nurek	[murek] [murɛk] – [nurek] [nurɛk]
35	wata – łata	[u̯ata] [wata] – [vata] [vata]
36	pieści – pięści	[pʲi̯eśći] [pʲjɛʨi] – [pʲi̯ɛ̃ɲśći] [pʲjɛ̃ɲʨi]
37	kosa – kąsa	[kosa] [kɔsa] – [kõnsa] [kɔ̃nsa]
38	łyżka – łóżka	[u̯yška] [wiʃka] – [u̯uška] [wuʃka]
39	wir – wór	[v̯ʲir] [vʲir] – [vur] [vur]
40	leki – loki	[leʲki] [lɛci] – [loʲki] [lɔci]
41	wyje – wije	[vy̯ie] [vijɛ] – [v̯ʲie] [vʲijɛ]
42	trawa – trasa	[trava] [trava] – [trasa] [trasa]

tympanometric tests, and intellectual disability was ruled out based on IQ assessments. The 1st group included children diagnosed with APD based on tests evaluating higher auditory functions. The 2nd group consisted of children whose testing did not indicate the presence of APD.

All participants underwent a diagnostic assessment of higher auditory functions, including the following test:

Adaptive Speech Understanding in Noise – Word Level: The child wears headphones and listens to speech babble noise in their native language. During this noise, a narrator presents single words, and the child's task is to repeat them. The noise level increases gradually until the child makes errors, allowing the determination of the signal-to-noise ratio (SNR) threshold.

Table 5. Basic descriptive statistics of the distributions of the 42 phoneme oppositions (DFF42) variables

Variable	n	Min	Max	M	SD	SE
DFF42	120	0.00	5.00	1.35	1.19	0.11

n – number; Min – minimum; Max – maximum; M – mean; SD – standard deviation; SE – standard error.

Table 6. Normality tests and measures of skewness for the distributions of the 42 phoneme oppositions (DFF42 variables)

Variable	KS		Measures of distribution symmetry	
	KS	p-value	skewness	kurtosis
DFF42	0.22	< 0.001	0.80	0.34

KS – Kolmogorov–Smirnov test statistic with Lilieforce's correction.

Table 7. Normality tests and measures of skewness for the distributions of the DFF42 variables in groups distinguished based on the 2 groups (children with and without auditory processing disorder (APD))

Variable	Group	KS		Measures of distribution symmetry	
		KS	p-value	skewness	kurtosis
DFF42	no APD	0.33	< 0.001	0.95	–0.30
	APD	0.25	< 0.001	1.05	0.47

APD – auditory processing disorder; KS – Kolmogorov–Smirnov test statistic with Lilieforce's correction.

Table 8. Differences between groups of children with and without auditory processing disorder (APD) in terms of the levels of the DFF42 variables

Dependent variable	No CAPD (a)					CAPD (b)					Mann–Whitney U test			rg
	n	M	SD	Me	Mrang	n	M	SD	Me	Mrang	U	p-value	Difference a vs b	
DFF42	60	0.73	0.94	0.00	42.18	60	1.97	1.09	2.00	78.82	701.00	< 0.001	a < b	0.61

Mrang – mean rank; U – Mann–Whitney U statistic; rg – Glass's effect size correlation test statistic; M – mean; SD – standard deviation; Me – median.

Adaptive Speech Understanding in Noise – Sentence Level: The child wears headphones and listens to speech babble noise in their native language. During this noise, a narrator presents short sentences, which the child repeats. The noise level gradually increases until errors occur, allowing the determination of the signal-to-noise ratio (SNR) threshold.

The dichotic Digit Test involves the child wearing headphones through which 4 digits are presented, 2 to each ear, almost simultaneously. The child's task is to repeat as many heard and remembered digits as possible. The results in this test are given separately for the right and left ear.

Auditory Reaction Test: The child wears headphones and listens to single sounds of the same frequency. The child's task is to react as quickly as possible whenever they hear the stimulus.

Frequency Pattern Test: The child wears headphones and hears a sequence of 3 sounds, each of high or low pitch. The child's task is to identify and name each sound in the correct order.

Difference Limen of Frequency test: The child wears headphones and hears a constant, irrelevant tone with occasional higher-pitched sounds interspersed. The child's task is to react when they detect the higher-frequency sound.

Gap Detection in Noise: The child listens to noise through headphones, with occasional silent gaps inserted. The child's task is to detect and react when they hear a break in the noise.

Next, all 120 children underwent a phonemic function assessment using an audiometric module containing 42 phonemic oppositions. The results are presented in the tables below, with disrupted phonemic oppositions highlighted in red. Table 1 presents the data for children diagnosed with APD, while Table 2 shows the results for children in whom APD was excluded.

Statistical analyses

To assess significant differences between the 2 groups – children diagnosed with APD and children with excluded APD – a Mann–Whitney U test was performed. Despite the variances of the DFF42 measurements being equal across groups ($F = 0.08$; $p = 0.772$), the non-parametric test was chosen due to the failure to meet normality assumptions both overall and within the subgroups. The total sample size was $n = 120$, with 60 children in each group.

The effect size was evaluated using Glass's biserial correlation measure. Descriptive statistics for the DFF42 measurements are presented in Table 5.

To verify the assumption of normality, the Kolmogorov–Smirnov test with Lilliefors correction was employed (appropriate for $n > 50$). Results indicated that normality

Table 9. The results of the phonemic opposition examination using the audiometric module in 60 patients with auditory processing disorder (APD)

Patient No.	DFF – 42 phonemic oppositions tests (children with APD)																																									
	1	2	3	4	5	6	7	8	9	10	11	12	13	14	15	16	17	18	19	20	21	22	23	24	25	26	27	28	29	30	31	32	33	34	35	36	37	38	39	40	41	42
	PB	PW	PK	BG	BW	BM	BT	TD	TC	TK	TS	DG	DZ	KG	GZ	SSz	SC	SF	SW	SŚ	SzŻ	SzCz	SzH	CzŻ	CCz	ZŻ	ZW	ŚŻ	ŚĆ	ĆDż	RL	RJ	MR	MH	MN	WŁ	EĘ	OĄ	YU	IU	EO	YI
1																																										x
2																												x														
3																												x							x							
4	x							x																																		
5	x					x						x																														
6																x								x				x														
7																																x										x
8																x																					x					
9		x			x								x																													
10																			x														x			x						
11														x	x	x					x																					
12										x				x													x															
13																																						x		x		
14																															x				x							
15																x																										
16		x						x																																		
17																x																										
18														x																												
19	x		x					x							x																											
20																			x																							
21														x																												
22						x				x		x			x																											
23																												x							x						x	
24																																			x							
25		x		x										x						x																						
26																								x		x				x									x	x		
27																																				x						x
28																x										x																
29	x															x																										
30																																										x
31																			x																							

Table 9. The results of the phonemic opposition examination using the audiometric module in 60 patients with auditory processing disorder (APD) – cont.

Patient No.	DFF – 42 phonemic oppositions tests (children with APD)																																									
	1	2	3	4	5	6	7	8	9	10	11	12	13	14	15	16	17	18	19	20	21	22	23	24	25	26	27	28	29	30	31	32	33	34	35	36	37	38	39	40	41	42
	PB	PW	PK	BG	BW	BM	BT	TD	TC	TK	TS	DG	DZ	KG	GZ	SSz	SC	SF	SW	SŚ	SzŻ	SzCz	SzH	CzŻ	CCz	ZŻ	ZW	ŚŻ	ŚĆ	ĆDź	RL	RJ	MR	MH	MN	WŁ	EĘ	OĄ	YU	IU	EO	YI
32							x					x			x																											
33														x																												
34								x																																		
35	x							x																																		
36																x																										
37																																			x							
38													x																													
39																x	x																									
40							x						x																													
41									x																																	
42															x																											
43	x			x																																					
44																		x			x																					
45															x	x						x		x		x																
46																x																										
47																												x							x							
48												x																														
49																x					x																					
50						x																																			
51	x						x							x																											
52	x																																								
53																x																										
54																			x											x							x				
55																																		x								
56													x		x																											
57																																									x
58																x																										
59					x										x																											
60																																								x	

x – disrupted phonemic oppositions.

Table 10. The results of the phonemic opposition examination using the audiometric module in 60 patients with excluded auditory processing disorder (APD)

Patient No.	DFF – 42 phonemic oppositions tests (children without APD)																																								
	1	2	3	4	5	6	7	8	9	10	11	12	13	14	15	16	17	18	19	20	21	22	23	24	25	26	27	28	29	30	31	32	33	34	35	36	37	38	39	40	41	42
	PB	PW	PK	BG	BW	BM	BT	TD	TC	TK	TS	DG	DZ	KG	GZ	SSz	SC	SF	SW	SŚ	SzŻ	SzCz	SzH	CzŻ	CCz	ZŻ	ZW	ŚŹ	ŚĆ	ĆDź	RL	RJ	MR	MH	MN	WŁ	EĘ	OĄ	YU	IU	EO	YI
1						x																																				
2																																										x
3																																										
4								x																																		
5								x																																		
6				x								x																														
7																																										
8																												x						x								
9																																										
10	x															x								x																		
11																																										
12																				x	x																					
13																																										
14																								x		x																
15																x																										
16																																										
17																		x																								
18																				xx																						
19																																										
20																																										
21																				x																						
22																x										x																
23																																										
24																																										
25																																										
26																																										
27																																										
28																										x																
29																																										
30	x																														x	x										
31													x	x																												

Table 10. The results of the phonemic opposition examination using the audiometric module in 60 patients with excluded auditory processing disorder (APD) – cont.

Patient No.	DFF – 42 phonemic oppositions tests (children without APD)																																									
	1	2	3	4	5	6	7	8	9	10	11	12	13	14	15	16	17	18	19	20	21	22	23	24	25	26	27	28	29	30	31	32	33	34	35	36	37	38	39	40	41	42
	PB	PW	PK	BG	BW	BM	BT	TD	TC	TK	TS	DG	DZ	KG	GZ	SSz	SC	SF	SW	SŚ	SzŻ	SzCz	SzH	CzŻ	CCz	ZŻ	ZW	ŚŹ	ŚĆ	ĆDź	RL	RJ	MR	MH	MN	WŁ	EĘ	OĄ	YU	IU	EO	YI
32																																										
33																																										
34																																										
35																																										
36																																										
37	x															x																										
38																																										
39																																										
40																																										
41																												x														
42																																										
43																																										
44																														x			x		x							
45																																										
46								x				x																														
47																																										
48																																										
49																																										x
50																																x			x							
51																																										
52																																										
53																		x	x																							
54																																										
55															x																											
56																																									x	
57																			x																		x					
58																																										
59																																										
60																																										

x – disrupted phonemic oppositions.

was not met in the overall sample (KS = 0.22; p < 0.001), nor within either subgroup: children with excluded APD (KS = 0.33; p < 0.001) and children with diagnosed APD (KS = 0.25; p < 0.001). These results, along with measures of skewness and descriptive statistics, are summarized in Tables 6,7. Between-group comparisons are shown in Table 8. Table 9 displays the phonemic opposition results from the audiometric assessment in children with APD. The average number of incorrectly identified phoneme positions in this group was 1.97 per person (SD = 1.09).

Table 10 presents the results for children without APD, with an average of 0.73 incorrect phoneme identifications (SD = 0.94).

Mann–Whitney U test revealed a significant difference between the groups (U = 701.00; p < 0.001). The APD group scored higher (mean rank = 78.82), indicating more errors, while the non-APD group scored lower (mean rank = 42.18). The effect size was large (r_g = 0.61). The results are visually summarized in Fig. 3.

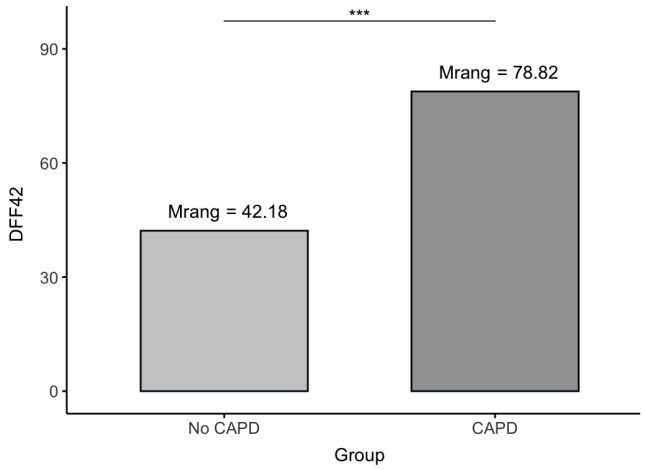

Fig. 3. Differences between of children with and without auditory processing disorder (APD) in terms of the levels of the DFF42 variable

Limitations

Several limitations of this study should be acknowledged. First, the research sample was limited to children aged 8–12 years, which restricts the generalizability of the findings to other age groups. Second, there is a notable lack of comparable studies in this area, making it difficult to contextualize the results within the broader literature. Given these limitations, future research should investigate similar issues in both adolescent and adult populations.

Conclusions

Variability in sound intensity during phonemic hearing tests – observed in a group of 20 specialists operating under different acoustic conditions – underscored the need for an objective diagnostic tool. These differences were primarily attributed to inconsistencies in the vocal intensity of diagnosticians. In response, an audiometric module for phonemic hearing assessment was developed. This tool ensures standardized presentation of verbal stimuli, thereby enhancing the reliability and repeatability of diagnostic results.

The study revealed a highly significant (p < 0.001) difference between the phonemic hearing assessment results of children with APD and those without. Among the 60 children with APD, phonemic hearing deficits were more frequent and more pronounced – indicating that more phonemic oppositions were not heard by these patients – while in the group of 60 children without APD, the number of incorrectly identified oppositions was reduced by 62.9%. Nevertheless, phonemic hearing difficulties were also observed in children without a diagnosis of APD. Such deficits may result in substantial challenges in both learning and everyday functioning.

These preliminary findings suggest the importance of developing targeted therapeutic procedures for children with phonemic hearing deficits. Special attention should be given to children with both APD and phonemic hearing disorders, as their coexistence can severely impact academic performance and peer relationships. This can result in lowered self-esteem and, in some cases, psychological issues – such as behavioral problems, outbursts of aggression, tearfulness, and, in extreme cases, self-harm and suicide attempts. These issues have been particularly evident following periods of remote learning during the COVID-19 pandemic.

Data availability

The datasets generated and/or analyzed during the current study are available from the corresponding author on reasonable request.

Consent for publication

All authors agree to publish personal information about an individual.

Use of AI and AI-assisted technologies

Not applicable.

ORCID iDs

Anna Kasprzyk https://orcid.org/0000-0001-6804-3611
Grażyna Mielnik-Niedzielska https://orcid.org/0000-0002-0818-9771
Artur Niedzielski https://orcid.org/0000-0001-9062-040

References

1. Luria A. *Travmaticheskaya Afaziia*. Moscow, Russia: Izdatelstvo Akademii Meditsinskikh Nauk SSSR; 1947.
2. Kilpatrick DA. *Equipped for Reading Success: A Comprehensive, Step-by-Step Program for Developing Phoneme Awareness and Fluent Word Recognition*. Reprinted with minor text changes and corrections. Syracuse, USA: Casey & Kirsch Publishers; 2023. ISBN:978-0-9646903-6-3.

3. Moats LC. *Speech to Print: Language Essentials for Teachers*. 3rd ed. Baltimore, USA: Paul H. Brookes Publishing Co; 2020. ISBN:978-1-68125-330-5.
4. Odowska-Szlachcic B, Mierzejewska B. *Wzrok i Słuch: Zmysły Wiodące w Uczeniu Się w Aspekcie Integracji Sensorycznej*. Gdańsk, Poland: Harmonia Universalis; 2013. ISBN:978-83-7744-045-2.
5. Milewski S. *Lingwistyczne i Dydaktyczne Aspekty Analizy Fonemowej*. Lublin, Poland: Wydawn. Uniwersytetu Marii Curie-Skłodowskiej; 1999. ISBN:978-83-227-1335-8.
6. Wepman JM. *Auditory Discrimination Test*. Chicago, USA: Language Research Associates; 1958.
7. Sunderland M. *Helping Children with Low Self-Esteem: A Guidebook*. London, UK: Taylor & Francis Group; 2003. ISBN:978-0-86388-466-5, 978-1-351-69295-3
8. Katz J. *Therapy for Auditory Processing Disorders: Simple Effective Procedures*. Prairie Village, USA: J. Katz ; Distributed by Educational Audiology Association; 2009. ISBN:978-0-9841511-0-3.
9. Geffner D, Goldman M. *Auditory Skills Assessment (ASA)*. London, UK: Pearson Publishing; 2010.
10. Robertson C, Salter W. *Phonological Awareness Test – Second Edition (PAT-2)*. Novato, USA: Academic Therapy Press; 2007.
11. Porayski-Pomsta J. *Znaki fonetyczne do zapisu poprawnych i zdeformowanych realizacji fonemów języka polskiego w alfabetach międzynarodowym i slawistycznym*. Gdańsk, Poland: Glottispol; 2013. ISBN:978-83-86804-81-8.
12. Styczek I. *Badanie i Kształtowanie Słuchu Fonematycznego: Komentarz i Tablice*. Warsaw, Poland: Wydawnictwa Szkolne i Pedagogiczne; 1982. ISBN:978-83-02-00052-2.
13. Baas E. Educational audiology: Methodology for auditory processing disorders. *J Hear Sci*. 2011;1(3):52–53. https://www.journalofhearingscience.com/pdf-120881-49534?filename=49534.pdf. Accessed March 1, 2025
14. International Organization for Standardization (ISO). International standard ISO 8253-3:2022(E) – Acoustics – Audiometric test methods – Part 3: Speech audiometry (ISO 8253-3:2022). Third edition 2022-01. 2022. https://www.iso.org/standard/74049.html. Accessed March 1, 2025.
15. Włodarczyk EA, Szkiełkowska A, Skarżyński H, Miaśkiewicz B, Skarżyński PH. Reference values for psychoacoustic tests on Polish school children 7–10 years old. *PLoS One*. 2019;14(8):e0221689. doi:10.1371/journal.pone.0221689
16. Skarżyński H, Bieńkowska K, Gos E, et al. Cross-cultural adaptation of the Scale of Auditory Behaviors Questionnaire. *Lang Speech Hear Serv Sch*. 2019;50(4):683–692. doi:10.1044/2019_LSHSS-19-0014

Cisplatin-induced *WWP1*-eccDNA expression contributes to ovarian cancer resistance

Chenyang Lu[1,B–D], Li Han[2,3,A,E,F], Xiaojuan Guo[2,3,B–D], Ruijuan Du[2,3,B–D], Hui Zhang[2,3,B–D], Kelei Guo[2,3,B–D], Yunfei Tu[4,B–D], Ruifang Li[1,A,E,F]

[1] College of Basic Medicine and Forensic Medicine, Henan University of Science and Technology, China
[2] Zhang Zhongjing College of Chinese Medicine, Nanyang Institute of Technology, China
[3] Henan Key Laboratory of Zhang Zhongjing Formulae and Herbs for Immunoregulation, Nanyang Institute of Technology, China
[4] Department of Surgery, The Second Affiliated Hospital of Nanyang Medical College, China

A – research concept and design; B – collection and/or assembly of data; C – data analysis and interpretation; D – writing the article; E – critical revision of the article; F – final approval of the article

Advances in Clinical and Experimental Medicine, ISSN 1899–5276 (print), ISSN 2451–2680 (online) *Adv Clin Exp Med*. 2026;35(2):279–290

Address for correspondence
Rui-Fang Li
E-mail: ylliruifang@163.com

Funding sources
This work was funded by the National Natural Science Foundation of China (grant No. 82074076), the Natural Science Foundation of Henan Province (grant No. 202300410022), and the Science and Technology Project of Henan Province (grant No. 242102311268).

Conflict of interest
None declared

Received on December 5, 2024
Reviewed on March 15, 2025
Accepted on April 15, 2025

Published online on September 4, 2025

Abstract

Background. Multidrug resistance remains a major obstacle in the treatment of ovarian cancer (OC) patients. Recent research has underscored the critical role of extrachromosomal circular DNA (eccDNA) in tumor initiation and progression. However, there is limited comprehensive understanding of the role eccDNA plays in tumor resistance.

Objectives. This study investigates the involvement of *WWP1*-eccDNA in the resistance mechanisms of OC.

Materials and methods. Human OC cells (SKOV3 and cisplatin-resistant SKOV3/DDP) were cultured and high-throughput sequencing was performed, leading to the identification of eccDNA in SKOV3/DDP cells. Female BALB/cA-nu nude mice with SKOV3 and SKOV3/DDP xenografts received cisplatin (5.5 mg/kg), hydroxyurea (50 mg/kg) or saline for 14 days, followed by tumor weight assessment. Digital droplet polymerase chain reaction (ddPCR) and real-time quantitative polymerase chain reaction (qPCR) were used to quantify *WWP1*-eccDNA, evaluating their sensitivity and accuracy. Linear DNA removal and BsmI digestion were tested to improve eccDNA detection.

Results. *WWP1*-eccDNA was among the top upregulated eccDNA in SKOV3/DDP cells. Both cisplatin and hydroxyurea reduced tumor growth in mice, with cisplatin showing limited efficacy in resistant tumors. The ddPCR outperformed RT-qPCR in sensitivity, and linear DNA removal improved *WWP1*-eccDNA detection. *WWP1*-eccDNA levels were significantly elevated in SKOV3/DDP tumors. Treatment with cisplatin further increased its expression, whereas hydroxyurea led to a reduction in *WWP1*-eccDNA levels.

Conclusions. *WWP1*-eccDNA is critical in OC resistance, with cisplatin treatment increasing *WWP1*-eccDNA levels, contributing to resistance. The ddPCR proves to be a superior method for eccDNA detection.

Key words: ovarian cancer, chemoresistance, *WWP1*, extrachromosomal circular DNA, droplet digital PCR

Cite as
Lu CY, Han L, Guo XJ, et al. Cisplatin-induced *WWP1*-eccDNA expression contributes to ovarian cancer resistance. *Adv Clin Exp Med*. 2026;35(2):279–290. doi:10.17219/acem/204077

DOI
10.17219/acem/204077

Highlights

- *WWP1*-eccDNA drives ovarian cancer (OC) drug resistance: Elevated extrachromosomal circular DNA of the *WWP1* gene promotes chemotherapy evasion in ovarian tumors.
- ddPCR outperforms qPCR for eccDNA quantification: Digital droplet PCR delivers higher sensitivity and accuracy when measuring low-abundance *WWP1*-eccDNA.
- Cisplatin treatment upregulates *WWP1*-eccDNA levels: Platinum-based chemotherapy significantly increases *WWP1*-eccDNA in resistant OC cells.
- Hydroxyurea reduces *WWP1*-eccDNA abundance: DNA synthesis inhibition with hydroxyurea lowers eccDNA copy number, suggesting a strategy to counteract resistance.
- *WWP1*-eccDNA as a therapeutic target: Targeting eccDNA biogenesis or stability offers a novel approach to reverse OC drug resistance.

Background

Ovarian cancer (OC) is the most lethal gynecological malignancy, with the highest mortality rate among related diseases. Around 70% of patients are diagnosed at advanced stages after substantial disease progression.[1] Consequently, the 5-year survival rate for these patients is alarmingly low, at around 30%.[2] Currently, chemotherapy represents the primary therapeutic strategy for OC; however, its effectiveness is significantly compromised by both inherent and acquired resistance of tumor cells to chemotherapeutic agents, as well as their strong tendency to metastasize. Multidrug resistance (MDR) plays a central role in reducing chemotherapy efficacy, leading to treatment failure and cancer recurrence. Notably, more than 90% of OC deaths are linked to drug resistance.[3]

WWP1, a HECT-type (homologous to the E6-AP carboxyl terminus) E3 ubiquitin ligase, regulates the ubiquitination of multiple substrates. It is frequently overexpressed or aberrantly activated in various cancers and is associated with poor clinical prognosis.[4] Recent preclinical studies have identified *WWP1* as a promising therapeutic target in cancer and other diseases. The overexpression of *WWP1* is particularly detrimental because it promotes the polyubiquitination of the tumor suppressor gene *PTEN*, leading to its functional inactivation. This gene, often mutated, deleted, downregulated, or silenced in cancers, is critical for regulating cell growth. The alteration of *PTEN* by *WWP1* impedes its dimerization and membrane localization, compromising its tumor suppressor function. Consequently, this deregulation activates the PI3K/AKT signaling pathway, enhancing tumor cell survival and contributing to MDR. Intriguingly, inhibiting *WWP1* has been shown to restore *PTEN*'s tumor suppressor function, regardless of the gene's mutational status, thereby inhibiting tumor growth and potentially reversing MDR.[5] *WWP1* is frequently overexpressed or mutated in multiple malignancies, such as colorectal, liver and breast cancers.[6–8] Although *WWP1*'s role in other malignancies is well documented, its contribution to OC and treatment resistance remains unknown. Our study addresses this gap by exploring its eccDNA-mediated regulatory mechanisms.

Extrachromosomal circular DNA (eccDNA) is a form of circular DNA that exists independently of chromosomes and is associated with oncogene amplification, as well as its strong tendency to promote tumor metastasis. Eccentric circular DNA (eccDNA) molecules were first identified in 1965 through optical microscopy in malignant tumor cells of children. These structures were frequently observed in pairs and became known as double minutes (DMs). The significance of eccDNA in cancer development has gained recognition in recent years thanks to advances in next-generation sequencing and ultra-high-resolution imaging technologies. These studies have established a clear link between oncogene amplification in eccDNA and adverse outcomes in cancer patients.[9] The eccDNA contributes to tumor pathology by amplifying oncogenes, supporting the synthesis of proteins that promote tumor growth, mutations and cellular invasion. This oncogenic overexpression is a crucial factor in the aggressive behavior of tumors.[10] For instance, a recent study showed that eccDNA-induced RAB3B promotes autophagy, thereby increasing resistance to cisplatin in hypopharyngeal squamous cell carcinoma. These findings suggest that targeting eccDNA may represent a promising strategy to overcome tumor drug resistance.[11] However, current methods for detecting eccDNA are still limited.

Droplet digital PCR (ddPCR) has emerged as a transformative technology in scientific research, particularly for precise quantification of nucleic acids. Unlike real-time quantitative polymerase chain reaction (qPCR), ddPCR enhances accuracy by partitioning the sample into tens of thousands of separate reaction compartments, each containing a tiny volume of the reaction mixture. This partitioning ensures that each compartment likely contains 0 or 1 nucleic acid template molecule. After amplification, fluorescent signals from each compartment are measured. These data are then used to calculate the concentration or copy number of the target molecule using the Poisson distribution.[12] This method provides

absolute quantification of nucleic acids in a sample, making it a powerful tool in medical research, especially in oncology, where it is used to analyze genetic variations in cancers such as breast and gastric cancers.[13–15]

Objectives

In this study, we performed sequencing of extrachromosomal circular DNA (eccDNA) from the OC cell lines SKOV3/DDP and SKOV3, which led to the identification of eccDNA encoding *WWP1*. To validate these findings, we employed the advanced droplet digital PCR (ddPCR) technique.

Materials and methods

Cell culture

Human OC cell line SKOV3 and its cisplatin-resistant variant SKOV3/DDP were acquired from Zhejiang Meisen Cell Technology Co. (Zhejiang, China; cat. No. CTCC-001-0011). The cells were cultured in Dulbecco's modified Eagle's medium (DMEM), supplemented with 10% fetal bovine serum (FBS) and 1% penicillin–streptomycin solution, both purchased from Thermo Fisher Scientific (Waltham, USA). Cultures were maintained in a BINDER cell thermostatic incubator (BINDER GmbH Co, Tuttlingen, Germany) set at 37°C with an atmosphere containing 5% CO_2. The culture medium was replaced every other day, and cells were passaged every 3–4 days to maintain optimal growth conditions. To preserve the cisplatin resistance phenotype, a concentration of 0.2 μg/mL cisplatin was continuously present in the culture medium of the SKOV3/DDP cells.

High-throughput sequencing of eccDNA

The SKOV3 and SKOV3/DDP cells were resuspended in L1 buffer from the Plasmid Mini AX kit (A&A Biotechnology Inc., Gdańsk, Poland), which included protease K from Thermo Fisher Scientific, and were digested overnight at 50°C. Following digestion, the samples underwent alkaline treatment and were purified using a column according to the instructions provided with the Plasmid Mini AX kit. The column-purified DNA was treated with FastDigest MssI enzyme (Thermo Fisher Scientific) at 37°C for 16 h to eliminate mitochondrial circular DNA. Subsequently, Plasmid-Safe ATP-dependent DNase (Epicentre Biotechnologies, Madison, USA) was added. Thirty units of the enzyme and the appropriate amount of adenosine triphosphate (ATP) were supplemented every 24 h for a total incubation of 1 week to ensure complete removal of residual linear DNA. These enzymatically treated samples served as templates for amplifying eccDNA using the RCA DNA Amplification Kit (GenSeq Inc., Shanghai, China). The amplified eccDNA was purified with the MinElute Reaction Cleanup Kit (Qiagen Inc., Hilden, Germany). This purified DNA was utilized to construct a library using the GenSeq® Rapid DNA Lib Prep Kit (GenSeq Inc.), which was subsequently sequenced using the NovaSeq 6000 system (IlluminaInc., San Diego, USA) in a 150bp paired-end format. The sequencing data was filtered using SOAPnuke v. 2.1.9 (BGI Research,Beijing, China) to obtain clean reads. HISAT2 v. 2.2.1 (Johns Hopkins University, Baltimore, USA) was then employed to align these clean reads to the reference genome. Circle-map v. 1.1.4 (University of Copenhagen, Copenhagen, Denmark) was used to identify eccDNA across all samples. Samtools v. 1.21 (Wellcome Sanger Institute, Cambridge, UK) calculated the number of soft-clip reads overlapping with breakpoints to generate raw count numbers. Finally, differential eccDNA expression analysis was performed using edgeR v. 4.2.2 (R Foundation for Statistical Computing, Vienna, Austria) with a biological coefficient of variation (BCV) parameter set to less than or equal to 0.4 for human data based on the methodological specifications outlined in the official edgeR documentation.[16] The pipeline included data normalization, calculation of intergroup fold changes and statistical significance assessment through p-value determination, enabling systematic identification of differentially expressed eccDNAs. The presence and characteristics of identified eccDNA signals were validated using the Integrated Genome Browser (IGB) v. 10.10 (University of North Carolina at Charlotte, Charlotte, USA), a specialized software platform for genomic data visualization and analysis.

Establishment of a nude mice ovarian cancer model

A total of 25 female BALB/cA-nu mice, aged 4–5 weeks, were obtained from Henan SCBS Biotechnology Co., Ltd. (Anyang, China; license No. SCXK2020-0005). Ethical approval for the study (No. NYDLS-2023-004) was granted by the Experimental Animal Ethics Committee of Nanyang Institute of Technology (China) on 13 April 2023. SKOV3 and SKOV3/DDP cells were harvested during the logarithmic growth phase. The cells were enzymatically dissociated using trypsin and gently pipetted to obtain a single-cell suspension. Following centrifugation at 1,500 rpm for 6 min, the supernatant was discarded, and the cells were washed 3 times with PBS. The final cell concentration was adjusted to 5×10^6 cells/mL using 0.9% sodium chloride solution. A total of 300 μL of the prepared cell suspension was subcutaneously injected into the flank of each mouse after alcohol disinfection of the injection site. The mice were housed under controlled environmental conditions, including a temperature of 25°C, relative humidity of 50 ±10% and a 12-h light/dark cycle. Tumor formation was typically detectable by palpation at the injection site within 6–7 days post-injection. The health status and general condition of the mice were closely monitored daily throughout the experiment.

Grouping and administration of nude mice

Therapeutic treatment began 7–10 days after the inoculation of subcutaneous tumor cells. Mice inoculated with SKOV3 cells were randomly assigned to either the control group or the cisplatin group. Mice inoculated with SKOV3/DDP cells were divided into 3 groups: the control group, the cisplatin group and the hydroxyurea group, with 5 mice in each group.

Control group: Mice were treated with 0.9% sodium chloride solution, 0.1 mL per 10 g of body weight, administered daily for 14 days.

Cisplatin group: Mice received cisplatin (5.5 mg/kg, CSNpharm Inc., Chicago, USA) in a volume of 0.1 mL per 10 g of body weight, administered every other day for 14 days.

Hydroxyurea group: Mice received hydroxyurea (50 mg/kg, CSNpharm Inc.) in a volume of 0.1 mL per 10 g of body weight, administered every other day for 14 days.

Tumor dissection

Mice were euthanized the day after the final drug administration. Tumors were dissected under sterile conditions, and their weights were recorded. The tumors were subsequently stored at −80°C for future analysis.

Extraction of genomic DNA

Tumors stored at −80°C were retrieved and thoroughly washed with PBS. The tumor tissues were then homogenized using a high-speed, low-temperature tissue grinder to ensure uniform disruption. Genomic DNA was subsequently extracted from the homogenized samples according to the manufacturer's instructions using the MagAttract High Molecular Weight DNA Kit (Qiagen Inc.). Proteinase K and RNase A were added to the tissue sample. The mixture was incubated at room temperature for 30 min. DNA purification magnetic beads were then added. The solution was thoroughly mixed using a mixer. Then, the supernatant was carefully transferred to a new container. The supernatant was washed. Finally, the DNA was eluted using the appropriate elution buffer. The extracted DNA was stored at −20°C for subsequent analysis.

Synthesis of primers and probes

All primers and probes used in this study were synthesized by Beijing Tsingke Biotech Co., Ltd. (Beijing, China), including those for ACTB:
(forward: TGCACCTCCCACCG;
reverse: ACAGAGCTTCCCTCCAAGAC;
probe: ACCGTGTTCAGGGTCCCTGTCC-FAM)
and *WWP1*:
(forward: ACCCTGACCTAGTCAC;
reverse: GAGATTTTAAAAGGATTTATGAAAAATAGG;
probe: TCATGCCTGGTGACCAGGTCACT-VIC).

Linear experiment

ACTB and *WWP1* plasmids, each at a concentration of 0.01 ng/μL, containing sequences cloned into the PUC57 vector based on identified eccDNA coordinates (ACTB: chr7:5532553-5533915; *WWP1*: chr8:86395371-86395928, data from High-Throughput eccDNA sequencing, as shown in Fig. 1). These plasmids were digested with Bsml endonuclease (New England Biolabs, NEB Inc., Ipswich, USA). The digested plasmids were subsequently diluted 20-fold with deionized water. The plasmids were partitioned into 8 serial dilutions, ranging from 10,000 to 5 copies per μL. These dilutions were analyzed using both RT-qPCR and

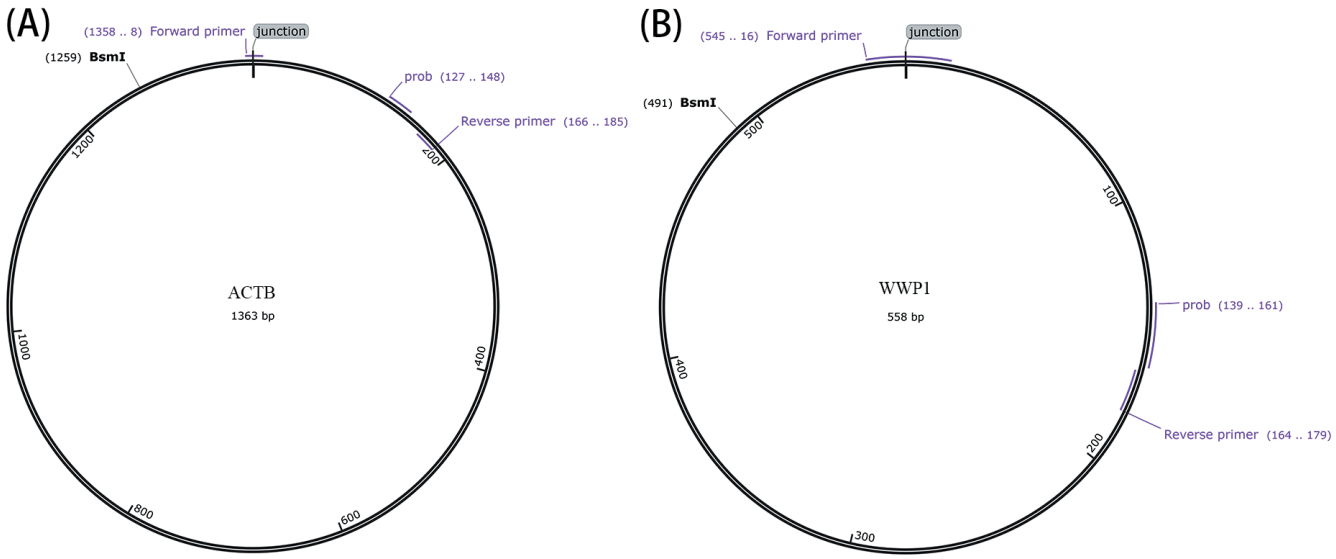

Fig. 1. Design diagram of primers and probes for ACTB and *WWP1* plasmids

ddPCR to assess the sensitivity. The digital PCR system (TargetingOne Inc. TD-1; Beijing Xinyi Biological Technology Co., Beijing, China) used a reaction mixture consisting of 7.5 μL of 4 × SuperMix (TargetingOne Corporation, Ltd.), 1.2 μL each of forward and reverse primers (400 nM), 200 nM probe and 50 ng DNA template in a total volume of 30 μL. Cycling conditions were: initial denaturation at 95°C for 10 min; 40 cycles of 94°C for 30 s and 58°C for 30 s; and a final hold at 12°C for 5 min. Real-time quantitative polymerase chain reaction was performed using the CFX Opus96 system (Bio-Rad Inc., Hercules, USA) under similar conditions.

Repeatability experiment

Plasmids containing ACTB and *WWP1* sequences were used as templates for ddPCR and RT-qPCR amplification at concentrations of approx. 10,000, 5,000, 1,000, 500, and 100 copies/μL.

Each concentration was tested in triplicate across 3 independent inter-batch experiments, and the coefficient of variation (CV) was calculated to assess the repeatability of the method. The reaction systems, primer and probe concentrations, and amplification conditions were consistent with those used in the linearity experiment.

Comparison before and after removal of linear DNA from circular DNA

Genomic DNA extracted from the tumor tissues of the cisplatin-treated SKOV3 nude mice model was divided into 3 aliquots. The 1st sample contained unmodified genomic DNA. In the 2nd sample, linear DNA was removed using the MinElute Reaction Cleanup Kit (Qiagen Inc.). The genomic DNA was added to the buffer solution, and then the resultant liquid was transferred to an adsorption column. Following centrifugation, a washing buffer was introduced. After allowing the system to stand for a defined period, a 2nd centrifugation step was carried out. Finally, an elution buffer was employed to elute the purified product. The 3rd sample, after linear DNA removal, was further treated with Bsml endonuclease. The DNA was incubated at 65°C for 10 min, followed by 80°C for 20 min in a thermal cycler. The presence of *WWP1*-eccDNA and ACTB-eccDNA in all 3 samples was evaluated using ddPCR. All samples were loaded with a final DNA concentration of 200 ng. The reaction system, primer and probe concentrations, and amplification conditions remained identical to those used in previous experiments.

Comparison of eccDNA in different treatment groups

The extracted genomic DNA from each group was retrieved from storage at –20°C, and linear DNA was subsequently removed. The DNA was then digested with Bsml endonuclease, and ddPCR analysis was performed. The final DNA loading concentration for each sample was 200 ng. The reaction system and amplification conditions remained consistent with those described previously.

Statistical analyses

Data analysis was performed using GraphPad Prism v. 8.0 (GraphPad Software, San Diego, USA). Given the small sample size ($n \leq 10$), normality testing was intentionally omitted due to insufficient statistical power, and nonparametric methods were uniformly applied. For comparisons between 2 groups, the Mann–Whitney U test was applied. Multi-group comparisons were performed using the Kruskal–Wallis test, followed by Dunn's post hoc test with Bonferroni correction to adjust for multiple comparisons. Results were expressed as median (min–max). Statistical significance was set at a p-value of less than 0.05.

Results

eccDNA differences between SKOV3/DDP and SKOV3 cells

Volcano plot analysis of eccDNA profiling for high-throughput sequencing (Fig. 2A) revealed 1,563 differentially expressed eccDNAs meeting predefined thresholds (|log2(fold change)| >1 and FDR-adjusted $p < 0.01$) between SKOV3 and SKOV3/DDP cells. Of these, 578 eccDNAs (37%) exhibited upregulation (depicted in red), while 986 eccDNAs (63%) showed downregulation (highlighted in blue). Notably, *WWP1*-eccDNA ranked among the top 10 most significantly upregulated species (log2(fold change) = 11.1, p = 6.36 × 10^–5). The IGB browser analysis of sequencing data confirmed elevated *WWP1*-eccDNA copy numbers in SKOV3/DDP cells compared to parental SKOV3 cells (Fig. 2B). Given the potential role of *WWP1* in tumor resistance,[5] we further investigated the presence and significance of *WWP1*-eccDNA in the tumor tissues of nude mice models. This was done following linear and reproducibility experiments designed to detect *WWP1*-eccDNA in plasmid samples.

The effects of different treatments on tumor weight

In nude mice models of SKOV3 and SKOV3/DDP, both the cisplatin and the hydroxyurea treatment showed inhibitory effects on tumor growth compared to the control group. The tumor inhibition effect of cisplatin was less pronounced in the SKOV3/DDP model than in the SKOV3 model (Fig. 3, Tables 1,2), indicating that the SKOV3/DDP mice exhibited resistance to cisplatin ($p < 0.05$).

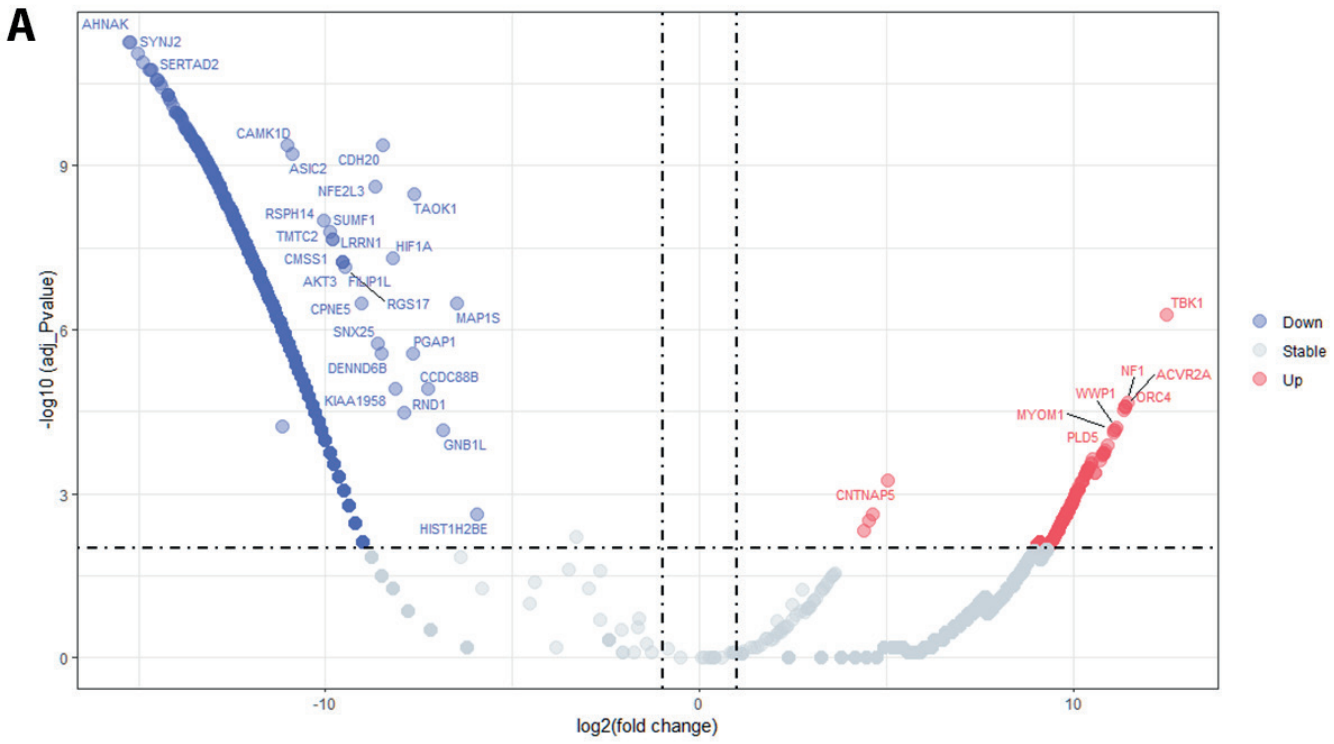

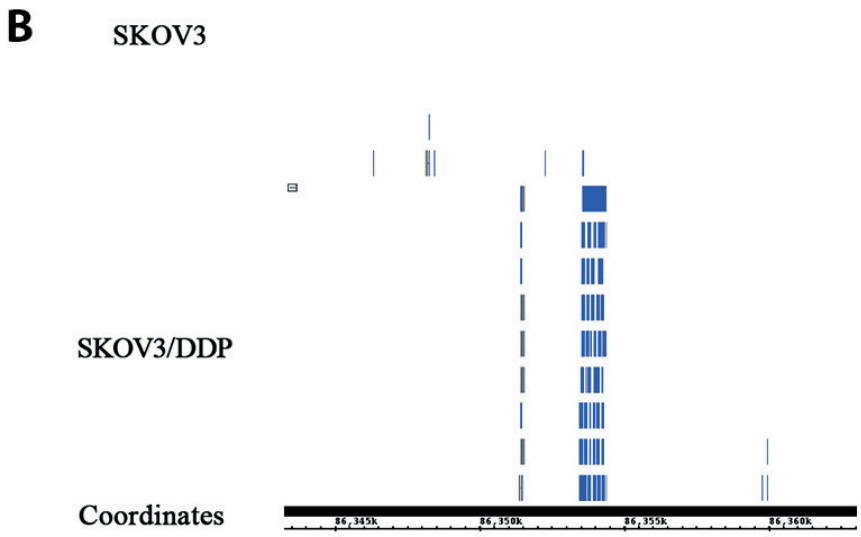

Fig. 2. The differentially expressed eccDNA between SKOV3 and SKOV3/DDP cells. A: Volcano plot; B: IGB view for *WWP1*-eccDNA

SKOV3 – human ovarian cancer cell line; SKOV3/DDP – cisplatin-resistant of human ovarian cancer cell line; *WWP1* – WW domain-containing ubiquitin E3 ligase 1 eccDNA – extrachromosomal circular DNAIGB: Integrated Genome Browser.

Table 1. Effects of cisplatin on tumor weight in SKOV3 nude mice models (median, min–max)

Tumor type	Group	Weight [mg]	p-value	95% CI of mean
Nude mice model of SKOV3	control	43.9 (33.8–53.6)	–	34.39–53.69
	cisplatin	9.3 (6.8–18.3)	0.008*	5.32–16.40

The differences in tumor weight between the 2 groups were analyzed using Mann–Whitney U test, *p < 0.01 vs control group. n = 5. Mann–Whitney U test: p = 0.008; 95% CI – 95% confidence interval.

Table 2. Effects of cisplatin and hydroxyurea on tumor weight in SKOV3/DDP nude mice models (median, min–max)

Tumor type	Group	Weight [mg]	p-value	95% CI of mean
Nude mice model of SKOV3/DDP	control	37.6 (33.4–78.6)	–	23.88–70.36
	cisplatin	17.5 (10.0–21.3)	0.014*	9.26–22.58
	hydroxyurea	12.1 (10.3–31.9)	0.040*	5.65–28.99

Differences in tumor weight among the 3 groups were analyzed using the Kruskal–Wallis test, and conducted post hoc analysis using Dunn's multiple comparison test; *p < 0.05 vs control group; n = 5. Kruskal–Wallis test: p = 0.002; 95% CI – 95% confidence interval.

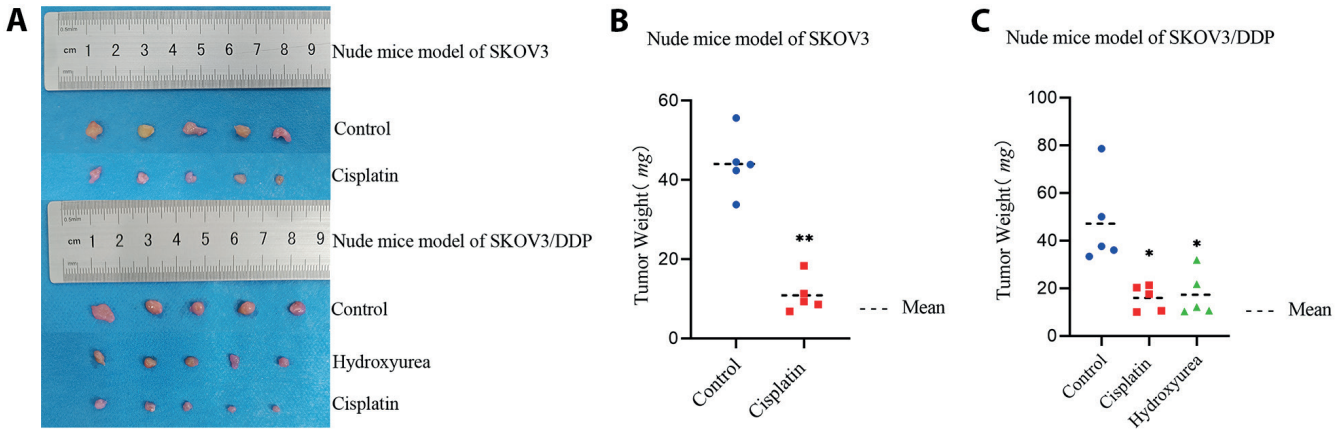

Fig. 3. Effects of cisplatin and hydroxyurea on tumor weight in SKOV3 and SKOV3/DDP nude mice models. A. Tumors dissected from nude mice; B. Tumor weights in SKOV3 nude mice model; C. Tumor weights in SKOV3/DDP nude mice model

*p < 0.05 vs corresponding control group. **p < 0.01 vs corresponding control group. n = 5.
SKOV3 – human ovarian cancer cell line; SKOV3/DDP – cisplatin-resistant of human ovarian cancer cell line

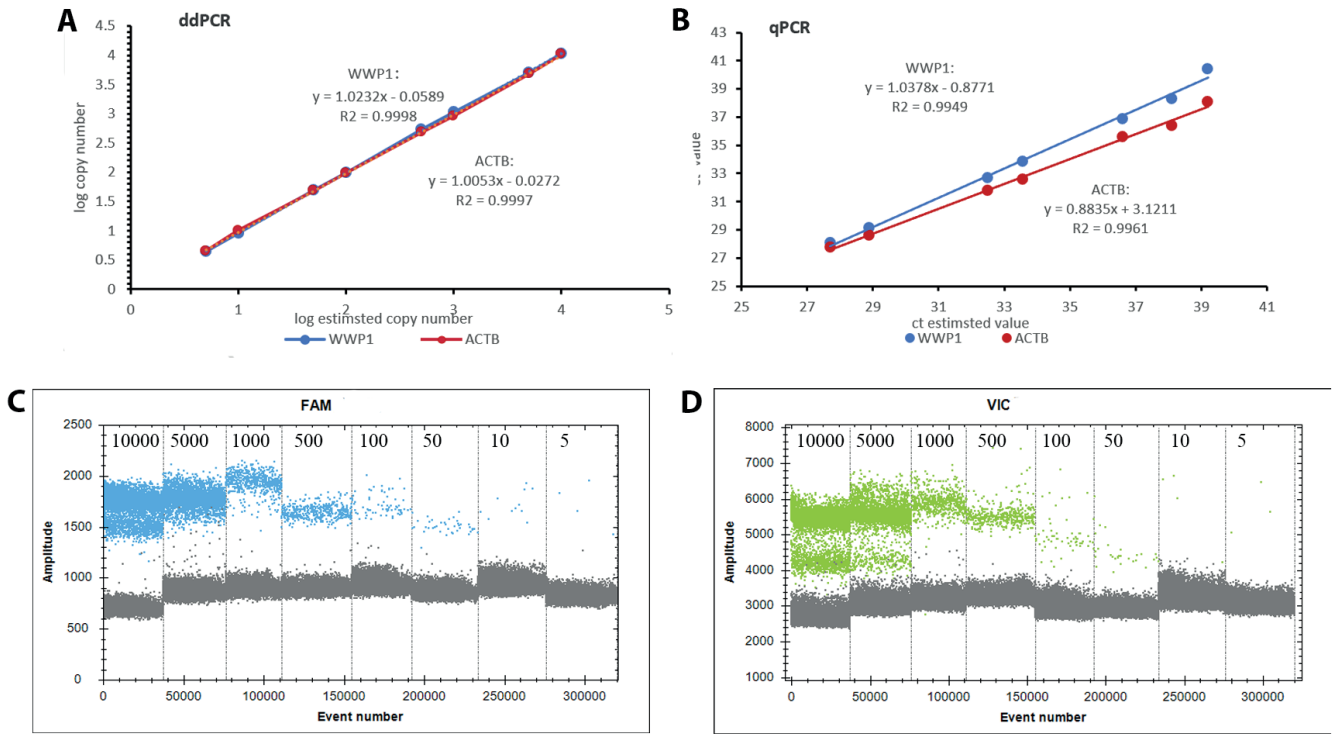

Fig. 4. Comparison of linear experimental results between ddPCR and RT-qPCR. A. ddPCR linear results; B. qPCR linear results; C. 1-D fluorescence amplitude plot of ACTB plasmids in ddPCR; D. 1-D fluorescence amplitude plot of *WWP1* plasmids in ddPCR. The estimated copy numbers (copies/μL) were 10,000, 5,000, 1,000, 500, 100, 50, 10, and 5

ddPCR – digital droplet polymerase chain reaction; qPCR – real-time quantitative polymerase chain reaction; ACTB – beta-actin; *WWP1* – WW domain-containing ubiquitin E3 ligase 1.

Increased sensitivity for plasmids detection using ddPCR

Analysis of the standard curve generated using RT-qPCR showed that the *WWP1* plasmids yielded a curve with the equation y = 1.0378x – 0.8771, resulting in an R^2 of 0.9949. Similarly, the standard curve for the ACTB plasmids was y = 0.8835x + 3.1211, with an R^2 of 0.9961. In comparison, the ddPCR method established in this study exhibited superior sensitivity and linearity. The standard curve for the *WWP1* plasmids was represented by the equation y = 1.0232x – 0.0589, with an impressive R^2 of 0.9998. For the ACTB plasmids, the standard curve equation was y = 1.0053x – 0.0272, also showing a high R^2 of 0.9997 (Fig. 4).

Table 3. The repeated experimental results of ACTB plasmids

Concentration of ACTB plasmids log(copies/μL)	ddPCR inter-assay variation (reproducibility)					qPCR inter-assay variation (reproducibility)				
	Rep. 1 log(copies/μL)	Rep.2 log(copies/μL)	Rep.3 log(copies/μL)	SD	CV	Rep.1(Ct)	Rep.2(Ct)	Rep.3(Ct)	SD	CV
3.70	3.71	3.71	3.71	0.002	0.05%	27.77	27.66	27.82	0.082	0.29%
3.40	3.41	3.41	3.41	0.001	0.04%	29.03	28.99	29.18	0.100	0.34%
2.70	2.74	2.69	2.72	0.024	0.89%	32.27	31.99	32.14	0.140	0.44%
2.00	1.98	2.02	1.99	0.018	0.90%	33.09	34.29	33.1	0.690	2.06%
1.30	1.31	1.31	1.31	0.008	0.63%	35.73	36.86	36.07	0.580	1.60%

SD – standard deviation; CV – coefficient of variation; ddPCR – digital droplet polymerase chain reaction; qPCR – real-time quantitative polymerase chain reaction; ACTB – beta-actin; *WWP1* – WW domain-containing ubiquitin E3 ligase 1; Rep – representative; SD – standard deviation; CV – coefficient of variation.

Table 4. The repeated experimental results of *WWP1* plasmids

Concentration of *WWP1* plasmids log(copies/μL)	ddPCR inter-assay variation (reproducibility)					qPCR inter-assay variation (reproducibility)				
	Rep.1 log(copies/μL)	Rep.2 log(copies/μL)	Rep.3 log(copies/μL)	SD	CV	Rep.1(Ct)	Rep.2(Ct)	Rep.3(Ct)	SD	CV
3.95	3.96	3.96	3.95	0.004	0.11%	29.58	29.81	29.78	0.125	0.42%
3.65	3.66	3.65	3.66	0.005	0.14%	31.15	31	31.49	0.251	0.80%
2.95	2.96	2.96	2.94	0.010	0.35%	34.85	34.41	34.27	0.303	0.88%
2.26	2.27	2.26	2.25	0.011	0.50%	35.69	36.95	36.15	0.638	1.76%
1.56	1.55	1.52	1.56	0.019	1.23%	38.61	39.41	38.82	0.415	1.06%

SD – standard deviation; CV – coefficient of variation; ddPCR – digital droplet polymerase chain reaction; qPCR – real-time quantitative polymerase chain reaction; ACTB – beta-actin; *WWP1* – WW domain-containing ubiquitin E3 ligase 1; Rep – representative; SD – standard deviation; CV – coefficient of variation.

Higher reproducibility for plasmids detection with ddPCR

For the inter-batch reproducibility assessment, ddPCR demonstrated superior precision, with an average CV of 0.50% and 0.47% for ACTB and *WWP1* plasmids, respectively. In contrast, RT-qPCR showed higher variability, with an average CV of 0.95% and 0.99% for ACTB and *WWP1* plasmids, respectively. Compared with RT-qPCR, ddPCR had better repeatability and accuracy (Tables 3,4).

Linearization and restriction endonuclease treatment enhance eccDNA detectability

As shown in Fig. 5, eccDNA detectability varied significantly across samples with different methods. Initially, eccDNA was almost undetectable in samples without linearization or restriction endonuclease digestion. This suggests that the presence of linear DNA may interfere with eccDNA detection, potentially affecting amplification efficiency and leading to inaccurate results. Following the removal of linear DNA and cleavage at the BsmI site, *WWP1*-eccDNA was consistently amplified and accurately detected in the samples. These results underscore the importance of removing linear DNA to preserve the integrity and accuracy of eccDNA amplification in our experimental setup.

Cisplatin increases *WWP1*-eccDNA level

Digital droplet PCR analysis revealed notable differences in the copy numbers of *WWP1*-eccDNA across various treatment groups. Specifically, in the SKOV3 and SKOV3/DDP nude mice models, the cisplatin treatment significantly increased the copy number of *WWP1*-eccDNA compared to the control group. In contrast, the hydroxyurea treatment notably decreased *WWP1*-eccDNA levels in the SKOV3/DDP model. Additionally, the *WWP1*-eccDNA copy number in the control group of the SKOV3/DDP model was significantly higher than in the control group of the SKOV3 model ($p < 0.01$). These findings underscore the differential effects of cisplatin and hydroxyurea on *WWP1*-eccDNA abundance, indicating a potential mechanism through which these treatments modulate drug resistance profiles in the OC nude mice model (Fig. 6, Table 5).

Discussion

The primary objective of this study was to establish a highly sensitive and accurate ddPCR methodology for quantifying eccDNA copy numbers and to assess how different chemotherapeutic agents impact the copy number of *WWP1*-eccDNA in OC. The results of our linearity and

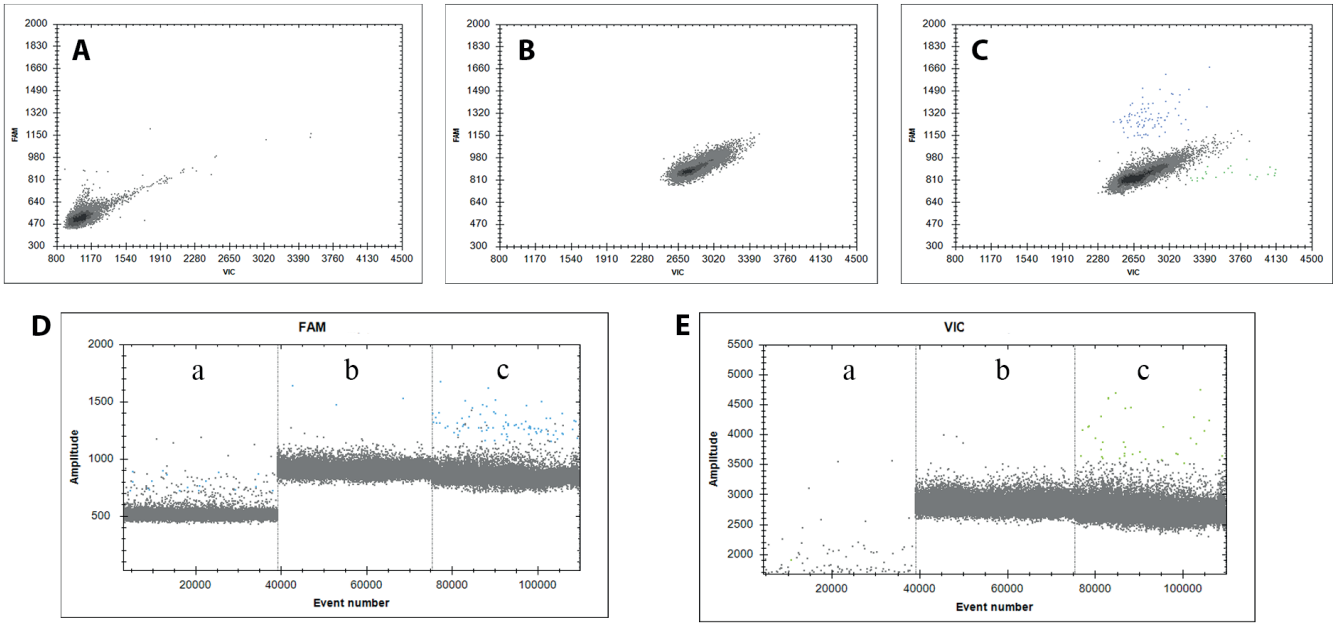

Fig. 5. Impact of linear DNA removal and restriction digestion on *WWP1*-eccDNA detection. A. Raw DNA (no treatment); B. Linear DNA removed (no BsmI digestion); C. Linear DNA removed + BsmI digestion; D. 1-D fluorescence amplitude plot of ACTB-eccDNA, E: 1-D fluorescence amplitude plot of *WWP1*-eccDNA

ACTB – beta-actin; *WWP1* – WW domain-containing ubiquitin E3 ligase 1; eccDNA – extrachromosomal circular DNA; BsmI – endonuclease.

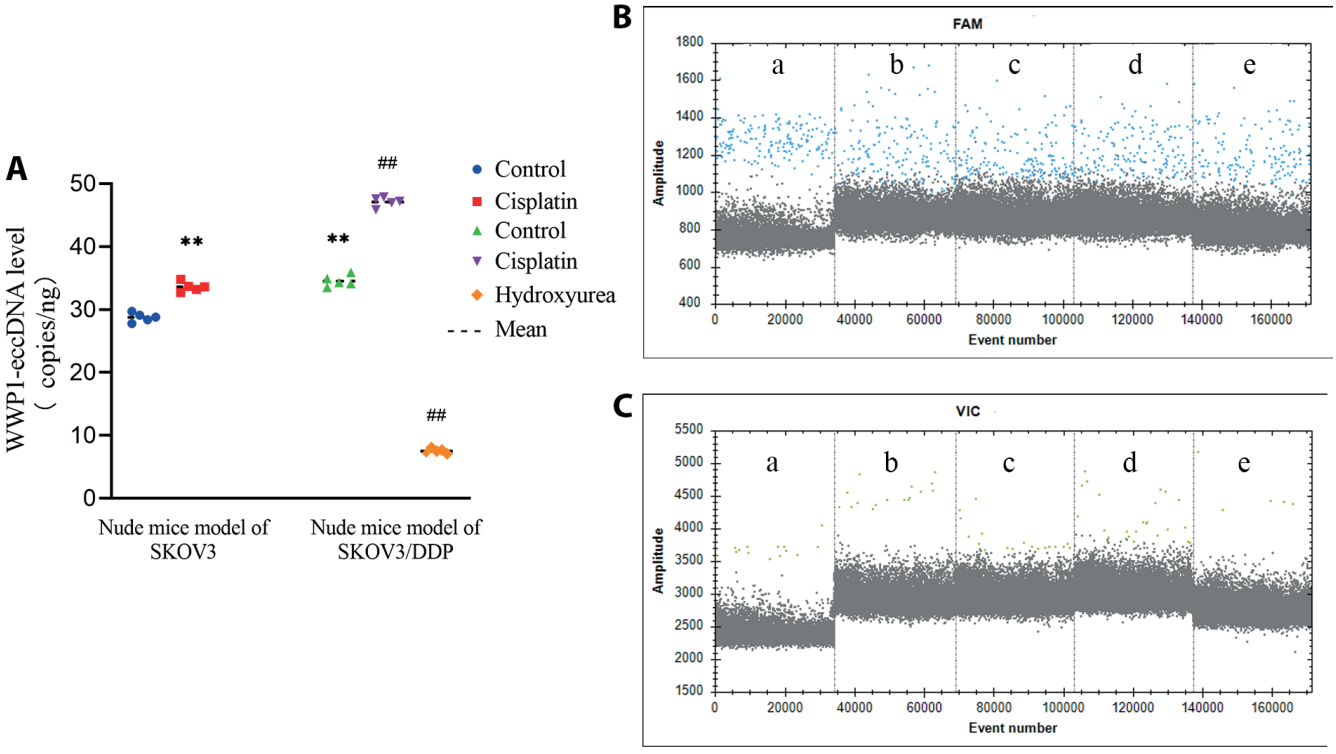

Fig. 6. *WWP1*-eccDNA – c number modulations in response to chemotherapy. A. Analysis of *WWP1*-eccDNA levels across treatment groups; B. 1-D fluorescence amplitude plot of ACTB-eccDNA; C. 1-D fluorescence amplitude plot of *WWP1*-eccDNA. Groups: a – control group of SKOV3 nude mice; b – cisplatin-treated SKOV3 nude mice; c – control group of SKOV3/DDP nude mice; d – cisplatin-treated SKOV3/DDP nude mice; e – hydroxyurea-treated SKOV3/DDP nude mice

**$p < 0.01$ vs control group of SKOV3 nude mice, ##$p < 0.01$ vs control group of SKOV3/DDP nude mice. n = 5. ACTB – beta-actin; *WWP1* – WW domain-containing ubiquitin E3 ligase 1; eccDNA – extrachromosomal circular DNA; SKOV3 – human ovarian cancer cell line; SKOV3/DDP – cisplatin-resistant of human ovarian cancer cell line.

Table 5. The effects of different drug administrations on the expression of *WWP1*-eccDNA (median, min–max)

Tumor type	Group	*WWP1*-eccDNA level (copies/ng)	p-value	95% CI of mean
Nude mice model of SKOV3	control	28.8 (27.8–29.7)	–	27.87–29.65
	cisplatin	33.6 (32.7–34.8)	0.008**	32.63–34.57
Nude mice model of SKOV3/DDP	control	34.3 (33.5–35.9)	0.008**	33.41–35.67
	cisplatin	47.2 (45.9–47.9)	0.008##	46.14–47.94
	hydroxyurea	7.5 (7.1–8.1)	0.008##	6.887–7.993

The Mann–Whitney U test was used to compare the expression levels of *WWP1*-eccDNA in tumor tissues between different drug administration groups. **p < 0.01 vs control group of SKOV3 nude mice; ##p < 0.01 vs control group of SKOV3/DDP nude mice; n = 5. Mann–Whitney U test: p = 0.008.

reproducibility experiments unequivocally demonstrate that ddPCR outperforms traditional RT-qPCR in sensitivity and accuracy. Specifically, ddPCR achieved reliable detection of eccDNA at concentrations as low as 5 copies/μL, a marked improvement over RT-qPCR, which only provided consistent results starting at 100 copies/μL. These findings underscore the key advantages of ddPCR in oncological research, particularly when studying low-abundance genetic targets like eccDNA, which is pivotal in understanding tumor biology and resistance mechanisms.

Moreover, this study pioneers the application of ddPCR for the detection of genetic mutations in preserved clinical samples from asymptomatic individuals at high risk for OC.[17] This innovative use of ddPCR holds considerable promise not only as a research tool but also for clinical applications, particularly in the early detection of genetic alterations associated with OC. By enabling the detection of low-level genetic markers in blood or other biosamples, ddPCR could facilitate early diagnosis and more timely therapeutic interventions, potentially improving patient outcomes.

Tumor MDR remains a critical challenge in cancer treatment, significantly affecting prognosis and treatment efficacy. Identifying and targeting novel molecular mechanisms involved in drug resistance is crucial for advancing therapeutic strategies. *WWP1*, an E3 ubiquitin ligase and proto-oncogene, is overexpressed or amplified in various cancers, including gastric, breast, liver, lung, and prostate cancers.[7,18–20] In these cancers, *WWP1* primarily exerts its oncogenic effects by inhibiting the tumor suppressor PTEN, which leads to the activation of the PI3K/AKT signaling pathway – an essential driver of MDR.[21] These findings indicate that *WWP1* may play a critical role in mediating drug resistance by modulating key signaling pathways that influence cell survival, proliferation and apoptosis.

In addition to its role in PTEN regulation, *WWP1* has been shown to interact with miR-452, a microRNA involved in cancer cell migration and invasion, particularly in prostate cancer.[22] This interaction further reinforces the multifaceted role of *WWP1* in driving tumorigenesis and metastatic potential. In some hematological malignancies, such as acute myeloid leukemia (AML), *WWP1* has been clearly identified as an oncogene. It can promote the progression of the cell cycle and help tumor cells evade apoptosis, thus maintaining the continuous proliferation of tumor cells.[23] *WWP1* is also involved in regulating other important cellular processes. During the epithelial-mesenchymal transition (EMT) of tumor cells, *WWP1* promotes the acquisition of mesenchymal characteristics by regulating the stability and activity of related proteins, thereby enhancing cell migration and invasion. This process contributes to tumor metastasis and drug resistance development.[4] Given the central role of *WWP1* in promoting cancer progression and MDR, developing inhibitors that target *WWP1* could represent an effective therapeutic strategy to reverse drug resistance in cancer, potentially enhancing the efficacy of current chemotherapy regimens and improving clinical outcomes.

EccDNA, as a prevalent form of extrachromosomal genetic material, is implicated in the amplification of oncogenes and the regulation of tumor-associated genes. A recent study by Kim et al. conducted a comprehensive analysis of whole-genome sequencing data from 3,212 cancer patients, revealing that oncogenes are significantly enriched on eccDNA, particularly in cases involving gene amplification.[24] This amplification is often associated with recurrent oncogenes and poor prognosis, indicating a strong link between eccDNA presence and increased tumor invasiveness. This widespread phenomenon across different cancer types further supports the potential importance of eccDNA in cancer biology.

Another key study highlighted the role of eccDNA in cross-resistance, especially through the amplification of the *MYC* oncogene.[25] *MYC*, a key regulator of cellular processes such as growth and metabolism, is often amplified on eccDNA, contributing to resistance mechanisms that affect multiple chemotherapy drugs. The interaction between *MYC* and *WWP1* is crucial in this context, as *MYC*-driven amplification of *WWP1*-eccDNA could significantly impact tumor resistance to chemotherapy. This underscores the importance of using ddPCR to evaluate the effects of different treatments on *WWP1*-eccDNA dynamics in cancer cells.

Hydroxyurea, a cell cycle-specific chemotherapeutic agent that inhibits nucleoside diphosphate reductase and prevents DNA synthesis during the S phase,[26] was included in this study as a positive control. Research has shown that hydroxyurea can reduce tumor heterogeneity by eliminating eccDNA-containing *MYC* amplifications,[27] bolstering its utility as a modulator of eccDNA expression. In this study, we observed that while cisplatin treatment increased *WWP1*-eccDNA levels, hydroxyurea treatment reduced them. This indicates that hydroxyurea's ability to inhibit *MYC*-driven eccDNA amplification may contribute to reversing tumor resistance. These results provide insights into the differential impacts of chemotherapeutic agents on eccDNA biology and their potential to modulate drug resistance in OC.

Limitations

Despite its advantages in sensitivity and specificity, the ddPCR methodology used in this study has several notable limitations. The relatively high cost of consumables – such as fluorescent probes and droplet-generation chips – and the lower throughput compared to RT-qPCR may limit its feasibility for large-scale studies or routine use in resource-constrained clinical settings. Additionally, the linearization of circular DNA may be incomplete, leading to residual circular or partially linearized DNA species. To address these issues, future work will focus on optimizing reagent usage (e.g., reduced reaction volumes) and integrating automated platforms to enhance throughput. Collaborative efforts with clinical laboratories will also be prioritized to standardize protocols and improve technical proficiency.

Conclusions

Our study provides compelling evidence that *WWP1*-eccDNA plays a central role in mediating chemotherapy resistance in OC. The ability to accurately quantify *WWP1*-eccDNA levels using ddPCR presents new opportunities for monitoring drug resistance and assessing treatment efficacy. The enhanced sensitivity of ddPCR also has significant implications for early detection and monitoring of genetic alterations in cancer, offering a promising strategy for improving patient outcomes and advancing precision medicine in oncology. However, the current research is still at the animal model stage. In the future, further clinical data are needed to verify its broader applicability. Future studies should explore *WWP1* inhibitors to reverse resistance. Clinically, ddPCR could monitor *WWP1*-eccDNA in liquid biopsies for early intervention, and our results indicate that targeting *WWP1* and its associated eccDNA may offer a novel approach for overcoming drug resistance in OC.

Data Availability Statement

Data sharing is not applicable to this article, as all data are already included in the manuscript.

Consent for publication

Not applicable.

Use of AI and AI-assisted technologies

Not applicable.

ORCID iDs

Chenyang Lu https://orcid.org/0009-0003-8383-0885
Li Han https://orcid.org/0000-0002-4486-0534
Xiaojuan Guo https://orcid.org/0000-0003-2554-4752
Ruijuan Du https://orcid.org/0000-0001-8544-0029
Hui Zhang https://orcid.org/0000-0003-3286-8122
Kelei Guo https://orcid.org/0009-0007-5730-8769
Yunfei Tu https://orcid.org/0009-0000-9089-2417
Ruifang Li https://orcid.org/0000-0002-1861-1809

References

1. Armstrong DK, Alvarez RD, Backes FJ, et al. NCCN Guidelines® Insights: Ovarian Cancer, Version 3.2022. Featured Updates to the NCCN Guidelines. *J Natl Compr Canc Netw*. 2022;20(9):972–980. doi:10.6004/jnccn.2022.0047
2. Konstantinopoulos PA, Matulonis UA. Clinical and translational advances in ovarian cancer therapy. *Nat Cancer*. 2023;4(9):1239–1257. doi:10.1038/s43018-023-00617-9
3. Chen T, Xiao Z, Liu X, et al. Natural products for combating multidrug resistance in cancer. *Pharmacol Res*. 2024;202:107099. doi:10.1016/j.phrs.2024.107099
4. Behera A, Reddy ABM. WWP1 E3 ligase at the crossroads of health and disease. *Cell Death Dis*. 2023;14(12):853. doi:10.1038/s41419-023-06380-0
5. Lee YR, Chen M, Lee JD, et al. Reactivation of PTEN tumor suppressor for cancer treatment through inhibition of a MYC-WWP1 inhibitory pathway. *Science*. 2019;364(6441):eaau0159. doi:10.1126/science.aau0159
6. Fan H, Hu X, Cao F, et al. WWP1 inhibition increases SHP2 inhibitor efficacy in colorectal cancer. *NPJ Precis Oncol*. 2024;8(1):144. doi:10.1038/s41698-024-00650-6
7. Zhang C, Wang W, Wu B. Molecular mechanism of WWP1-mediated ubiquitination modification affecting proliferation and invasion/migration of liver cancer cells. *Kaohsiung J Med Sci*. 2024;40(3):255–268. doi:10.1002/kjm2.12786
8. Zhou Z, Liu R, Chen C. The WWP1 ubiquitin E3 ligase increases TRAIL resistance in breast cancer. *Int J Cancer*. 2012;130(7):1504–1510. doi:10.1002/ijc.26122
9. Wu S, Bafna V, Chang HY, Mischel PS. Extrachromosomal DNA: An emerging hallmark in human cancer. *Annu Rev Pathol Mech Dis*. 2022;17(1):367–386. doi:10.1146/annurev-pathmechdis-051821-114223
10. Wang Y, Wang M, Zhang Y. Purification, full-length sequencing and genomic origin mapping of eccDNA. *Nat Protoc*. 2023;18(3):683–699. doi:10.1038/s41596-022-00783-7
11. Lin C, Chen Y, Zhang F, Liu B, Xie C, Song Y. Encoding gene *RAB3B* exists in linear chromosomal and circular extrachromosomal DNA and contributes to cisplatin resistance of hypopharyngeal squamous cell carcinoma via inducing autophagy. *Cell Death Dis*. 2022;13(2):171. doi:10.1038/s41419-022-04627-w
12. Pomari E, Matucci A, Accordini S, et al. ddPCR for the detection and absolute quantification of oropouche virus. *Viruses*. 2024;16(9):1426. doi:10.3390/v16091426
13. Sánchez-Martín V, López-López E, Reguero-Paredes D, et al. Comparative study of droplet-digital PCR and absolute Q digital PCR for ctDNA detection in early-stage breast cancer patients. *Clin Chim Acta*. 2024;552:117673. doi:10.1016/j.cca.2023.117673

14. Venetis K, Pepe F, Pescia C, et al. ESR1 mutations in HR+/HER2-metastatic breast cancer: Enhancing the accuracy of ctDNA testing. *Cancer Treat Rev*. 2023;121:102642. doi:10.1016/j.ctrv.2023.102642
15. Yu D, Zhang J, Wang M, et al. Exosomal miRNAs from neutrophils act as accurate biomarkers for gastric cancer diagnosis. *Clin Chim Acta*. 2024;554:117773. doi:10.1016/j.cca.2024.117773
16. Chen Y, Chen L, Lun ATL, Baldoni PL, Smyth GK. edgeR v4: Powerful differential analysis of sequencing data with expanded functionality and improved support for small counts and larger datasets. *Nucleic Acids Res*. 2025;53(2):gkaf018. doi:10.1093/nar/gkaf018
17. Arildsen NS, Martin De La Fuente L, Måsbäck A, et al. Detecting TP53 mutations in diagnostic and archival liquid-based Pap samples from ovarian cancer patients using an ultra-sensitive ddPCR method. *Sci Rep*. 2019;9(1):15506. doi:10.1038/s41598-019-51697-6
18. Kishikawa T, Higuchi H, Wang L, et al. WWP1 inactivation enhances efficacy of PI3K inhibitors while suppressing their toxicities in breast cancer models. *J Clin Invest*. 2021;131(24):e140436. doi:10.1172/JCI140436
19. Tung CH, Huang MF, Liang CH, et al. α-catulin promotes cancer stemness by antagonizing WWP1-mediated KLF5 degradation in lung cancer. *Theranostics*. 2022;12(3):1173–1186. doi:10.7150/thno.63627
20. Wang X, Bi Y, Liu X, et al. High expression of *WWP1* associates with tumor progression in papillary thyroid cancer. *Cancer Biother Radiopharm*. 2022;37(4):313–323. doi:10.1089/cbr.2020.4148
21. Lee YR, Yehia L, Kishikawa T, et al. WWP1 gain-of-function inactivation of PTEN in cancer predisposition. *N Engl J Med*. 2020;382(22):2103–2116. doi:10.1056/NEJMoa1914919
22. Goto Y, Kojima S, Kurozumi A, et al. Regulation of E3 ubiquitin ligase-1 (WWP1) by microRNA-452 inhibits cancer cell migration and invasion in prostate cancer. *Br J Cancer*. 2016;114(10):1135–1144. doi:10.1038/bjc.2016.95
23. Giovannini S, Li Y, Pecorari R, et al. Thioredoxin-interacting protein (TXNIP) is a substrate of the NEDD4-like E3 ubiquitin-protein ligase WWP1 in cellular redox state regulation of acute myeloid leukemia cells. *Mol Oncol*. 2025;19(1):133–150. doi:10.1002/1878-0261.13722
24. Kim H, Nguyen NP, Turner K, et al. Extrachromosomal DNA is associated with oncogene amplification and poor outcome across multiple cancers. *Nat Genet*. 2020;52(9):891–897. doi:10.1038/s41588-020-0678-2
25. Pal Choudhuri S, Girard L, Lim JYS, et al. Acquired cross-resistance in small cell lung cancer due to extrachromosomal DNA amplification of *MYC* paralogs. *Cancer Discov*. 2024;14(5):804–827. doi:10.1158/2159-8290.CD-23-0656
26. Ding C, Su B, Li Q, et al. Histone deacetylase inhibitor 2-hexyl-4-pentynoic acid enhances hydroxyurea therapeutic effect in triple-negative breast cancer cells. *Mutat Res Genet Toxicol Environ Mutagen*. 2022;873:503422. doi:10.1016/j.mrgentox.2021.503422
27. Luo J, Li Y, Zhang T, et al. Extrachromosomal circular DNA in cancer drug resistance and its potential clinical implications. *Front Oncol*. 2023;12:1092705. doi:10.3389/fonc.2022.1092705

Screening of metabolic markers related to molecular typing of breast cancer based on ^{1}H NMR metabonomics

*Man Xu[1,A,D], *Wenbin Huang[2,B], Xinping Huang[1,C], Hailong Shu[3,B], Weixiao Ke[3,C], Yongcheng Zhang[2,F], Yongxia Yang[3,4,F]

[1] College of Basic Medicine, Guangdong Pharmaceutical University, Guangzhou, China
[2] Department of Breast Care Surgery, The First Affiliated Hospital of Guangdong Pharmaceutical University, Guangzhou, China
[3] College of Medical Information Engineering, Guangdong Pharmaceutical University, Guangzhou, China
[4] Guangdong Province Precise Medicine Big Data of Traditional Chinese Medicine Engineering Technology Research Center, Guangzhou, China

A – research concept and design; B – collection and/or assembly of data; C – data analysis and interpretation;
D – writing the article; E – critical revision of the article; F – final approval of the article

Advances in Clinical and Experimental Medicine, ISSN 1899–5276 (print), ISSN 2451–2680 (online) *Adv Clin Exp Med*. 2026;35(2):291–306

Address for correspondence
Yongxia Yang
E-mail: yangyongxia@gdpu.edu.cn

Funding sources
This work was supported by the National Natural Science Foundation of China (grants No. 22074024 and No. 21005022) and the Natural Science Foundation of Guangdong Province (grants No. 2022A1515012045 and No. 2023A1515012573).

Conflict of interest
None declared

*Man Xu and Wenbin Huang contributed equally to this work.

Received on December 26, 2024
Reviewed on March 20, 2025
Accepted on April 24, 2025

Published online on January 12, 2026

Abstract

Background. Breast cancer (BC) is a heterogeneous disease classified into 4 molecular subtypes, each with distinct molecular characteristics that influence treatment strategies, clinical outcomes and prognosis. These subtypes are associated with specific changes in cellular metabolism, which may play a crucial role in tumor development and progression.

Objectives. To identify distinctive serum metabolic biomarkers for each molecular BC subtype and to evaluate their associations with estrogen receptor (ER) and human epidermal growth factor 2 (HER2) receptor status, thereby refining molecular classification and informing personalized treatment strategies.

Materials and methods. The study utilized the proton nuclear magnetic resonance (^{1}H NMR) metabolomics method to collect serum metabolic profiles from BC patients. Pattern recognition analysis was employed to analyze the metabolic data. Metabolic markers specific to each molecular subtype were selected, and Kyoto Encyclopedia of Genes and Genomes (KEGG) pathway enrichment analysis was employed to explore serum metabolic pathway heterogeneity.

Results. Distinct metabolic markers were identified for each molecular subtype, demonstrating strong discriminatory power. Additionally, we identified specific serum metabolites whose levels correlate with ER and HER2 expression profiles. The KEGG pathway analysis revealed significant heterogeneity in serum metabolic pathways across different subtypes.

Conclusions. This study demonstrates pronounced metabolic differences across BC subtypes that mirror their distinct molecular profiles and may underlie variations in therapeutic response. These metabolomic insights hold promise for refining tumor classification, improving diagnostic accuracy and guiding more personalized treatment strategies.

Key words: ^{1}H NMR, breast cancer, molecular typing, metabolic markers

Cite as
Xu M, Huang W, Huang X, et al. Screening of metabolic markers related to molecular typing of breast cancer based on ^{1}H NMR metabonomics. *Adv Clin Exp Med*. 2026;35(2):291–306. doi:10.17219/acem/204347

DOI
10.17219/acem/204347

Highlights

- Proton nuclear magnetic resonance (^{1}H NMR) metabolomics identifies distinct serum metabolic markers for 4 breast cancer (BC) molecular subtypes.
- Choline and glycerophosphorylcholine levels significantly change across all subtypes, indicating altered glycerophospholipid metabolism.
- Metabolic markers associated with estrogen receptor (ER) and human epidermal growth factor 2 (HER2) receptor expression demonstrate strong predictive value for molecular typing.
- Pathway analysis highlights subtype-specific disturbances in energy, amino acid and lipid metabolism.
- Findings suggest that serum metabolite profiles may guide personalized diagnosis and treatment of BC patients.

Introduction

Breast cancer (BC) is among the most common malignancies worldwide. According to the International Agency for Research on Cancer (IARC) of the World Health Organization (WHO), in 2022, BC became the most frequently diagnosed cancer globally – surpassing lung cancer – with 2.3 million new cases and nearly 665,000 deaths.[1] Since the mid-2000s, the incidence of female BC has steadily increased by approx. 0.6% per year.[2,3]

Breast cancer treatment has evolved dramatically over the past several decades and now encompasses a multimodal approach, including surgery combined with systemic therapies – chemotherapy, endocrine therapy and targeted agents – as well as radiotherapy. These integrated strategies have substantially improved patient survival; however, significant heterogeneity remains in treatment responses and long-term outcomes across different patient subgroups.[4]

Breast cancer is a heterogeneous disease classified into 4 main molecular subtypes based on the expression of estrogen receptor (ER), progesterone receptor (PR), human epidermal growth factor receptor 2 (HER2), and the proliferation marker Ki-67.[5] Luminal A tumors are ER-positive, HER2-negative, have PR expression ≥20%, and Ki-67 ≤14%; luminal B tumors are also ER-positive but may be HER2-negative or -positive, with PR <20% or Ki-67 >14%; the HER2-enriched subtype is ER-negative, PR-negative and HER2-positive; and triple-negative BCs (TNBCs) lack ER, PR and HER2 expression. Clinical presentation, tumor biology and therapeutic responsiveness vary markedly across molecular subtypes,[6] making subtype classification a cornerstone of treatment decision-making.[7] Luminal A tumors – the most common subtype – exhibit robust responses to endocrine therapy but derive minimal benefit from chemotherapy,[8] whereas luminal B cancers typically necessitate combined hormone therapy and cytotoxic chemotherapy to achieve optimal outcomes.[9]

HER2-positive/ER-negative tumors are often associated with aggressive, advanced disease and require targeted anti-HER2 therapies.[10] Triple-negative BC, which accounts for roughly 20% of all BC, is typically more aggressive than other subtypes; it disproportionately affects younger patients, presents with poorly differentiated histology and advanced stage at diagnosis, and carries a high risk of local recurrence and distant metastasis, resulting in poorer outcomes and survival.[11]

The heterogeneous treatment responses across these molecular subtypes underscore the imperative for personalized therapeutic strategies. Surgical intervention is the primary therapy for early-stage disease, whereas systemic therapies are used in both adjuvant and neoadjuvant settings. Endocrine therapy continues to be the cornerstone for hormone receptor-positive BC, while HER2-targeted agents have revolutionized outcomes in HER2-positive disease, and emerging immunotherapies are showing enhanced efficacy in TNBC. Optimizing treatment approaches on the basis of each subtype is crucial for achieving the most favorable results for patients.

Metabolomics is the comprehensive characterization of small-molecule metabolites in cells, tissues, organs, and whole organisms that respond to intrinsic or extrinsic factors.[12] Metabolomics, a powerful "omics" approach, has the potential to facilitate early disease detection and uncover novel therapeutic targets by profiling metabolites downstream of gene and protein activity.[13] Beyond revealing biochemical alterations, it uniquely captures in vivo phenotypic changes that may be missed by genomic and proteomic analyses.

Recent metabolomic approaches have greatly improved our understanding of BC biology. TBK1-mediated metabolic processes in cancer cells have emerged as a hallmark of metabolic reprogramming, with each molecular subtype exhibiting a distinct metabolic signature.[14] For example, an liquid chromatography–high-resolution mass spectrometry (LC-HRMS)-based plasma metabolomic study in BC patients revealed subtype-specific alterations in the porphyrin, chlorophyll and glycerophospholipid metabolic pathways.[15] The use of metabolomics in BC has grown exponentially in recent years. These alterations in cellular metabolism have been characterized into several important pathways that are critical for BC initiation and progression.[16] Enhanced aerobic glycolysis, the classic Warburg effect, is a consistent feature of aggressive BC subtypes. Metabolomic profiling has also uncovered distinctive alterations in amino acid turnover and fatty acid β-oxidation that map to specific molecular subtypes, highlighting their unique metabolic reprogramming.[17]

Objectives

Recent investigations have identified metabolic signatures that predict both treatment response and resistance. For instance, specific alterations in metabolic pathways have been linked to endocrine therapy resistance in hormone receptor-positive BC.[18] Moreover, the combination of metabolomics with other omics data has provided new therapeutic targets and a better understanding of drug resistance.[19] The metabolic features that underlie the different molecular subtypes of BC are still poorly understood, despite progress in BC treatment. We hypothesized that distinct molecular subtypes of BC have unique metabolic signatures detectable in the serum of patients and that these metabolic profiles correlate closely with the expression status of key receptors, ER and HER2. Moreover, the detection of these subtype-specific metabolic signatures may offer valuable information regarding BC biology and help guide individualized treatment initiatives.

This study aimed to reveal metabolic differences between BC patients and healthy controls and explore the biochemical pathways affected by different molecular subtypes of BC patients.

Materials and methods

Study population

A total of 117 BC patients and 55 healthy control subjects were enrolled at the First Affiliated Hospital of Guangdong Pharmaceutical University (Guangzhou, China) between January 2020 and December 2024. Sample size was determined with power analysis ($\alpha = 0.05$, power = 0.8) to ensure the detection of clinically meaningful metabolic differences.

The patient inclusion criteria were as follows: 1) histologically confirmed, newly diagnosed BC with molecular subtype determined with ER, PR, HER2, and Ki-67 status; 2) no prior oncologic treatment; and 3) absence of other malignancies or serious systemic illnesses. Healthy controls were age-matched healthy women with normal clinical examinations and no history of cancer or severe disease.

This study was approved by the Medical Ethics Committee of the First Affiliated Hospital of Guangdong Pharmaceutical University (approval No. 2022KT81).

Biological material collection and processing

Blood samples were collected from all participants after 12 h of fasting and centrifuged at 4°C at 3,000 rpm for 10 min to obtain the serum. For nuclear magnetic resonance (NMR) analysis, 300 µL of serum was mixed with 150 µL of phosphate-buffered saline (PBS) (0.2 mol/L, pH 7.4) and 100 µL of D_2O in 5 mm NMR tubes after recentrifugation (3,000 rpm, 10 min, 4°C).

Assay methods and data preprocessing

High-resolution proton NMR spectra were acquired on a Bruker AVANCE III 500 MHz superconducting NMR spectrometer (Bruker Inc., Karlsruhe, Germany). The pulse sequence was Carr–Purcell–Meiboom–Gill (CPMG). Proton NMR spectra were acquired at 298 K with an echo time of 100 ms and a relaxation delay of 3 s. The spectral width was set to 10 kHz, and 128 scans were collected for each spectrum. Data were processed in TopSpin 4.1 (Bruker Inc.), where manual phase correction and baseline adjustment were performed. Chemical shifts were calibrated using the lactate methyl doublet at 1.33 ppm. Spectral integration was performed in AMIX v. 4.0.2 (Bruker Inc.) using 0.004 ppm buckets across the 0.5–9.0 ppm range. The 4.7–5.5 ppm region was excluded to remove residual water signals, and the resulting integrals were normalized to the total spectral area.

Metabolic marker selection and analysis

Previous studies have demonstrated that BC is characterized by dysregulation of key metabolic pathways, including glucose metabolism, amino acid metabolism and lipid metabolism, which together reflect hallmark features of malignancy such as the Warburg effect, altered protein synthesis and membrane lipid remodeling. The metabolic markers were identified through signals in the proton nuclear magnetic resonance (^{1}H NMR) spectra, which represent metabolites in the serum samples. The integral data of these metabolites were used for orthogonal partial least squares discriminant analysis (OPLS-DA) analysis to distinguish between healthy controls and patients with BC. Specifically, we analyzed signals in the range of 0.5–9.0 ppm, with the integral from 4.7–5.5 ppm set to 0 to eliminate the influence of residual water signals.

Outcome measures

The study outcome measures focused on the metabolic differences between healthy controls and BC patients, as assessed through OPLS-DA. These measurements include integral data from ^{1}H spectra obtained using NMR technology, as well as characteristic metabolites of different BC molecular subtypes analyzed via MetaboAnalyst 6.0 (http://www.metaboanalyst.ca) and the Kyoto Encyclopedia of Genes and Genomes (KEGG) database (https://www.kegg.jp) .

Statistical analyses

The processed spectral data from 172 participants (55 healthy controls, 30 luminal A, 46 luminal B, 23 HER2-positive, and 18 triple-negative (TN) patients) were analyzed using OPLS-DA in MetaboAnalyst 6.0. As an exploratory metabolomics approach, we constructed OPLS-DA models for 2 sets of comparisons. We first compared healthy

controls (n = 55) with each BC molecular subtype – luminal A (n = 30), luminal B (n = 46), HER2-positive (n = 23), and TN (n = 18), and then stratified patients by receptor status and compared controls with ER-positive (n = 76), ER-negative (n = 41), HER2-positive (n = 40), and HER2-negative (n = 77) groups. Model performance was validated using 7-fold cross-validation, evaluating explained variance in the predictors (R^2X), explained variance in the responses (R^2Y) and the model's predictive ability (Q^2). Following OPLS-DA model construction, score plots were generated via MetaboAnalyst 6.0 for data visualization.

Potential differentially abundant metabolites were selected on the basis of variable importance in projection (VIP) scores greater than 1.0. For univariate analysis, we first tested the normality assumption via the Shapiro–Wilk test and the homogeneity of variances via Levene's test. The discriminatory ability of different metabolite combinations between BC subtypes and healthy controls was evaluated by calculating the area under the receiver operating characteristic (ROC) curve (AUC). Venn diagrams were constructed to identify shared and unique metabolites among different BC subtypes.

Although this exploratory approach entails multiple comparisons and may increase the risk of type I errors, we applied the Benjamini–Hochberg false discovery rate correction, a more permissive method, to maximize the identification of potential metabolic alterations, defining statistical significance as an adjusted $p < 0.05$.

For metabolic pathway analysis, we utilized both the KEGG database (http://www.kegg.jp) and the MetaboAnalyst 6.0 online service. The KEGG analysis was performed via KEGG Mapper 2.5, with a focus on *Homo sapiens* pathways. In MetaboAnalyst, pathway analysis was conducted via the *H. sapiens* KEGG pathway library.

Pathway analysis was performed using 2 complementary methods: enrichment analysis via the hypergeometric test to identify pathways overrepresented among the differentially abundant metabolites, and topology analysis based on relative-betweenness centrality to gauge each metabolite's network importance. Pathways with impact values greater than 0.1 and false discovery rate (FDR)-adjusted p-values below 0.05 were considered significantly altered.

Results

Clinical characteristics of patients and healthy controls

A total of 172 participants were enrolled: 55 healthy controls and 117 BC patients, stratified by molecular subtype into 30 luminal A, 46 luminal B, 23 HER2-positive, and 18 TNBC cases. Baseline demographic and clinical characteristics are summarized in Table 1.

Independent 2-tailed t-tests demonstrated no significant differences in mean age between healthy controls and each BC subtype: luminal A ($t_{83} = 1.54$, $p = 0.127$), luminal B ($t_{99} = 0.33$, $p = 0.740$), HER2-positive ($t_{76} = 0.68$, $p = 0.500$), or TNBC ($t_{71} = 0.92$, $p = 0.361$). Likewise, body mass index (BMI) did not differ significantly between controls and patients across subtypes: luminal A ($t_{83} = 1.25$, $p = 0.216$), luminal B ($t_{99} = 1.50$, $p = 0.136$), HER2-positive ($t_{76} = 1.50$, $p = 0.136$), or TNBC ($t_{71} = 0.38$, $p = 0.703$).

Serum ^{1}H-NMR spectra pattern recognition analysis and characteristic metabolite identification

The representative serum ^{1}H-NMR spectra from healthy controls and patients with 4 subtypes of BC are presented in Fig. 1. On the basis of the Human Metabolome Database (HMDB; https://www.hmdb.ca)) and related literature reports,[20,21] 24 endogenous metabolites were identified. The OPLS-DA results of the ^{1}H-NMR data

Table 1. Clinical characteristics of healthy control participants and breast cancer patients of different subtypes

Characteristics	Healthy control (n = 55)	Luminal A (n = 30)	Luminal B (n = 46)	HER2 (n = 23)	TN (n = 18)
Age [years] Mean ±SD	55.22 ±14.83	61.29 ±16.43	54.17 ±13.56	58.18 ±19.18	51.20 ±16.97
BMI [kg/m^2] Mean ±SD	22.33 ±3.11	23.58 ±2.41	23.26 ±2.92	24.93 ±7.87	21.90 ±4.33
TNM stage Tis, n (%)	–	6 (20.0)	1 (2.2)	2 (8.7)	0 (0)
TNM stage I, n (%)	–	8 (26.7)	9 (19.6)	2 (8.7)	2 (11.1)
TNM stage II, n (%)	–	12 (40.0)	25 (54.3)	12 (52.2)	10 (55.6)
TNM stage III, n (%)	–	4 (13.3)	6 (13.0)	7 (30.4)	6 (33.3)
TNM stage IV, n (%)	–	0 (0)	5 (10.9)	0 (0)	0 (0)

SD – standard deviation; TN – triple negative type; TNM – tumor node metastasis; BMI – body mass index; Tis – tumor in situ; HER2 – human epidermal growth factor 2.

from healthy controls and patients with BC are shown in Fig. 2. The score plots revealed significant metabolic differences between the serum samples of the 4 MSs and healthy controls. Metabolites with VIP ≥1 were subjected to Student's t test, and the results are summarized in Table 2. Serum metabolic markers of the 4 MSs were subsequently screened on the basis of the VIP values and statistical analysis results. In the luminal A subtype cohort, metabolomic profiling revealed significant elevations in glutamate (t[83] = 3.49, FDR-p = 0.002), glutamine (t[83] = 5.61, FDR-p < 0.001), citrate (t[83] = 3.75, FDR-p = 0.001), phosphorylcholine/glycerophosphorylcholine (PC/GPC; t[83] = 6.46, FDR-p < 0.001), glycine (t[83] = 3.78, FDR-p < 0.001), threonine (t[83] = 4.23, FDR-p < 0.001), choline (t[83] = 6.54, FDR-p < 0.001), creatine/phosphocreatine (Cr/Pcr; t[83] = 4.70, FDR-p < 0.001), 1-methylhistidine (t[83] = 5.61, FDR-p < 0.001), and methionine (t[83] = 4.00, FDR-p < 0.001) relative to controls.

Conversely, the luminal B subgroup exhibited distinct metabolic patterns with increased lactate (t[99] = 3.37, FDR-p = 0.003) and acetate (t[99] = 4.28, FDR-p < 0.001), alongside significant reductions in citrate (t[99] = 5.27, FDR-p < 0.001), phosphorylcholine/glycerophosphorylcholine (PC/GPC) (t[99] = 7.74, FDR-p < 0.001), trimethylamine oxide (TMAO)/taurine (t[99] = 3.21, FDR-p = 0.004), taurine (t[99] = 3.94, FDR-p = 0.0008), glucose (t[99] = 4.67, FDR-p < 0.0008), choline (t[99] = 7.63, FDR-p < 0.001), Cr/Pcr (t[99]=4.07, FDR-p < 0.001), and 1-methylhistidine (t[99] = 5.34, FDR-p < 0.001) (Table 2).

HER2-positive tumors demonstrated characteristic metabolic perturbations, marked by elevated lactate (t[76] = 3.87, FDR-p < 0.001) and diminished levels of citrate (t[76] = 3.37, FDR-p = 0.003), PC/GPC (t[76] = 5.31, FDR-p < 0.001), choline (t[76] = 5.48, FDR-p < 0.001), Cr/Pcr (t[76] = 3.27, FDR-p = 0.004), and 1-methylhistidine (t[76] = 4.01, FDR-p < 0.001).

The TNBC cohort displayed the most pronounced metabolic dysregulation, featuring increased lactate (t[71] = 2.24, FDR-p = 0.043) alongside decreased concentrations of glutamine (t[71] = 2.22, FDR-p = 0.045), PC/GPC (t[71] = 3.13, FDR-p = 0.005), taurine (t[71] = 3.11, FDR-p = 0.005), glucose (t[71] = 3.02, FDR-p = 0.007), threonine (t[71] = 2.12, FDR-p = 0.043), and choline (t[71] = 3.25, FDR-p = 0.004).

Venn diagram of metabolic markers related to molecular subtypes

Figure 3 shows that choline and the phosphocholine/glycerophosphocholine (PC/GPC) ratio was significantly dysregulated across all BC subtypes. In the hormone-receptor-positive

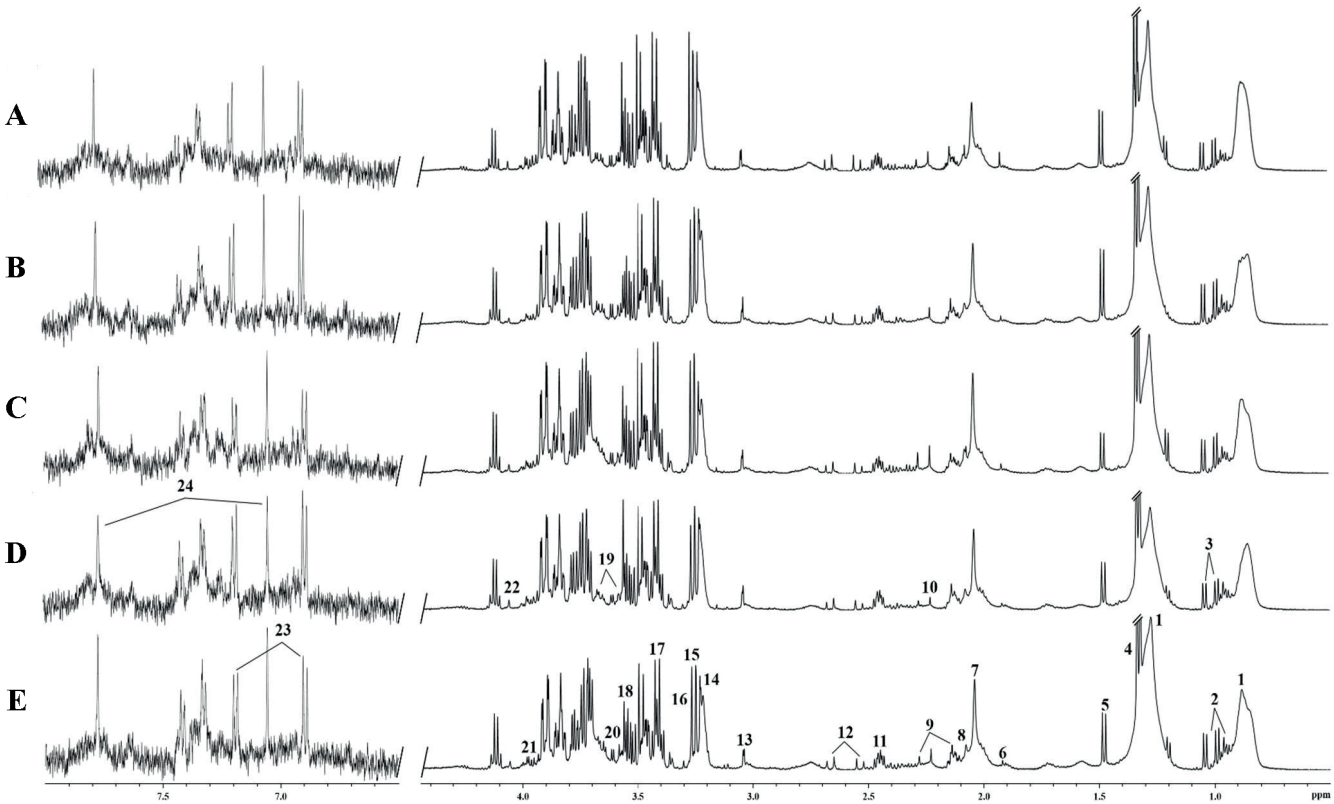

Fig. 1. Representative Carr–Purcell–Meiboom–Gill (CPMG) nuclear magnetic resonance (NMR) ^{1}H spectra of sera from different participants. A. Representative NMR ^{1}H spectra of sera from healthy controls; B. Representative NMR ^{1}H spectra of sera from luminal A breast cancer (BC) patients; C. Representative NMR ^{1}H spectra of sera from luminal B BC patients; D. Representative NMR ^{1}H spectra of sera from human epidermal growth factor 2 (HER2) BC patients; E. Representative NMR ^{1}H spectra of sera from triple-negative breast cancer (TNBC) patients. The metabolites identified in the spectrum are labeled as follows: 1. lipids, 2. leucine/isoleucine, 3. valine, 4. lactate, 5. alanine, 6. acetate, 7. N-acetyl compound, 8. methionine, 9. glutamate, 10. acetoacetate, 11. glutamine, 12. citrate, 13. creatine/Pcr, 14. choline, 15. phosphocholine/glycerophosphocholine, 16. trimethylamine N-oxide/taurine, 17. taurine, 18. glycine, 19. myo-inositol, 20. threonine, 21. glucose, 22. creatinine, 23. tyrosine, 24. 1-methylhistidine

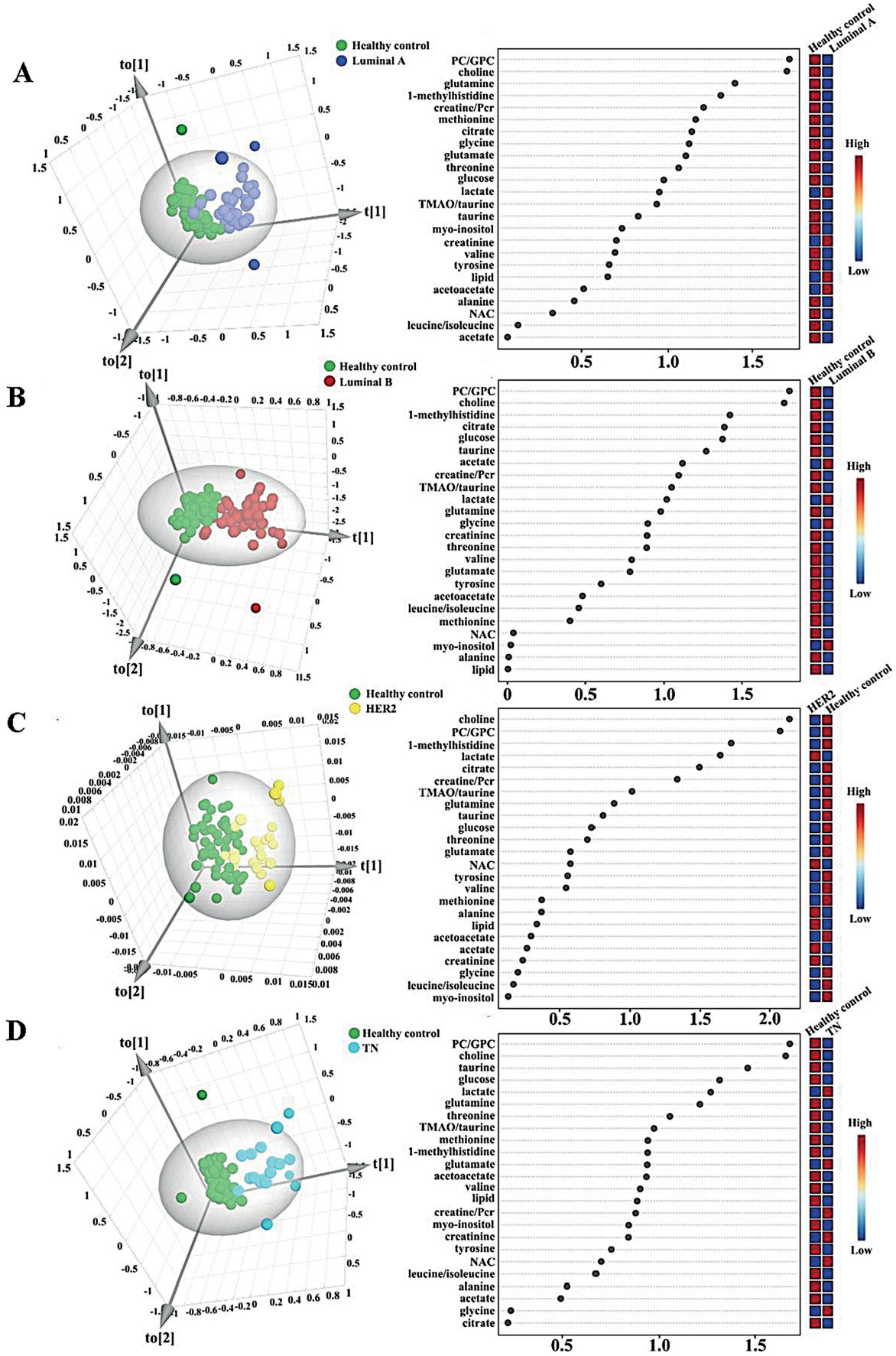

Fig. 2. Orthogonal partial least squares discriminant analysis (OPLS-DA) score plots for ^{1}H-NMR spectra of sera and variable importance in projection (VIP) values of metabolites between healthy controls and 4 subtypes of breast cancer (BC) patients. A. OPLS-DA score plot and VIP values of metabolites for healthy controls and luminal A BC patients, $R^2X = 0.327$, $R^2Y = 0.82$, $Q^2 = 0.650$; B. OPLS-DA score plot and VIP values of metabolites for healthy controls and luminal B BC patients, $R^2X = 0.360$, $R^2Y = 0.801$, $Q^2 = 0.669$; C. OPLS-DA score plot and VIP values of metabolites for healthy controls and human epidermal growth factor 2 (HER2) BC patients, $R^2X = 0.526$, $R^2Y = 0.724$, $Q^2 = 0.515$; D. OPLS-DA score plot and VIP values of metabolites for healthy controls and triple-negative breast cancer (TNBC) patients, $R^2X = 0.27$, $R^2Y = 0.838$, $Q^2 = 0.518$

R^2X – explained variance in the predictors; R^2Y – explained variance in the responses; Q^2 – model's predictive ability.

Table 2. Univariate analysis of potential serum biomarkers between 4 subtypes of breast cancer patients and healthy controls

Metabolites	Luminal A vs healthy controls		Luminal B vs healthy controls		HER2 vs healthy controls		TNBC vs healthy controls	
	SMD (95% CI)	adjusted p-value for t-test	SMD (95% CI)	adjusted p-value for t-test	SMD (95% CI)	adjusted p-value for t-test	SMD (95% CI)	adjusted p-value for t-test
Lactate	0.76 (0.31, 1.21)	0.003	0.67 (0.28, 1.07)	0.003	0.96 (0.46, 1.46)	<0.001	0.58 (0.06, 1.09)	0.043
Glutamate	–0.79 (–1.25, –0.34)	0.002	–0.57 (–0.96, –0.17)	0.009	–0.37 (–0.86, 0.13)	0.167	–0.60 (–1.14, –0.05)	0.046
Glutamine	–1.27 (–1.73, –0.82)	<0.001	–0.77 (–1.16, –0.37)	<0.001	–0.49 (–0.99, 0.02)	0.078	–0.60 (–1.14, –0.06)	0.045
Citrate	–0.85 (–1.30, –0.40)	0.001	–1.05 (–1.45, –0.66)	<0.001	–0.84 (–1.33, –0.34)	0.003	–0.10 (–0.64, 0.45)	0.744
PC/GPC	–1.47 (–1.92, –1.02)	<0.001	–1.55 (–1.94, –1.15)	<0.001	–1.32 (–1.82, –0.82)	<0.001	–0.85 (–1.39, –0.31)	0.005
TMAO/taurine	–0.76 (–1.21, –0.30)	0.003	–0.64 (–1.04, –0.24)	0.004	–0.53 (–1.02, –0.03)	0.053	–0.46 (–1.00, 0.08)	0.121
Taurine	–0.64 (–1.09, –0.18)	0.011	–0.79 (–1.18, –0.39)	<0.001	–0.41 (–0.91, 0.09)	0.125	–0.85 (–1.39, –0.30)	0.005
Glycine	–0.86 (–1.31, –0.40)	<0.001	–0.50 (–0.87, –0.13)	0.014	–0.13 (–0.62, 0.37)	0.648	–0.04 (–0.58, 0.50)	0.885
Glucose	–0.80 (–1.26, –0.35)	0.002	–0.93 (–1.33, –0.54)	<0.001	–0.42 (–0.91, 0.08)	0.122	–0.82 (–1.36, –0.28)	0.007
Threonine	–0.96 (–1.41, –0.51)	<0.001	–0.72 (–1.11, –0.32)	0.001	–0.38 (–0.87, 0.12)	0.158	–0.57 (–1.12, –0.03)	0.043
Choline	–1.48 (–1.94, –1.03)	<0.001	–1.52 (–1.92, –1.13)	<0.001	–1.36 (–1.86, –0.86)	<0.001	–0.88 (–1.42, –0.34)	0.004
Creatine/Pcr	–1.07 (–1.52, –0.61)	<0.001	–0.81 (–1.21, –0.42)	<0.001	–0.81 (–1.31, –0.32)	0.004	–0.57 (–1.12, 0.03)	0.052
1-Methylhistidine	–1.25 (–1.70, –0.80)	<0.001	–1.07 (–1.46, –0.67)	<0.001	–1.00 (–1.49, –0.50)	<0.001	–0.66 (–1.20, –0.12)	0.028
Methionine	–0.91 (–1.36, –0.45)	<0.001	–0.27 (–0.66, 0.13)	0.208	–0.24 (–0.74, 0.25)	0.358	–0.46 (–1.00, 0.09)	0.123
Acetate	0.07 (–0.38, 0.53)	0.757	0.85 (0.46, 1.25)	<0.001	0.14 (–0.36, 0.63)	0.621	–0.35 (–0.90, 0.19)	0.219

TNBC – triple-negative breast cancer; SMD – standardized mean difference; 95% CI – 95% confidence interval; PC/GPC – phosphorylcholine/glycerophosphorylcholine; TMAO – trimethylamine oxide; Pcr – phosphocreatine; p-values were adjusted using the Benjamini–Hochberg procedure to control the false discovery rate.

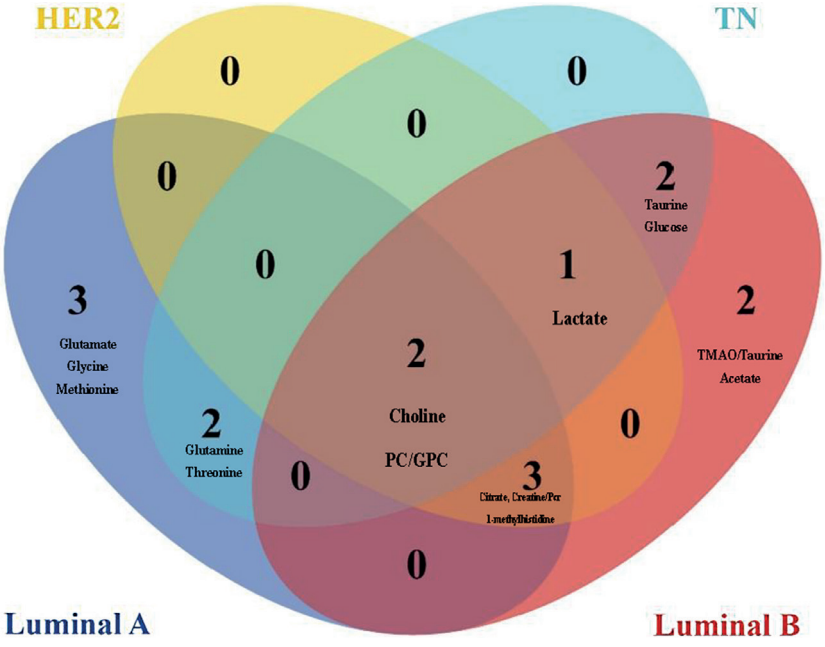

Fig. 3. Venn diagram of the serum metabolic markers of luminal A, luminal B, human epidermal growth factor 2 (HER2), and triple-negative breast cancer (TNBC)

luminal A and B tumors, we additionally observed consistent alterations in citrate, creatine/phosphocreatine and 1-methylhistidine levels alongside PC/GPC and choline, reflecting a shared metabolic phenotype in endocrine-responsive cancers. However, each subtype presented distinct metabolic patterns. Luminal A is characterized by unique alterations in glutamate, glutamine, glycine, threonine, and methionine, whereas luminal B displays specific changes in lactate, TMAO, taurine, glucose, and acetate. In the HER2-enriched and TN subtypes, we observed consistent elevations

Table 3. Pathway alteration in different molecular subtypes of breast cancer

Pathway name	Matched metabolites	Molecular subtype
Glycerophospholipid metabolism	PC/GPC choline	luminal A, luminal B, HER2, TN
Glyoxylate and dicarboxylate metabolism	citrate glycine glutamate glutamine	luminal A, luminal B, HER2
Citrate cycle	citrate	luminal A, luminal B, HER2
Arginine and proline metabolism	creatine/Pcr glutamate	luminal A, luminal B, HER2
Primary bile acid biosynthesis	glycine	luminal A, luminal B, TN
Alanine, aspartate and glutamate metabolism	glutamate glutamine citrate	luminal A, TN
Taurine and hypotaurine metabolism	taurine	luminal B, TN
Starch and sucrose metabolism	glucose	luminal B, TN
Galactose metabolism	glucose	luminal B, TN
Glycine, serine and threonine metabolism	choline glycine threonine creatine/Pcr	luminal A
Arginine biosynthesis	glutamate glutamine	luminal A
Glutathione metabolism	glycine glutamate	luminal A
Cysteine and methionine metabolism	methionine	luminal A
Lipoic acid metabolism	glycine	luminal A
Pyruvate metabolism	lactate acetate	luminal B
Glycolysis/ gluconeogenesis	lactate acetate	luminal B

PC/GPC – phosphorylcholine/glycerophosphorylcholine; TN – triple-negative; Pcr – phosphocreatine; HER2 – human epidermal growth factor 2.

in lactate alongside dysregulated choline metabolism, as evidenced by altered PC/GPC ratios and choline levels. Moreover, HER2-enriched tumors exhibited unique perturbations in citrate, creatine/phosphocreatine and 1-methylhistidine, whereas TNBC were distinguished by altered levels of glutamine, taurine, glucose, and threonine.

Diagnostic discrimination of metabolic markers related to molecular subtypes

The predictive value of metabolic markers for BC molecular subtypes was assessed through ROC curve analysis (Fig. 4). For the luminal A subtype, the combined metabolite panel exhibited outstanding discrimination, with an AUC of 0.983 (95% confidence interval (95% CI): 0.918–0.997), while the subset of subtype-specific metabolites also showed strong predictive performance (AUC = 0.858; 95% CI: 0.766–0.950). For the luminal B subtype, the combined metabolite panel similarly demonstrated excellent discrimination, with an AUC of 0.967 (95% CI: 0.908–0.989), while the subtype-specific marker set achieved an AUC of 0.770 (95% CI: 0.678–0.842). Similar strong predictive performance was observed for the HER2 (AUC = 0.970; 95% CI: 0.898–0.992) and TN (AUC = 0.846; 95% CI: 0.744–0.912) subtypes.

Pathway analysis of metabolic markers related to molecular subtypes

As demonstrated in Fig. 5 and Table 3, KEGG pathway enrichment of subtype-associated metabolites revealed glycerophospholipid metabolism to be a common alteration across all BC molecular subtypes. In the hormone-responsive luminal A and B subtypes, additional shared pathways included glyoxylate and dicarboxylate metabolism, the citrate (TCA) cycle, arginine and proline metabolism, and primary bile acid biosynthesis.

We found that luminal A tumors uniquely engage multiple amino acid-related pathways – namely alanine, aspartate and glutamate metabolism; glycine, serine and threonine metabolism; and arginine biosynthesis – alongside enriched glutathione metabolism as well as cysteine, methionine and lipoic acid metabolic routes. In contrast, the luminal B subtype was characterized by distinctive alterations in energy-related pathways, including taurine and hypotaurine metabolism, starch and sucrose metabolism, galactose metabolism, pyruvate metabolism, and glycolysis/gluconeogenesis. For HER2-positive tumors, the dominant metabolic signatures involved glyoxylate and dicarboxylate metabolism, the TCA cycle, and arginine and proline metabolism.

The TN subtype is characterized by involvement in primary bile acid biosynthesis; alanine, aspartate and glutamate metabolism; taurine and hypotaurine metabolism; starch and sucrose metabolism; and galactose metabolism.

Serum metabolic markers related to ER and HER2 receptor expression

To assess how ER and HER2 receptor status shapes the metabolic landscape in BC, we applied OPLS-DA to the serum metabolomic profiles of patients stratified by ER and HER2 expression. Metabolites with high VIP scores and statistically significant differences according to t-test were deemed differentially abundant (Fig. 6; Table 4). With respect to ER status, glutamine, citrate, the PC/GPC ratio, the TMAO/taurine ratio, choline, creatine/phosphocreatine, and 1-methylhistidine were consistently dysregulated between ER-positive and ER-negative groups (Fig. 7). Some metabolites were uniquely altered by group: Taurine, glucose and creatinine were specific

Table 4. Univariate analysis of potential serum biomarkers between different receptor status of breast cancer patients and healthy controls

Metabolites	ER-positive vs healthy controls		ER-negative vs healthy controls		HER2-positive vs healthy controls		HER2-negative vs healthy controls	
	SMD (95% CI)	adjusted p-value for t-test	SMD (95% CI)	adjusted p-value for t-test	SMD (95% CI)	adjusted p-value for t-test	SMD (95% CI)	adjusted p-value for t-test
Valine	−0.65 (−1.00, −0.30)	<0.001	−0.47 (−0.88, −0.07)	0.028	−0.73 (−1.14, −0.31)	0.001	−0.55 (−0.94, −0.20)	0.003
Lactate	1.00 (0.65, 1.35)	<0.001	0.75 (0.34, 1.16)	<0.001	0.81 (0.40, 1.23)	<0.001	0.64 (0.29, 0.99)	<0.001
Glutamine	−0.86 (−1.21, −0.51)	<0.001	−0.55 (−0.97, −0.14)	0.011	−0.86 (−1.28, −0.45)	<0.001	−0.77 (−1.12, −0.42)	<0.001
Citrate	−0.98 (−1.33, −0.62)	<0.001	−0.50 (−0.91, −0.09)	0.021	−1.21 (−1.63, −0.80)	<0.001	−0.68 (−1.03, −0.33)	<0.001
PC/GPC	−1.50 (−1.85, −1.15)	<0.001	−1.15 (−1.56, −0.74)	<0.001	−1.68 (−2.09, −1.27)	<0.001	−1.30 (−1.65, −0.95)	<0.001
TMAO/taurine	−0.66 (−1.01, −0.31)	<0.001	−0.53 (−0.94, −0.12)	0.014	−0.85 (−1.26, −0.43)	<0.001	−0.54 (−0.89, −0.19)	0.004
Taurine	−0.72 (−1.07, −0.37)	<0.001	−0.63 (−1.04, −0.22)	0.004	−0.72 (−1.13, −0.30)	0.001	−0.71 (−1.06, −0.36)	<0.001
Glucose	−0.88 (−1.23, −0.52)	<0.001	−0.60 (−1.01, −0.20)	0.005	−0.80 (−1.22, −0.39)	<0.001	−0.84 (−1.19, −0.49)	<0.001
Choline	−1.45 (−1.80, −1.10)	<0.001	−1.18 (−1.59, −0.76)	<0.001	−1.72 (−2.14, −1.31)	<0.001	−1.26 (−1.61, −0.91)	<0.001
Creatinine	0.43 (0.08, 0.78)	0.019	0.20 (−0.21, 0.61)	0.337	0.28 (−0.13, 0.70)	0.183	0.44 (0.09, 0.79)	0.016
Creatine/Pcr	−0.87 (−1.22, −0.52)	<0.001	−0.75 (−1.16, −0.34)	<0.001	−1.02 (−1.43, −0.61)	<0.001	−0.77 (−1.12, −0.42)	<0.001
1-methylhistidine	−1.08 (−1.43, −0.73)	<0.001	−0.93 (−1.34, −0.51)	<0.001	−1.34 (−1.76, −0.93)	<0.001	−0.94 (−1.29, −0.59)	<0.001

ER – estrogen receptor; HER2 – human epidermal growth factor 2; SMD – standardized mean difference; 95% CI – 95% confidence interval; PC/GPC – phosphorylcholine/glycerophosphorylcholine; TMAO – trimethylamine oxide; Pcr – phosphocreatine; p-values were adjusted based on Benjamini–Hochberg false discovery rate correction.

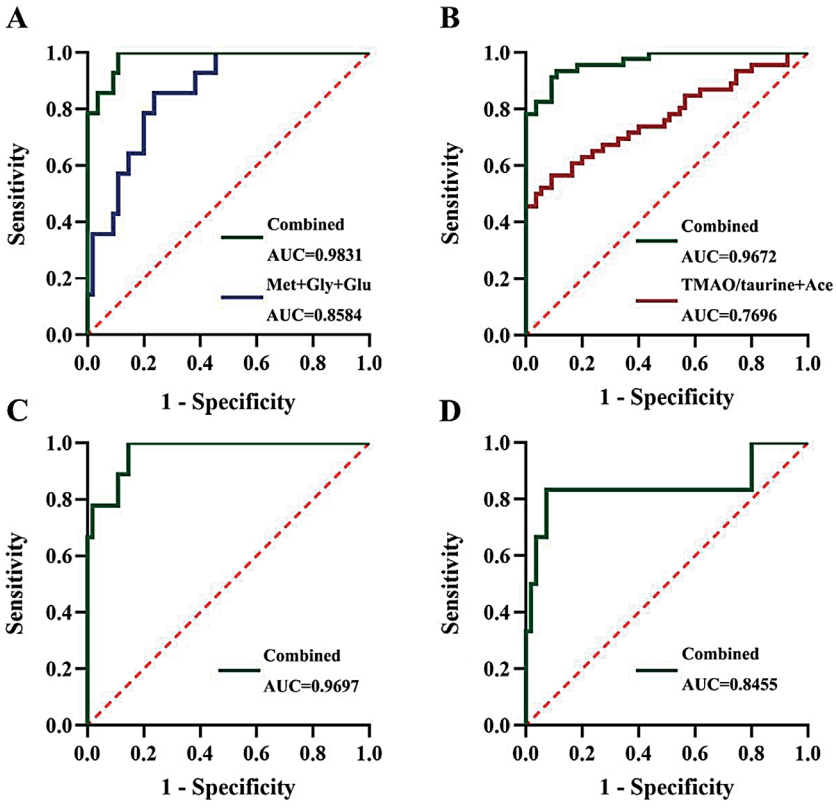

Fig. 4. Receiver operating characteristic (ROC) curves of metabolic markers for the prediction of breast cancer (BC) molecular subtypes; A. ROC curves of different combinations of metabolic markers for luminal A BC prediction; B. ROC curves of different combinations of metabolic markers for luminal B BC prediction; C. ROC curve of a combination of metabolic markers for human epidermal growth factor 2 (HER2)-related BC prediction; D. ROC curve of a combination of metabolic markers for triple-negative breast cancer (TNBC) prediction

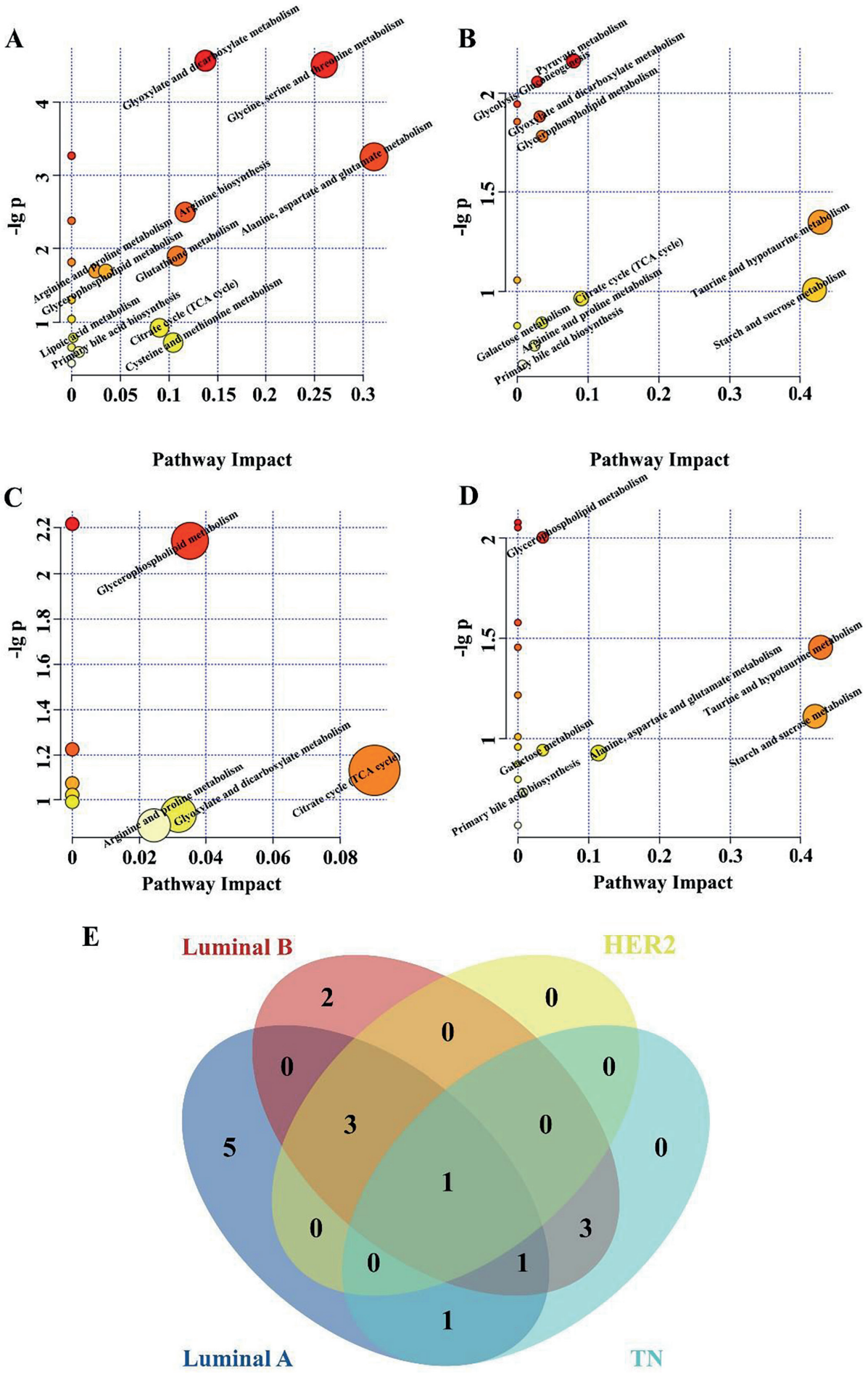

Fig. 5. Metabolic pathway alterations in different breast cancer (BC) molecular subtypes. A. Metabolic pathway alterations in the luminal A subtype; B. Metabolic pathway alterations in the luminal B subtype; C. Metabolic pathway alterations in the human epidermal growth factor 2 (HER2) subtype; D. Metabolic pathway alterations in the triple-negative (TN) subtype; E. Venn diagram of metabolic pathway alterations in luminal A, luminal B, HER2, and TNBC

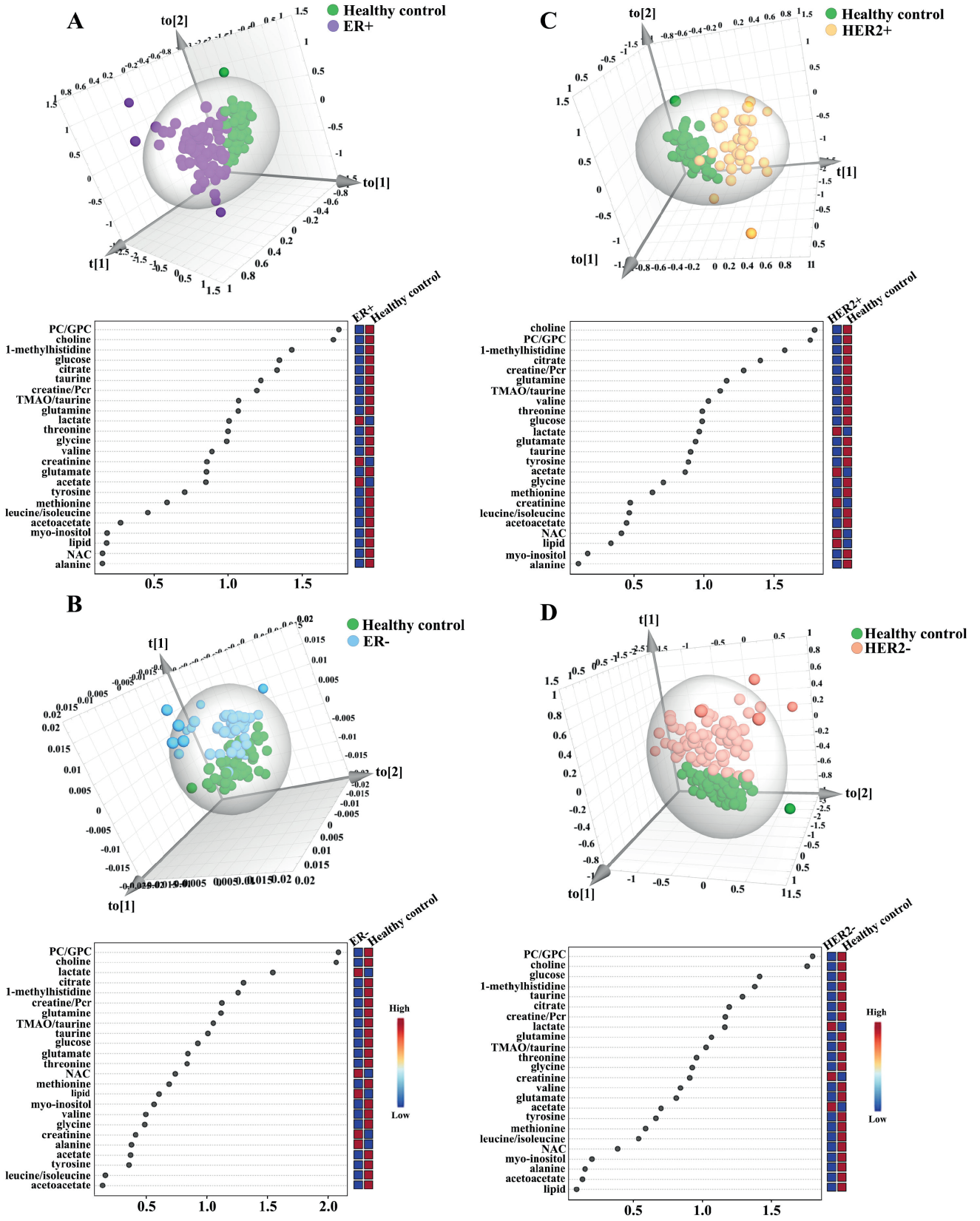

Fig. 6. Orthogonal partial least squares discriminant analysis (OPLS-DA) score plots for ^{1}H-NMR spectra of sera and variable importance in projection (VIP) values of metabolites between healthy controls and breast cancer (BC) patients with different estrogen receptor (ER) and human epidermal growth factor 2 (HER2) expression statuses. A. OPLS-DA score plot and VIP values of metabolites for healthy controls and BC patients with ER+, $R^2X = 0.387$, $R^2Y = 0.747$, and $Q^2 = 0.641$; B. OPLS-DA score plot and VIP values of metabolites for healthy controls and BC patients with ER–, $R^2X = 0.575$, $R^2Y = 0.635$, and $Q^2 = 0.532$; C. OPLS-DA score plot and VIP values of metabolites for healthy controls and BC patients with HER2+, $R^2X = 0.312$, $R^2Y = 0.796$, and $Q^2 = 0.631$; D. OPLS-DA score plot and VIP values of metabolites for healthy controls and BC patients with Her2-, $R^2X = 0.362$, $R^2Y = 0.712$, and $Q^2 = 0.553$

R^2X – explained variance in the predictors; R^2Y – explained variance in the responses; Q^2 – model's predictive ability.

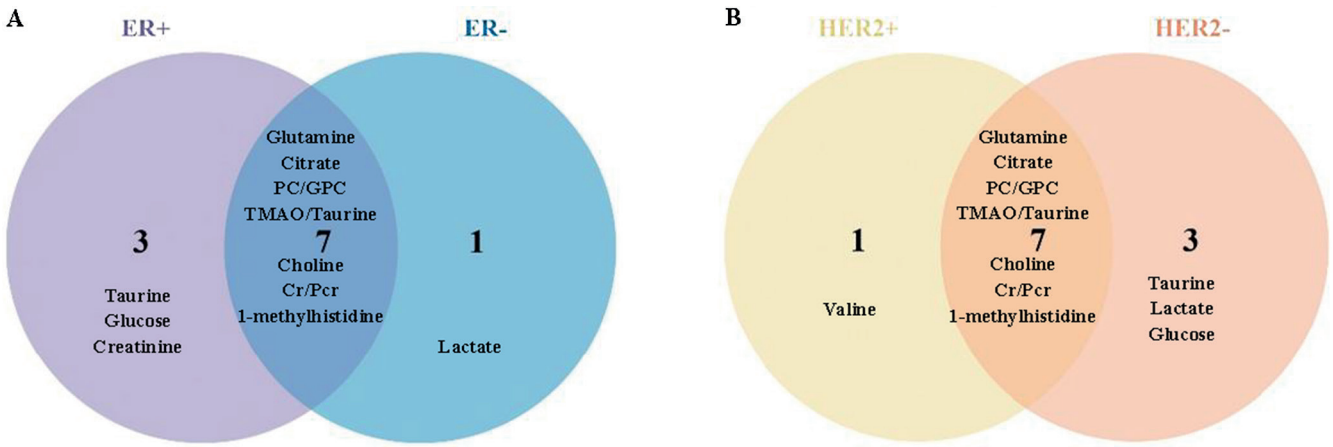

Fig. 7. Venn map of the serum metabolic markers of breast cancer (BC) patients with different estrogen receptor (ER) and human epidermal growth factor 2 (HER2) expression statuses. A. Venn map of the serum metabolic markers of BC patients who are ER positive or ER negative; B. Venn map of the serum metabolic markers of HER2 positive or HER2 negative BC patients

to the ER-positive group, and lactate was unique to the ER-negative group. Similarly, common metabolic changes in the HER2-positive and HER2-negative groups, including glutamine, citrate, PC/GPC, TMAO/taurine, choline, creatine/Pcr, and 1-methylhistidine, were observed for HER2 receptor status. Changes specific to groups were observed: valine was specific for the HER2-positive group, and lactate, taurine and glucose were specific for the HER2-negative group.

ER and HER2 receptor-related metabolomic pathway analysis

The functions and biological pathways predicted and significantly enriched by the KEGG pathway analysis are presented in Fig. 8 and Table 5, which indicate the metabolic pathways related to ER and HER2 receptor status in BC patients. In ER-luminal patients, the most significantly enriched pathways were taurine and hypotaurine metabolism; starch and sucrose metabolism; alanine, aspartate and glutamate metabolism; the citrate cycle; glycerophospholipid metabolism; galactose metabolism; glyoxylate and dicarboxylate metabolism; arginine and proline metabolism; and primary bile acid biosynthesis. Estrogen receptor-negative patients presented similar pathway enrichment patterns, except that taurine and hypotaurine metabolism, starch and sucrose metabolism, galactose metabolism, and primary cholic acid biosynthesis were not significantly affected in this group. The top enriched pathways for HER2-positive individuals were alanine, aspartate and glutamate metabolism; the citrate cycle; glycerophospholipid metabolism; glyoxylate and dicarboxylate metabolism; and arginine and proline metabolism. The HER2-negative patients included all the pathways detected in the HER2-positive patients, with further enrichment in taurine and hypotaurine metabolism, starch and sucrose metabolism, galactose metabolism, and primary bile acid biosynthesis.

Table 5. Pathway alteration in breast cancer with different ER and HER2 receptor expression

Pathway name	Matched metabolites	Molecular subtype
Alanine, aspartate and glutamate metabolism	glutamine citrate	ER+ ER– HER2+ HER2–
Glyoxylate and dicarboxylate metabolism	citrate glutamine	ER+ ER– HER2+ HER2–
Glycerophospholipid metabolism	PC/GPC choline	ER+ ER– HER2+ HER2-
Citrate cycle (TCA cycle)	citrate	ER+ ER– HER2+ HER2–
Arginine and proline metabolism	creatine/Pcr	ER+ ER– HER2+ HER2–
Starch and sucrose metabolism	glucose	ER+ HER2–
Primary bile acid biosynthesis	taurine	ER+ HER2–
Taurine and hypotaurine metabolism	taurine	ER+ HER2–
Galactose metabolism	glucose	ER+ HER2–

PC/GPC – phosphorylcholine/glycerophosphorylcholine; Pcr – phosphocreatine; HER2 – human epidermal growth factor 2; ER – estrogen receptor.

Discussion

Breast cancer exhibits pronounced molecular heterogeneity, which critically influences both therapeutic response and prognosis. Current molecular classification hinges on immunohistochemical assessment of ER, PR, HER2, and Ki-67; however, intratumoral heterogeneity means that biopsy specimens may not fully capture the complexity of the entire tumor. Metabolomics has recently emerged as a powerful tool for probing the tumor microenvironment – an important determinant of disease progression and treatment efficacy.[22] By profiling dynamic fluctuations in metabolites, this approach integrates information on tumor biology, genetic alterations and environmental exposures, offering a more comprehensive view of cancer behavior than static tissue markers alone.

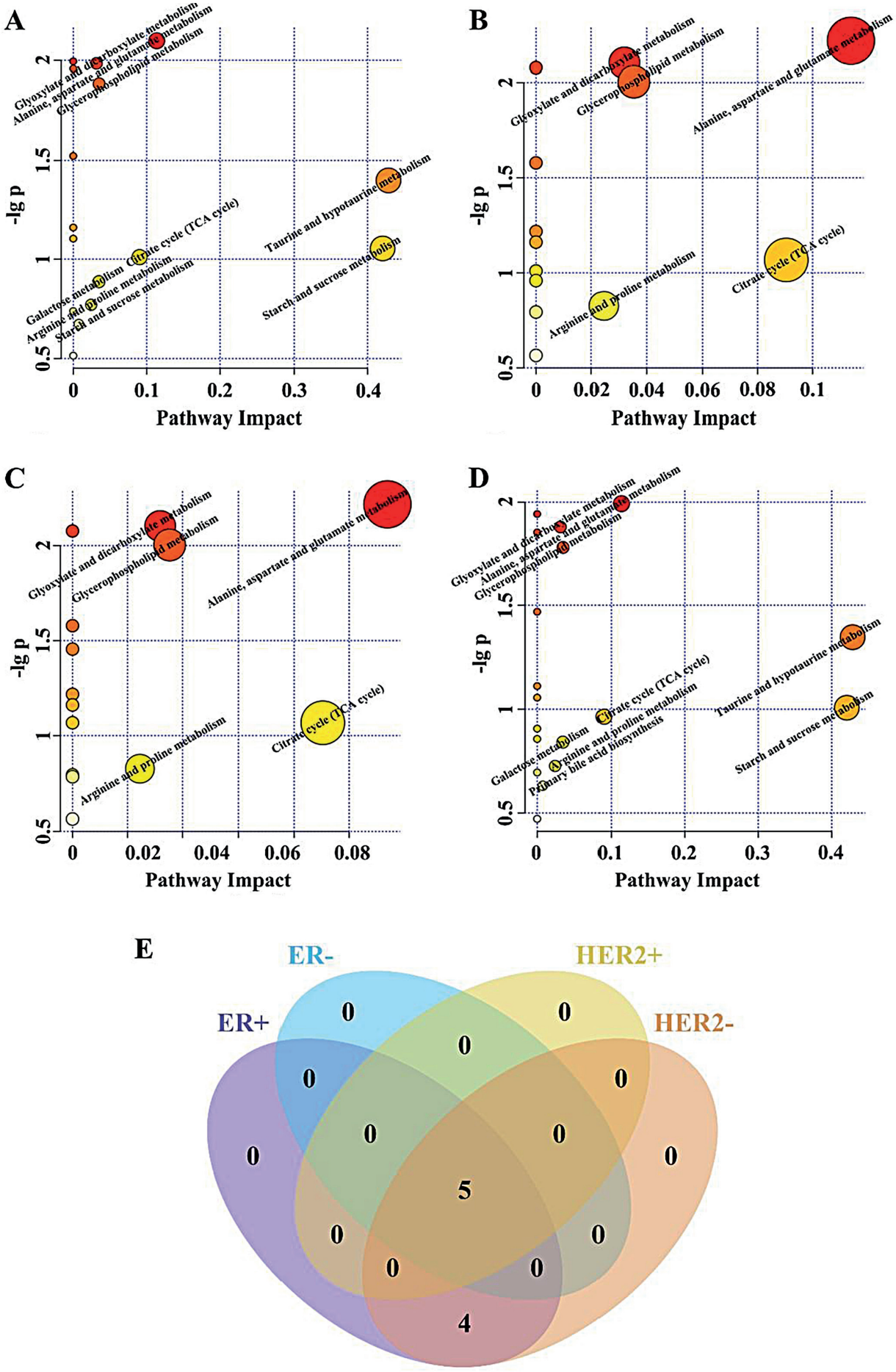

Fig. 8. Metabolic pathway alterations in molecular breast cancer (BC) patients with different estrogen receptor (ER) and human epidermal growth factor 2 (HER2) expression statuses. A. Metabolic pathway alterations in ER-positive BC patients; B. Metabolic pathway alterations in ER-negative BC patients; C. Metabolic pathway alterations in HER2-positive BC patients; D. Metabolic pathway alterations in HER2-negative BC patients; E. Venn diagram of metabolic pathway alterations in molecular BC patients with different ER and HER2 expression statuses

In this study, we investigated the serum metabolic profiles of 4 molecular subtypes of BC patients and compared them with those of healthy controls, confirming that the identified metabolic signatures can discriminate among subtypes with high predictive performance. Receiver operating characteristic curve analyses confirmed that these serum metabolic signatures exhibited excellent discriminatory and predictive performance for molecular typing. Moreover, we discovered metabolic markers linked to ER and HER2 receptor status, revealing varying metabolic profiles between the receptor-positive and receptor-negative cohorts. Pathways related to energy metabolism, amino acid metabolism and phospholipid metabolism were significantly different in terms of the metabolic heterogeneity of each BC subtype.

The 4 molecular subtypes presented different metabolite compositions. Distinct metabolic signatures were identified for each subtype as promising biomarkers. Previous studies have shown that serum levels of amino acids in less aggressive luminal A cancers are lower than those in more aggressive TNBCs.[23,24] Our results corroborate these reports, as the luminal A-specific metabolic alterations mainly included amino acids, indicating subtype-specific amino acid metabolism.

Importantly, excessive acetate accumulation was specifically observed in luminal B patients, suggesting a disturbance in the level of acetate-acetyl-CoA conversion. All 4 subtypes had decreased glucose levels and increased lactate levels, with HER2-positive tumors having the greatest increase in lactate. This finding is consistent with our recent work showing an increased Warburg effect in HER2-positive BC cells,[25,26] emphasizing the metabolic heterogeneity between molecular subtypes.

Common alterations in phospholipid metabolism, particularly with respect to PC/GPC and choline, were present across all subtypes. Other studies have shown similar phenomena in several types of cancer, implying that phospholipid metabolism plays a vital role in cancer development.[27–29] Notably, BC cells showed reduced ^13C-labeled choline and phosphocholine levels relative to normal mammary epithelial cells, suggesting an enhanced metabolic flux from membrane phosphatidylcholine toward free choline and phosphate in malignancy.[30]

In luminal BC, we identified 7 metabolic pathways that were uniquely and highly enriched: glycine, serine and threonine metabolism; arginine biosynthesis; glutathione metabolism; cysteine and methionine metabolism; lipoic acid metabolism; pyruvate metabolism; and glycolysis/gluconeogenesis.

Tumors stratified by ER status (luminal vs non-luminal) exhibited distinct metabolic signatures, with significant enrichment in pathways such as starch and sucrose metabolism, protocholic acid biosynthesis, taurine and hypotaurine metabolism, and galactose metabolism.

However, hormone receptor-positive BC cells are typically more differentiated and exhibit higher levels of proliferation-associated metabolites than hormone receptor-negative TNBC cells.[31–33] We also identified distinct metabolite accumulation patterns in HER2-positive BC patients compared to healthy controls, implicating pathways such as glycerophospholipid metabolism, glyoxylate and dicarboxylate metabolism, the TCA cycle, and arginine and proline metabolism. Notably, these same pathways were enriched in luminal B tumors, likely reflecting the subset of luminal B cancers that co-express HER2 and thus share similar metabolic phenotypes.[34]

The serum metabolic characteristics of these molecular subtypes may provide a noninvasive diagnostic tool to complement immunohistochemical typing, especially when tumor tissue is limited or heterogeneous. These findings indicate that our subtype-specific metabolic signature can be used for targeted therapy development, e.g., by targeting amino acid metabolism in luminal subtypes and inhibiting the glycolysis pathway in HER2-positive patients. Furthermore, longitudinal profiling of these metabolic biomarkers may enable real-time monitoring of therapeutic response and disease trajectory, facilitating the early detection of emerging drug resistance or tumor recurrence. Markers correlated with ER and HER2 status may also predict responsiveness to endocrine or HER2-targeted therapies, enabling more personalized treatment strategies.

Interestingly, we observed a strong overlap between the metabolic pathways distinguishing HER2-positive from HER2-negative patients and those differentiating ER-positive from ER-negative cases; notably, these shared pathways include starch and sucrose metabolism, primary bile acid biosynthesis, taurine and hypotaurine metabolism, and galactose metabolism. This novel finding indicates potential crosstalk between receptor signaling and metabolic regulation,[35] which needs to be further investigated at the molecular level.

Limitations

Despite these promising results, several limitations warrant consideration. First, our relatively small, single-center cohort limits statistical power and the generalizability of our findings to broader patient populations. Second, the cross-sectional design prevents us from drawing causal inferences about how metabolic alterations evolve with disease progression or in response to therapy; longitudinal sampling would be required to capture these dynamics. Third, although we detected a wide range of metabolites, current analytical platforms may have missed other relevant compounds, and the high cost of metabolomic assays poses practical challenges for large-scale validation. Finally, unmeasured confounders, such as variations in diet, concomitant medications and comorbid conditions, were not fully controlled and could have influenced the observed metabolic signatures. Future studies should address these issues by enrolling larger,

multicenter cohorts, incorporating longitudinal designs and standardizing preanalytical variables to confirm and extend our findings.

Conclusions

In this study, we utilized ^{1}H NMR metabolomics to identify serum metabolic signatures in patients with various molecular subtypes of BC. Through comprehensive metabolomic profiling, we explored the distinct metabolic features and pathways linked to each subtype, as well as the relationship between serum metabolites and the expression levels of ER and HER2 receptors. Our findings contribute to a deeper understanding of subtype-specific metabolic reprogramming in BC and may help uncover novel biomarkers for molecular-based classification.

Our analysis identified distinct serum metabolomic signatures corresponding to BC molecular subtypes and receptor profiles, demonstrating metabolomics' promise as a noninvasive tool for tumor classification. These subtype-specific metabolic patterns offer complementary insights to conventional diagnostics and could guide the personalization of therapy. The markers we describe warrant further validation for enhancing patient stratification and optimizing treatment selection.

The next steps toward clinical translation include validating these metabolic markers in larger, multicenter cohorts, establishing population-specific cutoff values, and assessing their ability to predict treatment response in prospective clinical trials. Ultimately, metabolic profiling could offer powerful, noninvasive insights for BC diagnosis, real-time treatment monitoring, and the identification of novel therapeutic targets, thereby enriching patient care.

Data Availability Statement

The datasets supporting the findings of this study are openly available in Figshare at https://figshare.com/s/1af283918b208d404822 (doi:10.6084/m9.figshare.30073258).

Consent for publication

Not applicable.

Use of AI and AI-assisted technologies

Not applicable.

ORCID iDs

Man Xu https://orcid.org/0009-0001-2014-5501
Wenbin Huang https://orcid.org/0000-0003-4925-1524
Xinping Huang https://orcid.org/0009-0003-5888-2157
Hailong Shu https://orcid.org/0009-0006-5814-3487
Weixiao Ke https://orcid.org/0009-0003-5163-779X
Yongcheng Zhang https://orcid.org/0009-0000-4414-5912
Yongxia Yang https://orcid.org/0000-0003-1887-4358

References

1. Alabdulkareem H, Pinchinat T, Khan S, et al. The impact of molecular subtype on breast cancer recurrence in young women treated with contemporary adjuvant therapy. *Breast J*. 2018;24(2):148–153. doi:10.1111/tbj.12853
2. Coles CE, Earl H, Anderson BO, et al. The Lancet Breast Cancer Commission. *Lancet*. 2024;403(10439):1895–1950. doi:10.1016/S0140-6736(24)00747-5
3. Giaquinto AN, Sung H, Newman LA, et al. Breast cancer statistics 2024. *CA Cancer J Clin*. 2024;74(6):477–495. doi:10.3322/caac.21863
4. Waks AG, Winer EP. Breast cancer treatment: A review. *JAMA*. 2019;321(3):288. doi:10.1001/jama.2018.19323
5. Qi G, Zhang X, Gai X, Yan X. Retrospective analysis of estrogen receptor (ER), progesterone receptor (PR), human epidermal growth factor receptor-2 (HER2), Ki67 changes and their clinical significance between primary breast cancer and metastatic tumors. *PeerJ*. 2024;12:e17377. doi:10.7717/peerj.17377
6. Testa U, Castelli G, Pelosi E. Breast cancer: A molecularly heterogenous disease needing subtype-specific treatments. *Med Sci (Basel)*. 2020;8(1):18. doi:10.3390/medsci8010018
7. Dai X, Li T, Bai Z, et al. Breast cancer intrinsic subtype classification, clinical use and future trends. *Am J Cancer Res*. 2015;5(10):2929–2943. PMID:26693050. PMCID:PMC4656721.
8. Gao JJ, Swain SM. Luminal A breast cancer and molecular assays: A review. *Oncologist*. 2018;23(5):556–565. doi:10.1634/theoncologist.2017-0535
9. Dieci MV, Guarneri V, Tosi A, et al. Neoadjuvant chemotherapy and immunotherapy in luminal B-like breast vancer: Results of the phase II GIADA trial. *Clin Cancer Res*. 2022;28(2):308–317. doi:10.1158/1078-0432.CCR-21-2260
10. Swain SM, Shastry M, Hamilton E. Targeting HER2-positive breast cancer: Advances and future directions. *Nat Rev Drug Discov*. 2023;22(2):101–126. doi:10.1038/s41573-022-00579-0
11. Zagami P, Carey LA. Triple negative breast cancer: Pitfalls and progress. *NPJ Breast Cancer*. 2022;8(1):95. doi:10.1038/s41523-022-00468-0
12. Xiao Y, Bi M, Guo H, Li M. Multi-omics approaches for biomarker discovery in early ovarian cancer diagnosis. *eBioMedicine*. 2022;79:104001. doi:10.1016/j.ebiom.2022.104001
13. Wishart DS. Emerging applications of metabolomics in drug discovery and precision medicine. *Nat Rev Drug Discov*. 2016;15(7):473–484. doi:10.1038/nrd.2016.32
14. Singh S, Sarma DK, Verma V, Nagpal R, Kumar M. Unveiling the future of metabolic medicine: Omics technologies driving personalized solutions for precision treatment of metabolic disorders. *Biochem Biophys Res Commun*. 2023;682:1–20. doi:10.1016/j.bbrc.2023.09.064
15. Zhang Y, Zhang R, Liang F, Zhang L, Liang X. Identification of metabolism-associated prostate cancer subtypes and construction of a prognostic risk model. *Front Oncol*. 2020;10:598801. doi:10.3389/fonc.2020.598801
16. Díaz-Beltrán L, González-Olmedo C, Luque-Caro N, et al. Human plasma metabolomics for biomarker discovery: Targeting the molecular subtypes in breast cancer. *Cancers (Basel)*. 2021;13(1):147. doi:10.3390/cancers13010147
17. Chen W, Li Q, Hou R, Liang H, Zhang Y, Yang Y. An integrated metabonomics study to reveal the inhibitory effect and metabolism regulation of taurine on breast cancer. *J Pharm Biomed Anal*. 2022;214:114711. doi:10.1016/j.jpba.2022.114711
18. Zhang X, Xia B, Zheng H, et al. Identification of characteristic metabolic panels for different stages of prostate cancer by ^{1}H NMR-based metabolomics analysis. *J Transl Med*. 2022;20(1):275. doi:10.1186/s12967-022-03478-5
19. Tayyari F, Gowda GAN, Olopade OF, et al. Metabolic profiles of triple-negative and luminal A breast cancer subtypes in African-American identify key metabolic differences. *Oncotarget*. 2018;9(14):11677–11690. doi:10.18632/oncotarget.24433
20. Bose S, Ramesh V, Locasale JW. Acetate metabolism in physiology, cancer, and beyond. *Trends Cell Biol*. 2019;29(9):695–703. doi:10.1016/j.tcb.2019.05.005
21. Klawitter J, Klawitter J, Gurshtein J, et al. Bezielle (BZL101)-induced oxidative stress damage followed by redistribution of metabolic fluxes in breast cancer cells: A combined proteomic and metabolomic study. *Int J Cancer*. 2011;129(12):2945–2957. doi:10.1002/ijc.25965

22. Zhang X, Zhu X, Wang C, Zhang H, Cai Z. Non-targeted and targeted metabolomics approaches to diagnosing lung cancer and predicting patient prognosis. *Oncotarget*. 2016;7(39):63437–63448. doi:10.18632/oncotarget.11521
23. Glunde K, Jie C, Bhujwalla ZM. Molecular causes of the aberrant choline phospholipid metabolism in breast cancer. *Cancer Res*. 2004; 64(12):4270–4276. doi:10.1158/0008-5472.CAN-03-3829
24. Stewart DA, Winnike JH, McRitchie SL, Clark RF, Pathmasiri WW, Sumner SJ. Metabolomics analysis of hormone-responsive and triple-negative breast cancer cell responses to paclitaxel identify key metabolic differences. *J Proteome Res*. 2016;15(9):3225–3240. doi:10.1021/acs.jproteome.6b00430
25. Cheang MCU, Chia SK, Voduc D, et al. Ki67 index, HER2 status, and prognosis of patients with luminal B breast cancer. *J Nat Cancer Inst*. 2009;101(10):736–750. doi:10.1093/jnci/djp082
26. Fan Y, Zhou X, Xia TS, et al. Human plasma metabolomics for identifying differential metabolites and predicting molecular subtypes of breast cancer. *Oncotarget*. 2016;7(9):9925–9938. doi:10.18632/oncotarget.7155
27. Faur IF, Dobrescu A, Clim IA, et al. Lipid metabolism and breast cancer: A narrative review of the prognostic implications and chemotherapy-induced dyslipidemia. *Life*. 2025;15(5):689. doi:10.3390/life15050689
28. Cai XX, Zhang ZZ, Yang XX, et al. Unveiling the impact of lipid metabolism on triple-negative breast cancer growth and treatment options. *Front Oncol*. 2025;15:1579423. doi:10.3389/fonc.2025.1579423
29. Wan M, Pan S, Shan B, et al. Lipid metabolic reprograming: The unsung hero in breast cancer progression and tumor microenvironment. *Mol Cancer*. 2025;24(1):61. doi:10.1186/s12943-025-02258-1
30. Jonker PB, Muir A. Metabolic ripple effects: Deciphering how lipid metabolism in cancer interfaces with the tumor microenvironment. *Dis Model Mech*. 2024;17(9):dmm050814. doi:10.1242/dmm.050814
31. Zipinotti Dos Santos D, de Souza JC, Pimenta TM, et al. The impact of lipid metabolism on breast cancer: A review about its role in tumorigenesis and immune escape. *Cell Commun Signal*. 2023;21(1):161. doi:10.1186/s12964-023-01178-1
32. Santana MDFM, Sawada MIBAC, Junior DRS, et al. Proteomic profiling of HDL in newly diagnosed breast cancer based on tumor molecular classification and clinical stage of disease. *Cells*. 2024;13(16):1327. doi:10.3390/cells13161327
33. Hussein S, Khanna P, Yunus N, Gatza ML. Nuclear receptor-mediated metabolic reprogramming and the impact on HR+ breast cancer. *Cancers (Basel)*. 2021;13(19):4808. doi:10.3390/cancers13194808
34. Holloway RW, Marignani PA. Targeting mTOR and glycolysis in HER2-positive breast cancer. *Cancers (Basel)*. 2021;13(12):2922. doi:10.3390/cancers13122922
35. Mao C, Wang M, Li L, Tang J. Circulating metabolites serve as diagnostic biomarkers for HER2-positive breast cancer and have predictive value for trastuzumab therapy outcomes. *Clin Lab Anal*. 2022; 36(2):e24212. doi:10.1002/jcla.24212

Expression profile of circular RNA in angiotensin II-mediated abdominal aortic aneurysm in mice: A microarray analysis

Jiangjie Lou[1,2,A–F], Shaoze Wu[2,A–C,E,F], Ting Lin[3,A–C,E,F], Guangzhong Zeng[3,A–C,E,F]

[1] Department of Cardiology, The Affiliated Hospital of Jiaxing University, China
[2] Department of Cardiology, Zhejiang Hospital, Hangzhou, China
[3] Department of Cardiology, People's Hospital of Pingxiang, China

A – research concept and design; B – collection and/or assembly of data; C – data analysis and interpretation;
D – writing the article; E – critical revision of the article; F – final approval of the article

Advances in Clinical and Experimental Medicine, ISSN 1899–5276 (print), ISSN 2451–2680 (online) *Adv Clin Exp Med*. 2026;35(2):307–318

Address for correspondence
Guangzhong Zeng
E-mail: zgggzg163@163.com

Funding sources
This work was supported by the Scientific and Technological Projects for Medicine and Health of Zhejiang Province (grant No. 2021KY426).

Conflict of interest
None declared

Received on July 30, 2024
Reviewed on December 2, 2024
Accepted on March 19, 2025

Published online onFebruary 9, 2026

Abstract

Background. Abdominal aortic aneurysm (AAA) is a cardiovascular condition characterized by the abnormal dilation of the abdominal aorta.

Objectives. A circular RNA (circRNA) microarray was utilized to identify differentially expressed circRNAs in angiotensin II (Ang II)-stimulated AAA mice.

Materials and methods. Male apolipoprotein E-deficient (apoE$^{-/-}$) mice were randomly assigned to 2 groups and subjected to 28 days of infusion with either Ang II or saline. At the end of the experiment, the mice were euthanized via exsanguination under anesthesia. The periadventitial tissues were carefully removed from the aortic wall to measure the maximal external diameter of the suprarenal aorta, and then stored for further analysis. Samples from both the control and AAA groups were used for circRNA expression profiling. The R package Bioconductor was employed to perform Gene Ontology (GO) analysis and Kyoto Encyclopedia of Genes and Genomes (KEGG) pathway enrichment analysis. Arraystar's proprietary miRNA target prediction software, integrating miRanda and TargetScan, was used to predict the circRNA/miRNA interactions. Reverse transcription quantitative polymerase chain reaction (RT-qPCR) was employed to confirm the reliability of the microarray results.

Results. A total of 13,103 circRNAs were detected. Compared to the control group, 90 circRNAs were upregulated and 234 were downregulated in the Ang II-induced AAA group. Gene Ontology analysis indicated that the target genes associated with the differentially expressed circRNAs were involved in a variety of biological processes. The KEGG pathway analysis revealed that the differentially expressed circRNAs influenced several critical pathways, including the MAPK signaling pathway, insulin signaling pathway, Ras signaling pathway, and autophagy. The results of RT-qPCR showed that the expression levels of circRNA_30395, circRNA_30398 and circRNA_012594 were significantly increased in AAA, while circRNA_006097 and circRNA_009932 were notably decreased. The top 5 miRNAs related to each validated circRNA were identified through bioinformatic analysis. Among these differentially expressed circRNAs, miR-136-5p was predicted to be the target gene of circRNA_30398 with high probability.

Conclusions. The differential expression of various circRNAs identified in AAA suggests that the circRNA-miRNA-mRNA axis may serve as a potential molecular regulatory mechanism for AAA.

Key words: gene expression profiling, circular RNA, abdominal aortic aneurysm, angiotensin II, mmu_circRNA_30398

Cite as
Lou J, Wu S, Lin T, Zeng G. Expression profile of circular RNA in angiotensin II-mediated abdominal aortic aneurysm in mice: A microarray analysis. *Adv Clin Exp Med*. 2026;35(2):307–318. doi:10.17219/acem/203098

DOI
10.17219/acem/203098

Highlights

- Significant circRNA expression changes in abdominal aortic aneurysm (AAA): A total of 324 circRNAs were differentially expressed in angiotensin (Ang) II-induced AAA mice (90 upregulated, 234 downregulated), suggesting a strong molecular response associated with aneurysm development.
- Pathway involvement identified: Gene Ontology (GO) and Kyoto Encyclopedia of Genes and Genomes (KEGG) analyses revealed that these circRNAs are involved in crucial biological and signaling pathways, including MAPK, insulin, Ras signaling, and autophagy.
- Validation of key circRNAs: RT-qPCR confirmed significant expression changes in several circRNAs – circRNA_30395, circRNA_30398 and circRNA_012594 were upregulated, while circRNA_006097 and circRNA_009932 were downregulated.
- Potential circRNA-miRNA interaction identified: Bioinformatics predicted miR-136-5p as a likely target of circRNA_30398, supporting the hypothesis that the circRNA–miRNA–mRNA axis may play a regulatory role in AAA pathogenesis.

Background

Abdominal aortic aneurysm (AAA) is an asymptomatic and potentially life-threatening cardiovascular disorder, characterized by a localized dilation of the abdominal aortic wall that exceeds 1.5 times its normal diameter or surpasses 3 cm.[1] It typically progresses asymptomatically and slowly until rupture occurs. Globally, the prevalence of asymptomatic AAA ranges from 4% to 8%, with rupture occurring at a rate of 4–13 cases per 100,000 individuals annually.[2] The condition predominantly affects elderly individuals, particularly those with a history of smoking.[3] Once rupture occurs, it can lead to massive internal bleeding, with mortality rates approaching 90%.[4]

To prevent rupture, surgical repair – either through endovascular aneurysm repair (EVAR) or open repair – is commonly employed. However, both approaches carry considerable perioperative risks and a high rate of postoperative re-intervention.[5] From both an economic and clinical standpoint, monitoring and managing small aneurysms to delay or avoid surgical intervention is of greater importance. Based on experiments in rodent models of AAA, successful intervention targets include tissue remodeling, vascular inflammation, lipid metabolism, and blood pressure regulation.[5] Although certain clinical studies suggest the possibility of stabilizing growing AAAs through medical intervention, these findings have not been confirmed in larger, controlled trials. Currently, there is no approved pharmacological treatment to slow the progression of small AAAs.[6]

Circular RNAs (circRNAs) are a class of non-coding RNAs produced through the back-splicing of precursor mRNA exons.[7] CircRNAs, with their circular structure and absence of free ends, are more stable than linear RNAs in extracellular plasma, making them well-suited as diagnostic biomarkers.[8] Emerging evidence suggests that a subset of circRNAs can act as sponges for microRNAs (miRNAs) due to their miRNA response elements (MREs), thereby preventing miRNAs from binding to their mRNA targets.[9,10] This mechanism is referred to as the competing endogenous RNA (ceRNA) theory.[11] Nuclear-resident circRNAs have been shown to influence gene expression at both the transcriptional and splicing levels.[12] Recent research has uncovered diverse biological functions of circRNAs in the cardiovascular system, including angiogenesis, vascular smooth muscle cell (VSMC) apoptosis, VSMC proliferation, and endothelial cell migration.[13–17] Given the growing evidence linking circRNAs to cardiovascular regulation, it is plausible that they also play a significant role in the development and progression of AAA.

Notably, the angiotensin II (Ang II)-induced AAA mouse model is the most widely used in vivo system for investigating AAA pathogenesis.[18]

Objectives

This study aimed to identify differentially expressed circular RNAs (circRNAs) in Ang II-induced AAA mouse models using a circRNA microarray platform. The expression levels of selected circRNAs were further validated by reverse transcription quantitative polymerase chain reaction (RT-qPCR). Additionally, a custom bioinformatics tool, integrating the miRanda and TargetScan algorithms, was used to predict potential circRNA/miRNA interaction networks.

Materials and methods

Study design and participants

Models of mice

Thirty male apoE$^{-/-}$ mice (12 weeks old, C57BL/6 background) were obtained from GemPharmatech Co., Ltd. (Nanjing, China). All animals were housed under specific

pathogen-free (SPF) conditions at the Zhejiang Academy of Medical Sciences (Hangzhou, China). Experimental procedures and animal handling were performed in accordance with the Guide for the Care and Use of Laboratory Animals issued by the U.S. National Institutes of Health (NIH Publication number 85–23, revised 1996: National Institutes of Health (NIH), Bethesda, USA), as well as the guidelines approved by the Laboratory Animal Welfare and Ethics Committee of the Zhejiang Academy of Medical Sciences.

Throughout the experiment, the mice were monitored daily for signs of distress, including changes in behavior, body weight and mobility. The mice were randomly assigned to 2 groups. In the AAA group, the mice received a subcutaneous implantation of an Alzet osmotic minipump (model 2004; ALZET Scientific Products, Mountain View, USA) delivering Ang II at a rate of 1,000 ng/kg/min (Sigma Chemical Co., St. Louis, USA) for 28 consecutive days.[18] In contrast, mice in the control group received normal saline in the pumps.

Minipump implantation

The procedure for micropump implantation was performed as previously described by Lu et al.[19] Prior to implantation, each mouse was weighed, and the midpoint body weight was calculated for each animal to determine the appropriate dosage of Ang II, based on its release rate. The total volume of Ang II required for all mice was subsequently calculated. During the implantation procedure, the mice were anesthetized with isoflurane (Yipin, Shijiazhuang, China), and an incision approx. 1 cm long was made perpendicular to the tail, behind the ear, over the shoulder blade of the foreleg. A subcutaneous pocket was created by inserting the tip of a hemostat toward the tail. The preloaded Alzet osmotic minipump was then carefully inserted into the pocket and advanced fully. The incision was closed with sutures to ensure complete wound closure.

Following surgery, the mice were placed in individual cages with unrestricted access to food and water. Analgesics were provided as needed to manage pain, and the incision site was inspected daily for signs of infection or improper healing. Behavioral assessments were performed regularly to detect any postoperative complications. Mice exhibiting signs of significant distress or health deterioration were evaluated by a veterinarian. Upon confirmation of recovery, the mice were returned to standard housing conditions, and daily welfare checks continued throughout the 28-day Ang II infusion period.

Sample collection

Upon completion of the research, the mice were anesthetized with isoflurane, and blood samples were collected from the right ventricle for subsequent analysis. Following systemic perfusion with cold saline, the aortic tissues were dissected from the ascending aorta to the iliac bifurcation. The gross appearance of the aortic tissues was captured through digital photography after peripheral fat was carefully removed. Immediately thereafter, the cleaned aortic tissues were snap-frozen in liquid nitrogen and stored at –80°C until further analysis.

Data sources and measurement

Total RNA separation and microarray hybridization

Three aortic tissue samples from each of the AAA and sham groups were selected for RNA extraction. Total RNA was isolated using Trizol reagent (Invitrogen Life Technologies, Carlsbad, USA), following the manufacturer's instructions. RNA concentration and purity were quantified using the NanoDrop ND-1000 spectrophotometer (Thermo Fisher Scientific, Waltham, USA). Subsequent microarray hybridization and sample preparation were conducted according to the standard protocols provided by Arraystar (Rockville, USA). Briefly, the total RNA samples were treated with RNase R (Epicentre, Inc, Madison, USA) to remove linear RNAs and enrich for circRNAs. The enriched circRNAs were then reverse-transcribed and amplified into fluorescently labeled complementary RNA (cRNA) using the random priming method provided in the Arraystar Super RNA Labeling Kit. The labeled cRNAs were hybridized to the Arraystar Mouse circRNA Array V2 (8 × 15K; Arraystar). After washing, the microarray slides were scanned using the Agilent Scanner G2505C (Agilent Technologies, Santa Clara, USA).

Identification of differentially expressed circRNAs

The acquired array images were processed and analyzed using Agilent Feature Extraction software (v. 11.0.1.1; Agilent Technologies). Quantile normalization and statistical analysis were performed using the limma package in R software (R Foundation for Statistical Computing, Vienna, Austria). A $p < 0.05$ and a fold change ≥1.5, estimated through a t-test, were used to identify differentially expressed circRNAs between the 2 groups. Discernible circRNA expression patterns among the specimens were visualized via hierarchical clustering.

Real-time polymerase chain reaction validation

To validate the circRNA expression profiles obtained from the microarray analysis, fluorescence-based RT-qPCR was performed using the C1000 system (Applied Biosystems, Waltham, USA). A total of 3 downregulated and 3 upregulated circRNAs were selected for analysis. GAPDH was used as the internal reference gene. The specific primer sequences used for RT-qPCR are listed in Supplementary Table 1. Relative expression levels were calculated using the $2^{-\Delta\Delta Ct}$ method.

Computational bioinformatics analysis

The interactions between differentially expressed circRNAs and their potential target miRNAs were predicted using an in-house miRNA target prediction tool, which integrates both miRanda and TargetScan algorithms. A circRNA/miRNA interaction network involving 5 putative miRNA partners and circRNAs was established based on the predicted miRNA binding sites. To further explore the functional implications of the dysregulated circRNAs, Gene Ontology (GO; https://geneontology.org) enrichment analysis was performed using Bioconductor packages in R, with annotations categorized into biological process, cellular component and molecular function. Additionally, Kyoto Encyclopedia of Genes and Genomes (KEGG; https://www.genome.jp/kegg) pathway enrichment analysis was conducted to identify relevant biological pathways associated with the parental genes of the dysregulated circRNAs.

Statistical analyses

The Shapiro–Wilk test was used to assess the normality of data distribution. For comparisons between groups, an unpaired t-test was applied to datasets with a normal distribution. A $p < 0.05$ was considered statistically significant. All statistical analyses were performed using IBM SPSS v. 23.0 (IBM Corp., Armonk, USA).

Results

Expression profiles of circRNA in mouse tissues of AAA

The Ang II-infusion AAA mouse model closely resembles human AAA in several key pathological features, including medial degeneration, atherosclerosis, increased endothelial permeability, thrombus formation, leukocyte and phagocyte extravasation, and matrix sensitivity to proteolysis.[20] In this study, AAA was induced via continuous Ang II infusion in apoE$^{-/-}$ mice to examine the circRNA expression profiles (Fig. 1). In the AAA group, 7 mice developed typical AAA (with 1 case of rupture-related death), 4 mice exhibited arterial dilation without meeting AAA diagnostic criteria, and 4 mice showed minimal abdominal aorta dilation. In total, 13,103 circRNAs were detected across all samples.

Differentially expressed circRNAs between the Ang II-induced AAA group and the control group were identified using Student's t-test and fold-change filtering (fold change ≥1.5; $p < 0.05$), resulting in 90 upregulated and 234 downregulated circRNAs. The volcano plot and hierarchical clustering revealed the circRNA expression profiles between the AAA group and the control group (Fig. 1).

Analysis of GO and KEGG pathways in differentially expressed circRNAs

Previous studies have demonstrated that circRNAs can act as miRNA sponges to modulate gene expression. Based on this regulatory mechanism, we performed a bioinformatics analysis using miRanda (https://www.microrna.org) and TargetScan (https://www.targetscan.org) to predict potential miRNA targets of the differentially expressed circRNAs. Subsequently, the predicted target genes were subjected to GO and KEGG pathway enrichment analyses. Gene Ontology enrichment analysis of the upregulated target genes revealed significant enrichment in several processes, including cellular macromolecule metabolism and nitrogen compound metabolism (Fig. 2A). Regarding cellular components, these genes were primarily associated with intracellular membrane-bounded organelles and the nucleus (Fig. 2B). The most enriched molecular functions were carbohydrate derivative binding and ATP binding (Fig. 2C).

In contrast, the downregulated target genes were primarily enriched in primary metabolic processes and the establishment of localization (Fig. 2D). In the cellular component category, they were enriched in membrane-bounded organelles and membranes (Fig. 2E), while molecular functions were enriched in cation binding and heterocyclic compound binding (Fig. 2F). The KEGG pathway analysis further revealed that 39 pathways were associated with the upregulated mRNAs and 127 pathways with the downregulated mRNAs. Notably, several crucial pathways, such as the insulin signaling pathway, Ras signaling pathway, MAPK signaling pathway, and autophagy, were potentially influenced by the altered circRNAs (Fig. 3).

qRT-PCR confirmation of circRNAs' differential expression

To validate the microarray results, 6 notably altered circRNAs, including circRNA_006097, circRNA_002457, circRNA_009932, circRNA_30395, circRNA_30398, and circRNA_012594, were assessed using RT-qPCR (Fig. 4). The results demonstrated that the expression levels of cir- cRNA_006097 and circRNA_009932 were markedly downregulated (Tables 1,2, Supplementary Tables 2–5). Conversely, circRNA_30395, circRNA_30398

Table 1. Unpaired t-test results for group comparisons of circRNA_006097 mRNA expression. The results are presented as n, Me (min–max) in Fig. 4A

AAA	Sham	t	p-value	df
3, 0.0001 (0.0001–0.0002)	3,0.0003 (0.0002–0.0003)	3.85	0.018	4

AAA – abdominal aortic aneurysm; n – number of observation; Me (min–max) – median (min–max); t – t-statistic; df – degrees of freedom.

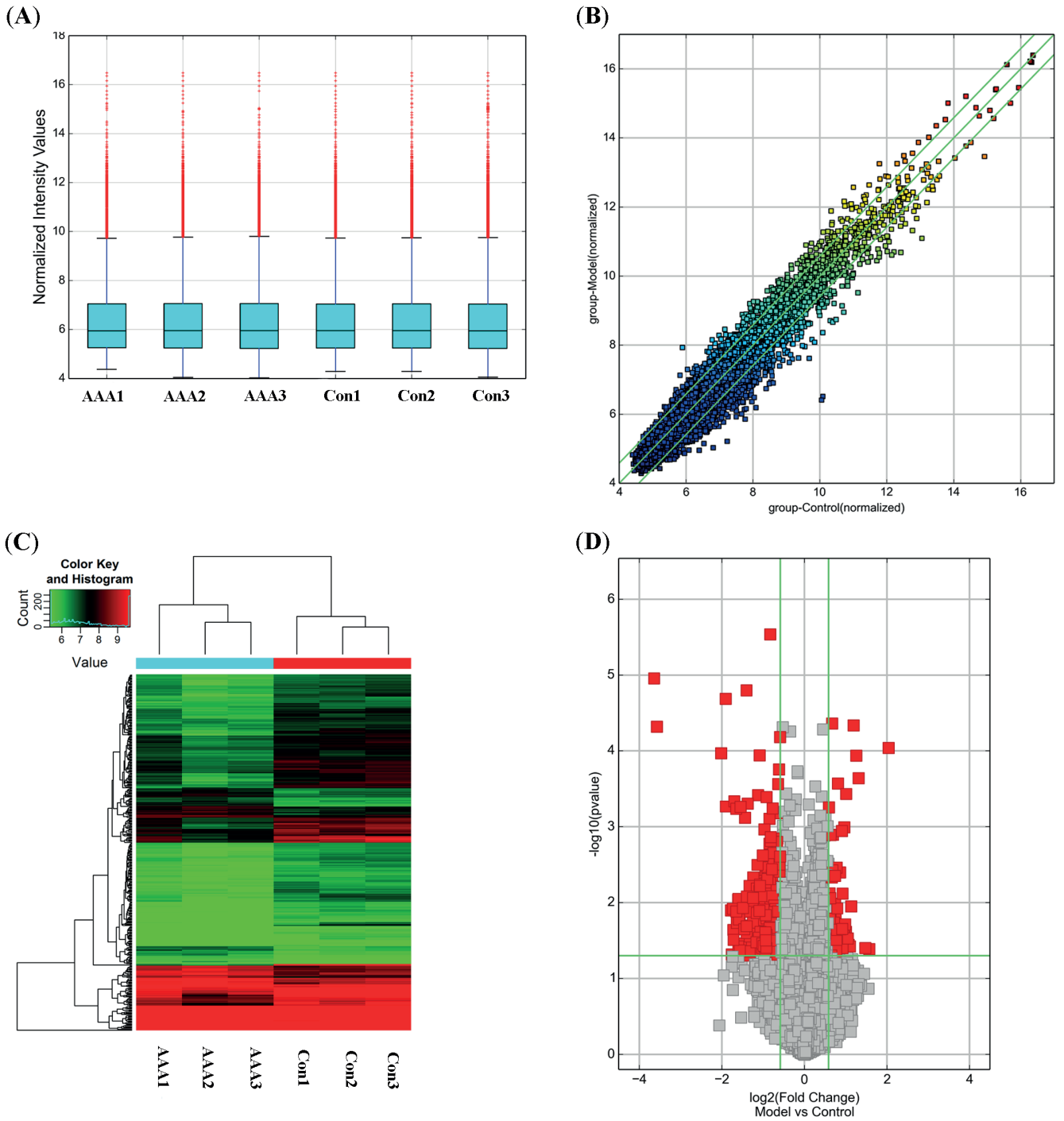

Fig. 1. Comparison of circRNA expression profile between the Ang II-induced AAA group and control group. A. Box plot showing normalized $\log_2$ ratio distributions of circRNA expression across samples. The uniform distribution indicates successful normalization; B. Scatter plot comparing average normalized $\log_2$ values between the AAA and control groups. Green lines represent the fold change threshold (×1.5); circRNAs above or below the threshold indicate significant differential expression; C. Hierarchical cluster analysis of all target circRNAs. 324 circRNAs were significantly differentially expressed ($p < 0.05$, fold change ≥1.5) between Ang II-induced AAA group and the control group; D. Volcano plot shows differential circRNAs expression between the 2 groups. The red parts indicated ≥1.5-fold change expression of the dysregulated circRNAs in AAA tissues ($p < 0.05$)

AAA – abdominal aortic aneurysm.

and circRNA_012594 were significantly upregulated in the AAA group (Tables 3–5, Supplementary Tables 6–11). Conversely, circRNA_006097 and circRNA_009932 were markedly downregulated (Tables 1,2, Supplementary Tables 2–5). In contrast, circRNA_002457 showed no significant difference in expression between the AAA and control groups (Table 6, Supplementary Table 12,13) Overall, the RT-qPCR results were consistent with the microarray data, supporting the reliability of the expression profiles obtained from the circRNA microarray analysis.

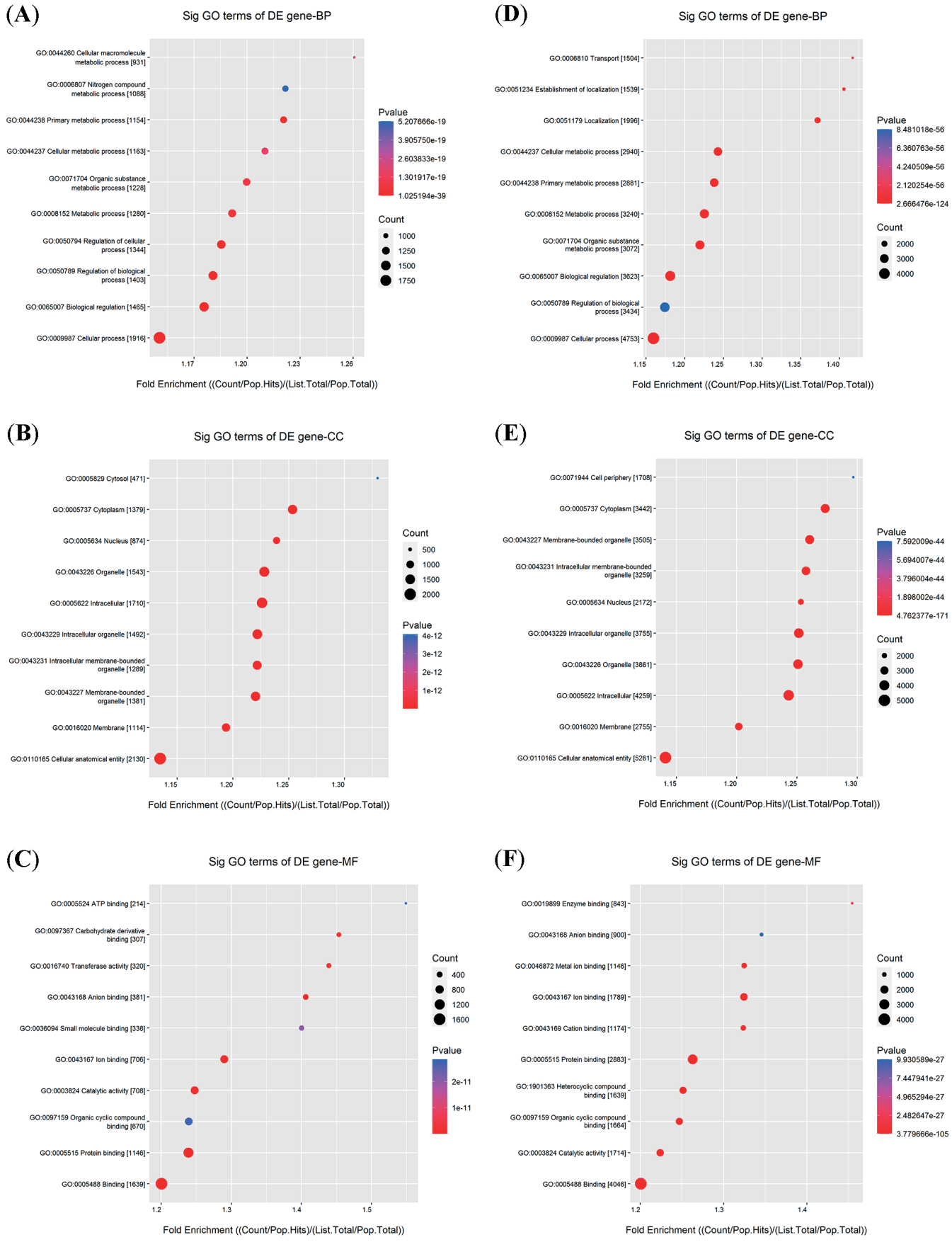

Fig. 2. Gene Ontology (GO) enrichment analysis for target mRNAs of differentially expressed circRNAs in AAA. Gene ontology annotation of upregulated (A, B, C) and downregulated (D, E, F) mRNAs

BP – biological process; CC – cellular component; MF – molecular function; AAA – abdominal aortic aneurysm; DE – differentially expressed.

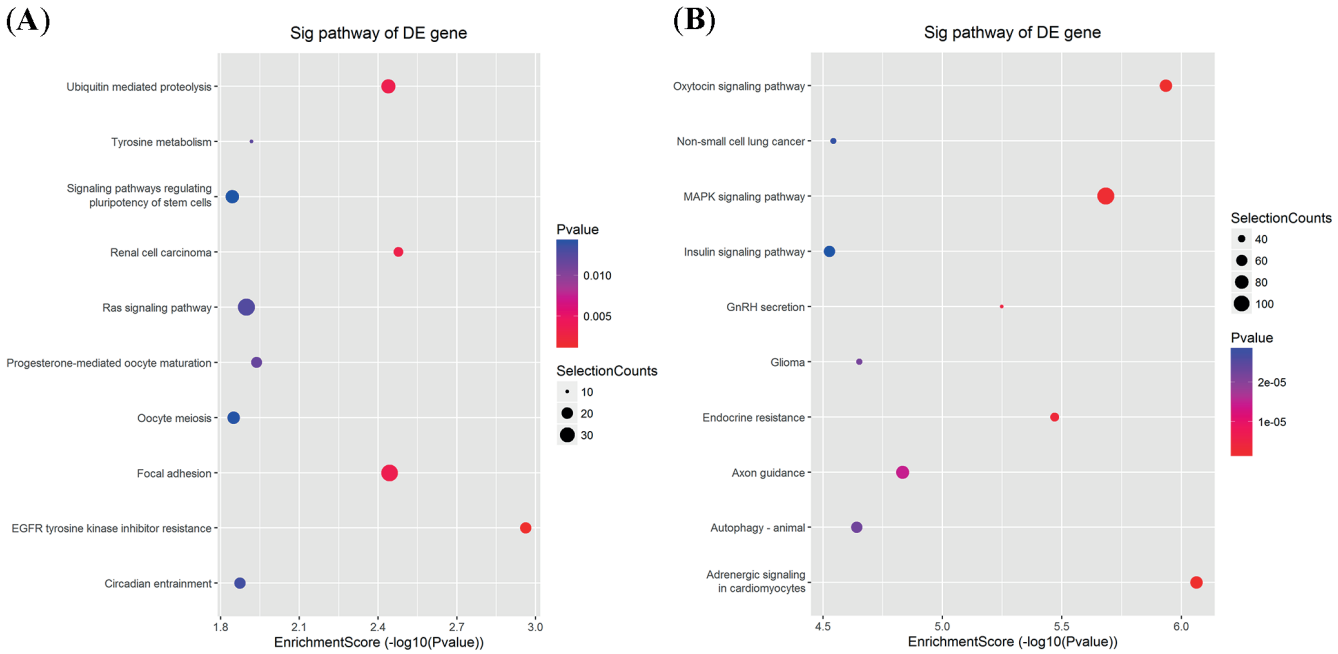

Fig. 3. Kyoto Encyclopedia of Genes and Genomes (KEGG) pathway analysis for target mRNAs of differentially expressed circRNAs in AAA. The top 10 significant pathways associated with the upregulated mRNAs (A) and downregulated mRNAs (B)

AAA – abdominal aortic aneurysm; DE – differentially expressed.

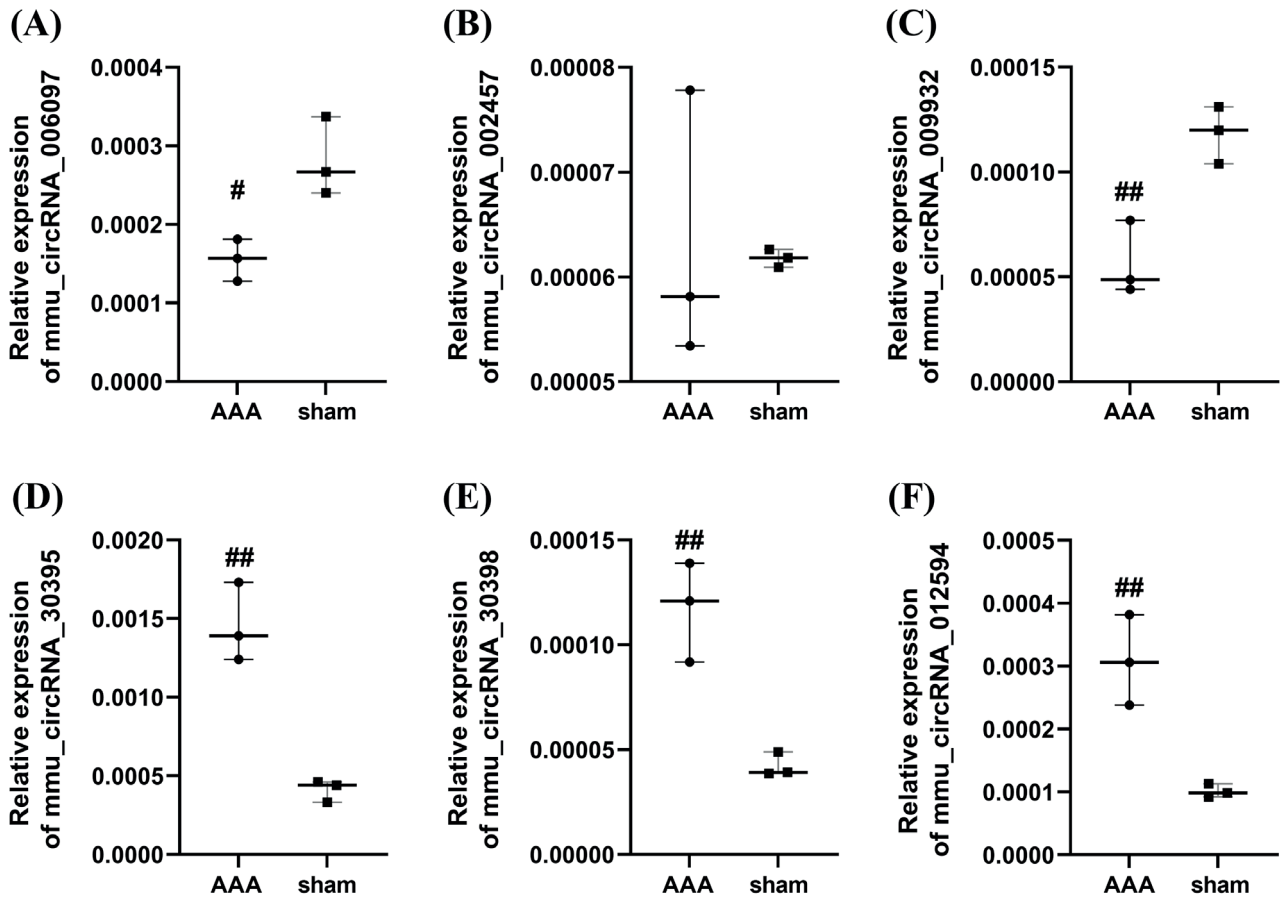

Fig. 4. Validation of differentially expressed candidate circRNAs. The expression levels of circRNAs were detected using reverse transcription quantitative polymerase chain reaction (RT-qPCR) (circRNA_006097, circRNA_002457, circRNA_009932, circRNA_30395, circRNA_30398, and circRNA_012594). CircRNA expression was quantified using the $2^{-\Delta\Delta Ct}$ method with normalization to GAPDH expression levels. Values are expressed as the mean ±SEM ($^{\#}p < 0.05$, $^{\#\#}p < 0.01$ vs control group)

SEM – standard error of the mean; AAA – abdominal aortic aneurysm; GADPH – glyceraldehyde 3-phosphate dehydrogenase.

Table 2. Unpaired t-test results for group comparisons of circRNA_009932 mRNA expression. The results are presented as n, Me (min–max) in Fig. 4C

AAA	Sham	t	p-value	df
3, 0.000049 (0.000044–0.000077)	3, 0.000060 (0.000040–0.000070)	4.77	0.009	4

AAA – abdominal aortic aneurysm; n – number of observation; Me (min–max) – median (min–max); t – t-statistic; df – degrees of freedom.

Table 3. Unpaired t-test results for group comparisons of circRNA_30395 mRNA expression. The results are presented as n, Me (min–max) in Fig. 4D

AAA	Sham	t	p-value	df
3, 0.0014 (0.0012–0.0017)	3,0.0004 (0.0003–0.0005)	6.93	0.002	4

AAA – abdominal aortic aneurysm; n – number of observation; Me (min–max) – median (min–max); t – t-statistic; df – degrees of freedom.

Table 4. Unpaired t-test results for group comparisons of circRNA_30398 mRNA expression. The results are presented as n, Me (min–max) in Fig. 4E

AAA	Sham	t	p-value	df
3, 0.000121 (0.000092–0.000139)	3, 0.000039 (0.000039–0.000049)	5.30	0.006	4

AAA – abdominal aortic aneurysm; n – number of observation; Me (min–max) – median (min–max); t – t-statistic; df – degrees of freedom.

Table 5. Unpaired t-test results for group comparisons of circRNA_012594 mRNA expression. The results are presented as n, Me (min–max) in Fig. 4F

AAA	Sham	t	p-value	df
3, 0.000360 (0.000238–0.000382)	3,0.000099 (0.000092–0.000113)	4.93	0.008	4

AAA – abdominal aortic aneurysm; n – number of observation; Me (min–max) – median (min–max); t – t-statistic; df – degrees of freedom.

Table 6. Unpaired t-test results for group comparisons of circRNA_002457 mRNA expression. The results are presented as n, Me (min–max) in Fig. 4B

AAA	Sham	t	p-value	df
3, 0.00006 (0.000053–0.000078)	3,0.00006 (0.000062–0.000063)	0.18	0.867	4

AAA – abdominal aortic aneurysm; n – number of observation; Me (min–max) – median (min–max); t – t-statistic; df – degrees of freedom.

Competing endogenous RNA (ceRNA) network construction

To further elucidate the potential regulatory mechanisms of the validated circRNAs, a circRNA–miRNA–mRNA interaction network was constructed using Cytoscape software (https://cytoscape.org) (Fig. 5). This network was based on predicted miRNA binding relationships and included the top 5 miRNA candidates associated with each confirmed circRNA, as summarized in Supplementary Table 14.

Discussion

Advancements in RNA-sequencing technologies have revealed that circRNAs constitute a distinct class of non-coding RNA molecules expressed across a wide range of mammalian tissues.[21] Recent studies have highlighted their potential roles as both therapeutic agents and disease biomarkers in various pathological conditions.[22] Acting as miRNA sponges, circRNAs can modulate post-transcriptional gene regulation by preventing miRNAs from binding to their target mRNAs. In addition to their interactions with RNA molecules, circRNAs are also capable of binding specific proteins, thereby influencing their localization or activity. Moreover, some circRNAs regulate transcription within the nucleus, serve as templates for translation, and even compete with linear mRNA splicing.[23] Due to their covalently closed-loop structure, circRNAs exhibit enhanced stability compared to linear RNAs, further supporting their potential as circulating biomarkers. Accumulating evidence suggests that circRNAs play important roles in cardiovascular biology and disease.[22,24]

Given the absence of effective pharmacological treatments for AAA, surgical interventions (either open or endovascular) remain the only available options. Developing effective medical therapies for small AAAs or for patients unsuitable for AAA repair would significantly enhance the existing approach to patient management. In this study, we established an AAA mouse model through continuous subcutaneous infusion of Ang II in apoE$^{-/-}$ mice and systemically profiled circRNA expression in the aorta using circRNA microarray technology. Ninety circRNAs were found to be upregulated and 234 downregulated in the AAA group compared with controls. The predicted target genes of these differentially expressed circRNAs were functionally annotated through GO and KEGG pathway enrichment analyses.

Gene Ontology analysis revealed the involvement of differentially expressed circRNAs in diverse biological processes, such as nitrogen compound metabolism

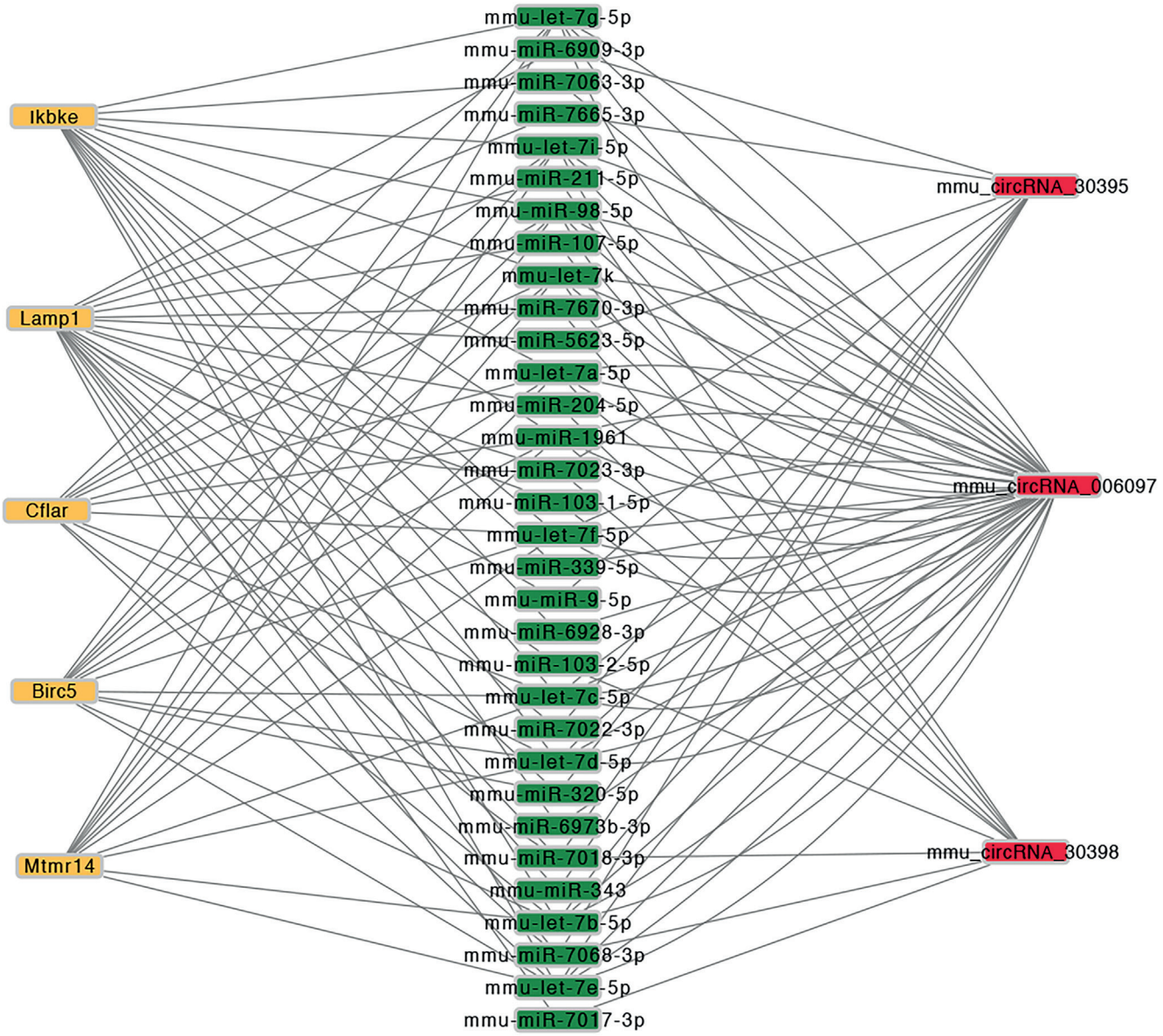

Fig. 5. Prediction of the circRNA/microRNA/mRNA interaction network of RT-qPCR-confirmed dysregulated circRNAs. The brown nodes represent circRNAs (mmu_circRNA_30395, mmu_circRNA_30398, mmu_circRNA_012594, mmu_circRNA_006097, and mmu_circRNA_009932), the red nodes represent miRNAs and the blue nodes represent mRNAs

RT-qPCR – reverse transcription quantitative polymerase chain reaction.

and the establishment of localization. Meanwhile, KEGG analysis highlighted enrichment in key pathways, including the MAPK, Ras, insulin signaling, and autophagy pathways. Among these, the MAPK signaling pathway was notably associated with the upregulated circRNAs in AAA. Jun amino-terminal kinases (JNK1/2/3), a major kinase in the MAPK family, have been implicated in AAA formation. Previous studies demonstrated that JNK inhibition attenuates AAA formation induced by Ang II or calcium chloride in mouse models.[25,26] Additionally, extracellular signal-regulated kinases (ERK), another key kinase in the MAPK family, have been shown to be elevated in human AAA tissues, as reported by Groeneveld et al.[27]

Autophagy, a critical cellular mechanism for degrading dysfunctional organelles and proteins, contributes to cellular homeostasis[28] and has been increasingly linked to AAA pathogenesis.[29] Associations between autophagy and established AAA risk factors, such as senescence,[30] gender[31] and cigarette smoking,[32] have been documented. Furthermore, both pharmacological agents[33,34] and genetic interventions[35,36] targeting autophagy have shown efficacy in small animal models of AAA. In the current study, 6 candidate circRNAs were selected for RT-qPCR verification. The results demonstrated that the expression levels of mmu_circRNA_30395, mmu_circRNA_30398, mmu_circRNA_012594, mmu_circRNA_006097, and mmu_circRNA_009932 were significantly dysregulated, in accordance with the microarray analysis.

To identify the most informative candidates, the 5 validated circRNAs were used to construct a comprehensive ceRNA regulatory network. As mentioned earlier, autophagy plays a significant role in AAA pathogenesis, so we focused on autophagy-related target genes. Further bioinformatics analysis revealed that the target genes of mmu_circRNA_30398, mmu_circRNA_006097 and mmu_circRNA_30395 were predominantly enriched in the autophagy pathway. The downstream target genes of circRNAs involved in autophagy in this ceRNA network include Birc5, Cflar, Ikbke, Mtmr14, and Lamp1.

Further inspection of the ceRNA network revealed additional axes likely involved in AAA progression. Matrix metalloproteinases (MMPs), particularly MMP-2, are known contributors to extracellular matrix (ECM) degradation[37] and AAA pathogenesis.[38] Elevated MMP-2 activity in the aorta has been linked to Ang II and CaCl2 stimulation.[39] Notably, Liu et al. reported that circ_MMP-2 promotes hepatocellular carcinoma metastasis by sponging miR-136-5p, resulting in MMP-2 upregulation.[40] Our analysis identified miR-136-5p as a likely target miRNA of circRNA_30398, supporting the hypothesis that mmu_circRNA_30398 may facilitate AAA progression via the circRNA_30398/miR-136-5p/MMP-2 axis.

Additionally, miR-448-3p, miR-337-3p and miR-432 were predicted as potential targets of circRNA_006097. Notably, miR-448-3p has been shown to be dysregulated in intracranial aneurysms, suggesting a role in vascular pathogenesis.[41] The AAA development is also closely linked to VSMC apoptosis and phenotypic changes, processes in which circRNAs are increasingly recognized as regulators.[42] Structural deterioration of the arterial wall, including ECM degradation and VSMC loss, is a primary cause of aortic dilation and rupture. Several studies have highlighted the involvement of circRNAs in VSMC apoptosis and proliferation.[43,44] For instance, miR-432 has been shown to suppress PI3K/AKT/mTOR signaling by downregulating P55PIK, inhibiting myoblast proliferation and differentiation.[45]

Similarly, miR-337-3p modulates myosin 10 expression, impacting pulmonary artery smooth muscle cell proliferation.[46] These findings suggest that circRNA_006097 may influence AAA formation by regulating VSMC function.[47] Moreover, circRNA_009932 may exert similar effects through its predicted target, miR-222-5p, which inhibits smooth muscle cell differentiation by suppressing ROCK2 and α-smooth muscle actin expression.

Limitations

This study has several limitations. First, the construction of the circRNA–miRNA–mRNA interaction network was based solely on bioinformatics analysis, which requires further experimental validation. Second, although RT-qPCR confirmed the differential expression of selected circRNAs, their functional roles in AAA pathogenesis were not assessed through knockdown or overexpression experiments. Such mechanistic investigations are essential to establish causal relationships. Finally, emerging evidence suggests that circRNAs may also interact with RNA-binding proteins or serve as templates for translation, aspects that were not explored in the current study.

Conclusions

In this study, circRNA expression profiles in AAA were characterized based on an Ang II-induced mouse model. Five circRNAs were selected and verified with RT-qPCR. Our findings provide evidence that the circRNA-miRNA-mRNA axis may play a critical role in the molecular pathogenesis of AAA. Further experimental research is needed to elucidate the regulatory mechanisms of the circRNA_30398/miR-136-5p/MMP-2 axis. Understanding these mechanisms could reveal potential therapeutic targets for AAA.

Supplementary data

The supplementary materials are available at https://doi.org/10.5281/zenodo.15744894. The package includes the following files:

Supplementary Table 1. Primers used for RT-qPCR.

Supplementary Table 2. Shapiro–Wilk test results for circRNA_006097 mRNA expression in the AAA and sham groups (see Fig. 4A).

Supplementary Table 3. F-test for equality of variances for circRNA_006097 mRNA expression in the AAA and sham groups (see Fig. 4A).

Supplementary Table 4. Shapiro–Wilk test results for circRNA_009932 mRNA expression in the AAA and sham groups (see Fig. 4C).

Supplementary Table 5. F-test for equality of variances for circRNA_009932 mRNA expression in the AAA and sham groups (see Fig. 4C).

Supplementary Table 6. Shapiro–Wilk test results for circRNA_30395 mRNA expression in the AAA and sham groups (see Fig. 4D).

Supplementary Table 7. F-test for equality of variances for circRNA_30395 mRNA expression in the AAA and sham groups (see Fig. 4D).

Supplementary Table 8. Shapiro–Wilk test results for circRNA_30398 mRNA expression in the AAA and sham groups (see Fig. 4E).

Supplementary Table 9. F-test for equality of variances for circRNA_30398 mRNA expression in the AAA and sham groups (see Fig. 4E).

Supplementary Table 10. Shapiro–Wilk test results for circRNA_012594 mRNA expression in the AAA and sham groups (see Fig. 4F).

Supplementary Table 11. F-test for equality of variances for circRNA_012594 mRNA expression in the AAA and sham groups (see Fig. 4F).

Supplementary Table 12. Shapiro–Wilk test results for circRNA_002457 mRNA expression in the AAA and sham groups (see Fig. 4B).

Supplementary Table 13. F-test for equality of variances for circRNA_002457 mRNA expression in the AAA and sham groups (see Fig. 4B).

Supplementary Table 14. The top 5 predicted targets of RT-qPCR confirmed dysregulated circRNAs.

Data availability

The datasets generated and/or analyzed during the current study are available from the corresponding author on reasonable request.

Consent for publication

Not applicable.

Use of AI and AI-assisted technologies

Not applicable.

ORCID iDs

Jiangjie Lou https://orcid.org/0000-0002-2917-7518
Shaoze Wu https://orcid.org/0000-0002-7274-3095
Ting Lin https://orcid.org/0009-0006-2705-625X
Guangzhong Zeng https://orcid.org/0009-0000-9623-2663

References

1. Johnston KW, Rutherford RB, Tilson MD, Shah DM, Hollier L, Stanley JC. Suggested standards for reporting on arterial aneurysms. *J Vasc Surg*. 1991;13(3):452–458. doi:10.1067/mva.1991.26737
2. Howard DPJ, Banerjee A, Fairhead JF, Handa A, Silver LE, Rothwell PM. Age-specific incidence, risk factors and outcome of acute abdominal aortic aneurysms in a defined population. *Br J Surg*. 2015;102(8):907–915. doi:10.1002/bjs.9838
3. Vardulaki KA, Walker NM, Day NE, Duffy SW, Ashton HA, Scott RAP. Quantifying the risks of hypertension, age, sex and smoking in patients with abdominal aortic aneurysm. *J Br Surg*. 2000;87(2):195–200. doi:10.1046/j.1365-2168.2000.01353.x
4. Kent KC. Abdominal aortic aneurysms. *N Engl J Med*. 2014;371(22):2101–2108. doi:10.1056/NEJMcp1401430
5. Lindeman JH, Matsumura JS. Pharmacologic management of aneurysms. *Circ Res*. 2019;124(4):631–646. doi:10.1161/CIRCRESAHA.118.312439
6. Golledge J. Abdominal aortic aneurysm: Update on pathogenesis and medical treatments. *Nat Rev Cardiol*. 2019;16(4):225–242. doi:10.1038/s41569-018-0114-9
7. Kristensen LS, Andersen MS, Stagsted LVW, Ebbesen KK, Hansen TB, Kjems J. The biogenesis, biology and characterization of circular RNAs. *Nat Rev Genet*. 2019;20(11):675–691. doi:10.1038/s41576-019-0158-7
8. Memczak S, Papavasileiou P, Peters O, Rajewsky N. Identification and characterization of circular RNAs as a new class of putative biomarkers in human blood. *PLoS One*. 2015;10(10):e0141214. doi:10.1371/journal.pone.0141214
9. Du WW, Yang W, Chen Y, et al. Foxo3 circular RNA promotes cardiac senescence by modulating multiple factors associated with stress and senescence responses. *Eur Heart J*. 2016;38(18):1402–1412. doi:10.1093/eurheartj/ehw001
10. Hansen TB, Jensen TI, Clausen BH, et al. Natural RNA circles function as efficient microRNA sponges. *Nature*. 2013;495(7441):384–388. doi:10.1038/nature11993
11. Rong D, Sun H, Li Z, et al. An emerging function of circRNA-miRNAs-mRNA axis in human diseases. *Oncotarget*. 2017;8(42):73271–73281. doi:10.18632/oncotarget.19154
12. Li X, Yang L, Chen LL. The biogenesis, functions, and challenges of circular RNAs. *Mol Cell*. 2018;71(3):428–442. doi:10.1016/j.molcel.2018.06.034
13. Boeckel JN, Jaé N, Heumüller AW, et al. Identification and characterization of hypoxia-regulated endothelial circular RNA. *Circ Res*. 2015;117(10):884–890. doi:10.1161/CIRCRESAHA.115.306319
14. Holdt LM, Stahringer A, Sass K, et al. Circular non-coding RNA ANRIL modulates ribosomal RNA maturation and atherosclerosis in humans. *Nat Commun*. 2016;7(1):12429. doi:10.1038/ncomms12429
15. Chen J, Cui L, Yuan J, Zhang Y, Sang H. Circular RNA WDR77 target FGF-2 to regulate vascular smooth muscle cells proliferation and migration by sponging miR-124. *Biochem Biophys Res Commun*. 2017;494(1–2):126–132. doi:10.1016/j.bbrc.2017.10.068
16. Zhang SJ, Chen X, Li CP, et al. Identification and characterization of circular RNAs as a new class of putative biomarkers in diabetes retinopathy. *Invest Ophthalmol Vis Sci*. 2017;58(14):6500. doi:10.1167/iovs.17-22698
17. He Q, Zhao L, Liu Y, et al. circ-SHKBP1 regulates the angiogenesis of U87 glioma-exposed endothelial cells through miR-544a/FOXP1 and miR-379/FOXP2 pathways. *Mol Ther Nucleic Acids*. 2018;10:331–348. doi:10.1016/j.omtn.2017.12.014
18. Daugherty A, Manning MW, Cassis LA. Angiotensin II promotes atherosclerotic lesions and aneurysms in apolipoprotein E-deficient mice. *J Clin Invest*. 2000;105(11):1605–1612. doi:10.1172/JCI7818
19. Lu H, Howatt DA, Balakrishnan A, et al. Subcutaneous angiotensin II infusion using osmotic pumps induces aortic aneurysms in mice. *J Vis Exp*. 2015;103:53191. doi:10.3791/53191
20. Sénémaud J, Caligiuri G, Etienne H, Delbosc S, Michel JB, Coscas R. Translational relevance and recent advances of animal models of abdominal aortic aneurysm. *Arterioscler Thromb Vasc Biol*. 2017;37(3):401–410. doi:10.1161/ATVBAHA.116.308534
21. Memczak S, Jens M, Elefsinioti A, et al. Circular RNAs are a large class of animal RNAs with regulatory potency. *Nature*. 2013;495(7441):333–338. doi:10.1038/nature11928
22. Holdt LM, Kohlmaier A, Teupser D. Circular RNAs as therapeutic agents and targets. *Front Physiol*. 2018;9:1262. doi:10.3389/fphys.2018.01262
23. Aufiero S, Reckman YJ, Pinto YM, Creemers EE. Circular RNAs open a new chapter in cardiovascular biology. *Nat Rev Cardiol*. 2019;16(8):503–514. doi:10.1038/s41569-019-0185-2
24. Kishore R, Garikipati VNS, Gonzalez C. Role of circular RNAs in cardiovascular disease. *J Cardiovasc Pharmacol*. 2020;76(2):128–137. doi:10.1097/FJC.0000000000000841
25. Yoshimura K, Aoki H, Ikeda Y, et al. Regression of abdominal aortic aneurysm by inhibition of c-Jun N-terminal kinase. *Nat Med*. 2005;11(12):1330–1338. doi:10.1038/nm1335
26. Guo ZZ, Cao QA, Li ZZ, et al. SP600125 attenuates nicotine-related aortic aneurysm formation by inhibiting matrix metalloproteinase production and CC chemokine-mediated macrophage migration. *Mediators Inflamm*. 2016;2016:9142425. doi:10.1155/2016/9142425
27. Groeneveld ME, Van Burink MV, Begieneman MPV, et al. Activation of extracellular signal-related kinase in abdominal aortic aneurysm. *Eur J Clin Invest*. 2016;46(5):440–447. doi:10.1111/eci.12618
28. Mizushima N, Levine B, Cuervo AM, Klionsky DJ. Autophagy fights disease through cellular self-digestion. *Nature*. 2008;451(7182):1069–1075. doi:10.1038/nature06639
29. Wang L, Liu S, Pan B, et al. The role of autophagy in abdominal aortic aneurysm: Protective but dysfunctional. *Cell Cycle*. 2020;19(21):2749–2759. doi:10.1080/15384101.2020.1823731
30. Ren J, Sowers JR, Zhang Y. Metabolic stress, autophagy, and cardiovascular aging: From pathophysiology to therapeutics. *Trends Endocrinol Metab*. 2018;29(10):699–711. doi:10.1016/j.tem.2018.08.001
31. Tyutyunyk-Massey L, Gewirtz DA. Roles of autophagy in breast cancer treatment: Target, bystander or benefactor. *Semin Cancer Biol*. 2020;66:155–162. doi:10.1016/j.semcancer.2019.11.008
32. Wang Z, Liu B, Zhu J, Wang D, Wang Y. Nicotine-mediated autophagy of vascular smooth muscle cell accelerates atherosclerosis via nAChRs/ROS/NF-κB signaling pathway. *Atherosclerosis*. 2019;284:1–10. doi:10.1016/j.atherosclerosis.2019.02.008
33. Wang Z, Guo J, Han X, et al. Metformin represses the pathophysiology of AAA by suppressing the activation of PI3K/AKT/mTOR/autophagy pathway in ApoE$^{-/-}$ mice. *Cell Biosci*. 2019;9(1):68. doi:10.1186/s13578-019-0332-9

34. Li G, Qin L, Wang L, et al. Inhibition of the mTOR pathway in abdominal aortic aneurysm: Implications of smooth muscle cell contractile phenotype, inflammation, and aneurysm expansion. *Am J Physiol Heart Circ Physiol*. 2017;312(6):H1110–H1119. doi:10.1152/ajpheart.00677.2016
35. Peng J, He X, Zhang L, Liu P. MicroRNA-26a protects vascular smooth muscle cells against H_2O_2-induced injury through activation of the PTEN/AKT/mTOR pathway. *Int J Mol Med*. 2018;42(3):1367–1378. doi:10.3892/ijmm.2018.3746
36. Zhao L, Huang J, Zhu Y, et al. miR-33-5p knockdown attenuates abdominal aortic aneurysm progression via promoting target adenosine triphosphate-binding cassette transporter A1 expression and activating the PI3K/Akt signaling pathway. *Perfusion*. 2020;35(1):57–65. doi:10.1177/0267659119850685
37. Nagase H, Visse R, Murphy G. Structure and function of matrix metalloproteinases and TIMPs. *Cardiovasc Res*. 2006;69(3):562–573. doi:10.1016/j.cardiores.2005.12.002
38. Rabkin SW. The role of matrix metalloproteinases in the production of aortic aneurysm. *Prog Mol Biol Transl Sci*. 2017;147:239–265. doi:10.1016/bs.pmbts.2017.02.002
39. Quintana RA, Taylor WR. Cellular mechanisms of aortic aneurysm formation. *Circ Res*. 2019;124(4):607–618. doi:10.1161/CIRCRESAHA.118.313187
40. Liu D, Kang H, Gao M, et al. Exosome-transmitted circ_MMP2 promotes hepatocellular carcinoma metastasis by upregulating MMP2. *Mol Oncol*. 2020;14(6):1365–1380. doi:10.1002/1878-0261.12637
41. Zhang JZ, Chen D, Lv LQ, et al. miR-448-3p controls intracranial aneurysm by regulating KLF5 expression. *Biochem Biophys Res Commun*. 2018;505(4):1211–1215. doi:10.1016/j.bbrc.2018.10.032
42. Wang J, Sun H, Zhou Y, et al. Circular RNA microarray expression profile in 3,4-benzopyrene/angiotensin II-induced abdominal aortic aneurysm in mice. *J Cell Biochem*. 2019;120(6):10484–10494. doi:10.1002/jcb.28333
43. Zheng C, Niu H, Li M, et al. Cyclic RNA has-circ-000595 regulates apoptosis of aortic smooth muscle cells. *Mol Med Rep*. 2015;12(5):6656–6662. doi:10.3892/mmr.2015.4264
44. Yue J, Zhu T, Yang J, et al. CircCBFB-mediated miR-28-5p facilitates abdominal aortic aneurysm via LYPD3 and GRIA4. *Life Sci*. 2020;253:117533. doi:10.1016/j.lfs.2020.117533
45. Ma M, Wang X, Chen X, et al. MicroRNA-432 targeting *E2F3* and *P55PIK* inhibits myogenesis through PI3K/AKT/mTOR signaling pathway. *RNA Biol*. 2017;14(3):347–360. doi:10.1080/15476286.2017.1279786
46. Zhang J, Li Y, Qi J, et al. Circ-*calm4* serves as an *miR-337-3p* sponge to regulate Myo10 (myosin 10) and promote pulmonary artery smooth muscle proliferation. *Hypertension*. 2020;75(3):668–679. doi:10.1161/HYPERTENSIONAHA.119.13715
47. Gu W, Hong X, Le Bras A, et al. Smooth muscle cells differentiated from mesenchymal stem cells are regulated by microRNAs and suitable for vascular tissue grafts. *J Biol Chem*. 2018;293(21):8089–8102. doi:10.1074/jbc.RA118.001739

Single-cell pseudotime and cell communication analysis of pancreatic cancer

Chengming Ni[1,2,A,D], Xiaohang Wang[3,B], Zhensheng Cai[1,2,B], Yang Chen[1,2,C], Huan Wang[1,2,C], Qianqian Wang[1,2,B,C], Hao Lin[4,B], Yunting Zhou[5,B], Yang Yuan[1,2,B], Bo Sun[6,C], Zilin Sun[1,2,F]

[1] Department of Endocrinology, Zhongda Hospital, Institute of Diabetes, School of Medicine, Southeast University, Nanjing, China
[2] Institute of Diabetes, School of Medicine, Southeast University, Nanjing, China
[3] Institute of Translational Medicine, Jiangsu Key Laboratory of Integrated Traditional Chinese and Western Medicine for Prevention and Treatment of Senile Diseases, Medical College, Yangzhou University, China
[4] Department of Clinical Science and Research, Zhongda Hospital, School of Medicine, Southeast University, Nanjing, China
[5] Department of Endocrinology, Nanjing First Hospital, Nanjing Medical University, China
[6] State Key Laboratory of Bioelectronics, School of Biological Science and Medical Engineering, Southeast University, Nanjing, China

A – research concept and design; B – collection and/or assembly of data; C – data analysis and interpretation; D – writing the article; E – critical revision of the article; F – final approval of the article

Advances in Clinical and Experimental Medicine, ISSN 1899–5276 (print), ISSN 2451–2680 (online) *Adv Clin Exp Med*. 2026;35(2):319–332

Address for correspondence
Zilin Sun
E-mail: sunzilin1963@seu.edu.cn

Funding sources
This research was funded by the National Natural Science Foundation of China (grant No. NSFC-82270848), Southeast University Global Engagement of Excellence Fund and Lvyang Jinfeng Talent Program.

Conflict of interest
None declared

Acknowledgements
We would like to express our sincere gratitude to the staff of the Biobank at Zhongda Hospital, affiliated with Southeast University, for their technical assistance.

Received on November 11, 2024
Reviewed on December 22, 2024
Accepted on March 30, 2025

Published online on February 9, 2026

Cite as
Ni C, Wang X, Cai Z et al. Single-cell pseudotime and cell communication analysis of pancreatic cancer. *Adv Clin Exp Med*. 2026;35(2):319–332. doi:10.17219/acem/203156

DOI
10.17219/acem/203156

Abstract

Background. Pancreatic cancer (PC) is among the most aggressive and lethal malignancies, characterized by development within a complex tumor microenvironment (TME) that includes a desmoplastic stroma composed of extracellular matrix (ECM) and various cellular components.

Objectives. This study aims to elucidate the cellular and molecular mechanisms regulating PC progression through an integrated analysis of single-cell pseudotime trajectories and intercellular communication.

Materials and methods. We constructed pseudotime trajectories using single-cell RNA sequencing (scRNA-seq) data from PC tissues to trace the developmental progression of cancer cells. Transitional cell states and critical genes involved in the shift from early-to-advanced disease stages were identified. Through a comprehensive analysis, we pinpointed key transcription factors and signaling pathways implicated in tumor progression. Expression of stemness-associated genes in pancreatic stellate cells (PSC) was validated using immunofluorescence and transmission electron microscopy (TEM). Additionally, cell–cell communication analysis was performed to examine interactions within the TME, with particular emphasis on ligand–receptor pairings.

Results. Our analysis identified key transcription factors and signaling pathways that drive the cellular transitions associated with cancer progression. The findings revealed extensive intercellular crosstalk between cancer cells, stromal fibroblasts, and diverse immune cell subpopulations. Notably, the study underscored the distinct functional contributions of these cell populations to tumor development, immune evasion and metastatic dissemination.

Conclusions. The study uncovers the complex cellular diversity and intercellular crosstalk in PC, providing novel avenues for therapeutic interventions and early predictive markers in diagnosis. These findings support the potential for more targeted, personalized treatment strategies in combating PC.

Key words: pancreatic cancer, core genes, scRNA-seq, cell communication

Highlights

- Single-cell RNA sequencing (scRNA-seq) exposes fine-scale cellular heterogeneity and lineage routes in pancreatic cancer (PC).
- Pseudotime trajectory analysis spots the genes that drive PC progression from early lesions to invasive disease.
- High-resolution tumor-microenvironment mapping reveals cross-talk among malignant, stromal and immune cells, highlighting druggable signaling hubs.
- Immunofluorescence and TEM confirm stemness markers in pancreatic stellate cells (PSC), validating a stem-like niche within the tumor stroma.
- The resulting single-cell atlas uncovers novel biomarkers and therapeutic targets for earlier diagnosis and precision treatment of PC.

Background

Pancreatic cancer (PC) is associated with one of the highest mortality rates due to its aggressive nature and poor overall prognosis. The 5-year survival rate for patients with PC remains approx. 9%, with minimal improvement over recent decades. This is partly attributed to late detection and a tumor microenvironment (TME) that supports cancer progression and therapy resistance. Understanding the cellular and molecular events associated with the emergence of PC is crucial for developing more effective diagnostic and therapeutic strategies.[1–3]

Emerging technologies, such as Single-cell RNA sequencing (scRNA-seq), have dramatically transformed our ability to uncover the complexity of cancer in detail. Unlike bulk RNA sequencing, which averages gene expression profiles over a large population of cells, scRNA-seq allows for the analysis of gene expression at the individual cell level. This technology has revealed the diversity of cellular composition and states within tumors, highlighting the functional roles that various cell types play throughout cancer progression.[4–7] Clinically, these insights are vital for tailoring personalized treatment approaches and enhancing early detection methods. By understanding the unique cellular interactions and resistance mechanisms in PC, researchers and clinicians can develop targeted therapies that more effectively disrupt tumor growth and dissemination. This could potentially lead to improved survival rates and enhanced quality of life for patients.

This catalog aims to provide a molecular atlas for the cellular heterogeneity and intercellular communication that characterize PC. To achieve this, scRNA-seq approaches were employed to analyze PC tissues at single-cell resolution to define developmental trajectories in this study, enhancing understanding of how various cell populations within the TME interact. By utilizing pseudotime trajectories, the evolution of individual cancer cells from early to late stages of the disease was traced. This method identified key transitional states and the genes driving these transitions, elucidating the hierarchical organization and temporal dynamics of tumor evolution.[8–11] In addition, a cell communication analysis was conducted to examine interactions between cancer cells and stromal and immune cells. Various cell types are known to affect tumor progression and inhibition through immune evasion, metastasis and therapy resistance in the TME. The analysis of ligand–receptor interactions uncovered widespread intercellular crosstalk and emphasized the intricate signaling networks that maintain the TME.[12–15]

To further support our single-cell analysis, we combined immunofluorescence and transmission electron microscopy (TEM) to identify the expression of stemness genes in pancreatic stellate cells (PSC). These methods confirmed and spatially contextualized our findings, highlighting the role of stemness in PC pathogenesis.

These discoveries offer additional therapeutic targets and biomarkers for early detection and treatment. These discoveries emphasize the critical role that single-cell technologies can play in advancing our understanding of cancer biology and driving precision oncology.

Objectives

The study aims to elucidate the cellular and molecular features regulating PC progression through an integrated analysis of single-cell pseudotime and cell communication.

Materials and methods

Patients

The study included PC patients sourced from public databases (such as The Cancer Genome Atlas (TCGA) https://www.cancer.gov/ccg/research/genome-sequencing/tcga, Gene Expression Omnibus (GEO) https://www.ncbi.nlm.nih.gov/geo, GSM8541021, GSM8541020). Inclusion criteria comprised confirmed cases of PC with documented patient characteristics, including age, sex, geographic location, and stage at diagnosis. Exclusion criteria encompassed patients with incomplete clinical or demographic data.[16–18]

Specimen characteristics

Gene expression data from PC patients were collected from the GEO database. Control samples were obtained from the same datasets, consisting of non-cancerous tissue from PC patients. The datasets used were publicly available and underwent quality control in their respective studies. Data storage complied with open-source data-sharing standards.

Gene expression analysis

RNA-seq and microarray data were utilized for expression profiling. Data were processed with normalization techniques to account for batch effects and technical variability. The analysis focused on differentially expressed genes (DEGs) related to PC. All assays were conducted blinded to clinical endpoints, ensuring unbiased interpretation.

Study design

The study was retrospective and utilized data from the GEO database. The analysis concentrated on immune infiltration and intercellular communication in PC. The primary endpoint focused on exploring gene expression differences in the TME using single-cell sequencing data. The secondary endpoint centered on intercellular communication pathways. Variables initially considered included gene expression levels, selected based on their relevance in PC prognosis. A large dataset from the GEO database was used to ensure adequate statistical power.

Statistical analyses

The clustering and annotation process for single-cell data was performed as follows: First, the Seurat package (v. 4.4.0; https://github.com/satijalab/seurat) was used to filter, perform quality control, normalize, reduce dimensionality, and cluster the single-cell data from GSM854102 and GSM8541020. The steps involved are outlined below:

1. Data preprocessing: The CreateSeuratObject function was employed to filter the single-cell sequencing data, retaining genes expressed in at least 3 cells and cells detecting more than 350 genes (parameters set to min.cell = 3 and min.features = 350).

2. Mitochondrial and ribosomal gene scoring: The PercentageFeatureSet function was utilized to calculate the mitochondrial and ribosomal gene scores based on the expression data of mitochondrial and ribosomal genes, respectively. A robust gene expression window was established, excluding cells with fewer than 200 or more than 2,500 unique genes. This approach mitigated the risk of including cell doublets and excluded low-quality cells that could compromise subsequent analyses. Furthermore, mitochondrial gene expression was assessed, and cells with more than 5% mitochondrial transcript expression were systematically removed. This step helped identify and exclude cells potentially undergoing stress or apoptosis, which could distort analytical outcomes. Only cells with mitochondrial and ribosomal gene scores below 20% were retained for analysis.

3. Data normalization and variable gene identification: The SCTransform function was used to normalize the data and identify the top 3,000 highly variable genes (variable.features.n = 3000).

4. Principal component analysis and dimensionality reduction: Principal component analysis (PCA) was performed, and an elbow plot was generated to determine the optimal number of dimensions. Principal components up to the inflection point were selected for further analysis. The first 15 principal components were chosen, and batch effects were removed using the Canonical Correlation Analysis (CCA) method in Seurat. The FindNeighbors and FindClusters functions were then used for unsupervised cluster analysis of the data, following batch removal. The optimal resolution parameter was determined using the "clustree" function to assess cluster stability across different resolutions. In this study, the optimal resolution was set to 0.7, resulting in the identification of 26 clusters. Uniform manifold approximation and projection (UMAP) visualization was employed for cluster representation. Cells were annotated based on reference marker genes provided by CellMarker,[13] and the proportions of annotated cells were computed and visualized using ggplot2.[19–22]

5. Cell communication analysis: To assess cell communication, the interaction between ligands and receptors, along with the activation of specific cell signaling pathways, was analyzed. The CellChat package was used to predict differences in cell communication between groups with high and low Müller ratings. Ligand-receptor pairs were selected for analysis, with a threshold p-value of less than 0.05 considered statistically significant. Only membrane-bound ligand-receptor pairs were analyzed, and the expression of these pairs in different cell types was evaluated.

6. Immunofluorescence: Cells were fixed using either pre-warmed 4% paraformaldehyde (PFA) or cold methanol for 20 min. The PFA-fixed cells were then permeabilized with 0.1% Triton X-100 in phosphate-buffered saline (PBS) for 8 min. A pre-boiled ethylenediaminetetraacetic acid (EDTA) solution (1 mM EDTA) was added to the PFA-fixed cells in a LabTek 8-well chambered coverglass and incubated for 10 min at room temperature. This procedure was repeated 3 times. Following fixation and permeabilization, cells were blocked with 3% bovine serum albumin (BSA) in PBS for 30 min. Primary antibodies were incubated at 4°C overnight, diluted 1:500 in 3% BSA/PBS. After washing, secondary antibodies (also diluted 1:500) were incubated for 1 h at room temperature. Nuclear DNA was stained using DAPI (4′,6-diamidino-2-phenylindole;

1 μg/mL). Samples were then analyzed using an LSM800 GaAsP laser scanning confocal microscope with Zen software (Carl Zeiss AG, Jena, Germany).[23–25]

All statistical analyses were performed using R v. 4.0.3 (R Foundation for Statistical Computing, Vienna, Austria). Differences were considered statistically significant when the p-value was less than 0.05, unless otherwise specified.

Results

Analysis of single-cell RNA sequencing data comparing normal and tumor cells

Figure 1 presents a comprehensive analysis of scRNA-seq data comparing normal and tumor cells. Panels A–D display density plots of various metrics, whereas panels E, F present results from PCA. The density plot illustrates the distribution of total RNA counts per cell for normal (blue) and tumor (red) cells, revealing a broader and higher distribution of RNA counts in tumor cells, indicative of increased transcriptional activity (Fig. 1A). This plot demonstrates the distribution of the number of detected genes per cell, with tumor cells exhibiting a higher number of detected genes, suggesting increased gene expression diversity (Fig. 1B). The density plot depicting mitochondrial gene expression percentage shows a similar distribution for both normal and tumor cells, although tumor cells exhibit a slight shift towards higher mitochondrial gene expression, potentially indicating altered metabolic states (Fig. 1C). The plot representing hemoglobin gene expression percentage shows overlapping distributions for normal and tumor cells, with tumor cells displaying slightly higher hemoglobin gene expression (Fig. 1D). The scree plot illustrates the variance explained by each principal component, with the first few principal components accounting for the majority of variance in the data. Although p-values are provided for each principal component, they indicate statistical significance rather than effect magnitude. The relative importance of principal compotents is better assessed by the proportion of variance they explain, as visualized in the scree plot (Fig. 1E). The scatter

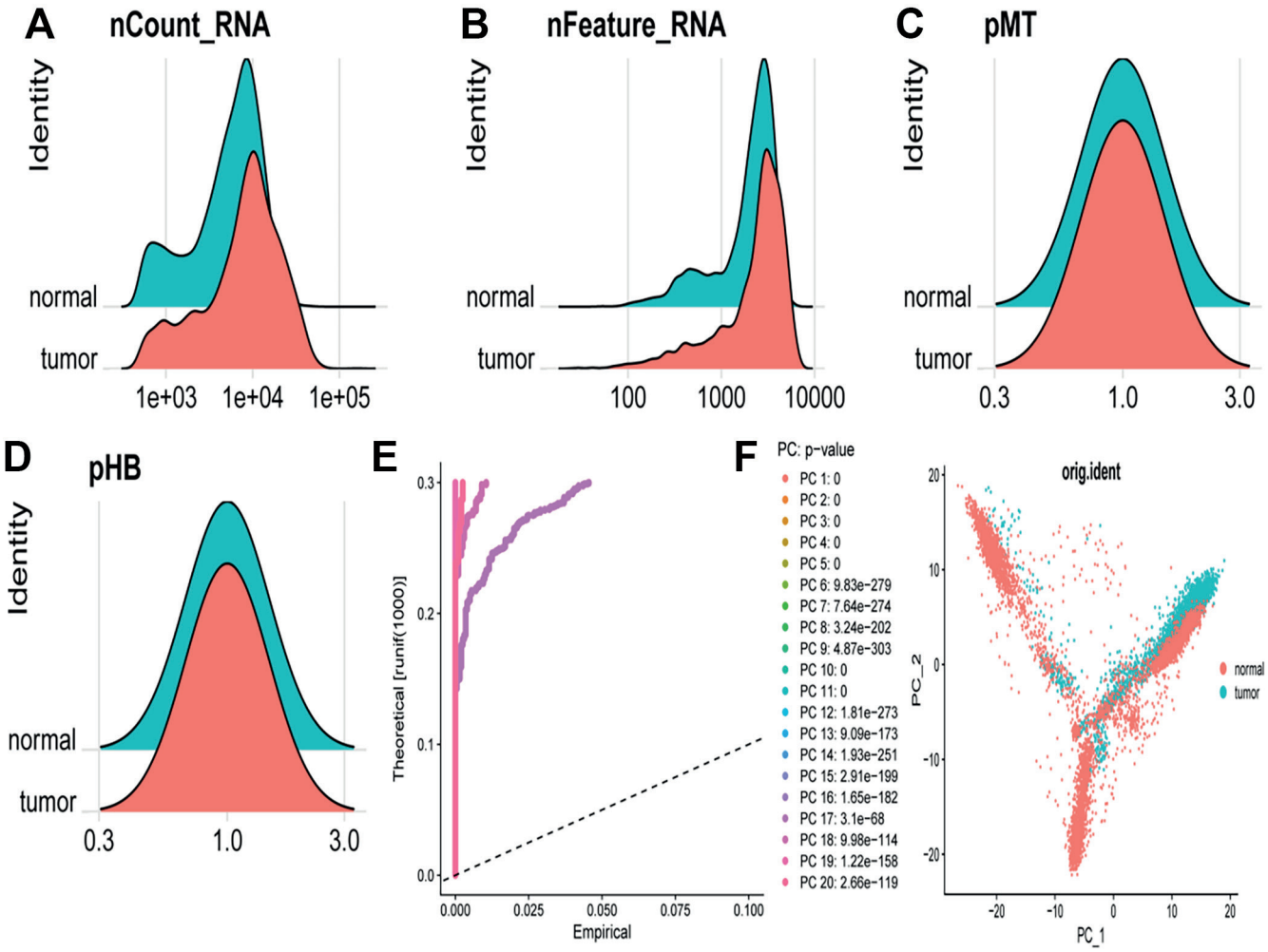

Fig. 1. Analysis of single-cell RNA sequencing (scRNA-seq) data comparing normal and tumor cells. A, B. Tumor cells exhibit higher RNA content and transcriptional diversity compared to normal cells; C. A slight increase in mitochondrial gene expression in tumor cells; D. Marginally higher hemoglobin gene expression in normal cells; E. Significant principal components that capture variance in the data; F. Transcriptional profiles of normal and tumor cells, emphasizing the separation between these 2 groups

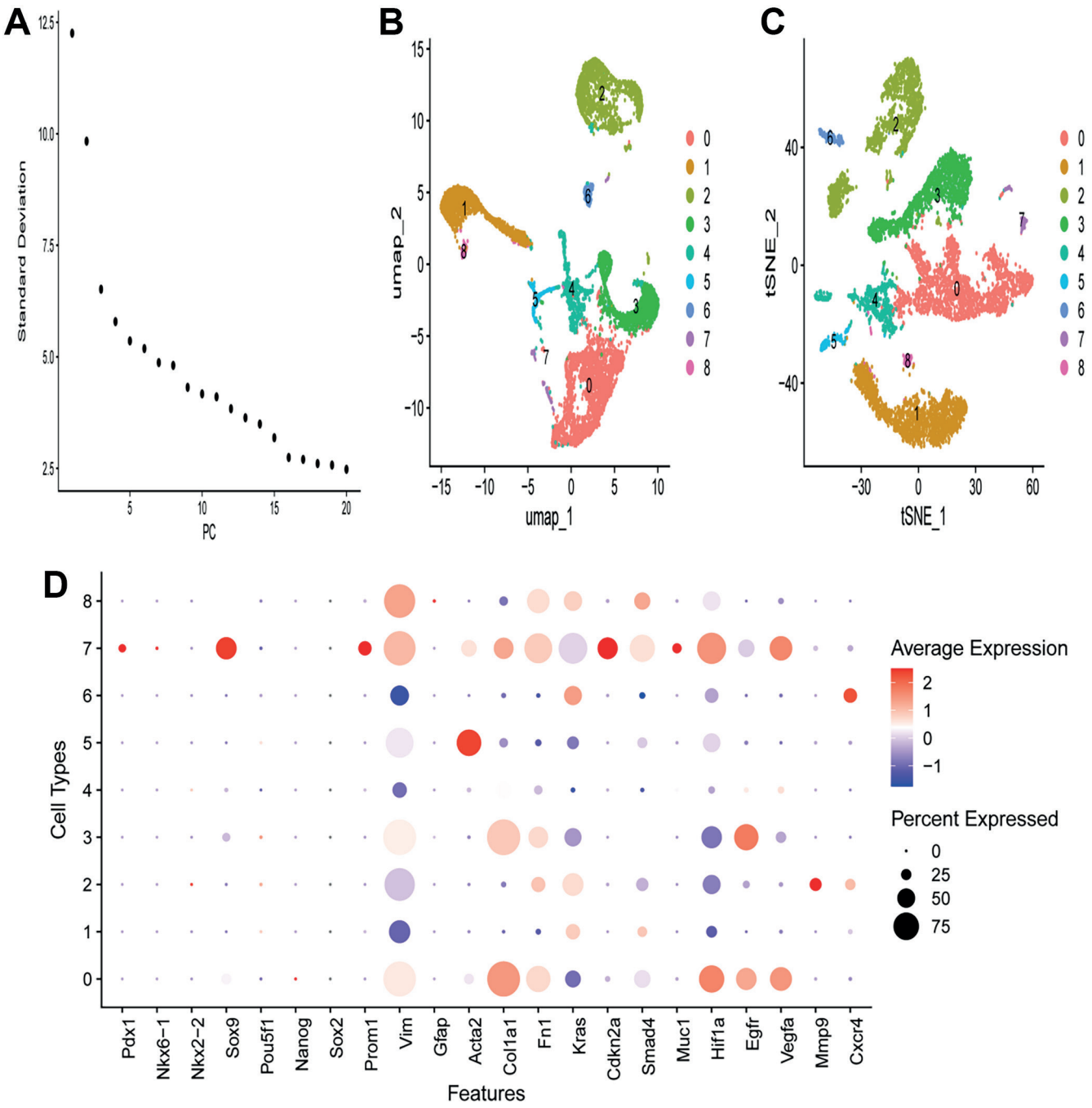

Fig. 2. Principal component analysis and dimensionality reduction techniques. A. The principal component analysis (PCA) scree plot illustrates that the initial principal components account for the majority of the variance in the data, indicating that these components are adequate for subsequent analysis; B. The uniform manifold approximation and projection (UMAP) plot displays a clear separation of cells into varied clusters, revealing the heterogeneity and different cellular states or types within the dataset; C. The t-SNE plot supports the UMAP findings, offering an additional visualization of the cell clusters and their interrelations. The dot plot conveys the expression patterns of key genes across different cell types. Genes such as *Pdgfr*β, *Sox9*, *Nanog*, and *Vim* demonstrate varied expression across the clusters, highlighting their roles in various cellular states or types

plot visualizes the PCA results, with cells plotted according to their scores on the first 2 principal components. Normal (blue) and tumor (red) cells formed distinct clusters, indicating substantial differences in their gene expression profiles. The separation along principal compotent 1 and principal component 2 suggests that these principal components capture the major sources of variation between normal and tumor cells (Fig. 1F).

Principal component analysis and dimensionality reduction techniques

The scree plot (Fig. 2A) illustrates the standard deviation (SD) of the principal components, indicating that the first few principal components capture the most variance. As the number of principal components increases, the SD decreases, suggesting that later principal components

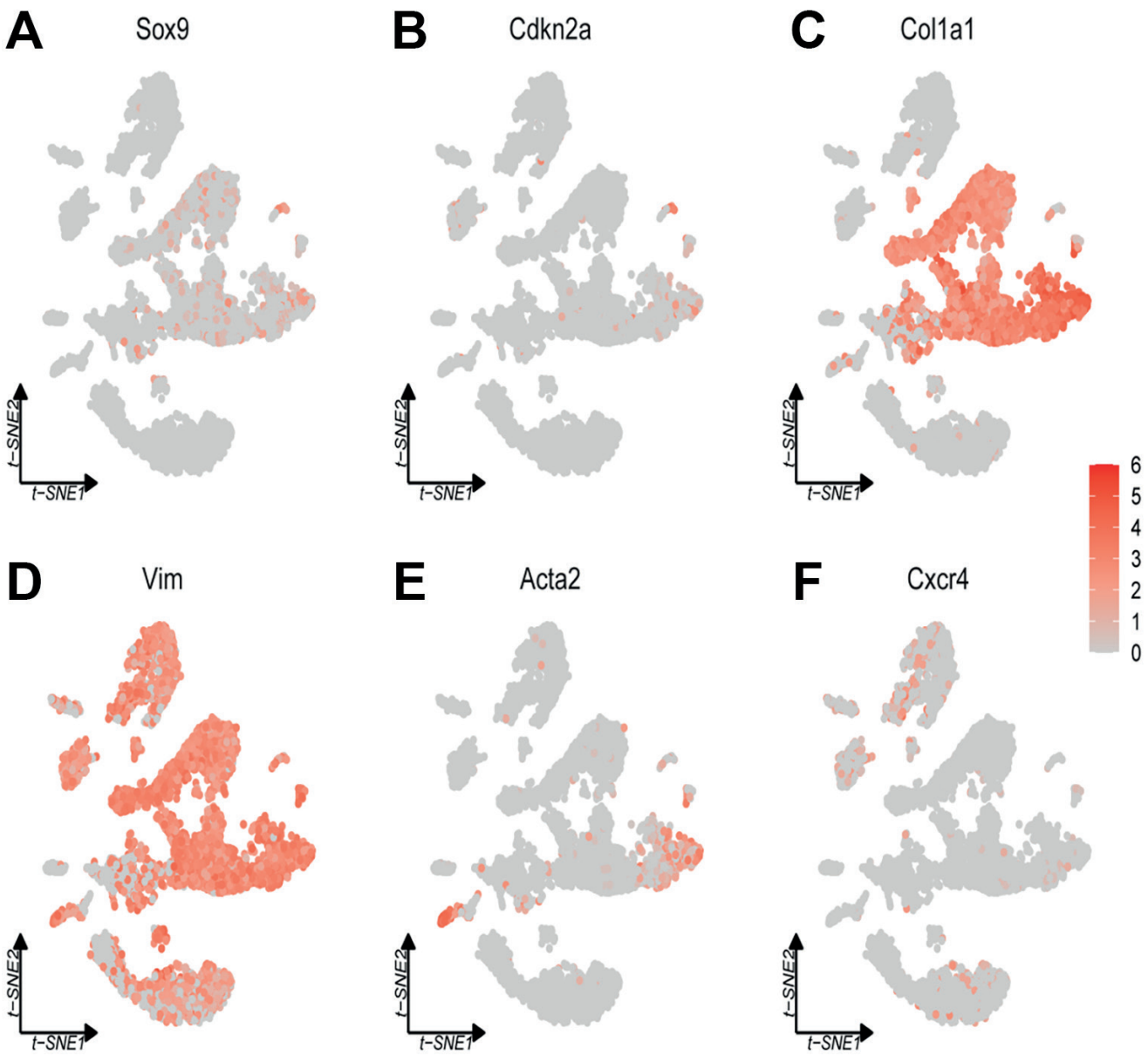

Fig. 3. The expression of specific genes across different cell populations in single-cell RNA sequencing. A. ***Sox9*** reveals distinct clusters of high expression, signifying its role in stem cell maintenance and differentiation; B. ***Cdkn2a*** exhibits scattered high expression, emphasizing its role in cell cycle regulation; C. ***Col1a1*** demonstrates strong expression in specific clusters, highlighting its significance in extracellular matrix formation; D. ***Vim*** is broadly expressed in mesenchymal cells, indicating its role in cellular integrity and motility; E. ***Acta2*** shows high expression in clusters associated with muscle contraction; F. ***Cxcr4*** displays scattered high expression, suggesting its role in cell migration and signaling

contribute less to overall variance (Fig. 2A). The UMAP plot visualizes the scRNA-seq data in a 2-dimensional space, where each dot represents a single cell colored based on assigned clusters (0–8). The distinct clusters indicate different cell populations, with spatial separation suggesting differences in gene expression profiles (Fig. 2B). The t-distributed stochastic neighbor embedding (t-SNE) plot also visualizes the scRNA-seq data in 2 dimensions. Similar to the UMAP plot, cells are colored by clusters (0–8), further confirming the separation of cell populations and highlighting heterogeneity within the dataset (Fig. 2C). The dot plot displays expression levels of selected genes across different cell types, where the size of each dot represents the percentage of cells expressing the gene, and the color indicates the average expression level. Notable observations show that certain genes are highly expressed in specific cell types, as indicated by larger and darker dots (Fig. 2D). For example, Sox2 and Prom1 show high expression in cell type 7, whereas Egfr and Vegfa are broadly expressed across multiple cell types. The differential expression patterns provide insights into the functional roles of these genes in various cell populations.

Figure 3 presents t-SNE plots illustrating the expression of specific genes across various cell populations in a scRNA-seq dataset. The t-SNE plot for *Sox9* gene expression reveals that Sox9 is present in multiple, yet discrete clusters. The staining intensities vary among clusters, with some clusters exhibiting higher levels of *Sox9*

expression (Fig. 3A). The visualization of Cdkn2a expression in the t-SNE plot indicates a more cluster-specific expression pattern, suggesting a cell-type-dependent expression profile. Each major group of genes (*MGA-D*, *MGB-E* and *2GGs*) is ordered by peak expression time within each cluster, with shades of gray representing expression levels. Gene Ontology (GO) term analysis was performed for each functional map, consistently applying a threshold or flag-based criteria at the boundaries of the last exons.

Figure 3C displays the expression of *Col1a1*, which is concentrated in specific regions of the dataset, indicating that *Col1a1* is expressed at lower levels throughout much of the brain, suggesting that *Col1a* promoter-driven Cre recombinase primarily exists in specific cell populations, such as those producing extracellular matrix (ECM; Fig. 3C). The t-SNE plot for *Vim* demonstrates broad expression across various clusters, with several regions exhibiting higher expression levels. The lower cluster is enriched with cell types similar to mesenchymal cells, characterized by the expression of their derived marker, *Vim* (Fig. 3D). The Acta2 expression plot indicates that *Acta2* is concentrated in specific clusters, suggesting predominant expression in certain cell populations, potentially smooth muscle cells or myofibroblasts, due to its role in actin filament formation (Fig. 3E). The expression of *Cxcr4* is depicted in the t-SNE plot, showing scattered and relatively low expression across the clusters, indicating that this gene is expressed at lower levels or in fewer cell populations compared to the other genes illustrated (Fig. 3F).

The proportions of different cell types in each group

The t-SNE plot (Fig. 4) visualizes the distribution of normal cells within a 2-dimensional space, with each dot representing a single cell. The clustering pattern illustrates the presence of distinct cell populations within the normal tissue, with spatial separation suggesting heterogeneity among normal cells (Fig. 4A). Another t-SNE plot displays the distribution of tumor cells, where each dot again represents a single cell. The clustering pattern indicates the presence of various cell populations within the tumor tissue. In comparison to normal cells, tumor cells appear more densely packed and less dispersed, indicating alterations in cellular composition and gene expression profiles (Fig. 4B). A bar plot compares the proportions of different cell types across the total, normal, and tumor groups. The cell types are color-coded as follows: activated stellate cells (orange), cancer-associated fibroblasts (CAF) (green), embryonic stem cell-like cells (cyan), endothelial cells (blue), immune cells (purple), other mesenchymal cells (brown), PC cells (dark pink), pancreatic progenitor cells (light blue), and PSC (pink). In the normal group, PSC and other cell types are well-represented. Conversely, in the tumor group, PC cells dominate, accompanied by a noticeable increase in CAF and a decrease in other cell types such as PSC.

Using pseudotime trajectories to explore cellular differentiation and transitions

Figure 5 presents visualizations of cell type distributions along pseudotime and comparisons between normal and tumor cells. This plot displays the pseudotime trajectory of cells, color-coded by cell types. The trajectory is represented in a 2-dimensional space, with components 1 and 2 indicating the PC. The cell types are color-coded: activated stellate cells (orange), CAF (green), embryonic stem cell-like cells (cyan), endothelial cells (blue), immune cells (purple), other mesenchymal cells (brown), PC cells (dark pink), pancreatic progenitor cells (light blue), and PSC (pink). The trajectory suggests a progression from one cell type to another, implying a potential differentiation pathway or cellular transition process (Fig. 5A).

A subsequent plot shows the same pseudotime trajectory as in panel A, with cells colored according to their pseudotime values, ranging from 0 to 50 (light to dark blue). Key transition points (1, 2 and 3) are marked along the trajectory, indicating significant stages in the progression of cellular states (Fig. 5B). Additional plots compare the pseudotime trajectories of normal and tumor cells, with cells colored by their respective types. The left plot illustrates the trajectory for normal cells, whereas the right plot depicts the trajectory for tumor cells. Observed differences in the trajectories suggest varying differentiation pathways or cellular transitions between normal and tumor cells. Notably, tumor cells exhibit a more pronounced clustering of PC cells and CAF (Fig. 5C). This combined plot presents pseudotime trajectories for both normal and tumor cells in a single view, with cells colored by their types. The trajectories are aligned to emphasize the differences and similarities in the progression of cell states between normal and tumor conditions. The transitions and clustering patterns provide insights into how cellular states evolve differently within the TME compared to normal tissue (Fig. 5D).

Using pseudotime analysis to understand the progression and differentiation of various cell types

The UMAP plot (Fig. 6A) illustrates the distribution of cells in 2-dimensional space, color-coded by cell type. The pseudotime trajectory is overlaid, demonstrating the progression of cells through various states. The cell types are color-coded as follows: activated stellate cells (orange), CAF (green), embryonic stem cell-like cells (cyan), endothelial cells (blue), immune cells (purple), other mesenchymal cells (brown), PC cells (dark pink), pancreatic progenitor cells (light blue), and PSC (pink). The trajectory lines connect different clusters, suggesting pathways of cellular differentiation or transition. This plot also depicts the density of various cell types along the pseudotime axis, with each cell type represented by a different color,

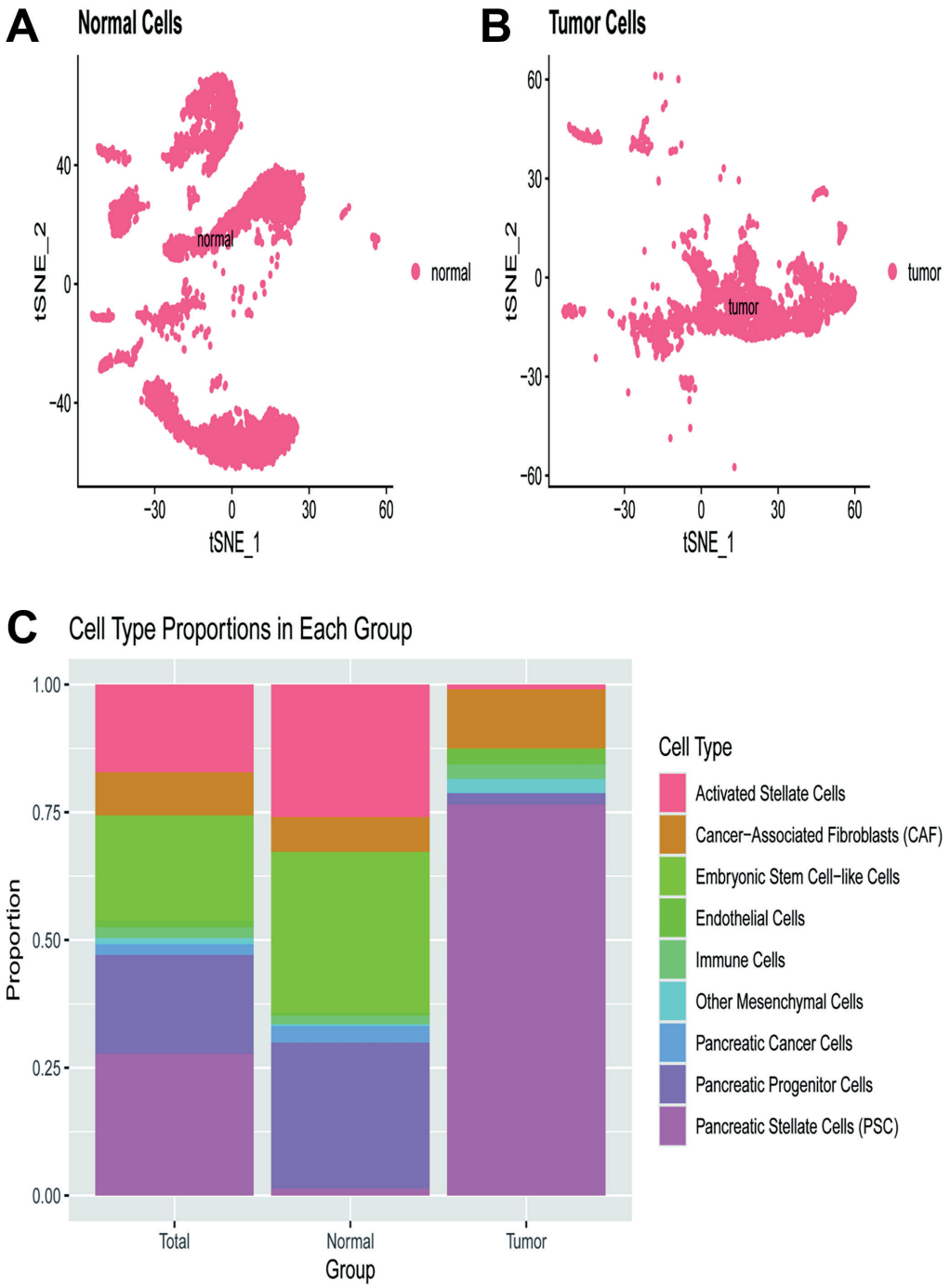

Fig. 4. The proportions of different cell types in each group. A. The t-distributed stochastic neighbor embedding (t-SNE) plot of normal cells reveals distinct clusters, indicating the presence of various subpopulations within the normal cell population; B. The t-SNE plot of tumor cells also shows distinct clusters, albeit with different patterns compared to normal cells. This suggests significant transcriptional heterogeneity within the tumor cell population, reflecting the complexity of tumor biology; C. The bar plot of cell type proportions reveals differences in the composition of cell types among the total, normal and tumor groups

consistent with those in Fig. 6A. The density peaks indicate where specific cell types are most prevalent along the pseudotime trajectory. For instance, PC cells (dark pink) and cancer-associated fibroblasts (CAFs; green) exhibit distinct expression peaks, suggesting critical transition points in their progression. These plots illustrate the expression levels of 4 genes (*Lypla1*, *Mrpl15*, *Sox17*, and *Tcea1*) over pseudotime, with each dot representing a single cell colored by its state (1–7) (Fig. 6B). The black line represents the smoothed trend of gene expression over pseudotime. Key observations include: *Lypla1* shows high expression early in pseudotime, decreasing as pseudotime progresses; *Mrpl15* exhibits peak expression around the midpoint of the pseudotime trajectory; *Sox17* displays a distinct peak in expression later in pseudotime, indicating its role in a specific state; *Tcea1* has high expression early in pseudotime, followed by a gradual decrease (Fig. 6C).

UMAP plots illustrating the expression of specific genes across different cell populations in a single-cell RNA sequencing dataset

As shown in Fig. 7, each UMAP plot demonstrates the distribution of cells in 2-dimensional space, with gene expression levels indicated by color intensity. The color gradient

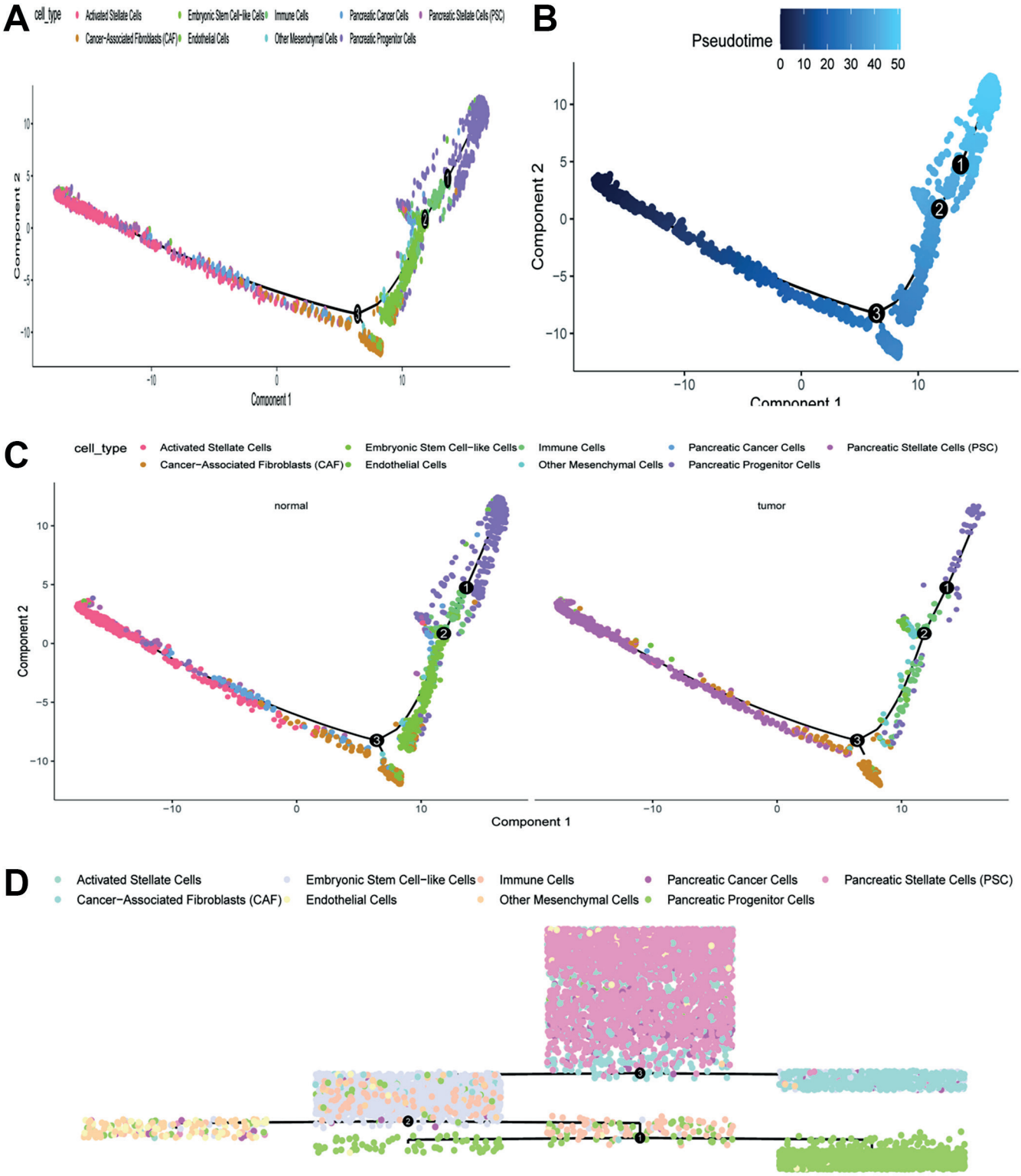

Fig. 5. Pseudotime trajectories used to explore cellular differentiation and transitions. A. The trajectory plot illustrates the differentiation path of cells, with distinct clusters representing different cell types; B. The pseudotime plot highlights the temporal progression of cells along the differentiation path, with key transition points marked; C. The separate trajectory plots for normal and tumor cells reveal differences in their differentiation paths, reflecting the altered progression in tumor cells; D. The linear trajectory plot simplifies the visualization of the differentiation process, showing the sequential progression of cells along the trajectory

ranges from purple (low expression) to green (high expression), representing the percentage of maximum expression for each gene. Areas of high expression (green) exhibit a punctate pattern, implying roles in specific cell types. *Col3a1* (collagen type III alpha 1 chain) shows expression in the same clusters as its paralog in certain regions (75), indicating an association with the ECM and connective tissue. Decorin (Dcn) exhibits scattered expression across

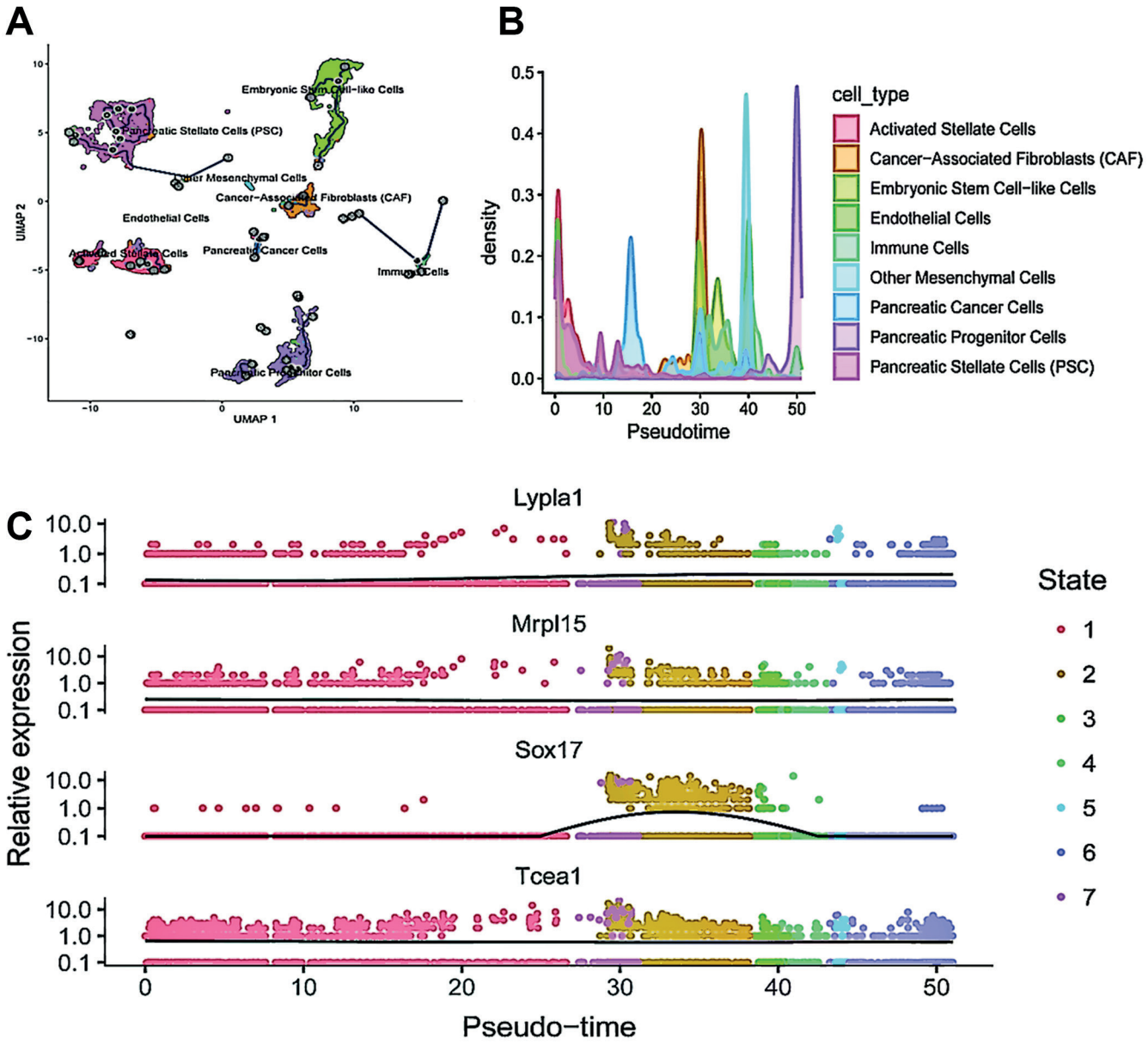

Fig. 6. Pseudotime analysis used to understand the progression and differentiation of various cell types. A. The uniform manifold approximation and projection (UMAP) plot with trajectory inference displays the differentiation path of cells, with distinct clusters representing different cell types. The trajectory line indicates the progression and transitions between these cell types; B. The density plot reveals the distribution of cell types along pseudotime, highlighting key transition points where certain cell types are more prevalent; C. The gene expression trends over pseudotime illustrate how selected genes are regulated during the differentiation process. Each gene exhibits unique expression patterns, reflecting their specific roles at different stages of cell differentiation

multiple clusters, with some regions showing higher levels, highlighting its role in collagen fibrillogenesis and ECM organization. Serping1 (decreased expression in cluster L10 but similar levels to P7) displays a highly restricted expression pattern, with high fractional spike-ins limiting its detection. *Csf1r* (colony stimulating factor 1 receptor) is expressed in existing clusters, indicating its association with specific cell types likely associated with macrophage differentiation and function. *C1qc* (complement C1q C chain) is uniquely expressed, with clear enrichment in clusters associated with immune response and the complement system.

Surface markers of PSC and its differentiation characteristics

Figure 8 presents a comprehensive list of marker expression in PSC and their differentiation capacity. The top immunofluorescence images depict specific markers indicating co-expression in PSC (Vimentin and GFAP), corresponding to embryonic stem cell markers (*Oct4*, *Nanog* and *CD133*) and pancreatic progenitor cell markers (*Ngn3* and *Sox9*) (Fig. 8). The extent to which PSC differentiate into osteogenic, adipogenic, hepatic, and chondrogenic lineages is illustrated through phase-contrast microscopy

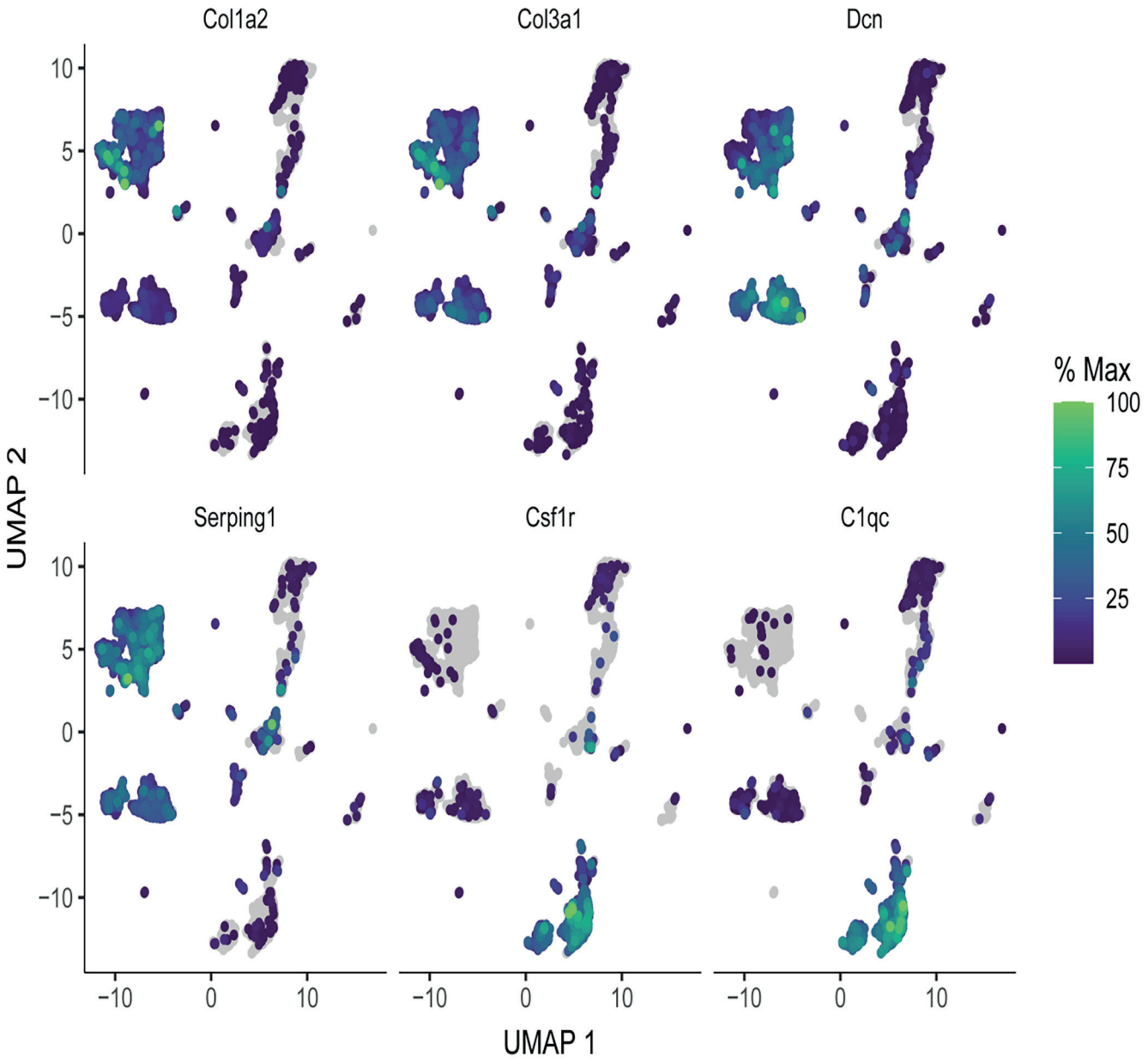

Fig. 7. The uniform manifold approximation and projection (UMAP) plots illustrating the expression of specific genes across different cell populations in a scRNA-seq dataset. The UMAP plots provide a comprehensive visualization of the expression patterns of key genes across various cell populations in the scRNA-seq dataset. Each gene exhibits a unique distribution, reflecting its specific roles and functions within the tissue

images, which show the morphological changes associated with each differentiated state (Fig. 8). Collectively, these analyses provide valuable insights into the cellular heterogeneity within PSC and their differentiation potential.

Discussion

Pancreatic cancer is among the most lethal forms of cancer, characterized by a dismal prognosis and aggressive behavior. Despite some advancements in medical research, the 5-year relative survival rate for individuals diagnosed with PC remains only 7%.[26–28]

The scRNA-seq of pancreatic ductal adenocarcinomas was conducted to provide an extensive analysis of cellular heterogeneity and intercellular communications within the TME. The application of scRNA-seq is rapidly yielding unprecedented insights into cellular dynamics, revealing potential advancements and druggable targets in PC. The construction of pseudotime trajectories has been essential for tracing the developmental pathways of individual cancer cells, identifying critical intermediate states and key regulatory genes that drive these transitions. This has provided a profound understanding of the temporal dynamics of tumor evolution – an essential concept for comprehending the progression of PC from early stages to advanced malignancy. Immunofluorescence studies

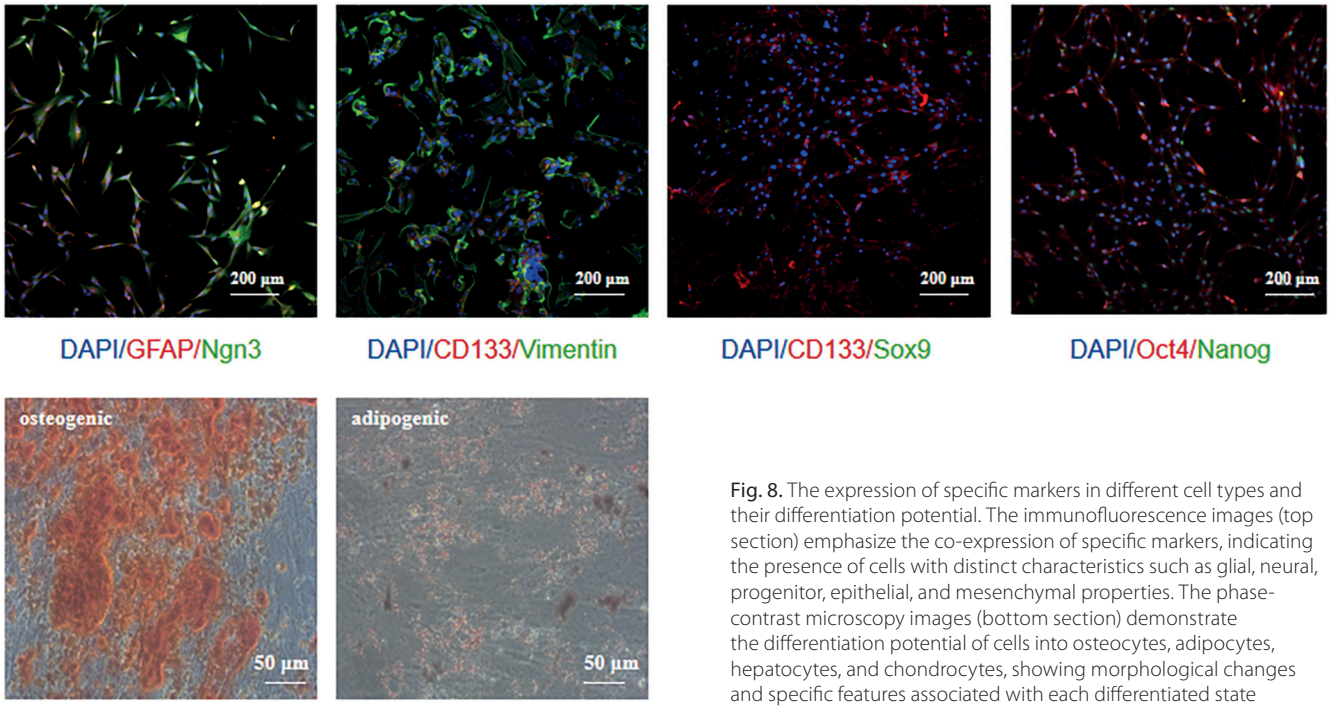

Fig. 8. The expression of specific markers in different cell types and their differentiation potential. The immunofluorescence images (top section) emphasize the co-expression of specific markers, indicating the presence of cells with distinct characteristics such as glial, neural, progenitor, epithelial, and mesenchymal properties. The phase-contrast microscopy images (bottom section) demonstrate the differentiation potential of cells into osteocytes, adipocytes, hepatocytes, and chondrocytes, showing morphological changes and specific features associated with each differentiated state

corroborate the spatial context of scRNA-seq data, particularly regarding the examination of stemness genes. The co-expression of vimentin and GFAP, markers characteristic of PSC, with embryonic stem cell markers (*Oct4*, *Nanog* and *CD133*) and pancreatic progenitor markers (*Ngn3* and *Sox9*), suggests an unrecognized pluripotent potential in these cells. These findings highlight the role of stemness in tumor activity, with implications for various aspects such as cancer recurrence and therapeutic resistance. Pseudotime analysis is pivotal in scRNA-seq studies, as it illuminates the developmental trajectories of cancer cells, identifies key intermediate states, and reveals essential genes that govern these transitions. This analytical framework provides unprecedented insights into the temporal dynamics of tumor evolution, which is crucial for understanding the progression of PC from early disease to advanced malignant states. The selection of parameter settings is critical for validating the results of pseudotime analysis. Several factors must be considered, including biological variability, technical biases and inter-sample variability. For example, methods based on PCA, such as scran and Seurat, perform competitively with default parameters, whereas more sophisticated models like ZinbWave, DCA, and scVI demonstrate enhanced performance with parameter optimization. This indicates that parameter adjustment is a crucial step in optimizing results for various analytical approaches.

CellChat offers ligand-receptor databases for humans and mice, containing extensive validated molecular interaction data essential for understanding and predicting intercellular communication. By comparing ligand and receptor expression across different cell populations or conditions, key molecules related to specific biological processes can be identified. This differential analysis may reveal changes in cell states and variations in intercellular communication.

Our investigation of cell communication has elucidated complex interactions among cancer cells, the stromal compartment, and immune cells within the TME. The findings have illuminated the roles of various cell populations that contribute to tumorigenesis, immune suppression and metastasis by identifying significant signaling crosstalk through ligand-receptor interactions. Understanding the functions of these diverse cell types is critical for developing targeted therapies that address the complexities of the TME. By dissecting cellular heterogeneity, researchers can pinpoint specific cellular interactions and pathways that drive cancer progression, leading to more effective and personalized treatment strategies. Although mutations in genes such as *KRAS*, *TP53* and *SMAD4* are prevalent in PC, the specific mutation patterns and their interactions can differ significantly from those in other cancers.

The identification of critical transcription factors and signaling pathways controlling cellular transitions offers potential therapeutic targets. Furthermore, our research has identified disease markers that may facilitate early detection of PC, thereby significantly enhancing patient survival. The findings highlight the efficacy of single-cell technologies in elucidating cancer characteristics and their contribution to precision oncology. These technologies provide a more detailed understanding of the TME, which is essential for personalized treatment approaches.

The integration of these findings into clinical practice will rely on validation in larger cohorts and through clinical trials. A prerequisite for employing this concept,

even in its preliminary form, will likely require defining specific genes or pathways modified by these critical drivers (and perhaps several additional alterations) so that targeted agents can be developed. The identification of biomarkers and therapeutic targets has the potential to enable precision diagnostics, prognostics and treatment strategies that could significantly improve patient care. Ultimately, such advances may contribute to increased survival rates and enhanced quality of life for individuals affected by PC.

Limitations

Despite the intriguing results of the study, several limitations exist. Single-cell transcriptome analyses yield highly detailed data but may not capture the dynamic and time-resolved nature of cellular interactions within the TME. Although we identified individual cells as representing fresh and aged states, more dynamic studies must incorporate longitudinal sample collections to map transitions between cellular states.

Conclusions

This study contributes to the growing body of knowledge on PC and demonstrates the potential of single-cell technologies in elucidating, with remarkable clarity, the features that underlie its biology. Immunofluorescence data confirmed the stem-like properties of PSC, revealing their pluripotent potential in tumor dynamics. Analyzing key cellular transitions and intercellular communication provides a foundation for developing innovative therapeutic strategies and underscores the need for further studies to translate these insights into clinically relevant outcomes.. Continued research is essential to validate findings related to personalized treatment and prognostic biomarkers, with the goal of advancing clinical applications and improving patient selection, particularly in the effective management of cancer. This ongoing research is essential for transforming scientific discoveries into effective clinical solutions.

Data Availability Statement

The datasets supporting the findings of this study are openly available in Figshare at https://figshare.com/s/d51989569cd0bf8a0fce.

Consent for publication

Not applicable.

Use of AI and AI-assisted technologies

Not applicable.

ORCID iDs

Chengming Ni https://orcid.org/0009-0006-7277-2108
Xiaohang Wang https://orcid.org/0000-0003-2111-9601
Zhensheng Cai https://orcid.org/0000-0003-2964-0565
Yang Chen https://orcid.org/0009-0000-5258-6662
Huan Wang https://orcid.org/0009-0009-7343-0478
Qianqian Wang https://orcid.org/0009-0001-9098-1062
Hao Lin https://orcid.org/0000-0001-7981-7707
Yunting Zhou https://orcid.org/0000-0002-1385-3841
Yang Yuan https://orcid.org/0000-0003-2873-1262
Bo Sun https://orcid.org/0009-0001-5483-0910
Zilin Sun https://orcid.org/0000-0001-7936-0196

References

1. Jiang J, Krishna SG. Early detection of concomitant pancreatic cancer during intraductal papillary mucinous neoplasms surveillance. *Gland Surg*. 2024;13(9):1659–1661. doi:10.21037/gs-24-158
2. Kinoshita S, Terai T, Nagai M, et al. Clinical significance and therapeutic implication of CD200 in pancreatic cancer. *Pancreatology*. 2024;24(8):1280–1287. doi:10.1016/j.pan.2024.10.007
3. Li R, Liu R, Xu Y, et al. Suppressing pancreatic cancer survival and immune escape via nanoparticle-modulated STING/STAT3 axis regulation. *Bioconjugate Chem*. 2024;35(11):1815–1822. doi:10.1021/acs.bioconjchem.4c00379
4. Ding S, Yi X, Gao J, et al. Prognostic risk model of LIHC T-cells based on scRNA-seq and RNA-seq and the regulation of the tumor immune microenvironment. *Discov Oncol*. 2024;15(1):540. doi:10.1007/s12672-024-01424-z
5. Lou Z, Wei X, Hu Y, Hu S, Wu Y, Tian Z. Clustering scRNA-seq data with the cross-view collaborative information fusion strategy. *Brief Bioinform*. 2024;25(6):bbae511. doi:10.1093/bib/bbae511
6. Tang M, Xiong L, Cai J, et al. Comprehensive analysis of scRNA-Seq and bulk RNA-Seq reveals transcriptional signatures of macrophages in intrahepatic cholestasis of pregnancy. *J Inflamm Res*. 2024;17:6863–6874. doi:10.2147/JIR.S471374
7. Wang H, Torous W, Gong B, Purdom E. Visualizing scRNA-Seq data at population scale with GloScope. *Genome Biol*. 2024;25(1):259. doi:10.1186/s13059-024-03398-1
8. Cao L, Zhang S, Yao D, et al. Comparative analyses of the prognosis, tumor immune microenvironment, and drug treatment response between left-sided and right-sided colon cancer by integrating scRNA-seq and bulk RNA-seq data. *Aging*. 2023;15(14):7098–7123. doi:10.18632/aging.204894
9. Guo G, Zhou Z, Chen S, et al. Characterization of the prognosis and tumor microenvironment of cellular senescence-related genes through scRNA-seq and bulk RNA-seq analysisin GC. *Recent Pat Anticancer Drug Discov*. 2024;19(4):530–542. doi:10.2174/0115748928255417230924191157
10. Lin Z, Li X, Shi H, et al. Decoding the tumor microenvironment and molecular mechanism: Unraveling cervical cancer subpopulations and prognostic signatures through scRNA-Seq and bulk RNA-seq analyses. *Front Immunol*. 2024;15:1351287. doi:10.3389/fimmu.2024.1351287
11. Zhong J, Sun Y, Wu S, et al. The impact of the Hedgehog signal pathway on the tumor immune microenvironment of gastric adenocarcinoma by integrated analysis of scRNA-seq and RNA-seq datasets. *Funct Integr Genomics*. 2023;23(3):258. doi:10.1007/s10142-023-01187-w
12. Jiang X, Chen N, Wei Q, et al. Single-cell RNA sequencing and cell–cell communication analysis reveal tumor microenvironment associated with chemotherapy responsiveness in ovarian cancer. *Clin Transl Oncol*. 2024;27(3):1000–1012. doi:10.1007/s12094-024-03655-6
13. Lyu N, Wu J, Dai Y, et al. Identification of feature genes and molecular mechanisms involved in cell communication in uveal melanoma through analysis of single-cell sequencing data. *Oncol Lett*. 2024;28(5):503. doi:10.3892/ol.2024.14636
14. Xie S, Xu J, Chen L, Qi Y, Yang H, Tan B. Single-cell transcriptomic analysis revealed the cell population changes and cell–cell communication in the liver of a carnivorous fish in response to high-carbohydrate diet. *J Nutr*. 2024;154(8):2381–2395. doi:10.1016/j.tjnut.2024.06.016

15. Zhao Z, Wu Y, Geng X, Yuan C, Yang G. Single-cell analysis reveals histone deacetylation factor guide intercellular communication of tumor microenvironment that contribute to colorectal cancer progression and immunotherapy [published online as ahead of print on April 18, 2024]. *Biochem Genet*. 2024. doi:10.1007/s10528-024-10730-8
16. Shen C, Geng R, Zhu S, et al. Characterization of tumor suppressors and oncogenes evaluated from TCGA cancers. *Am J Clin Exp Immunol*. 2024;13(4):187–194. doi:10.62347/XMZW6604
17. Cheng X, Lin J, Wang B, Huang S, Liu M, Yang J. Clinical characteristics and influencing factors of anti-PD-1/PD-L1-related severe cardiac adverse event: Based on FAERS and TCGA databases. *Sci Rep*. 2024;14(1):22199. doi:10.1038/s41598-024-72864-4
18. Lin B, Wang K, Yuan Y, et al. A novel approach to the analysis of overall survival (OS) as response with progression-free interval (PFI) as condition based on the RNA-seq expression data in The Cancer Genome Atlas (TCGA). *BMC Bioinformatics*. 2024;25(1):300. doi:10.1186/s12859-024-05897-1
19. Ding Q, Yang W, Xue G, et al. Dimension reduction, cell clustering, and cell–cell communication inference for single-cell transcriptomics with DcjComm. *Genome Biol*. 2024;25(1):241. doi:10.1186/s13059-024-03385-6
20. Pagnotta SM. Unsupervised single-cell clustering with asymmetric within-sample transformation and per-cluster supervised features selection. *Methods Mol Biol*. 2024;2812:155–168. doi:10.1007/978-1-0716-3886-6_8
21. Sun Y, Kong L, Huang J, et al. A comprehensive survey of dimensionality reduction and clustering methods for single-cell and spatial transcriptomics data. *Brief Funct Genomics*. 2024;23(6):733–744. doi:10.1093/bfgp/elae023
22. Yao Z, Li B, Lu Y, Yau ST. Single-cell analysis via manifold fitting: A framework for RNA clustering and beyond. *Proc Natl Acad Sci U S A*. 2024;121(37):e2400002121. doi:10.1073/pnas.2400002121
23. Hsieh Y, Chen S. Visualization and analysis of neuromuscular junctions using immunofluorescence. *Bio Protoc*. 2024;14(1354):e5076. doi:10.21769/BioProtoc.5076
24. Lin CCJ, Jaafar N, Tanzi RE. Protocol to characterize mouse dural mast cells by flow cytometry and immunofluorescence. *STAR Protoc*. 2024;5(4):103364. doi:10.1016/j.xpro.2024.103364
25. Wang Y, Bai W, Wang X. Progress on three-dimensional visualizing skin architecture with multiple immunofluorescence staining and tissue-clearing approaches [published online as ahead of print on September 16, 2024]. *Histol Histopathol*. 2024. doi:10.14670/HH-18-815
26. Wang Q, Wang J, Xu K, Luo Z. Targeting the CSF1/CSF1R signaling pathway: An innovative strategy for ultrasound combined with macrophage exhaustion in pancreatic cancer therapy. *Front Immunol*. 2024;15:1481247. doi:10.3389/fimmu.2024.1481247
27. Yang DH, Park SH, Yoon S. Differential diagnosis of pancreatic cancer and its mimicking lesions. *J Korean Soc Radiol*. 2024;85(5):902. doi:10.3348/jksr.2023.0100
28. Yee KX, Lee YC, Nguyen HD, et al. Uncovering the role of *FXYD3* as a potential oncogene and early biomarker in pancreatic cancer. *Am J Cancer Res*. 2024;14(9):4353–4366. doi:10.62347/LUDE7524

Enhancing professional outcome in nursing and midwifery: A systematic review of competency-based education's impact on performance, self-confidence and anxiety reduction

Gaxue Jiang[1,A–F], Liqiong Hou[2,A–C,E,F]

[1] Department of Cardiology, The First Hospital of Lanzhou University, China
[2] Department of Rheumatology and Immunology, The First Hospital of Lanzhou University, China

A – research concept and design; B – collection and/or assembly of data; C – data analysis and interpretation;
D – writing the article; E – critical revision of the article; F – final approval of the article

Advances in Clinical and Experimental Medicine, ISSN 1899–5276 (print), ISSN 2451–2680 (online) *Adv Clin Exp Med*. 2026;35(2):333–342

Address for correspondence
Liqiong Hou
E-mail: chuandahouliqiong@163.com

Funding sources
None declared

Conflict of interest
None declared

Received on August 6, 2024
Reviewed on February 3, 2025
Accepted on February 18, 2025

Published online on February 9, 2026

Abstract

Clinical skills refresher courses focusing on competence are essential for enhancing the clinical performance of healthcare providers. These courses play a pivotal role in nursing and midwifery education, offering students initial exposure to clinical environments and preparing them for subsequent internships. This systematic review aimed to assess the effectiveness of clinical skills refresher courses on clinical performance, particularly focusing on competency-based supplementary clinical skills courses.

A comprehensive literature search was conducted across articles published in the last 15 years, utilizing PubMed, Embase, Cochrane Library, Web of Science, and Cumulative Index of Nursing and Allied Health Literature (CINAHL) databases with specific keywords. This extensive search yielded 1,751 records, of which 13 were selected based on strict inclusion and exclusion criteria. Of these, 5 studies examined the effect of competency-based education (CBE) on the quality of clinical skills, 5 studies assessed clinical skills in detail, and 3 studies discussed other variables related to nursing skills, such as anxiety. The results indicate that CBE significantly enhances clinical skills and self-efficacy among nursing students, addressing gaps in practical training and psychological readiness for clinical internships.

This review recommends the implementation of well-organized competency-based training courses in nursing and midwifery education. By bridging the gap between theoretical knowledge and practical experience, this approach equips nurses and midwives to effectively address contemporary healthcare challenges, ultimately improving patient outcomes, enhancing professional confidence and ensuring adherence to healthcare standards.

Key words: nurses, midwives, clinical skills, competency-based education, refresher course

Cite as
Jiang G, Hou L. Enhancing professional outcome in nursing and midwifery: A systematic review of competence-based education's impact on performance, self-confidence, and anxiety reduction. *Adv Clin Exp Med*. 2026;35(2):333–342. doi:10.17219/acem/202001

DOI
10.17219/acem/202001

Highlights

- Clinical skill refresher courses effectively enhance clinical performance, alleviate anxiety and prepare nurses and midwives for their ongoing professional performance.
- Competency-based education (CBE), focusing on short-term supplementary courses, emphasizes flexibility, personalized learning and individualized innovation, and aligns with professional demands.
- The integration of theoretical knowledge and practical skills through competency-based training courses can enhance healthcare outcomes and prepare nursing and midwife students for real-world challenges.
- Simulating training courses in a competency-based way for nurses and midwives is crucial for mastery of clinical skills, high-quality performance and confidence in healthcare demands.
- Students who receive CBE show higher motivation and performance in theoretical and practical courses than those who receive traditional education.

Introduction

Learning is the fundamental foundation of human progress in today's world. Literacy improves people's attitudes and performance, and it is further enhanced through new, practical methods in learning curriculum design. The curriculum is a cornerstone of educational sciences, and its pivotal role in educational practices cannot be overlooked.[1] Improving the quality of education by aligning educational goals with performance and activities is essential for developing educational programs that meet societal health needs. To address these demands, both the theoretical and practical components of an effective educational system must be continuously updated.[2–4]

The "Clinical Skills" foundational course is designed to introduce nursing and midwifery students to real-world clinical experiences. It is essential to assess both existing practices and ideal benchmarks across theoretical, practical and clinical aspects of education within this course. This serves as students' initial exposure to the clinical environment, helping to prepare them for future internships.[5,6] Alternatively, nursing students receive clinical skills training in the nursing school's clinical laboratory during their 1st semester. Following this, they participate in a range of supervised exercises in hospitals and other clinical settings. In preparation for their final year, students engage in a 2-semester internship, in addition to part-time, unsupervised classes. The goal of this internship program is to help students transition from an academic setting to a clinical setting.[7]

Unfortunately, some students do not fully experience all the necessary clinical nursing abilities, and some may gradually deviate from standard practice procedures due to inadequacies and issues inherent in various clinical environments.[8] Accordingly, improper learning in clinical courses was identified by Aein et al. as a major issue in clinical nursing education programs.[9] Numerous studies from Iran, China, Australia, and the UK have demonstrated that nursing students lack psychological readiness for clinical internships. Senior nursing students and recently graduated nurses are acutely aware of their clinical incapacity, which causes them to feel anxious and lack confidence. A student's last year of study may be less educationally beneficial if they join an internship program with such uncertainty and worry.[10–12]

To ensure a seamless transition into professional practice, final-year nursing students should enhance their clinical skills by participating in competency-based supplementary training courses. In other words, the final year serves as a preparatory phase that helps nursing students solidify their clinical abilities while cultivating favorable work attitudes and professional traits. To support final-year clinical students, several educational approaches and initiatives have been proposed in the form of competency-based supplementary courses. These instructional strategies positively impact students' approaches and clinical abilities by reducing their sense of inadequacy.[13–15]

Short-term supplemental courses designed to enhance clinical skills can help students feel less anxious before starting their internships. The primary cause of stress among newly graduated nurses is the perception of their clinical incapacity to perform clinical duties.[16] Throughout the final year of the nursing bachelor's program, feelings of inadequacy in performing professional nursing tasks, along with associated anxiety, often lead to considerations of leaving the profession. These emotions are frequently triggered when students become aware of their limitations and upcoming legal responsibilities.[17] In many countries, nursing students inevitably encounter unsuitable role models in clinical settings. Therefore, it is crucial for students to have an opportunity to refresh their clinical knowledge before graduation.

Short, additional courses on clinical skills, based on competence, can help nursing students become more proficient in the field, feel more confident in their abilities and experience less anxiety.[7,18] Ongoing challenges in healthcare education, particularly those highlighted by emerging medical issues such as the COVID-19 pandemic, have made competency-based education (CBE) a timely and

relevant approach. Competency-based education addresses many limitations of traditional educational models by emphasizing flexibility, personalized learning, alignment with workforce demands, and mastery of skills.[19] As healthcare systems adapt to new realities, CBE provides a pathway for preparing competent professionals to effectively meet future challenges.

As mentioned above, CBE provides a valuable approach that focuses on improving specific skills and competencies, rather than adhering to a fixed curriculum or schedule. This method is especially important in nursing and midwifery, where the ability to apply theoretical knowledge in real-world scenarios is essential for delivering high-quality patient care.

Objectives

This study aims to examine the significance of CBE for nurses and midwives by systematically analyzing recent literature, with the goal of offering valuable insights to educational administrators for improving healthcare outcomes.

Materials and methods

An extensive literature review was conducted across various databases covering the past 15 years, using targeted keywords associated with CBE and clinical performance. Out of 1,751 identified records, 13 studies were chosen after applying stringent inclusion criteria.

Systematic preprocessing workflow

Data processing involved the following main steps: 1) initial search, 2) literature screening, 3) full-text evaluation, 4) initial data extraction, 5) quality assessment, and 6) data synthesis. The final step, data synthesis, involved incorporating summaries of findings from the selected literature and preparing them for interpretation.

Search strategy and initial preprocessing

The initial literature search included a primary screening of the literature in the database based on search queries and Boolean operators (AND, OR, and NOT). A comprehensive literature search was performed on original English-language research publications during the last 15 years from databases including PubMed, Embase, Cochrane Library, Web of Science (WoS), and Cumulative Index of Nursing and Allied Health Literature (CINAHL). Based on the predetermined aim of the study and the Preferred Reporting Items for Systematic Review (PRISMA) search strategy, literature searching was initiated using the relevant search queries and keywords as follows (alphabetically ordered): "basic clinical skills", "clinical performance", "clinical practice", "clinical skills", "clinical training", "competency", "competency enhancement", "competency-based education", "competency-based training", "health professional competence", "midwife competence", "midwife education", "nurse", "nursing competence", "nursing education", "professional development", "refresher course", "self-efficacy", and "skills". Additionally, mentioned search terms were used in combination with Boolean operators such as "AND" and "OR".

Screening and article selection

Screening was conducted independently by 2 trained authors in 2 steps. First, they assessed the titles and abstracts of the searched articles for relevance to the study's aim. Second, they evaluated each article based on inclusion and exclusion criteria, quality and relevance to the review's objectives. The abstract of each article was examined, and the full text was obtained for any article that could not be excluded based on the title or abstract. Duplicates were identified and excluded.

Inclusion and exclusion criteria

Published literature, including original research articles, quasi-experimental studies, case-control studies, and cohort studies, were included in the study selection. The focus was on evaluating the effectiveness of clinical skills refresher courses by measuring clinical performance and competency enhancement in nurses and midwives, regardless of factors such as age, weight, etc. Studies that assessed clinical skills and related parameters in evaluating nurse education with an emphasis on competency or the development of competence were also considered.

Articles that were not available in full text, including editorials, review articles and those included into nurses or midwives, or that did not evaluate refresher training in clinical skills, competency development or clinical performance in the targeted study population, were excluded from the analysis. Additionally, studies that were not published in full text were also excluded.

Full-data extraction

After screening, the full texts of the selected literature were downloaded, and the complete text and details of the reviewed results were obtained. Articles that met all inclusion criteria and were of sufficient quality were chosen for final evaluation. The goal of the study and data collection were determined using the PRISMA framework, which included the analysis technique and interpretation (Fig. 1). Data extraction was performed by 2 trained reviewers, focusing on study design, sample size, participant ethnicity, outcome assessment, and key findings.

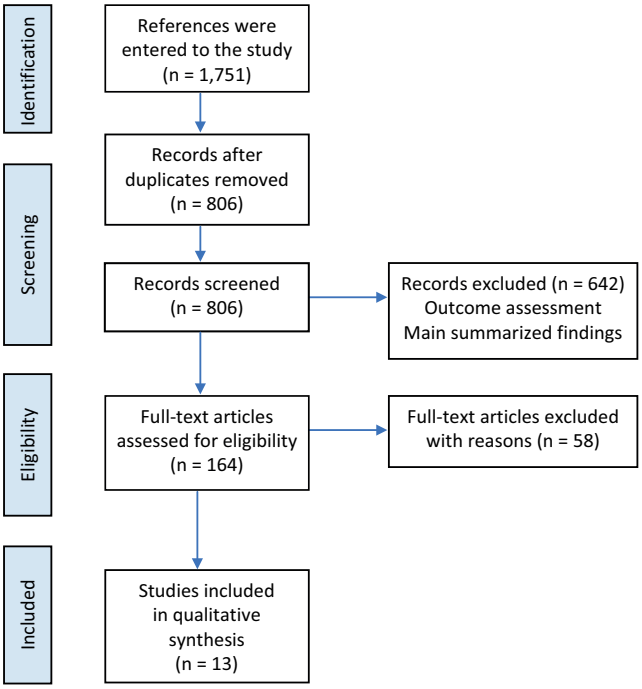

Fig. 1. Article selection based on Preferred Reporting Items for Systematic Reviews and Meta-Analyses (PRISMA) diagram

Checking articles quality

Two academics with backgrounds in systematic review research and nursing themes independently assessed the quality of the downloaded publications. The results were then addressed during meetings and in situations where there were disagreements, the conversation continued until 2 evaluators came to a final consensus. Quality assessment of resources was performed using the Cochrane Risk of Bias tool, which is an effective instrument for systematically evaluating the robustness of included publications. It considers key determinants of various biases, including selection, performance, detection, attrition, and reporting.[20] In terms of selection bias, the researcher evaluated the adequacy of methodology in randomization to generate allocation sequence as well as sufficient description in methodology (random sequence generation (RSG)), and whether the allocation sequence was concealed from participants (allocation concealment). Performance and detection biases express the blindness of participants, assessors or both. In attrition bias, the author searches whether missing data were addressed well, and finally, in reporting bias, the researcher checks if all achieved data were reported in some of them removed selectively (selective outcome reporting). All 6 parameters were scored as "Low risk" and "High risk". If it was not reported in the main resource, then we put "Unclear." A lower summation of the risk of bias was favored for evaluation.

Results

In the initial search, 1,751 records were obtained by examining the article text, inclusion and exclusion criteria, and subject relevance. A total of 13 studies were selected for further examination (Fig. 1). Regarding study type, 12 semi-experimental articles and 1 randomized clinical trial (RCT) were included, with all studies being case-control ones (Table 1).[7,21–32] Six studies were conducted on Chinese nurses,[21–26] 4 studies were conducted on Iranian nursing students,[7,27–29] 2 studies were conducted on Taiwanese nurses,[30,31] and 1 study was conducted on South Korean nurses.[32] In 5 studies, attention was paid to the effect of CBE on clinical skills.[22,24,27,30,31] The outcomes of CBE were assessed using 2 main approaches: first, through formal assessments of nurses and midwives, enabling them to demonstrate their improvement and performance; and second, through assessment tools such as technical improvement evaluations, strategic examinations and self-report questionnaires. In 5 studies, clinical skills were examined alongside other variables.[7,23,26,28,32] In 3 studies, other variables related to nursing skills were also examined.[21,25,29] In 10 studies, the effect of CBE on improving clinical skills was reported.[22,28,30,32]

Risk of bias in individual studies

The Cochrane Collaboration Risk of Bias scale was used to assess the quality of the 13 articles included in the systematic review. Table 2 presents the quality evaluation results of these articles.[7,21–32] According to the Cochrane evaluation scale, 3 studies had a risk of bias in 3 areas, while 5 studies had a risk of bias in 1 area. The remaining studies did not show clear evidence of risk in the areas of selection, performance, reporting, or other forms of bias.

Discussion

This study suggests that clinical skills refresher courses can significantly improve clinical performance, reduce anxiety and better prepare nurses and midwives for their ongoing professional roles. Therefore, it is strongly recommended to implement integrated short-term refresher programs that focus on competency to enhance training outcomes more effectively. Nursing education includes both theoretical and clinical training, with the expectation that graduates will possess the necessary competencies for professional nursing practice. Additionally, participating in clinical skills enhancement courses can increase nurses' self-confidence and improve their clinical proficiency.[32] The results indicate that emphasizing supplementary training on nursing competence can significantly influence the development of clinical skills over time[18]; however, the scope of this matter remains highly significant.

Table 1. Articles reviewed

Measurement	Summarized key findings	Outcome assessment	Type of study, population, country	Authors and reference
Anxiety, clinical self-efficacy and clinical skills	The undergraduate nursing curriculum can be enhanced with a basic clinical skills course. This training course can bridge the theory–practice gap and provide a better transition from the role of student to nurse.	The intervention was a 3-day refresher course directed by nurse instructors for intervention group focused on 10 basic nursing procedures in the clinical skill lab.	A quasi-experimental study; 160 nursing students Iran	Shahsavari et al., 2017[7]
General clinical knowledge; satisfaction level	The level of comprehensive knowledge and satisfaction improved.	General clinical knowledge and level of satisfaction were investigated in 2 groups under competence training and control.	A quasi-experimental design; 84 nursing students China	Ali et al., 2024 [21]
Performance	Clinical skills of nurses were improved.	Nurses were examined in terms of clinical skills during a period of 2 training and control groups.	A quasi-experimental design; 88 nursing students China	Danting and Yinyu, 2018[22]
Cooperation and clinical skills of nurses	The communication ability of nurses was improved.	After a course of clinical skills training of nurses, focusing on competency in nurses' communication ability, this skill was investigated.	A quasi-experimental design; 63 nursing students China	Hanqin et al., 2024[23]
Performance	Levels of comprehensive knowledge, interpersonal security skills, clinical nursing care improved after the training course.	After standardized training for new nurses, variables related to nurses' efficiency were evaluated based on job competence.	A quasi-experimental design; 120 nursing students China	Wang et al., 2025[24]
Comprehensive knowledge, interpersonal ability, community and nurses' point of view	Comprehensive knowledge improved in nurses under training.	After the training model of professional nurses oriented by core nursing competence, comprehensive knowledge, the interpersonal and community abilities of nurses were evaluated.	A quasi-experimental design; 120 nursing students China	Feng et al., 2016[25]
Clinical nursing skills and clinical competence	The performance in the health information collection, physical assessment and communication in the experimental group were higher.	The students who had received the nursing core competence standard training were selected as the experimental group.	A quasi-experimental design; 73 nursing students China	Wu et al., 2014[26]
Performance	The clinical performance of experimental group students was higher both in terms of specific clinical performance and skill.	The control group received conventional education and the experiment group received competency-based education for their CCU course.	A quasi-experimental post-test study; 34 nursing students Iran	Soheili et al., 2015[27]
Clinical nursing skills and clinical competence	Clinical skills and cognitive skills were higher in the group receiving competency-based education.	The experimental group received competency-based education and the control group received traditional instruction in a medical-surgical nursing course.	A quasi-experimental study; 28 nursing students Iran	Nadery et al., 2012[28]
Clinical nursing skills	The clinical performance of experimental group students was higher both in terms of specific clinical performance and skill.	The experimental group received competency-based education and the control group received traditional instruction in a medical-surgical nursing course.	A quasi-experimental study; 26 nursing students Iran	Valizadeh et al., 2009[29]
Performance	A significant increase in the average nursing competency scores was observed in both groups from the pre-test to the post-test.	The experimental group experienced the competency-based lesson plan, while the control group was only subjected to lectures based on routine training	Randomized clinical trial (RCT); 213 nursing students Taiwan	Hsu et al., 2016[30]
Performance	Students who received competency-based training had higher performance in course and practical course of medical-surgical nursing.	The experimental group received competency-based education and the control group received traditional instruction in a medical-surgical nursing course.	A quasi-experimental design; 312 nursing students Taiwan	Fan et al., 2015[31]
Self-confidence and clinical nursing skills and clinical competence	The mean scores in self-confidence and clinical competence were higher in the experimental group than in the control group.	During the course, students repeatedly practiced the 20 items that make up the core basic nursing skills using clinical scenarios. Their clinical competence with these skills was measured using the Core Clinical Nursing Skills checklist.	A quasi-experimental study; 162 senior nursing students South Korea	Park, 2017[32]

Table 2. Study quality scores (Cochrane Collaboration Risk of Bias)

Authors, year, reference	Selective bias		Participants blinding	Assessor blinding	Incomplete outcome date	Selective outcome reporting
	RSG	AC				
Shahsavari et al., 2017[7]	L	U	U	L	L	L
Ali et al., 2024[21]	U	U	U	L	U	L
Danting and Yinyu, 2018[22]	L	U	U	L	L	L
Hanqin et al., 2020[23]	L	U	L	L	L	L
Wang et al., 2017[24]	L	U	L	L	L	L
Feng et al., 2016[25]	L	U	L	L	L	L
Wu et al., 2014[26]	U	U	U	U	L	L
Soheili et al., 2015 [27]	U	U	U	U	L	L
Nadery et al., 2012[28]	L	U	L	U	L	L
Valizadeh et al., 2009[29]	L	U	L	L	L	L
Hsu et al., 2016[30]	L	U	L	U	L	L
Fan et al., 2015[31]	U	U	L	L	L	L
Park, 2017[32]	L	U	U	L	U	L

U – unclear; L – low; H – high; RSG – random sequence generation; AC – allocation concealment.

In nursing and midwifery practice, CBE plays a crucial role in improving patient safety and healthcare quality. This approach ensures that healthcare professionals acquire essential skills, enhance their clinical decision-making abilities and adhere to standardized protocols. As a result, patients experience better outcomes, healthcare services become more efficient and overall satisfaction increases. Additionally, this educational model fosters professional growth and helps practitioners meet regulatory requirements.

This study highlights the importance of CBE and its effective implementation in real-world clinical training. Several key strategies can support the successful application of this educational model.[33] First, it is essential to determine whether the training course is appropriate and built upon a well-structured curriculum. A curriculum should be designed around a set of competencies that encompass clinical skills, critical thinking and effective communication essential for nurses and midwives. Incorporating real-world experiences, maintaining continuous assessment and fostering collaboration with clinical institutes are also critical steps. Practical exposure in healthcare settings allows well-trained students to gain valuable experience. Instructors can use simulated competency-based training to engage students in unrealistic situations that reflect patient care expertise. Finally, evaluating the training program and collecting feedback through structured questionnaires can help educators refine and improve their training method.[34]

The present systematic study was conducted to investigate the effectiveness of competency-based clinical skills supplementary courses on nurses' clinical performance. In the reviewed studies, the impact of CBE on improving clinical skills was confirmed. Shahsavari et al. demonstrated the positive effect of a clinical skills refresher course on clinical skills, although the focus of the course was not specifically on merit. They suggested that the undergraduate nursing curriculum could be strengthened with a supplementary course on basic clinical skills. This training course can bridge the gap between theoretical knowledge and practical application, providing a smoother transition from a student's role to that of a nurse.[7] Another study reported that students who received CBE had higher performance in theoretical and practical courses in medical-surgical nursing.[31] They were better in terms of clinical performance.[27] Additionally, based on another semi-experimental study, it was found that clinical and cognitive skills were higher in the group receiving CBE.[28]

This systematic review strongly emphasizes the importance of incorporating a competency-based approach into nursing education. Given the critical role that nurses and midwives play in patient care outcomes, such an approach is likely to enhance their professional performance and increase their self-confidence in clinical practice.

There are serious gaps between theoretical learning and its clinical applications in healthcare educational systems.[35] A well-identified approach to overcoming these faults can increase the integration and frequency of practical experiences, reinforce theoretical knowledge through training courses, enhance critical thinking, problem-solving and emergency management, and acknowledge CBE.[36,37] The results highlight the crucial role of supplementary clinical training in undergraduate nursing programs. Newly graduated nurses often experience significant stress due to a lack of confidence in their clinical abilities. Among the various challenges faced in nursing, anxiety is closely linked to perceived clinical incompetence, which emerges as a key concern affecting professional readiness.[16,38] Nursing educators and curriculum developers play a crucial role in easing students' anxiety during training. Therefore,

strategies aimed at reducing or managing this distressing experience should be thoughtfully implemented.[7] Research by Valizadeh et al.[29] indicates that CBE enhances both cognitive and behavioral skills in nursing students. Their findings showed that students in the experimental group demonstrated notable improvements in these areas. Moreover, these students exhibited higher levels of clinical competence compared to those taught through traditional methods. Their study concludes that outcome-focused educational approaches are more effective in building essential nursing competencies than conventional teaching strategies.[29]

It has been observed in various surveys that focusing on competence in the training courses can have a positive effect on nurses' competence.[30] In the meantime, patient safety competence is a critical issue, as nurses are responsible for patient care 24 h a day.[39] On the other hand, the implementation of supplementary courses and education types in advanced countries has made the skills and self-confidence of nurses acceptable. A study in Italy reported the competence of nursing students in the patient safety field at a high level.[40] In her review, Park considered the effectiveness of additional clinical skills courses on clinical practice to be important. She stated that learning clinical skills provides an opportunity for students to improve their clinical and communication skills by using a variety of teaching aids, models and mannequins. In fact, the clinical skills center creates a link between theoretical content and practical skills.[32] In a study by Danting et al., it was found that competency training has a positive effect on nurses' ability, innovation, performance and clinical performance.[22]

Harvey et al. conducted an in-depth study to design a foundational training program tailored for nurses, midwives and other healthcare professionals. The initiative included an 8-day course, with its effectiveness assessed through participant feedback, as well as evaluations of knowledge, skill development and confidence. The program featured clearly articulated learning goals and was designed to allow participants to implement what they had learned between sessions. Emphasizing a strengths-based approach, it built on participants' existing capabilities and integrated both theoretical instruction and hands-on practice.[41]

Evidence suggests that simulation-based training and supplementary courses are among the most effective strategies for maintaining clinical skills. However, drawing firm conclusions about other types of interventions is challenging due to inconsistencies in research quality and design. The existing literature shows considerable variability, limiting the generalizability of the findings. Therefore, well-designed RCTs are urgently needed to identify the most effective methods for resuscitation training and long-term skill retention.[42] A study in Iran showed that emergency nurses' knowledge was at a relatively high level, whereas the skills, attitudes and overall patient safety competence of nurses working in emergencies were at a relatively favorable level. They reported that a basic understanding of competence and nurses' working skills in the emergency room is important for improving nursing quality, and additional clinical skills courses designed in the field of nurses' safety competence based on evaluations can enhance treatment quality.[43] A study conducted in Iran highlighted that professional self-efficacy among nursing students falls within a moderate range, indicating a need to revise nursing graduate curricula. Emphasis should be placed on fostering clinical and professional competencies, and these elements should be actively incorporated into nursing assessments. Our systematic review supports the idea that competency-based refresher programs can significantly improve nurses' practical abilities, knowledge and professional outlook. Overall, the evidence suggests that CBE plays a vital role in enhancing the clinical performance of healthcare practitioners.[18]

Another systematic review examining the impact of the CBE model in training newly graduated nurses found that emphasizing competency development in educational programs significantly enhances various professional abilities. These include improved clinical care performance, stronger critical thinking and innovation, better interpersonal communication, greater professional growth, increased knowledge, and more refined personal attributes. Furthermore, the benefits of competency-based training have also been observed among physicians, where such programs have been shown to enhance clinical skills and overall professional effectiveness.[44–47] Continuing professional development (CPD) should be implemented to enhance nursing competence. However, attention must also be given to the challenges encountered in clinical skills training. The findings identified 2 key obstacles in this area: the lack of effective clinical education facilitators and the presence of various barriers that hinder practical learning experiences.[48,49]

Recent research has demonstrated the substantial impact of CBE in improving clinical performance among nursing students. Those who engaged in CBE exhibited improved clinical abilities and greater self-confidence compared to those trained through conventional methods. This study emphasizes the value of CBE in equipping nursing students to face real-world clinical scenarios effectively.[50,51] Similarly, refresher programs have proven successful in increasing nurses' skills while also attenuating the anxiety levels linked with clinical responsibilities. These findings support the conclusions of our review and, further advocate for the integration of CBE in nursing curricula to better prepare students for real-world clinical challenges.[52] Furthermore, existing literature suggests that ongoing professional development combined with CBE is essential for ensuring that nurses remain equipped to handle the evolving demands of modern healthcare. Through the implementation of these educational strategies, institutions can foster both clinical performance and

confidence of current and upcoming nursing students, ultimately contributing to improved patient care.

Numerous studies have reported that nursing students and recent graduates often experience heightened anxiety, self-doubt and feelings of inadequacy as they transition into clinical practice and hospital internships.[16] One widely recognized approach to alleviating this anxiety involves incorporating curriculum models that emphasize hands-on clinical skill development. Simulated clinical environments, in particular, have been shown to enhance practical skills while also reducing anxiety levels.[7] Integrating such approaches within a CBE framework may further enhance the effectiveness of clinical skill acquisition. Learning is an ongoing and dynamic process through which individuals gain knowledge, refine skills and shift their attitudes and performance. A central goal of nursing education is to continuously enhance its programs by introducing innovative and practical strategies. By participating in supplementary courses that focus on competency development, nurses can improve their knowledge base, attitudes and professional performance, ultimately contributing to higher levels of clinical competence.

Limitations

Reanalyzing the data presented several challenges, primarily due to insufficient resources for constructing a robust CBE model. Additionally, the limited number of studies focused on a single competency framework, combined with various confounding factors such as differences in foundational clinical skills, cognitive abilities and procedural expertise, made the interpretation of the findings more complex. A key limitation of the current systematic review was the scarcity of research specifically targeting competence. Furthermore, we lacked detailed insight into the students' training environments, which may have introduced variables that influenced the outcomes. However, the strength of our study lies in the critical evaluation of article quality and the quasi-experimental designs employed, which enhanced the credibility of the findings. Another limitation was the limited focus on the long-term retention and practical application of competencies acquired through follow-up programs.

Conclusions

This study provides a deeper understanding of the importance of training improvement in healthcare providers, especially nurses and midwives, owing to their crucial role in responding to patients by highlighting the beneficial outcomes of CBE as a good approach. Although the current research provides a systematic review of publications in this field, the heterogeneity in the study details of the selected articles made it impossible to perform a meta-analysis.

Performing comparative studies in future cohort studies with more detail and distinct categorization in participants is beneficial to confirm the results. This study highlights several innovative elements of the proposed CBE model for nurses and midwives. These include the integration of theoretical knowledge with hands-on experience, consideration of personalized learning styles to address specific skill gaps, the use of simulation-based interventions to enhance practical abilities, and emphasis on developing core competencies to improve patient care.

Our study strongly advocates for the adoption of structured competency-based training programs by nursing educators and healthcare professionals aimed at addressing the specific professional gaps commonly observed among nursing students. Competency-based education bridges the gap between academic learning and clinical applications, equipping students to effectively navigate the dynamic challenges of today's healthcare landscape.

Use of AI and AI-assisted technologies

Not applicable.

ORCID iDs

Gaxue Jiang https://orcid.org/0009-0004-9072-6442
Liqiong Hou https://orcid.org/0000-0001-8410-5595

References

1. Nouhi E, Sabzevari S, Hosainrezaee H. Improvement of the quality of basic clinical skills training and evaluation of the efficacy of Objective Structured Clinical Examination (OSCE): An action research with a mixed method. *Strides Dev Med Educ*. 2018;15(1):e64982. doi:10.5812/sdme.64982
2. Efendi N. Implementation of total quality management and curriculum on the education quality. *J Soc Studies Educ Res*. 2022;13(3):120–149. https://www.learntechlib.org/p/222921. Accessed August 15, 2024.
3. Karami M, Hashemi N, Van Merrienboer J. Medical educators' beliefs about learning goals, teaching, and assessment in the context of curriculum changes: A qualitative study conducted at an Iranian medical school. *BMC Med Educ*. 2021;21(1):446. doi:10.1186/s12909-021-02878-3
4. Papapanou M, Routsi E, Tsamakis K, et al. Medical education challenges and innovations during COVID-19 pandemic. *Postgrad Med J*. 2022;98(1159):321–327. doi:10.1136/postgradmedj-2021-140032
5. Kim SC, Jillapali R, Boyd S. Impacts of peer tutoring on academic performance of first-year baccalaureate nursing students: A quasi-experimental study. *Nurse Educ Today*. 2021;96:104658. doi:10.1016/j.nedt.2020.104658
6. Saab MM, Hegarty J, Murphy D, Landers M. Incorporating virtual reality in nurse education: A qualitative study of nursing students' perspectives. *Nurse Educ Today*. 2021;105:105045. doi:10.1016/j.nedt.2021.105045
7. Shahsavari H, Ghiyasvandian S, Houser ML, Zakerimoghadam M, Kermanshahi SSN, Torabi S. Effect of a clinical skills refresher course on the clinical performance, anxiety and self-efficacy of the final year undergraduate nursing students. *Nurse Educ Pract*. 2017;27:151–156. doi:10.1016/j.nepr.2017.08.006
8. Ford K, Watson FA, Ross A, et al. Understanding the experiences of transition for newly qualified mental health nurses and their potential to stay in the role: A qualitative exploration. *Nurse Educ Pract*. 2024;80:104105. doi:10.1016/j.nepr.2024.104105
9. Aein F, Alhani F, Anoosheh M. The experiences of nursing students, instructors, and hospital administrators of nursing clerkship. *Iran J Med Educ*. 2010;9(3):191–200. https://ijme.mui.ac.ir/browse.php?a_id=1050&slc_lang=en&sid=1&printcase=1&hbnr=1&hmb=1. Accessed August 15, 2024.

10. Ahmadi S, Abdi A, Nazarianpirdosti M, Rajati F, Rahmati M, Abdi A. Challenges of clinical nursing training through internship approach: A qualitative study. *J Multidiscip Healthc*. 2020;13:891–900. doi:10.2147/JMDH.S258112
11. Liao RX, Liu YH. The impact of structural empowerment and psychological capital on competence among Chinese baccalaureate nursing students: A questionnaire survey. *Nurse Educ Today*. 2016;36:31–36. doi:10.1016/j.nedt.2015.07.003
12. Song Y, McCreary LL. New graduate nurses' self-assessed competencies: An integrative review. *Nurse Educ Pract*. 2020;45:102801. doi:10.1016/j.nepr.2020.102801
13. Ulupinar S, Aydogan Y. New graduate nurses' satisfaction, adaptation and intention to leave in their first year: A descriptive study. *J Nurs Manag*. 2021;29(6):1830–1840. doi:10.1111/jonm.13296
14. Herrman JW. *Creative Teaching Strategies for the Nurse Educator*. 4th ed. Philadelphia, USA: F.A. Davis; 2024. ISBN:978-1-7196-5055-7.
15. Wolf A. Adapting nursing programs to competency-based education. *Nursing*. 2022;52(2):12–13. doi:10.1097/01.NURSE.0000806200.13094.90
16. Christensen M, Aubeeluck A, Fergusson D, et al. Do student nurses experience imposter phenomenon? An international comparison of final year undergraduate nursing students readiness for registration. *J Adv Nurs*. 2016;72(11):2784–2793. doi:10.1111/jan.13034
17. Vázquez-Calatayud M, Errasti-Ibarrondo B, Choperena A. Nurses' continuing professional development: A systematic literature review. *Nurse Educ Pract*. 2021;50:102963. doi:10.1016/j.nepr.2020.102963
18. Imanipour M, Ebadi A, Monadi Ziarat H, Mohammadi MM. The effect of competency-based education on clinical performance of health care providers: A systematic review and meta-analysis. *Int J Nurs Pract*. 2022;28(1):e13003. doi:10.1111/ijn.13003
19. Ryan MS, Holmboe ES, Chandra S. Competency-based medical education: Considering its past, present and a post-COVID-19 era. *Acad Med*. 2022;97(3 Suppl):S90–S97. doi:10.1097/ACM.0000000000004535
20. Flemyng E, Moore TH, Boutron I, et al. Using Risk of Bias 2 to assess results from randomised controlled trials: Guidance from Cochrane. *BMJ Evid Based Med*. 2023;28(4):260–266. doi:10.1136/bmjebm-2022-112102
21. Kamal Ali F, Abdel-Wahab Afifi Araby Ali O, Mansour Abdel Azeem Barakat F. Effect of competency-based education on maternity nurses' performance and quality of care regarding management of first stage of labor. *Egypt J Health Care*. 2024;15(2):149–170. doi:10.21608/ejhc.2024.350819
22. Danting Z, Yinyun C. Application of job competency training in pre-job training for new nurses [in Chinese]. *Chin J Prim Med Pharm*. 2018;25(1):128–130. http://wprim.whocc.org.cn/admin/article/articleDetail?WPRIMID=701676&articleId=702161. Accessed August 15, 2024.
23. Hanqin D, Cailan H, Xiajun H, Qiuling H, Yueya W. Job competency of new nurses in the open ward of the psychiatric department of a general hospital: Construction of assessment and evaluation indicators [in Chinese]. *J Nurs (China)*. 2020, 27: 9–13. https://chn.oversea.cnki.net/kcms/detail/detail.aspx?filename=NFHL202005004&dbcode=CJFQ&dbname=CJFDLAST2020&uniplatform=NZKP. Accessed August 15, 2024.
24. Wang L, Fan L, Huang S, Lu Z. Practice of standardized training for new nurses in stomatological hospitals [in Chinese]. *Chin Nurs Educ* 2025; 22: 153–157. https://jy.zhhlzzs.com/EN/10.3761/j.issn.1672-9234.2025.02.004. Accessed August 15, 2024.
25. Feng XY, Zhou YL, Cao YC, Chen L, Deng Y, Duan MH. The clinical application of a training model of neurological professional nurses oriented by core nursing competence [in Chinese]. *Health Vocational Education*. 2016;34(18):104–105. https://www.zhangqiaokeyan.com/academic-journal-cn_health-vocational-education_thesis/0201210910916.html. Accessed August 15, 2024.
26. Wu FQ, Wang YL, Wu Y, Guo M. Application of nursing core competency standard education in the training of nursing undergraduates. *Int J Nurs Sci*. 2014;1(4):367–370. doi:10.1016/j.ijnss.2014.10.010
27. Soheili A, Hemmati Maslak M, Mohammadpour Y, Khalkhali H, Rahmani A. The effect of implementing competency based education model on nursing students' clinical performance in coronary care unit. *Nurs Midwifery J*. 2015;13(9):728–738. http://unmf.umsu.ac.ir/article-1-2525-en.html. Accessed August 15, 2024.
28. Naderi A, Baghaei R, Por YM, Aliramaei N, Zadeh KG. Comparison of the effect of competency-based education model and traditional teaching on cognitive and clinical skills learning among ICU nursing students. *Iran J Med Educ*. 2012;12:698–708. https://ijme.mui.ac.ir/browse.php?a_id=1982&slc_lang=en&sid=1&printcase=1&hbnr=1&hmb=1. Accessed August 15, 2024.
29. Valizadeh S, Mohammadpour Y, Parvan K, Lakdizaji S. The effect of outcome-based education on nursing students' clinical competency. *Iran J Med Educ*. 2009;9(2):157–166. https://ijme.mui.ac.ir/browse.php?a_id=975&slc_lang=en&sid=1&printcase=1&hbnr=1&hmb=1. Accessed August 15, 2024.
30. Hsu LL, Pan HC, Hsieh SI. Randomized comparison between objective-based lectures and outcome-based concept mapping for teaching neurological care to nursing students. *Nurse Educ Today*. 2016;37:83–90. doi:10.1016/j.nedt.2015.11.032
31. Fan JY, Wang YH, Chao LF, Jane SW, Hsu LL. Performance evaluation of nursing students following competency-based education. *Nurse Educ Today*. 2015;35(1):97–103. doi:10.1016/j.nedt.2014.07.002
32. Park S. Effects of an intensive clinical skills course on senior nursing students' self-confidence and clinical competence: A quasi-experimental post-test study. *Nurse Educ Today*. 2018;61:182–186. doi:10.1016/j.nedt.2017.11.028
33. Curry L, Docherty M. Implementing competency-based education. *Collected Essays on Learning and Teaching*. 2017;10:61–74. doi:10.22329/celt.v10i0.4716
34. Ige WB, Ngcobo WB, Afolabi O. Implementation of competency-based education for quality midwifery programmes in Africa: A scoping review. *BMC Nurs*. 2024;23(1):685. doi:10.1186/s12912-024-02333-w
35. Moradian ST, Nehrir B, Khaghanizade M. Strategies for reducing theory practice gap in nursing education: An integrative review. *J Nurs Educ*. 2019;8(2):58–64. http://jne.ir/article-1-930-en.html. Accessed August 15, 2024.
36. Saifan A, Devadas B, Daradkeh F, Abdel-Fattah H, Aljabery M, Michael LM. Solutions to bridge the theory-practice gap in nursing education in the UAE: A qualitative study. *BMC Med Educ*. 2021;21(1):490. doi:10.1186/s12909-021-02919-x
37. Vosoughi MN, Zamanzadeh V, Valizadeh L, et al. An introduction to the TPSN model: A comprehensive approach to reducing the theory-practice gap in nursing. *BMC Nurs*. 2022;21(1):261. doi:10.1186/s12912-022-01030-w
38. Contreras JA, Edwards-Maddox S, Hall A, Lee MA. Effects of reflective practice on baccalaureate nursing students' stress, anxiety and competency: An integrative review. *Worldviews Evid Based Nurs*. 2020;17(3):239–245. doi:10.1111/wvn.12438
39. Han JH, Roh YS. Teamwork, psychological safety, and patient safety competency among emergency nurses. *Int Emerg Nurs*. 2020;51:100892. doi:10.1016/j.ienj.2020.100892
40. Stevanin S, Bressan V, Bulfone G, Zanini A, Dante A, Palese A. Knowledge and competence with patient safety as perceived by nursing students: The findings of a cross-sectional study. *Nurse Educ Today*. 2015;35(8):926–934. doi:10.1016/j.nedt.2015.04.002
41. Harvey S, Spurr P, Sidebotham M, Fenwick J. Describing and evaluating a foundational education/training program preparing nurses, midwives and other helping professionals as supervisors of clinical supervision using the Role Development Model. *Nurse Educ Pract*. 2020;42:102671. doi:10.1016/j.nepr.2019.102671
42. Au K, Lam D, Garg N, et al. Improving skills retention after advanced structured resuscitation training: A systematic review of randomized controlled trials. *Resuscitation*. 2019;138:284–296. doi:10.1016/j.resuscitation.2019.03.031
43. Najafi Ghezeljeh T, Keyvanloo Shahrestanaki S, Mohammadbeigi T, et al. Patient safety competency in emergency nurses in educational-medical centers of Iran University of Medical Sciences, 2020. *Iran J Nurs*. 2022;34(134):60–73. doi:10.32598/ijn.34.6.5
44. Hassankhani H, Mohajjel Aghdam A, Rahmani A, Mohammadpoorfard Z. The relationship between learning motivation and self-efficacy among nursing students. *Res Dev Med Educ*. 2015;4(1):97–101. doi:10.15171/rdme.2015.016
45. Chen S, Zhang C, Li W. The effects of competency-based training model in the training of new nurses: A meta-analysis and systematic review. *PLoS One*. 2022;17(11):e0277484. doi:10.1371/journal.pone.0277484

46. Chen G, Wang H, Zhou L, Yang J, Xu L, Liang Y. Development and applications of graduate outcome-based curriculum for basic medical education. *Front Med (Lausanne)*. 2024;11:1400811. doi:10.3389/fmed.2024.1400811
47. Hong M, Rozenblit JW, Hamilton AJ. Simulation-based surgical training systems in laparoscopic surgery: A current review. *Virtual Reality*. 2021;25(2):491–510. doi:10.1007/s10055-020-00469-z
48. Ma H, Niu A, Sun L, Luo Y. Development and evaluation of competency-based curriculum for continuing professional development among military nurses: A mixed methods study. *BMC Med Educ*. 2022;22(1):793. doi:10.1186/s12909-022-03846-1
49. Ahmari Tehran H, Gaeeni M, Rezaei M, Khoramirad A, Parizad A. The challenges of clinical education in nursing: A qualitative analysis of nursing students and clinical instructors' perspectives. *J Nurs Midwifery Sci*. 2021;8(4):260. https://brieflands.com/articles/jnms-140709.pdf. Accessed August 15, 2024.
50. Lee H, Song Y. Kirkpatrick model evaluation of accelerated second-degree nursing programs: A scoping review. *J Nurs Educ*. 2021;60(5):265–271. doi:10.3928/01484834-20210420-05
51. Alsalamah A, Callinan C. The Kirkpatrick model for training evaluation: Bibliometric analysis after 60 years (1959–2020). *Industrial and Commercial Training*. 2022;54(1):36–63. doi:10.1108/ICT-12-2020-0115
52. Mlambo M, Silén C, McGrath C. Lifelong learning and nurses' continuing professional development: A metasynthesis of the literature. *BMC Nurs*. 2021;20(1):62. doi:10.1186/s12912-021-00579-2

Basket trial designs in oncology: A comprehensive systematic review

Mikołaj Bartoszkiewicz[1,A–D,F], Joanna Kufel-Grabowska[2,D–F], Paweł Burchardt[3,E,F]

[1] Department of Immunobiology, Poznan University of Medical Sciences, Poland
[2] Department and Clinic of Oncology and Radiotherapy, Medical University of Gdańsk, Poland
[3] Department of Hypertension, Angiology and Internal Diseases, Poznan University of Medical Sciences, Poland

A – research concept and design; B – collection and/or assembly of data; C – data analysis and interpretation; D – writing the article; E – critical revision of the article; F – final approval of the article

Advances in Clinical and Experimental Medicine, ISSN 1899–5276 (print), ISSN 2451–2680 (online) *Adv Clin Exp Med*. 2026;35(2):343–350

Address for correspondence
Mikołaj Bartoszkiewicz
E-mail: m.bartoszkiewicz@ump.edu.pl

Funding sources
None declared

Conflict of interest
None declared

Received on June 3, 2024
Reviewed on February 17, 2025
Accepted on May 8, 2025

Published online on September 4, 2025

Abstract

Background. Basket trials are an innovative type of clinical trial primarily used in oncology. A distinctive feature of these studies is the grouping of patients based on specific molecular characteristics, such as genetic mutations or immunological subtypes, rather than traditional criteria like the type of cancer.

Materials and methods. This review was conducted in accordance with the Preferred Reporting Items for Systematic Reviews and Meta-Analyses (PRISMA) guidelines. Medical databases were searched for studies published between 2014 and 2024. The inclusion criteria focused on basket trials as a clinical trial model in oncology.

Objectives. This work aims to outline the principles of conducting basket trials in oncology, analyze basket trials from the past decade, and highlight the emerging trends in this type of trial.

Results. The analysis of 76 articles meeting the inclusion criteria revealed that most of these studies are conducted as phase II clinical trials. The average duration of the basket trials in the analysis was 5.9 years (mean = 5.05), with an average recruitment target of 326 patients (mean = 123.5). Most of these studies were conducted in the USA, and the majority of basket trials focused on patients with solid tumors.

Conclusions. The systematic review confirms that basket trials have significant potential as a clinical trial model, as evidenced by the increasing number of basket trial projects being conducted.

Key words: cancer clinical trials, basket trials, basket and umbrella trials

Cite as
Bartoszkiewicz M, Kufel-Grabowska J, Burchardt P. Basket trial designs in oncology: A comprehensive systematic review. *Adv Clin Exp Med*. 2026;35(2):343–350. doi:10.17219/acem/204832

DOI
10.17219/acem/204832

Highlights

- Molecularly driven basket trials in oncology group patients by shared biomarkers rather than tumor origin, advancing precision medicine.
- Systematic review of 76 basket trials (2014–2024) reveals design trends, patient selection strategies and outcome metrics.
- Phase II studies dominate, with a primary focus on solid tumors, validating biomarker-guided therapeutic approaches.
- Average trial duration of 5.9 years and 326-patient recruitment targets highlight the scale and timelines of modern basket trials.
- USA-based leadership in basket-trial research – the majority of studies are conducted in the USA, showcasing regional expertise in precision oncology.

Background

Basket trials are an innovative type of clinical trial primarily used in oncology. A key feature of these studies is the grouping of patients based on specific molecular characteristics, such as genetic mutations or immunological subtypes, rather than traditional criteria like the type of cancer.[1] The growing use of precision medicine to identify and develop effective targeted therapies defines the current landscape of pharmaceutical drug development. This innovative approach aims to enhance treatment effectiveness by tailoring therapy to the patient's unique molecular profile, rather than relying on standard treatment regimens designed for patients with cancer in a particular location, such as lung or colorectal cancer.

Innovations in biotechnology, clinical trials and advanced computational tools have the potential to accelerate the discovery and development of new targeted therapies. One example of methodological innovation is the design of master protocols[2] – studies that simultaneously assess the effects of multiple investigational drugs across various cancer types within a single overarching framework. The main protocols in oncology enable the identification of specific signaling pathways closely associated with gene variants responsible for tumor development, growth, and progression of cancer cells.[3] Designs of these master protocols, such as basket trials or umbrella trials, facilitate the personalization of patient therapy, which may lead to improved clinical outcomes and better optimization of available drugs.

Basket trials aim to use therapies targeting specific molecular changes in cancer patients, regardless of the tumor's origin in the body.[4] One example of a basket trial is the use of imatinib across various histological subtypes of advanced sarcoma,[5] or vemurafenib in the treatment of cancers other than melanoma that harbor the BRAF V600 mutation.[6]

Basket trials represent the next stage in the evolution of precision medicine, enabling clinicians to select effective treatments based on a patient's genetic, environmental, and lifestyle factors. As precision medicine advances, the role of artificial intelligence (AI) has become increasingly important. AI-based solutions can enhance cancer treatment and management, which is why their use is recommended in various areas, including personalized medicine.[7] Despite these advancements, significant gaps remain in understanding the broader implications of basket trial designs in clinical practice. While numerous studies have demonstrated the potential of basket trials in specific tumor types, comprehensive reviews addressing their overall efficacy, methodological challenges and emerging trends in oncology remain limited.

Basket trial study model

A basket trial design selects patients based on specific molecular biomarkers, grouping them according to common molecular characteristics, and then treating all patients in a given group with the same therapy or a set of different drugs. Basket trials can be single-arm or multi-arm, where each arm represents a separate 'basket' that, regardless of the disease type, brings together patients to test a specific treatment based on their shared genetic characteristics.[8,9] The term 'basket' thus refers to the grouping of potentially different cancers into one unified disease at the molecular level (Fig. 1).

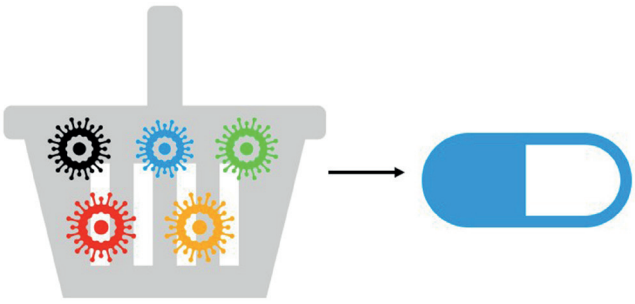

Fig. 1. Basket trial model

Objectives

This study aims to address these gaps by conducting a systematic review of basket trials published between January 2014 and June 2024. Specifically, it seeks to provide

an overview of the methodological principles underlying basket trials in oncology, as well as analyze the scope, effectiveness and geographical distribution of these trials to identify trends and areas requiring further exploration, and highlight the role of AI and technological advancements in enhancing the design and outcomes of these trials. By examining the evolving landscape of basket trials, this study aims to provide critical insights into their potential as a cornerstone of precision oncology, while contributing to the advancement of molecular profiling applications in clinical practice.

Methods

In March 2024, a systematic review of basket studies conducted between January 2014 and June 2024 was performed following the Preferred Reporting Items for Systematic Reviews and Meta-Analyses (PRISMA) guidelines. A total of 241 records were identified (Fig. 2). The review was conducted across four major databases (PubMed, Scopus, Web of Science, and Google Scholar) as well as the clinical trial registry ClinicalTrials.gov.

Eligibility criteria

The study analyzed relevant publications from January 2014 to June 2024. The inclusion criteria were as follows: 1) the basket trial model was clearly described in the abstract or title of the publication, 2) the study involved cancer clinical trials and 3) the publication was in English.

Search strategy

The database search strategy was defined using keywords in the title or abstract, including "basket trials", "clinical trials", "basket trial", and "basket study". The concept of a basket study had to be clearly defined in the title or abstract of the study. The results were filtered by language,

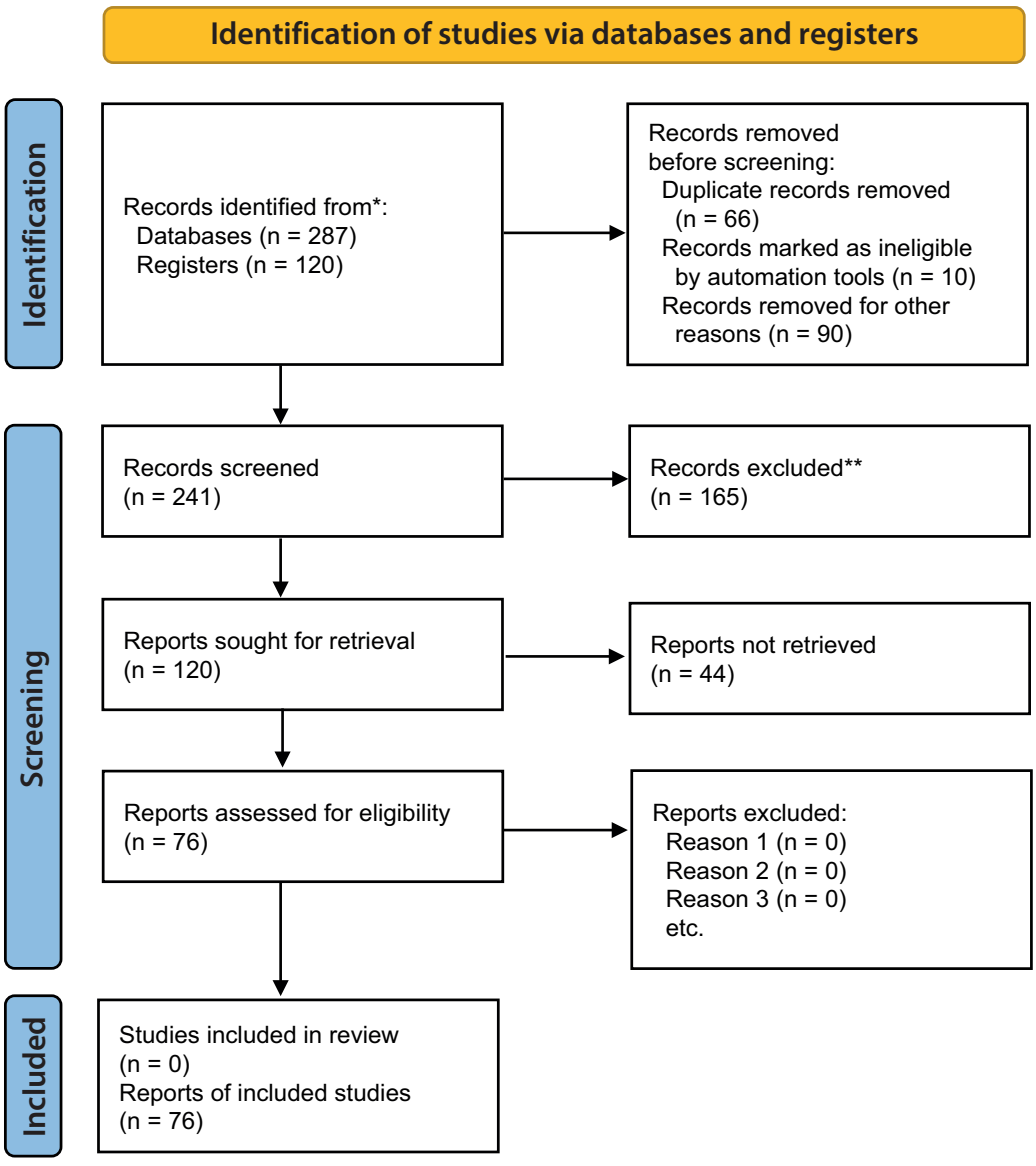

Fig. 2. Preferred Reporting Items for Systematic reviews and Meta-Analyses (PRISMA) diagram

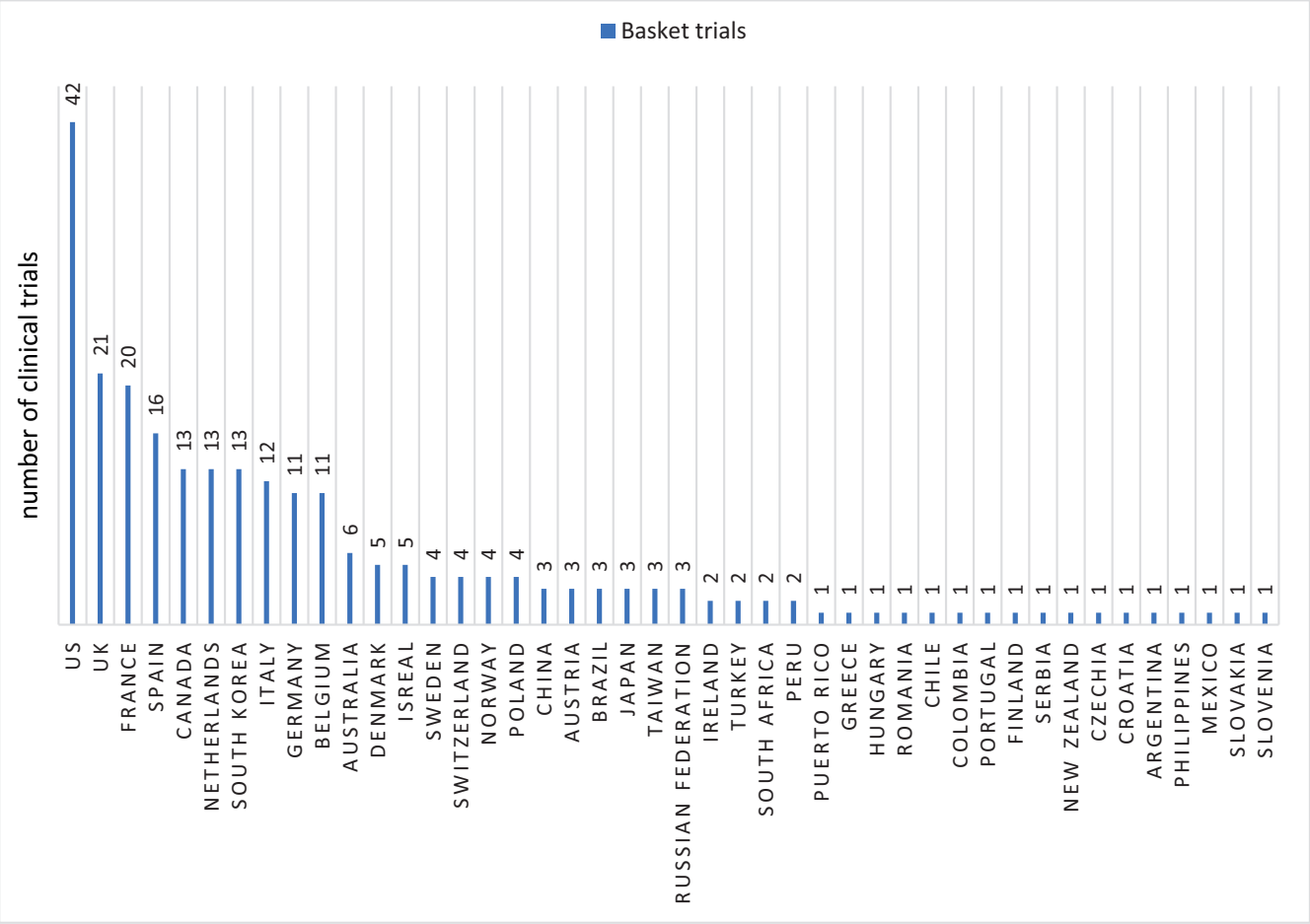

Fig. 3. Basket trials by countries

and only studies published in English were included. Four databases were used: PubMed, Scopus, Web of Science, and Google Scholar, as well as the clinical trial registry database ClinicalTrials.gov. The same keywords were used to search for publications across each database.

The articles found in the databases were initially screened by reviewing their titles and abstracts. The authors assessed the inclusion criteria to select publications that could meet these criteria. Articles deemed relevant to the proposed topic were then read in full. Below, basket studies conducted among patients with the most common and rare cancers will be briefly summarized.

Results

The analysis identified 76 basket studies that met the criteria for inclusion in the systematic review. The majority of these studies were phase II trials (n = 45, 76%), with nearly 1/5 (n = 15, 19%) being early extended phase I/II studies. The remaining studies included phase I trials (n = 6, 7.6%) and phase III trials (n = 2, 2.6%). One study (n = 1, 1.3%) was observational. Most of the studies were conducted in an open-label model (n = 70, 92.1%), and 9.2% were performed as academic research.

The average duration of basket trials in the included analysis is 5.9 years (mean = 5.05), while the average recruitment target is 326 patients (median = 123.5). On average, approx. 3 countries were involved in conducting each basket trial. Additionally, an average of 3.1 treatments were used in the studies. The USA accounted for the largest number of basket studies in the analysis (n = 42, 55.2%), followed by the UK (n = 21, 27.6%) and France (n = 20, 26.3%). The chart below shows all countries where basket trials in oncology have been conducted (Fig. 3).

In basket studies, there is typically no fundamental division of cancer based on the location of the primary tumor. Therefore, the table below includes the cancer types listed as inclusion criteria in the basket study. Most basket trials are focused on patients with solid tumors (n = 69, 90%) (Fig. 4). The trend of the basket trial model in oncology was also analyzed. In 2023, 0.9% of oncology studies were conducted using the basket model. Since 2020, the number of studies conducted in the basket model has averaged 10.2 per year in oncology (Fig. 5).

One example of a basket study in the above analysis is the NCT02693535 study. The Targeted Agent and Profiling Utilization Registry (TAPUR) study is a non-randomized clinical trial designed to determine the safety and effectiveness of commercially available targeted anticancer

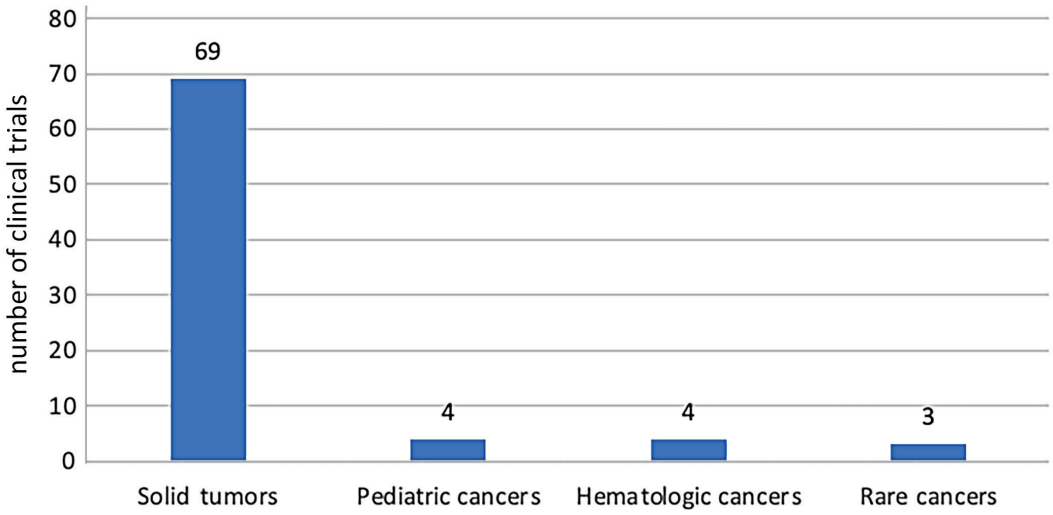

Fig. 4. Basket trials divided into types of cancer

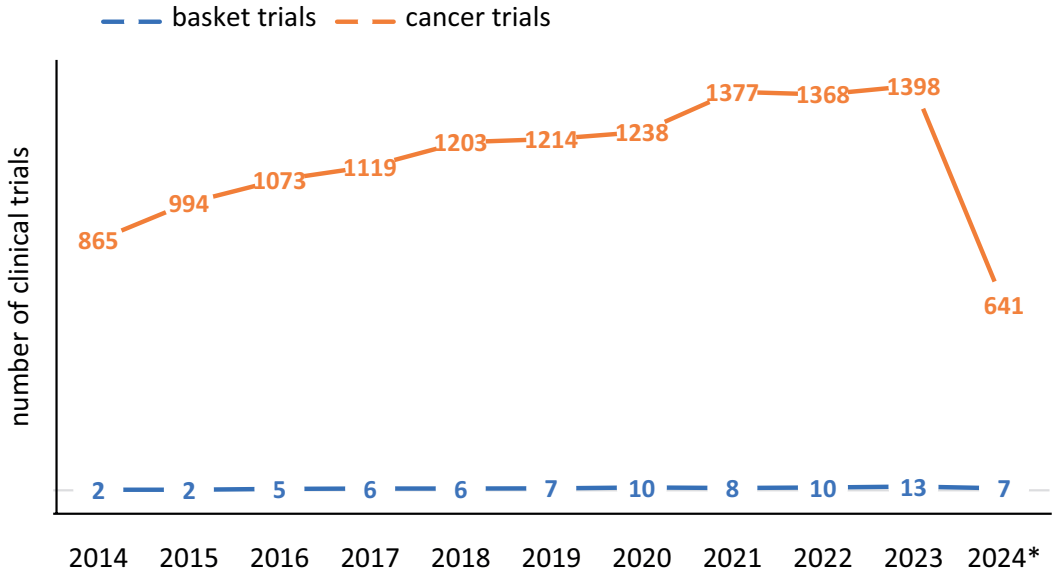

Fig. 5. Basket trials model and clinical trials in oncology

drugs in the treatment of patients with advanced cancer that has a potentially actionable genomic variant.

The TAPUR trial aims to analyze U.S. Food and Drug Administration (FDA)-approved targeted therapies developed by collaborating pharmaceutical companies, catalog clinical oncologists' molecular profiling test selections, and generate hypotheses for additional clinical trials. The study's recruitment goal is 3,791 patients, the largest number of patients in any basket study included in this analysis. The study is scheduled to last 9 years and 6 months. Fisher et al. presented partial results from the TAPUR trial for patients with advanced breast cancer, non-small cell lung cancer, and ovarian cancer using cetuximab therapy. Patients with breast cancer (n = 10), non-small-cell lung cancer (n = 10) and ovarian cancer (n = 29) were enrolled in the study between June 2016 and September 2018. No objective responses or disease stabilization for at least 16 weeks were observed in any cohort of patients without *KRAS*, *NRAS*, or *BRAF* mutations (Table 1).[10–14]

Chung et al. presented partial results from the KEYNOTE-158 phase II basket trial, which recruited patients with advanced cervical cancer who had previously undergone therapy due to tumor dissemination. The study included 90 patients who received pembrolizumab 200 mg every 3 weeks for up to 2 years or until progression, intolerable toxicity, or discontinuation by the physician or patient. Pembrolizumab monotherapy demonstrated durable antitumor activity and manageable safety in patients with advanced cervical cancer. Based on these results, FDA granted accelerated approval of pembrolizumab for patients with PD-L1-positive advanced cervical cancer who progressed during or after chemotherapy.[12] The total recruitment target for the NCT02628067 Advanced Solid Tumor Basket Study is 1,609 patients, and the study is scheduled to last 10 years and 10 months.

Another example of a basket study of advanced solid tumors is the study by Sweeney et al., which focused on cancer patients with *HER2* amplification, overexpression, and/or activating variants. The study (NCT02091141)

Table 1. Solid tumors basket trials

CT number	Author	Type of cancer	Phase	Blinding	Screened	Duration	Countries	Intervention
NCT02693535	Yang, et al.[11]	advanced solid tumors	II	open-label	3791	9 years and 6 months	1	1
NCT02628067	Chung, et al.[12]	advanced solid tumors	II	open-label	1609	10 years and 10 months	23	2
NCT02091141	Sweeney et al.[13]	advanced solid tumors	II	open-label	346	9 years and 1 month	1	8
NCT01953926	Hyman, et al.[14]	solid tumors harboring somatic *HER2* or *EGFR* exon 18 mutations	II	open-label	582	11 years and 10 months	13	3

CT – clinical trial.

included 346 patients. The study demonstrated that pertuzumab + trastuzumab had activity in various cancers with *HER2* amplification and/or overexpression and wild-type *KRAS*, with a range of efficacy depending on the tumor type. However, it also showed limited activity in patients with *KRAS* variants, variants in the *HER2* gene, or in those with *HER2*-low (Score 1+) or ultra-low (Score 0) status.[13]

Oaknin et al. also presented partial results of a study on variants in the *HER2* gene in this case of cervical cancer. The SUMMIT trial (NCT01953926) is a phase II study evaluating the efficacy and safety of neratinib as monotherapy or in combination with other therapies in participants with solid tumors with a variant in the *HER* gene (*EGFR, HER2*). The study included 16 patients with cervical adenocarcinoma. Neratinib monotherapy showed activity in previously intensively treated patients with cervical cancer with a variant in the *HER2* gene.[15] The overall recruitment goal of the SUMMIT study is 582 patients. The SUMMIT trial was terminated at the beginning of 2023.

Others basket trials

Pediatric cancers

One example of a basket study in a pediatric group is the NCT03363217 study described by Perreault et al. This is a phase II study of trametinib in patients with pediatric glioma or plexiform neurofibroma, specifically those with treatment-resistant tumors and activation of the MAPK/ERK: TRAM-0 pathway. The main objective of the study is to determine the objective response rate to trametinib as a single agent in the treatment of progressive/refractory cancers with MAPK/ERK pathway activation.[16] The recruitment target is 114 patients, and the study is planned to last 9 years. A clinical trial is ongoing.

Rare cancers

Rare cancers pose a significant challenge for accurate diagnosis and treatment. While there is no universal definition, the American Cancer Society (ACS) defines rare cancers as those with an incidence of fewer than 6 cases per 100,000 people per year.[17] Basket trials present an opportunity to identify appropriate molecularly targeted treatments for patients with rare cancers.

In the phase II study NCT02721732, patients with advanced rare cancers who had progressed on standard therapies within the last 6 months were enrolled in 9 cohorts of cancer patients, with a 10th cohort for those diagnosed with other rare lesions. The study included 127 patients who received pembrolizumab at a dose of 200 mg intravenously every 21 days. The favorable toxicity profile and antitumor activity observed in patients diagnosed with cutaneous squamous cell carcinoma, adenoid cystic carcinoma, cancer of unknown primary, and paraganglioma-pheochromocytoma support further evaluation of pembrolizumab in this patient population.[18]

Hematological cancers

Another group of cancers in which the basket model of a clinical trial is used is hematological cancers. The phase II trial NCT00866047, published by Pro et al., evaluated the safety and efficacy of brentuximab vedotin in patients with relapsed or refractory (R/R) systemic anaplastic large cell lymphoma (ALCL). Fifty-eight patients were included in the study; brentuximab was administered to patients every

Table 2. Others basket trials

CT number	Author	Type of cancer	Phase	Blinding	Screened	Duration	Countries	Intervention
NCT03363217	Perreault, et al.[16]	pediatric glioma or plexiform neurofibroma	II	open-label	114	9 years and 5 months	1	1
NCT02721732	How, et al.[18]	rare tumors	II	open-label	127	9 years and 4 months	1	1
NCT00866047	Pro et al.[19]	large cell lymphoma	II	open-label	58	7 years and 3 months	5	1

CT – clinical trial.

three weeks as a 30-min intravenous infusion for a maximum of 16 treatment cycles. The results showed a high rate of resolution of peripheral neuropathy symptoms and durable remissions in the subgroup of patients with R/R systemic ALCL, indicating that brentuximab vedotin monotherapy may be a potentially effective therapeutic option (Table 2).[19]

Discussion

The master protocol is a project tool designed to develop a clinical trial that can evaluate multiple research hypotheses and, most importantly, enhance the effectiveness of the clinical trial. The study above focused on one type of primary protocol, a basket trial, in which the efficacy and safety of targeted therapies are assessed in cancer patients with a specific molecular target, regardless of the tumor's primary origin. In addition to identifying therapeutic options, precision oncology tracks tumor response to intervention at the molecular level and detects drug resistance and the mechanisms underlying its development.[20–22]

The USA, France, and the UK are the countries where the largest number of basket trials in oncology are conducted, reflecting the global trend in new research initiatives. The USA leads in the total number of clinical trials globally, while France is the leader in Europe. The fact that these trials typically involve 3 or more countries (on average) underscores the global nature of oncology research and the international collaboration required to address complex, rare and diverse cancer types. Most basket studies are early-phase I/II trials, highlighting that master protocol models are still relatively new concepts in clinical research. Pharmaceutical companies aim to expand the scope of implementing a single project across multiple therapeutic areas while reducing the costs of conducting clinical trials through master protocol research models.

The basket studies included in the systematic review primarily focus on solid cancers. Ongoing studies have defined "baskets" specific to particular molecular targets, aiming to determine the effectiveness of drugs acting on specific molecular pathways, including those used to treat other diseases. A basket study, which incorporates multiple independent, two-stage designs (1 per basket), is characterized by a higher false-positive rate compared to a typical phase II trial (i.e., there is a greater chance that a drug will be found effective in at least one basket, even if it is actually ineffective). The ability of basket trials to identify molecular subtypes across different solid tumors is particularly valuable, as demonstrated by the various targeted therapies evaluated in the reviewed trials, including those aimed at HER2 amplification, PD-L1 expression and MAPK/ERK pathway activation.

The success of such trials is exemplified by studies like KEYNOTE-158, which investigated pembrolizumab for advanced cervical cancer. The results of this trial led to FDA approval, underscoring the basket trial model's potential to quickly translate genomic discoveries into clinical applications. Similarly, the study on pertuzumab and trastuzumab for HER2-positive cancers further highlights the importance of targeting specific molecular aberrations, regardless of tumor site.

Another significant finding was the inclusion of rare and pediatric cancers in the basket trial model. These populations, which often have limited treatment options due to small patient numbers and heterogeneous genetic profiles, stand to benefit from the precision medicine approach offered by basket trials. For example, the NCT03363217 study evaluating trametinib in pediatric glioma and plexiform neurofibroma highlights how basket trials can address the unmet need for effective therapies in younger populations with rare tumor types.

Basket trials have become a prominent approach in oncology, providing a valuable opportunity for patients who do not respond to standard anticancer therapies. The focus on molecular drug delivery targets differs from the traditional approach, which centers on the location of the primary tumor. The concept of molecular tumor profiling will enable cancer patients with specific molecular pathway alterations, regardless of tumor histology, to benefit from modern targeted therapies or immunotherapies. The growing trend of basket trials in oncology is promising, but further refinement in trial methodology, patient selection and biomarker-driven therapeutic development is essential to fully realize their potential.

For basket trials to be more effectively implemented in clinical practice, advancements are needed in patient selection, regulatory frameworks, data sharing, statistical analysis, and patient education. By improving access to diagnostics, fostering collaboration across disciplines and refining methodologies, basket trials can enable more targeted, personalized treatments across a wide range of diseases. With these improvements, basket trials have the potential to revolutionize clinical practice and reshape the broader landscape of precision medicine[23].

Limitations

Our study has several limitations. The systematic review included only clinical trials from recent decades, and the articles were searched exclusively in English. Additionally, some basket clinical trials may not have been registered in the ClinicalTrials.gov database.

Conclusions

The systematic review confirms that basket trials have significant potential as a clinical trial model, as evidenced by the increasing number of basket trial projects being conducted. Their effective use could lead to a deeper understanding of the pathogenesis of cancer, better assessment

of therapy effectiveness, and more personalized patient care. These trials have shown considerable promise in improving outcomes across a variety of cancer types, from common solid tumors to rare cancers and pediatric malignancies. However, for basket trials to reach their full potential, continuous efforts are needed to refine trial designs, standardize methodologies, and ensure broad global participation. With the ongoing expansion of molecular profiling and targeted therapies, basket trials are poised to play an increasingly crucial role in the future of cancer treatment. Further methodological refinements and global collaboration are essential to fully realize the potential of basket trials in advancing personalized cancer care.

Use of AI and AI-assisted technologies

During the preparation of this work the authors used OpenAI – ChatGPT in order to improve the language and readability of their paper. After using this tool, the authors reviewed and edited the content as needed and takes full responsibility for the content of the publication.

ORCID iDs

Mikołaj Bartoszkiewicz https://orcid.org/0000-0002-8728-5998
Joanna Kufel-Grabowska https://orcid.org/0000-0002-5724-9961
Paweł Burchardt https://orcid.org/0000-0003-0353-3470

References

1. La Thangue NB, Kerr DJ. Predictive biomarkers: A paradigm shift towards personalized cancer medicine. *Nat Rev Clin Oncol*. 2011;8(10):587–596. doi:10.1038/nrclinonc.2011.121
2. Woodcock J, LaVange LM. Master protocols to study multiple therapies, multiple diseases, or both. *N Engl J Med*. 2017;377(1):62–70. doi:10.1056/NEJMra1510062
3. Hirakawa A, Asano J, Sato H, Teramukai S. Master protocol trials in oncology: Review and new trial designs. *Contemp Clin Trials Commun*. 2018;12:1–8. doi:10.1016/j.conctc.2018.08.009
4. Zhou T, Ji Y. Bayesian methods for information borrowing in basket trials: An overview. *Cancers (Basel)*. 2024;16(2):251. doi:10.3390/cancers16020251
5. Chugh R, Wathen JK, Maki RG, et al. Phase II multicenter trial of imatinib in 10 histologic subtypes of sarcoma using a Bayesian hierarchical statistical model. *J Clin Oncol*. 2009;27(19):3148–3153. doi:10.1200/JCO.2008.20.5054
6. Hyman DM, Puzanov I, Subbiah V, et al. Vemurafenib in multiple nonmelanoma cancers with *BRAF* V600 mutations. *N Engl J Med*. 2015;373(8):726–736. doi:10.1056/NEJMoa1502309
7. Rezayi S, R Niakan Kalhori S, Saeedi S. Effectiveness of artificial intelligence for personalized medicine in neoplasms: A systematic review. *Biomed Res Int*. 2022;2022(1):7842566. doi:10.1155/2022/7842566
8. Renfro LA, Mandrekar SJ. Definitions and statistical properties of master protocols for personalized medicine in oncology. *J Biopharm Stat*. 2018;28(2):217–228. doi:10.1080/10543406.2017.1372778
9. West HJ. Novel precision medicine trial designs: Umbrellas and baskets. *JAMA Oncol*. 2017;3(3):423. doi:10.1001/jamaoncol.2016.5299
10. Fisher JG, Tait D, Garrett-Mayer E, et al. Cetuximab in patients with breast cancer, non-small cell lung cancer, and ovarian cancer without KRAS, NRAS, or BRAF mutations: Results from the Targeted Agent and Profiling Utilization Registry (TAPUR) study. *Target Oncol*. 2020;15(6):733–741. doi:10.1007/s11523-020-00753-7
11. Yang ES, Halabi S, Rothe M, et al. Olaparib in patients with metastatic prostate cancer with *BRCA1/2* mutation: Results from the TAPUR study. *JCO Precis Oncol*. 2023;7:e2200505. doi:10.1200/PO.22.00505
12. Chung HC, Ros W, Delord JP, et al. Efficacy and safety of pembrolizumab in previously treated advanced cervical cancer: Results from the phase II KEYNOTE-158 study. *J Clin Oncol*. 2019;37(17):1470–1478. doi:10.1200/JCO.18.01265
13. Sweeney CJ, Hainsworth JD, Bose R, et al. MyPathway human epidermal growth factor receptor 2 basket study: Pertuzumab + trastuzumab treatment of a tissue-agnostic cohort of patients with human epidermal growth factor receptor 2–altered advanced solid tumors. *J Clin Oncol*. 2024;42(3):258–265. doi:10.1200/JCO.22.02636
14. Hyman DM, Piha-Paul SA, Won H, et al. HER kinase inhibition in patients with HER2- and HER3-mutant cancers [Erratum in: *Nature*. 2019;566(7745):E11–E12. doi:10.1038/s41586-019-0974-0]. *Nature*. 2018;554(7691):189–194. doi:10.1038/nature25475
15. Oaknin A, Friedman CF, Roman LD, et al. Neratinib in patients with HER2-mutant, metastatic cervical cancer: Findings from the phase 2 SUMMIT basket trial. *Gynecol Oncol*. 2020;159(1):150–156. doi:10.1016/j.ygyno.2020.07.025
16. Perreault S, Larouche V, Tabori U, et al. A phase 2 study of trametinib for patients with pediatric glioma or plexiform neurofibroma with refractory tumor and activation of the MAPK/ERK pathway: TRAM-01. *BMC Cancer*. 2019;19(1):1250. doi:10.1186/s12885-019-6442-2
17. American Cancer Society (ACS). American Cancer Society Special section: Rare cancers in adults. Cancer facts & figures 2017. Atlanta, USA: American Cancer Society (ACS); 2017. https://www.cancer.org/content/dam/cancer-org/research/cancer-facts-and-statistics/annual-cancer-facts-and-figures/2017/cancer-facts-and-figures-2017-special-section-rare-cancers-in-adults.pdf. Accessed May 15, 2024.
18. How JA, Jazaeri AA, Soliman PT, et al. Pembrolizumab in vaginal and vulvar squamous cell carcinoma: A case series from a phase II basket trial. *Sci Rep*. 2021;11(1):3667. doi:10.1038/s41598-021-83317-7
19. Pro B, Advani R, Brice P, et al. Five-year results of brentuximab vedotin in patients with relapsed or refractory systemic anaplastic large cell lymphoma [Erratum in: *Blood*. 2018;132(4):458–459. doi:10.1182/blood-2018-05-853192]. *Blood*. 2017;130(25):2709–2717. doi:10.1182/blood-2017-05-780049
20. Kumar-Sinha C, Chinnaiyan AM. Precision oncology in the age of integrative genomics. *Nat Biotechnol*. 2018;36(1):46–60. doi:10.1038/nbt.4017
21. Heckman-Stoddard BM, Smith JJ. Precision medicine clinical trials: Defining new treatment strategies. *Semin Oncol Nurs*. 2014;30(2):109–116. doi:10.1016/j.soncn.2014.03.004
22. Collins FS, Varmus H. A new initiative on precision medicine. *N Engl J Med*. 2015;372(9):793–795. doi:10.1056/NEJMp1500523
23. Cunanan KM, Gonen M, Shen R, et al. Basket trials in oncology: A trade-off between complexity and efficiency. *J Clin Oncol*. 2017;35(3):271–273. doi:10.1200/JCO.2016.69.9751

Immunogenic mutanome of breast cancer: Advances, challenges and future directions in neoantigen-based immunotherapy

Almohanad A. Alkayyal[A,B,D–F], Nizar H. Saeedi[A,D–F], Mamdouh S. Moawadh[A,D–F]

Department of Medical Laboratory Technology, Faculty of Applied Medical Sciences, University of Tabuk, Saudi Arabia

A – research concept and design; B – collection and/or assembly of data; C – data analysis and interpretation;
D – writing the article; E – critical revision of the article; F – final approval of the article

Advances in Clinical and Experimental Medicine, ISSN 1899–5276 (print), ISSN 2451–2680 (online) *Adv Clin Exp Med*. 2026;35(2):351–359

Address for correspondence
Almohanad A. Alkayyal
E-mail: aalkayyal@ut.edu.sa

Funding sources
This work was supported by the Deputyship for Research & Innovation, Ministry of Education, Saudi Arabia (project No. 0026-1442-S).

Conflict of interest
None declared

Received on March 10, 2025
Reviewed on April 9, 2025
Accepted on May 12, 2025

Published online on August 1, 2025

Abstract

Breast cancer (BC) remains a leading cause of cancer-related mortality worldwide, underscoring the need for novel, more effective therapies. Neoantigen-based immunotherapy – which harnesses tumor-specific somatic mutations to boost immune recognition – has emerged as a particularly promising strategy. Advances in next-generation sequencing and computational immunopeptidomics now allow systematic mapping of the tumor mutanome and rapid identification of immunogenic neoantigens, enabling personalized vaccine design and more precise deployment of immune-checkpoint blockade. However, intratumor heterogeneity, immune-escape mechanisms and the often-limited intrinsic immunogenicity of individual neoepitopes continue to constrain clinical efficacy. This review synthesizes the current landscape of neoantigen-targeted immunotherapies in BC, outlines the principal obstacles to their broader impact and highlights emerging solutions – including improved epitope-prediction algorithms, multi-epitope vaccine constructs and synergistic combination regimens. A deeper understanding of the immunogenic mutanome is expected to translate into more durable and widely applicable treatments for patients with breast cancer.

Key words: breast cancer, personalized immunotherapy, neoantigens, tumor mutanome, tumor mutational burden (TMB)

Cite as
Alkayyal AA, Saeedi NH, Moawadh MS. Immunogenic mutanome of breast cancer: Advances, challenges and future directions in neoantigen-based immunotherapy. *Adv Clin Exp Med*. 2026;35(2):351–359. doi:10.17219/acem/205014

DOI
10.17219/acem/205014

Highlights

- Tumor heterogeneity, mutational burden and immune modulation dictate neoantigen immunogenicity, steering both treatment success and immune escape in breast cancer.
- Neoantigen vaccines and adoptive T cell therapies show promise but must overcome antigen loss and intratumoral diversity to achieve durable responses.
- Dual-strategy treatments that pair neoantigen targeting with checkpoint inhibitors amplify antitumor immunity, offering a path to stronger, more consistent clinical outcomes.

Introduction

Breast cancer (BC) is the most commonly diagnosed cancer in women worldwide, accounting for nearly 25% of all cancer cases.[1] Despite significant advancements in early detection and treatment, BC remains a leading cause of cancer-related mortality, particularly in cases of metastatic or recurrent disease.[1] The heterogeneity of BC, characterized by distinct molecular subtypes such as hormone receptor-positive (HR+), human epidermal growth factor receptor 2-positive (HER2+) and triple-negative BC (TNBC), poses a major challenge for the development of universally effective therapies.[2] While targeted therapies and immunotherapies have shown promise, resistance mechanisms and the immunosuppressive tumor microenvironment (TME) often limit their efficacy.[3]

In recent years, the concept of the tumor mutanome – the complete set of somatic mutations within a tumor – has emerged as a critical determinant of tumor immunogenicity.[4–6] Mutations in coding regions of the genome can give rise to neoantigens, which are novel peptides presented on the cell surface by major histocompatibility complex (MHC) class I molecules.[7] These neoantigens are recognized as foreign by the immune system, eliciting a T cell-mediated anti-tumor response.[4–7] The identification of neoantigens has opened new horizons for personalized cancer immunotherapy by offering the potential for highly specific and efficacious treatments.

The immunogenic mutanome is particularly relevant in BC, where the mutational burden varies widely across subtypes. For example, TNBC, which is associated with a higher tumor mutational burden (TMB), has been shown to harbor a greater number of neoantigens compared to HR+ BC.[8,9] This difference in mutational load may explain the observed variability in immune infiltration and response to immunotherapy among BC subtypes. However, the relationship between the mutanome and immunogenicity is complex and usually influenced by factors such as MHC diversity, T cell receptor (TCR) repertoire and the composition of the TME.[9–11]

Objectives

This review aims to examine the immunogenic mutanome of BC and its role in shaping neoantigen-targeted immunotherapy. Specifically, it: 1) Analyzes tumor-intrinsic and host factors influencing neoantigen immunogenicity and immune escape mechanisms; 2) Explores neoantigen-based therapeutic strategies, including personalized vaccines, adoptive T cell therapy and immune checkpoint inhibitors; 3) Identifies key challenges such as tumor heterogeneity, antigen loss and limitations in neoantigen prediction; 4) Discusses future directions involving antigen discovery, multi-omics biomarker integration and combination immunotherapy strategies.

Literature search strategy

This review was conducted as a narrative synthesis of recent literature on the immunogenic mutanome of BC and its implications for neoantigen-based immunotherapy. Studies were selected for their relevance, scientific impact, and contributions to neoantigen discovery, tumor immunology and therapeutic applications. The authors prioritized peer-reviewed original research, review and translational articles published in high-impact journals between 2017 and 2024. While no formal systematic search or Boolean strategy was employed, efforts were made to include a representative range of perspectives and recent advancements in the field. No statistical analyses were conducted, as this is a narrative review based on previously published studies. This is not a systematic review; however, we strived to incorporate diverse perspectives and landmark studies shaping the field of neoantigen-directed immunotherapy in BC.

The mutanome in breast cancer

Breast cancer's genomic landscape is sculpted by diverse mutational processes, including environmental exposures, DNA-repair deficiencies and endogenous cellular mechanisms.[12,13] These processes contribute to the accumulation of somatic mutations, which collectively constitute

the tumor mutanome.[12,13] The mutanome is highly variable between patients, reflecting the unique genetic and environmental factors that influence tumor development.[14,15]

Breast cancer is traditionally stratified into molecular subtypes according to the expression levels of hormone receptors – estrogen (ER) and progesterone (PR) – and the human epidermal growth factor receptor 2 (HER2).[16] These subtypes exhibit distinct mutational profiles and clinical behaviors.[17–19] For example, HR+ BCs, which account for approx. 70% of cases, are characterized by a lower TMB and a predominance of mutations in genes such as *PIK3CA* and *GATA3*.[19,20] In contrast, TNBC, which lacks expression of ER, PR and HER2, is associated with a higher TMB and mutations in genes such as *TP53* and *BRCA1/2*.[21–23] HER2+ BCs, which are driven by amplification of the *HER2* gene, exhibit intermediate TMB and a unique mutational signature.[24]

The mutational processes underlying these subtypes are influenced by both intrinsic and extrinsic factors. Endogenous processes, such as errors in DNA replication and repair, contribute to the accumulation of point mutations and small insertions/deletions.[25] Exogenous factors, such as exposure to ultraviolet (UV) radiation or tobacco smoke, can induce specific mutational signatures.[26] In BC, defects in DNA-repair pathways, especially homologous-recombination deficiency (HRD), drive genomic instability and increase TMB.[27–29]

Tumor mutational burden, defined as the total number of somatic mutations per megabase of DNA, has emerged as a key biomarker for predicting response to immunotherapy.[30] A high TMB is linked to a larger neoantigen repertoire and more robust immune infiltration, especially in cancers such as melanoma and non-small-cell lung cancer (NSCLC).[31,32] In BC, the relationship between TMB and immunogenicity is more complex, with TNBC exhibiting higher TMB and greater immune infiltration compared to HR+ BC.[33–35] However, even within TNBC, there is significant variability in TMB and immune response, highlighting the need for more precise biomarkers.[33–35]

Neoantigen discovery starts with comprehensive somatic-mutation profiling by whole-exome sequencing (WES) or whole-genome sequencing (WGS), which identify single-nucleotide variants, insertions/deletions and structural rearrangements capable of generating tumor-specific neoantigens. However, not all mutations are equally likely to generate immunogenic neoantigens.[36] The immunogenicity of a mutation depends on several factors, including its genomic location, its impact on protein structure and its capacity to be presented by MHC molecules.[37] Computational algorithms play a critical role in predicting which mutations are likely to generate neoantigens.[38] These algorithms use sequence-based and structural-based approaches to predict MHC binding affinity, peptide processing and TCR recognition.[38,39] Commonly used tools include NetMHC, NetMHCpan and MuPeXI, which integrate genomic and transcriptomic data to prioritize neoantigens for experimental validation. Despite advances in computational prediction, the accuracy of these tools remains limited by the complexity of antigen processing and presentation, as well as the diversity of MHC alleles in the human population.

Experimental validation of neoantigens is a critical step in the development of mutanome-based therapies. In vitro assays, such as MHC-peptide binding assays and T cell activation assays, are used to confirm the immunogenicity of predicted neoantigens. The in vivo tumor models including syngeneic mouse models and patient-derived xenografts (PDXs), provide additional insights into the anti-tumor activity of neoantigen-specific T cells. However, these models have limitations, particularly in mimicking the complexity of the human immune system and the TME.

Neoantigen discovery and validation

The discovery of neoantigens begins with the comprehensive genomic profiling of tumor tissue. Whole-exome sequencing remains the standard approach for detecting somatic mutations, given its focus on protein-coding regions of the genome, where most neoantigens originate.[36] However, WGS provides a more complete picture of the mutational landscape, including non-coding regions that may also contribute to neoantigen generation.[40,41]

RNA sequencing (RNA-seq) is another vital tool as it provides information on the levels of gene expression, ensuring that only mutations in certain genes are included for neoantigen prediction.[42,43] Additionally, proteomics-based approaches, such as mass spectrometry, can directly identify peptides presented on the cell surface by MHC molecules, offering a more direct assessment of neoantigen presentation.[44,45]

Despite advances in sequencing technologies, several challenges remain in accurately predicting neoantigens. One major challenge is the broad spectrum of MHC alleles in the human population.[46] Each individual expresses unique MHC molecules, which vary in their ability to bind and present specific peptides. Computational tools must account for this diversity, often requiring population-specific databases and algorithms.

Another challenge is distinguishing between clonal and subclonal mutations. Clonal mutations, present in all tumor cells, are more likely to generate neoantigens that can elicit a broad anti-tumor response. In contrast, subclonal mutations, present in only a subset of tumor cells, may contribute to immune escape and therapeutic resistance. Advanced algorithms, such as those incorporating tumor phylogeny, are being developed to address this issue.

Experimental validation is a critical step in confirming the immunogenicity of predicted neoantigens. To assess the affinity of neoantigens for MHC molecules, in vitro

approaches such as MHC–peptide binding assays are commonly utilized. T cell activation assays, including ELISpot and intracellular cytokine staining, are used to measure the ability of neoantigens to stimulate T cell responses.[47]

Although syngeneic mouse models and PDXs have been instrumental in evaluating neoantigen-specific T cell responses, they fall short in replicating the complexity of human immune–tumor interactions. Emerging humanized mouse model platforms may offer more clinically relevant insights into therapeutic efficacy in human settings.[48] Humanized mouse models, which are engrafted with human immune cells, offer a more physiologically relevant system for studying neoantigen immunogenicity.[49]

The therapeutic potential of neoantigen-based approaches in bladder cancer has been highlighted by several studies. Notably, a phase 1b trial by Ott et al. assessed the personalized neoantigen vaccine NEO-PV-01 combined with nivolumab in patients with advanced melanoma, NSCLC and bladder cancer, demonstrating safety, feasibility and immunogenicity. The study demonstrated that the regimen was safe and capable of inducing robust neoantigen-specific $CD4^+$ and $CD8^+$ T cell responses, which persisted long-term and exhibited cytotoxic potential.[50] Vaccine-induced T cells successfully trafficked to tumors, mediating tumor killing and triggering epitope spreading, an indicator of vaccine-driven tumor destruction.[50] Patients with epitope spreading had significantly longer progression-free survival (PFS), and some achieved major pathological responses (MPR), demonstrating substantial tumor reduction.[50] Similarly, a recent clinical study identified neoantigens in a patient with metastatic TNBC and used them to generate personalized T cell therapies.[51] This study demonstrated that metastatic BC is immunogenic, with most patients generating immune responses to somatic tumor mutations.[51] In this phase II trial, adoptive transfer of tumor-infiltrating lymphocytes (TILs) reactive to patient-specific neoantigens, combined with pembrolizumab, led to objective tumor regression in 3 of 6 patients, including 1 complete response lasting over 5.5 years. The majority of neoantigen-reactive TILs were $CD4^+$ T cells, highlighting a distinct immunogenic profile in BC.[51] Immune escape mechanisms, including human leukocyte antigen (HLA) loss of heterozygosity and downregulation of antigen presentation, were observed in progressing tumors.[51] These findings support personalized TIL therapy as a promising approach for treatment-refractory metastatic breast cancer (mBrCa) and warrant further investigation to enhance response rates and overcome immune resistance.[51] These findings highlight the potential of personalized neoantigen vaccination to enhance anti-tumor immunity and synergize with PD-1 blockade, supporting its development as an effective immunotherapeutic approach for metastatic solid tumors.[50] Discussed studies highlight the potential of mutanome-based therapies in BC and provide a framework for future research.

Immunogenicity of the breast cancer mutanome

Factors influencing neoantigen immunogenicity

The immunogenicity of neoantigens is governed by a dynamic interaction between tumor-intrinsic properties and host immune factors, ultimately influencing the strength and effectiveness of anti-tumor immune responses. Tumor-intrinsic factors include the binding affinity of neoantigens to MHC molecules, the stability of the peptide–MHC complex and the abundance of neoantigen presentation – all of which influence the likelihood of T cell recognition.[52,53] The efficiency of antigen processing, proteasomal cleavage, and TAP-mediated transport further modulates the availability of neoantigen peptides for immune recognition.[54] In addition, tumors may develop immune escape mechanisms, such as MHC downregulation, antigen loss variants and altered antigen-processing machinery (APM), to evade immune detection.[46] Host factors, including TCR repertoire diversity, the presence of pre-existing T cell clones and the composition of the TME, critically influence immune responses. A diverse TCR repertoire enhances the recognition of neoantigens, while pre-existing T cell clones may provide a rapid and effective immune response.[53] Nevertheless, TME exerts immunosuppressive pressure through mechanisms including regulatory T cells, myeloid-derived suppressor cells and immune checkpoint expression, thereby impairing effective anti-tumor immunity and limiting tumor eradication.[46] The interplay between TMB and TME composition determines response to immune checkpoint inhibitors and neoantigen-directed immunotherapies.[54] Mechanistically, high-affinity neoantigens and a permissive TME support strong T cell responses, while low immunogenicity and immune evasion contribute to poor immune recognition and immunotherapy resistance.[52] Understanding these factors is essential for optimizing neoantigen-based immunotherapies – such as personalized neoantigen vaccines and adoptive T cell therapies – to enhance immune recognition and overcome treatment resistance.

The TME plays a critical role in modulating the immune response to neoantigens. Immune-suppressive elements, such as regulatory T cells (Tregs), myeloid-derived suppressor cells (MDSCs) and inhibitory cytokines (e.g., tumor growth factor beta (TGF-β) and interleukin 10 (IL-10)), can dampen the anti-tumor immune response.[55,56] Conversely, the presence of TILs, particularly $CD8^+$ T cells, is associated with enhanced immunogenicity and improved clinical outcomes.[57–60]

The spatial distribution of immune cells within the TME is also important. For example, the presence of tertiary lymphoid structures (TLS), which are organized aggregates of immune cells, is associated with increased

neoantigen-specific T cell responses and better prognosis in BC.[61–64] Understanding the spatial and temporal dynamics of the TME is critical for optimizing neoantigen-based therapies.

Immune escape mechanisms

Tumors employ a variety of mechanisms to evade immune detection and destruction. One primary strategy is the downregulation or complete loss of MHC class I molecules, which prevents the presentation of tumor neoantigens to cytotoxic T lymphocytes (CTLs), thereby reducing immune recognition. Some tumors also selectively alter the APM, including defects in TAP1/TAP2 transporters, β2-microglobulin (B2M) mutations and impaired proteasomal processing, further diminishing neoantigen display.[10,65–67] Additionally, tumors upregulate immune checkpoint molecules, such as programmed death ligand 1 (PD-L1), cytotoxic T cell antigen 4 (CTLA-4), TIM-3, and LAG-3, which suppress effector T cell function by engaging inhibitory receptors on T cells, leading to T cell exhaustion and immune tolerance.[10,65–67]

Beyond checkpoint regulation, tumors also secrete immunosuppressive factors, including TGF-β, IL-10 and vascular endothelial growth factor (VEGF), which create an immunosuppressive microenvironment by recruiting Tregs and myeloid-derived suppressor cells (MDSCs), both of which dampen anti-tumor immune responses.[68] Another major mechanism of immune evasion is immunoediting, where the immune system selectively eliminates highly immunogenic tumor cells, leading to the outgrowth of less immunogenic clones with reduced or altered neoantigen expression.[69] This process, which involves clonal selection under immune pressure, results in tumors that become progressively more resistant to immune attack and less responsive to neoantigen-based therapies.[69–71]

Biomarkers of immunogenicity

Several biomarkers have been proposed to predict the immunogenicity of the BC mutanome.[72,73] These include TMB, which reflects the total number of somatic mutations in a tumor, and PD-L1 expression, a key regulator of immune evasion that influences the response to checkpoint blockade therapy.[72,73] Additionally, the presence of TILs serves as a critical indicator of immune activation and correlates with improved prognosis in BC.[74] However, these biomarkers have limitations; e.g., TMB does not always correlate with the presence of highly immunogenic neoantigens, and PD-L1 expression is subject to intratumoral heterogeneity, reducing its predictive power.[75] Emerging evidence suggests that a more comprehensive biomarker strategy is required, integrating genomic, transcriptomic and proteomic data to better characterize the immune landscape of BC.

Therapeutic strategies exploiting the mutanome

Neoantigen vaccines

Various neoantigen vaccine platforms are being explored – such as peptide-based, mRNA-based, DNA-based, and dendritic cell-based approaches – each with unique strengths and challenges. Peptide-based vaccines offer favorable safety and stability profiles but typically necessitate the use of adjuvants to elicit a robust immune response.[76] mRNA-based vaccines have gained attention due to their rapid and flexible manufacturing, but challenges remain in ensuring efficient delivery and stability.[76] DNA-based vaccines offer durable antigen expression but have lower immunogenicity and potential safety concerns related to genomic integration.[76] Dendritic cell-based vaccines leverage the body's antigen-presenting cells to elicit robust T cell responses but are complex and expensive to produce.[76] Recent studies highlight the potential of combining neoantigen vaccines with immune checkpoint inhibitors or oncolytic viruses to enhance immunogenicity and sustain anti-tumor responses.[4,76] Ongoing clinical trials are assessing the safety and efficacy of these approaches in BC, particularly in TNBC, which has a high mutational burden and greater potential for neoantigen-targeted therapies.[4] Mechanistically, the efficacy of neoantigen vaccines relies on optimal antigen selection, MHC binding affinity and T cell priming, emphasizing the need for personalized vaccine strategies to overcome immune evasion and enhance therapeutic efficacy.[76,77]

Adoptive cell therapy

Adoptive cell therapy (ACT) involves the ex vivo expansion of neoantigen-specific T cells, which are then reinfused back into the patient. This approach has shown remarkable success in other cancers, such as melanoma, and is now being explored in BC. Challenges include the identification and validation of suitable neoantigens and the optimization of T cell expansion protocols. A recent study investigates the challenges associated with expanding neoantigen-reactive TILs in solid epithelial cancers, including BC, where such cells are often rare and exhibit an exhausted phenotype.[78] Conventional TIL expansion protocols using anti-CD3 (OKT3) and high-dose IL-2 were found to reduce the frequency of neoantigen-reactive TILs, particularly in BC, due to the outgrowth of bystander T cells and further differentiation toward an exhausted state.[78] To address this limitation, the study introduces NeoExpand, a neoantigen-specific stimulation method that selectively expands neoantigen-reactive $CD4^+$ and $CD8^+$ TILs while preserving their stem-like memory phenotypes, which are crucial for sustained anti-tumor immunity.[78] In BC-derived TILs, NeoExpand facilitated

the recovery and enrichment of p53-reactive T cell clones, which were lost during conventional expansion methods.[78] These findings highlight the potential of neoantigen-specific stimulation strategies to enhance the efficacy of adoptive TIL therapy in BC by improving the expansion, persistence and functional capacity of tumor-reactive T cell populations.

Immune checkpoint inhibitors

Immune checkpoint inhibitors (ICIs), such as anti-PD-1, anti-PDL-1 and anti-CTLA-4 antibodies, have transformed the treatment landscape for several cancers. In BC, ICIs have shown efficacy in TNBC, particularly in patients with high TMB or PD-L1 expression. Combining ICIs with neoantigen-based therapies may enhance anti-tumor immunity and overcome resistance mechanisms. A study explores the role of TMB as a biomarker for predicting the response of BC to ICIs, emphasizing its limitations and potential clinical utility. While TMB reflects the number of somatic mutations per megabase, only a fraction of these mutations generate immunogenic neoantigens, limiting its predictive accuracy.[30] Breast cancer generally exhibits a low TMB, with only 5% of cases exceeding the threshold (≥10 mutations per megabase) associated with improved ICI response.[79] However, higher TMB in HER2-positive and TNBCs suggests a greater likelihood of neoantigen presentation, enhanced tumor immunogenicity and increased TILs, which can potentiate responses to checkpoint blockade.[80–82] Mechanistically, the combination of TMB with ICIs, particularly anti-PD-1/PD-L1 therapies (e.g., pembrolizumab, atezolizumab), enhances T cell activation and tumor clearance.[83] Despite these associations, TMB alone is an imperfect predictor of immunotherapy response, as factors such as neoantigen quality, HLA diversity, immune gene signatures, and the TME also influence outcomes.[83] These findings support the notion that combining TMB with complementary immune biomarkers, including PD-L1 expression, TIL density and spatial immune architecture, could refine patient selection and optimize the therapeutic benefit of checkpoint inhibitors in bladder cancer.

Limitations

Tumor heterogeneity, both within individual tumors (intratumoral heterogeneity) and across different patients (interpatient heterogeneity), adds another layer of complexity in the identification of universal neoantigens.[84] This variability limits the treatment efficacy of shared off-the-shelf neoantigen vaccines, necessitating highly personalized approaches. Additionally, clonal evolution under immune pressure can lead to the emergence of antigen-loss subclones, reducing the durability of neoantigen-targeted therapies and enabling immune escape.[85]

Developing neoantigen-based therapies requires high-throughput sequencing, computational neoantigen prediction models and experimental validation, all of which are time-consuming, costly and technically demanding.[38] Key limitations include inaccuracies in MHC-binding predictions, variable tumor antigen presentation and lack of robust preclinical models to validate neoantigen immunogenicity. These factors hinder the widespread clinical translation of neoantigen-based vaccines and adoptive cell therapies.

Additionally, the nature of neoantigen therapies as a personalized approach raises concerns regarding cost, scalability and accessibility. Efforts to develop off-the-shelf neoantigen vaccines based on publicly shared recurrent mutations and optimize mRNA-based neoantigen platforms may help improve accessibility. Furthermore, artificial intelligence (AI)-driven neoantigen discovery, validations and advancements in bioinformatics pipelines aim to streamline production to enhance patient selection. Overcoming these challenges is critical to scale up the clinical application of neoantigen-based cancer immunotherapies.

Conclusions

The integration of AI and machine learning into neoantigen prediction algorithms and software holds great promise for improving accuracy and efficiency.[86] These tools can analyze large datasets, identify patterns and prioritize neoantigens for experimental validation. Combining genomic, transcriptomic and proteomic data provides a more comprehensive understanding of neoantigen and epitope presentation along with their immunogenicity. Multi-omics approaches can identify novel neoantigens and biomarkers, guiding the development of personalized therapies. Furthermore, off-the-shelf neoantigen vaccines that target shared neoantigens expressed in multiple patients, even across different cancer indications, offer a more scalable and cost-effective alternative to personalized vaccines. These vaccines are being explored in clinical trials and have the potential to revolutionize BC immunotherapy.[87]

The immunogenic mutanome of BC represents a rich source of therapeutic targets with the potential to transform BC treatment. By leveraging advances in genomics, immunology and bioinformatics, significant strides are being made in the development of personalized immunotherapies. While challenges remain, the continued exploration of the mutanome and its interaction with the immune system holds great promise for improving outcomes for patients with BC. A multidisciplinary approach that integrates basic science, clinical data and technological innovation will be essential to fully exploit the immunogenic potential of the BC mutanome.

Consent for publication

Not applicable.

Use of AI and AI-assisted technologies

Not applicable.

ORCID iDs

Almohanad A Alkayyal https://orcid.org/0000-0001-7042-5985
Nizar H. Saeedi https://orcid.org/0000-0002-9281-1550

References

1. Arnold M, Morgan E, Rumgay H, et al. Current and future burden of breast cancer: Global statistics for 2020 and 2040. *Breast*. 2022; 66:15–23. doi:10.1016/j.breast.2022.08.010
2. Zheng M. Tumor mutation burden for predicting immune checkpoint blockade response: The more, the better. *J Immunother Cancer*. 2022;10(1):e003087. doi:10.1136/jitc-2021-003087
3. Chapdelaine AG, Sun G. Challenges and opportunities in developing targeted therapies for triple negative breast cancer. *Biomolecules*. 2023;13(8):1207. doi:10.3390/biom13081207
4. Kundu M, Butti R, Panda VK, et al. Modulation of the tumor microenvironment and mechanism of immunotherapy-based drug resistance in breast cancer. *Mol Cancer*. 2024;23(1):92. doi:10.1186/s12943-024-01990-4
5. Brito Baleeiro R, Liu P, Chard Dunmall LS, et al. Personalized neoantigen viro-immunotherapy platform for triple-negative breast cancer. *J Immunother Cancer*. 2023;11(8):e007336. doi:10.1136/jitc-2023-007336
6. Riaz N, Morris L, Havel JJ, Makarov V, Desrichard A, Chan TA. The role of neoantigens in response to immune checkpoint blockade. *Int Immunol*. 2016;28(8):411–419. doi:10.1093/intimm/dxw019
7. Arlen PM. Neoantigens in the immuno-oncology space. *Future Oncol*. 2017;13(25):2209–2211. doi:10.2217/fon-2017-0349
8. De Mattos-Arruda L, Blanco-Heredia J, Aguilar-Gurrieri C, Carrillo J, Blanco J. New emerging targets in cancer immunotherapy: The role of neoantigens. *ESMO Open*. 2019;4:e000684. doi:10.1136/esmoopen-2020-000684
9. Barroso-Sousa R, Pacífico JP, Sammons S, Tolaney SM. Tumor mutational burden in breast cancer: Current evidence, challenges, and opportunities. *Cancers (Basel)*. 2023;15(15):3997. doi:10.3390/cancers15153997
10. Xu J, Bao H, Wu X, Wang X, Shao Y, Sun T. Elevated tumor mutation burden and immunogenic activity in patients with hormone receptor-negative or human epidermal growth factor receptor 2-positive breast cancer. *Oncol Lett*. 2019;18(1):449–455. doi:10.3892/ol.2019.10287
11. Wu X, Li T, Jiang R, Yang X, Guo H, Yang R. Targeting MHC-I molecules for cancer: Function, mechanism, and therapeutic prospects. *Mol Cancer*. 2023;22(1):194. doi:10.1186/s12943-023-01899-4
12. Goodman AM, Castro A, Pyke RM, et al. MHC-I genotype and tumor mutational burden predict response to immunotherapy. *Genome Med*. 2020;12(1):45. doi:10.1186/s13073-020-00743-4
13. Chen C, Lin CJ, Pei YC, et al. Comprehensive genomic profiling of breast cancers characterizes germline-somatic mutation interactions mediating therapeutic vulnerabilities. *Cell Discov*. 2023;9(1):125. doi:10.1038/s41421-023-00614-3
14. Davis JD, Lin. DNA damage and breast cancer. *World J Clin Oncol*. 2011;2(9):329. doi:10.5306/wjco.v2.i9.329
15. Blass E, Ott PA. Advances in the development of personalized neoantigen-based therapeutic cancer vaccines. *Nat Rev Clin Oncol*. 2021; 18(4):215–229. doi:10.1038/s41571-020-00460-2
16. Yu G, He X, Li X, Wu Y. Driving neoantigen-based cancer vaccines for personalized immunotherapy into clinic: A burdensome journey to promising land. *Biomed Pharmacother*. 2022;153:113464. doi:10.1016/j.biopha.2022.113464
17. Yersal O, Barutca S. Biological subtypes of breast cancer: Prognostic and therapeutic implications. *World J Clin Oncol*. 2014;5(3):412. doi:10.5306/wjco.v5.i3.412
18. Pareja F, Bhargava R, Borges VF, et al. Unraveling complexity and leveraging opportunities in uncommon breast cancer subtypes. *NPJ Breast Cancer*. 2025;11(1):6. doi:10.1038/s41523-025-00719-w
19. Li RQ, Yan L, Zhang L, et al. Genomic characterization reveals distinct mutational landscapes and therapeutic implications between different molecular subtypes of triple-negative breast cancer. *Sci Rep*. 2024;14(1):12386. doi:10.1038/s41598-024-62991-3
20. Jönsson G, Staaf J, Vallon-Christersson J, et al. Genomic subtypes of breast cancer identified by array-comparative genomic hybridization display distinct molecular and clinical characteristics. *Breast Cancer Res*. 2010;12(3):R42. doi:10.1186/bcr2596
21. Testa U, Castelli G, Pelosi E. Breast cancer: A molecularly heterogenous disease needing subtype-specific treatments. *Med Sci (Basel)*. 2020;8(1):18. doi:10.3390/medsci8010018
22. Sukumar J, Gast K, Quiroga D, Lustberg M, Williams N. Triple-negative breast cancer: Promising prognostic biomarkers currently in development. *Exp Rev Anticancer Ther*. 2021;21(2):135–148. doi:10.1080/14737140.2021.1840984
23. Zagami P, Carey LA. Triple negative breast cancer: Pitfalls and progress. *NPJ Breast Cancer*. 2022;8(1):95. doi:10.1038/s41523-022-00468-0
24. Han Y, Rovella V, Smirnov A, et al. A *BRCA2* germline mutation and high expression of immune checkpoints in a TNBC patient. *Cell Death Discov*. 2023;9(1):370. doi:10.1038/s41420-023-01651-3
25. Verschoor N, Smid M, Jager A, Sleijfer S, Wilting SM, Martens JWM. Integrative whole-genome and transcriptome analysis of HER2-amplified metastatic breast cancer. *Breast Cancer Res*. 2023;25(1):145. doi:10.1186/s13058-023-01743-z
26. Chatterjee N, Walker GC. Mechanisms of DNA damage, repair, and mutagenesis. *Environ Mol Mutagen*. 2017;58(5):235–263. doi:10.1002/em.22087
27. Australian Pancreatic Cancer Genome Initiative, ICGC Breast Cancer Consortium, ICGC MMML-Seq Consortium, et al. Signatures of mutational processes in human cancer. *Nature*. 2013;500(7463):415–421. doi:10.1038/nature12477
28. Mekonnen N, Yang H, Shin YK. Homologous recombination deficiency in ovarian, breast, colorectal, pancreatic, non-small cell lung and prostate cancers, and the mechanisms of resistance to PARP inhibitors. *Front Oncol*. 2022;12:880643. doi:10.3389/fonc.2022.880643
29. Van Wilpe S, Tolmeijer SH, Koornstra RHT, et al. Homologous recombination repair deficiency and implications for tumor immunogenicity. *Cancers (Basel)*. 2021;13(9):2249. doi:10.3390/cancers13092249
30. Incorvaia L, Bazan Russo TD, Gristina V, et al. The intersection of homologous recombination (HR) and mismatch repair (MMR) pathways in DNA repair-defective tumors. *NPJ Precis Oncol*. 2024;8(1):190. doi:10.1038/s41698-024-00672-0
31. Sha D, Jin Z, Budczies J, Kluck K, Stenzinger A, Sinicrope FA. Tumor mutational burden as a predictive biomarker in solid tumors. *Cancer Discov*. 2020;10(12):1808–1825. doi:10.1158/2159-8290.CD-20-0522
32. Shao C, Li G, Huang L, et al. Prevalence of high tumor mutational burden and association with survival in patients with less common solid tumors. *JAMA Netw Open*. 2020;3(10):e2025109. doi:10.1001/jamanetworkopen.2020.25109
33. Ibrahim E, Diab E, Hayek R, Hoyek K, Kourie H. Triple-negative breast cancer: Tumor immunogenicity and beyond. *Int J Breast Cancer*. 2024; 2024(1):2097920. doi:10.1155/2024/2097920
34. Dieci MV, Miglietta F, Guarneri V. Immune infiltrates in breast cancer: Recent updates and clinical implications. *Cells*. 2021;10(2):223. doi:10.3390/cells10020223
35. Goldberg J, Pastorello RG, Vallius T, et al. The immunology of hormone receptor positive breast cancer. *Front Immunol*. 2021;12:674192. doi:10.3389/fimmu.2021.674192
36. Xie N, Shen G, Gao W, Huang Z, Huang C, Fu L. Neoantigens: Promising targets for cancer therapy. *Sig Transduct Target Ther*. 2023;8(1):9. doi:10.1038/s41392-022-01270-x
37. Kuriakose A, Chirmule N, Nair P. Immunogenicity of biotherapeutics: Causes and association with posttranslational modifications. *J Immunol Res*. 2016;2016:1298473. doi:10.1155/2016/1298473
38. De Mattos-Arruda L, Vazquez M, Finotello F, et al. Neoantigen prediction and computational perspectives towards clinical benefit: Recommendations from the ESMO Precision Medicine Working Group. *Ann Oncol*. 2020;31(8):978–990. doi:10.1016/j.annonc.2020.05.008
39. Dhusia K, Su Z, Wu Y. A structural-based machine learning method to classify binding affinities between TCR and peptide-MHC complexes. *Mol Immunol*. 2021;139:76–86. doi:10.1016/j.molimm.2021.07.020

40. Zhao EY, Jones M, Jones SJM. Whole-genome sequencing in cancer. *Cold Spring Harb Perspect Med*. 2019;9(3):a034579. doi:10.1101/cshperspect.a034579
41. Nguyen BQT, Tran TPD, Nguyen HT, et al. Improvement in neoantigen prediction via integration of RNA sequencing data for variant calling. *Front Immunol*. 2023;14:1251603. doi:10.3389/fimmu.2023.1251603
42. Nakagawa H, Fujita M. Whole genome sequencing analysis for cancer genomics and precision medicine. *Cancer Sci*. 2018;109(3):513–522. doi:10.1111/cas.13505
43. Tang G, Liu X, Cho M, Li Y, Tran DH, Wang X. Pan-cancer discovery of somatic mutations from RNA sequencing data. *Commun Biol*. 2024; 7(1):619. doi:10.1038/s42003-024-06326-y
44. Kote S, Pirog A, Bedran G, Alfaro J, Dapic I. Mass spectrometry-based identification of MHC-associated peptides. *Cancers (Basel)*. 2020; 12(3):535. doi:10.3390/cancers12030535
45. Huber F, Arnaud M, Stevenson BJ, et al. A comprehensive proteogenomic pipeline for neoantigen discovery to advance personalized cancer immunotherapy [published online as ahead of print on October 11, 2024]. *Nat Biotechnol*. 2024. doi:10.1038/s41587-024-02420-y
46. Lybaert L, Lefever S, Fant B, et al. Challenges in neoantigen-directed therapeutics. *Cancer Cell*. 2023;41(1):15–40. doi:10.1016/j.ccell.2022.10.013
47. Danilova L, Anagnostou V, Caushi JX, et al. The Mutation-Associated Neoantigen Functional Expansion of Specific T Cells (MANAFEST) Assay: A sensitive platform for monitoring antitumor immunity. *Cancer Immunol Res*. 2018;6(8):888–899. doi:10.1158/2326-6066.CIR-18-0129
48. Models for immuno-oncology research. *Cancer Cell*. 2020;38(2): 145–147. doi:10.1016/j.ccell.2020.07.010
49. Mian SA, Anjos-Afonso F, Bonnet D. Advances in human immune system mouse models for studying human hematopoiesis and cancer immunotherapy. *Front Immunol*. 2021;11:619236. doi:10.3389/fimmu.2020.619236
50. Ott PA, Hu-Lieskovan S, Chmielowski B, et al. A phase Ib trial of personalized neoantigen therapy plus anti-PD-1 in patients with advanced melanoma, non-small cell lung cancer, or bladder cancer. *Cell*. 2020; 183(2):347–362.e24. doi:10.1016/j.cell.2020.08.053
51. Zacharakis N, Huq LM, Seitter SJ, et al. Breast cancers are immunogenic: Immunologic analyses and a phase II pilot clinical trial using mutation-reactive autologous lymphocytes. *J Clin Oncol*. 2022;40(16): 1741–1754. doi:10.1200/JCO.21.02170
52. Gopanenko AV, Kosobokova EN, Kosorukov VS. Main strategies for the identification of neoantigens. *Cancers (Basel)*. 2020;12(10):2879. doi:10.3390/cancers12102879
53. Carri I, Schwab E, Podaza E, et al. Beyond MHC binding: Immunogenicity prediction tools to refine neoantigen selection in cancer patients. *Explor Immunol*. 2023;3:82–103. doi:10.37349/ei.2023.00091
54. Lang F, Schrörs B, Löwer M, Türeci Ö, Sahin U. Identification of neoantigens for individualized therapeutic cancer vaccines. *Nat Rev Drug Discov*. 2022;21(4):261–282. doi:10.1038/s41573-021-00387-y
55. Czajka-Francuz P, Prendes MJ, Mankan A, et al. Mechanisms of immune modulation in the tumor microenvironment and implications for targeted therapy. *Front Oncol*. 2023;13:1200646. doi:10.3389/fonc.2023.1200646
56. Giraldo NA, Sanchez-Salas R, Peske JD, et al. The clinical role of the TME in solid cancer. *Br J Cancer*. 2019;120(1):45–53. doi:10.1038/s41416-018-0327-z
57. Li F, Li C, Cai X, et al. The association between $CD8^+$ tumor-infiltrating lymphocytes and the clinical outcome of cancer immunotherapy: A systematic review and meta-analysis. *eClinicalMedicine*. 2021; 41:101134. doi:10.1016/j.eclinm.2021.101134
58. Wang J, Tian S, Sun J, Zhang J, Lin L, Hu C. The presence of tumour-infiltrating lymphocytes (TILs) and the ratios between different subsets serve as prognostic factors in advanced hypopharyngeal squamous cell carcinoma. *BMC Cancer*. 2020;20(1):731. doi:10.1186/s12885-020-07234-0
59. Sharma P, Shen Y, Wen S, et al. CD8 tumor-infiltrating lymphocytes are predictive of survival in muscle-invasive urothelial carcinoma. *Proc Natl Acad Sci U S A*. 2007;104(10):3967–3972. doi:10.1073/pnas.0611618104
60. Liang H, Huang J, Li H, et al. Spatial proximity of $CD8^+$ T cells to tumor cells predicts neoadjuvant therapy efficacy in breast cancer. *NPJ Breast Cancer*. 2025;11(1):13. doi:10.1038/s41523-025-00728-9
61. Chung SY, Yeh YC, Huang CJ, et al. Comparative impact of tertiary lymphoid structures and tumor-infiltrating lymphocytes in cholangiocarcinoma. *J Immunother Cancer*. 2025;13(1):e010173. doi:10.1136/jitc-2024-010173
62. Petroni G, Pillozzi S, Antonuzzo L. Exploiting tertiary lymphoid structures to stimulate antitumor immunity and improve immunotherapy efficacy. *Cancer Res*. 2024;84(8):1199–1209. doi:10.1158/0008-5472.CAN-23-3325
63. Li Z, Liu S, Liu D, Yang K, Xiong J, Fang Z. Multiple mechanisms and applications of tertiary lymphoid structures and immune checkpoint blockade. *J Exp Clin Cancer Res*. 2025;44(1):84. doi:10.1186/s13046-025-03318-6
64. Zou X, Lin X, Cheng H, et al. Characterization of intratumoral tertiary lymphoid structures in pancreatic ductal adenocarcinoma: Cellular properties and prognostic significance. *J Immunother Cancer*. 2023;11(6):e006698. doi:10.1136/jitc-2023-006698
65. Wang L, Geng H, Liu Y, et al. Hot and cold tumors: Immunological features and the therapeutic strategies. *MedComm*. 2023;4(5):e343. doi:10.1002/mco2.343
66. Cornel AM, Mimpen IL, Nierkens S. MHC class I downregulation in cancer: Underlying mechanisms and potential targets for cancer immunotherapy. *Cancers (Basel)*. 2020;12(7):1760. doi:10.3390/cancers12071760
67. Cui JW, Li Y, Yang Y, et al. Tumor immunotherapy resistance: Revealing the mechanism of PD-1/PD-L1-mediated tumor immune escape. *Biomed Pharmacother*. 2024;171:116203. doi:10.1016/j.biopha.2024.116203
68. Krishnamoorthy M, Gerhardt L, Maleki Vareki S. Immunosuppressive effects of myeloid-derived suppressor cells in cancer and immunotherapy. *Cells*. 2021;10(5):1170. doi:10.3390/cells10051170
69. Galassi C, Chan TA, Vitale I, Galluzzi L. The hallmarks of cancer immune evasion. *Cancer Cell*. 2024;42(11):1825–1863. doi:10.1016/j.ccell.2024.09.010
70. Zolkind P, Dunn GP, Lin T, Griffith M, Griffith OL, Uppaluri R. Neoantigens in immunotherapy and personalized vaccines: Implications for head and neck squamous cell carcinoma. *Oral Oncol*. 2017;71:169–176. doi:10.1016/j.oraloncology.2016.09.010
71. Zhang Z, Lu M, Qin Y, et al. Neoantigen: A new breakthrough in tumor immunotherapy. *Front Immunol*. 2021;12:672356. doi:10.3389/fimmu.2021.672356
72. Passaro A, Al Bakir M, Hamilton EG, et al. Cancer biomarkers: Emerging trends and clinical implications for personalized treatment. *Cell*. 2024;187(7):1617–1635. doi:10.1016/j.cell.2024.02.041
73. Jardim DL, Goodman A, De Melo Gagliato D, Kurzrock R. The challenges of tumor mutational burden as an immunotherapy biomarker. *Cancer Cell*. 2021;39(2):154–173. doi:10.1016/j.ccell.2020.10.001
74. Obeagu EI, Obeagu GU. Lymphocyte infiltration in breast cancer: A promising prognostic indicator. *Medicine (Baltimore)*. 2024;103(49): e40845. doi:10.1097/MD.0000000000040845
75. McGrail DJ, Pilié PG, Rashid NU, et al. High tumor mutation burden fails to predict immune checkpoint blockade response across all cancer types. *Ann Oncol*. 2021;32(5):661–672. doi:10.1016/j.annonc.2021.02.006
76. Zhang L, Zhou X, Sha H, Xie L, Liu B. Recent progress on therapeutic vaccines for breast cancer. *Front Oncol*. 2022;12:905832. doi:10.3389/fonc.2022.905832
77. Huff AL, Longway G, Mitchell JT, et al. CD4 T cell–activating neoantigens enhance personalized cancer vaccine efficacy. *JCI Insight*. 2023;8(23):e174027. doi:10.1172/jci.insight.174027
78. Levin N, Kim SP, Marquardt CA, et al. Neoantigen-specific stimulation of tumor-infiltrating lymphocytes enables effective TCR isolation and expansion while preserving stem-like memory phenotypes. *J Immunother Cancer*. 2024;12(5):e008645. doi:10.1136/jitc-2023-008645
79. Barroso-Sousa R, Jain E, Cohen O, et al. Prevalence and mutational determinants of high tumor mutation burden in breast cancer. *Ann Oncol*. 2020;31(3):387–394. doi:10.1016/j.annonc.2019.11.010
80. Qureshi S, Chan N, George M, Ganesan S, Toppmeyer D, Omene C. Immune checkpoint inhibitors in triple negative breast cancer: The search for the optimal biomarker. *Biomark Insights*. 2022;17:11772719221078774. doi:10.1177/11772719221078774
81. Moragon S, Hernando C, Martinez-Martinez MT, et al. Immunological landscape of HER-2 positive breast cancer. *Cancers (Basel)*. 2022; 14(13):3167. doi:10.3390/cancers14133167

82. Bai X, Ni J, Beretov J, Graham P, Li Y. Immunotherapy for triple-negative breast cancer: A molecular insight into the microenvironment, treatment, and resistance. *J Nat Cancer Center*. 2021;1(3):75–87. doi:10.1016/j.jncc.2021.06.001
83. Kossai M, Radosevic-Robin N, Penault-Llorca F. Refining patient selection for breast cancer immunotherapy: Beyond PD-L1. *ESMO Open*. 2021;6(5):100257. doi:10.1016/j.esmoop.2021.100257
84. Marusyk A, Janiszewska M, Polyak K. Intratumor heterogeneity: The Rosetta Stone of therapy resistance. *Cancer Cell*. 2020;37(4):471–484. doi:10.1016/j.ccell.2020.03.007
85. Anagnostou V, Smith KN, Forde PM, et al. Evolution of neoantigen landscape during immune checkpoint blockade in non-small cell lung cancer. *Cancer Discov*. 2017;7(3):264–276. doi:10.1158/2159-8290.CD-16-0828
86. Cai Y, Chen R, Gao S, et al. Artificial intelligence applied in neoantigen identification facilitates personalized cancer immunotherapy. *Front Oncol*. 2023;12:1054231. doi:10.3389/fonc.2022.1054231
87. Ruangapirom L, Sutivijit N, Teerapakpinyo C, Mutirangura A, Doungkamchan C. Identification of shared neoantigens in BRCA1-related breast cancer. *Vaccines (Basel)*. 2022;10(10):1597. doi:10.3390/vaccines10101597

Matrix metalloproteinases and tissue inhibitors of metalloproteinases as potential biomarkers for pulmonary arterial hypertension: A review

Wiktoria U. Kozłowska[1,A–D,F], Jakub Łomzik[1,A–D,F], Karol Kamiński[2,3,A,E,F], Remigiusz Kazimierczyk[2,A,D–F]

[1] Students' Scientific Society, Department of Cardiology, Medical University of Bialystok, Poland
[2] Department of Cardiology and Internal Medicine with Cardiac Intensive Care Unit, Medical University of Bialystok, Poland
[3] Department of Population Medicine and Lifestyle Diseases Prevention, Medical University of Bialystok, Poland

A – research concept and design; B – collection and/or assembly of data; C – data analysis and interpretation;
D – writing the article; E – critical revision of the article; F – final approval of the article

Advances in Clinical and Experimental Medicine, ISSN 1899–5276 (print), ISSN 2451–2680 (online) *Adv Clin Exp Med*. 2026;35(2):361–376

Address for correspondence
Remigiusz Kazimierczyk
E-mail: remigiuszk1989@gmail.com

Funding sources
None declared

Conflict of interest
None declared

Received on February 7, 2025
Reviewed on April 5, 2025
Accepted on May 8, 2025

Published online on August 1, 2025

Abstract

Pulmonary arterial hypertension (PAH) is a rare and progressive syndrome that is frequently diagnosed at an advanced stage due to the nonspecific nature of its symptoms. Current research aims to identify novel diagnostic tools, including biomarkers, to facilitate earlier detection and differentiation of pulmonary hypertension (PH) subtypes. Matrix metalloproteinases (MMPs) play a critical role in the pathogenesis of PAH through extracellular matrix (ECM) remodeling, with their activity tightly regulated by tissue inhibitors of metalloproteinases (TIMPs). This review summarizes existing studies on the potential of MMPs and TIMPs as biomarkers for PAH. Our analysis highlights significant differences in MMP concentrations between PAH patients and healthy controls. In particular, MMP-2, MMP-7 and MMP-9 exhibit promising prognostic value, which could contribute to risk stratification and support clinical decision-making in the future. However, large-scale, randomized prospective studies involving well-characterized patient cohorts are necessary to confirm their clinical utility and clarify their mechanistic roles in PAH pathogenesis.

Key words: prognosis, biomarkers, pulmonary hypertension, tissue inhibitors of metalloproteinases, metalloproteinases

Cite as
Kozłowska WU, Łomzik J, Kamiński K, Kazimierczyk R. Matrix metalloproteinases (MMPs) and tissue inhibitors of metalloproteinases (TIMPs) as potential biomarkers for pulmonary arterial hypertension: A review. *Adv Clin Exp Med*. 2026;35(2):361–376. doi:10.17219/acem/204831

DOI
10.17219/acem/204831

Highlights

- Late-stage pulmonary arterial hypertension (PAH) diagnosis delays treatment: Nonspecific symptoms often result in advanced disease at presentation, worsening prognosis.
- Matrix metalloproteinases (MMPs) and tissue inhibitors (TIMPs) as PAH biomarkers: Emerging evidence positions MMP/TIMP profiling for early detection and prognostic assessment.
- MMP-2, MMP-7 and MMP-9 show the strongest prognostic value in PAH: These specific MMPs outperform others in predicting disease progression and patient outcomes.
- Significant biomarker concentration differences distinguish PAH from other pulmonary hypertension types: Multiple studies confirm diagnostic specificity for MMP/TIMP levels.
- Prospective studies are crucial to validate MMP/TIMP profiling in PAH: Ongoing research aims to integrate these biomarkers into clinical diagnostic and prognostic workflows.

Introduction

Pulmonary arterial hypertension (PAH) is a progressive disorder marked by dysregulated endothelial-derived vasoactive factors, chronic inflammation and structural remodeling of the pulmonary vasculature.[1] These pathological changes ultimately contribute to right ventricular (RV) failure.[2] Hemodynamically, PAH is defined by a mean pulmonary arterial pressure (mPAP) >20 mm Hg, pulmonary vascular resistance (PVR) >2 Wood units and pulmonary arterial wedge pressure (PAWP) ≤15 mm Hg, as determined by right heart catheterization (RHC).[3,4]

Despite the growing number of available treatment options, the management of PAH remains a significant clinical challenge worldwide. Identifying novel biomarkers is essential for enhancing diagnostic accuracy and recognizing patient subgroups at higher risk of poor outcomes. Among the various molecular pathways implicated in PAH, matrix metalloproteinases (MMPs) and their endogenous inhibitors – tissue inhibitors of metalloproteinases (TIMPs) – represent a promising area of ongoing research. A deeper understanding of these molecules may offer valuable insights into disease pathogenesis and help guide the development of future therapeutic strategies.

Objectives

This review synthesizes current evidence on the role of MMPs and TIMPs in PAH, with a focus on their implications for pathophysiology and their utility as biomarkers of this disease.

Methodology

A comprehensive literature search was conducted using the PubMed and Scopus electronic databases from their inception through July 31, 2024. The search strategy incorporated Medical Subject Headings (MeSH) terms, including "pulmonary arterial hypertension metalloproteinases" and "pulmonary arterial hypertension biomarkers." A total of 3,231 potentially relevant articles were initially identified. All manuscripts were independently screened by 2 reviewers. Studies were excluded based on the following criteria: 1) not relevant to the selected topic, 2) case reports, 3) non-English language publications, 4) duplicate records, 5) lack of full-text availability, 6) animal studies, and 7) pediatric studies. After applying these exclusion criteria, 22 manuscripts were deemed eligible for inclusion in the analysis.

Interplay between MMPs and TIMPs

Matrix metalloproteinases are a family of zinc-dependent endoproteases that play a central role in the degradation and remodeling of extracellular matrix (ECM) components.[5,6] Their activity is tightly regulated through several mechanisms, including modulation of gene expression,[7] activation of proenzymes,[8] inhibition by TIMPs,[9] subcellular compartmentalization,[10] and formation of protein complexes.[11] Most MMPs are not constitutively expressed; rather, their transcription is induced in response to proinflammatory cytokines such as tumor necrosis factor alpha (TNF-α), interleukin 1 (IL-1) and various growth factors.[12,13]

Additionally, certain MMPs are stored in the granules of inflammatory cells, thereby restricting their enzymatic activity to specific microenvironments.[14] Dysregulated MMP expression and activity have been implicated in the pathogenesis of various diseases, particularly cardiovascular disorders.[15,16] These endoproteases are initially synthesized as pre-proMMPs; during translation, the signal peptide is cleaved to produce the latent proMMP form. In this inactive state, the cysteine residue within the propeptide maintains coordination with a Zn^{2+} ion at the catalytic site through the "cysteine switch" mechanism, thereby preventing enzymatic activity. Activation

occurs when this switch is disrupted, typically via proteolytic cleavage by enzymes such as serine proteases, furin endopeptidases, plasmin, or other MMPs.[13,17]

The expression and activity of MMPs are tightly regulated by TIMPs.[18] The TIMPs are the principal endogenous inhibitors of the MMP family, exhibiting varying inhibitory efficacy against different MMPs, along with distinct patterns of tissue expression and regulatory control.[19] This family comprises 4 members – TIMP-1 through TIMP-4.[6,14] Despite their relatively small size, TIMPs serve multiple biochemical and physiological functions, including inhibition of active MMPs, activation of proMMPs, promotion of cell proliferation, matrix binding, and regulation of angiogenesis and apoptosis.[14,20] The TIMPs are distributed across various cellular compartments: TIMP-1, -2, -3, and -4 can localize to the cell surface; TIMP-3 is also found in the ECM; and TIMP-1, -2 and -4 can exist in soluble forms. This spatial diversity enables TIMPs to modulate a broad range of cellular signaling pathways.[19]

The TIMPs are composed of 2 adjacent domains, each stabilized by 3 intramolecular disulfide bonds. The N-terminal domain, referred to as the "inhibitory domain", is primarily responsible for MMP inhibition, as it alone is sufficient to suppress MMP activity. The highly conserved core epitope within this domain – centered around the N-terminal strand and characterized by a "Cys-X-Cys" motif – forms the principal interaction site with the catalytic domain of MMPs. This binding involves coordination with the catalytic zinc ion at the MMP active site, effectively blocking the substrate-binding cleft.[21,22] In addition to TIMPs, other molecules, such as α2-macroglobulin and amyloid β precursor protein, have also been identified as inhibitors of MMP activity.[23,24]

The balance between MMPs and TIMPs largely influences the ECM composition, which tightly regulates MMP activity.[25] Published evidence suggests that MMPs may contribute to the pathophysiology of PAH.[26,27] The early pathological progression of PAH primarily involves endothelial cells (ECs) and smooth muscle cells (SMCs) in the vascular wall, as well as pulmonary artery smooth muscle cells (PASMCs).[28,29] The PASMCs are critically involved in disease advancement.[30] The pathological state of PASMCs is associated with PASMC phenotypic switching.[28]

Several mechanisms have been proposed as potential initiating events in PAH, including increased blood flow and shear stress, hypoxia, inflammation, oxidative stress, and altered bone morphogenetic protein receptor 2 signaling. These factors lead to endothelial/mesenchymal transition, in which ECs adopt a mesenchymal phenotype and express gene profiles characteristic of SMCs.[28,31] In fact, phenotypic switching is an early vascular self-repair mechanism in response to stimulation.[1] During this process, ECs lose their intercellular junctions and detach from the intimal monolayer. Subsequently, they migrate into the medial layer, where they undergo dedifferentiation into myofibroblast-like mesenchymal cells.[25] These cells exhibit increased secretion of α-smooth muscle actin, collagen, vimentin, and MMPs, as well as serine elastases and lysyl oxidases, while simultaneously showing reduced expression of their endogenous inhibitors, including TIMPs.[25,31,32] Myofibroblast-like cells contribute to ECM remodeling through enhanced collagen deposition and cross-linking.[25]

Oxidative stress, exacerbated by inflammation, has also been implicated in MMP dysregulation. Reactive oxygen species (ROS) generated in response to inflammation have been shown to increase MMP secretion while downregulating TIMP expression in SMCs, ECs and fibroblasts. Furthermore, pro-inflammatory cytokines stimulate the recruitment and activation of macrophages and neutrophils, which subsequently secrete MMPs and serine elastases. The degradation products of collagen and elastin generated by heightened proteolytic activity exhibit pro-inflammatory properties, thereby sustaining inflammation through a positive feedback loop.[25,33]

Notably, the upregulation of MMP-1 and MMP-9 has been observed, enhancing the migratory capacity of adventitial fibroblasts.[34] Deregulation of MMPs has been implicated in multiple pathological processes, including ECs and SMCs migration, hyperplasia, adventitial fibroblast transdifferentiation, increased ECM turnover, and inflammatory cell recruitment. These changes collectively contribute to increased vascular stiffness, preceding abnormal pulmonary arterial pressure and elevated PVR.[25] Additionally, ECM degradation products and growth factors further stimulate MMP secretion,[25] exacerbating vascular remodeling in small to medium-sized pulmonary vessels, ultimately leading to RV hypertrophy and right-sided heart failure (HF).[35]

Due to the non-specificity of the symptoms, PAH is frequently diagnosed at a late stage.[36] At present, the only routinely used clinical markers that correlate with myocardial stress and provide prognostic information are brain natriuretic peptide and N-terminal pro B-type natriuretic peptide (NT-proBNP).[3,37] However, these are not specific to pulmonary hypertension (PH), as they can be elevated in other heart diseases, showing significant variability.[3] Research is now focusing on identifying new diagnostic methods, including biomarkers that allow for prognosis, diagnosis and differentiation of PH subtypes.[38] Among the compounds under investigation are MMPs and their inhibitors, which may potentially fulfil this role.

Metalloproteinases

Matrix metalloproteinase 1

Matrix metalloproteinase 1 (MMP-1), a collagenase-1, acts on various substrates, including collagen types I, II, III, VII, VIII, and X, as well as gelatin, aggrecan, casein, nidogen, serpins, versican, perlecan, proteoglycan link protein, and tenascin-C.[26,39] Its expression is stimulated by high

glucose levels in cultured ECs and macrophages[40] and by C-reactive protein (CRP).[41] Pulmonary arterial hypertension is often associated with glucose metabolism disorders,[42,43] and increased concentrations of this molecule in the lungs of PAH patients,[42] but unchanged circulating levels have been observed.[44] Furthermore, inflammation has been implicated in the pathophysiology of PAH,[33] including its role in pulmonary vascular remodeling,[45] as reflected by elevated CRP levels in PAH patients.[46]

Functionally, MMP-1 has been shown to induce the expression of a subset of proangiogenic genes in human microvascular ECs.[47] Furthermore, it enhances vascular endothelial growth factor receptor-2 (VEGF-2) expression and ECs proliferation via protease-activated receptor 1 (PAR-1)[48] signaling, a mechanism that may also contribute to pulmonary arterial vasoconstriction.[49]

Elevated serum concentrations of MMP-1 have been demonstrated in PAH patients.[27,50] Additionally, when monocytes were isolated, M1-polarized macrophages from PAH patients, but not from healthy controls, exhibited significantly higher MMP-1 protein levels compared to M0 and M2-polarized macrophages. Immunohistochemical assessment of lung tissue from PAH patients showed notably increased MMP-1 immunoreactivity compared to control samples.[27] However, quantitative real-time polymerase chain reaction (qPCR) analysis has not revealed significant differences in *MMP-1* transcript expression between cells obtained from lung tissue from patients with idiopathic PAH (IPAH) during lung transplantation and samples from lobectomy of patients with localized lung cancer.[51] Similarly, no difference in *MMP-1* expression has been observed between pulmonary arteries of IPAH patients and downsized non-tumorous, non-transplanted donor lungs used as controls.[52]

Matrix metalloproteinase 2

Matrix metalloproteinase 2 (MMP-2), a member of the gelatinase subfamily of MMPs, degrades a broad range of substrates, including collagen types I, IV, V, VII, X, XI, XIV, as well as gelatin, aggrecan, elastin, fibronectin, laminin, nidogen, proteoglycan link protein, and versican.[39,53] This MMP directly affects various cellular functions by modulating the activity of biologically active molecules or interacting with cell surface receptors.[54] It is secreted as an inactive proenzyme, which undergoes activation via membrane type 1-matrix metalloproteinase (MT1-MMP). This process is tightly regulated by TIMP-2 at the cell surface at the site where activation is required.[55] Several alternative pathways for MT1-MMP-dependent of MMP-2 have been described, involving proteases such as neutrophil elastase, cathepsin G, proteinase-3,[56] and plasmin.[57] In addition to these pathways, a TIMP-independent activation route has been described, mediated by MT1-MMP and claudin-5.[58] Furthermore, the generation of ROS by nicotinamide adenine dinucleotide phosphate oxidase, induced by mechanical stretch, increases *MMP-2* messenger RNA (mRNA) expression and pro-MMP-2 release.[59]

A significantly elevated concentration of MMP-2 has been demonstrated in patients with PAH compared to the control group of healthy volunteers.[60] Comparable results were observed in individuals with PH, where 19 out of 36 individuals included in the analysis were diagnosed with IPAH or associated PAH (APAH).[61] Plasma circulating levels of MMP-2 were substantially increased in PH patients compared to healthy controls.[61] Remodeling biomarkers, including MMP-2, and NT-proBNP, did not show significant differences in concentration between patients with PAH and those with other forms of PH.[61] A study investigating patients with PH, including IPAH, PAH associated with connective tissue disease (PAH-CTD), chronic thromboembolic PH (CTEPH), PH due to left heart disease (PH-LHD), and non-PH controls (individuals suspected of PH who underwent RHC and had a mPAP <25 mm Hg), demonstrated that mean plasma circulating levels of MMP-2 were significantly higher in PAH-CTD and PH-LHD patients compared to non-PH controls.[62] Furthermore, in PH patients, MMP-2 concentrations exhibited a weak but statistically significant correlation with cardiac output, PAWP and 6-minute walking distance (6MWD). Next, patients with plasma MMP-2 levels in the 1st (below 176 ng/mL) and 2nd quartiles (176–206 ng/mL) had significantly better 5-year survival and time to clinical worsening (TTCW) than those in the 4th quartile (≥246 ng/mL).[62] These findings were further confirmed by Arvidsson et al., who linked elevated serum MMP-2 concentrations to an unfavorable prognosis in PAH.[63] Increased circulating MMP-2 levels at the time of diagnosis correlated with higher European Society of Cardiology (ESC) and European Respiratory Society (ERS) risk scores, as well as with mean right atrial pressure, NT-proBNP, and 6MWD, indicating worsening right heart function and reduced exercise capacity. MMP-2 was identified as a valuable negative prognostic marker.[63]

Moreover, Karamanian et al. presented a study based on plasma analyses in PAH patients and healthy volunteers, in which it was shown that MMP-2 circulating levels were elevated in the plasma of non-IPAH patients, but not in the plasma of IPAH patients.[64]

Studies were also conducted on pulmonary artery tissue from patients undergoing lung transplantation for IPAH and from patients treated by lobectomy for localized lung cancer, who served as controls. In cultured PASMCs derived from patients with IPAH, MMP-2 activity is elevated, attributable to both elevated total MMP-2 expression and a higher proportion of its active form. In situ zymography and immunolocalization showed that MMP-2 was associated with SMCs and elastic fibers. Furthermore, in the arteries of IPAH patients, pronounced gelatinolytic activity and MMP-2 immunostaining were observed along the internal elastic lamina, extending even to its disruption.[51] In contrast, the latent MMP-2 levels in IPAH cells remained indistinguishable from those in control cells.[51] Conversely, another study

reported no significant variation in *MMP-2* expression levels in the pulmonary arteries of IPAH patients.[52]

A notable observation in one study was the elevated concentration of circulating $CD34^+CD133^+$ bone marrow-derived proangiogenic precursors in the peripheral blood of IPAH patients compared to healthy controls, with levels correlating with PAP. However, resident endothelial progenitor levels in the pulmonary arteries of IPAH patients were comparable to those in the control group. Colony-forming units of ECs derived from $CD34^+CD133^+$ bone marrow precursors of IPAH patients exhibited increased MMP-2 secretion, a greater affinity for angiogenic tube formation, and a tendency to form disorganized cell clusters spontaneously.[65]

Notably, no significant differences in pro-MMP-2 content were found between PAH patients and those with chronic obstructive pulmonary disease or CTEPH. Additionally, no correlation was observed between pro-MMP-2 levels and PH severity indices.[66]

Concerning patients with systemic sclerosis-associated PAH (PAH-SSc), MMP-2 concentrations were significantly higher compared to the group of systemic sclerosis (SSc) patients without elevated pulmonary pressure.[67] Another study involving 35 SSc patients, of whom 12 had PAH, found that MMP-2 circulating levels were similar in SSc patients with or without PAH.[68]

Matrix metalloproteinase 3

Matrix metalloproteinase 3 (MMP-3), or stromelysin-1, is involved in the degradation of various ECM components, including matrix proteins, growth factors, proteases, surface receptors, and adhesion molecules. Notably, this metalloproteinase can activate various pro-MMPs, making the synthesis and activation of MMP-3 a fundamental initiating event in the MMP-mediated degradation process.[26,69]

Cells derived from IPAH patients demonstrated a marked reduction in MMP-3 production compared to control cells obtained from lung tissue excised during lobectomy for localized lung cancer in 6 individuals. Additionally, immunostaining for MMP-3 was detected exclusively in the media of pulmonary arteries in the control group.[51] These findings are further supported by another study,[60] which reported significantly lower serum MMP-3 concentrations in PAH patients compared to other subgroups of PH: CTEPH, PH due to HF with preserved ejection fraction (HFpEF-PH), PH due to HF with reduced ejection fraction (HFrEF-PH), and HF without PH (HF-NON-PH).[60]

Matrix metalloproteinase 7

Matrix metalloproteinase 7 (MMP-7) belongs to the matrilysins, which lack a hemopexin domain and act on many cell surface molecules.[26] It is responsible for the degradation of collagen types I, II, III, V, IV, and X, aggrecan, casein, elastin, enactin, laminin, and proteoglycan link protein.[39] Matrix metalloproteinase 7 degrades recombinant and native soluble vascular endothelial growth factor receptor-1 (sVEGFR-1), leading to the release of vascular endothelial growth factor (VEGF) from sequestration by sVEGFR-1. In vitro assays demonstrate that MMP-7 promotes VEGF-driven angiogenesis by degrading sVEGFR-1, which otherwise sequesters VEGF and inhibits its activity. Additionally, this metalloproteinase releases VEGF from sVEGFR-1 secreted by human ECs, providing a regulatory mechanism for VEGF bioavailability within the local endothelial microenvironment.[70] Elevated concentrations of MMP-7 have been observed in comparison with healthy volunteers without RHC; however, these levels remain lower than those measured in other patient groups (CTEPH, HFpEF-PH, HFrEF-PH, and HF-NON-PH). Receiver operating characteristic (ROC) analysis of plasma MMP-7 concentrations in PAH compared to other PH groups and HF-NON-PH showed an area under the curve (AUC) of 0.75, with a sensitivity of 58.7% and specificity of 83.3%.[60] It is noteworthy that plasma levels of MMP-7 increase with age,[71] and patients with PAH were generally the oldest among the assessed PH groups. Nevertheless, relatively lower concentrations of MMP-7 were noted compared to other disease groups.[60] Arvidsson et al.[60] further demonstrated that plasma MMP-7 can differentiate PAH from other causes of dyspnea, including HF with or without PH, as well as from healthy controls, suggesting its potential utility as a novel diagnostic biomarker.

Matrix metalloproteinase 8

Matrix metalloproteinase 8 (MMP-8), a neutrophil-derived collagenase-2, is critically involved in the degradation of ECM components, targeting collagen types I, II, III, V, VII, VIII, and X, as well as gelatin, aggrecan, laminin, and nidogen.[39] It is one of the MMPs participating in stem/progenitor cell mobilization and recruitment in blood vessel formation and vascular remodeling.[26] Additionally, MMP-8 counteracts pathological mechanobiological feedback by modifying matrix composition and disrupting integrin-β3/FAK and YAP/TAZ-dependent mechanical signaling in PASMCs.[72]

Dieffenbach et al. conducted a study involving a diverse group of patients, including those with IPAH and APAH, which they categorized into a combined group of patients with PAH, PH, and healthy volunteers. Their findings revealed that the mean plasma concentration of MMP-8 was 18 times higher in PAH patients compared to controls. Furthermore, immunofluorescence staining demonstrated increased MMP-8 expression in PASMCs and the pulmonary endothelium of PAH patients relative to the control group.[72]

Matrix metalloproteinase 9

Matrix metalloproteinase 9 (MMP-9), a gelatinase-B enzyme, is responsible for the degradation of collagen types IV, V, VII, X, and XIV, fibronectin, laminin, nidogen,

proteoglycan link protein, and versican.[39] Its secretion is stimulated by high glucose levels.[40] Notably, a reduction in the number of NK cells has been observed in PAH lung tissue, accompanied by functional impairments and overexpression of MMP-9.[73] Elevated circulating levels of MMP-9 have been detected in the plasma of individuals with PAH,[60,74] suggesting a potential role in pulmonary vascular remodeling. Furthermore, for IPAH, study results are inconsistent, showing both increased levels of MMP-9[64,75] and unchanged concentrations.[62] Moreover, no statistical correlation was found between plasma MMP-9 levels and hemodynamic parameters or 6MWD, and no statistically meaningful association with survival was detected.[62]

It is of particular relevance that MMP-9 may be produced by macrophages.[76] Chi et al. examined monocytes isolated from PAH patients and healthy donors, differentiating them into M0, M1 or M2 macrophage phenotypes. After differentiation with macrophage colony-stimulating factor into macrophages (M0), *MMP-9* mRNA expression was significantly upregulated in PAH patients compared to controls. Similarly, *MMP-9* mRNA levels were elevated in M0 and M1 macrophages derived from PAH patients relative to their counterparts in the control group.[27]

In a subset of patients with PAH related to PAH-CTD and PAH associated with congenital heart disease (PAH-CHD), circulating levels of examined compounds, including MMP-9, were high and did not significantly differ from concentrations in patients with idiopathic, hereditary and anorexigenic PAH. These results suggest that elevated concentrations are markers of disease presence rather than markers of PAH etiology.[74] Gene expression profiling of peripheral blood mononuclear cells from patients with IPAH, PAH-SSc, and healthy controls identified MMP-9-related genes, which were further analyzed using RT-PCR. This analysis revealed a clinically significant upregulation of these genes in patients with mild PAH compared to healthy controls, whereas no differences were observed in those with severe PAH.[77] Interestingly, circulating MMP-9 concentrations were found to be higher in SSc patients without PAH than in those with PAH involvement.[68] Vascular remodeling in CHD-associated APAH and IPAH, as well as in donor lung tissue, was analyzed for mRNA and protein expression patterns. Changes in vascular tissue demonstrated increased mRNA levels of *MMP-9* in comparison with adjacent remodeled pulmonary arteries. While plexiform lesions in IPAH and APAH demonstrated only minor differences in remodeling-associated gene regulation, *MMP-9* expression was upregulated in APAH compared to adjacent arteries, with a similar but statistically nonsignificant trend observed in IPAH. Importantly, hemodynamic parameters, including mPAP and PVR values measured prior to lung transplantation, had no effect on remodeling-associated gene expression in plexiform lesions.[78]

Pro-MMP-9 levels in circulating monocytes were found to correlate with key indices of severity of PH-induced cardiac failure but not with PVR or mPAP, suggesting a link between the pro-MMP-9 content of circulating monocytes and HF rather than pulmonary artery remodeling. Subgroup analysis further demonstrated that pro-MMP-9 was lower in patients with HF, defined by a right atrial pressure (P_{ra}) >8 mm Hg and a cardiac index (CI) <2.5 L/min/m^2, than in patients without HF.[66]

Matrix metalloproteinase 10

Matrix metalloproteinase 10 (MMP-10), a stromelysin-2 enzyme, acts on various substrates, including collagen types III, IV, V, gelatin, fibronectin, laminin, nidogen,[39] and participates in pro-MMPs proteolysis.[26] Increased serum concentrations of MMP-10 have been observed in PAH patients compared to healthy controls, with strong expression detected in the media and adventitia of human pulmonary arteries.[27] Notably, MMP-10 expression was significantly reduced in the intima and media, as well as in perivascular tissue, of pulmonary arteries from IPAH patients. To explore the potential prognostic significance of regulated collagens and collagen-processing enzymes, circulating levels of MMP-10 were compared between donors and patients with IPAH. Both groups showed similar concentrations of MMP-10.[52]

Matrix metalloproteinase 12

Matrix metalloproteinase 12 (MMP-12), a macrophage metalloelastase,[39] is involved in macrophage infiltration during inflammation. By facilitating macrophage migration across basement membranes, this enzyme enables their recruitment to inflamed tissues, thereby amplifying and sustaining the inflammatory cascade.[79] Notably, circulating MMP-12 concentrations were significantly elevated in patients with PAH compared to the control group.[60]

Matrix metalloproteinase 19

The catalytic domain of matrix metalloproteinase 19 (MMP-19) exhibits proteolytic activity against a broad spectrum of ECM components, including collagen type IV, laminin, nidogen, large tenascin-C isoform, fibronectin, gelatin type I in vitro. These findings suggest its potential involvement in ECM remodeling.[13,80] Matrix metalloproteinase 19 is inhibited by TIMP-3 and, to a lesser extent, TIMP-1. Its expression was significantly elevated only in the intima + media of IPAH vessels compared to donor vessels.[52]

Table 1 summarizes the studies discussed above regarding the potential utility of MMPs as biomarkers for PAH. The table includes the PAH subtype and the number of patients enrolled in each study.

Table 1. Summary of research on matrix metalloproteinase (MMP) concentrations in pulmonary arterial hypertension (PAH)

Molecule	Studied groups	Sample	Groups size	Change in concentration	Reference
MMP-1	PAH	plasma lung tissue	$n_{PAH} = 39$ $n_{HealthyControl} = 30$	Increase in PAH compared to the control.	Chi et al., 2022[27]
	IPAH PAH-SSc	plasma lung tissue	$n_{IPAH} = 27$ $n_{PAH\text{-}SSc} = 27$ $n_{HealthyControl} = 6$	Increase in IPAH and PAH-SSc compared to the control.	Mickael et al., 2022[50]
	IPAH	lung tissue	$n_{IPAH} = 5$ $n_{LungCancerControl} = 6$	No difference between groups.	Lepetit et al., 2005[51]
	IPAH	lung tissue	$n_{IPAH} = 20$ $n_{LungDonorControl} = 22$	No difference between groups.	Hoffmann et al., 2015[52]
MMP-2	IPAH	lung tissue	$n_{IPAH} = 5$ $n_{LungCancerControl} = 6$	Increase in IPAH compared to the control.	Lepetit et al., 2005[51]
	IPAH	lung tissue	$n_{IPAH} = 20$ $n_{LungDonorControl} = 22$	No difference between groups.	Hoffmann et al., 2015[52]
	PAH CTEPH HFpEF-PH HFrEF-PH	plasma	$n_{PAH} = 48$ $n_{CTEPH} = 20$ $n_{HFpEF\text{-}PH} = 33$ $n_{HFrEF\text{-}PH} = 36$ $n_{HF\text{-}NON\text{-}PH} = 15$ $n_{HealthyControl} = 20$	Increase in PAH and PH groups (CTEPH, HFpEF-PH, HFrEF-PH) compared to the control.	Arvidsson et al., 2019[60]
	IPAH APAH group 2 PH group 3 PH CTEPH	plasma	$n_{IPAH} = 16$ $n_{APAH} = 3$ $n_{Group2PH} = 2$ $n_{Group3PH} = 4$ $n_{CTEPH} = 11$ $n_{HealthyControl} = 44$	Increase in PH groups (IPAH, APAH, group 2 and 3 PH, CTEPH) compared to the control.	Schumann et al., 2010[61]
	IPAH PAH-CTD CTEPH PH-LHD	plasma	$n_{IPAH} = 42$ $n_{PAH\text{-}CTD} = 42$ $n_{CTEPH} = 43$ $n_{PH\text{-}LHD} = 33$ $n_{Non\text{-}PHControl} = 44$	Increase in PAH-CTD and PH-LHD compared to the non-PH control.	Tiede et al., 2016[62]
	IPAH HPAH PAH-SSc PPHTN DPAH PAH-CHD	plasma	$n_{IPAH} = 58$ $n_{HPAH} = 5$ $n_{PAH\text{-}SSc} = 15$ $n_{SLE\text{-}PAH} = 3$ $n_{PPHTN} = 13$ $n_{DPAH} = 6$ $n_{PAH\text{-}CHD} = 5$ $n_{HealthyControl} = 51$	Increase in PAH groups (without IPAH) compared to the control.	Karamanian et al., 2014[64]
	PAH-SSc	plasma	$n_{PAH\text{-}SSc} = 77$ $n_{SSc\text{-}non\text{-}PHControl} = 80$	Increase in PAH-SSc compared to the control.	Bauer et al., 2021[67]
	PAH-SSc	plasma	$n_{PAH\text{-}SSc} = 12$ $n_{SSc\text{-}non\text{-}PAH} = 23$	No difference between groups.	Giannelli et al., 2005[68]
Pro-MMP-2	IPAH PPHTN PAH-CHD anorexigen associated PAH PH-COPD CTEPH	lung tissue	$n_{IPAH} = 2$ $n_{PPHTN} = 1$ $n_{PAH\text{-}CHD} = 2$ $n_{Anorexigen\ associatedPAH} = 3$ $n_{PH\text{-}COPD} = 6$ $n_{CPTE} = 3$	No difference between groups.	Cantini-Salignac et al., 2006[66]
MMP-3	IPAH	lung tissue	$n_{IPAH} = 5$ $n_{LungCancerControl} = 6$	Decrease in IPAH compared to the control.	Lepetit et al., 2005[51]
	PAH CTEPH HFpEF-PH HFrEF-PH	plasma	$n_{PAH} = 48$ $n_{CTEPH} = 20$ $n_{HFpEF\text{-}PH} = 33$ $n_{HFrEF\text{-}PH} = 36$ $n_{HF\text{-}NON\text{-}PH} = 15$ $n_{HealthyControl} = 20$	Decrease in PAH compared to PH groups (CTEPH, HFpEF-PH, HFrEF-PH).	Arvidsson et al., 2019[60]
MMP-7	IPAH	lung tissue	$n_{IPAH} = 20$ $n_{LungDonorControl} = 22$	No difference between groups.	Hoffmann et al., 2015[52]
	PAH CTEPH HFpEF-PH HFrEF-PH	plasma	$n_{PAH} = 48$ $n_{CTEPH} = 20$ $n_{HFpEF\text{-}PH} = 33$ $n_{HFrEF\text{-}PH} = 36$ $n_{HF\text{-}NON\text{-}PH} = 15$ $n_{HealthyControl} = 20$	Increase in PH groups (PAH, CTEPH, HFpEF-PH, HFrEF-PH) compared to the control.	Arvidsson et al., 2019[60]

Table 1. Summary of research on matrix metalloproteinase (MMP) concentrations in pulmonary arterial hypertension (PAH) – cont.

Molecule	Studied groups	Sample	Groups size	Change in concentration	Reference
MMP-8	IPAH APAH group 2 PH group 3 PH group 4 PH	plasma lung tissue	$n_{IPAH} = 10$ $n_{APAH} = 7$ $n_{Group2PH} = 1$ $n_{Group3PH} = 19$ $n_{Group4PH} = 2$ $n_{HealthyControl} = 12$	Increase in PAH (IPAH, APAH) compared to the PH groups (group 2, 3, 4 PH) and the control.	Dieffenbach et al., 2021[72]
MMP-9	PAH	lung tissue	$n_{PAH} = 39$ $n_{HealthyControl} = 30$	Increase in PAH compared to the control.	Chi et al., 2022[27]
	PAH CTEPH HFpEF-PH HFrEF-PH	plasma	$n_{PAH} = 48$ $n_{CTEPH} = 20$ $n_{HFpEF-PH} = 33$ $n_{HFrEF-PH} = 36$ $n_{HF-NON-PH} = 15$ $n_{HealthyControl} = 20$	Increase in PH groups (PAH, CTEPH, HFpEF-PH, HFrEF-PH) compared to the control.	Arvidsson et al., 2019[60]
	IPAH PAH-CTD CTEPH PH-LHD	plasma	$n_{IPAH} = 42$ $n_{PAH-CTD} = 42$ $n_{CTEPH} = 43$ $n_{PH-LHD} = 33$ $n_{Non-PHControl} = 44$	No difference between groups.	Tiede et al., 2016[62]
	IPAH HPAH PAH-SSc PPHTN DPAH PAH-CHD	plasma	$n_{IPAH} = 58$ $n_{HPAH} = 5$ $n_{PAH-SSc} = 15$ $n_{SLE-PAH} = 3$ $n_{PPHTN} = 13$ $n_{DPAH} = 6$ $n_{PAH-CHD} = 5$ $n_{HealthyControl} = 51$	Increase in PAH groups (IPAH, HPAH, PAH-SSc, PPHTN, DPAH, PAH-CHD) compared to the control.	Karamanian et al., 2014[64]
	PAH-SSc	plasma	$n_{PAH-SSc} = 12$ $n_{SSc-non-PAH} = 23$	Decrease in PAH-SSc compared to the SSc-non-PAH.	Giannelli et al., 2005[68]
	IPAH anorexigen associated PAH HPAH	plasma	$n_{PAH} = 68$ $n_{HealthyControl} = 37$	Increase in PAH (IPAH, HPAH, Anorexigen associated PAH) compared to the control.	Safdar et al., 2014[74]
	IPAH CVD-PAH	plasma	$n_{IPAH} = 42$ $n_{CVD-PAH} = 2$	Increase in IPAH compared to the manufacturer -supplied reference.	Hiremath et al., 2010[75]
	IPAH PAH-SSc	plasma	$n_{IPAH} = 9$ $n_{PAH-SSc} = 10$ $n_{HealthyControl} = 5$	Increase in mild PAH (WHO I & II IPAH and PAH-SSc) compared to the control.	Grigoryev et al., 2008[77]
Pro-MMP-9	IPAH PPHTN PAH-CHD anorexigen associated PAH PH-COPD CPTE	lung tissue	$n_{IPAH} = 2$ $n_{PPHTN} = 1$ $n_{PAH-CHD} = 2$ $n_{AnorexigenassociatedPAH} = 3$ $n_{PH-COPD} = 6$ $n_{CPTE} = 3$	No difference between groups.	Cantini-Salignac et al., 2006[66]
MMP-10	PAH	lung tissue plasma	$n_{PAH} = 39$ $n_{HealthyControl} = 30$	Increase in PAH compared to the control.	Chi et al., 2022[27]
	IPAH	plasma	$n_{IPAH} = 40$ $n_{LungDonorControl} = 40$	No difference between groups.	Hoffmann et al., 2015[52]
	IPAH	lung tissue	$n_{IPAH} = 20$ $n_{LungDonorControl} = 22$	Decrease in IPAH compared to the control.	Hoffmann et al., 2015[52]
MMP-12	PAH CTEPH HFpEF-PH HFrEF-PH	plasma	$n_{PAH} = 48$ $n_{CTEPH} = 20$ $n_{HFpEF-PH} = 33$ $n_{HFrEF-PH} = 36$ $n_{HF-NON-PH} = 15$ $n_{HealthyControl} = 20$	Increase in PH groups (PAH, CTEPH, HFpEF-PH, HFrEF-PH) compared to the control.	Arvidsson et al., 2019[60]
MMP-19	IPAH	lung tissue	$n_{IPAH} = 20$ $n_{LungDonorControl} = 22$	Increase in IPAH compared to the control.	Hoffmann et al., 2015[52]

APAH – associated pulmonary arterial hypertension; PAH-CHD – congenital heart disease pulmonary arterial hypertension; CPTE – chronic pulmonary thromboembolism; CTEPH – chronic thromboembolic pulmonary hypertension; CVD-PAH – collagen vascular disease pulmonary arterial hypertension; DPAH – drug- and toxin-associated pulmonary arterial hypertension; HF-NON-PH – heart failure without pulmonary hypertension; HFpEF-PH – pulmonary hypertension due to heart failure with preserved ejection fraction; HFrEF-PH – pulmonary hypertension due to heart failure with reduced ejection fraction; HPAH – heritable pulmonary arterial hypertension; IPAH – idiopathic pulmonary arterial hypertension; PAH-CTD – pulmonary arterial hypertension associated with connective tissue diseases; PAH-SSc – systemic sclerosis-associated pulmonary arterial hypertension; PH – pulmonary hypertension; PH-COPD – chronic obstructive pulmonary disease-associated pulmonary hypertension; PH-LHD – pulmonary hypertension due to left heart disease; PPHTN – portopulmonary hypertension; SLE-PAH – systemic lupus erythematosus-associated pulmonary arterial hypertension.

Tissue inhibitors of metalloproteinase

Tissue inhibitor of metalloproteinase 1

Tissue inhibitors of metalloproteinase 1 (TIMP-1) have been shown to exhibit multiple functions in regulating biological processes such as cell growth, apoptosis and differentiation.[81] Independent of its metalloproteinase inhibitory activity, it exerts these effects through the activation of p38, mitogen-activated protein kinase and c-Jun N-terminal kinase.[82] The inhibitor suppresses the activity of most MMPs.[83] Furthermore, plasma TIMP-1 correlates with markers of left ventricular diastolic filling and serves as a potential noninvasive marker of fibrosis.[84] Notably, its circulating concentrations increase with age and are higher in males, individuals who smoke and those with diabetes.[85] While TIMPs exhibit limited specificity towards individual MMPs, TIMP-1 preferentially binds to MMP-9,[86] and their levels indicate a positive correlation.[87]

Higher concentrations of circulating TIMP-1 have been reported in the blood of PAH patients compared to age- and sex-matched healthy controls.[62,74,88] In a subset of patients with PAH-CTD and PAH-CHD, circulating levels of TIMP-1 were high but did not differ significantly from those in individuals with idiopathic, hereditary and anorexigenic PAH.[74] In a study focusing on patients with limited systemic sclerosis (lSSc), increases in TIMP-1 were found compared to healthy controls. It is worth emphasizing that the concentration of this molecule was higher in lSSc patients with PAH (PAH-lSSc) compared to those without PAH, underscoring its relevance as a biomarker for PAH-lSSc.[89]

An imbalance between MMP and TIMP was identified in cultured PASMCs derived from patients with IPAH through increased expression of TIMP-1. Immunostaining for this compound was observed in pulmonary arteries obtained from both control individuals and patients with IPAH. Furthermore, the same study showed a reduction in MMP-3 expression. This imbalance between MMP-3 and TIMP-1 may be responsible for promoting ECM accumulation.[51] Notably, a significant correlation was observed between TIMP-1 and PAWP as well as the 6MWD. TIMP-1 plasma concentrations also increased with the rising New York Heart Association (NYHA) functional class. Moreover, patients with TIMP-1 plasma circulating levels above the median exhibited significantly lower 5-year survival and a higher risk of death compared to those with concentrations below the median. This molecule demonstrates prognostic potential in the described cohort.[62] In opposition to previous results, MMP-2/TIMP-1 and MMP-9/TIMP-1 ratios did not correlate with hemodynamic or clinical parameters, such as mPAP, PAWP, CI, or PVR, in IPAH patients.[90] Multianalyte profiling analysis revealed increased circulating TIMP-1 levels in both IPAH and non-IPAH patients compared to healthy controls. Variations in inhibitor concentrations were observed across patient subgroups, with the highest levels detected in IPAH patients.[64] In contrast to the aforementioned studies, *TIMP-1* expression was reduced in the intima and media of pulmonary artery profiles from IPAH patient lungs, and its blood levels did not differ significantly between PAH patients and healthy volunteers.[52] In the intima+media of IPAH vessels, collagens (COL4A5, COL14A1 and COL18A1), MMP-19 and a disintegrin and metalloprotease (ADAM) 33 were higher expressed, whereas MMP-10, ADAM17, TIMP1, and TIMP3 were less abundant.

Tissue inhibitor of metalloproteinase 2

Tissue inhibitor of metalloproteinase 2 (TIMP-2) is constitutively expressed in most tissues, but it is not inducible by growth factors.[19] This inhibitor exhibits antiangiogenic and antiapoptotic activities.[20] In addition to inhibiting most MMPs, it also suppresses a disintegrin and metalloproteinase 12 (ADAM12).[91] A key function of TIMP-2 is its participation in the formation of the ternary complex responsible for proMMP-2 activation at the cell surface.[92]

In IPAH, no significant alterations in TIMP-2 expression were detected in cultured PASMCs; however, increased TIMP-2 transcript expression was observed in PASMCs from IPAH patients compared to controls.[51] Moreover, no differences in *TIMP-2* expression were found between the lung tissue of patients with IPAH and the control group.[52] In a study focused on patients with lSSc, RT-PCR confirmed an increased expression of 9 genes, including *TIMP-2*, in PAH-lSSc patients. A significant difference in *TIMP-2* expression was noted between the PAH-lSSc and lSSc without PAH samples, which persisted between these groups even after excluding patients with extensive pulmonary fibrosis or mildly elevated pulmonary capillary wedge pressure. This suggests that these PAH biomarkers are not primarily caused by pulmonary fibrosis or HF.[89]

Tissue inhibitor of metalloproteinase 3

Tissue inhibitor of metalloproteinase 3 (TIMP-3) is distinguished by its ability to bind directly to ECM proteins, potentially stabilizing MMP-TIMP complexes within the interstitial space.[32] It has the broadest range of substrates, including MMPs,[19,93] as well as several ADAMs: ADAM-17 (TNF-α-converting enzyme),[19] ADAM-10, ADAM-12,[9] and a disintegrin and metalloproteinase with thrombospondin motifs (ADAMTSs): ADAMTS-4 and ADAMTS-5.[94] An increase in TIMP-3 levels and the quantity of this protein in lung tissue from patients with IPAH has been observed compared to normal lung tissue. The majority of MMP inhibitor expression in the lungs is likely attributable to SMCs of the bronchi and pulmonary artery, as well as adult pulmonary fibroblasts. *TIMP-3* expression has also been documented in lung ECs, ECs from placental microvessels and umbilical

veins, and non-adherent blood-derived cell lines.[95] In contrast to these findings, significantly lower gene expression of the aforementioned inhibitor was reported in the perivascular tissue of IPAH patients.[52] TIMP3 expression was significantly lower in perivascular tissue of IPAH patients.

Tissue inhibitor of metalloproteinase 4

Tissue inhibitor of metalloproteinase 4 (TIMP-4) is the largest identified human MMP inhibitor[96] and has been associated with inflammation in cardiovascular disease, suggesting its potential role as a systemic biomarker of vascular inflammatory activity. Beyond its ability to inhibit MMPs, TIMP-4 also suppresses ADAM28.[97] Elevated circulating TIMP-4 levels have been observed in patients with increased pulmonary artery systolic pressure measurements on echocardiography among patients with SSc, where pulmonary artery systolic pressure is considered elevated if it reaches or exceeds 40 mm Hg.[98]

In healthy individuals, plasma TIMP-4 concentrations are not influenced by sex or age.[60] Schumann et al. confirmed that plasma TIMP-4 concentrations were significantly elevated in PH patients compared with healthy age- and sex-matched volunteers. The remodeling biomarkers, including TIMP-4, were not statistically significantly different between PAH and other forms of PH.[61] The concentration of the metalloproteinase inhibitor was significantly higher in patients with PAH compared to the control group.[60] This contradicted findings by Tiede et al., where mean circulating levels of TIMP-4 in plasma were notably lower in patients with IPAH compared with non-PH controls and patients with PH-LHD.[62] These discrepancies may be attributable to differences in study populations; the first cited included both IPAH and PAH-SSc patients. Additionally, TIMP-4 exhibited modest yet significant correlations with mPAP, PAWP, PVR, and 6MWD,[62] and its elevated concentrations are associated with unfavorable prognosis in PAH.[63] No differences in *TIMP-4* expression were found in the pulmonary arteries between IPAH patients and the control group.[52] Within a subgroup selected from the previously mentioned cohort,[62] the MMP2/TIMP-4 ratio was assessed, which showed a notable correlation with mPAP, PVR, estimated glomerular filtration rate (eGFR), and tricuspid annular plane systolic excursion, while MMP9/TIMP-4 showed significant correlation with mPAP and eGFR. Moreover, MMP2/TIMP-4 demonstrated considerable results in the ROC analysis predicting death and cardiovascular events.[90]

ADAM, ADAMTS and ADAMTSL

The equilibrium between ECM degradation and remodeling is regulated not only by MMPs but also by a disintegrin and metalloproteinases (ADAMs) and ADAMTSs,[92] which are proteases closely related to MMPs.[99] These molecules carry MMP and disintegrin-like domains, giving them the properties of both proteases and adhesion molecules.[100,101] Crucially, they can also be inhibited by TIMPs.[14] ADAMTS8 has been implicated in PAH pathogenesis and RV failure, along with the expansion of PASMCs, ECM remodeling and endothelial dysfunction in an autocrine/paracrine manner.[102]

In a cohort of patients with IPAH, no significant differences in *ADAMTS1* and *ADAMTS13* expression were observed when compared to healthy volunteers.[52] Upregulation of ADAMTS8 has been demonstrated in areas of α-smooth muscle actin, along with increased levels of this compound in the lungs of patients with PAH. Furthermore, RT-PCR has shown that the *ADAMTS8* gene is more strongly expressed in PASMCs from PAH patients (PAH-PASMCs) than in control PASMCs. Notably, no significant difference in the expression of this protease was observed between control pulmonary artery endothelial cells (PAEC) and those from patients with pulmonary arterial hypertension (PAH-PAEC). Moreover, the expression levels were comparable in both PAH-PAEC and PAH-PASMCs.[102] These findings indicate that ADAMTS8 upregulation in PASMCs may contribute to the pathogenesis of PAH through PASMCs proliferation and migration, increased MMP activity and mitochondrial dysfunction.[103]

In patients with IPAH, no differences in ADAMTS13 expression were found compared to healthy controls, although the pulmonary embolism group exhibited slightly lower concentrations. Additionally, there was no correlation with sex or ethnic identity.[104] Plasma samples from patients with incidentally diagnosed untreated PAH, as well as those with CTEPH, HFpEF, and a control population with dyspnea or HF without PH (dyspnea/HF-non-PH), were analyzed, alongside samples from 20 healthy controls. In contrast to previous reports, ADAMTS13 concentrations were significantly lower in PAH patients compared to individuals with CTEPH, HFpEF-PH, HFrEF-PH, dyspnea/HF-non-PH, and healthy controls. No differences were observed between subgroups analyzing IPAH and SSc-PAH. Furthermore, a correlation between ADAMTS13 levels and PAWP was established. The study concluded that using a multifactorial logistic regression model, incorporating age- and sex-adjusted ADAMTS13 concentrations, effectively differentiated PAH patients from other dyspnea-related disease groups, achieving AUC of 0.91, with a sensitivity of 87.5% and specificity of 78.4%.[105]

In a study on ADAMTSL4, Li et al.[106] confirmed that plasma ADAMTSL4 protein concentrations were significantly elevated in patients with IPAH and CTEPH compared to healthy controls. It is noteworthy that the AUC for ADAMTSL4 was 0.947 for the PH group (IPAH and CTEPH combined) and 0.981 for the IPAH subgroup. Furthermore, plasma ADAMTSL4 concentrations exhibited a positive correlation with mPAP.

ADAM-10 and ADAM-17 play a critical role in the inflammatory response by promoting the release of pro-inflammatory

cytokines, such as TNF-α and IL-6, from peripheral blood macrophages and ECs.[107] ADAM33 is involved in promoting angiogenesis, as well as stimulating cell proliferation and differentiation.[108] No changes in *ADAM10* expression were found in the media or intima of pulmonary arteries in patients with IPAH, but a significant reduction in expression of *ADAM17* and upregulation of *ADAM33* was observed.[52] Additionally, plasma ADAM33 concentrations remained unchanged in IPAH patients compared to controls.[52]

Table 2 provides a summary of the studies examining the potential role of TIMPs as biomarkers in PAH. It outlines the PAH subtype investigated and the corresponding number of patients included in each study.

Discussion

The described compounds offer promising possibilities for more advanced diagnosis and for assessing prognosis in this challenging condition. Metalloproteinases exert a fundamental role in the pathogenesis of PAH through ECM remodeling. The concentrations of specific MMPs differ significantly between PAH patients and healthy individuals. Particularly, MMP-2, MMP-7 and MMP-9 exhibit considerable prognostic potential, which may help in clinical decisions in the future. Furthermore, TIMP-1 and TIMP-2, when assessed in conjunction with a panel of 7 additional circulating proteins, have been shown to effectively identify PAH patients at high risk of mortality.[109] A potential biomarker, it can refer not only to the concentration of a particular molecule but also to their proportion to one another, for instance, MMP-2/TIMP-4 and MMP-9/TIMP-4, which correlate with clinical outcomes. In addition, manuscripts have shown differences in biomarker concentrations between PAH and other causes of PH. These findings, along with comparisons of biomarker concentrations between PAH and other causes of PH, have been drawn from Table 1 and Table 2, which summarize and contrast the referenced studies. Notably, the small sample sizes in many studies, an inherent limitation given

Table 2. Summary of research on tissue inhibitor of metalloproteinases (TIMPs), A disintegrin and metalloproteinase (ADAM) and ADAM with thrombospondin motifs (ADAMTS) concentrations in pulmonary arterial hypertension (PAH)

Molecule	Studied groups	Sample	Group size	Change in concentration	Reference
TIMP-1	IPAH	lung tissue	$n_{IPAH} = 5$ $n_{LungCancerControl} = 6$	Increase in IPAH compared to the control.	Lepetit et al., 2005[51]
	IPAH	plasma	$n_{IPAH} = 40$ $n_{LungDonorControls} = 40$	No difference between groups.	Hoffmann et al., 2015[52]
	IPAH	lung tissue	$n_{IPAH} = 20$ $n_{LungDonorControls} = 22$	Decrease in IPAH compared to the control.	Hoffmann et al., 2015[52]
	IPAH PAH-CTD CTEPH PH-LHD	plasma	$n_{IPAH} = 42$ $n_{PAH-CTD} = 42$ $n_{CTEPH} = 43$ $n_{PH-LHD} = 33$ $n_{Non-PHControl} = 44$	Increase in PAH-CTD compared to the CTEPH and control.	Tiede et al., 2016[62]
	IPAH HPAH PAH-SSc PPHTN DPAH PAH-CHD	plasma	$n_{IPAH} = 58$ $n_{HPAH} = 5$ $n_{PAH-SSc} = 15$ $n_{SLE-PAH} = 3$ $n_{PPHTN} = 13$ $n_{DPAH} = 6$ $n_{PAH-CHD} = 5$ $n_{HealthyControl} = 51$	Increase in PAH groups (IPAH, HPAH, PAH-SSc, PPHTN, DPAH, PAH-CHD) compared to the control.	Karamanian et al., 2014[64]
	IPAH anorexigen-associated PAH HPAH	plasma	$n_{PAH} = 68$ $n_{HealthyControl} = 37$	Increase in PAH (IPAH, HPAH, anorexigen associated PAH) compared to the control.	Safdar et al., 2014[74]
	IPAH CTD-PAH	plasma	$n_{IPAH} = 12$ $n_{CTD-PAH} = 3$ $n_{HealthyControl} = 10$	Increase in PAH (IPAH, CTD-PAH) compared to the control.	Fenster et al., 2016[88]
	PAH-ISSc	plasma	$n_{-PAH-ISSc} = 15$ $n_{ISSc-noPAH} = 21$ $n_{HealthyControl} = 10$	Increase in PAH-ISSc compared to the ISSc-noPAH and control.	Pendergrass et al., 2010[89]
TIMP-2	IPAH	lung tissue	$n_{IPAH} = 5$ $n_{LungCancerControl} = 6$	No difference between groups.	Lepetit et al., 2005[51]
	IPAH	lung tissue	$n_{IPAH} = 20$ $n_{LungDonorControls} = 22$	No difference between groups.	Hoffmann et al., 2015[52]
	PAH-ISSc	plasma	$n_{PAH-ISSc} = 15$ $n_{ISSc-noPAH} = 21$ $n_{HealthyControl} = 10$	Increase in PAH-ISSc compared to the ISSc-noPAH and control.	Pendergrass et al., 2010[89]

Table 2. Summary of research on tissue inhibitor of metalloproteinases (TIMPs), A disintegrin and metalloproteinase (ADAM) and ADAM with thrombospondin motifs (ADAMTS) concentrations in pulmonary arterial hypertension (PAH) – cont.

Molecule	Studied groups	Sample	Group size	Change in concentration	Reference
TIMP-3	IPAH	lung tissue	$n_{IPAH} = 20$ $n_{LungDonorControls} = 22$	Decrease in IPAH compared to the control.	Hoffmann et al., 2015[52]
	IPAH	lung tissue	$n_{IPAH} = 4$ $n_{HealthyControl} = 4$	Increase in IPAH compared to the control.	Edgar et al., 2006[95]
TIMP-4	IPAH	lung tissue	$n_{IPAH} = 20$ $n_{LungDonorControls} = 22$	No difference between groups.	Hoffmann et al., 2015[52]
	PAH CTEPH HFpEF-PH HFrEF-PH	plasma	$n_{PAH} = 48$ $n_{CTEPH} = 20$ $n_{HFpEF-PH} = 33$ $n_{HFrEF-PH} = 36$ $n_{HF-NON-PH} = 15$ $n_{HealthyControl} = 20$	Increase in PAH and PH groups (CTEPH, HFpEF-PH, HFrEF-PH) compared to the control.	Arvidsson et al., 2019[60]
	IPAH APAH group 2 PH group 3 PH CTEPH	plasma	$n_{IPAH} = 16$ $n_{APAH} = 3$ $n_{Group2PH} = 2$ $n_{Group3PH} = 4$ $n_{CTEPH} = 11$ $n_{HealthyControl} = 44$	Increased in PH groups (IPAH, APAH, group 2 and 3 PH, CTEPH) compared to the control.	Schumann et al., 2010[61]
	IPAH PAH-CTD CTEPH PH-LHD	plasma	$n_{IPAH} = 42$ $n_{PAH-CTD} = 42$ $n_{CTEPH} = 43$ $n_{PH-LHD} = 33$ $n_{Non-PHControl} = 44$	Decrease in IPAH compared to the non-PH control and PH-LHD.	Tiede et al., 2016[62]
ADAMTS1	IPAH	lung tissue	$n_{IPAH} = 20$ $n_{LungDonorControls} = 22$	No difference between groups.	Hoffmann et al., 2015[52]
ADAMTS8	PAH	lung tissue	$n_{PAH} = 6$ $n_{ControlPASMCs} = 5$	Increase in PAH compared to the control.	Omura et al., 2019[102]
ADAMTS13	IPAH	lung tissue	$n_{IPAH} = 20$ $n_{LungDonorControls} = 22$	No difference between groups.	Hoffmann et al., 2015[52]
	CTEPH CTED IPAH PE	plasma	$n_{CTEPH} = 208$ $n_{CTED} = 35$ $n_{IPAH} = 30$ $n_{PE} = 28$ $n_{HealthyControl} = 68$	No difference between IPAH and the control.	Newnham et al., 2019[104]
	IPAH FPAH PAH-SSc PAH-CTD CTEPH HFpEF-PH HFrEF-PH	plasma	$n_{IPAH} = 21$ $n_{FPAH} = 2$ $n_{PAH-SSc} = 21$ $n_{PAH-CTD} = 4$ $n_{CTEPH} = 20$ $n_{HFpEF-PH} = 31$ $n_{HFrEF-PH} = 36$ $n_{HFrEF} = 8$ $n_{HFpEF} = 7$ $n_{HealthyControl} = 20$	Decrease in PAH (IPAH, FPAH, PAH-SSc, PAH-CTD) compared to the CTEPH, HFpEF-PH, HFrEF-PH and control.	Ahmed et al., 2021[105]
ADAMTSL4	IPAH	plasma	$n_{IPAH} = 8$ $n_{HealthyControl} = 9$	Increase in IPAH compared to the control.	Li et al., 2023[106]
ADAM10	IPAH	lung tissue	$n_{IPAH} = 20$ $n_{LungDonorControls} = 22$	No difference between groups.	Hoffmann et al., 2015[52]
ADAM17	IPAH	lung tissue	$n_{IPAH} = 20$ $n_{LungDonorControls} = 22$	Decrease in IPAH compared to the control.	Hoffmann et al., 2015[52]
ADAM33	IPAH	lung tissue	$n_{IPAH} = 20$ $n_{LungDonorControls} = 22$	Increase in IPAH compared to the control.	Hoffmann et al., 2015[52]
	IPAH	plasma	$n_{IPAH} = 40$ $n_{LungDonorControls} = 40$	No difference between groups.	Hoffmann et al., 2015[52]

APAH – associated pulmonary arterial hypertension; PAH-CHD – congenital heart disease pulmonary arterial hypertension; CPTE – chronic pulmonary thromboembolism; CTEPH – chronic thromboembolic pulmonary hypertension; CVD-PAH – collagen vascular disease pulmonary arterial hypertension; DPAH – drug- and toxin-associated pulmonary arterial hypertension; HF-NON-PH – heart failure without pulmonary hypertension; HFpEF-PH – pulmonary hypertension due to heart failure with preserved ejection fraction; HFrEF-PH – pulmonary hypertension due to heart failure with reduced ejection fraction; HPAH – heritable pulmonary arterial hypertension; IPAH – idiopathic pulmonary arterial hypertension; PAH-CTD – pulmonary arterial hypertension associated with connective tissue diseases; PAH-SSc – systemic sclerosis-associated pulmonary arterial hypertension; PH – pulmonary hypertension; PH-COPD – chronic obstructive pulmonary disease-associated pulmonary hypertension; PH-LHD – pulmonary hypertension due to left heart disease; PPHTN – portopulmonary hypertension; SLE-PAH – systemic lupus erythematosus-associated pulmonary arterial hypertension.

the rarity of PAH, present challenges in formulating clinically valid conclusions. Furthermore, a significant proportion of investigations have relied on lung tissue samples, restricting the practical application of potential biomarkers due to the invasive nature of tissue sampling. Future research should prioritize less-invasive biomarkers to facilitate broader clinical implementation.

Phenotypic switching, which plays a unique and pivotal role in the initiation of PAH, is considered a critical early marker of pulmonary vascular remodeling and disease progression.[28] Identifying biomarkers capable of capturing the onset of PAH could enable risk stratification and facilitate earlier therapeutic intervention. Emerging therapies, such as sotatercept, have been shown to improve quality of life and potentially extend survival in patients with PAH. A delay of 2 years in initiating sotatercept therapy could result in a loss of 4.1 life years per patient,[110] underscoring the essential requirement for early diagnosis and treatment initiation.

Advancements in the understanding of MMPs and their inhibitors have contributed to the identification of novel therapeutic targets for PAH. Lercanidipine, a vasoselective dihydropyridine calcium channel blocker, has demonstrated potential clinical benefits in PAH by reducing serum MMP-9 levels and improving survival without affecting proMMP-2 activity or TIMP-1 levels.[111] Meanwhile, the endogenous elastase inhibitor – elafin – has been postulated to exert protective effects against PAH by suppressing MMP-9 activity. Experimental models of PAH have consistently shown increased elastase activity, and elafin is now progressing through clinical evaluation, with initial trials assessing its safety and tolerability in healthy volunteers.[112]

Limitations

Our analysis was limited to 2 databases, which may have restricted the number of studies identified. However, PubMed and Scopus are the 2 largest databases primarily focused on medical research, ensuring broad coverage of relevant literature. The screening process was conducted independently by 2 reviewers, who subsequently compared the included studies, thereby minimizing the risk of selection bias. All studies meeting the inclusion criteria were considered, which resulted in variability in sample sizes and PAH subtypes included. These differences were systematically presented in tables, allowing for a more objective comparison of the reported findings.

Conclusions

These findings highlight the pivotal role of MMP-related pathways in the pathophysiology of PAH and suggest that targeted modulation of these mechanisms may offer promising therapeutic avenues. However, to determine the clinical applicability of MMP-targeted therapies and their potential to alter disease progression, rigorous evaluation through prospective, controlled trials is essential. Large-scale studies are required to validate these initial observations, with particular emphasis on the standardization of biomarker measurement protocols – including sample collection, processing and analytical methods – to ensure reproducibility and comparability across research settings. As our understanding of PAH deepens, the integration of validated biomarker assessments into clinical practice may enhance patient outcomes through more precise, personalized therapeutic strategies.

Use of AI and AI-assisted technology

Not applicable.

ORCID iDs

Wiktoria U. Kozłowska https://orcid.org/0009-0003-0362-0336
Jakub Łomzik https://orcid.org/0009-0009-9676-3400
Karol Kamiński https://orcid.org/0000-0002-9465-2581
Remigiusz Kazimierczyk https://orcid.org/0000-0003-4517-1498

References

1. Schermuly RT, Ghofrani HA, Wilkins MR, Grimminger F. Mechanisms of disease: Pulmonary arterial hypertension. *Nat Rev Cardiol*. 2011;8(8):443–455. doi:10.1038/nrcardio.2011.87
2. Naeije R, Richter MJ, Rubin LJ. The physiological basis of pulmonary arterial hypertension. *Eur Respir J*. 2022;59(6):2102334. doi:10.1183/13993003.02334-2021
3. Humbert M, Kovacs G, Hoeper MM, et al. 2022 ESC/ERS Guidelines for the diagnosis and treatment of pulmonary hypertension. *Eur Heart J*. 2022;43(38):3618–3731. doi:10.1093/eurheartj/ehac237
4. Maron BA. Revised definition of pulmonary hypertension and approach to management: A clinical primer. *JAHA*. 2023;12(8):e029024. doi:10.1161/JAHA.122.029024
5. Löffek S, Schilling O, Franzke CW. Biological role of matrix metalloproteinases: A critical balance. *Eur Respir J*. 2011;38(1):191–208. doi:10.1183/09031936.00146510
6. Visse R, Nagase H. Matrix metalloproteinases and tissue inhibitors of metalloproteinases: Structure, function, and biochemistry. *Circ Res*. 2003;92(8):827–839. doi:10.1161/01.RES.0000070112.80711.3D
7. Yan C, Boyd DD. Regulation of matrix metalloproteinase gene expression. *J Cell Physiol*. 2007;211(1):19–26. doi:10.1002/jcp.20948
8. Murphy G, Stanton H, Cowell S, et al. Mechanisms for pro matrix metalloproteinase activation. *APMIS*. 1999;107(1–6):38–44. doi:10.1111/j.1699-0463.1999.tb01524.x
9. Ramnath N, Creaven PJ. Matrix metalloproteinase inhibitors. *Curr Oncol Rep*. 2004;6(2):96–102. doi:10.1007/s11912-004-0020-7
10. Mannello F, Medda V. Nuclear localization of matrix metalloproteinases. *Prog Histochem Cytochem*. 2012;47(1):27–58. doi:10.1016/j.proghi.2011.12.002
11. Hadler-Olsen E, Fadnes B, Sylte I, Uhlin-Hansen L, Winberg J. Regulation of matrix metalloproteinase activity in health and disease. *FEBS J*. 2011;278(1):28–45. doi:10.1111/j.1742-4658.2010.07920.x
12. Zitka O, Kukacka J, Krizkov S, et al. Matrix metalloproteinases. *Curr Med Chem*. 2010;17(31):3751–3768. doi:10.2174/092986710793213724
13. Simões G, Pereira T, Caseiro A. Matrix metaloproteinases in vascular pathology. *Microvasc Res*. 2022;143:104398. doi:10.1016/j.mvr.2022.104398
14. Tallant C, Marrero A, Gomis-Rüth FX. Matrix metalloproteinases: Fold and function of their catalytic domains. *Biochim Biophys Acta Mol Cell Res*. 2010;1803(1):20–28. doi:10.1016/j.bbamcr.2009.04.003
15. Yabluchanskiy A, Ma Y, Iyer RP, Hall ME, Lindsey ML. Matrix metalloproteinase-9: Many shades of function in cardiovascular disease. *Physiology*. 2013;28(6):391–403. doi:10.1152/physiol.00029.2013

16. Tayebjee MH, Nadar S, Blann AD, Gareth Beevers D, MacFadyen RJ, Lip GYH. Matrix metalloproteinase-9 and tissue inhibitor of metalloproteinase-1 in hypertension and their relationship to cardiovascular risk and treatment: A substudy of the Anglo-Scandinavian Cardiac Outcomes Trial (ASCOT). *Am J Hypertens*. 2004;17(9):764–769. doi:10.1016/j.amjhyper.2004.05.019
17. Laronha H, Caldeira J. Structure and function of human matrix metalloproteinases. *Cells*. 2020;9(5):1076. doi:10.3390/cells9051076
18. Cui N, Hu M, Khalil RA. Biochemical and biological attributes of matrix metalloproteinases. *Prog Mol Biol Transl Sci*. 2017;147:1–73. doi:10.1016/bs.pmbts.2017.02.005
19. Cabral-Pacheco GA, Garza-Veloz I, Castruita-De La Rosa C, et al. The roles of matrix metalloproteinases and their inhibitors in human diseases. *Int J Mol Sci*. 2020;21(24):9739. doi:10.3390/ijms21249739
20. Costanzo L, Soto B, Meier R, Geraghty P. The biology and function of tissue inhibitor of metalloproteinase 2 in the lungs. *Pulm Med*. 2022;2022:3632764. doi:10.1155/2022/3632764
21. Raeeszadeh-Sarmazdeh M, Do L, Hritz B. Metalloproteinases and their inhibitors: Potential for the development of new therapeutics. *Cells*. 2020;9(5):1313. doi:10.3390/cells9051313
22. Li K, Tay FR, Yiu CKY. The past, present and future perspectives of matrix metalloproteinase inhibitors. *Pharmacol Ther*. 2020;207:107465. doi:10.1016/j.pharmthera.2019.107465
23. Wang X, Khalil RA. Matrix metalloproteinases, vascular remodeling, and vascular disease. *Adv Pharmacol*. 2018;81:241–330. doix:10.1016/bs.apha.2017.08.002
24. Hopps E, Lo Presti R, Caimi G. Matrix metalloproteases in arterial hypertension and their trend after antihypertensive treatment. *Kidney Blood Press Res*. 2017;42(2):347–357. doi:10.1159/000477785
25. Thenappan T, Chan SY, Weir EK. Role of extracellular matrix in the pathogenesis of pulmonary arterial hypertension. *Am J Physiol Heart Circ Physiol*. 2018;315(5):H1322–H1331. doi:10.1152/ajpheart.00136.2018
26. Chen Q, Jin M, Yang F, Zhu J, Xiao Q, Zhang L. Matrix metalloproteinases: Inflammatory regulators of cell behaviors in vascular formation and remodeling. *Mediators Inflamm*. 2013;2013:928315. doi:10.1155/2013/928315
27. Chi PL, Cheng CC, Hung CC, et al. MMP-10 from M1 macrophages promotes pulmonary vascular remodeling and pulmonary arterial hypertension. *Int J Biol Sci*. 2022;18(1):331–348. doi:10.7150/ijbs.66472
28. Ma B, Cao Y, Qin J, Chen Z, Hu G, Li Q. Pulmonary artery smooth muscle cell phenotypic switching: A key event in the early stage of pulmonary artery hypertension. *Drug Discov Today*. 2023;28(5):103559. doi:10.1016/j.drudis.2023.103559
29. Zhang D, Gou Z, Qu Y, Su X. Understanding how methyltransferase-like 3 functions in lung diseases: From pathogenesis to clinical application. *Biomed Pharmacother*. 2024;179:117421. doi:10.1016/j.biopha.2024.117421
30. Gao Y, Chen T, Raj JU. Endothelial and smooth muscle cell interactions in the pathobiology of pulmonary hypertension. *Am J Respir Cell Mol Biol*. 2016;54(4):451–460. doi:10.1165/rcmb.2015-0323TR
31. Stenmark KR, Frid M, Perros F. Endothelial-to-mesenchymal transition: An evolving paradigm and a promising therapeutic target in PAH. *Circulation*. 2016;133(18):1734–1737. doi:10.1161/CIRCULATIONAHA.116.022479
32. Chelladurai P, Seeger W, Pullamsetti SS. Matrix metalloproteinases and their inhibitors in pulmonary hypertension. *Eur Respir J*. 2012;40(3):766–782. doi:10.1183/09031936.00209911
33. Kumar R, Graham B. How does inflammation contribute to pulmonary hypertension? *Eur Respir J*. 2018;51(1):1702403. doi:10.1183/13993003.02403-2017
34. Devendran A, Kar S, Bailey R, Trivieri MG. The role of bone morphogenetic protein receptor type 2 (BMPR2) and the prospects of utilizing induced pluripotent stem cells (iPSCs) in pulmonary arterial hypertension disease modeling. *Cells*. 2022;11(23):3823. doi:10.3390/cells11233823
35. Humbert M, Sitbon O, Chaouat A, et al. Survival in patients with idiopathic, familial, and anorexigen-associated pulmonary arterial hypertension in the modern management era. *Circulation*. 2010;122(2):156–163. doi:10.1161/CIRCULATIONAHA.109.911818
36. Humbert M, Gerry Coghlan J, Khanna D. Early detection and management of pulmonary arterial hypertension. *Eur Respir Rev*. 2012;21(126):306–312. doi:10.1183/09059180.00005112
37. Foris V, Kovacs G, Tscherner M, Olschewski A, Olschewski H. Biomarkers in pulmonary hypertension. *Chest*. 2013;144(1):274–283. doi:10.1378/chest.12-1246
38. Kazimierczyk R, Błaszczak P, Kowal K, et al. The significance of diminished sTWEAK and P-selectin content in platelets of patients with pulmonary arterial hypertension. *Cytokine*. 2018;107:52–58. doi:10.1016/j.cyto.2017.11.014
39. Newby A. Matrix metalloproteinases regulate migration, proliferation, and death of vascular smooth muscle cells by degrading matrix and non-matrix substrates. *Cardiovasc Res*. 2006;69(3):614–624. doi:10.1016/j.cardiores.2005.08.002
40. Bohara S, Bagheri A, Ertugral EG, et al. Integrative analysis of gene expression, protein abundance, and metabolomic profiling elucidates complex relationships in chronic hyperglycemia-induced changes in human aortic smooth muscle cells. *J Biol Eng*. 2024;18(1):61. doi:10.1186/s13036-024-00457-w
41. Kirkgöz K. C-reactive protein in atherosclerosis: More than a biomarker, but not just a culprit. *Rev Cardiovasc Med*. 2023;24(10):297. doi:10.31083/j.rcm2410297
42. Zhao Y, Peng J, Lu C, et al. Metabolomic heterogeneity of pulmonary arterial hypertension. *PLoS One*. 2014;9(2):e88727. doi:10.1371/journal.pone.0088727
43. Kazimierczyk R, Szumowski P, Nekolla SG, et al. Prognostic role of PET/MRI hybrid imaging in patients with pulmonary arterial hypertension. *Heart*. 2021;107(1):54–60. doi:10.1136/heartjnl-2020-316741
44. Hemnes AR, Luther JM, Rhodes CJ, et al. Human PAH is characterized by a pattern of lipid-related insulin resistance. *JCI Insight*. 2019;4(1):e123611. doi:10.1172/jci.insight.123611
45. Hassoun PM, Mouthon L, Barberà JA, et al. Inflammation, growth factors, and pulmonary vascular remodeling. *J Am Coll Cardiol*. 2009;54(1 Suppl):S10–S19. doi:10.1016/j.jacc.2009.04.006
46. Malhotra R, Paskin-Flerlage S, Zamanian RT, et al. Circulating angiogenic modulatory factors predict survival and functional class in pulmonary arterial hypertension. *Pulm Circ*. 2013;3(2):369–380. doi:10.4103/2045-8932.110445
47. Blackburn JS, Brinckerhoff CE. Matrix metalloproteinase-1 and thrombin differentially activate gene expression in endothelial cells via PAR-1 and promote angiogenesis. *Am J Pathol*. 2008;173(6):1736–1746. doi:10.2353/ajpath.2008.080512
48. Mazor R, Alsaigh T, Shaked H, et al. Matrix metalloproteinase-1-mediated up-regulation of vascular endothelial growth factor-2 in endothelial cells. *J Biol Chem*. 2013;288(1):598–607. doi:10.1074/jbc.M112.417451
49. Merkus D, Van Beusekom HMM, Boomars KA. Protease-activated receptor 1 as potential therapeutic target in pulmonary arterial hypertension. *Cardiovasc Res*. 2019;115(8):1260–1261. doi:10.1093/cvr/cvz071
50. Mickael C, Kheyfets VO, Langouët-Astrié C, et al. Peripheral blood inflammation profile of patients with pulmonary arterial hypertension using the High-Throughput Olink Proteomics Platform. *Am J Respir Cell Mol Biol*. 2022;66(5):580–581. doi:10.1165/rcmb.2021-0369LE
51. Lepetit H, Eddahibi S, Fadel E, et al. Smooth muscle cell matrix metalloproteinases in idiopathic pulmonary arterial hypertension. *Eur Respir J*. 2005;25(5):834–842. doi:10.1183/09031936.05.00072504
52. Hoffmann J, Marsh LM, Pieper M, et al. Compartment-specific expression of collagens and their processing enzymes in intrapulmonary arteries of IPAH patients. *Am J Physiol Lung Cell Mol Physiol*. 2015;308(10):L1002–L1013. doi:10.1152/ajplung.00383.2014
53. Lenci E, Cosottini L, Trabocchi A. Novel matrix metalloproteinase inhibitors: An updated patent review (2014–2020). *Exp Opin Ther Patents*. 2021;31(6):509–523. doi:10.1080/13543776.2021.1881481
54. Hardy E, Hardy-Sosa A, Fernandez-Patron C. MMP-2: Is too low as bad as too high in the cardiovascular system? *Am J Physiol Heart Circ Physiol*. 2018;315(5):H1332–H1340. doi:10.1152/ajpheart.00198.2018
55. Chakraborti S, Sarkar J, Pramanik PK, Chakraborti T. Role of proteases in lung disease: A brief overview. In: Chakraborti S, Chakraborti T, Dhalla NS, eds. *Proteases in Human Diseases*. Singapore: Springer Singapore; 2017:333–374. doi:10.1007/978-981-10-3162-5_16
56. Shamamian P, Schwartz JD, Pocock BJZ, et al. Activation of progelatinase A (MMP-2) by neutrophil elastase, cathepsin G, and proteinase-3: A role for inflammatory cells in tumor invasion and angiogenesis. *J Cell Physiol*. 2001;189(2):197–206. doi:10.1002/jcp.10014

57. Monea S, Lehti K, Keski-Oja J, Mignatti P. Plasmin activates pro-matrix metalloproteinase-2 with a membrane-type 1 matrix metalloproteinase-dependent mechanism. *J Cell Physiol*. 2002;192(2):160–170. doi:10.1002/jcp.10126
58. Miyamori H, Takino T, Kobayashi Y, et al. Claudin promotes activation of pro-matrix metalloproteinase-2 mediated by membrane-type matrix metalloproteinases. *J Biol Chem*. 2001;276(30):28204–28211. doi:10.1074/jbc.M103083200
59. Grote K, Flach I, Luchtefeld M, et al. Mechanical stretch enhances mRNA expression and proenzyme release of matrix metalloproteinase-2 (MMP-2) via NAD(P)H oxidase-derived reactive oxygen species. *Circ Res*. 2003;92(11):e80–86. doi:10.1161/01.RES.0000077044.60138.7C
60. Arvidsson M, Ahmed A, Bouzina H, Rådegran G. Matrix metalloproteinase 7 in diagnosis and differentiation of pulmonary arterial hypertension. *Pulm Circ*. 2019;9(4):2045894019895414. doi:10.1177/2045894019895414
61. Schumann C, Lepper PM, Frank H, et al. Circulating biomarkers of tissue remodelling in pulmonary hypertension. *Biomarkers*. 2010;15(6):523–532. doi:10.3109/1354750X.2010.492431
62. Tiede SL, Wassenberg M, Christ K, et al. Biomarkers of tissue remodeling predict survival in patients with pulmonary hypertension. *Int J Cardiol*. 2016;223:821–826. doi:10.1016/j.ijcard.2016.08.240
63. Arvidsson M, Ahmed A, Säleby J, Hesselstrand R, Rådegran G. Plasma matrix metalloproteinase 2 is associated with severity and mortality in pulmonary arterial hypertension. *Pulm Circ*. 2022;12(1):e12041. doi:10.1002/pul2.12041
64. Karamanian VA, Harhay M, Grant GR, et al. Erythropoietin upregulation in pulmonary arterial hypertension. *Pulm Circ*. 2014;4(2):269–279. doi:10.1086/675990
65. Asosingh K, Aldred MA, Vasanji A, et al. Circulating angiogenic precursors in idiopathic pulmonary arterial hypertension. *Am J Pathol*. 2008;172(3):615–627. doi:10.2353/ajpath.2008.070705
66. Cantini-Salignac C, Lartaud I, Schrijen F, Atkinson J, Chabot F. Metalloproteinase-9 in circulating monocytes in pulmonary hypertension. *Fundam Clin Pharmacol*. 2006;20(4):405–410. doi:10.1111/j.1472-8206.2006.00417.x
67. Bauer Y, De Bernard S, Hickey P, et al. Identifying early pulmonary arterial hypertension biomarkers in systemic sclerosis: Machine learning on proteomics from the DETECT cohort. *Eur Respir J*. 2021;57(6):2002591. doi:10.1183/13993003.02591-2020
68. Giannelli G, Iannone F, Marinosci F, Lapadula G, Antonaci S. The effect of bosentan on matrix metalloproteinase-9 levels in patients with systemic sclerosis-induced pulmonary hypertension. *Curr Med Res Opin*. 2005;21(3):327–332. doi:10.1185/030079905X30680
69. Wan J, Zhang G, Li X, et al. Matrix metalloproteinase 3: A promoting and destabilizing factor in the pathogenesis of disease and cell differentiation. *Front Physiol*. 2021;12:663978. doi:10.3389/fphys.2021.663978
70. Ito TK, Ishii G, Saito S, et al. Degradation of soluble VEGF receptor-1 by MMP-7 allows VEGF access to endothelial cells. *Blood*. 2009;5;113(10):2363-9. doi: 10.1182/blood-2008-08-172742
71. Bonnema DD, Webb CS, Pennington WR, et al. Effects of age on plasma matrix metalloproteinases (MMPs) and tissue inhibitor of metalloproteinases (TIMPs). *J Cardiac Fail*. 2007;13(7):530–540. doi:10.1016/j.cardfail.2007.04.010
72. Dieffenbach PB, Mallarino Haeger C, Rehman R, et al. A novel protective role for matrix metalloproteinase-8 in the pulmonary vasculature. *Am J Respir Crit Care Med*. 2021;204(12):1433–1451. doi:10.1164/rccm.202108-1863OC
73. Ge Q, Zhang T, Yu J, et al. A new perspective on targeting pulmonary arterial hypertension: Programmed cell death pathways (autophagy, pyroptosis, ferroptosis) [Erratum in: *Biomed Pharmacother*. 2024;181:117741. doi:10.1016/j.biopha.2024.117741]. *Biomed Pharmacother*. 2024;181:117706. doi:10.1016/j.biopha.2024.117706
74. Safdar Z, Tamez E, Chan W, et al. Circulating collagen biomarkers as indicators of disease severity in pulmonary arterial hypertension. *JACC Heart Fail*. 2014;2(4):412–421. doi:10.1016/j.jchf.2014.03.013
75. Hiremath J, Thanikachalam S, Parikh K, et al. Exercise improvement and plasma biomarker changes with intravenous treprostinil therapy for pulmonary arterial hypertension: A placebo-controlled trial. *J Heart Lung Transplant*. 2010;29(2):137–149. doi:10.1016/j.healun.2009.09.005
76. Vandooren J, Van Den Steen PE, Opdenakker G. Biochemistry and molecular biology of gelatinase B or matrix metalloproteinase-9 (MMP-9): The next decade. *Crit Rev Biochem Mol Biol*. 2013;48(3):222–272. doi:10.3109/10409238.2013.770819
77. Grigoryev DN, Mathai SC, Fisher MR, et al. Identification of candidate genes in scleroderma-related pulmonary arterial hypertension. *Transl Res*. 2008;151(4):197–207. doi:10.1016/j.trsl.2007.12.010
78. Jonigk D, Golpon H, Bockmeyer CL, et al. Plexiform lesions in pulmonary arterial hypertension. *Am J Pathol*. 2011;179(1):167–179. doi:10.1016/j.ajpath.2011.03.040
79. Garbacki N, Di Valentin E, Piette J, Cataldo D, Crahay C, Colige A. Matrix metalloproteinase 12 silencing: A therapeutic approach to treat pathological lung tissue remodeling? *Pulm Pharmacol Ther*. 2009;22(4):267–278. doi:10.1016/j.pupt.2009.03.001
80. Stracke JO, Hutton M, Stewart M, et al. Biochemical characterization of the catalytic domain of human matrix metalloproteinase 19. *J Biol Chem*. 2000;275(20):14809–14816. doi:10.1074/jbc.275.20.14809
81. Ries C. Cytokine functions of TIMP-1. *Cell Mol Life Sci*. 2014;71(4):659–672. doi:10.1007/s00018-013-1457-3
82. Almuntashiri S, Alhumaid A, Zhu Y, et al. TIMP-1 and its potential diagnostic and prognostic value in pulmonary diseases. *Chin Med J Pulm Crit Care Med*. 2023;1(2):67–76. doi:10.1016/j.pccm.2023.05.002
83. Fassina G, Ferrari N, Brigati C, et al. Tissue inhibitors of metalloproteases: Regulation and biological activities. *Clin Exp Metastasis*. 2000;18(2):111–120. doi:10.1023/a:1006797522521
84. Lindsay MM, Maxwell P, Dunn FG. TIMP-1: A marker of left ventricular diastolic dysfunction and fibrosis in hypertension. *Hypertension*. 2002;40(2):136–141. doi:10.1161/01.HYP.0000024573.17293.23
85. Sundström J, Evans JC, Benjamin EJ, et al. Relations of plasma total TIMP-1 levels to cardiovascular risk factors and echocardiographic measures: The Framingham Heart Study. *Eur Heart J*. 2004;25(17):1509–1516. doi:10.1016/j.ehj.2004.05.029
86. Caimi G, Hopps E, Montana M, et al. The function of matrix metalloproteinase-9 (MMP-9) and its tissue inhibitor (TIMP-1) in several clinical conditions: Results and analysis of our survey. *Clin Hemorheol Microcirc*. 2021;78(4):401–416. doi:10.3233/CH-201094
87. Cavusoglu E, Ruwende C, Chopra V, et al. Tissue inhibitor of metalloproteinase-1 (TIMP-1) is an independent predictor of all-cause mortality, cardiac mortality, and myocardial infarction. *Am Heart J*. 2006;151(5):1101.e1–1101.e8. doi:10.1016/j.ahj.2006.02.029
88. Fenster BE, Lasalvia L, Schroeder JD, et al. Galectin-3 levels are associated with right ventricular functional and morphologic changes in pulmonary arterial hypertension. *Heart Vessels*. 2016;31(6):939–946. doi:10.1007/s00380-015-0691-z
89. Pendergrass SA, Hayes E, Farina G, et al. Limited systemic sclerosis patients with pulmonary arterial hypertension show biomarkers of inflammation and vascular injury. *PLoS One*. 2010;5(8):e12106. doi:10.1371/journal.pone.0012106
90. Wetzl V, Tiede SL, Faerber L, et al. Plasma MMP2/TIMP4 ratio at follow-up assessment predicts disease progression of idiopathic pulmonary arterial hypertension. *Lung*. 2017;195(4):489–496. doi:10.1007/s00408-017-0014-5
91. Jacobsen J, Visse R, Sørensen HP, et al. Catalytic properties of ADAM12 and its domain deletion mutants. *Biochemistry (Moscow)*. 2008;47(2):537–547. doi:10.1021/bi701629c
92. Boon L, Ugarte-Berzal E, Vandooren J, Opdenakker G. Protease propeptide structures, mechanisms of activation, and functions. *Crit Rev Biochem Mol Biol*. 2020;55(2):111–165. doi:10.1080/10409238.2020.1742090
93. Moore L, Fan D, Basu R, Kandalam V, Kassiri Z. Tissue inhibitor of metalloproteinases (TIMPs) in heart failure. *Heart Fail Rev*. 2012;17(4–5):693–706. doi:10.1007/s10741-011-9266-y
94. Kashiwagi M, Tortorella M, Nagase H, Brew K. TIMP-3 is a potent inhibitor of aggrecanase 1 (ADAM-TS4) and aggrecanase 2 (ADAM-TS5). *J Biol Chem*. 2001;276(16):12501–12504. doi:10.1074/jbc.C000848200
95. Edgar AJ, Chacón MR, Bishop AE, Yacoub MH, Polak JM. Upregulated genes in sporadic, idiopathic pulmonary arterial hypertension. *Respir Res*. 2006;7(1):1. doi:10.1186/1465-9921-7-1
96. Melendez-Zajgla J, Pozo L, Ceballos G, Maldonado V. Tissue inhibitor of metalloproteinases-4: The road less traveled. *Mol Cancer*. 2008;7(1):85. doi:10.1186/1476-4598-7-85

97. Mochizuki S, Shimoda M, Shiomi T, Fujii Y, Okada Y. ADAM28 is activated by MMP-7 (matrilysin-1) and cleaves insulin-like growth factor binding protein-3. *Biochem Biophys Res Commun*. 2004;315(1):79–84. doi:10.1016/j.bbrc.2004.01.022
98. Elias GJ, Ioannis M, Theodora P, et al. Circulating tissue inhibitor of matrix metalloproteinase-4 (TIMP-4) in systemic sclerosis patients with elevated pulmonary arterial pressure. *Mediators Inflamm*. 2008;164134. doi: 10.1155/2008/164134
99. Paulissen G, Rocks N, Gueders MM, et al. Role of ADAM and ADAMTS metalloproteinases in airway diseases. *Respir Res*. 2009;10(1):127. doi:10.1186/1465-9921-10-127
100. Black RA, White JM. ADAMs: focus on the protease domain. *Curr Opin Cell Biol*. 1998;10(5):654–659. doi:10.1016/S0955-0674(98)80042-2
101. Zhong S, Khalil RA. A disintegrin and metalloproteinase (ADAM) and ADAM with thrombospondin motifs (ADAMTS) family in vascular biology and disease. *Biochem Pharmacol*. 2019;164:188–204. doi:10.1016/j.bcp.2019.03.033
102. Omura J, Satoh K, Kikuchi N, et al. ADAMTS8 promotes the development of pulmonary arterial hypertension and right ventricular failure: A possible novel therapeutic target. *Circ Res*. 2019;125(10):884–906. doi:10.1161/CIRCRESAHA.119.315398
103. Satoh K. Drug discovery focused on novel pathogenic proteins for pulmonary arterial hypertension. *J Cardiol*. 2021;78(1):1–11. doi:10.1016/j.jjcc.2021.01.009
104. Newnham M, South K, Bleda M, et al. The ADAMTS13–VWF axis is dysregulated in chronic thromboembolic pulmonary hypertension. *Eur Respir J*. 2019;53(3):1801805. doi:10.1183/13993003.01805-2018
105. Ahmed A, Ahmed S, Rådegran G. Plasma ADAMTS13 and von Willebrand factor in diagnosis and prediction of prognosis in pulmonary arterial hypertension. *Pulm Circ*. 2021;11(4):20458940211041500. doi:10.1177/20458940211041500
106. Li Y, Chen Y, Yang L, et al. Increased plasma expression of a disintegrin and metalloproteinase with thrombospondin motifs like 4 in patients with idiopathic pulmonary arterial hypertension and chronic thromboembolic pulmonary hypertension. *Pulm Circ*. 2023;13(3):e12267. doi:10.1002/pul2.12267
107. Liao S, Lin Y, Liu L, et al. ADAM10, a "multitasker" in sepsis: Focus on its posttranslational target. *Inflamm Res*. 2023;72(3):395–423. doi:10.1007/s00011-022-01673-0
108. Tripathi P, Awasthi S, Gao P. ADAM metallopeptidase domain 33 (ADAM33): A promising target for asthma. *Mediators Inflamm*. 2014;2014:572025. doi:10.1155/2014/572025
109. Rhodes CJ, Wharton J, Ghataorhe P, et al. Plasma proteome analysis in patients with pulmonary arterial hypertension: An observational cohort study. *Lancet Respir Med*. 2017;5(9):717–726. doi:10.1016/S2213-2600(17)30161-3
110. Kopeć G, Skride A, Ereminiene E, et al. Emerging therapies and new directions in the treatment of pulmonary arterial hypertension. *Pol Heart J*. 2025;83(1):18–26. doi:10.33963/v.phj.104053
111. Zolty R. Novel experimental therapies for treatment of pulmonary arterial hypertension. *J Exp Pharmacol*. 2021;13:817–857. doi:10.2147/JEP.S236743
112. Shah AJ, Beckmann T, Vorla M, Kalra DK. New drugs and therapies in pulmonary arterial hypertension. *Int J Mol Sci*. 2023;24(6):5850. doi:10.3390/ijms24065850

Simple, low-cost in vitro protocol for differentiating mesenchymal stem cells into cardiomyocyte-like cells

Ariyani Noviantari[1,2,A–F], Elrade Rofaani[3,B,C,E,F], Radiana Dhewayani Antarianto[4,5,B,C,E,F], Mulyadi M. Djer[6,E,F]

[1] Doctoral Program in Biomedical Science, Faculty of Medicine, Universitas Indonesia, Jakarta, Indonesia
[2] Center for Biomedical Research, Research Organization for Health, National Research and Innovation Agency (BRIN), Cibinong, Bogor, Indonesia
[3] Group of Trend Analysis and Foresight, Directorate for Measurement and Indicators of Research, Technology and Innovation, National Research and Innovation Agency (BRIN), Jakarta, Indonesia
[4] Department of Histology, Faculty of Medicine, Universitas Indonesia, Jakarta, Indonesia
[5] Stem Cell and Tissue Engineering Research Cluster, Indonesian Medical Education and Research Institute (IMERI), Faculty of Medicine, Universitas Indonesia, Jakarta, Indonesia
[6] Department of Pediatrics, Dr. Cipto Mangunkusumo National Central Hospital, Faculty of Medicine, Universitas Indonesia, Jakarta, Indonesia

Received on June 7, 2024
Reviewed on January 5, 2025
Accepted on April 16, 2025

Published online on January 12, 2026

A – research concept and design; B – collection and/or assembly of data; C – data analysis and interpretation;
D – writing the article; E – critical revision of the article; F – final approval of the article

Advances in Clinical and Experimental Medicine, ISSN 1899–5276 (print), ISSN 2451–2680 (online) *Adv Clin Exp Med*. 2026;35(2):377–392

Address for correspondence
Radiana Dhewayani Antarianto
E-mail: radiana.dhewayani@ui.ac.id

Funding sources
This work has received support from research grants from Publikasi Terindeks Internasional (PUTI) Q1, Universitas Indonesia, under contract No. PENG-001/UN2.RST/PPM.00.00/2023, and Rumah Program Research Organization for Health, National Research and Innovation Agency (BRIN), under contracts No. 23/III.9/HK/2023, 6/III.9/HK/2024 and 5/III.9/HK/2025.

Conflict of interest
None declared

Acknowledgements
The authors would like to express gratitude to the Chairman of Research Organization for Health and Head of Center for Biomedical Research, National Research and Innovation Agency (BRIN), Indonesia for providing a working environment to conduct and support this research. The authors also would like to thank Prof. Yong Chen from École Normale Superieure, Université Paris Sciences et Lettres (PSL), France, as an external collaborator for PUTI Q1 Universitas Indonesia 2023 grant obtainment.

Cite as
Noviantari A, Rofaani E, Dhewayani Antarianto R, Djer MM. Simple, low-cost in vitro protocol for differentiating mesenchymal stem cells into cardiomyocyte-like cells. *Adv Clin Exp Med*. 2026;35(2):377–392. doi:10.17219/acem/204112

DOI
10.17219/acem/204112

Abstract

Congenital heart disease (CHD) remains the foremost cause of mortality in children under 20 years of age. Given their ease of harvest, robust proliferative capacity and multilineage differentiation potential, stem cells (SCs) have emerged as a promising therapeutic alternative. In particular, mesenchymal stem cells (MSCs) derived from Wharton's jelly in the umbilical cord, i.e., an abundant byproduct of childbirth, especially in low- and middle-income settings, can be induced toward a cardiomyocyte lineage, making them an attractive cell source for cardiac regeneration. Although MSCs can be directed toward a cardiomyocyte lineage using growth factors or chemical cues, most in vitro-differentiated cells remain developmentally immature, with only a small fraction achieving the structural, functional and metabolic maturity required for therapeutic use. In resource-limited laboratories, the primary challenge is to develop a simple, cost-effective protocol that reliably differentiates MSCs into structurally, functionally and metabolically mature cardiomyocytes. This review presents a streamlined, cost-effective in vitro differentiation protocol for umbilical-cord MSCs into cardiomyocytes, designed for laboratories with minimal resources, involving 3 sequential stages. First, induce cardiac mesoderm commitment by treating umbilical cord-derived MSCs (UC-MSCs) with 5-azacytidine (5-Aza) or bone morphogenetic protein (BMP). Next, specify cardiac progenitor cells by adding a Wnt-pathway inhibitor (e.g., IWP-2). Finally, drive cardiomyocyte maturation by supplementing the culture with insulin-like growth factors (IGFs). In laboratories lacking complex bioreactors, seeding the cells onto a simple biocompatible scaffold, such as a collagen or fibrin hydrogel, can further boost differentiation efficiency and promote tissue-like organization.

Key words: cardiomyocyte, cell- and tissue-based therapy, differentiation, growth factor, mesenchymal stem cells

Highlights

- In vitro cardiomyocyte differentiation of pluripotent/multipotent stem cells progresses through sequential stages that mirror in vivo cardiac development.
- Key stages include cardiac mesoderm, cardiac progenitor cells, and immature and mature cardiomyocytes.
- A simple, low-cost differentiation protocol for resource-limited laboratories uses 5-Aza or BMP-2 to induce cardiac mesoderm, a Wnt inhibitor to promote cardiac progenitors, and insulin-like growth factor (IGF) to generate immature cardiomyocytes.
- A hybrid scaffold is recommended to support in vitro cardiomyocyte maturation under limited-resource laboratory conditions.

Introduction

Cardiovascular disease is the leading cause of death worldwide, accounting for 17.9 million deaths annually.[1] Congenital heart disease (CHD) is the most common cause of mortality in children and adolescents under 20 years of age. A key challenge in CHD management is the heart's inability to regenerate cardiomyocytes irreversibly lost after myocardial infarction. Myocarditis and cardiomyopathy, although typically acquired rather than congenital, are important contributors to pediatric heart disease, affecting approx. 1 in 100,000 individuals under 20 years of age. Structural cardiac malformations and cardiomyopathic changes that impair myocardial function often lead to heart failure in this population. Although heart transplantation remains the definitive treatment for end-stage disease, its use is severely limited by the scarcity of suitable donor organs.[2–4]

Children with CHD experience high mortality rates in the first 4 years of life, with few surviving to their 5th birthday owing to serious complications and comorbidities.[5] This burden falls disproportionately on low- and lower-middle-income countries (LICs and LMICs), where the birth prevalence of CHD continues to rise even as diagnostic infrastructure and trained personnel remain scarce. Although timely surgical interventions can significantly reduce mortality, many health systems in these regions lack the resources required to provide them.[6]

However, cardiomyocytes are terminally differentiated and possess only a limited capacity for proliferation. Because primary adult human cardiomyocytes are difficult to obtain and embryonic stem cells (SCs) raise ethical and biological concerns, mesenchymal stem cells (MSCs), which are multipotent, readily available and exhibit low immunogenicity, offer a promising alternative for cardiac regenerative therapies.[7] Mesenchymal stem cells can be harvested from a variety of tissues, including endometrium, placenta, dental pulp, amniotic fluid, adipose tissue, Wharton's jelly (from the umbilical cord), bone marrow, and dermis, and can differentiate in vitro into osteocytes, adipocytes, neurons, chondrocytes, and cardiomyocytes.[8,9] Wharton's jelly is especially attractive as an MSC source because it is readily available as medical waste, facilitates easy isolation and expansion, and exhibits a high proliferative capacity, making it particularly valuable for cardiac regenerative applications in LICs and LMICs.

Functionally mature cardiomyocytes display spontaneous contractile activity in vitro, a property that is essential for modeling cardiac pathophysiology.[10,11] In addition to serving as a research platform, these cells offer the potential to replace damaged myocardium.[12] Consequently, SC-based therapies, chosen for their accessibility, robust proliferative capacity and multilineage differentiation potential, are under investigation as novel approaches for cardiac regeneration.[7]

Similar to the in vivo procedure, MSCs can differentiate into cardiomyocytes in vitro with initial induction towards the mesoderm, cardiac progenitor cells or pre-cardioblasts, immature cardiomyocytes or cardioblasts, and mature cardiomyocytes.[13] Several studies show that the MSCs can develop into cardiomyocytes in vitro by showing the expression of specific markers like cardiac troponin I (cTnI), cardiac troponin-T (cTnT), desmin, Nkx2.5, GATA-4, and connexin 43 (Cx43).[14,15] The cells grow in combination on a biomaterial scaffold with the proper biophysics and chemical signaling in the triad of tissue engineering techniques to generate a specific tissue.[16]

Protocols for directing pluripotent SCs toward differentiating into cardiomyocytes are under development. Several approaches have been established to induce cardiomyogenic differentiation in both induced pluripotent SCs (iPSCs) and MSCs. Previous studies have demonstrated MSC differentiation efficiencies of 20–50%,[17–19] often achieved by treating cells with the DNA demethylating agent 5-azacytidine (5-Aza) to trigger cardiomyogenic commitment.[20,21]

Although protocols for differentiating MSCs into cardiomyocytes are rapidly advancing, their broader application is hindered by a lack of standardized methodologies across research laboratories.[22] Moreover, current differentiation protocols yield predominantly immature cardiomyocytes, with only a small fraction achieving the structural, functional and metabolic maturity required for therapeutic applications.

Therefore, the biggest hurdle for laboratories with limited resources is to find a simple and cost-effective method for differentiating MSCs into mature cardiomyocytes. This

method should use accessible reagents, rely on a sustainable in-house differentiation medium and maintain optimal efficiency.

Objectives

This article aims to provide a simple protocol for differentiating the umbilical cord MSCs into cardiomyocytes in a laboratory with limited resources.

Materials and methods

This review is based on a comprehensive literature search conducted in the PubMed database. We searched PubMed (up to 2023) to identify relevant studies with the key words: "mesenchymal stem cell*" OR "mesenchymal progenitor cell*" OR "mesenchymal stromal cell*" AND "differentiat*" AND "cardiomyocyte*" OR "cardiac cell*" OR "cardiovascular" OR "heart muscle cell*" AND "in vitro" NOT "in vivo" (Table 1). Articles from the last 10 years were collected and selected based on the recommended topic; then, inclusion criteria were applied to filter the literature search results. We included peer-reviewed articles published in the last 10 years indexed in PubMed using relevant key words for MSC-to-cardiomyocyte differentiation, and excluded studies that did not employ defined induction factors. The initial search retrieved 86 articles; after title and abstract screening, 63 were deemed irrelevant, leaving 23 for full-text review. Six of these failed to meet our inclusion criteria, resulting in 17 studies ultimately incorporated into this analysis (Fig. 1).

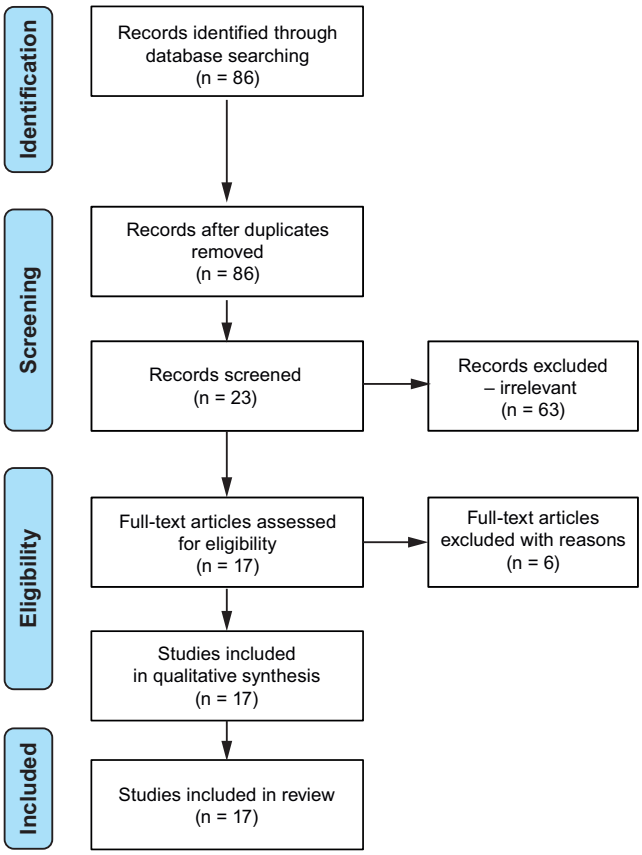

Fig. 1. Study selection process

Results

Mesenchymal stem cells can be directed in vitro to differentiate into mesoderm-derived lineages such as cardiomyocytes by applying tailored cocktails of growth factors and small molecules that mimic cardiac development signals. Commonly used inducers include basic fibroblast growth factor (bFGF), salvianolic acid B, transforming growth factor-β1 (TGF-β1), vascular endothelial growth factor (VEGF), insulin-like growth factor 1 (IGF-1), bone morphogenetic protein 2 (BMP-2), demethylating agent 5-Aza, neuregulin-1 (NRG-1), forskolin, angiotensin II (Ang-II), and an oligosaccharide extract of *Rehmannia glutinosa* (RGO). Each component contributes to cardiac mesoderm specification, activation of cardiogenic gene networks, and promotion of structural and functional maturation (Table 2,3).[17–19,23–37]

Table 1. In vitro differentiation of mesenchymal stem cells (MSCs) into cardiomyocytes

No.	Query	Results
1	((mesenchymal stem cell*[Title/Abstract]) OR (mesenchymal progenitor cell*[Title/Abstract])) OR (mesenchymal stromal cell*[Title/Abstract])	23,065
2	differentiat*[Title/Abstract]	176,624
3	(((cardiomyocyte*[Title/Abstract]) OR (cardiac cell*[Title/Abstract])) OR (cardiovascular[Title/Abstract])) OR (heart muscle cell*[Title/Abstract])	143,836
4	in vitro[Title/Abstract]	267,786
5	in vivo[Title/Abstract]	216,999
6	((((((mesenchymal stem cell*[Title/Abstract]) OR (mesenchymal progenitor cell*[Title/Abstract])) OR (mesenchymal stromal cell*[Title/Abstract]) AND ((y_10[Filter]) AND (data[Filter]))) AND (differentiat*[Title/Abstract] AND ((y_10[Filter]) AND (data[Filter])))) AND ((((cardiomyocyte*[Title/Abstract]) OR (cardiac cell*[Title/Abstract])) OR (cardiovascular[Title/Abstract])) OR (heart muscle cell*[Title/Abstract]) AND ((y_10[Filter]) AND (data[Filter])))) AND (in vitro[Title/Abstract] AND ((y_10[Filter]) AND (data[Filter])))) NOT (in vivo[Title/Abstract] AND ((y_10[Filter]) AND (data[Filter])))	86

Table 2. In vitro differentiation of mesenchymal stem cells (MSCs) into cardiomyocytes – induction factor

No.	Source of MSCs	Induction factor											Other treatment	Authors, year
		5-Aza	bFGF	Ang-II	TGF-β1	BMP-2	Sal-B	VEGF	IGF-1	RGO	forskolin	neuregulin-1		
1	rat BM-MSCs	√				√							–	Hou et al.[17] 2013
2	mice AD-MSCs	√											–	Li et al.[18] 2013
3	rat BM-MSCs				√		√						–	Lv et al.[19] 2018
4	porcine EMSCs	√		√									–	Subbarao et al.[23] 2019
5	rat olfactory bulbs		√								√	√	coculture with cardiomyocyte	Huang et al.[24] 2013
6	rat BM-MSCs	√								√			–	Wang et al.[25] 2016
7	human UC-MSCs	√											–	Zhu et al.[27] 2015
8	human BM-MSCs	√											–	Yu et al.[28] 2016
9	rat BM-MSCs	√											nano-sized collagen I molecules	Kang et al.[29] 2013
10	BM-MSCs of Mongolian sheep	√											–	Liu et al.[30] 2014
11	rat BM-MSCs	√			√								–	Shi et al.[31] 2016
12	human AD-MSCs	√	√	√									–	Song et al.[32] 2013
13	rat BM-MSCs					√	√						–	Lv et al.[33] 2017
14	human UC-MSCs		√		√			√	√				scaffold	Sekula et al.[34] 2021
15	human WJ-MSCs	√											H_2O_2	Nimsanor et al.[35] 2017
16	rat BM-MSCs	√			√								electrical stimulation (ES)	He et al.[36] 2019
17	rat AD-MSCs												MethoCult GF M3534 + Y-27632	Zhao et al.[37] 2014

AD-MSCs – adipose tissue; Ang-II – angiotensin II; bFGF – basic fibroblast growth factor; BM-MSCs – bone marrow mesenchymal stem cells; BMP-2 – bone morphogenetic protein 2; cTnI – cardiac troponin I; cTnT – cardiac troponin T; Cx43 – connexin-43; EMSCs – endometrial mesenchymal stem cells; hUC-MSCs – human umbilical cord mesenchymal stem cells; IGF-1 – insulin-like growth factor 1; MEF-2C – myocyte-specific enhancer factor 2C; MHC – myosin heavy chain; RGO – *Rehmannia glutinosa* oligosaccharide; Sal-B – salvianolic acid B; TGF-β1 – transforming growth factor-β1; VEGF – vascular endothelial growth factor; WJ-MSCs – Wharton's jelly mesenchymal stem cells; 5-Aza – 5-azacytidine.

Cardiovascular diseases in children

The most common form of CHD is the non-cyanotic type, which presents without cyanosis and typically arises from an intracardiac septal defect that creates a left-to-right shunt. In this condition, a gap in the septum allows oxygenated blood to flow from one heart chamber to another.[38] Congenital heart disease results from disrupted cardiac morphogenesis during early gestation – typically around the 6th week – when the fetal heart and great vessels are forming. It remains the leading cause of mortality among newborns with congenital anomalies.[39,40]

Congenital heart disease may result from a septal defect – such as an atrial or ventricular septal defect – that allows abnormal shunting of blood between the heart chambers. It can also arise from a patent ductus arteriosus, in which the fetal vessel connecting the pulmonary artery to the aorta fails to close after birth. Other forms include anomalous pulmonary venous return and transposition of the great arteries, where the aorta and pulmonary artery are reversed in position.[41]

Congenital heart disease spans a spectrum from asymptomatic, mild lesions – often undetected on routine physical examination – to critical defects that present immediately after birth and require urgent intervention.

Table 3. In vitro differentiation of mesenchymal stem cells (MSCs) into cardiomyocytes – markers

No.	Source of MSCs	Marker									Beating of cells	Authors, year
		GATA-4	MEF-2C	Nkx 2.5	MHC	Cx43	cTnT	cTnI	α-actin	desmin		
1	rat BM-MSCs					√		√			x	Hou et al.[17] 2013
2	mice AD-MSCs	√		√			√				x	Li et al.[18] 2013
3	rat BM-MSCs	√		√				√	√		x	Lv et al.[19] 2018
4	porcine EMSCs						√		√	√	x	Subbarao et al.[23] 2019
5	rat olfactory bulbs	√		√	√	√		√	√		√	Huang et al.[24] 2013
6	rat BM-MSCs					√		√			x	Wang et al.[25] 2016
7	human UC-MSCs							√			x	Zhu et al.[27] 2015
8	human BM-MSCs	√		√			√		√		x	Yu et al.[28] 2016
9	rat BM-MSCs	√		√	√			√	√		x	Kang et al.[29] 2013
10	BM-MSCs of Mongolian sheep	√		√							x	Liu et al.[30] 2014
11	rat BM-MSCs				√	√		√	√		x	Shi et al.[31] 2016
12	human AD-MSCs				√	√		√			x	Song et al.[32] 2013
13	rat BM-MSCs	√		√		√	√			√	x	Lv et al.[33] 2017
14	human UC-MSCs	√	√						√		x	Sekula et al.[34] 2021
15	human WJ-MSCs	√		√			√		√		x	Nimsanor et al.[35] 2017
16	rat BM-MSCs					√			√		x	He et al.[36] 2019
17	rat AD-MSCs	√	√		√		√		√		√	Zhao et al.[37] 2014

AD-MSCs – adipose tissue; Ang-II – angiotensin II; bFGF – basic fibroblast growth factor; BM-MSCs – bone marrow mesenchymal stem cells; BMP-2 – bone morphogenetic protein 2; cTnI – cardiac troponin I; cTnT – cardiac troponin T; Cx43 – connexin-43; EMSCs – endometrial mesenchymal stem cells; hUC-MSCs – human umbilical cord mesenchymal stem cells; IGF-1 – insulin-like growth factor 1; MEF-2C – myocyte-specific enhancer factor 2C; MHC – myosin heavy chain; RGO – *Rehmannia glutinosa* oligosaccharide; Sal-B – salvianolic acid B; TGF-β1 – transforming growth factor-β1; VEGF – vascular endothelial growth factor; WJ-MSCs – Wharton's jelly mesenchymal stem cells; 5-Aza – 5-azacytidine.

While subtle cases can go unnoticed without imaging, advances in echocardiography now enable reliable detection of most septal defects, patent ductus arteriosus, anomalous pulmonary venous return, and transposition of the great arteries, facilitating timely diagnosis and management.[39]

The mortality rate among CHD patients is highest during the 1st year of life.[42] The LICs and LMICs are especially impacted, and congenital disabilities have been related to increased newborn mortality rates. The birth prevalence of CHD is increasing in LICs and LMICs, and there is substantial evidence that surgery reduces the disease burden. In many LICs and LMICs, the identification of CHD is hampered by under-resourced health systems and a shortage of trained personnel.[6]

Current management of CHD

Treatment of CHD aims to correct anatomic defects and manage their sequelae. Intervention should be undertaken at the earliest feasible opportunity, with surgical repair representing the standard of care. However, not all patients are candidates for corrective surgery.[43] The following strategies may be employed in CHD management:

Drug usage

Medication regimens, including β-blockers, diuretics, prostaglandins, digoxin, and sacubitril, are tailored in dose and timing to the specific cardiac lesion to reduce

myocardial workload and enhance ventricular function.[44] When bradyarrhythmias or conduction defects impair cardiac output, implantation of a pacemaker or implantable cardioverter-defibrillator provides essential rhythm support and helps prevent complications associated with congenital conduction abnormalities.[45]

Catheter-based interventions

Catheter-based interventional cardiology enables the repair of CHD without open surgery. Under fluoroscopic and echocardiographic guidance, a thin, flexible catheter is introduced – typically via the femoral vessels – and navigated to the cardiac lesion. Once in position, specialized devices (such as balloons, occlusion plugs or stents) are delivered through the catheter to correct septal defects, relieve valvular stenosis or address vascular obstructions. This minimally invasive approach allows for avoiding surgical incisions, minimizes tissue trauma and generally reduces hospital stays and overall costs.[46–49] World Bank estimates indicate that Asia and Africa each have fewer than 1 cardiac catheterization laboratory per 1,000,000 inhabitants. Many low-income African nations lack any functional cardiac catheterization laboratory, leaving large portions of their populations without access to essential tertiary cardiac care.[6]

Heart surgery

When catheter-based interventions are insufficient to correct CHD, open-heart surgery becomes necessary. Surgical procedures aim to repair or replace malformed valves, enlarge constricted vessels and close intracardiac septal defects. While coronary artery bypass grafting (CABG) is an example of cardiac surgery, congenital anomalies such as Tetralogy of Fallot and coarctation of the aorta are routinely managed through specialized corrective operations.[43] However, access to cardiac surgery is often constrained, and most patients present late, or for the first time, with comorbid infections, severe malnutrition and impaired growth and development in LICs and LMICs.[6]

Heart transplantation

If medications or other treatment options cannot resolve the cardiac problem, a heart transplant may be the best option. The process known as a heart transplant involves removing a damaged heart and replacing it with a healthy donor heart.[43]

There are significant differences between LICs and LMICs and high-income countries (HICs) in terms of CHD prevalence, status and concerns. In HICs, most children with CHD are detected during antenatal screening, infancy or childhood. Over 90% of those born with CHD survive into maturity due to available intervention facilities. In most LMICs, CHD diagnosis relies on health systems and specialized personnel – which remain severely limited in the lowest-income regions.[6]

Mesenchymal stem cells as a promising strategy in congenital heart disease

Stem cells are unique cells defined by their capacity for unlimited self-renewal, their undifferentiated state and their ability to differentiate into multiple specialized cell types. These characteristics make them promising candidates for cell-based therapies aimed at treating degenerative conditions such as diabetes mellitus, cardiovascular disease and beyond.[46]

Stem cells can be broadly divided into embryonic SCs (ESCs) and adult (somatic) SCs (ASCs). Based on their developmental potential, they are further classified into 4 categories. Totipotent SCs – such as the zygote – can give rise to all embryonic and extraembryonic tissues. Pluripotent SCs – including ESCs and iPSCs – are capable of differentiating into derivatives of the 3 germ layers (endoderm, mesoderm and ectoderm) but cannot form extraembryonic structures like the placenta or umbilical cord. Multipotent SCs – such as MSCs and hematopoietic SCs (HSCs) – can differentiate into a limited range of cell lineages, whereas unipotent SCs, like renal stem/progenitor cells (RSPCs), are restricted to producing a single specialized cell type while still retaining the capacity for self-renewal.[47,48]

The ASCs consist of HSCs and MSCs. Furthermore, MSCs are commonly isolated from cord blood, peripheral blood, bone marrow, and fat tissue. When cultured, the cells will produce a cell line that morphologically resembles a fibroblast (fibroblast-like cell). In research, SCs can act as diagnostic cells where they can be applied to screen new drugs and test for cell damage due to viral infection.[47]

According to the International Society for Cellular Therapy, MSCs must meet 3 criteria: they must adhere to plastic under standard culture conditions; they must express CD105, CD73 and CD90 while lacking surface expression of CD45, CD34, CD14 (or CD11b), CD79α (or CD19), and HLA-DR; and they must demonstrate the capacity to differentiate in vitro into adipocytes, chondrocytes and osteoblasts.[49]

Friedenstein et al. were the first to isolate MSCs from mouse bone marrow, noting their fibroblast-like morphology and plastic adherence. Subsequent studies have identified MSCs in bone marrow as well as in umbilical cord blood, adipose tissue, peripheral blood, amniotic fluid, Wharton's jelly, placenta, dental pulp, and dermis. Prior to experimental use, confluent MSC cultures – grown as a uniform monolayer – must be passaged to maintain optimal growth conditions.[50]

Mesenchymal stem cell therapy has been shown to improve cardiac function and reduce scar formation in patients with heart disease. These benefits are mediated primarily through enhancement of endogenous repair mechanisms, improving tissue perfusion, modulating the immune response, inhibiting fibrosis, and promoting proliferation of resident cardiac cells. In animal models,

rare instances of MSC differentiation into cardiomyocytes and vascular components have also been documented.[51]

Owing to their unique properties – including differentiation into cardiovascular lineages, immunomodulatory and antifibrotic effects, and the promotion of neovascularization – MSCs play a key role in the treatment of cardiovascular diseases. Autologous MSC transplantation has been shown to be safe in patients with cardiomyopathy, and allogeneic MSCs can likewise be administered with minimal immunogenicity.[51]

Despite these advancements demonstrating the potential of stem cell transplantation, neither preclinical nor clinical research has yet achieved complete cardiac recovery. To reach this goal, novel cell-based treatment strategies are required. Current research focuses on integrating MSCs with biomaterials, employing cell combinations, applying genetic modification, or preconditioning MSCs to enhance the secretion of paracrine factors such as growth factors, exosomes and microRNAs.[48] Mesenchymal stem cells used for cardiomyocyte differentiation have been isolated from diverse sources, including Wharton's jelly (umbilical cord), adipose tissue, bone marrow, endometrium, and even from olfactory bulbs of rats, mice, sheep, porcine species, and humans.[17–19,23–37] During growth factor-induced cardiomyogenic differentiation, MSC-specific markers decline while cardiac-specific markers are upregulated. Moreover, MSCs derived from umbilical cord tissue differentiate into cardiomyocytes more efficiently than those from bone marrow.[52]

Mesenchymal stem cells derived from Wharton's jelly of the umbilical cord (UC-MSCs) represent a primary and practical cell source. Due to their noninvasive collection from abundant medical waste, ease of isolation and expansion, and high proliferative capacity, UC-MSCs are particularly suitable for LICs and LMICs.[53,54] Moreover, unlike ESCs, UC-MSCs are non-tumorigenic, exhibit low immunogenicity and pose minimal ethical concerns.[55,56]

The application of SCs is promising in future regenerative medicine.[46] The human iPSC-derived cardiomyocytes can be used as diagnostic cells, heart disease models, for drug discovery, developmental biology, and regenerative medicine.[57] Other type of stem cells such as iPSCs, ESCs and ASCs could be use as the source of cellular therapy in CHD. The use of iPSCs in cardiovascular disease has raised the risk of arrhythmogenesis, tumor growth and immune reaction rejection. Induced pluripotent SCs can differentiate into cardiomyocytes in vitro when exposed to growth factors such as VEGF, bFGF, TGF-β1, BMPs, or retinoic acid (RA).[47] However, to develop into cardiomyocytes, iPSCs must be reprogrammed from somatic cells, which is costly and time-consuming.[48]

Stem cell-based therapies hold great promise for future regenerative medicine.[46] Human iPSC-derived cardiomyocytes can serve as diagnostic tools, in vitro disease models, platforms for drug discovery and developmental biology, and ultimately as regenerative treatments.[58] In addition to iPSCs, ESCs and ASCs are valuable sources for cellular therapies in CHD. However, iPSC-based cardiovascular approaches carry risks of arrhythmogenesis, tumorigenicity and immune rejection. The iPSC differentiation into cardiomyocytes can be driven in vitro by growth factors such as VEGF, bFGF, TGF-β1, BMPs, or RA.[59] Nevertheless, reprogramming somatic cells into iPSCs remains costly and time-consuming.[55]

Mesenchymal stem cells are a promising therapy for CHD because they are multipotent and can differentiate into various cell types, including cardiomyocytes. This capacity enables them to regenerate damaged cardiac tissue.[60] Studies have shown that MSCs can reduce myocardial fibrosis and improve left ventricular ejection fraction (LVEF) and endothelial function without increasing the risk of malignancy or arrhythmia. Furthermore, MSCs from multiple sources, such as bone marrow, adipose tissue, placenta, and umbilical cord, are suitable for allogeneic use.[48] Mesenchymal stem cell therapy contributes to myocardial repair by promoting cardiomyocyte regeneration and has not been associated with adverse effects on myocardial integrity or tissue viability. Moreover, MSCs exert paracrine actions that enhance cardiac function and reduce scar burden, myocardial fibrosis and infarct size. Mesenchymal stem cells release a broad spectrum of bioactive mediators – such as cytokines, growth factors, chemokines, and microRNAs – that underpin their paracrine actions.[51]

They also exhibit anti-inflammatory properties, which can mitigate tissue injury resulting from chronic inflammation, a common feature of CHD. Furthermore, MSCs enhance angiogenesis by promoting new vessel formation, thereby improving blood supply to ischemic myocardium. In cell therapy applications, MSCs act as immunomodulators, regulating host immune responses to minimize the risk of graft rejection.[52]

Mesenchymal stem cells can ameliorate myocardial infarction by promoting angiogenesis and neovascularization, enhancing myocardial repair, inhibiting cardiomyocyte apoptosis, and replacing injured cardiomyocytes. Numerous phase I and II clinical trials have reported promising results for MSC-based regenerative therapies. Key factors in developing standardized MSC therapy protocols include selecting the optimal cell source, standardizing preparation procedures, determining the ideal dose and administration route, and ensuring reproducible clinical outcomes.

The results of phase III clinical trials are crucial for validating the therapeutic application of MSCs in cardiovascular medicine. Preconditioning techniques have enhanced engraftment, proliferation, differentiation, and survival of transplanted MSCs, thereby improving therapeutic efficacy.[51]

Signalling pathways regulating in vitro differentiation of MSCs into cardiomyocytes

Mesenchymal stem cells are self-renewing, multipotent progenitors capable of differentiating into cardiomyocytes as well as other mesodermal lineages. In vitro,

MSC-to-cardiomyocyte differentiation can be driven by paracrine factors such as Wnt ligands, hepatocyte growth factor (HGF), platelet-derived growth factor (PDGF), and activation of Notch signaling.[61,62] According to Raman et al., signaling pathways such as HGF, PDGF and Notch regulate the differentiation of MSCs into cardiomyocytes.[63]

Cardiomyocytes, endothelial cells and vascular smooth muscle cells (VSMCs) derive from cardiac progenitor cells (CPCs) through migration, proliferation and differentiation processes that are stimulated by HGF secreted by MSCs. The Notch1 receptor and HGF/Met regulate the cell fate of CPCs. The Met tyrosine kinase receptor and HGF activation pathways lead to the induction of ERK1/2, p38 mitogen-activated protein kinase (MAPK) and phosphatidylinositide-3 kinase (PI3K/Akt) activities. In the early phases of cardiomyocyte maturation, HGF and Met receptors express transcription factors and structural genes such as *Mef2C*, *TEF1-α*, *GATA-4*, *α-MHC*, and *desmin*. Wnt receptors and the hepatocyte growth factor–immunoglobulin G (HGF–IgG) complex initiate biochemical signaling that drives epithelial–mesenchymal transition (EMT) and subsequent differentiation into cardiomyocytes.[63,64]

The final stage of heart development, i.e., maturation, follows mesoderm formation and cardiac progenitor cell specification. Maturation is characterized by structural, transcriptomic, metabolic, and functional specialization of cardiomyocytes, enabling the heart to generate strong, efficient and enduring contractile force. Insulin-like growth factors regulate cardiomyocyte maturation via receptor tyrosine kinases, including the insulin-like growth factor 1 receptor (IGF1R) and the insulin receptor (INSR), which activate the PI3K–AKT and RAF–MEK–ERK signaling cascades.[65]

In vitro differentiation of MSCs into cardiomyocytes mimics in vivo cardiomyogenesis

Mesenchymal stem cells differentiate into cardiomyocytes only when specific signaling pathways are modulated and the requisite combination of growth factors, small molecules and extracellular matrix (ECM) components is present. Thus, these factors must be administered at defined concentrations and for precise durations to effectively drive differentiation.[62]

The differentiation of stem cells into cardiomyocytes in vitro is similar to the process of cardiomyogenesis in vivo. The mechanism starts from mesoderm induction, and then continues to cardiac progenitor cells or precardiomyoblasts, immature cardiomyocytes or cardiomyoblasts, and mature cardiomyocytes.[13,66]

Wnt, Activin, NODAL, and bone morphogenetic protein (BMP) signals impact early cardiomyogenesis. Several transcription factors have a role in early cardiomyogenesis, including Nkx2.5, GATA-4 and Tbx5. Other molecular cues, including Wnt pathway inhibitors and differentiation inducers such as fibroblast growth factors (FGFs) and BMPs, play critical roles in cardiac specification and differentiation.[67,68] Differentiation towards the cardiac mesoderm lineage depends on the amount and timing of certain factors, such as BMP-4, TGF-β1, family member Nodal (or Activin A as a substitute of Nodal), and Wnt modulators.[67,68]

During embryonic development, Wnt has a biphasic form, inhibiting cardiac induction at later stages and promoting cardiac gene expression at the early stage of mesoderm formation.[69] Previous research showed that 5-Aza and Sal-B can improve early mesodermal commitment by increasing Wnt/β signaling.[70,71] Even though Wnt plays a role in differentiation to early cardiomyocyte, the latest study has shown that adding Wnt inhibitors (such as IWR-1, IWP-3 or XAV939) enhanced cell differentiation in the late-phase of differentiation to the cardiac progenitor cell stage.[22] The administration of neuregulin, fibroblast growth factor 1 (FGF-1), IGF-1, and periostin peptide can be used to promote postnatal cardiomyocyte cycling or late-stage cardiomyocyte.[72]

Under defined in vitro conditions, MSCs can differentiate into mesodermal cell types, including cardiomyocytes, when exposed to tailored "cocktails" of small molecules and growth factors that precisely direct lineage specification. For example, a defined cocktail of factors, including bFGF, Sal-B, TGF-β1, BMP-2, 5-Aza, NRG-1, forskolin, and Ang-II, induces MSC differentiation into cardiomyocytes.[17–19,23–37] The expression of cardiomyocyte-specific genes and proteins is evidence for in vitro differentiation. Soluble chemical factors in the culture medium initiate signaling cascades that regulate cell differentiation.

Chemical inducer for in vitro differentiation of MSCs into cardiomyocytes

5-azacytidine

5-azacytidine is commonly used to induce MSCs to differentiate into cardiomyocytes in vitro. It can also be used in stem cell laboratories in LMICs. 5-azacytidine is a cytidine nucleoside analog and DNA demethylating agent primarily used to induce MSC differentiation into cardiomyocytes in vitro. It inhibits DNA methyltransferases, thereby modulating chromatin structure, gene expression and processes such as X-chromosome inactivation. A potent inhibitor of DNA (cytosine-5)-methyltransferases (DNMTs), 5-Aza promotes DNA demethylation and activates cardiac gene expression.[21] The concentration of 5-Aza used to induce MSC differentiation into cardiomyocytes is typically 10 μmol/L for 24 h, resulting in upregulation of cardiac markers such as Cx43 and cTnT.[15,18,23,25,31]

Further research showed that 5-Aza administration in human UC-MSCs induced the activation of extracellular signal-related kinases (ERK) but did not affect protein kinase C.

A particular ERK inhibitor, U0126, can potentially prevent human UC-MSCs from expressing cardiac-specific proteins and genes when 5-Aza is present. These findings indicate that persistent activation of the ERK pathway by 5-Aza induces in vitro differentiation of human UC-MSCs into cardiomyocytes.[73] Differentiation of cardio-sphere-derived cells (CDCs) into cardiomyogenic cells can be induced with 5-Aza by upregulating cardiac-specific genes like *Nkx2.5, α-sarcomeric actin* and *GATA-4*. The phosphorylation of β-catenin is negatively regulated by the Wnt pathway.[69]

During development, the pathway of Wnt/β-catenin-dependent controls important elements of polarity, migration, organogenesis, and patterning. Similarly, Wnt/β-catenin signaling is crucial for the maturation of cardiomyocyte-derived MSCs. The Wnt/β-catenin signaling can stimulate the mouse bone marrow-derived MSCs (BM-MSCs) to differentiate into cardiomyocytes and upregulate the myogenic regulatory factors (*MRFs*). Nevertheless, 5-Aza significantly upregulates glycogen synthase kinase-3 (GSK-3), thereby modulating cardiogenesis.[61]

Neuregulin-1

Neuregulin-1 is an epidermal growth factor (EGF) that promotes proliferation, differentiation and survival in several tissues, such as breast epithelial cells, glial cells, neurons, and myocytes. A group of tyrosine kinase receptors (ErbB2, ErbB3 and ErbB4) exerts its biological effects by dimerizing upon ligand binding, which results in phosphorylation and subsequent signaling. NRG-1/ErbB signaling is most recognized for its critical function in developing neurons and the embryonic and adult heart.[74,75]

Neuregulin-1 promotes the development and survival of embryonic stem cell-derived cardiomyocytes and directs their differentiation into cardiac conduction system cells. When the endocardial endothelium produces NRG-1, the surrounding cardiomyocytes express ErbB2 and ErbB4 in the embryonic heart. On the other hand, aside from its function in ventricular trabeculation and cardiac cushion creation, the ErbB3 receptor is not expressed in the endocardium or the myocardium.[74]

In the adult heart, NRG-1 is expressed by cardiac endothelial cells adjacent to cardiomyocytes, specifically within the endocardium and myocardial microvasculature, whereas cardiomyocytes express ErbB2 and ErbB4 receptors but lack ErbB3. Angiotensin II and epinephrine raise blood pressure and inhibit endothelial production, while endothelin-1 and mechanical strain promote it. Neuregulin-1 binds to ErbB4 receptors on cardiomyocytes, inducing either ErbB4 homodimerization or ErbB4/ErbB2 heterodimerization. This receptor dimerization activates the Akt and ERK signaling pathways, resulting in growth-promoting and cytoprotective effects. Moreover, cooperative signaling between M2 muscarinic receptors and activation of cardiomyocyte nitric oxide synthase (NOS) modulates cardiac contractility and adrenergic responsiveness.[74]

Basic fibroblast growth factor, NRG-1 and cyclic adenosine monophosphate (cAMP) regulate signaling pathways that direct myocardial cell specification. In ESCs, these factors stimulate cardiac-specific transcription factors such as GATA4 and Nkx2.5. Neuregulin-1, bFGF and forskolin have been implicated in regulating cardiac cell-fate determination and heart development. These factors influence both cardiomyocyte differentiation and the cardiac microenvironment. Since all growth factors were applied simultaneously, the relative contribution of each component to myocardial specification remains unclear. For MSC induction into cardiomyocytes, NRG-1 is administered at 50 ng/mL (1.92×10^{-6} M).[24]

Forskolin

Forskolin, a cell-permeable diterpenoid, activates adenylate cyclase and protein kinase A, thereby elevating intracellular cyclic adenosine monophosphate (cAMP) levels. It possesses antihypertensive and positive inotropic effects. The forskolin-induced response in embryonic cardiomyocytes indicates a functional cAMP signaling pathway. Moreover, forskolin modulates calcium transport and currents and stimulates adrenergic receptors in culture, leading to hypertrophic responses. It increases the expression of cardiomyocyte markers, *cTnT* and myocyte enhancer factor 2C (*Mef2c*), while suppressing mesodermal and cardiac progenitor markers.[76,77] Forskolin treatment enhances the beating frequency of cardiomyocytes. Forskolin is administered at a concentration of 10 mM to induce MSC differentiation into cardiomyocytes.[24]

Basic fibroblast growth factor

The bFGF is required for the initial development of the embryo, especially to maintain mesoderm lineages during cardiac organogenesis. It is a potent mitogen that controls stem cell migration, differentiation, proliferation, and survival. The bFGF promotes the ESCs to differentiate into early maturation cardiomyocytes and expresses cardiac markers of α-cardiac myosin heavy chain (MHC) and β-MHC. These findings suggest that bFGF must act synergistically with additional factors to drive MSC differentiation into cardiomyocytes. Basic fibroblast growth factor also enhances the migration capacity of MSCs by activating the Akt signaling pathway.[21,78,79] The concentrations of bFGF used to induce MSC differentiation into cardiomyocytes are 10 ng/mL and 20 ng/mL when applied in combination with other factors.[24,32]

The bFGF is expressed in cardiac progenitor cells; it plays an important role in early cardiomyogenesis and directly influences cardiomyocyte formation. Before downregulating the early phase of vertebrate cardiac development in vivo, bFGF is involved in the autoregulatory mechanisms of cardiomyocyte proliferation and differentiation. During the tubular stage of cardiogenesis, bFGF and FGF

receptor-mediated signaling govern cardiomyocyte formation. However, beyond the 2nd week of embryogenesis, myocyte development becomes independent of bFGF.[79]

Transforming growth factor-β1

Transforming growth factor-β1 is a pleiotropic cytokine that regulates multiple aspects of cellular and tissue physiology. The TGF-β1 is a cytokine with several functions that influence the survival, proliferation and differentiation of several kinds of cells.[19] The development of the ventricular myocardium and the formation of the coronary vasculature during embryogenesis are influenced by TGF.[21] Previous studies have shown that TGF-β1 can drive the differentiation of BM-MSCs and ESCs into cardiomyocytes, and that TGF-β1 is essential for embryonic heart development.[80]

TGF-β1 is more effective in expressing α-actin, Cx43, MHC, and cTnI when combined with other factors like 5-Aza. Additionally, TGF-β1 and Sal-B increase the expression of cardiac markers like GATA-4 and Nkx2.5 compared to either factor alone. The dose of TGF-β1 for inducing rat BM-MSCs to cardiomyocytes is 5 ng/mL and 10 ng/mL.[19,31] Rat BM-MSCs exhibited significantly increased mRNA expression of *Cx43*, *myocyte enhancer factor 2C* (*MEF2C*), *α-actinin 2* (*ACTN2*) and *cardiac troponin T* (*TNNT2*) in response to TGF-β1, electrical stimulation (ES) and combined TGF-β1 + ES treatments compared with control.[36]

Bone morphogenetic protein 2

The BMP superfamily has gained significant attention since the discovery in 1988 that BMP-2 potently induces bone and cartilage formation in vertebrate skeletal biology.[81] Undifferentiated MSCs are converted into chondrocytes and osteoblasts as well as osteoprogenitors into osteoblasts through the action of the BMP. The use of BMP-2 therapy is to improve cardiomyocyte contractility and prevent cell death, leading to significant implications for treating myocardial ischemia.[17,33] Therefore, in LMICs, BMP could be a growth factor that induces MSCs to differentiate into cardiomyocytes.

Mesenchymal cells from bone marrow can be converted into cardiomyocytes using BMP-2. According to Lv et al., Sal-B combined with BMP-2 at 250 mg/L and 200 ng/L, respectively, enhanced cardiomyocyte differentiation compared to single treatments.[33] Conversely, Hou et al. showed that the combination of 10 μg/L BMP-2 and 10 μmol/L 5-Aza significantly increased the rate of cardiac differentiation and showed reduced effects on cell damage.[17]

BMP-2 has shown therapeutic promise in treating myocardial disease by preventing the death of cells and enhancing cardiomyocyte contractility. It promoted the phosphorylation of the Smad1/5/8 protein, which saved adult cardiomyocytes from oxidative stress and long-term hypoxia-induced cell damage without activating the cardiodepressant TGF-β pathway.[82]

A previous study documented that after being treated with BMP-2, BM-MSCs showed enhanced differentiation to cardiomyocytes by identifying cardiomyocyte-specific protein expression, ultrastructural characterization and transcription factor mRNA expression. Additionally, Sal-B, extracted from *Salvia miltiorrhiza*, when combined with BMP-2, may enhance the efficiency of cardiomyocyte differentiation.[33]

Angiotensin II

Angiotensin II is a bioactive substance present in myocardial cell lysate and has many biological effects in addition to aiding in the development of the myocardium microenvironment. Angiotensin I is transformed by the angiotensin-converting enzyme (ACE) into Ang-II, activating Ang-II receptors to modulate various cardiovascular responses, such as vasoconstriction and heart growth.[83]

The dose of Ang-II is 0.2 mg/mL or 0.2 mmol/L and 0.1 mmol/L is used to induce MSCs in cardiomyocytes for 24 h.[23,32] Angiotensinogen is formed by the liver and transformed into angiotensin I and II. The action of the renin–angiotensin system (RAS) can be initiated by Ang-II binding to the angiotensin II receptor type 1 and type 2 (AT1R and AT2R), or it can be further degraded or altered to produce the cardioprotective peptides angiotensin, angiotensin IV and alamandine, which operate by binding to Mas-related G protein-coupled receptor member D (MrgD), AT4R and MasR receptors, respectively. N-acetyl-seryl-aspartyl-lysyl-proline (Ac-SKDP), apelin and angioprotectin have been discovered as novel cardioprotective RAS peptides. As a result, the RAS can have both pathogenic and cardioprotective effects on the heart, with the relative importance of each defining the cardiovascular system's overall impact. The interaction of Ang-II with AT1R results in the activation of numerous intracellular signaling pathways, including MAPK, β-arrestin, G protein-independent, JAK/STAT, protein kinase C (PKC), scaffold proteins, numerous tyrosine kinases, and the transactivation of growth factor receptors.[84]

Salvianolic acid B

Salvianolic acid B is a water-soluble phenolic compound isolated from *Salvia miltiorrhiza*, a traditional Chinese medicinal herb used for centuries to treat various cardiac disorders. It has been shown to inhibit apoptosis induced by combined hyperglycemia and hypoxia in cardiomyocytes derived from ASCs. Lv et. al. described that Sal-B inhibited apoptosis by reducing the levels Bcl-2/adenovirus E1B 19-kDa-interacting protein 3 (BNIP3), hypoxia inducible factor 1 subunit alpha (HIF1α) and cleaved caspase 3. Salvianolic acid B has been proven in trials to stimulate human MSCs' osteogenesis without cytotoxicity,

making it a viable therapeutic agent for the treatment of osteoporosis.[33]

Shu et. al. explained that Sal-B protects iPSC-derived neuron SCs (NSCs) exposed to H_2O_2, while Gao et al. suggested that Sal-B enhances the ability of BM-MSCs to differentiate into type I alveolar epithelial cells.[85,86] According to the study by Lv et al., MSCs treated with Sal-B and TGF-β1 expressed higher levels of cardiac-specific markers – including Nkx2.5, GATA-4 and cTnI – compared with the control group. TGF-β1 and Sal-B can be used effectively to reduce apoptosis. In the study by Lv et al., Sal-B demonstrated cardioprotective effects in acute myocardial infarction, making it a potentially valuable therapeutic adjunct. Their western blot analyses of proteins related to autophagy, apoptosis and angiogenesis further supported the cardioprotective role of Sal-B. Owing to these properties, Sal-B represents a relatively safe and promising trigger for cardioprotection.[19]

Lv et al. and Chan et al. found that Sal-B alone had minimal impact. However, when Sal-B is combined with TGF-β1 or vitamin C, it can promote MSCs or other SCs to differentiate into cardiomyocytes and increase the expression of cardiomyocyte maturation markers in a dose-dependent manner. The switch between neurogenesis and cardiomyogenesis in SC differentiation can be regulated by p38 MAP kinase activity. The dose of Sal-B to induce differentiation to cardiomyocytes is 250 mg/L for 72 h.[33,87] Salvianolic acid B also increased the expression of Wnt signaling proteins while reducing the expression of transcription factors associated with the Notch signaling pathway.[71]

Insulin-like growth factor

Insulin-like growth factor 1 is a 70-amino-acid, single-chain protein critical for cardiomyocyte development. It inhibits apoptosis and necrosis while promoting the growth, proliferation and differentiation of diverse cell types, both in vivo and in vitro, including vascular smooth muscle cells and cardiomyocytes. Upon binding to its receptor, the IGF1R, IGF-1 engages the receptor's intrinsic tyrosine kinase activity, triggering downstream signaling cascades such as the MAPK and PI3K/Akt pathways.[88]

In co-cultured myocardium and BM-MSCs, HGF and IGF-1 stimulated the cardiac-specific transcription factor GATA4 expression, representing myocardial differentiation.[89] Insulin-like growth factors can be essential for LICs because they play a significant role in stem cell biology, which can either improve differentiation or enhance proliferation and self-renewal.[90]

Other treatment for in vitro differentiation MSCs to cardiomyocyte

Even though there are numerous methods for inducing MSCs to differentiate into cardiomyocytes, the results of differentiation in 2D culture might occasionally be insufficient, immature and unpure.[62] In addition to supplementary growth factors, several adjunctive strategies – such as ES, controlled hypoxia, co-culture with cardiomyocytes, and 3D approaches using hydrogels or scaffolds – are employed to enhance the efficiency of MSC-to-cardiomyocyte differentiation (Fig. 2).

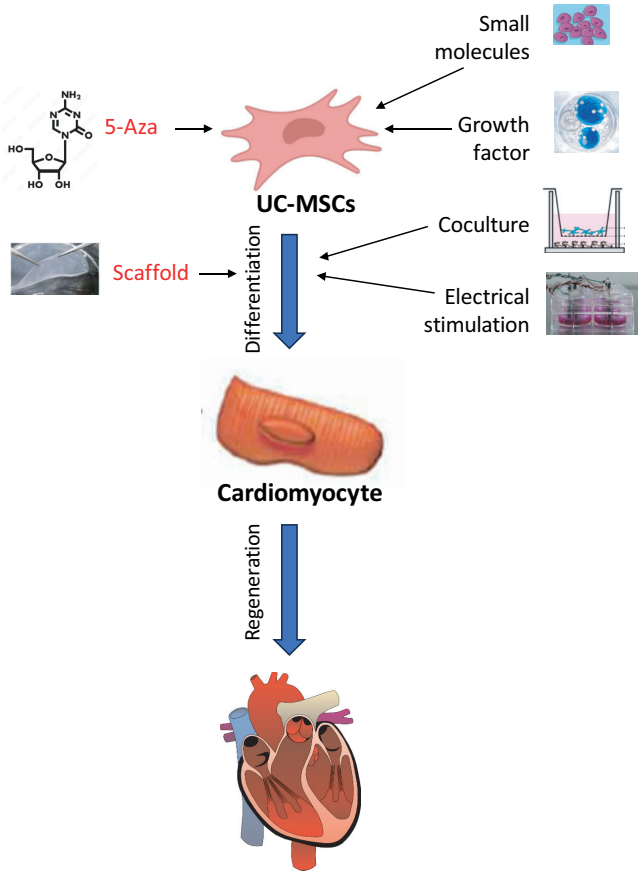

Fig. 2. An additional technique to differentiate UC-MSCs into cardiomyocytes.

UC-MSCs – umbilical cord mesenchymal stem cells; 5-Aza – 5-azacytidine.

Co-culture of cells

Co-culture involves growing MSCs with other cell types to promote intercellular communication through direct cell–cell interaction, paracrine signaling and soluble molecules.[91] Previous research showed that MSCs co-cultured with cardiomyocytes can differentiate into these cells. It is suggested that one of the factors influencing the differentiation of MSCs into cardiomyocytes is direct cell-to-cell contact. The co-culture technique enables research into physical and paracrine variables influencing cardiac cell fate and differentiation.[24]

Co-culturing MSCs with cardiomyocytes in vitro produced direct contact between both types of cells. They formed gap junctions, which reverse-facilitated the low-resistance transmission of electrical and chemical signals between neighboring cells, a process linked to cardiomyogenic differentiation. Co-culturing MSCs with cardiomyocytes also promoted MSC expression cardiac-specific

markers, like Cx43, Nkx2.5, GATA-4, sarcomeric α-actin, MHC, cTnI, and atrial natriuretic peptide, because the adult heart tissue environment expresses the right signals that encourage SCs to differentiate into cardiomyocytes. Co-culture MSCs with neonatal cardiomyocytes and the addition of growth factors such as neuregulin, forskolin and bFGF can differentiate into cardiomyocytes and show synchronous contractions.[24,92]

Electrical stimulation

An essential component of the cardiomyocyte microenvironment is the electrical milieu: in vitro, this is created by connecting the culture well plate to electrodes and applying voltage across the medium. According to He et al., ES can promote SC differentiation toward both cardiogenic and neurogenic lineages. Electrical stimulation enhances the expression of cardiac transcription factors Nkx2.5 and GATA4, which are critical during early myocardial development. In rat BM-MSCs, ES promotes cardiomyocyte differentiation by upregulating TGF-β1 and increasing the expression of Cx43 and α-sarcomeric actinin.[36]

Scaffold

The cell requires a scaffold that provides rigidity and biological support to differentiate into cardiomyocytes. A combination of cells, scaffolds and growth factors can regulate cellular activity and cell differentiation.[93] Scaffolds are essential in tissue engineering because they can support and provide resilience to SCs by creating an appropriate microenvironment that aids cell transplantation and regeneration.[8] Biological scaffolds facilitate the growth, development and implantation of SCs in injured cardiac tissue. The scaffold can be applied in LICs and LMICs due to its potential advantages. This increases the efficacy of stem SC-based therapies and makes them more widely available and reasonably priced.[94]

Graphene oxide (GO)-based scaffolds reported as innovative scaffolds to enhance the in vitro differentiation capacity of human UC-MSCs. Graphene oxide may engage cellular mechanotransduction pathways and modulate how cells respond to external stimuli. Derivatives of graphene may be used as cell mechanical stimulation inducers to improve the efficiency of angiogenic and cardiogenic differentiation in human UC-MSCs.[34]

During the differentiation of MSCs into cardiomyocytes, the specific marker proteins are expressed in the cell membrane. Mesenchymal stem cells are positive for CD90, CD73 and CD105, and negative for CD34 and CD45.[95] Thus, a specific cell surface marker on BM-MSCs can identify their cardiomyogenic differentiation. Spontaneous contractions combined with expression of cardiomyocyte-specific markers confirm MSC differentiation into functional cardiomyocytes. Cardiac-specific markers encompass transcription factors (Nkx2.5 and GATA4), gap-junction protein Cx43, MEF2C, sarcomeric proteins (α-MHC, titin, desmin, α-cardiac actin), and cardiac peptides such as ANP, cTnI and cTnT.[17–19,23–37]

Discussion

Mesenchymal stem cells have emerged as a promising option for regenerating injured cardiac tissue, garnering increasing attention in recent years.[96] In CHD, MSCs offer new therapeutic possibilities. In this review, we comprehensively analyzed growth factors, with particular emphasis on individual factors and their combinations, that can trigger MSC differentiation into cardiomyocytes. Moreover, we propose a streamlined, scaffold-based in vitro protocol to enhance MSC-to-cardiomyocyte differentiation, tailored for stem cell laboratories in LMICs.

Mesenchymal stem cells derived from diverse sources, including the olfactory bulb, endometrium, adipose tissue, Wharton's jelly of the umbilical cord, and bone marrow, can differentiate into cardiomyocytes in vitro. The MSC-to-cardiomyocyte differentiation is induced by administering specific growth factors and small molecules, such as RA, 5-Aza, Ang-II, bFGF, Sal-B, TGF-β1, BMP-2, forskolin, and NRG-1.[17–19,23–37] Various induction "cocktails" have been evaluated for MSC-to-cardiomyocyte differentiation, including: 5-Aza with TGF-β1; 5-Aza with BMP-2; Sal-B with BMP-2; bFGF, forskolin and NRG-1; TGF-β1 with Sal-B, TGF-β1 combined with bFGF, IGF-1 and VEGF; TGF-β1 with ES; and 5-Aza with Ang-II and TGF-β1.

All the studies mentioned above[17–19,23–37] indicate that using cocktails to differentiate MSCs into cardiomyocytes can improve cardiomyocyte marker expression compared to single factors. The efficiency of differentiation can be verified using qualitative data from immunofluorescence or immunohistochemistry (IHC). Hou et al. found that BMP-2 and 5-Aza induced BM-MSC differentiation with an efficiency of 27.97 ±1.77%.[17] According to Lv et al., 5-Aza had an approx. 30% success rate in converting MSCs into cardiomyocytes.[19] Li et al. identified that the percentage of cTnT-positive cells, one of the cardiomyocyte markers, was approx. 46.3 ±2.1%.[18]

The mechanism that enables SCs to differentiate into cardiomyocytes in vitro is similar to the process of in vivo cardiogenesis, with the mesoderm being the initial target, followed by cardiac progenitor cells or pre-cardiomyoblasts, immature cardiomyocytes or cardiomyoblasts, and mature cardiomyocytes. GATA-4, MEF-2C, Nkx2.5, MHC, Cx43, cTnT, cTnI, α-actin, and desmin are frequently used cardiomyocyte markers. Nkx2.5, GATA4, Tbx5, Islet-1 (Isl-1), and myocyte enhancer factor 2C (MEF2C) serve as markers of cardiac progenitor cells. Nkx2.5 and Tbx5/20 remain expressed by immature cardiomyocytes or cardiomyoblasts, along with myosin heavy chain (*MYH*), GATA-4 and Hand 1/2. Mature cardiomyocytes express markers such as cTnT, α-sarcomeric actinin, myosin light chain 2a

(MLC2a), myosin light chain 2v (MLC2v), sodium channel subunit SCN5A, L-type calcium channel subunit CACNA1C, cardiac myosin heavy chain (cMHC), and Iroquois homeobox 4 (IRX4).[13,66]

A streamlined differentiation protocol minimizes the number of reagents needed to modulate each signaling pathway and prioritizes readily available chemicals, which is especially advantageous in LMIC settings. We propose a streamlined, stage-specific protocol for MSC-to-cardiomyocyte differentiation: first, induce cardiac mesoderm with 5-Aza; next, specify cardiac progenitor cells via Wnt pathway inhibition; and finally, drive cardiomyocyte maturation using IGF-1.

Huang et al. reported that MSCs co-cultured with rat neonatal cardiomyocytes in an induction medium supplemented with bFGF, forskolin and neuregulin exhibited spontaneous beating, demonstrating functional cardiomyocyte differentiation. Spontaneous contractions were also observed by Zhao et al. in MSCs treated with the Rho-associated protein kinase (ROCK) inhibitor Y-27632 in MethoCult medium.[24,37]

The cardiomyocyte differentiation protocol is suitable for laboratories or research centers with minimal facilities. Therefore, using fewer reagents that target key signaling pathways at each stage of differentiation is preferable. Employing readily available chemicals in LMICs and minimizing the use of additional techniques, such as selecting either scaffolds or 3D culture alone, offers a more practical and accessible approach.[97,98]

In monolayer, or two-dimensional (2D) culture systems, cell–cell interactions are confined to a single substrate layer during cardiomyocyte differentiation. The 2D approach is cost-effective and permits straightforward manipulation and precise arrangement of the culture. On the other hand, limitations include low throughput, reduced contact connections between cells and the ECM, and the absence of soluble growth agents. However, three-dimensional (3D) culture using a scaffold enhances cell proliferation and enables the ECM to recapitulate the native tissue microenvironment.[97,98]

In vitro, 3D cultures closely resemble the function of a miniature organ, with cells adhering tightly to one another and forming connections that facilitate signal transmission.[99] Developing 3D cultures is one of the techniques for promoting the maturation stage of cardiomyocytes derived from SCs.[100]

Limitations

Our review has several limitations. First, recent publications on MSC differentiation into cardiomyocytes are scarce, as research emphasis has shifted toward pluripotent SC applications. Second, many studies focus on advanced in vitro and in vivo models that may not translate easily to LIC/LMIC settings. Nevertheless, we believe this review provides a valuable foundation for future efforts to harness multipotent SCs in cardiovascular therapy, particularly for CHD. We also anticipate that forthcoming experiments will emphasize protocols and technologies accessible in LMICs and LLMICs.

Conclusions

Differentiation of MSCs into cardiomyocytes remains a key challenge in LICs and LMICs. Wharton's jelly-derived MSCs from the umbilical cord are particularly advantageous in these settings due to their noninvasive collection from abundant medical waste, ease of isolation and expansion, and high proliferative capacity. A straightforward, resource-efficient protocol for sequential cardiomyocyte differentiation involves inducing cardiac mesoderm with 5-Aza or BMP, followed by cardiac progenitor specification through Wnt pathway inhibition, and concluding with cardiomyocyte maturation promoted by IGFs. Finally, employing a 3D scaffold supports cell attachment and alignment and represents the most accessible technique for laboratories with limited infrastructure.

Use of AI and AI-assisted technologies

Not applicable.

ORCID iDs

Ariyani Noviantari https://orcid.org/0000-0001-7852-6983
Elrade Rofaani https://orcid.org/0009-0000-0922-8608
Radiana Dhewayani Antarianto https://orcid.org/0000-0002-8578-7505
Mulyadi M. Djer https://orcid.org/0000-0003-1235-1951

References

1. Roth GA, Johnson C, Abajobir A, et al. Global, regional, and national burden of cardiovascular diseases for 10 causes, 1990 to 2015. *J Am Coll Cardiol*. 2017;70(1):1–25. doi:10.1016/j.jacc.2017.04.052
2. Lodato V, Parlapiano G, Calì F, et al. Cardiomyopathies in children and systemic disorders: When is it useful to look beyond the heart? *J Cardiovasc Dev Dis*. 2022;9(2):47. doi:10.3390/jcdd9020047
3. Attenhofer Jost CH, Schmidt D, Huebler M, et al. Heart transplantation in congenital heart disease: In whom to consider and when? *J Transplant*. 2013;2013:376027. doi:10.1155/2013/376027
4. Edelson JB, Rossano JW. The difficult to transplant patient: Challenges and opportunities. *Prog Pediatr Cardiol*. 2019;54:101131. doi:10.1016/j.ppedcard.2019.101131
5. Mandalenakis Z, Giang KW, Eriksson P, et al. Survival in children with congenital heart disease: Have we reached a peak at 97%? *J Am Heart Assoc*. 2020;9(22):e017704. doi:10.1161/JAHA.120.017704
6. Zühlke L, Lawrenson J, Comitis G, et al. Congenital heart disease in low- and lower-middle-income countries: Current status and new opportunities. *Curr Cardiol Rep*. 2019;21(12):163. doi:10.1007/s11886-019-1248-z
7. Murata K, Masumoto H. Systems for the functional evaluation of human heart tissues derived from pluripotent stem cells. *Stem Cells*. 2022;40(6):537–545. doi:10.1093/stmcls/sxac022
8. Bagheri-Hosseinabadi Z, Salehinejad P, Mesbah-Namin SA. Differentiation of human adipose-derived stem cells into cardiomyocyte-like cells in fibrin scaffold by a histone deacetylase inhibitor. *Biomed Eng Online*. 2017;16(1):134. doi:10.1186/s12938-017-0423-y
9. Macrin D, Joseph JP, Pillai AA, Devi A. Eminent sources of adult mesenchymal stem cells and their therapeutic imminence. *Stem Cell Rev Rep*. 2017;13(6):741–756. doi:10.1007/s12015-017-9759-8

10. Rajasingh S, Isai DG, Samanta S, et al. Manipulation-free cultures of human iPSC-derived cardiomyocytes offer a novel screening method for cardiotoxicity. *Acta Pharmacol Sin*. 2018;39(10):1590–1603. doi:10.1038/aps.2017.183
11. Li J, Hua Y, Miyagawa S, et al. hiPSC-derived cardiac tissue for disease modeling and drug discovery. *Int J Mol Sci*. 2020;21(23):8893. doi:10.3390/ijms21238893
12. Karch SB, Fineschi V, Francia P, et al. Role of induced pluripotent stem cells in diagnostic cardiology. *World J Stem Cells*. 2021;13(5):331–341. doi:10.4252/wjsc.v13.i5.331
13. Jeziorowska D, Korniat A, Salem JE, Fish K, Hulot JS. Generating patient-specific induced pluripotent stem cells-derived cardiomyocytes for the treatment of cardiac diseases. *Exp Opin Biol Ther*. 2015;15(10):1399–1409. doi:10.1517/14712598.2015.1064109
14. Ruan Z, Zhu L, Yin Y, Chen G. Overexpressing NKx2.5 increases the differentiation of human umbilical cord drived mesenchymal stem cells into cardiomyocyte-like cells. *Biomed Pharmacother*. 2016;78:110–115. doi:10.1016/j.biopha.2016.01.020
15. Abd Emami B, Mahmoudi E, Shokrgozar MA, et al. Mechanical and chemical predifferentiation of mesenchymal stem cells into cardiomyocytes and their effectiveness on acute myocardial infarction. *Artif Organs*. 2018;42(6):E114–E126. doi:10.1111/aor.13091
16. Almouemen N, Kelly HM, O'Leary C. Tissue engineering: Understanding the role of biomaterials and biophysical forces on cell functionality through computational and structural biotechnology analytical methods. *Comput Struct Biotechnol J*. 2019;17:591–598. doi:10.1016/j.csbj.2019.04.008
17. Hou J, Lü A, Liu B, et al. Combination of BMP-2 and 5- AZA is advantageous in rat bone marrow-derived mesenchymal stem cells differentiation into cardiomyocytes. *Cell Biol Int*. 2013;37(12):1291–1299. doi:10.1002/cbin.10161
18. Li Q, Qi LJ, Guo ZK, Li H, Zuo HB, Li NN. $CD73^+$ adipose-derived mesenchymal stem cells possess higher potential to differentiate into cardiomyocytes in vitro. *J Mol Hist*. 2013;44(4):411–422. doi:10.1007/s10735-013-9492-9
19. Lv Y, Liu B, Liu Y, Wang H, Wang H. TGF-β1 combined with Sal-B promotes cardiomyocyte differentiation of rat mesenchymal stem cells. *Exp Ther Med*. 2018;15(6):5359–5364. doi:10.3892/etm.2018.6105
20. Guo X, Bai Y, Zhang L, et al. Cardiomyocyte differentiation of mesenchymal stem cells from bone marrow: New regulators and its implications. *Stem Cell Res Ther*. 2018;9(1):44. doi:10.1186/s13287-018-0773-9
21. Ramesh S, Govarthanan K, Ostrovidov S, et al. Cardiac differentiation of mesenchymal stem cells: Impact of biological and chemical inducers. *Stem Cell Rev Rep*. 2021;17(4):1343–1361. doi:10.1007/s12015-021-10165-3
22. Afjeh-Dana E, Naserzadeh P, Moradi E, Hosseini N, Seifalian AM, Ashtari B. Stem cell differentiation into cardiomyocytes: Current methods and emerging approaches. *Stem Cell Rev Rep*. 2022;18(8):2566–2592. doi:10.1007/s12015-021-10280-1
23. Subbarao RB, Shivakumar SB, Choe YH, et al. $CD105^+$ porcine endometrial stromal mesenchymal stem cells possess differentiation potential toward cardiomyocyte-like cells and insulin-producing β cell-like cells in vitro. *Reprod Sci*. 2019;26(5):669–682. doi:10.1177/1933719118786461
24. Huang YS, Li IH, Chueh SH, et al. Mesenchymal stem cells from rat olfactory bulbs can differentiate into cells with cardiomyocyte characteristics. *J Tissue Eng Regen Med*. 2015;9(12):E191–201. doi:10.1002/term.1684
25. Wang XH, Du HW, Guo XH, et al. *Rehmannia glutinosa* oligosaccharide induces differentiation of bone marrow mesenchymal stem cells into cardiomyocyte-like cells. *Genet Mol Res*. 2016;15(4):1–9. doi:10.4238/gmr15047795
26. Lee KS, Cha SH, Kang HW, et al. Effects of serial passage on the characteristics and chondrogenic differentiation of canine umbilical cord matrix derived mesenchymal stem cells. *Asian Australas J Anim Sci*. 2013;26(4):588–595. doi:10.5713/ajas.2012.12488
27. Zhu L, Ruan Z, Yin Y, Chen G. Expression and significance of DLL4-Notch signaling pathway in the differentiation of human umbilical cord derived mesenchymal stem cells into cardiomyocytes induced by 5-azacytidine. *Cell Biochem Biophys*. 2015;71(1):249–253. doi:10.1007/s12013-014-0191-2
28. Yu Z, Zou Y, Fan J, Li C, Ma L. Notch1 is associated with the differentiation of human bone marrow-derived mesenchymal stem cells to cardiomyocytes. *Mol Med Rep*. 2016;14(6):5065–5071. doi:10.3892/mmr.2016.5862
29. Kang P, Chen C, Chen SY, et al. Nano-sized collagen I molecules enhanced the differentiation of rat mesenchymal stem cells into cardiomyocytes. *J Biomed Mater Res*. 2013;101(10):2808–2816. doi:10.1002/jbm.a.34589
30. Liu Z, Wang W, Gao J, Zhou H, Zhang Y. Isolation, culture, and induced multiple differentiation of Mongolian sheep bone marrow-derived mesenchymal stem cells. *In Vitro Cell Dev Biol Anim*. 2014;50(5):464–474. doi:10.1007/s11626-013-9725-y
31. Shi S, Wu X, Wang X, et al. Differentiation of bone marrow mesenchymal stem cells to cardiomyocyte-like cells is regulated by the combined low dose treatment of transforming growth factor-β1 and 5-azacytidine. *Stem Cells Int*. 2016;2016(1):3816256. doi:10.1155/2016/3816256
32. Song K, Wang Z, Li W, Zhang C, Lim M, Liu T. In vitro culture, determination, and directed differentiation of adult adipose-derived stem cells towards cardiomyocyte-like cells induced by angiotensin II. *Appl Biochem Biotechnol*. 2013;170(2):459–470. doi:10.1007/s12010-013-0210-6
33. Lv Y, Gao C, Liu B, Wang H, Wang H. BMP-2 combined with salvianolic acid B promotes cardiomyocyte differentiation of rat bone marrow mesenchymal stem cells. *Kaohsiung J Med Sci*. 2017;33(10):477–485. doi:10.1016/j.kjms.2017.06.006
34. Sekuła-Stryjewska M, Noga S, Dźwigońska M, et al. Graphene-based materials enhance cardiomyogenic and angiogenic differentiation capacity of human mesenchymal stem cells in vitro: Focus on cardiac tissue regeneration. *Mater Sci Eng C Mater Biol Appl*. 2021;119:111614. doi:10.1016/j.msec.2020.111614
35. Nimsanor N, Phetfong J, Plabplueng C, Jangpatarapongsa K, Prachayasittikul V, Supokawej A. Inhibitory effect of oxidative damage on cardiomyocyte differentiation from Wharton's jelly-derived mesenchymal stem cells. *Exp Ther Med*. 2017;14(6):5329–5338. doi:10.3892/etm.2017.5249
36. He X, Li L, Tang M, Zeng Y, Li H, Yu X. Biomimetic electrical stimulation induces rat bone marrow mesenchymal stem cells to differentiate into cardiomyocyte-like cells via TGF-beta 1 in vitro. *Prog Biophys Mol Biol*. 2019;148:47–53. doi:10.1016/j.pbiomolbio.2017.09.023
37. Zhao L, Yang G, Zhao X. Rho-associated protein kinases play an important role in the differentiation of rat adipose-derived stromal cells into cardiomyocytes in vitro. *PLoS One*. 2014;9(12):e115191. doi:10.1371/journal.pone.0115191
38. Rao PS. Management of congenital heart disease: State of the art. Part I: Acyanotic heart defects. *Children (Basel)*. 2019;6(3):42. doi:10.3390/children6030042
39. Djer MM, Madiyono B. Tatalaksana Penyakit Jantung Bawaan. *Sari Pediatri*. 2016;2(3):155. doi:10.14238/sp2.3.2000.155-62
40. Schleich JM, Abdulla T, Summers R, Houyel L. An overview of cardiac morphogenesis. *Arch Cardiovasc Dis*. 2013;106(11):612–623. doi:10.1016/j.acvd.2013.07.001
41. Wernovsky G, Anderson RH, Kumar K, et al., eds. *Anderson's Pediatric Cardiology*. 4th ed. Philadelphia, USA: Elsevier; 2020. ISBN:978-0-7020-7608-4.
42. Best KE, Rankin J. Long-term survival of individuals born with congenital heart disease: A systematic review and meta-analysis. *J Am Heart Assoc*. 2016;5(6):e002846. doi:10.1161/JAHA.115.002846
43. Meng X, Song M, Zhang K, et al. Congenital heart disease: Types, pathophysiology, diagnosis, and treatment options. *MedComm*. 2024;5(7):e631. doi:10.1002/mco2.631
44. Varela-Chinchilla CD, Sánchez-Mejía DE, Trinidad-Calderón PA. Congenital heart disease: The state-of-the-art on its pharmacological therapeutics. *J Cardiovasc Dev Dis*. 2022;9(7):201. doi:10.3390/jcdd9070201
45. Chubb H, Rosenthal E. Implantable cardioverter-defibrillators in congenital heart disease. *Herzschrittmacherther Elektrophysiol*. 2016;27(2):95–103. doi:10.1007/s00399-016-0437-3
46. Steffens D, Lersch M, Rosa A, et al. A new biomaterial of nanofibers with the microalga *Spirulinaas* scaffolds to cultivate with stem cells for use in tissue engineering. *J Biomed Nanotechnol*. 2013;9(4):710–718. doi:10.1166/jbn.2013.1571

47. Morita Y, Kishino Y, Fukuda K, Tohyama S. Scalable manufacturing of clinical-grade differentiated cardiomyocytes derived from human-induced pluripotent stem cells for regenerative therapy. *Cell Prolif*. 2022;55(8):e13248. doi:10.1111/cpr.13248
48. Bagno L, Hatzistergos KE, Balkan W, Hare JM. Mesenchymal stem cell-based therapy for cardiovascular disease: Progress and challenges. *Mol Ther*. 2018;26(7):1610–1623. doi:10.1016/j.ymthe.2018.05.009
49. Mantakaki A, Fakoya AOJ, Sharifpanah F. Recent advances and challenges on application of tissue engineering for treatment of congenital heart disease. *PeerJ*. 2018;6:e5805. doi:10.7717/peerj.5805
50. Patel AA, Mohamed AH, Rizaev J, et al. Application of mesenchymal stem cells derived from the umbilical cord or Wharton's jelly and their extracellular vesicles in the treatment of various diseases. *Tissue Cell*. 2024;89:102415. doi:10.1016/j.tice.2024.102415
51. Matta A, Nader V, Lebrin M, et al. Pre-conditioning methods and novel approaches with mesenchymal stem cells therapy in cardiovascular disease. *Cells*. 2022;11(10):1620. doi:10.3390/cells11101620
52. Pedersen KW, Kierulf B, Neurauter A. Specific and generic isolation of extracellular vesicles with magnetic beads. *Methods Mol Biol*. 2017; 1660:65–87. doi:10.1007/978-1-4939-7253-1_7
53. Atewologun FA, Okesanya OJ, Okon II, et al. Examining the potentials of stem cell therapy in reducing the burden of selected non-communicable diseases in Africa. *Stem Cell Res Ther*. 2024;15(1):253. doi:10.1186/s13287-024-03864-4
54. Zakrzewski W, Dobrzyński M, Szymonowicz M, Rybak Z. Stem cells: Past, present, and future. *Stem Cell Res Ther*. 2019;10(1):68. doi:10.1186/s13287-019-1165-5
55. Abbaszadeh H, Ghorbani F, Derakhshani M, et al. Regenerative potential of Wharton's jelly-derived mesenchymal stem cells: A new horizon of stem cell therapy. *J Cell Physiol*. 2020;235(12):9230–9240. doi:10.1002/jcp.29810
56. Yin S, Ji C, Wu P, Jin C, Qian H. Human umbilical cord mesenchymal stem cells and exosomes: Bioactive ways of tissue injury repair. *Am J Transl Res*. 2019;11(3):1230–1240. PMID:30972158. PMCID:PMC6456565.
57. Lyra-Leite DM, Gutiérrez-Gutiérrez Ó, Wang M, Zhou Y, Cyganek L, Burridge PW. A review of protocols for human iPSC culture, cardiac differentiation, subtype-specification, maturation, and direct reprogramming. *STAR Protoc*. 2022;3(3):101560. doi:10.1016/j.xpro.2022.101560
58. Szaraz P, Gratch YS, Iqbal F, Librach CL. In vitro differentiation of human mesenchymal stem cells into functional cardiomyocyte-like cells. *J Vis Exp*. 2017;126:55757. doi:10.3791/55757
59. Batsali AK, Kastrinaki MC, Papadaki HA, Pontikoglou C. Mesenchymal stem cells derived from Wharton's jelly of the umbilical cord: Biological properties and emerging clinical applications. *Curr Stem Cell Res Ther*. 2013;8(2):144–155. doi:10.2174/1574888X11308020005
60. Hollweck T, Hartmann I, Eblenkamp M, et al. Cardiac differentiation of human Wharton's jelly stem cells: Experimental comparison of protocols. *Open Tissue Eng Regen Med J*. 2011;4(1):95–102. doi:10.2174/1875043501104010095
61. Farzaneh M, Rahimi F, Alishahi M, Khoshnam SE. Paracrine mechanisms involved in mesenchymal stem cell differentiation into cardiomyocytes. *Curr Stem Cell Res Ther*. 2019;14(1):9–13. doi:10.2174/1574888X13666180821160421
62. Naito AT, Shiojima I, Akazawa H, et al. Developmental stage-specific biphasic roles of Wnt/β-catenin signaling in cardiomyogenesis and hematopoiesis. *Proc Natl Acad Sci U S A*. 2006;103(52):19812–19817. doi:10.1073/pnas.0605768103
63. Raman N, Imran SAM, Ahmad Amin Noordin KB, Wan Kamarul Zaman WS, Nordin F. Mechanotransduction of mesenchymal stem cells (MSCs) during cardiomyocytes differentiation. *Heliyon*. 2022;8(11):e11624. doi:10.1016/j.heliyon.2022.e11624
64. Gallo S, Sala V, Gatti S, Crepaldi T. Cellular and molecular mechanisms of HGF/Met in the cardiovascular system. *Clin Sci (Lond)*. 2015; 129(12):1173–1193. doi:10.1042/CS20150502
65. Guo Y, Pu WT. Cardiomyocyte maturation: New phase in development. *Circ Res*. 2020;126(8):1086–1106. doi:10.1161/CIRCRESAHA.119.315862
66. Asumda FZ. Towards the development of a reliable protocol for mesenchymal stem cell cardiomyogenesis. *Stem Cell Discov*. 2013;3(1):13–21. doi:10.4236/scd.2013.31003
67. Leitolis A, Robert AW, Pereira IT, Correa A, Stimamiglio MA. Cardiomyogenesis modeling using pluripotent stem cells: The role of microenvironmental signaling. *Front Cell Dev Biol*. 2019;7:164. doi:10.3389/fcell.2019.00164
68. Rajala K, Pekkanen-Mattila M, Aalto-Setälä K. Cardiac differentiation of pluripotent stem cells. *Stem Cells Int*. 2011;2011:383709. doi:10.4061/2011/383709
69. Mundre RS, Koka P, Dhanaraj P, et al. Synergistic role of 5-azacytidine and ascorbic acid in directing cardiosphere derived cells to cardiomyocytes in vitro by downregulating Wnt signaling pathway via phosphorylation of β-catenin. *PLoS One*. 2017;12(11):e0188805. doi:10.1371/journal.pone.0188805
70. Shouman S, Zaher A, Abdelhameed A, et al. Cardiac progenitor cells. *Adv Exp Med Biol*. 2020;1312:51–73. doi:10.1007/5584_2020_594
71. Chen J, Tschudy-Seney B, Ma X, Zern MA, Liu P, Duan Y. Salvianolic acid B enhances hepatic differentiation of human embryonic stem cells through upregulation of WNT pathway and inhibition of Notch pathway. *Stem Cells Dev*. 2018;27(4):252–261. doi:10.1089/scd.2017.0168
72. Parodi EM, Kuhn B. Signalling between microvascular endothelium and cardiomyocytes through neuregulin. *Cardiovasc Res*. 2014; 102(2):194–204. doi:10.1093/cvr/cvu021
73. Qian Q, Qian H, Zhang X, et al. 5-azacytidine induces cardiac differentiation of human umbilical cord-derived mesenchymal stem cells by activating extracellular regulated kinase. *Stem Cells Dev*. 2012; 21(1):67–75. doi:10.1089/scd.2010.0519
74. Lemmens K, Doggen K, De Keulenaer GW. Role of neuregulin-1/ErbB signaling in cardiovascular physiology and disease: Implications for therapy of heart failure. *Circulation*. 2007;116(8):954–960. doi:10.1161/CIRCULATIONAHA.107.690487
75. Wang Z, Xu G, Wu Y, et al. Neuregulin-1 enhances differentiation of cardiomyocytes from embryonic stem cells. *Med Biol Eng Comput*. 2009;47(1):41–48. doi:10.1007/s11517-008-0383-2
76. Norström A, ÅKesson K, Hardarson T, Hamberger L, BjöRquist P, Sartipy P. Molecular and pharmacological properties of human embryonic stem cell-derived cardiomyocytes. *Exp Biol Med (Maywood)*. 2006;231(11):1753–1762. doi:10.1177/153537020623101113
77. Park G, Yoon BS, Kim YS, et al. Conversion of mouse fibroblasts into cardiomyocyte-like cells using small molecule treatments. *Biomaterials*. 2015;54:201–212. doi:10.1016/j.biomaterials.2015.02.029
78. Guo Y, Yu Y, Hu S, Chen Y, Shen Z. The therapeutic potential of mesenchymal stem cells for cardiovascular diseases. *Cell Death Dis*. 2020; 11(5):349. doi:10.1038/s41419-020-2542-9
79. Khezri S, Valojerdi MR, Sepehri H, Baharvand H. Effect of basic fibroblast growth factor on cardiomyocyte differentiation from mouse embryonic stem cells. *Saudi Med J*. 2007;28(2):181–186. PMID:17268693.
80. Ramesh S, Singh A, Cibi DM, Hausenloy DJ, Singh MK. In vitro culture of epicardial cells from mouse embryonic heart. *J Vis Exp*. 2016; 110:53993. doi:10.3791/53993
81. Salazar VS, Gamer LW, Rosen V. BMP signalling in skeletal development, disease and repair. *Nat Rev Endocrinol*. 2016;12(4):203–221. doi:10.1038/nrendo.2016.12
82. Ebelt H, Hillebrand I, Arlt S, et al. Treatment with bone morphogenetic protein 2 limits infarct size after myocardial infarction in mice. *Shock*. 2013;39(4):353–360. doi:10.1097/SHK.0b013e318289728a
83. Alves AJ, Eynon N, Oliveira J, Goldhammer E. RAAS and adrenergic genes in heart failure: Function, predisposition and survival implications. *World J Cardiol*. 2010;2(7):187–197. doi:10.4330/wjc.v2.i7.187
84. Adamcova M, Kawano I, Simko F. The impact of microRNAs in renin–angiotensin-system-induced cardiac remodelling. *Int J Mol Sci*. 2021; 22(9):4762. doi:10.3390/ijms22094762
85. Shu T, Pang M, Rong L, et al. Protective effects and mechanisms of salvianolic acid B against H_2O_2-induced injury in induced pluripotent stem cell-derived neural stem cells. *Neurochem Res*. 2015;40(6): 1133–1143. doi:10.1007/s11064-015-1573-6
86. Gao P, Yang J, Gao X, et al. Salvianolic acid B improves bone marrow-derived mesenchymal stem cell differentiation into alveolar epithelial cells type I via Wnt signaling. *Mol Med Rep*. 2015;12(2):1971–1976. doi:10.3892/mmr.2015.3632
87. Chan SSK, Chen JH, Hwang SM, et al. Salvianolic acid B–vitamin C synergy in cardiac differentiation from embryonic stem cells. *Biochem Biophys Res Commun*. 2009;387(4):723–728. doi:10.1016/j.bbrc.2009.07.122
88. Li J, Zhu K, Wang Y, et al. Combination of *IGF-1* gene manipulation and 5-AZA treatment promotes differentiation of mesenchymal stem cells into cardiomyocyte-like cells. *Mol Med Rep*. 2015;11(2):815–820. doi:10.3892/mmr.2014.2812

89. Zhang G, Gu T, Guan X, et al. HGF and IGF-1 promote protective effects of allogeneic BMSC transplantation in rabbit model of acute myocardial infarction. *Cell Prolif*. 2015;48(6):661–670. doi:10.1111/cpr.12219
90. Youssef A, Aboalola D, Han VKM. The roles of insulin-like growth factors in mesenchymal stem cell niche. *Stem Cells Int*. 2017;2017:9453108. doi:10.1155/2017/9453108
91. Rofaani E, Mardani MW, Yutiana PN, Amanda O, Darmawan N. Differentiation of mesenchymal stem cells into vascular endothelial cells in 3D culture: A mini review. *Mol Biol Rep*. 2024;51(1):781. doi:10.1007/s11033-024-09743-8
92. Gaafar T, Shawky S, Attia W, Hamza H, El Hawary R. The role of angiotensin II in cardiomyogenic differentiation of human adipose tissue-derived mesenchymal stem cells. *Comp Clin Pathol*. 2015;24(4):879–885. doi:10.1007/s00580-014-2001-z
93. Cetin Y, Sahin MG, Kok FN. Application potential of three-dimensional silk fibroin scaffold using mesenchymal stem cells for cardiac regeneration. *J Biomater Appl*. 2021;36(4):740–753. doi:10.1177/08853282211018529
94. Razavi ZS, Farokhi S, Mahmoudvand G, et al. Stem cells and bio scaffolds for the treatment of cardiovascular diseases: New insights. *Front Cell Dev Biol*. 2024;12:1472103. doi:10.3389/fcell.2024.1472103
95. Dominici M, Le Blanc K, Mueller I, et al. Minimal criteria for defining multipotent mesenchymal stromal cells: The International Society for Cellular Therapy position statement. *Cytotherapy*. 2006;8(4):315–317. doi:10.1080/14653240600855905
96. Avolio E, Caputo M, Madeddu P. Stem cell therapy and tissue engineering for correction of congenital heart disease. *Front Cell Dev Biol*. 2015;3:39. doi:10.3389/fcell.2015.00039
97. Gopal S, Rodrigues AL, Dordick JS. Exploiting CRISPR Cas9 in three-dimensional stem cell cultures to model disease. *Front Bioeng Biotechnol*. 2020;8:692. doi:10.3389/fbioe.2020.00692
98. McKee C, Chaudhry GR. Advances and challenges in stem cell culture. *Colloids Surf B Biointerfaces*. 2017;159:62–77. doi:10.1016/j.colsurfb.2017.07.051
99. Andrysiak K, Stępniewski J, Dulak J. Human-induced pluripotent stem cell-derived cardiomyocytes, 3D cardiac structures, and heart-on-a-chip as tools for drug research. *Pflugers Arch Eur J Physiol*. 2021;473(7):1061–1085. doi:10.1007/s00424-021-02536-z
100. Wang L, Hu S, Zhou B. Deciphering cardiac biology and disease by single-cell transcriptomic profiling. *Biomolecules*. 2022;12(4):566. doi:10.3390/biom12040566